


REPORT DOCUMENTATION PAGE	1. REPORT NO. NCEER-92-0004	2.	3.  PB94-142239
4. Title and Subtitle Proceedings from the First U.S. - Japan Workshop on Earthquake Protective Systems for Bridges		5. Report Date February 4, 1992	
7. Author(s) I.G. Buckle		6.	
9. Performing Organization Name and Address National Center for Earthquake Engineering Research State University of New York at Buffalo Red Jacket Quadrangle Buffalo, New York 14261		8. Performing Organization Rept. No.	
12. Sponsoring Organization Name and Address National Center for Earthquake Engineering Research State University of New York at Buffalo Red Jacket Quadrangle Buffalo, New York 14261		10. Project/Task/Work Unit No. 11. Contract(C) or Grant(G) No. (C) BCS 90-25010 and NYSSTF Grant No. (G) NEC-91029	
15. Supplementary Notes This workshop was conducted at the State University of New York at Buffalo. It was partially supported by the National Science Foundation under Grant No. BCS 90-25010 and the New York State Science and Technology Foundation under Grant No. NEC-91029.		13. Type of Report & Period Covered Technical Report	
16. Abstract (Limit: 300 words) This report offers the Proceedings of the First U.S.-Japan Workshop on Earthquake Protective Systems for Bridges, held in Buffalo, New York on September 4 and 5, 1991. This comprehensive workshop saw the presentation and discussion of 41 papers covering a wide range of topics: seismic isolation hardware, the testing of isolated bridges and components, active control and hybrid systems, design issues and applications, long span bridges, seismic retrofit and new construction. Of particular interest was the difference in philosophy between menshin design in Japan and seismic isolation as practiced in the United States. The need to lengthen the period of vibration is not so important (in Japan) as the requirement to keep joint clearances small. Other issues included joint design, displacement restraint devices, and durability of isolation hardware in the field. This report also contains a set of resolutions adopted at the meeting regarding future cooperation between the United States and Japan.			
17. Document Analysis a. Descriptors b. Identifiers/Open-Ended Terms Highway bridges. Seismic isolation. Base isolation. Rubber bearings. Joints. Sliding friction dampers. Steel dampers. Viscous dampers. Design methods. Elastomeric bearings. Dynamic response analysis. Sliding isolation systems. Lateral loads. Experimental tests. Pseudodynamic tests. Active control systems. Hybrid control systems. Retrofitting. Long span structures. United States. Japan. <small>c. COBARI Field/Group</small> Cable stayed bridges. Menshin design. Earthquake Engineering.			
18. Availability Statement Release Unlimited		19. Security Class (This Report) Unclassified	21. No. of Pages 614
		20. Security Class (This Page) Unclassified	22. Price

NOTICE

This report was prepared by the National Center for Earthquake Engineering Research (NCEER). Neither NCEER, associates of NCEER, its sponsors, nor any person acting on their behalf:

- a. makes any warranty, express or implied, with respect to the use of any information, apparatus, method, or process disclosed in this report or that such use may not infringe upon privately owned rights; or
- b. assumes any liabilities of whatsoever kind with respect to the use of, or the damage resulting from the use of, any information, apparatus, method or process disclosed in this report.

Any opinions, findings, and conclusions or recommendations expressed in this publication are those of the author(s) and do not necessarily reflect the views of the National Science Foundation, the New York State Science and Technology Foundation, or other sponsors.



FB94 - 142239

**Proceedings
from the
First U.S. - Japan Workshop on
Earthquake Protective Systems for Bridges**

**Held at the
State University of New York at Buffalo
September 4-5, 1991**

Technical Report NCEER-92-0004

**Edited by I. Buckle
February 4, 1992**

NCEER Project Number 90-6016

**NSF Master Contract Number BCS 90-25010
and
NYSSTF Grant Number NEC-91029**

**NATIONAL CENTER FOR EARTHQUAKE ENGINEERING RESEARCH
State University of New York at Buffalo
Red Jacket Quadrangle, Buffalo, NY 14261**

Preface

This report is the Proceedings from the First U.S.-Japan Workshop on Earthquake Protective Systems for Bridges, which was held in Buffalo, New York on September 4 and 5, 1991. Conducted under the auspices of Task Committee G on Passive, Active and Hybrid Controls of the UJNR Panel on Wind and Seismic Effects, the workshop was attended by 35 Japanese and 28 U.S. participants. In addition, four observers from Taiwan and People's Republic of China were in attendance. U.S. sponsorship for the meeting was provided by the National Center for Earthquake Engineering Research (NCEER), which is headquartered on the campus of the State University of New York at Buffalo. The organizer for the Japan-side was the Public Works Research Institute (PWRI) of the Ministry of Construction.

This comprehensive workshop comprised the presentation and discussion of 29 papers which covered a wide range of topics including seismic isolation hardware, the testing of isolated bridges and components, active control and hybrid systems, design issues and applications, long span bridges, seismic retrofit and new construction. Fruitful discussion on many issues of common concern took place. Of particular interest was the difference in philosophy between menshin design in Japan and seismic isolation as practiced in the United States. The need to lengthen the period of vibration is not so important (in Japan) as the requirement to keep joint clearances small. Other issues included joint design, displacement restraint devices, and durability of isolation hardware in the field. A set of resolutions were adopted by the meeting regarding future cooperation between the United States and Japan. These resolutions are contained herein.

In conjunction with the workshop, a study tour of base isolated bridges in the United States was undertaken by the Japanese participants. The purpose was to obtain first-hand knowledge about U.S. practice concerning the use of base isolation for seismic retrofit and the construction of new bridges.

Resolutions

1. There are many topics of common interest related to the development and implementation of these systems. It is therefore resolved that continued cooperation between researchers and bridge engineers in both countries be actively encouraged. The free exchange of research and design experience, in both the laboratory and field, will facilitate the advancement of this technology and its practical implementation in both countries.
2. In view of the success of this first workshop, the importance of this technology and the rapidly advancing state-of-the-art, it is resolved that a second U.S.-Japan Workshop on Earthquake Protective Systems for Bridges be held in Japan late in 1992.
3. It is further resolved that the second workshop be oriented towards research and application rather than state-of-the-art reviews. Topics to be covered should include: (1) innovative protective systems; (2) design methods for base isolated/menshin bridges; (3) design of utilities carried by isolated bridges so as to accommodate movement; and (4) full-scale verification of performance.

Another activity for the second workshop should be the comparison of U.S. and Japanese isolation/menshin designs for the same bridge. This project requires the design exercises to be completed before the next meeting, so that the results are available for presentation and discussion. For such an exercise to be useful, practitioners and designers should be active participants in the workshop.

TABLE OF CONTENTS

SECTION	TITLE	PAGE
1	OPENING SESSION AND OVERVIEW	1
	A Perspective of Menshin Design for Highway Bridges in Japan	3
	<i>K. Kawashima, K. Hasegawa and H. Nagashima</i>	
	History and Application of Seismic Isolation to Highway Bridges in the United States	27
	<i>I. Buckle and R. Mayes</i>	
2	SEISMIC ISOLATION HARDWARE	41
	Development of Textile-Reinforced Rubber Bearings for Menshin Bridges	43
	<i>N. Kawai, N. Doro and Y. Miyauchi</i>	
	Development of a Sliding Friction Damper	51
	<i>T. Iguchi</i>	
	Development of Steel Damper for Menshin Bridges	63
	<i>H. Kamiya, S. Iizuka and M. Takei</i>	
	Development of Viscous Damper for Menshin Bridges	77
	<i>K. Kawashima, J. Iseki, I. Shimoda and Y. Makiguchi</i>	
	Development of Finger Joint Movable in Horizontal Directions for Menshin Bridges	95
	<i>T. Kimishima, T. Harada and D. Ozaki</i>	
	Development of High Damping Rubber Bearing for Menshin Bridges	
	Part 1 - <i>Y. Suizu and C. Sudoh</i>	109
	Part 2 - <i>K. Kawashima, M. Koshitoge, K. Endo, C. Yamada and T. Nishimoto</i>	123
	Part 3 - <i>I. Nishikawa, N. Katoh, M. Itoh and Y. Muramatsu</i>	137
	Finite Element Analysis of Elastomeric Isolation Bearings for Different Connection Details	151
	<i>H. Liu and I. Buckle</i>	

TABLE OF CONTENTS (Cont'd)

SECTION	TITLE	PAGE
	Finite Element Analysis of Elastomeric Bearings <i>R. Shepherd and L.J. Billings</i>	169
	Development of Roller-Type Bearing for Menshin Bridges <i>T. Takaku, M. Shimada, N. Tsumura and S. Izuma</i>	177
	Sliding Isolation Systems for Bridges <i>M.C. Constantinou</i>	189
	Certification Test of Menshin Devices <i>K. Kawashima, K. Hasegawa, H. Nagashima, Y. Makiguchi and Y. Suizu</i>	205
	Investigation of Friction Pendulum Systems <i>S.A. Mahin</i>	213
	Lateral Loading Tests of Knock-Off Mechanism for Menshin Bridges <i>T. Kikuchi and Y. Goto</i>	221
	Development of Falling-Off Prevention Devices for Menshin Bridges <i>D. Ozaki and F. Matsumoto</i>	233
	Design Concept of Falling-Down Prevention Devices for Menshin Bridges <i>A. Hayashi, J. Izeki, K. Yoshikawa, T. Kikuchi, K. Matsubara and H. Koyama</i>	247
3	TESTING OF ISOLATED BRIDGES AND COMPONENTS	259
	Effect of Dynamic Property of Menshin Devices and Stiffness of Substructures on Seismic Response of Menshin Bridges <i>T. Takeda, Y. Hishiki and H. Okamoto</i>	261
	Experiment and Analysis on Seismic Response of Menshin Bridges <i>K. Kawashima, K. Hasegawa and H. Nagashima</i>	273

—

TABLE OF CONTENTS (Cont'd)

SECTION	TITLE	PAGE
	On-Line Earthquake Response Tests of High-Damping	299
	Rubber Bearings for Seismic Isolation <i>H. Iemura, Y. Yamada, W. Tanzo, Y. Uno and S. Nakamura</i>	
4	ACTIVE CONTROL AND HYBRID SYSTEMS FOR BRIDGES .	315
	Active Control for Bridge Applications: Case Studies	317
	<i>T.T. Soong</i>	
	A Hybrid Sliding Isolation System for Bridges	323
	<i>Q. Feng, M. Shinozuka, S. Fujii and T. Fujita</i>	
	Some Thoughts on Hybrid Control of Bridge Structures	337
	<i>J.N. Yang</i>	
5	DESIGN ISSUES AND APPLICATIONS	351
	Selecting Bedrock Motions for the Seismic Design of Bridges	353
	<i>A.W. Taylor and W.C. Stone</i>	
	AASHTO Seismic Isolation Design Requirements for	363
	Highway Bridges <i>R.L. Mayes, I.G. Buckle, T.E. Kelly and L.R. Jones</i>	
	Bridge Modeling Method in Menshin Design	379
	<i>M. Shimada, K. Dewa and T. Tamura</i>	
	Design and Construction of Miyagawa Bridge (First Menshin	389
	Bridge in Japan) <i>M. Yoshiro and H. Koji</i>	
	Equivalent Linearizing Method of Menshin Devices	407
	<i>K. Takahashi, D. Ozaki, K. Matsubara, Y. Takagi, Y. Makiguchi and Y. Suizu</i>	
	Simplified Determination Method of Substructure Dimensions	421
	of Menshin Bridges <i>Y. Sawauchi, Y. Hishiki and K. Utsugi</i>	
	Seismic Response Analysis Method of Menshin Bridges	431
	<i>Y. Hamazaki, O. Ohtani and H. Zui</i>	

TABLE OF CONTENTS (Cont'd)

SECTION	TITLE	PAGE
	Effect of Nonlinearity of Bridge Columns on Seismic Response of Menshin Bridges <i>T. Hirai and M. Sugimoto</i>	441
	Seismic Response of Curved Continuous Menshin Bridge <i>N. Hosoda, I. Kaneko and K. Kuroda</i>	457
	Comparative Design of a Steel Girder Bridge Using Three Different Bearing Systems <i>M. Okado, M. Komuro, M. Horikawa and F. Kawahara</i>	469
6	APPLICATIONS TO SEISMIC RETROFIT	479
	Application of Menshin Design to Seismic Retrofit of Existing Bridges By Concrete Slabs of Adjacent Girders <i>M. Yanagihara, Y. Makiguchi and I. Kawasaki</i>	481
	Advantages of Isolation Bearings for New Bridges <i>R. Anderson</i>	491
	Application of Menshin Design to Seismic Retrofitting of Highway Bridge Substructures <i>T. Tamura, M. Hirai, N. Higuchi and S. Masuda</i>	501
7	APPLICATIONS TO MEDIUM AND LONG-SPAN BRIDGES	517
	CALTRANS Seismic Isolation Design and Future Concepts <i>E. Thorkildsen</i>	519
	Earthquake Resistant Design of a Long-Span Cable-Stayed Bridge <i>Y. Yamada, K. Toki and M. Kitazawa</i>	531
	Passive Seismic Control of Cable-Stayed Bridges <i>H-E.M. Ali and A.M. Abdel-Ghaffar</i>	543
	Seismic Response of Multi-Span Continuous Bridge with Deck Length of 1 Km <i>Y. Goto, M. Tokunaga, T. Yosimura and M. Sintaku</i>	557

TABLE OF CONTENTS (Cont'd)

SECTION	TITLE	PAGE
	Application of Menshin Design to Bridges With Deck Length of 1000 M <i>H. Mashiko, H. Arai and Y. Fujiwara</i>	573
	Appendix A	583
	Workshop Program	585
	Workshop Participants	587

1. Opening Session and Overview

A Perspective of Menshin Design for Highway Bridges in Japan
K. Kawashima, K. Hasegawa and H. Nagashima

History and Application of Seismic Isolation to Highway Bridges in the United States
I. Buckle and R. Mayes

A PERSPECTIVE OF MENSHEIN DESIGN FOR HIGHWAY BRIDGES IN JAPAN

Kazuhiko KAWASHIMA, Kinji HASEGAWA and Hiroyuki NAGASHIMA

Earthquake Engineering Division, Public Works Research Institute

SUMMARY

Presented are current technical developments for the base isolation to ordinary size of highway bridges with span length from 10 m to 50 m in Japan. Seismic environment, history of seismic damage and formulation of seismic design codes are firstly described with emphasis on motivation for introducing the base isolation. Because elongation of natural period of bridges is quite difficult to be adopted due to various restrictions associated with deck displacement, a "Menshein Design" which aims even distribution of lateral force to each substructure as well as increase of energy dissipating capability is becoming to be incorporated. Existing and current efforts for developing the Menshein Design including pilot construction and a joint arch program of the Menshein Design is presented.

INTRODUCTION

Highways in Japan consist of Expressways (3,721 km), National Highways (46,661 km), Prefectural Roads (128,202 km) and Municipal Roads (925,138 km). Along the highways and roads, excluding the Municipal Roads, there are about 60,000 bridges with span length of 15 m or longer. Although the number of bridges constructed per year depends on the year and span length, it is about 6,000 for concrete bridges and 2,000 for steel bridges with the length of 15 m or longer.

Base isolation has been highlighted in Japan as a new technology to reduce seismic response of structures, and more than 30 base-isolated buildings have been constructed. The principles of base isolation is to elongation the natural period of a structure and enhance the energy dissipating capability with a base isolation device, which consist of an isolator and an energy dissipator. Although the base isolation has been applied to highway bridges in New Zealand and U.S.A.(Refs. 1 - 4), seismicity is higher and ground condition is softer in Japan, so that a specific research and development be inevitable for applying the base isolation to highway bridges in Japan.

This paper describes the current efforts for incorporating the base isolation to seismic design of highway bridges. Because design consideration is different with large bridges such as cable-stayed bridges, description is concentrated here to ordinary size of highway bridges with span length of 10 to 50 m. Overcrossing and viaduct in city area is also included here as "bridge". Seismic design philosophy of those highway bridges including the the history of bridge damage in the past and past revision of seismic design codes is presented with emphasis on the motivation for incorporating the base isolation. Because elongation of natural period is difficult to be adopted and

distribution of lateral force to substructures is now becoming considerably important, a slightly different concept with the base isolation is being introduced by taking advantages of energy dissipation and distribution of lateral force. It is referred as "Menshin Design". Outline of the existing and on-going researches including a joint program between the Public Works Research Institute and 28 private firms entitled "Development of Menshin Design of Highway Bridges" (Ref. 5) are also presented.

CURRENT SEISMIC DESIGN AND PHILOSOPHY OF HIGHWAY BRIDGES

History of Earthquake Damages Located along the Pacific Seismic Belt, Japan is one of the most seismically disastrous countries in the world and has often suffered significant damage from large earthquakes. Fig. 1 shows the largest magnitude of the earthquakes which occurred in the past (Ref. 6). It is recognized that the earthquakes with magnitude over 8 occurred with rather short recurrent period in and around Japan in the past. It should be noted that seismicity is especially high along the Pacific coast where large cities in population and industrial products such as Tokyo, Osaka and Nagoya are located.

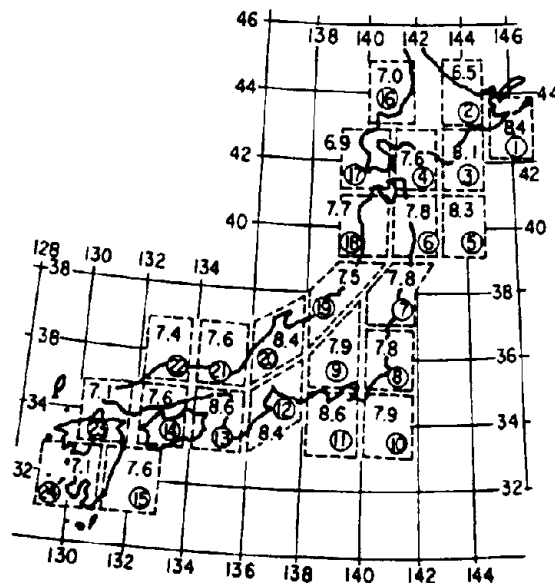


Fig. 1 Largest Earthquake Magnitude Which Occurred in the Past

Table 1 shows the highway bridges which suffered damages in the past earthquakes since the Kanto Earthquake of 1923 (Ref. 7). It should be noted that although there were many bridges which suffered damages due to earthquakes, number of bridges which fell down was only 15. It is important to note that damage types have been varying as shown in Table 2 in accordance with the progress of the seismic design method and improvement of construction practice. Seismic damage since the 1923 Kanto Earthquake may be classified into three stages from their significance (Refs. 8, 9).

**Table 1 Number of Highway Bridges Which Suffered Damage
in the Past Earthquakes after 1923 Kanto Earthquake**

DATE	EARTHQUAKE	MAGNITUDE	NUMBER OF BRIDGES DAMAGED	NUMBER OF BRIDGES WHICH FELL DOWN
1923. 9. 1	KANTO	7.9	1,785	6
1946.12.21	NANKAI	8.1	346	1
1948. 6.28	FUKUI	7.3	243	4
1949.12.26	IMAICHI	6.4	1	0
1952. 3. 4	TOKACHI-OKI	8.1	128	0
1962. 4.30	MIYAGI-KEN-HOKUBU	6.5	187	0
1964. 6.16	NIGATA	7.5	98	3
1968. 2.21	EBINO	6.1	10	0
1968. 5.16	TOKACHI-OKI	7.9	101	0
1978. 1.14	IZU-ONSHIMA	7.0	7	0
1978. 6.12	MIYAGI-KEN-OKI	7.4	95	1
1982. 3.21	URAKAWA-OKI	7.1	5	0
1983. 5.26	NIHON-KAI-CHUBU	7.7	176	0
1984. 9.14	NAGANO-KEN-SEIBU	6.8	14	0
TOTAL			3,191	15

Table 2 Change of Seismic Damage Mode

Year	Major Earthquakes	Change of Major Seismic Damage	Seismic Design Method	Seismic Inspection and Strengthening	
1920	1923 Kanto Earthquake (M7.9)		1926 Initiation of Seismic Design (Details of Road Structures)		
1930					
1940	1946 Nankai Earthquake (M8.1) 1948 Fukui Earthquake (M7.3)			1939 Introduction of Standard Seismic Coefficient (Design Specifications of Steel Highway Bridges)	
1950	1952 Tokachi-oki Earthquake (M8.1)			1956 Seismic Coefficient depending on Zone and Ground Condition (Design Specifications of Steel Highway Bridges)	
1960	1964 Niigata Earthquake (M7.5)				
1970	1978 Miyagi-ken-oki Earthquake (M7.4)		1971 • Seismic Coefficient depending on Zone, Ground Conditions, Importance and Structural Response • Introduction of Evaluation Method for Liquefaction (Specifications for Seismic Design)	1971 Seismic Inspection	
1980	1982 Utsunomiya-oki Earthquake (M7.1) 1983 Nihon-ko-i-chubu Earthquake (M7.7)		1980 • Part V Seismic Design, Specifications for Design of Highway Bridges • Introduction of New Evaluation Method for Liquefactions	1976 Seismic Inspection 1979 Seismic Inspection	
1990			1990 Part V Seismic Design, Specifications for Design of Highway Bridges	1986 Seismic Inspection	

1) Stage 1 - Damage due to Inadequate Strength of Foundations

After experiencing the destructive damage of the 1923 Kanto Earthquake, the first requirements for seismic design of highway bridges were included in the "Details of Road Structures (Draft)" issued in 1926. No seismic effects were considered for design of highway bridges prior to the Kanto Earthquake. Even after the first stipulations, seismic design was not adequate because the stipulations only described design force levels without providing detailed design method and design details. Therefore, seismic safety of bridges was short until the 1950's when seismic design for foundations and substructures came to be widely improved.

In those days when seismic effects were either disregarded or poorly considered, seismic damage was characterized by failure of foundations and substructures as shown in Photo 1. In most cases, foundations were tilted, moved or even overturned due to insufficient strength of the foundations and the surrounding subsoils, which led to falling-off of the superstructures (Ref. 10).



Photo 1 Damage of Nakazuno Bridge by the Fukui Earthquake of 1948

2) Stage 2 - Damage due to Soil Liquefaction

Although the damage due to inadequate strength of foundations became less frequent by the improvement of seismic design and construction methods for substructures, the next stage of earthquake damage encountered was soil failure in conjunction with liquefaction prominently observed during the 1964 Niigata earthquake. Photo 2 shows the falling-off of the decks of the Showa bridge in the earthquake. Extensive soil movement associated with liquefaction produced large lateral movements of the bent pile foundations, which caused the dropping-off of the deck (Ref. 11). Responding to the damage, the first stipulations for assessing vulnerability of liquefaction were introduced in the "Design Specifications for Seismic Design of Highway Bridges" in 1971 through extensive studies initiated after the earthquake.



Photo 2 Damage of Showa Bridge by the Niigata Earthquake of 1964

The other important lesson gained from the Niigata earthquake was that devices for preventing falling-off of superstructures from the crest of columns are unavoidable. It was considered that even if large relative movements between the deck and the substructures occurred due to soil failures such as soil liquefaction, critical failure causing falling-off of deck could be prevented by providing special devices. Various devices as shown in Fig. 2 were proposed then, and recommendations on design details were included in the 1971 Specifications.

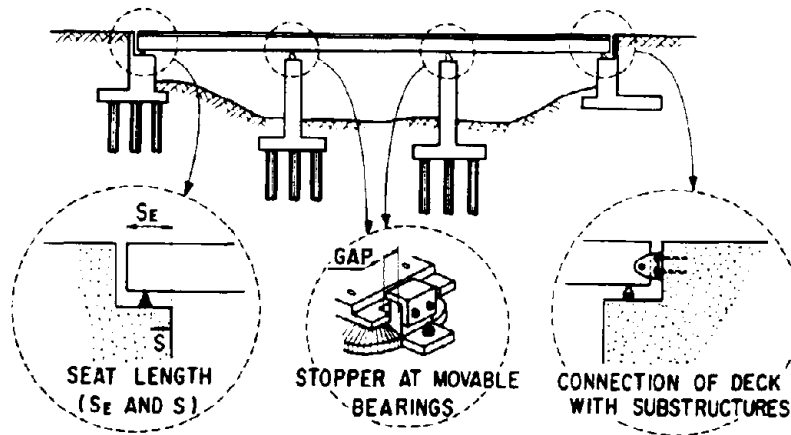


Fig.2 Devices for Preventing Superstructure from Falling

3) Stage 3 - Damage to Columns and Bearing Supports

In recent earthquakes including the 1978 Miyagi-ken-oki earthquake and the 1983 Nihon-kai-chubu earthquake, substantial damage due to shortage of foundation strength and effect of soil liquefaction was not developed in those bridges designed and constructed in accordance with the recent design specifications after 1971. However, damages to reinforced concrete columns and bearing supports, which were rarely suffered in the earlier earthquakes, were developed extensively as shown in **Photo 3**. This is due to the fact that old failure modes such as tilting or movement of the foundations, soil liquefaction and falling-off of superstructures were prevented by the new design recommendations.

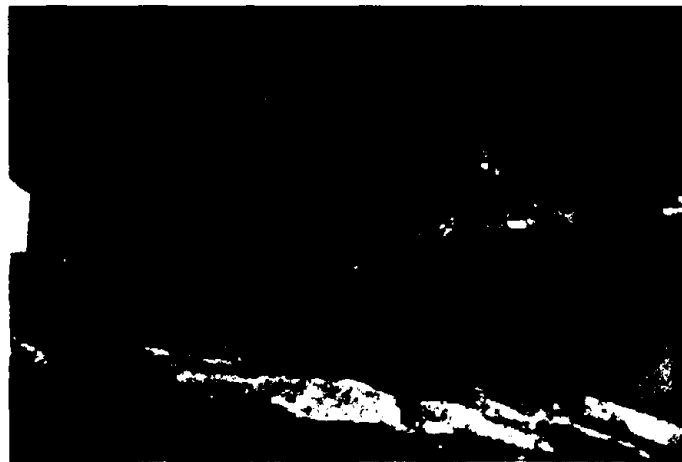


Photo 3 Damage to Reinforced Concrete Piers of Sendai Bridge by the Miyagi-ken-oki Earthquake in 1978

Through these evidences of seismic damage and effect of countermeasures, it is becoming apparent that certain types of failure developed in recent years at bearing supports and columns may not be prevented by only increasing the lateral force, although large lateral force has been adopted for seismic design of highway bridges. It may be effective to allow some relative displacement between deck and substructures for preventing the damage of bearings. Because lateral force developed during a destructive earthquake with the magnitude over 8 would be at least 3 times larger than the force level considered in the current seismic design based on the allowable stress design approach, occurrence of some damage may be unavoidable. Incorporation of structural members which develop stable energy dissipation under destructive seismic loading may be required. This is one of the motivations for incorporating the base isolation to highway bridges in Japan.

Seismic Design Philosophy of Highway Bridges The latest specifications were issued by the Ministry of Construction in February 1990 (Ref. 12). Major revisions introduced in the 1990 Specifications were unification of static lateral force method and the modified static lateral force method including the revision of the modification factors for design seismic force, a new method for computing inertia force for multi-span continuous bridges, a new ductility check for reinforced concrete columns, and detailed stipulations for dynamic response analysis. These revisions were incorporated based on the recent

studies for predicting earthquake ground motions and strength of reinforced concrete columns (Ref. 13).

The current specifications, with which highway bridges constructed in Japan with less than or equal to 200 m span length shall be designed in complete accordance, stipulates the principles of the seismic design of highway bridges as :

- 1) A highway bridge shall be designed to have sufficient stability against earthquakes not only as an individual superstructure and substructure but also as a whole structure by considering the structural characteristic of the bridge, topographical and geological conditions at the site, damage experiences in past earthquakes, importance and circumstances of the bridge.
- 2) The earthquake resistant design shall be based on the static lateral force method. The seismic safety of a bridge shall be evaluated by comparing the resultant values due to the static lateral force method with the allowable values such as allowable stresses, allowable bearing capacities, allowable displacements and safety factors.
- 3) A reinforced concrete column which is designed by the static lateral force method should be checked on the bearing capacity for lateral force to prevent the brittle failure from taking place.
- 4) A bridge which is designed by the static lateral force method and has complicated seismic response should be checked by the dynamic analysis.

The lateral force coefficient in the static lateral force method, which is equivalent to the fraction of design lateral response acceleration to the gravity acceleration, is stipulated as shown in Fig. 3. In which the zoning modification coefficient and the modification coefficient for importance are assumed as 1.0. The design lateral acceleration from 0.1 g to 0.3 g is taken into the seismic design. This represents the seismic force for moderate earthquakes which are supposed to take place with higher possibility.

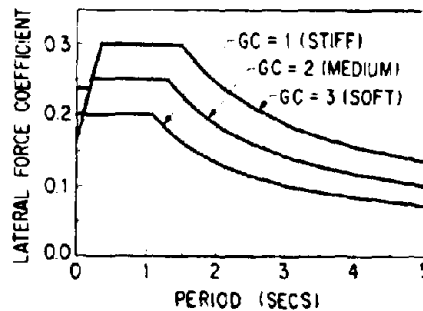


Fig. 3 Lateral Force Coefficient k_h for Static Lateral Force Method
($c_z = c_i = 1.0$)

The specifications adopt the allowable stress method, or working stress method. Although the ductility check of reinforced concrete columns for lateral force as shown in Fig. 4 objects larger earthquakes such as the 1923

Kanto earthquake which are supposed to take place rarely, basic philosophy of seismic design for highway bridges in Japan is to review the dynamic performance within elastic range. With the philosophy, it is difficult to come to use a energy dissipator aiming to reduce the seismic response. This is one of the reasons why base Isolation was not so interested in bridges, compared with buildings, in Japan.

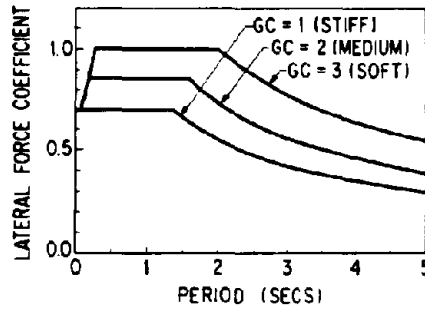


Fig. 4 Lateral Force Coefficient k_{ho} for Check of Bearing Capacity of Reinforced Concrete Piers for Lateral Force ($c_z = c_1 = 1.0$)

EXISTING EFFORTS TO MITIGATE SEISMIC RESPONSE OF HIGHWAY BRIDGES

Reduction of Lateral Force Efforts to reduce lateral force for design of substructures have been made in Japan (Ref. 14). The first attempt was to reduce lateral force by increasing energy dissipation capability. Viscous dampers such as cylinder type viscous dampers were tried to be adopted in early stage. Fig. 5 shows the result of an analytical study for a simple highway bridge. One of the two ends of the deck is supported by a fixed bearing with the other end being supported by roller. This is the usual way for supporting the deck. Viscous dampers were assumed to be provided between the deck and the column on the side where the deck is supported by the roller. The viscous dampers were assumed to have viscous coefficient of C.

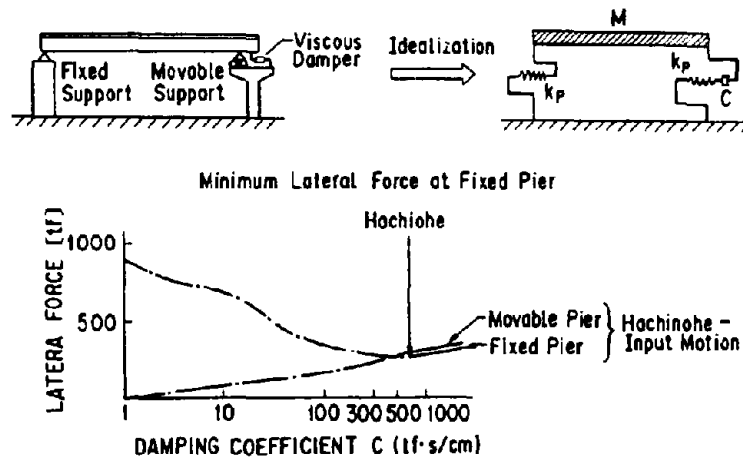


Fig. 5 Effect of Viscous Coefficient on Distribution and Reduction of Lateral Force

The maximum shear forces developed at the columns were computed for the Hachinohe record observed during the 1968 Tokachi-oki Earthquake (M=7.9). It can be seen in Fig. 5 that the lateral force developed at the column which supports the deck with roller and the viscous damper increases as the viscous damping coefficient C increases. It tends to support the half lateral force of the deck when the viscous damping coefficient C becomes infinitively large.

There is however a best viscous coefficient C which makes the total lateral force minimum. In the case presented in Fig. 5, 600 tf s/cm may be the best viscous coefficient.

However this type of finding was not incorporated into practice because of two reasons (Ref. 15). The first reason was that the optimum value of viscous coefficient significantly depends on ground motion. Adjustment of the viscous coefficient depending on ground motion was impossible. The other reason was temperature dependence of the viscous coefficient. The viscous coefficient significantly varied with temperature for materials available at those days.

Therefore, instead of aiming to reduce the lateral force, viscous damper has been adopted to distribute the lateral force. The viscous damper gives a resistive force when subjected to high-velocity motion such as the one encountered during an earthquake, and does not offer resistance to low-velocity motion such as the deck movement caused by temperature change. Hence, by providing the viscous damper the seismic lateral force may be more evenly carried by many columns without giving harmful effects due to temperature change. It should be noted that the temperature dependence of the viscous coefficient was no more significant for such high viscous coefficient range. In this mean, the viscous damper adopted in the past has been regarded as "damper stopper", because the dampers were used to work as a stopper instead of energy dissipator during an earthquake.

Various damper stoppers have been developed and adopted in the past (Refs. 16, 17). Some typical damper stoppers are presented in Fig. 6. Fig. 7 show an example of this type of damper installed in a five-span continuous bridge of the Tokyo Metropolitan Expressway. The bridge was designed for lateral force coefficient of 0.3 and its superstructure weighs of 3,000 tf. The total lateral force of 1,200 tf is expected to be almost evenly distributed to the ten columns through twenty dampers.

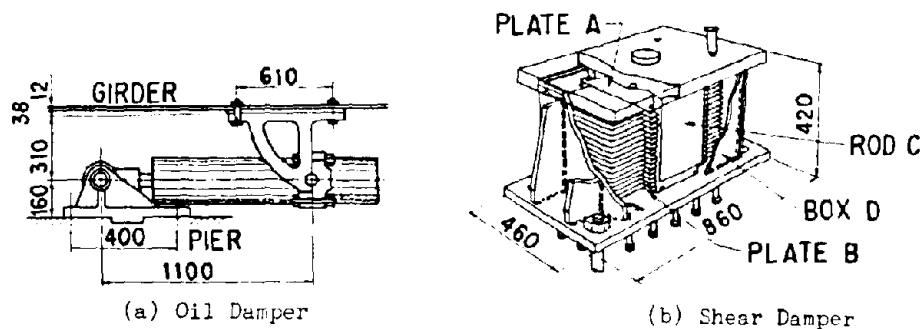


Fig. 6 Various Damper Stoppers Adopted to Highway Bridges

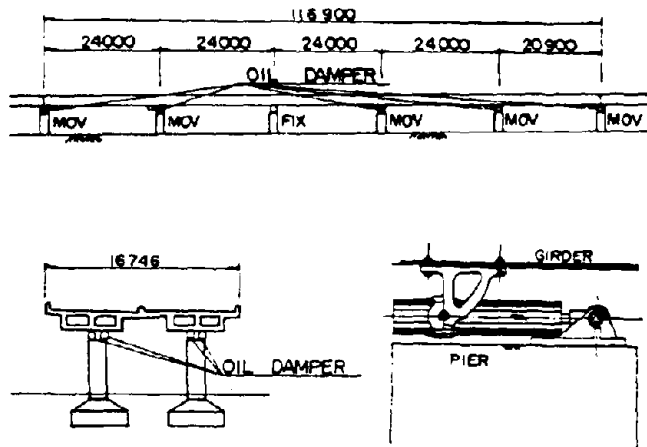


Fig. 7 5-Span Continuous Highway Bridge with Viscous Damper Stoppers

A unique device similar with the base isolation is the "SU Damper" as shown in Fig. 8 (Ref. 18). Original concept of the SU-Damper was to avoid the transmission of excessive lateral force larger than that considered in seismic design. Therefore the deck was supported by columns with friction bearings. For preventing excessive movement of the deck, prestressed strands which connect the deck and columns were provided. As well as the function of restrainer, the strands were considered as device to control the natural period of the bridge. The stiffness can be arbitrarily controlled by adjusting the length and size of the strands. The energy is dissipated by the friction developed at the bearings. Fig. 9 shows an analytical model to consider the effect of the SU Damper. Because of elongation of natural period and energy dissipation, the SU Damper may be considered as one of the base isolation devices. The SU Damper was firstly adopted in 1963 at an overcrossing on Route 1 of the Metropolitan Expressway. Photo 4. shows the SU Damper installed on the 9 span continuous prestressed concrete bridge of the Metropolitan Expressway.

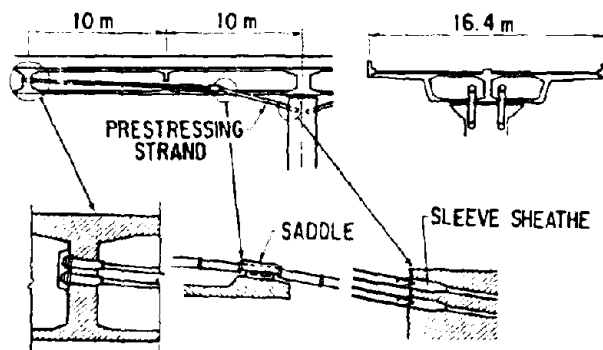


Fig. 8 SU-Damper

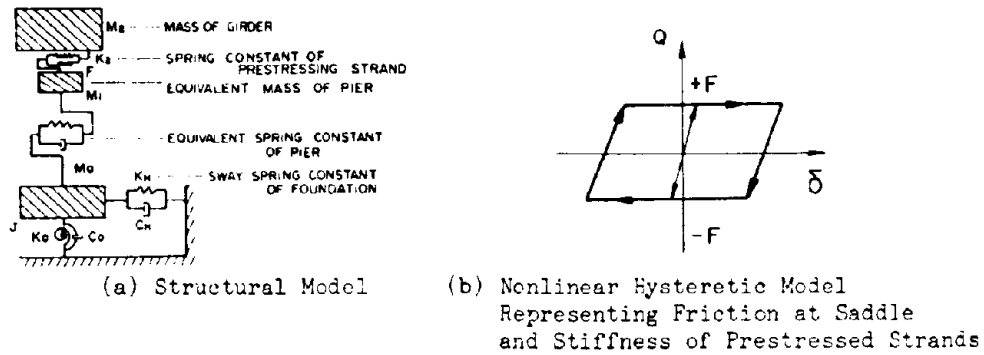


Fig. 9 Analytical Idealization of SU Damper



Photo 4 Bridge with SU Damper, Ukizuka Viaduct

Elongation of natural period has been adopted as a measure to reduce seismic lateral force. In particular for cable stayed bridges. Various devices have been developed to elongate natural period of cable stayed bridges. Deck was either isolated from tower (Ref. 19) or supported by links (Ref. 20) for making the deck being free to move in longitudinal direction. For either adjusting the natural period or preventing excessive deck movement, special devices has as springs (Ref. 21) and prestressed strands (Ref. 22) were used. Fig. 10 shows an example of such attempt in which the deck was supported by plate springs at the end.

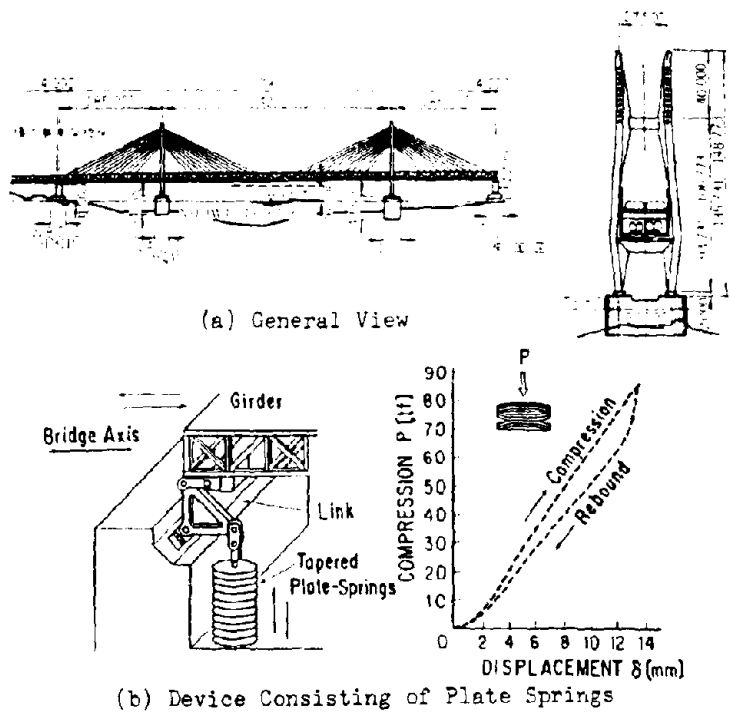


Fig. 10 Adoption of Elastic Spring to Prevent Excessive Deck Movement Associated with Elongation of Natural Period (Iitsuiishi-Iwaguro Bridge)

Distribution of Lateral Force Multi-span continuous highway bridges are likely to be constructed recently with demand of decreasing the number of expansion joints, which make annoying vibration and are vulnerable to traffic load, in order to secure comfortable driving with flat road surface and be released from bothersome maintenance work of the joints. Furthermore, multi-span continuous bridges are known to be more earthquake-resistant from past seismic experiences since they have larger degrees of redundancy than simple supported girder bridges.

However, the seismic lateral force in longitudinal direction for multi-span continuous bridges becomes extremely large as the number of the spans and/or the length of each individual span is extended. Traditionally, the lateral force was concentrated to a single substructure with a fixed bearing and the other substructures support only the vertical dead weight of the girder with movable bearings. However, the size of the single fixed substructure often becomes excessively large from the practical design point of view. To avoid such concentration of lateral force to a single substructure, various devices including rubber bearings have been developed and put into practice.

Distribution of lateral force to substructures can be performed by several methods (Ref. 14). The simplest method is to support the girder by fixed bearings at every piers. Although indeterminate lateral force will be

developed due to the elongation and shrinkage of the girder by thermal change, this method may be adopted unless the effect of the force is critical to design substructures. A highway bridge having as many as twelve continuous spans with a total deck length of 507 m has already been constructed (Ref. 23).

The second way is use of rubber bearing. Lateral stiffness of the rubber bearing can be easily adjusted by changing the rubber thickness or rubber material to intentionally modify the distribution ratio to each substructure. Many multi-span continuous bridges have been successfully constructed with use of rubber bearings for distribution of lateral force (Ref. 24). The third way is to adopt a viscous damper as described above.

PERSPECTIVE OF "MENSEIN DESIGN" IN JAPAN

Although elongation of the natural period and increase of energy dissipation capability of a structure are key factors in base-isolation, the elongation of the fundamental natural period for highway bridges leads to large relative displacement between the girder and the substructures, and requires the special expansion joints with large displacement capacity. Because the elongation of natural period has been attempted for cable stayed bridges, further technical development would be made. However for ordinary highway bridges in multi-span continuous type with span length of 10 m to 50 m, it is not appropriate to elongate the natural period so forcibly as in buildings, deeply related with various reasons constrained to highway bridges in Japan.

First reason is softer soil condition. Because most of populated areas are located on alluvial fan deposits, soils are very weak. Second reason is the high seismicity accompanying large earthquakes with magnitude over 8. These large earthquakes caused considerable damage in the past. Reflecting the occurrence of destructive earthquake as well as the worse soil condition, lateral force coefficient as shown in Figs. 3 and 4 are very high up to long natural period.

Third reason is difficulty to widen the clearance between decks. From the demand of driving comfort, maintenance problems and release from annoying noise and vibration, various efforts have been paid to develop expansion joint with small clearance. Even the regular expansion joints currently used cause considerable problems, increase of gap clearance can not be incorporated.

Fourth reason is the evaluation on collision developed either between abutment and deck or between adjacent decks. When enough clearance is not provided collision would be taken place. Actually collision frequently took place during the past earthquakes (Ref. 25). It should be noted from these past experiences that collision did not cause critical structural problems although expansion joints were often badly damaged. Although collision caused failure at contact face (Ref. 25) and/or bearings and stoppers, they were not serious. Although bearings have not been intentionally designed taking account of the fact that they would be damaged during a destructive earthquake, they did behave as a "fuse" to prevent the transmission of larger lateral force than that considered in seismic design. Therefore it may be said that the failure of bearing have been behaved as "isolator" (Ref. 26).

Now turning to the fourth reason, did collision cause serious problem to highway bridges ? The answer is "no" ! As long as enough seat length was provided, it caused no serious structural damage such as falling-off of superstructure. Attention has to be paid only when two adjacent decks with considerable different mass collides. In such case, the heavier deck tends to push the lighter deck, and damage is likely to be developed at the bearings and piers supporting the light deck (Ref. 25). Although the energy dissipating effect is not included in the current seismic design method, it constrains the deck response. It is effective to constrain deck response at early smaller stage of deck movement (Refs. 27, 28, 29). Therefore the superiority for causing collision would become clear if the energy dissipation and constrain of deck movement at small response stage were considered.

Based on these considerations, it seems preferable not to intentionally increase natural period and not to widen the gap clearance at joints in highway bridges in Japan. Therefore instead of intentionally increasing natural period, combination of increase of energy dissipating capability and distribution of seismic lateral force is considered to be preferred to highway bridges in Japan. It may be important to adjust natural period to avoid resonance with ground. This is an extension of the existing seismic design concept of highway bridge in Japan. The design concept in which bridges are designed taking advantage of the increase of energy dissipating capability and the distribution of seismic lateral force is proposed to be referred as "menschin design" (Ref. 5). Although the original meaning of "menschin" in Japanese is "base isolation", it is a little bit different with "base isolation" in design concept.

The followings are the basic principles considered required to activate menschin design in ordinary size of highway bridges in Japan :

- 1) Distribution of lateral seismic force should be attempted by adjusting the lateral stiffness of menschin bearings, while the lateral seismic force would be reduced by improving the energy dissipating capability with use of menschin bearings.
- 2) The fundamental natural period of menschin bridge should be adjusted to avoid the resonance with the ground, being balanced with the distribution effect. Attempt for elongating natural period so forcibly as buildings should not be made.
- 3) The menschin effect should be used not to make dimension and size of substructures small, but to improve the seismic performance of bridges.
- 4) Gap at an expansion joint should not be widened in menschin bridges, although a little larger relative displacement is expected to be developed between a girder and substructures during a destructive earthquake.
- 5) The menschin design should be adopted only at the site with stable soil behavior. The site vulnerable to soil liquefaction and other type of failure should be avoided.
- 6) The menschin design should be encouraged to construct super-multi-span continuous bridges with the effect of lateral force distribution.

EXISTING AND CURRENT EFFORTS FOR MENSCHIN DESIGN

Guidelines for Base Isolation Design of Highway Bridges For studying the application of base isolation to highway bridges, a committee chaired by

Professor Tsuneo Katayama, University of Tokyo, was formed through 1986 to 1989 at the Technology Research Center for National Land Development, which is the first public activity for the base isolation of highway bridges in Japan. Three programs were studied in the committee, i.e., 1) survey of base isolation devices which can be used for highway bridges, 2) study on the key points of the base isolation design of highway bridges, and 3) trial designs of base isolated highway bridges. As the final accomplishments of the three year study, "Guidelines for Base Isolation Design of Highway Bridges (Draft)" was published in 1989 (Ref. 30).

Pilot Construction Program of Menshin Bridges Five pilot menshin highway bridges as shown in Table 3 are under construction or completed under the supervision of the Ministry of Construction in order to verify the performance of the menshin highway bridges (Refs. 31,32,33). A working group is formulated in the Ministry of Construction for supervising the design and construction. One of them, Miyagawa Bridge in Shizuoka-ken, was completed and opened for the public traffic in March 15, 1991 as the first menshin highway bridge under the program (Ref. 32). Some other bridges following the first five are in design stage.

Table 3 Construction Program of Menshin Bridge

Owner	Name of Bridge	Type of Superstructure	Total Length
Hokkaido developing Bureau	On-netoh Bridge	Steel Girder	456 m
Tohoku Regional Construction Bureau, MOC	Nagakigawa Bridge	Steel Girder	97 m
Iwate-ken	Maruki Bridge	Prestressed Concrete	92 m
Tochigi-ken	Daiichi Karasuyama Bridge	Prestressed Concrete	250 m
Shizuoka-ken	Miyagawa Bridge	Steel Girder	110 m

Joint Research Program on Menshin Bridges The three-year joint research program on the menshin highway bridges is now under way between Public Works Research Institute and twenty eight private firms since July 1989 (Refs. 5, 34). The goal of the program is to develop the menshin design method and the new menshin devices for highway bridges in order to improve the seismic performance of new and existing bridges with less cost. Table 4 shows the research items and the contribution of each organization. The program will be accomplished in March 1992. "Design Manual of Menshin Design of Highway Bridges" is to be composed as fruits of the research program. There are four research topics in this joint program:

Table 4 Research Items and Organization of Joint Research between Public Works Research Institute and 28 Private Firms for Developing Menshin Systems for Highway Bridges

Research Theme	P	Ka	Sh	Ob	Ku	To	H	Ni	Su	M	G	Om	Ti	I	Ni	Ko	Ns	Os	Y	To	Bs	Bb	Sh	Pc	J	N	Chief	Sub-Chief
1. Development of Device for Isolation																												
1.1 High Energy Absorbing Rubber Bearing																												
1.2 Friction Damper																												
1.3 Steel Damper																												
1.4 Link Bearing Develop of																												
1.5 Viscous Damper																												
1.6 Test Method																												
2. Development of Expansion Joint and Falling-off Prevention Device for Isolated Bridge																												
2.1 Expansion Joint																												
2.2 Falling-off Prevention Device																												
3. Development of Design Method for Isolated Bridge																												
3.1 Design Philosophy																												
3.2 Dynamic Response Analysis Method																												
3.3 Design Method of Device for Isolation																												
3.4 Simplified Design Method																												
3.5 Design Method of Expansion Joint and Falling-off Prevention Device																												
4. Application of Base Isolation to Bridge																												
4.1 Application to Prestressed Concrete Bridge																												
4.2 Application to Steel Bridge																												
4.3 Application to Multiple Super-long Bridge																												
4.4 Application to Seismic Retrofit																												

P: Public Works Research Institute, Ka: Kajima, Si: Shimizu, Ob: Obayashi, Ku: Kumagai, Tr: Takenaka Doboiki + Takenaka, H: Hazama, Ni: Nishimatsu, Su: Sumitomo, M: Mitani, G: Goyoh, Ok: Okumura, Ti: Taisei + Tokyo Fabric + Nippon Chuzo, I: Ishikawajima Harima, Ni: NKK + Nippon Chuzo, Ko: Kobe Steel, Ns: Nippon Seiko, Os: Oshika, Y: Yokohama Rubber, To: Toyo Rubber, Bs: Bridgestone, Bb: BBM, Sh: Showa Denso, Pc: Pacific Consultants, J: Japan Engineering Consultant, N: New Structural Engineering Consultants.

1)Development of new menshin devices

The menshin devices for highway bridges have to be more compact and more weather-proof than the base-isolation devices for buildings since the menshin devices would be installed at narrow and exposed crests of bridge columns. The new menshin devices should be developed exclusively for menshin highway bridges to be effectively constructed. The following ten new devices in the six types are now being developed under the research program.

1) high damping rubber bearing -----	4 devices
2) sliding friction damper -----	2 devices
3) steel damper -----	1 device
4) roller menshin bearing -----	1 device
5) link bearing -----	1 device
6) viscous damper -----	1 device

All developed menshin devices but the link bearing were tested with use of the dynamic loading systems of PWRI under the same loading conditions to verify their performance as shown in **Photos 5** and **6**.

2)Development of expansion joints and restrainers for menshin bridges

The knock-off mechanism at an abutment to ease the impact force induced by the collision between the superstructure and the abutment, and the finger expansion joints which is distinguished from the regular finger joints by the transverse movement, are being developed. The restrainer which consists of the steel bar installed in the crest of the substructure and the steel casing with rubber inside is also being developed.

3)Development of menshin design method

Taking into account the high seismic activity and the philosophy of seismic design in Japan, the flow chart of the menshin design method illustrated in **Fig. 11** are proposed, in which two levels of design force are considered as limits states. The first level, called as Level 1, is equivalent to the design seismic force considered in the current static lateral force method (refer to **Fig. 3**). This represents the force level developed by moderate earthquakes. The second level, called as Level 2, is equivalent to the design seismic force for the check of the bearing capacity of the reinforced concrete columns for the lateral force (refer to **Fig. 4**), and this corresponds to larger earthquakes such as the 1923 Kanto Earthquake.

4)Application of menshin design

The menshin multi-span continuous bridge with the deck length over 1 km, which is called in the research program as a super multi-span continuous bridge, is examined as a crucial research item. Connecting of existing simple supported girders to lessen the number of troublesome expansion joints, and retrofitting of existing bridges to increase the seismic bearing capacity by using menshin bearings are also studied in the research program.



**Photo 5 Dynamic Loading Test of Menshin Devices at
Public Works Research Institute**

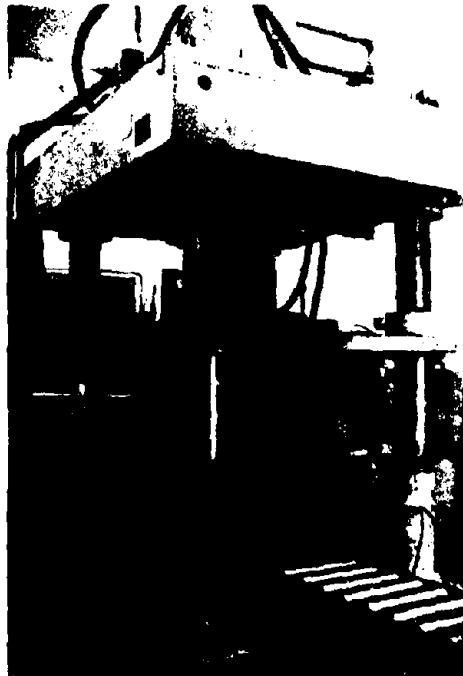


Photo 6 Cyclic Shear Test of Menshin Devices

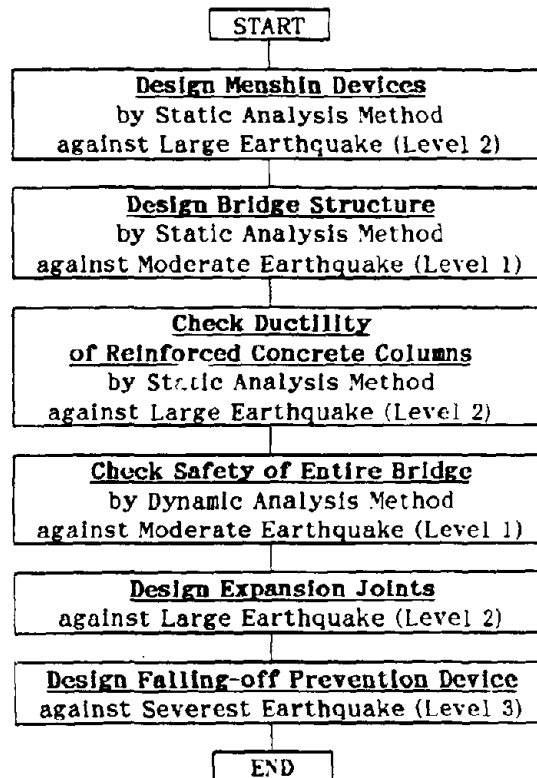


Fig. 11 Flow of Menshin Design of Highway Bridges

CONCLUDING REMARKS

Application of the base isolation to highway bridges in Japan was described in the preceding pages. Seismic damage has been decreased by improving seismic design method as well as construction practices by adopting large lateral force based on the allowable design approach. For further decreasing seismic damage at bearings and reinforced concrete piers, it is appropriate to provide a member where seismic damage would be intentionally concentrated. On the other hand, construction of multi-span continuous bridges is being pursued from the view point of driving comfort, maintenance and release from annoying noise and vibration.

Taking advantage of increasing energy dissipating capability and distribution of lateral force to many piers, the menshin design which is slightly different in concept is being introduced in Japan. The menshin design will be spotlighted in Japan as a new technology for making possible to easily construct multi-span continuous bridges as well as for reducing seismic lateral force.

ACKNOWLEDGEMENTS

For executing investigations presented here, various supports and suggestions have been obtained from many organizations and persons. Special thanks go to Professor I. Buckle, National Center for Earthquake Engineering Research, University of Buffalo, U.S.A., and Mr. Donald K. Kirkcaldie, Works and Development, New Zealand (former Visiting Researcher at PWRI), for their guidance and invaluable discussions on the base isolation. Special appreciation also goes to Professor T. Katayama, Institute of Industrial Science, University of Tokyo, for chairing the Committee formulated at the Technical Research Center for National Land Development for preparing the Guidelines for Base Isolation Design of Highway Bridges (Draft) in 1989. The authors express sincere thanks to all organizations and participants involved in the Joint Research with the Public Works Research Institute for studying the Menshin Design of Highway Bridges, with special appreciation to Mr. Y. Goto, Research Institute of Obayashi Corporation, for his endeavour to organize the research group.

REFERENCES

- 1)Buckle, I. G. and Mayes, R. L. : Seismic Isolation:History, Application and Performance -A World View, Earthquake Spectra, Vol. 6, No. 2, May 1990
- 2)McKay, G. R., Chapman, H.E. and Kirkcaldie, D. K. : Seismic Isolation : New Zealand Application, Earthquake Spectra, Vol. 6, No. 2, May 1990
- 3)Skinner, R.L., Tyler, R. G., Heine, A. J. and Robinson, W. H. : Hysteresis Dampers for the Protection of Structures from Earthquakes, Proc. New Zealand - Japan Workshop on Base Isolation of Highway Bridges, Wellington, New Zealand, December 1987
- 4)Billings, I. J. and Kirkcaldie, D. K. : Base Isolation of Bridges in New Zealand, Proc. New Zealand - Japan Workshop on Base Isolation of Highway Bridges, Wellington, New Zealand, December 1987
- 5)Public Works Research Institute : Report of Joint Research between PWRI and 28 Private Firms on Development of Menshin Systems for Highway Bridges.

- Technical Report of Cooperative Research, No. 44 and No. 60. March 1990 and March 1991 (in Japanese)
- 6) Arakawa, T. and Kawashima, K. : Seismicity and Maximum Possible Earthquake around Japan for Application to Seismic Risk Analysis, Technical Note No. 2098, Public Works Research Institute, March 1984 (in Japanese)
 - 7) Japan Road Association : Guide Specifications for Earthquake Hazard Mitigation for Transportation Facilities - Post-Earthquake Countermeasures-, February 1987 (in Japanese)
 - 8) Kawashima, K. : Seismic Design, Seismic Strengthening and Repair of Highway Bridges in Japan, Proc. U.S.-Japan Workshop on Seismic Retrofit of Bridges, Public Works Research Institute, Tsukuba, Japan, 1990
 - 9) Japan Road Association : Guide Specifications for Earthquake Hazard Mitigation for Transportation Facilities - Pre-Earthquake Countermeasures-, February 1987 (in Japanese)
 - 10) Iwasaki, T., Penzien, J. and Clough, R.W. : Literature Survey - Seismic Effects on Highway Bridges, Report No. EERC 71-11, Earthquake Engineering Research Center, University of California, Berkeley, 1972
 - 11) Public Works Research Institute : Report on Niigata Earthquake, Vol.125, June 1965 (in Japanese)
 - 12) Japan Road Associations : Design Specifications for Highway Bridges - Part V Seismic Design -, February 1990 (in Japanese)
 - 13) Iwasaki, T., Kawashima, K. and Hasegawa, K. : New Seismic Design Specifications of Highway Bridges in Japan, 22nd Joint Meeting, U.S.-Japan Panel on Wind and Seismic Effects, UJNR, Galthersburg, U.S.A., May 1990
 - 14) For example, Katayama, T., Kawashima, K., and Murakami, Y. : Current Design Considerations for Reducing Seismic Lateral Force of Highway Bridges in Japan, New Zealand - Japan Workshop on Base Isolation of Highway Bridges, Wellington, New Zealand, December, 1987 (Procs. are available from Technical Research Center for National Land Development, Tokyo, Japan)
 - 15) Yahagi, K. and Mizumoto, Y. : Past and Present of Seismic Design, Bridge and Foundation Engineering, Vol. 13, No. 10, 1979 (in Japanese)
 - 16) Matsumura, S., Fukuoka, S., Mizumoto, Y. and Nakata, T. : Seismic Design of Multi-span Continuous Bridge with Damper, Bridge and Foundation Engineering, Vol. 16, No. 5, 1982 (in Japanese)
 - 17) Iseki, J. : Viscous Damper, Society of PC Technology, Vol. 21, No. 4, August 1979 (in Japanese)
 - 18) Okamoto, S. and Uemae, Y. : Aseismic Bridge Structure by Elastic Supports Using Tie Members (SU Damper Method), Proc. Symposium on New Ideas in Structural Design, Japan Society of Civil Engineers and Architectural Institute of Japan, 1963 (in Japanese)
 - 19) Kitazawa, M., Ishizaki, H., Emi, S. and Nishimori, K. : Characteristics of Earthquake Responses and Design of Aseismic Design on the Long-period Cable-stayed Bridge (Higashi-Kobe Bridge) with All Movable Shoes in Longitudinal Direction, Procs. Japan Society of Civil Engineers, No. 422/I-14, October 1990 (in Japanese)
 - 20) Maeda, K. and Eya, S. : Adoption and Dynamic Characteristic of Short Link Bearing in Yokohama Bay Bridge, Bridge and Foundation Engineering, Vol.24, No.9, September 1990 (in Japanese)
 - 21) Kanemitsu, H. and Higuchi, K. : Displacement Control of Bridges with Suspended Girder, Technical Report of the Honshu-Shikoku Bridge Authority, 1981 (in Japanese)
 - 22) Kato, N., Hloka, Y. and Kawahito, T. : Design of Meiko-nishi Bridge, Bridge and Foundation Engineering, 1983 (in Japanese)

- 23)Fukuoka, S. : Design of Multi-span Continuous Highway Bridges with Use of Shear Viscous Damper, Bridge Engineering, 1980 (In Japanese)
- 24)Sakairi, Tominaga, Kiyota and Sasaki : Vibration Characteristics of 5-span Continuous Steel Box Girder Bridge Supported by Rubber Bearings, 44th Annual Meeting, Japan Society of Civil Engineering, September 1989 (in Japanese)
- 25)Public Works Research Institute : Report on the Disaster Caused by the Miyagi-ken-oki Earthquake of 1978, Vol. 159, March 1983 (in Japanese)
- 26)Personal Discussion with Mr. James Gate, California Department of Transportation, and Mr. Shoichi Saeki, Honshu Shikoku Bridge Authority
- 27)Williams, D. and Godden, W. G. : Experimental Model Studies on the Seismic Response of High Curved Overcrossings, Report No. EERC 76-18, Earthquake Engineering Research Center University of California, Berkeley, 197
- 28)Kawashima, K. and Penzien, J. : Correlative Investigation on Theoretical and Experimental Dynamic Behavior of A Model Bridge Structure, Report No. EERC 76-26, Earthquake Engineering Research Center, University of California, Berkeley, 1976
- 29)Kawashima, K. : An Analytical Model of Contact and Impact in Dynamic Response Analysis, Proc. Japan Society of Civil Engineers, Vol. 308, April 1981
- 30)Technology Research Center for National Land Development : Guidelines for Design of Base-Isolated Highway Bridges, Final Report of Base Isolation to Seismic Design of Highway Bridges (Chairperson : Professor T. Katayama), March, 1989 (in Japanese)
- 31)Kakizaki, H. and Ito, T. : Menshin Design of Nagaki-gawa Bridge, Bridge and Foundation Engineering, Vol. 90-9, September 1990 (In Japanese)
- 32)Matsuo, Y., Ooishi, A., Hara, K. and Yamashita, M. : Design and Construction of Miyagawa Bridge, Bridge and Foundation Engineering, Vol. 91-2, February 1991 (In Japanese)
- 33)Ikeda, T., Oozeki, K., Kumakura K. and Abe, N. : Design of Karasuyama No. 1 Bridge (Base Isolated Bridge), Bridge and Foundation Engineering, Vol. 25, No. 6, June 1991(In Japanese)
- 34)Kawashima, K., Hasegawa, K., Unjoh, S., Nagashima, H., and Shimizu, H. : Current Research Efforts in Japan for Passive and Active Control of Highway Bridges against Earthquake, 23rd Joint Meeting, U.S.-Japan Panel on Wind and Seismic Effects, U.J.N.R., Public Works Research Institute, Tsukuba, Japan, May 1991

APPENDIX

Chapter 1 INTRODUCTION

Chapter 2 BASIC CONCEPTS

Chapter 3 SEISMIC FORCE FOR MENSHIN DESIGN

3.1 General

3.2 Lateral Force Coefficient

3.3 Lateral Force for Ductility Check of RC Concrete Columns

Chapter 4 MENSHIN DESIGN

4.1 General

4.2 Lateral Force Coefficient Method

4.3 Ductility Check of RC Concrete Columns

Chapter 5 DESIGN METHOD OF MENSHIN DEVICES

5.1 General

5.2 Fundamental Displacement

5.3 Dynamic Characteristic

5.4 Static Characteristic

5.5 Rubber Bearing

5.6 Lead Rubber Bearing

5.7 High Damping Rubber Bearing

5.8 Steel Damper

5.9 Friction Damper

5.10 Viscous Damper

Chapter 6 SAFETY CHECK BY DYNAMIC ANALYSIS

6.1 General

6.2 Input Motion for Dynamic Analysis

6.3 Dynamic Analysis Method

6.4 Safety Check

Chapter 7 STRUCTURAL DETAILS OF MENSHIN BRIDGES

7.1 General

7.2 Restrainers

7.3 Structural Details of Menshin Devices

7.4 Structural Details of Expansion Joints

Chapter 8 CERTIFICATION TESTS OF MENSHIN DEVICES

8.1 General

8.2 Dynamic Loading Tests

8.3 Static Loading Tests

8.4 Ultimate State Tests

Chapter 9 RETROFITTING BY MENSHIN DESIGN

9.1 General

9.2 Construction of Menshin Devices

9.3 Structural Details of Retrofitting

Appendix I References for Design

Appendix II Design Examples

HISTORY AND APPLICATION OF SEISMIC ISOLATION TO HIGHWAY BRIDGES IN THE UNITED STATES

Ian G. Buckle
Department of Civil Engineering
State University of New York at Buffalo

Ronald L. Mayes
Dynamic Isolation Systems
Berkeley, California

ABSTRACT

Seismic isolation is used in buildings to decouple these structures from the damaging components of earthquake ground motion. It is also used in bridges where it involves the separation of the superstructure from the substructure, usually at the bent cap level. But unlike a building application the primary intent in a bridge is to protect the structure below the plane of isolation – the superstructure being relatively rigid to in-plane loads and of adequate strength to resist these loads.

Bridges are particularly suitable for isolation and literature surveys indicate that more than 90% of the world's isolated structures are, in fact, bridge structures. Applications include both new construction and retrofit work. Implementation within the United States has only occurred within the last few years and then predominantly as a retrofit measure rather than in new construction. This activity is reviewed in this paper along with some potential innovations in the use of isolators for protecting monolithic continuous bridges.

SEISMIC ISOLATION

Basic Principles The basic intent of seismic isolation is to increase the fundamental period of vibration such that a structure is subject to lower earthquake forces. However, this reduction in force is accompanied by an increase in displacement which must be accommodated within the flexible support. Furthermore, longer period bridges can be lively under service loads. To control these deflections and stiffen a bridge for service loads, hysteretic damping devices are included as part of the isolation system. Studies have shown that the cost of this isolation hardware can be offset against the savings in the substructures and foundations (because of the reduced forces) and the long term reduction in repair costs for seismic damage.

There are therefore three basic elements in a bridge isolation system, as follows:

- A flexible support so that the period of vibration of the bridge is lengthened sufficiently to reduce the force response;
- A damper or energy dissipator so that the relative deflections across the flexible support can be limited to a practical design level, and

- Rigidity at low (service) load levels such as wind and braking forces.

Design Principles The design principles for seismic isolation are illustrated in Figure 1. The solid uppermost line (curve (1)) is the realistic (elastic) ground response spectrum as recommended in the AASHTO Guide Specifications [1] for the highest seismic zone. This is the spectrum that is used to determine actual forces and displacements to which a bridge will be subjected. The lowest solid line (curve 4) is the design curve from the AASHTO Standard Specification [2]. It is seen to be approximately one-fifth of the realistic forces given by the Guide Specification. This reduction, to obtain the design forces, is consistent with an R-factor of 5 for a multicolumn bent [1].

Also shown in Figure 1 is curve (3), the probable overstrength of a bent designed to the AASHTO Standard Specification. This has been obtained by assuming an overstrength factor of 1.5. Curve (3) therefore represents the probable capacity of the bent.

The demand on this bent is represented by curve (1) and the difference between demand and capacity results in damage – possibly in the form of plastic hinging in the columns. This difference is highlighted in Figure 1 by the arrow and note just above the legend for curve (1).

Now if the bridge is isolated, the actual shear forces that the bridge will be subjected to may be represented by curve (2) (small dashed line). This curve corresponds to the same seismic input as curve (1) but it includes the effect of the substantial level of damping inherent in hysteretic isolation systems. If the period of the isolated bridge is in the 2.0 to 2.5 second range, it will be seen that the overstrength (actual capacity) of the bent exceeds the realistic forces (demand) for the isolated bridge. This area has been shaded in Figure 1. In this region there is no inelastic deformation or ductility required of the bent and elastic performance (without damage) is assured.

APPLICATIONS

Overview Seismic isolation may be applied to both the design of new bridge structures and the retrofit of existing structures. In general, implementation is straightforward since most bridges have bearings to accommodate thermal movements and the substitution of isolation bearings for these standard hardware items is routine.

For new construction, the reduction in realistic column forces by factors of 5 to 10 substantially removes the need for ductile detailing. There will be cost savings in both the columns and foundations, particularly if piled footings are used [3]. There will also be long-term reductions in the repair costs of seismic damage.

For existing bridges, seismic isolation is a solution to the three most common deficiencies in bridges built before the mid-1970's. These are

1. Inadequate strength of steel bearings and connections
2. Inadequate strength and ductility of columns and substructures

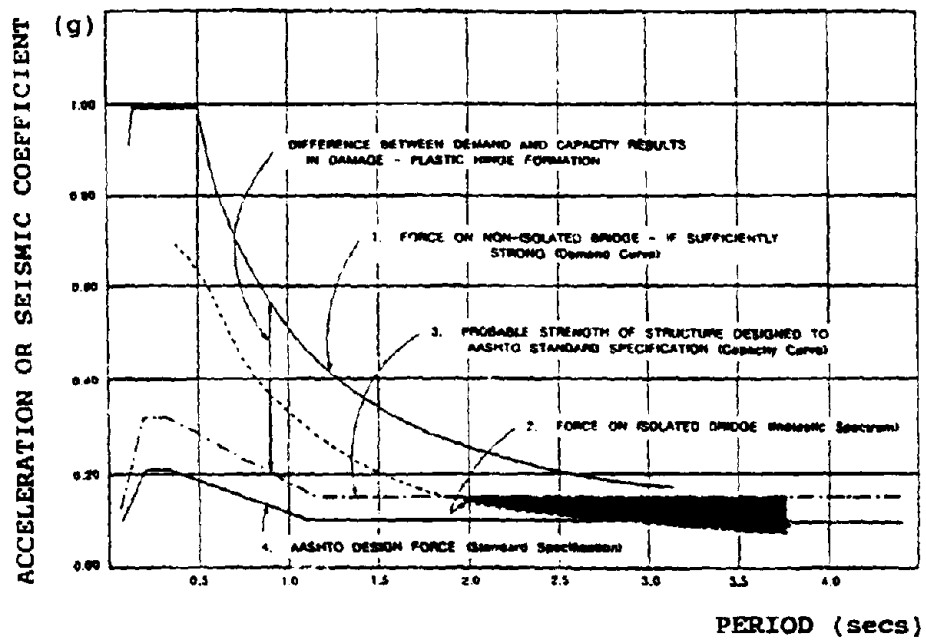


FIGURE 1: COMPARISON OF ELASTIC RESPONSE SPECTRA AND SEISMIC DESIGN COEFFICIENTS FOR BRIDGES

3. Inadequate support length for girders.

Item 3 is the area in which most of the current U.S. effort in bridge seismic retrofit has been carried out. Caltrans has pioneered this work and has so far concentrated on the provision of positive connections between the superstructure and supporting substructure [4,5]. Measures used to date include longitudinal joint restrainers, transverse bearing restrainers and vertical motion restrainers. Other concepts which have been proposed [5], include bearing seat extensions and the use of shear keys or stoppers.

Another solution to the above three problem areas is the replacement of vulnerable bearings with hysteretic isolation bearings which not only addresses the first problem, but also minimizes the importance of the other two due to the force reduction and displacement control features of these bearings.

Further, the use of elastomeric bearings of different size and stiffness permits a degree of control over the distribution of lateral load to the substructures of a bridge. This can be a particular advantage for bridges on variable soil conditions and/or bridges that have irregular stiffness or mass.

To date more than 30 bridges in the United States and Canada have been completed or are under construction using seismic isolation. A brief description of some of these applications follows.

Sierra Point Overhead The plan dimensions of the bridge are 616 feet long overall and 117 feet wide. The ten simply supported spans vary in length from 26 to 100 feet. The bridge is on a skew of approximately 60 degrees with respect to the highway traffic lanes.

The construction is concrete deck slab on a steel superstructure with concrete columns, 3 feet in diameter and approximately 25 feet high. There are a total of 27 columns, generally arranged in bents of 4 columns, reducing to 2 or 3 column bents at the ends of the bridge due to the skew.

The columns are nonductile and understrength for the maximum expected earthquake at the site. However, replacement of the existing steel bearings at the top of the column and at each abutment with lead-rubber isolators enabled the retention of these columns without the need for strengthening.

Analysis to determine the expected performance for the as-built, non-isolated, structure was also carried out, assuming the columns remain elastic. It was shown that the seismic demand exceeded the capacity by a factor of 4, and that severe damage, if not collapse, was inevitable for the existing structure. Isolation, however, reduced the demand to below the capacity of the columns and eliminated the need for strengthening.

Santa Ana River This bridge carries the Upper Feeder pipeline across the Santa Ana River for the Metropolitan Water District of Southern California. The pipe is 116 inches in diameter at this location and is supported over the river on 3 steel trusses, each 180 ft in span. There are a total of 10 approach spans bringing the overall length of the crossing to 1010 ft. Both the river spans and side spans are supported on reinforced concrete piers and

pedestals which are nonductile and of inadequate strength. Further, some of the truss members and connections were under capacity for the maximum expected earthquake for the site.

Removal of existing steel expansion bearings and their replacement with lead filled elastomeric isolators reduced the seismic forces to below the existing strength levels in the piers and the capacity of the truss members.

Eel River Bridge¹ During floods in the Eel River in 1986, 3 spans of this bridge at Rio Dell were damaged due to scour under the river piers. Two spans survived and these 300 ft trusses have since been incorporated into a new structure. The surviving piers are nonductile and to protect them against damage and potential collapse in an earthquake, isolation bearings have been installed under each truss. The design spectrum corresponded to a 0.5g peak ground acceleration on a type IV soils profile (more than 150 ft of alluvium). The site is within 12 miles of the Fresh Water fault. At the same time as installing the isolators, the spans were raised an average of 4 feet, so as to match the deck elevation with that of the new spans. Removal of the existing steel rocker bearings, to make room for the elastomeric bearings, was therefore not necessary. However, to ensure stability of the isolators at high shear strains, all existing pins and rockers were locked against movement by the installation of holding-down bolts and welded gusset plates. No other strengthening work was necessary.

Main Yard and Shops Vehicle Access Bridge This 2-span bridge across the Long Beach freeway is composed of dual 12 foot deep plate girders with steel floor beams spanning the 32 feet between the longitudinal girders. The single reinforced concrete pier is 2-column bent with an infill wall of about half the overall height of the columns. Non-ductile, with a potential for shear failure in the free standing portion of the columns, the pier was seismically vulnerable.

Each 128 foot span was originally supported on steel expansion bearings. These have now been removed and replaced with isolation bearings. Because the original steel bearings were almost 36 inches tall and the elastomeric isolators are just 17 inches high, the difference in height required the construction of new reinforced concrete pedestals under the isolators.

All American Canal Bridge This bridge was reconstructed using the existing concrete columns of the original structure. The new bridge is a continuous welded composite girder over 3 spans. It replaces a narrow reinforced concrete deck on the same alignment. The piers are a combination of steel columns for the portion above water and tapered concrete pedestals on spread footings below water. To protect these non-ductile columns against damage, where it will be difficult to inspect and repair, the isolators were placed at the interface between the steel and concrete i.e. at a three-quarter point in the overall column

¹ Since this paper was presented to the US-Japan Workshop in September, 1991, a series of moderate-to-large earthquakes (M=6.0 to 7.0) have occurred within 15 miles of the bridge site. Whereas nearby structures have been damaged, the bridge has been unaffected by these earthquakes. Deformations in the isolators of 8 inches longitudinally and 4 inches transversely have been reported, which are consistent with theoretical estimates for earthquakes of this size and distance.

height.

The site spectrum corresponds to a 0.6g ground acceleration on a type IV soils profile (more than 150 ft alluvium).

Sexton Creek The first new bridge to be isolated in the United States is located in the State of Illinois. It is a three-span continuous steel plate girder structure over Sexton Creek in Alexander County (Figure 2).

The spans are approximately 120-154-120 ft in length and 40 ft wide. A concrete deck and five, 54 inch deep plate girders make up the superstructure. Each girder is continuous over 2 piers and rest on seat-type abutments. Both the piers and the abutments are founded on piles footings.

Several alternative isolation schemes were developed for the bridge and these are summarized in Table 1. Scheme A has an equal distribution of thermal forces between the piers and the abutments but most of the seismic loads is resisted by the two piers. Scheme B reverses this situation and most of the seismic load is resisted by the abutments. This is achieved by concentrating the lead cores into the abutment bearings and removing them from the pier bearings. Scheme C was developed to equalize the distribution of seismic forces between the abutments and piers.

This adjustment of load distribution is one of several reasons for considering isolation in both new and retrofit situations. It is seen that by judicious choice of bearing stiffness, size and location of lead cores, it is possible to control the distribution of lateral load over a wide range. In this way seismic loads can be directed into those substructures with the capacity to resist them and away from those elements with inadequate strength or ductility. In each of the above schemes the total seismic shear and displacement has been kept the same. Only bearing stiffness and the size and location of the lead cores was changed from one scheme to another. After review of the options, the Illinois Department of Transportation chose Scheme B (seismic loads resisted primarily at the abutments).

Lacey V. Murrow Bridge West Approach This structure is part of the original floating bridge built in 1940 to carry former highway US-10 across Lake Washington between Seattle and Mercer Island, Washington. A new, adjacent floating bridge has been opened to eastbound and westbound traffic on highway I-90. The original structure has been closed for widening, rehabilitation and seismic upgrading and will become the eastbound lanes of highway I-90. Heading in the eastbound direction, the original west approach consists of a 237-foot, 3-span continuous monolithic concrete tee-girder structure, a 453-foot, 3-span continuous steel deck truss, and a 215-foot steel tied arch span leading to the transition span to the floating bridge. There is an identical steel tied arch span which is part of the east approach. The seismic requirement is AASHTO A=0.25 and Soil Profile Type II.

The concrete tee-beam spans were demolished and replaced with twin continuous haunched concrete box girders cast integrally with a multi-cell box deck structure. This new superstructure is isolated, with one isolator under each box girder at the new center piers and the existing east pier, and six at the rebuilt abutment. The steel rocker bearings under the deck truss and both tied arches were modified to incorporate isolators. The pin

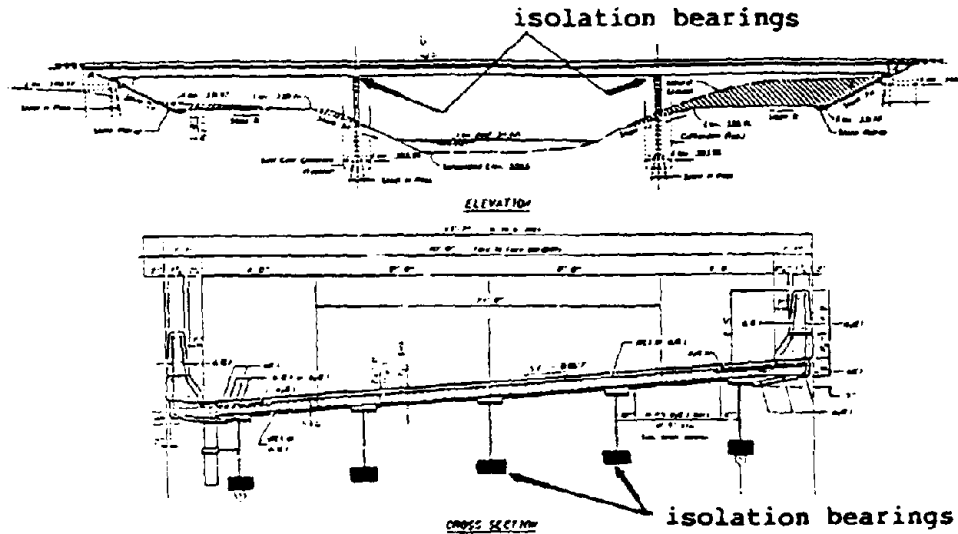


FIGURE 2: SEXTON CREEK BRIDGE
Elevation and section

SCHEME	SUBSTR. UNIT	BEARING SIZE L x W x H (inches)	LEAD CORE DIA. (inches)	Δ_{EQ} in.	F_{EQ}/D	F_{EQ} kips	Δ_{LT} in.	F_{LT} kips	F_{ST} (kips)	
									TRANS.	LONG.
A	Abut.	13 x 13 x 8-3/8	2	2.8	0.13	57.4	2.62	41.5		
	Pier	18 x 18 x 8-3/8	3-3/4	2.8	0.13	141.0	1.03	43.6		
B	Abut.	13 x 13 x 8-3/8	4-1/4	2.8	0.13	117.6	2.62	54.4	88.7	35.1
	Pier	18 x 18 x 8-3/8	none	2.8	0.13	80.8	1.03	28.9	16.5	5.0
C	Abut.	13 x 13 x 8-3/8	3-3/4	2.8	0.13	100.5	2.62	50.7		
	Pier	18 x 18 x 8-3/8	2	2.8	0.13	97.9	1.03	33.1		

- Δ_{EQ} = Seismic Displacement
- F_{EQ}/D = Seismic Force Coefficient
- F_{EQ} = Seismic Force
- Δ_{LT} = Non-Seismic Long-Term Displacement (Thermal)
- F_{LT} = Non-Seismic Long-Term Force
- F_{ST} = Non-Seismic Short-Term Force

TABLE 1: ALTERNATIVE ISOLATION SCHEMES FOR SEXTON CREEK BRIDGE

connection was retained and a new clevis weldment provided whose base plate is the interface with the top of the isolator. The pin connection was locked to prevent rotation so that all movement occurs as horizontal shear across the isolator.

The widening of the deck in the tied arch spans presented a special challenge. The cross members between the two arches were severed, the arches spread apart, and additional segments spliced into the cross members. The arches now rest on isolators which are mounted on large corbels added to the outboard sides of the pier columns.

Isolation design enabled the reuse of the existing piers in the structures over water. It reduced the elastic seismic forces by factors of 4 to 5. Detailed analyses showed that the existing piers of the isolated structure would respond elastically to the effects of the design earthquake. The seismic upgrade for the truss and tied arch spans then reduced itself to a bearing replacement.

Deas Slough Bridge This bridge is a 3-span continuous riveted haunched steel plate girder structure with spans of 90-140-90 feet and 10 girders in its cross section. It carries the Deas Island Throughway (Highway 99) across Deas Slough, part of the Fraser River delta south of Vancouver, British Columbia. Highway 99 is the main thoroughfare between the U.S. border and Vancouver. The superstructure was mounted on large steel rocker bearings, and the piers and abutments are on piled foundations. Seismic criteria are equivalent to AASHTO A=0.20 and Soil Profile Type III.

Isolation design was investigated to see if a bearing replacement would be a feasible means of seismically upgrading this bridge. The main objective was to unload the fixed pier which was attracting an inordinately high seismic load in the longitudinal direction. The elastic seismic forces were reduced by a factor of approximately 3 which, when combined with the force redistribution attributable to isolation design, was sufficient to meet this objective.

Cache River Bridge The Cache River Bridge was built in 1946 as a 2-lane, 3-span structure carrying Illinois Route 3 over the Cache River Diversion Channel in Alexander County. The span lengths are 86-108-86 feet, and the original width was 32 feet with six steel beams in the cross section. The ground response spectrum at the bridge site, which lies within the influence of the New Madrid Fault, was assumed to be equivalent to AASHTO acceleration coefficient, A, of 0.20 (Category C) and Soil Profile Type III. When it became a candidate for rehabilitation or replacement, it was decided to save as much of the existing structure as possible while widening the deck to 35 feet and bringing the bridge up to current seismic code. Another requirement was to construct the project in stages, keeping one lane open to traffic at all times.

It was decided to provide a new continuous superstructure with five lines of 42 inch deep steel plate girders. For the substructures, the objective was to retain the existing wall piers and replace the abutments utilizing the existing piling. Consideration was given to taking out most of the seismic forces at the abutments by fixing one abutment and providing for thermal movements at the other. While this scheme might minimize the seismic forces at the tops of the piers, it also results in a longitudinal force on the fixed abutment of over 800 kips, and transverse forces on both abutments of approximately 400 kips.

The initial isolation design reduced the overall seismic load by a factor greater than 3. Then, by adjusting the design of the isolators to redistribute the lateral forces, the pier forces were minimized, the longitudinal force at the fixed abutment was reduced by a factor of 9, and the transverse forces at both abutments were reduced by a factor of 4.5. Thus, the force reduction and force redistribution features of isolation design proved to be the most effective solution, avoiding the expense of replacing the piers and saving significant cost in the construction of the new abutments.

West Street Overpass This bridge, built in the 1950's, carries West Street over the northbound and southbound lanes of the I-95 New England Thruway in Harrison, Westchester County, New York. The bridge is part of an extensive Thruway rehabilitation and reconstruction project. There are four simple spans of 31.5-54.5-54.5-31.5 feet, with five steel beams supporting a 33-foot wide concrete deck. The two center spans cross the Thruway traffic lanes, and the shorter end spans cover the side slopes. It was considered essential to keep the Thruway open immediately after a seismic event. The criteria were based on AASHTO A=0.19 and Soil Profile Type III.

To ensure that the center spans would not collapse and block the Thruway traffic lanes, it was decided to replace the existing steel rocker bearings with lead-rubber isolators (Figure 3). This solved the problems of the vulnerable existing bearings and the lack of adequate support length for the beams, and reduced the overall seismic load by a factor of 2.5. This force reduction had a mitigating effect on the extent of rehabilitation work required on the substructures. Other work included replacement of the center pier and the cap beams of the side piers, and reconstruction of some of the abutment pedestals. Much of this work was required for non-seismic reasons.

Poplar Street Bridge East Approach Lying in the shadow of the Gateway Arch, the Poplar Street Bridge spans the Mississippi River, connecting East St. Louis, Illinois with St. Louis, Missouri. Constructed in 1966 as the first orthotropic steel plate deck structure in the U.S., this bridge carries 130,000 vehicles per day from highways I-44, I-55, I-64, I-70, and US-40. Immediately east of the bridge a six-span approach viaduct collects this maze of highway. Forty-five feet above the ground, the 856-foot long viaduct flares out in width from 113 feet to 180 feet.

Plans for rehabilitating this vital link to the Poplar Street Bridge were completed in 1989 and the work was under contract in 1990. Neither the original structure nor the planned rehabilitation included seismic design. Shortly after the Loma Prieta earthquake struck the San Francisco Bay Area in 1989, it was decided to include seismic retrofit in the general contract. This retrofitting was necessary to meet the demands of a Richter 7.5 or greater earthquake generated by the nearby New Madrid fault. The spectra at the site are equivalent to AASHTO A=0.12 and Soil Profile Type III.

Potential seismic retrofit options included strengthening the piers and foundations, and seismic isolation. The latter was selected as it easily proved to be the most cost effective and practical solution. The elastic seismic forces were reduced by a factor of approximately 4.5. Other construction alternatives would have cost considerably more, and would have interrupted traffic for an extended period of time, necessitating closure of half the lanes of the Poplar Street Bridge. Pier and foundation strengthening was avoided by combining the

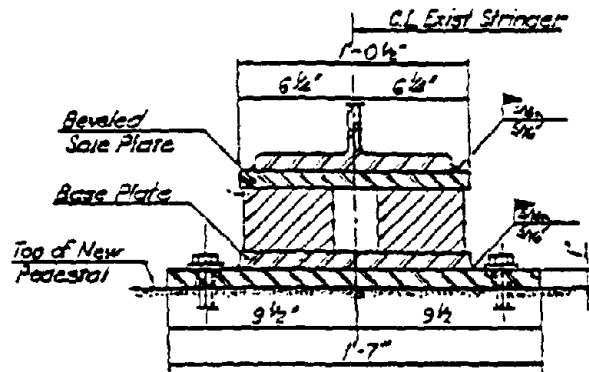


FIGURE 3: WEST STREET OVERPASS
 Welded isolator installation. Sole and base plates are bolted to isolator's internal load plates with countersunk bolts.

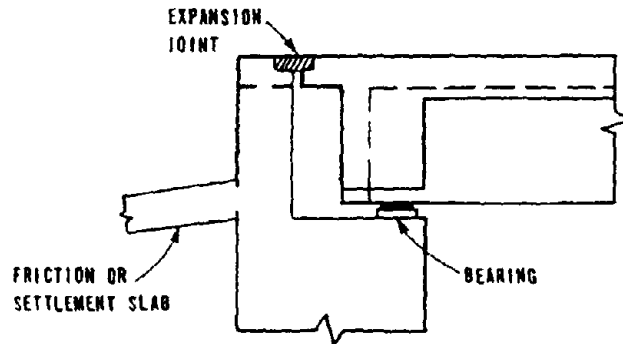


FIGURE 4: TYPICAL SEAT-TYPE ABUTMENT

force-lowering effect of isolation and the force-distribution technique of altering the isolator design appropriately. Replacement of 128 steel rocker bearings took less than six months and was accomplished without disruption of traffic.

ISOLATION BEARINGS AS ENERGY DISSIPATORS

It was stated earlier that most isolation systems comprise three elements: flexibility, energy dissipation and restraint for service loads. Although these elements are almost always used, it is not necessary that all three elements exist in every application. For example, flexibility alone (period shift) will usually achieve the required force reduction, although the displacements may be large.

Alternatively, energy dissipation may be used to reduce forces without additional flexibility. Although the force reduction is not as dramatic as that possible with period shift, the displacements are much less than for conventional (fully) isolated structures.

This strategy has particular application to monolithic bridges with seat - type abutments. Here it is possible to combine the advantages of a monolithic superstructure with some of the benefits of seismic isolation.

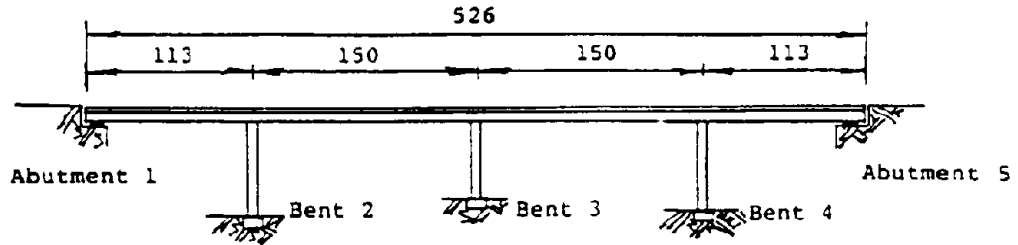
In this application the elastomeric bearing pads, normally used at the abutments to accommodate thermal and other movements (Figure 4), are replaced by isolation bearings with lead cores. Significant hysteretic energy dissipation is possible with these devices and reduced forces and displacements are the direct result. Since the columns remain monolithic with the superstructure, the fundamental period of vibration is virtually unchanged. But the energy dissipation introduced into the abutment bearings is sufficient to dampen the spectrum significantly even in the short period range, and useful force reductions are available. To illustrate this technique, an example is given below. It is a 4-span, 5-cell box girder bridge, subject to a 0.5g ARS spectrum on 10-80 ft. alluvium; backfill interaction is included.

Example

Geometry Figure 5 shows a four-span, continuous, monolithic bridge with seat - type abutments. This example is taken from Appendix A of the Caltrans Memo to Designers 15-10 (April 1982, Revised July 1984).

The span lengths, bent stiffness, and dead loads are as shown in this figure. The seismic loads correspond to a 0.5g ARS spectrum for 10-80 ft. of alluvium. All bents are assumed to perform elastically during this event.

Results The results of several analyses are shown in Table 2. These analyses include, in Column 1, the solution given in Memo 15-10, which is based on current Caltrans procedures for longitudinal response. These results, however, use an incorrect value for the strength of the combined abutment - bent spring model. A corrected set of results is given in Column 2 of Table 2.



	Dead Load (K)	Longitudinal Stiffness (K/in)
Abutment 1	869	-
Bent 2	3063	100
Bent 3	3132	218
Bent 4	3028	175
Abutment 5	865	-
TOTAL	10957	493

FIGURE 5: FOUR-SPAN, MULTICELL, MONOLITHIC BRIDGE

	Conventional Design		Isolation Designs	
	Memo 15-10	Revised	Energy Dissipators ²	Full Isolation ³
Column	1	2	3	4
BASIC RESPONSE				
Base shear (F/W)	0.98	1.00	0.42	0.19
Deflection (inches)	6.8	6.3	3.90	7.65
Period (Secs)	0.85	0.81	0.98	2.02
FORCE DISTRIBUTION (Kips)				
Abutment 1	(7800) ¹	(7800)	1334	197
Bent 2	680	630	394	562
Bent 3	1482	1373	826	562
Bent 4	1190	1103	676	562
Abutment 5	7800	7800	1334	197
Total	11,152	10,906	4,564	2,080

NOTE:

1. () means that this force is not included in the total figure at bottom of the Table. This is because only one abutment backfill is assumed to be effective at any instant in time.
2. 'Energy Dissipators' means isolation bearings are used as energy dissipators at the abutments.
3. 'Full Isolation' means isolation bearings are used at the abutments and at all bents.

TABLE 2: RESPONSE OF A 4-SPAN, MONOLITHIC CONTINUOUS BRIDGE
Showing conventional (fixed base) response compared to
energy dissipation solution and full seismic isolation

Column 3 presents the results when isolation bearings are used as energy dissipators at the abutments. The sizes of these bearings and their lead cores were chosen to limit the deflection to 4.0 inches. This target value was selected because a 4-inch clearance at the abutment was assumed in the previous analyses (Memo 15-10) and avoidance of impact on the backwall was considered desirable. If the gap size were different or limited impact was acceptable, different bearing sizes could be chosen. The results in this column were obtained by averaging the values from seven inelastic time history analyses (using the DRAIN computer program). Each time history was spectrum-compatible with the above, ARS 0.5g, spectrum

For comparative purposes, the response of a fully isolated design is given in Column 4 of Table 2. Here, isolation bearings are provided at each abutment and at each bent. In these circumstances, the structure is no longer monolithic with the bents, but the superstructure is still continuous from one abutment to the other.

Discussion

Deflections are reduced by about 40% to just under 4.0 inches. This is less than the specified gap width and no impact on the backwall is expected for this event. The response is not now dependent on the mobilization of backfill soil resistance (stiffness or strength). It is therefore more easily quantified and actual performance more accurately predicted. Repair of the backwall is also avoided.

The total base shear force is reduced by more than 50% due to the energy dissipation introduced at the abutments.

The abutment forces are smaller by almost a factor of 6, from 7800K to 1330K, and the bent forces are reduced by 40% (in direct proportion to the reduced deflections).

The results given in Table 2 are for longitudinal response only. Transverse response for both the isolation designs will be similar to the above, provided the bent stiffness in the transverse direction are of the same order of magnitude as in the longitudinal direction.

No significant period shift is possible with the energy dissipation solution. The force reductions that are obtained are due to the introduction of significant levels of hysteretic energy dissipation, which lead to a heavily damped design force spectrum, particularly in the short period range. If full isolation is used, force reductions due to both period shift and hysteretic damping are possible, as shown in Column 4 of Table 2.

CONCLUSIONS

Seismic isolation offers particular advantages to bridge structures. Reductions in earthquake loads can be significant and savings can be achieved in the foundations of new designs along with improved seismic performance (elastic response). Redistribution of load from one substructure to another can further enhance this performance.

Isolation also offers a solution to many of the common retrofit problems encountered

in existing bridges. Limited experience to date has shown that isolation can be adapted and implemented to meet a wide variety of different site and bridge conditions.

Isolation bearings may also be used as energy dissipators at the abutments of otherwise monolithic, continuous bridges. Although not as effective as full isolation, this arrangement can enhance the seismic performance of existing structures with a minimum of on-site construction work.

ACKNOWLEDGEMENTS

Acknowledgement is made of the authors' colleagues at Dynamic Isolation Systems for their respective contributions to this paper. Particular recognition is made of the work of Richard Knight, David Jones and Lindsay Jones.

REFERENCES

1. -----, "Guide Specifications for Seismic Design of Highway Bridges," American Association of State Highway and Transportation Officials (AASHTO), 1983.
2. -----, "Standard Specifications for Highway Bridges," American Association for State Highway and Transportation Officials (AASHTO), 13th Edition, 1983 and Interim Specifications 1984 and 1985.
3. Billings, I.J. and Kirkcaldie, D.K., "Base Isolation of Bridges in New Zealand," Proc. Joint US-New Zealand Workshop on Seismic Resistance of Highway Bridges, Applied Technology Council, Report 12-1, Redwood City, 1985.
4. Zelinski, R.J., "California Department of Transportation Bridge Earthquake Retrofitting Program," proc. Second Joint US-Japan Workshop on Performance and Strengthening of Bridge Structures and Research Needs, San Francisco, 1985, pp. 213-217.
5. -----, "Seismic Retrofitting Guidelines for Highway Bridges," Federal Highway Administration Report No. FHWA/RD-83/007, 1983, 205 pp.

2. Seismic Isolation Hardware

Development of Textile-Reinforced Rubber Bearings for Menshin Bridges

N. Kawai, N. Doro and Y. Miyauchi

Development of a Sliding Friction Damper

T. Iguchi

Development of Steel Damper for Menshin Bridges

H. Kamiya, S. Iizuka and M. Takei

Development of Viscous Damper for Menshin Bridges

K. Kawashima, J. Iseki, I. Shimoda and Y. Makiguchi

Development of Finger Joint Movable in Horizontal Directions for Menshin Bridges

T. Kimishima, T. Harada and D. Ozaki

Development of High Damping Rubber Bearing for Menshin Bridges

Part 1 - *Y. Suizu and C. Sudoh*

Part 2 - *K. Kawashima, M. Koshitoge, K. Endo, C. Yamada and T. Nishimoto*

Part 3 - *I. Nishikawa, N. Katoh, M. Itoh and Y. Muramatsu*

Finite Element Analysis of Elastomeric Isolation Bearings for Different Connection Details

H. Liu and I. Buckle

Finite Element Analysis of Elastomeric Bearings

R. Shepherd and L.J. Billings

Development of Roller-Type Bearing for Menshin Bridges

T. Takaku, M. Shimada, N. Tsumura and S. Izuma

Sliding Isolation Systems for Bridges

M.C. Constantinou

Certification Test of Menshin Devices

K. Kawashima, K. Hasegawa, H. Nagashima, Y. Makiguchi and Y. Suizu

Investigation of Friction Pendulum Systems

S.A. Mahin

Lateral Loading Tests of Knock-Off Mechanism for Menshin Bridges

T. Kikuchi and Y. Goto

Development of Falling-Off Prevention Devices for Menshin Bridges

D. Ozaki and F. Matsumoto

Design Concept of Falling-Down Prevention Devices for Menshin Bridges

A. Hayashi, J. Izei, K. Yoshikawa, T. Kikuchi, K. Matsubara and H. Koyama

DEVELOPMENT OF TEXTILE-REINFORCED RUBBER BEARINGS FOR MENSIN BRIDGES

Norio KAWAI¹ Nobuyuki DORO² Yasuhiro MIYAUCHI³

¹ Toyo Tire & Rubber Corporation, Inami-cho, Hyogo, Japan

² Toyo Tire & Rubber Corporation, Iruma-shi, Saitama, Japan

³ Toyo Tire & Rubber Corporation, Ibaraki-shi, Osaka, Japan

ABSTRACT

A new type of menshin device for bridge structures using textile-reinforced rubber bearings is developed. Unlike the steel-reinforced rubber bearings currently in use, the newly developed textile-reinforced rubber bearings (TR-RB hereafter) consist of alternating layers of rubber and textile reinforcements to form a laminated rubber bearing. In this paper, material properties of the natural rubber components and the fundamental properties of the TR-RB bearings are reported. In the initial test, 1/4 reduced scale models of the TR-RB bearings are tested. Influences of the variation in shear strain levels, bearing stress, and loading frequencies on damping capacity have been observed. In the second part, full-size models are tested as part of a joint project between the Public Work Research Institute (PWRI) and Toyo Tire & Rubber Corp. From the test results, it has been observed that the ratio of lateral stiffness to axial stiffness is about 1/1000 which is the about the same range for conventional isolator bearings used in seismic isolation of highway bridges. In addition, extensive tests for static cases up to 200% shear strain and for dynamic cases up to 150% shear strain have shown that the developed TR-RB bearings have stable hysteresis behavior suitable for seismic isolation purposes.

INTRODUCTION

In the conventional steel-reinforced rubber bearings, steel reinforcing plates are interleaved with rubber layers alternately to form a laminated bearing with high axial stiffness and yet flexible in the lateral direction to decouple the supported structure from the destructive earthquake ground motion. The fabrication process involves finishing of the steel plate surfaces and application of adhesives which need tedious labor and results in a heavy bearing. In the newly developed TR-RB bearings, textile mats are laid alternately with the rubber layers. In this series of tests, polyester fabric is used as the textile reinforcements. This results in a bearing which is 2/3 lighter than a steel-reinforced equivalent. In addition, finishing and applying adhesives are confined only to the two end plates. With the advantage of being lighter in weight, the developed TR-RB bearings possess similar seismic isolation properties as the conventional steel-reinforced rubber bearings. Furthermore, the TR-RB bearings can developed a little more damping capacity compared with the conventional types using the same rubber materials. And using a high-damping rubber material to further gain higher damping capacity is a next consideration. Since the textile reinforcements provide confinement to the rubber material, it is expected that the developed TR-RB bearings have excellent resistance to creep.

FUNDAMENTAL PROPERTIES OF TEXTILE-REINFORCED RUBBER BEARINGS

Fundamental Properties of Rubber Materials and Textile Reinforcements Results of fundamental test on rubber material done in accordance to the JIS-K6301 specifications are tabulated in Table 1. It can be observed from the table that the rubber material used possesses good physical properties for use as seismic isolation bearings.

Table 1 Physical Properties of Rubber Material

hardness	40 JIS A
shear modulus	5.2 kgf/cm ²
tensile strength	244 kgf/cm ²
elongation	690%
tear strength	64 kgf/cm ²
compression set	13%

For the textile reinforcements, a polyester fiber material with tensile strength above 20 kgf/cm² and an elongation of over 15% is used. Compression test was conducted on a textile model (Fig. 1) until fracture to verify its strength. Test result (Fig. 2) shows that the textile begins to fracture when bearing stress reaches about 1320 kgf/cm². Thus, the textile used has more than adequate strength when used in the isolator designed to have axial bearing stress below 100 kgf/cm².

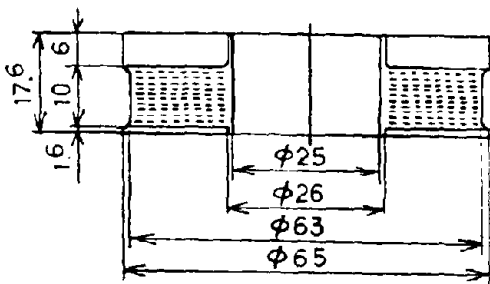


Fig. 1 Fracture Model for Textile Reinforcement Under Compression Test

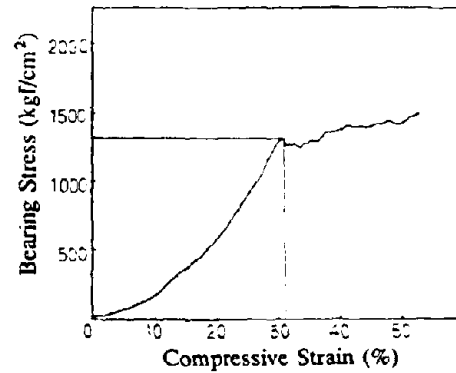


Fig. 2 Stress-Strain Curve of Textile Reinforcement Under Compression Test

Fundamental Properties of Textile-Reinforced Rubber Bearings

A 1/4-scale reduced model is shown in Fig. 3. It has a dead load resistance of 6 tonf using natural rubber component with shear modulus of 5.2 kg/cm² as noted in Table 1. Three series of tests are conducted (Table 2). Series 1 investigates the influence of different levels of shear strain. Series 2 investigates the influence of different levels of axial bearing pressure. Series 3 investigates the influence of frequency.

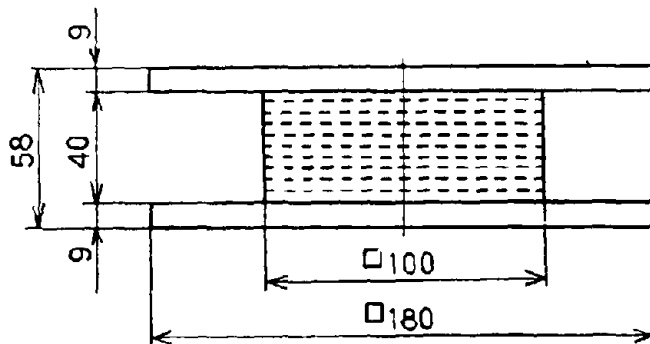


Fig. 3 A 1/4 Reduced Scale Model

Table 2 Outline of Tests on 1/4 Reduced TR-RB Scale Models

Series No.	Bearing Stress kg/cm ²	Frequency Hz	Strain %	Temperature °C
1	60	0.05	±25, ±50, ±75 ±100, ±125, ±150	+18
2	30, 60, 90	0.05	±100	+18
3	60	0.01, 0.05, 0.1, 0.5	±100	+18

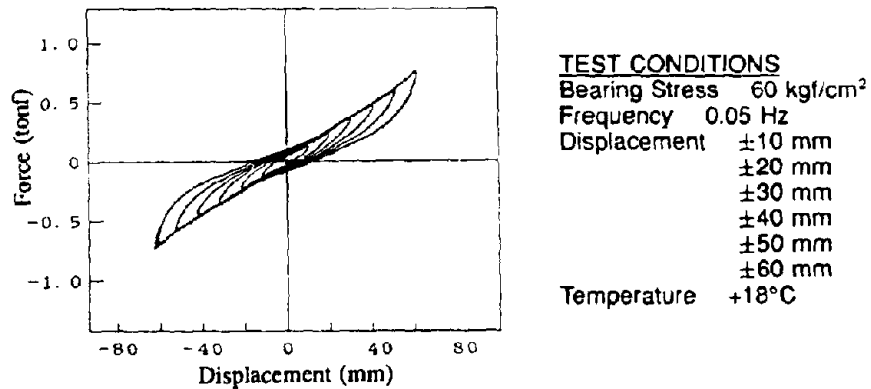


Fig. 4 Force-Displacement Hysteretic Loops of 1/4-Scale Reduced model

The force-displacement hysteretic loops under increasing amplitudes of shear strain is shown in Fig. 4. From the force-displacement hysteresis loops, shear modulus G_{eq} and damping ratio h_{eq} can be calculated by the following equations.

$$G_{eq} = \frac{K_{eq} \times t_R}{A_R} \quad (1)$$

$$h_{eq} = \frac{\Delta W}{2\pi W_e} \quad (2)$$

where K_{eq} is the effective stiffness defined by $(F_{max} - F_{min}) / (u_{max} - u_{min})$, A_R is the effective area of rubber section, t_R is the thickness of rubber, ΔW is the area enclosed in a hysteresis loop, and W_e is the potential energy (Fig. 5).

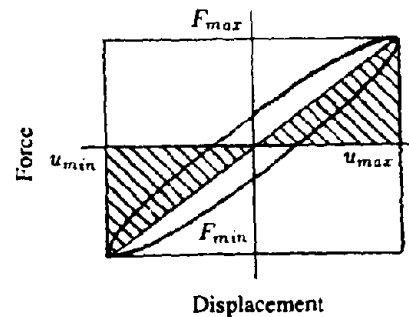


Fig. 5 Equivalent Damping Capacity

Influences of the variation in shear strain level, axial bearing stress, and frequency on the shear modulus and damping capacity are shown in Figs. 6–8. The results can be summarized as follows:

- The influence of shear strain levels on both shear modulus and damping capacity are shown to be small. The effective shear modulus is shown to agree with the shear modulus of the rubber material used. Effective damping ratio of about 10% is obtained although low damping rubber material is used in this set of models.
- While axial bearing stress has been observed to have no influence on the effective shear modulus G_{eq} , the effective damping ratio becomes significantly larger with increasing axial bearing stress.
- Loading frequency does not seem to affect the effective shear modulus G_{eq} , but the effective damping ratio h_{eq} increases with increasing frequency.

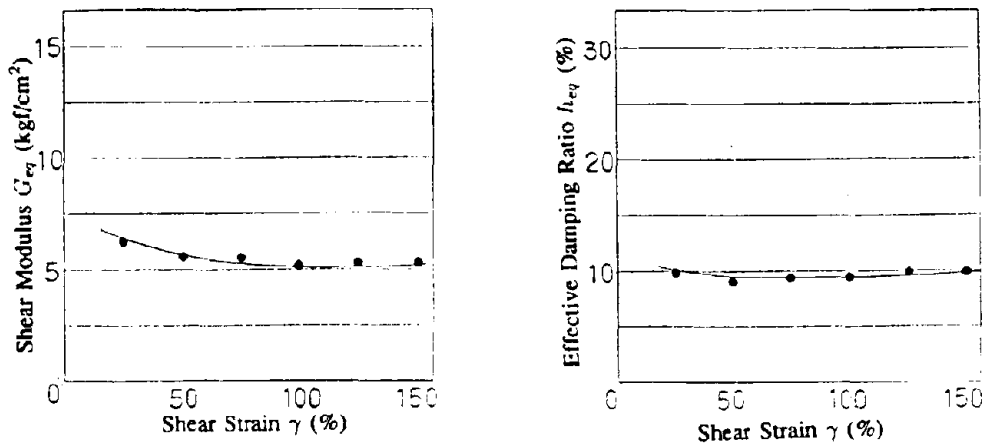


Fig. 6 Influence of Shear Strain on Shear Modulus and Damping Ratio (Test on Scaled Models)

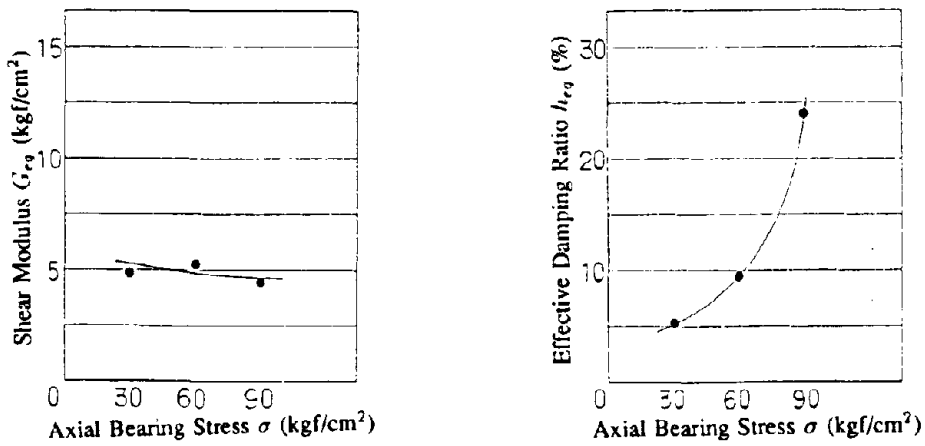


Fig. 7 Influence of Axial Bearing Stress on Shear Modulus and Damping Ratio (Test on Scaled Models)

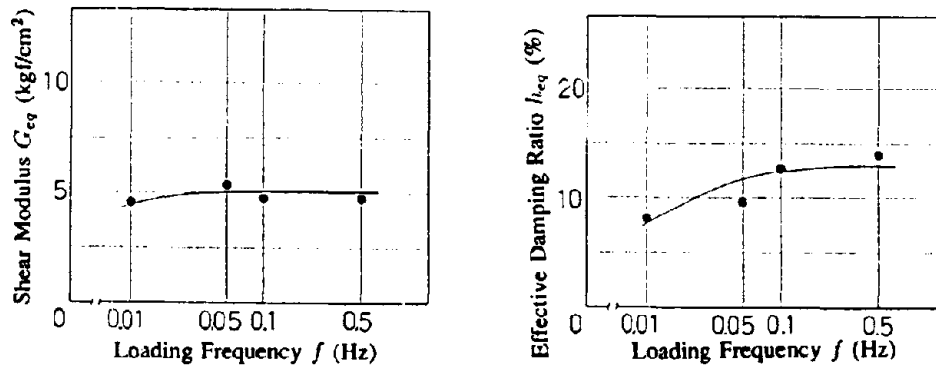


Fig. 8 Influence of Loading Frequency on Shear Modulus and Damping Ratio (Test on Scaled Models)

DYNAMIC LOADING TESTS AT PWRI

Outline of Tests Two full-scale models (Fig. 9) capable of supporting a dead load of 92 tonf were tested under the joint research program between the Public Work Research Institute (PWRI) and Toyo Tire & Rubber Corp.

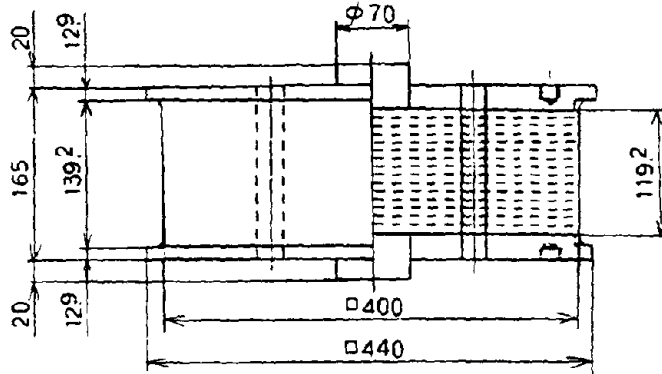


Fig. 9 A Full-Scale model for Dynamic Tests at PWRI

The rubber material used in these full-scale models is the same natural rubber material with a shear modulus of 5.2 kgf/cm². Model 1 was tested using test series 1 ~ 4 under lateral displacement histories and then using test series 5 and 6 under axial load histories. Model 2 was tested to evaluate endurance under repeated application of cyclic displacements by test no. 7 and then followed by test no. 8 three hours after the previous test. A summary of the test series is given in Table 3. During test, the room was controlled at a constant temperature of +20°C. A view of a model during test is shown in Photo 1.

Table 3 Outline of Dynamic Tests at PWRI

Test No.	Bearing Stress kgf/cm ²	Frequency Hz	Pre-Strain %	Strain alternate ± ranges %	No. of Cycles	model No.
1	60	0.1	0	25, 50, 100, 150, 200	10	1
2	60	0.1	0	25, 50, 100, 150, 200	10	1
3	60	1.0	0	25, 50, 100, 150	10	1
4	60	0.1	50	25, 50, 100, 150	10	1
5	0 ~ 80	—	0	—	3	1
6	60 ± 20	—	0	—	5	1
7	60	0.5	0	150	40	2
8	60	0.5	0	150	40	2

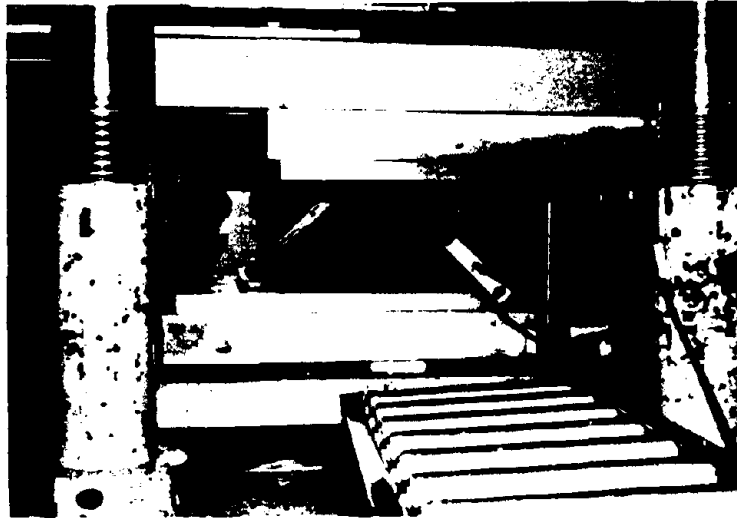


Photo 1 Dynamic Test of Full-Scale Model at PWRI

Test Results Fig. 10 shows the force-displacement hysteretic loops from test series 2. The influence of increasing shear strain on effective stiffness and effective damping ratio are shown in Fig. 11 using results from test series 1 and 2. Influence of repeated cycles on G_{eq} and h_{eq} is shown in Fig. 12 using results from the endurance tests of test series 7 and 8. From these, the following observations can be made:

- It can be noted from Fig. 10 that no stiffness hardening was noted even at shear strain level of 200%.
- It can be seen from Fig. 11 that level of shear strain does not significantly affect both the effective stiffness and the effective damping ratio. G_{eq} of 5.2 kgf/cm² closely matched that of the material shear modulus. Effective damping ratio of about 4% has been observed. This shows a relatively higher damping capacity than a conventional bearing using the same type of rubber material.
- Under endurance test series 7, dynamic loading at 150% shear strain for 40 cycles was conducted and then followed three hours later by endurance test series 8 under the same condition. The results plotted in Fig. 12 show very stable behavior for the developed TR-RB bearings.
- The lateral stiffness at 100% shear strain is about 570 kgf/cm and the axial stiffness under bearing stress of 40 ~ 80 kgf/cm² is about 560 tonf/cm. Therefore, the ratio of lateral to axial stiffnesses is in the 1/1000 range.

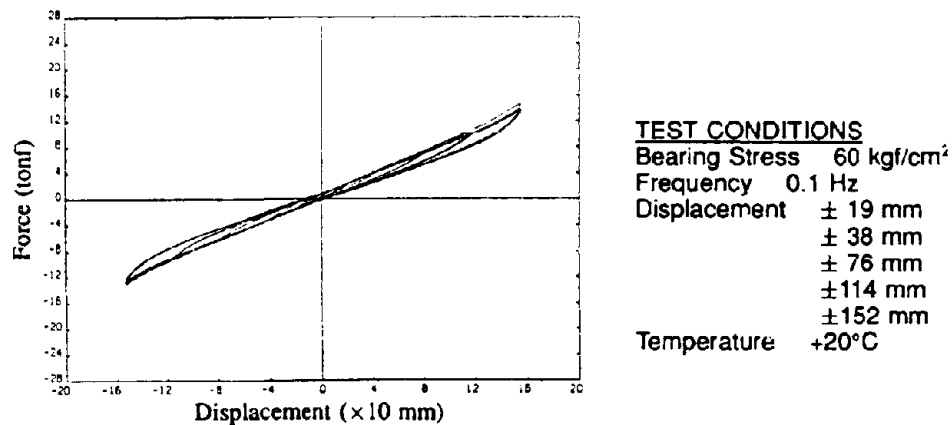


Fig. 10 Force-Displacement Hysteretic Loops of TR-RB Under Dynamic Test at PWRI

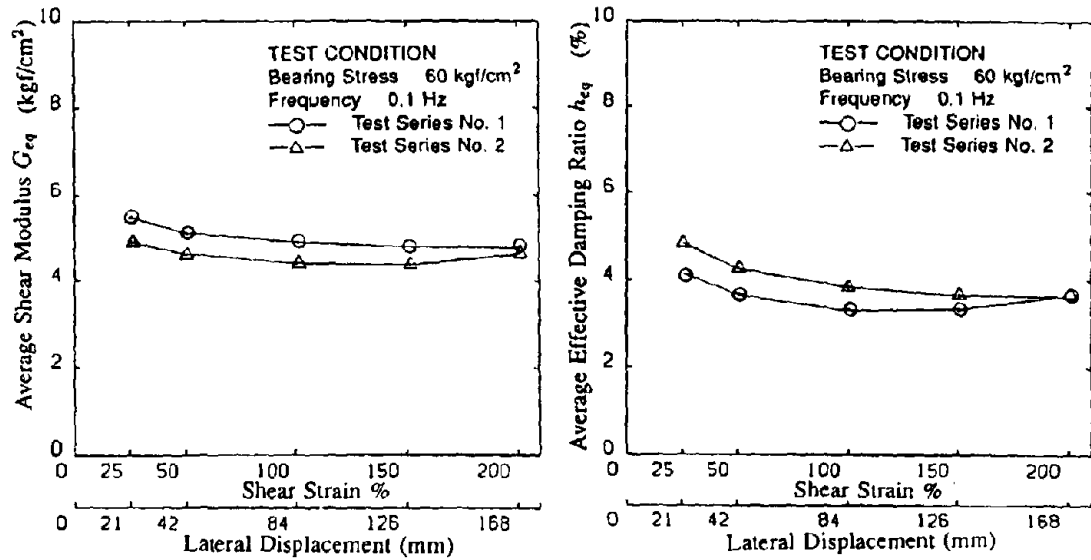


Fig. 11 Influence of Shear Strain on Shear Modulus and Damping Ratio (Dynamic Test at PWRI)

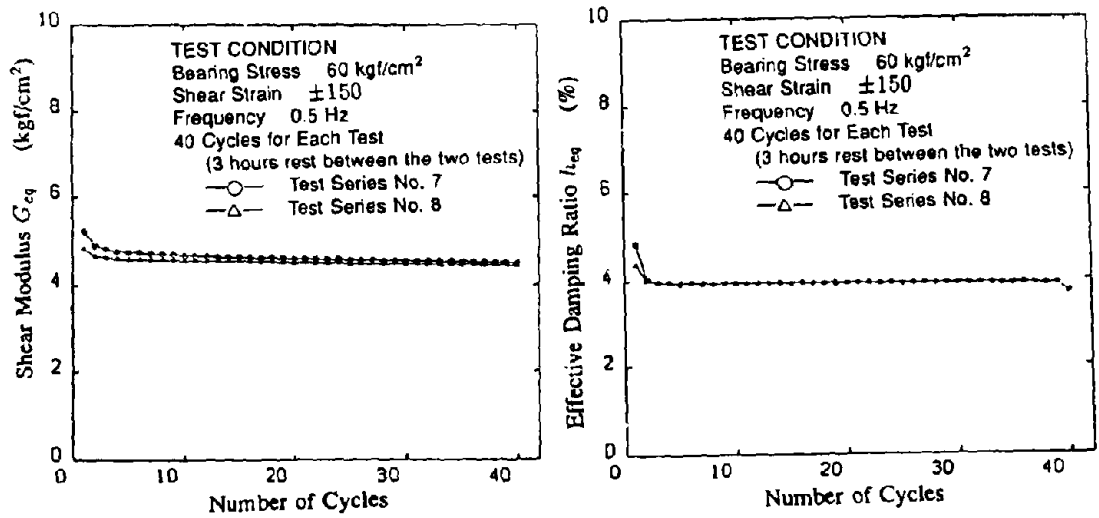


Fig. 12 Influence of Repeated Cycles on Shear Modulus and Damping Ratio (Endurance Test at PWRI)

SUMMARY AND CONCLUSIONS

Extensive tests were conducted on the newly developed textile-reinforced menshin bearings under both static and dynamic load conditions. Tests were first conducted on 1/4-scale reduced models to evaluate fundamental bearing properties, and then dynamic tests were conducted on full-scale models under the test program of the joint research project between PWRI and Toyo Tire & Rubber Corp. The results can be summarized as follows:

- The developed TR-RB bearings exhibit similar hysteresis loops as conventional menshin bearings.
- The ratio of lateral to axial stiffnesses of about 1/1000 range is suitable for use in seismic isolation purpose of highway bridges.
- Extensive static tests with displacement up to 200% shear strain and dynamic tests with displacement up to 150% have shown that the developed TR-RB bearings have stable hysteretic behavior.
- Although the same rubber material as in the scale models was used in the full-scale models tested at PWRI, high damping capacity was not exhibited. However, the damping capacity is still higher than for conventional bearings using the same rubber material.

In conclusions,

- The developed TR-RB bearings have been tested and shown to exhibit suitable properties for use as menshin device with the advantage of being lighter in weight. It is necessary to establish the parameters of lateral stiffness and damping for design application.
- In order to further increase the damping capacity of the TR-RB bearings, it is considered in the next step of the development project to replace the the common natural rubber material used in the tested models with high-damping rubber material.

ACKNOWLEDGEMENTS

The development of the textile-reinforced rubber bearings was made as part of the joint research program on "Development of Menshin Systems for Highway Bridges" between PWRI and Toyo Tire & Rubber Corp. We would like to gratefully acknowledge the cooperation of Dr. K. Kawashima, Mr. K. Hasegawa, Mr. S. Unjo, and Mr. H. Nagashima of the Earthquake Engineering Division of PWRI.

Development of A Sliding Friction Damper

Takamura IGUCHI¹⁾

¹⁾Manager Engineering Department
BBM Co., Ltd.
Chuo-ku, Tokyo, JAPAN

Summary

This paper describes a base Menshin bearing that has been developed by combining a rubber bearing with a sliding surface so as to form a module damper, and an experiment was made to verify its effective damping characteristics and the following was found: 1) Dependency of the friction resistance on the bearing stress was $\mu = 0.03 \sim 0.06$ at $\sigma_c = 30 \sim 120 \text{ kgf/cm}^2$, while its dependency on the velocity was $\mu = 0.07 \sim 0.09$ at 1 HZ. 2) Damping characteristic of approximately 50 % was confirmed. It was same even in the area of $\pm 25 \sim \pm 50 \%$. 3) The rubber packing located in the gap of the sliding surface restricts the slide in the large displacement zone, and a hysteresis curve was obtained with the secondary gradient caused by the shear deformation of the rubber bearing.

INTRODUCTION

A friction type energy dissipator with an elastmer bearing as shown in Fig.1 and 2 was developed for Menshin bearing of highway bridges.

The natural rubber is used for elastmeric bearing has been used in Japan, for the past 17 years, and bearing with as large as 1000 tf were adopted for multi-span continuous girder bridges. General structure of the elastmeric bearing is as:

- (1) Reinforced plate with thickness 6 to 19 mm
- (2) An opening of about 50 % is provided at the center and the rubber is set through of total structure of the bearing is laminated with rubber.

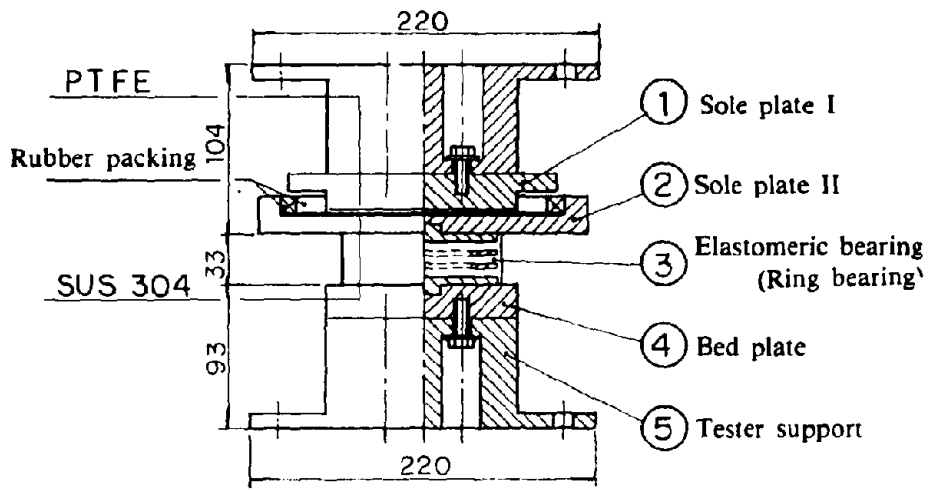


Figure 1. Small-scale model of sliding friction damper.

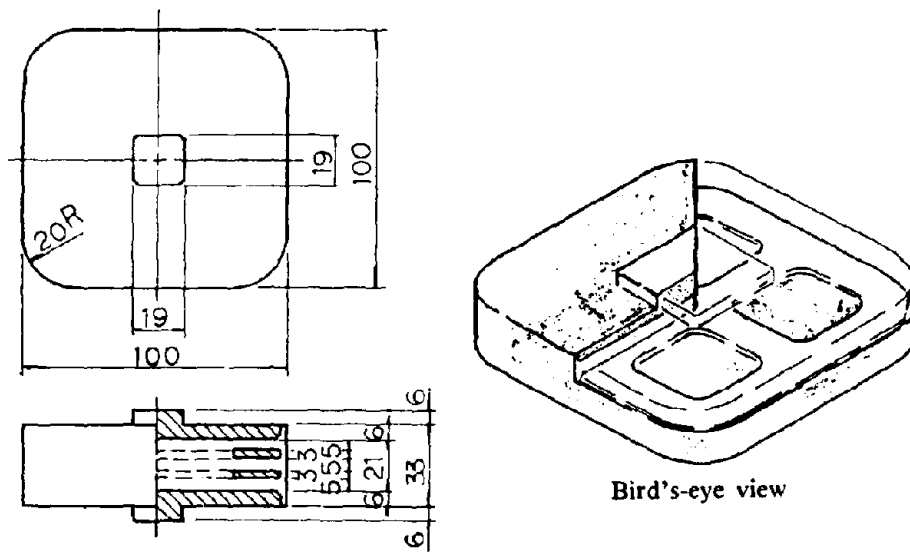


Figure 2. Ring bearing.

FUNDAMENTAL PROPERTIES OF SLIDING FRICTION DAMPER

Physical Properties of Rubber

The Ring bearing is used as the elastomeric bearing because it satisfies the specifications for the rubber material given in the bearing manual and its durability is already verified by the fatigue test, exposure tests, and acceleration tests in the room.

Testing Methods

A series of tests as shown in Table 1 were conducted to check the basic properties of the device.

Table 1 Testing conditions.

	Case (1)			Case (2)	Case (3)		
Vertical load (t.f)	2.9	5.8	7.7	5.8	2.9	5.8	7.7
Bedring Stress (kg.t/cm ²)	30	60	80	60	30	60	80
Frequency (Hz)	0.3	0.4	0.5	0.1	0.1		
	1.0	1.5	2.0				
Shear displacement rate (%)	±100			±100	±100		
	±150			±150			
PTFE	Pure teflon			containing glass fiber	containing glass fiber		
				containing graphite			

Test Results

- (1) The basic hysteresis curve as the sliding friction damper is confirmed.
- (2) The basic hysteresis curve is observed in the region $f < 1.0$ as the velocity dependence.
 In the region $f > 1.5$, the friction disappears and the shear deformation of the elastomeric bearing is dominant.
 In the region $f > 2.0$, the sliding face is almost still and the shear deformation of the elastomeric bearing only repeats.
- (3) The material containing glass fiber is the best in the abrasion resistance of PTFE
- (4) The packing material cannot be quantitatively evaluated by the scale model test. (At first, the low-elasticity rubber was planned to be used. However, its behavior shown in the test was not favorable; therefore, mold damping rubber damping packing was adopted.)

DYNAMIC LOADING TESTS AT PWRI

Testing Methods

To check the properties of the sliding friction damper, a series of dynamic loading tests were made at PWRI under the conditions presented in Table 2.

Table 2 Testing Conditions

Series No.	Bearing stress	Frequency Hz	Pre-strain %	Stain	Cycles	Model used
	kgf/cm ²			%		
1	30	0.1	0	±25	10	Rubber bearing 300x300x71
2				±50		
3				±100		
4				±150		
5				±200		
6	60	0.1	0	"	"	"
7						
8						
9						
10	120	0.1	0	"	"	"
11						
12						
13						
14						
15	60	1.0	0	"	"	"
16						
17						
18						
19						
20						

Fig. 3 shows the model used for the loading tests and Fig. 4 and 5 show the ring bearing and damping rubber packing used for the model. Test procedure is presented in Photo 1.

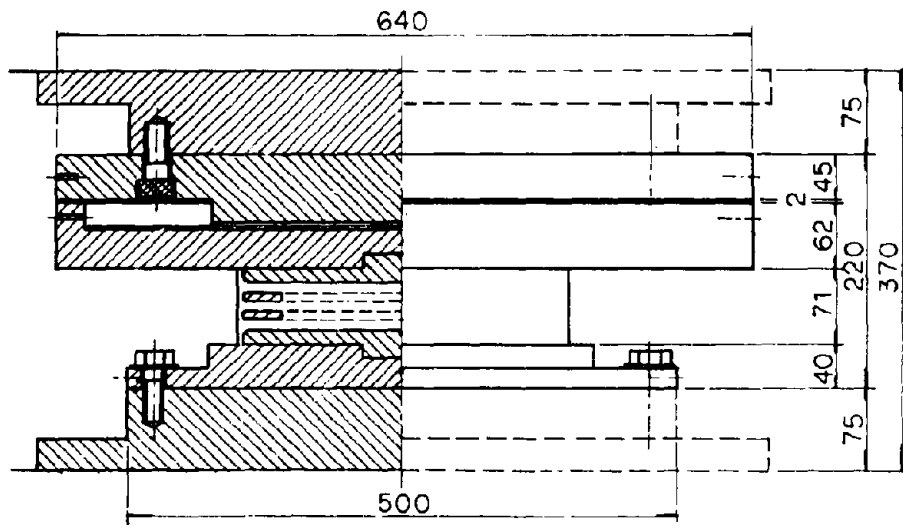


Figure 3. Dynamic loading test at PWRI.

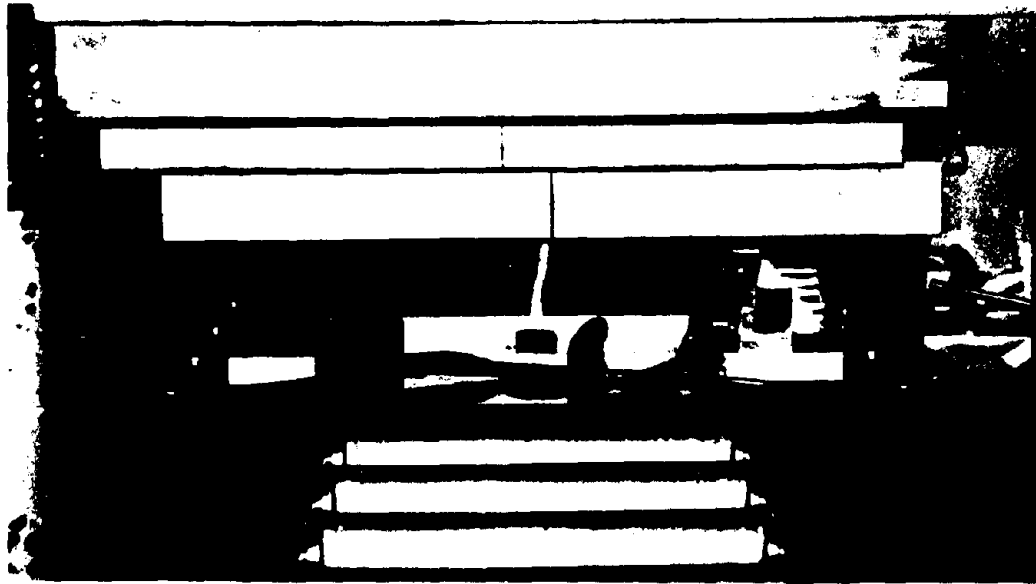


Photo 1. Dynamic loading test.

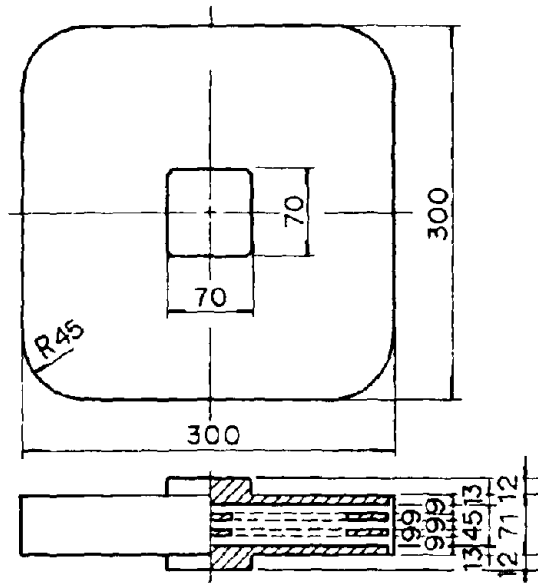


Figure 4. Ring bearing.

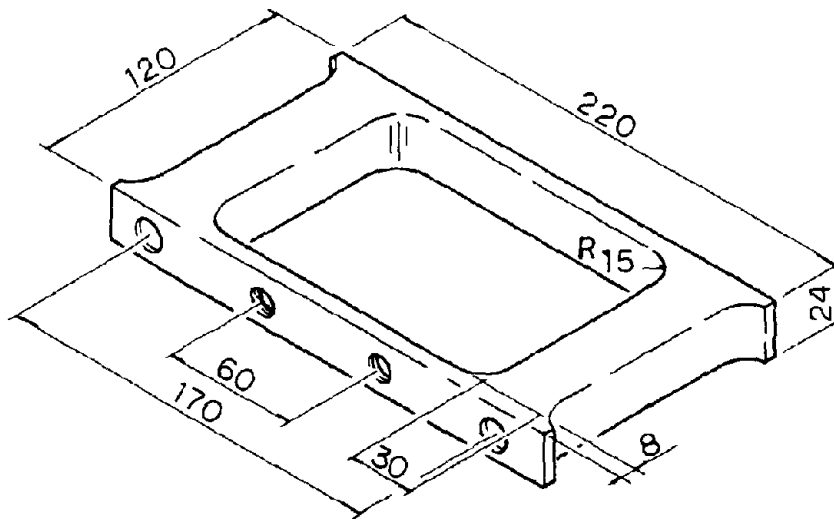


Figure 5. Damping rubber packing.

Test Results of a series of tests at PWRI

Major test results are presented in Table 3.

Table 3 Tests results

Test No.	Test results										
	Average bearing stress (kg/cm ²)	Average shear displacement		Shear properties							
		Strain rate (%)	Displacement (mm)	Effective stiffness (krf/cm)				Effective damping ratio (heq)			
				1 cycle	3 cycles	10 cycles	4 to 10 average	1 cycle	3 cycles	10 cycles	4 to 10 average
1	35.5	22.7	10.2	1.62 1.51	1.12 1.05	1.05 0.98	1.07 1.0	32.6 0.71	45.2 0.99	46.0 1.00	45.8 1.0
2	35.3	45.1	20.3	0.67 1.13	0.62 1.05	0.58 0.98	0.59 1.0	47.2 0.93	50.4 0.99	51.1 1.00	51.0 1.0
3	36.1	90.9	40.9	0.38 1.15	0.35 1.04	0.33 0.98	0.34 1.0	48.9 0.95	51.2 0.99	52.0 1.01	51.7 1.0
4	35.7	136.0	61.2	0.27 1.07	0.26 1.02	0.25 1.00	0.25 1.0	48.5 0.98	49.1 0.99	49.6 1.00	49.6 1.0
5	36.1	182.2	82.0	0.52 1.13	0.49 1.05	0.46 0.99	0.46 1.0	19.1 0.93	19.9 0.96	20.9 1.01	20.6 1.0
6	72.3	22.4	10.1	1.52 1.12	1.34 0.98	1.38 1.01	1.36 1.0	35.5 0.88	40.6 1.01	39.9 0.99	40.3 1.0
7	72.2	45.1	20.3	0.86 1.00	0.84 0.99	0.87 1.02	0.86 1.0	47.7 0.99	48.7 1.01	47.8 0.99	48.4 1.0
8	72.3	90.9	40.9	0.54 1.05	0.52 1.01	0.52 1.01	0.52 1.0	50.2 0.96	51.8 1.00	51.7 0.99	52.0 1.0
9	72.2	136.4	61.4	0.42 1.08	0.40 1.01	0.40 1.01	0.40 1.0	50.0 0.97	51.1 0.99	51.5 1.00	51.4 1.0
10	72.8	182.4	82.1	0.49 1.04	0.47 1.01	0.46 0.99	0.47 1.0	33.5 0.98	33.7 0.99	34.6 1.01	34.1 1.0
11	144.4	22.4	10.1	2.77 1.56	2.62 1.00	2.62 1.00	2.61 1.0	14.5 1.23	12.0 1.02	11.6 0.98	11.8 1.02
12	144.3	45.3	20.4	1.75 0.89	1.90 0.97	1.98 1.01	1.96 1.0	27.4 1.05	27.8 1.06	25.2 0.96	26.2 1.0
13	144.1	91.8	41.3	1.16 0.92	1.22 0.97	1.29 1.02	1.26 1.0	40.5 1.03	40.6 1.03	38.7 0.98	39.4 1.0
14	144.1	137.8	62.0	0.92 0.95	0.95 0.98	0.99 1.02	0.98 1.0	43.8 1.00	54.2 1.01	43.3 0.99	43.7 1.0
15	144.3	184.4	83.0	0.79 0.95	0.81 0.98	0.75 1.02	0.83 1.0	43.3 1.00	43.6 1.01	43.1 0.99	43.4 1.0
16	72.5	21.1	9.5	2.83 1.03	2.76 1.00	2.77 1.00	2.76 1.0	17.7 1.36	13.8 1.06	12.5 0.96	13.0 1.0
17	72.6	42.9	19.3	2.04 0.99	2.14 1.03	2.02 0.98	2.07 1.0	26.8 0.90	28.5 0.96	29.7 1.00	29.6 1.0
18	73.2	86.0	38.7	1.28 1.17	1.22 1.11	1.05 0.96	1.10 1.0	41.4 0.91	43.9 0.97	44.9 0.99	45.5 1.0
19	73.5	128.0	57.6	0.96 1.25	0.86 1.13	0.73 0.95	0.76 1.0	45.3 0.94	47.4 0.98	47.3 0.98	48.4 1.0
20	73.9	168.4	75.8	0.79 1.27	0.70 1.11	0.61 0.97	0.62 1.0	44.2 0.95	46.2 0.99	45.0 0.97	46.6 1.0

Stability of $h_{e,q}$ and $k_{e,q}$ to the Cyclic Loadings

- (1) In tests 1 to 20, dependence of $h_{e,q}$ on cyclic loading from 3 to 10 cycles is obtained, and it is about 96 to 102% of the average in 4 to 10 cycles.
- (2) The fatigue properties are checked by the following test.

Test conditions: $f = 0.5\text{Hz}$
 $\sigma_c = 71.8\text{kgf/cm}^2$
 $\epsilon = \pm 136\%$

The results are shown in Table 4. and 5.

Table 4 Test Result to the Cyclic Loadings

	1	3	10	20	30	40	Average 4 - 10
$h_{e,q}$ (%)	43.7	49.9	51.7	51.5	51.6	50.2	51.3
	0.64	0.93	1.00	1.01	1.01	0.98	1.0
$k_{e,q}$ (tf/cm)	0.55	0.42	0.37	0.37	0.38	0.39	0.39
	1.42	1.10	0.97	0.96	0.97	1.00	1.0

- (3) In 100 to 150% relative displacement region, which is important for the device, damping ratio $h_{e,q}$ obtained as 52.0 ~ 51.4% for tests 7 and 9.
- (4) Average damping ratio over test 2 ~ test 4, test 7 ~ test 9, test 17 ~ test 19 was evaluated as shown in Table 5. They are almost similar with the value averaged from 4 to 10 loading cycles.

Table 5 Stability of Effective Damping Ratio (%)

Test	± 50	± 100	± 150
Test case 2 - 4	47.2 (51.0)	48.9 (51.7)	48.5 (49.6)
Test case 7 - 9	47.7 (48.4)	50.2 (52.0)	50.0 (51.4)
Test case 17 - 19	26.8 (29.6)	41.4 (45.5)	45.3 (48.4)

Note) Average from N = 4 to 10 cycles () represents.

The tests results for hysteresis loop of standing friction damper as shown in Fig. 6 ~ 9.

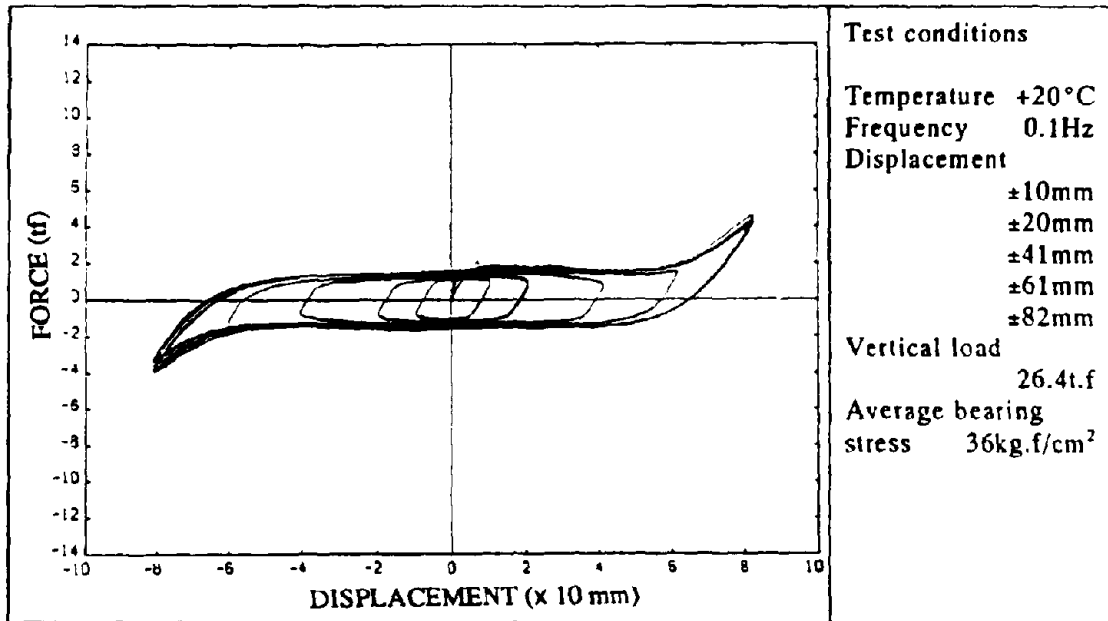


Figure 6. Force-displacement hysteresis loop of sliding friction damper (Test 1 - 5).

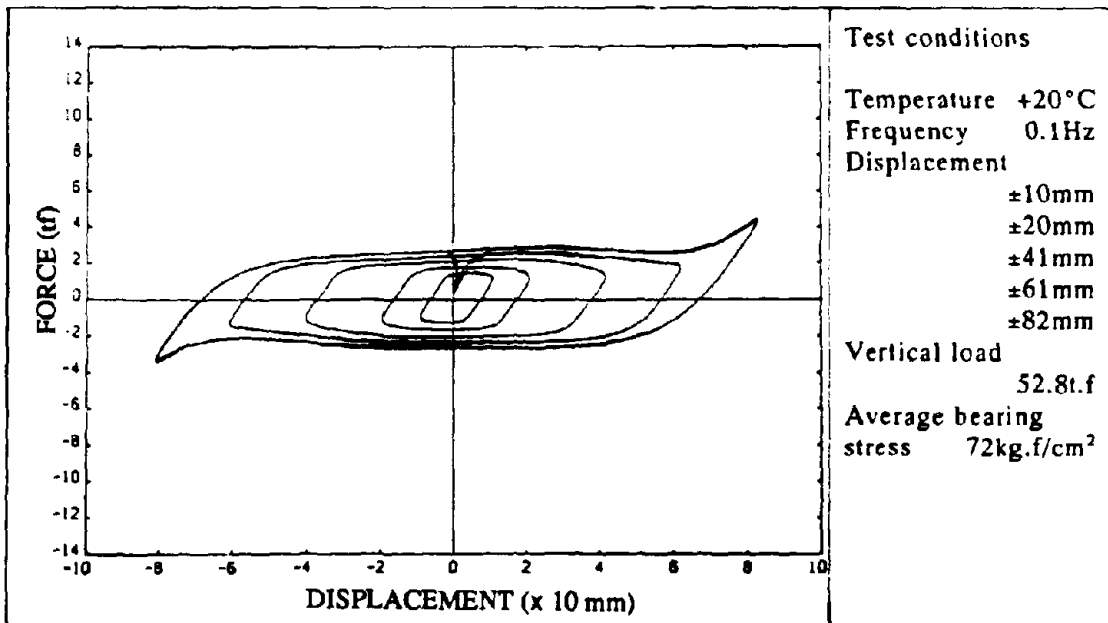


Figure 7. Force-displacement hysteresis loop of sliding friction damper (Test 6 - 10).

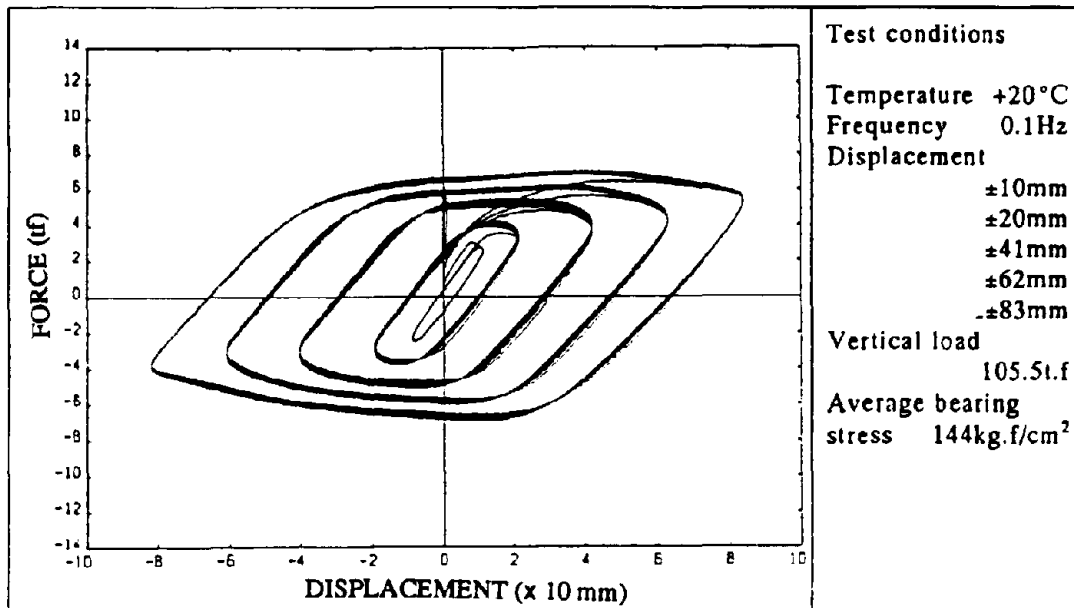


Figure 8. Force-displacement hysteresis loop of sliding friction damper (Test 11 - 15).

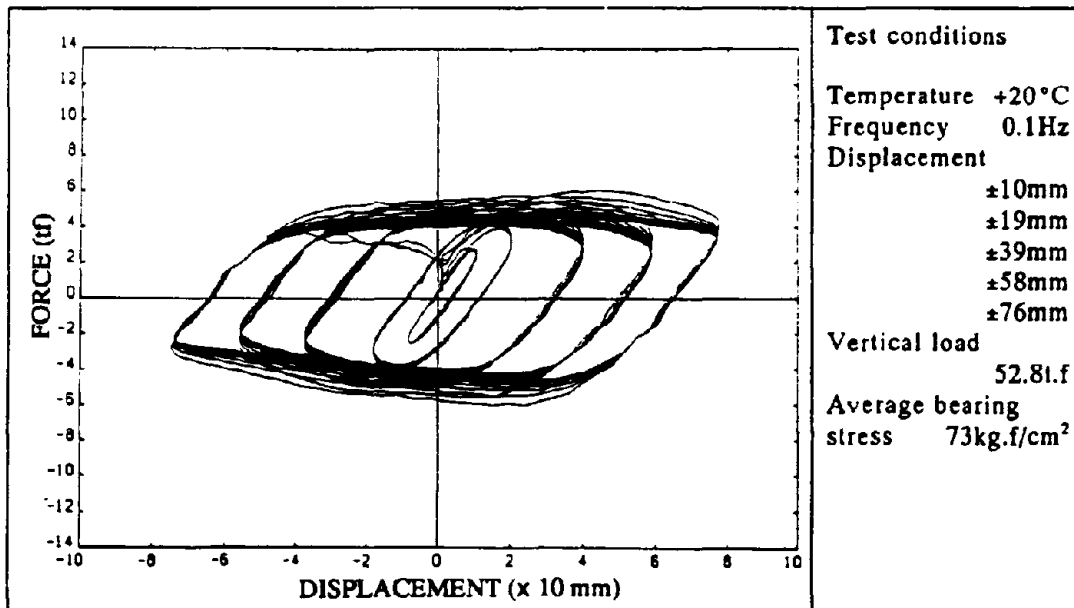


Figure 9. Force-displacement hysteresis loop of sliding friction damper (Test 16 - 20).

CONCLUSION

Following findings were obtained from the loading test presented herein:

- (1) A stable basic hysteresis curve was obtained as a module friction damper and as a Menshin device.
- (2) High performance with a high damping characteristic of approximately 50% was obtained.
- (3) Damping characteristic of approximately 40% was obtained even in the area where lateral displacement is less ($\pm 25\%$).
- (4) A test result of $\mu = 0.03 \sim 0.06$ was obtained for the dependency of the friction coefficient on the bearing stress.
- (5) A test result of $\mu = 0.07 \sim 0.09$ was obtained for the dependency of the friction coefficient on the velocity.
- (6) Wear-resistant characteristics against repeated lateral load was sufficient even at $N = 80$.

ACKNOWLEDGEMENTS

The development of sliding friction damper (Part 2) was made as a part of the joint research program on "Development of Menshin Systems of Highway Bridges" between PWRI and BBM Co., Ltd. Grateful acknowledgement is made to Dr. K. Kawashima, Mr. K. Hasegawa, Mr. S. Unjo and Mr. H. Nagashima of the Earthquake Engineering Division of PWRI for their cooperation.

DEVELOPMENT OF STEEL DAMPER FOR MENSIN BRIDGES

Hiroshi KAMIYA, Shin_ichi IIZUKA and Masataka TAKEI

Nishimatsu Construction Co. Ltd., Yamato-shi, Kanagawa, Japan

SUMMARY

A Steel damper was developed for energy dissipation for highway bridges. The steel damper is circular and made of stainless steel. Characteristic tests performed on the steel damper showed that it absorbs large deformation and has hysteresis damping capacity. The performance of the steel damper does not vary according to the velocity, frequency and temperature.

INTRODUCTION

The basic function of the steel damper is to absorb the energy of the earthquake through plastic deformation of the steel material. For the Menshin system, the laminated elastomeric bearing mainly bears dead load, while the steel damper bears part of the horizontal seismic force; it does not shoulder vertical forces.

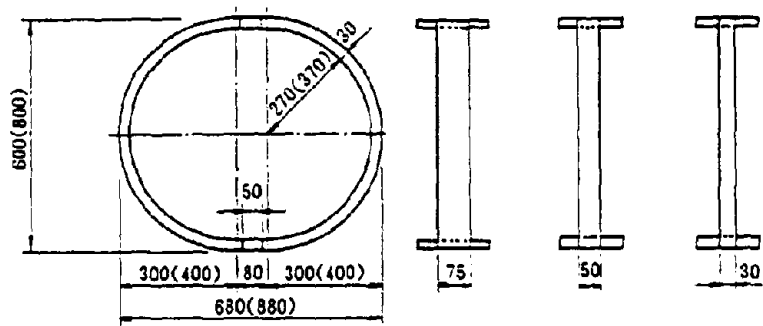
The steel damper that we developed uses a ring damper which is made by processing stainless steel (SUS 304) into a circular shape. Stainless steel is characteristically more resistant to corrosion and has higher strength and elongation. Static loading tests, dynamic loading tests, and dynamic loading tests at the Public Works Research Institute (PWRI) were performed to verify the fundamental properties of this steel damper.

FUNDAMENTAL PROPERTIES OF THE STEEL DAMPER

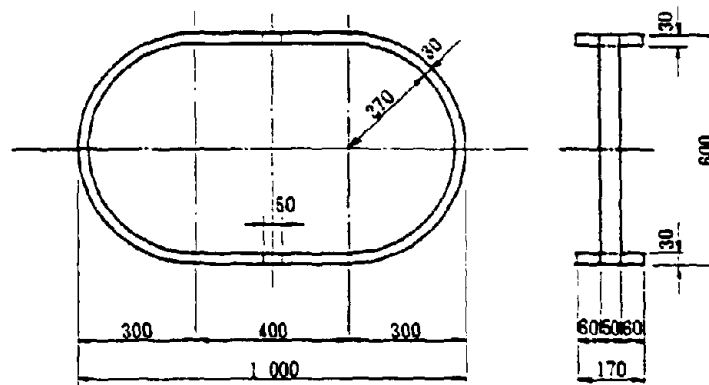
Test Models The shapes of the test models are shown in Figure 1. Test parameters are presented in Table 1. The test parameters were the diameter and the width of the test model. An actuator was used to apply static and dynamic forces. Static loading was applied by scheduling the displacement amplitude. Dynamic loading was applied sinusoidally while controlling the frequency and amplitude as parameters. Testing facilities are shown in Figure 2.

The arrangements of steel dampers are illustrated in Figure 3. One steel damper may exhibit directionality depending on where it is located. Therefore, sets of two or four steel dampers are considered the fundamental arrangement.

The loading tests were individually carried on, shear direction and compressive - tensile direction.



(a) Circular Type



(b) Oval Type

Figure 1 Shape of Steel Damper

Table 1 Test Parameters

(a) Static Loading

Test name	Loading Direction	Size of Damper(mm)	
		Diameter	Width
TC8030	C & T*	800	30
SS8030	Shear		30
TC8050	C & T*		50
SS8050	Shear		50
TC8075	C & T*		75
SS8075	Shear		75
TC850	C & T*	800	50
SS850	Shear		50
TC850	C & T*	600	50
SS850	Shear		50
TC875	C & T*		75
SS875	Shear		75
TC630	C & T*		30
SS630	Shear		30
TCL50	C & T*	(Oval)	50
SSL50	Shear		50

(b) Dynamic Loading

Test name	Loading Direction	Size of Damper(mm)		Freq. (Hz)	Amplitude (mm)
		Diameter	Width		
80-TC1	C & T*	800	30	1	±40
80-SS1	Shear				
80-TC2	C & T*			0.5	±40
80-SS2	Shear				
80-TC3	C & T*			0.5	±90
80-SS3	Shear				
80-TC4	C & T*			0.2	±90
80-SS4	Shear				
80-TC5	C & T*			0.2	±130
80-SS5	Shear				
60-TC1	C & T*	600	50	1	±20
60-SS1	Shear				
60-TC2	C & T*			1	±40
60-SS2	Shear				
60-TC3	C & T*			0.5	±40
60-SS3	Shear				
60-TC4	C & T*			0.5	±60
60-SS4	Shear				
60-TC5	C & T*			0.2	±60
60-SS5	Shear				
L-TC1	C & T*	(Oval)	50	0.5	±60
L-SS1	Shear				

*C & T Compressive - Tensile direction

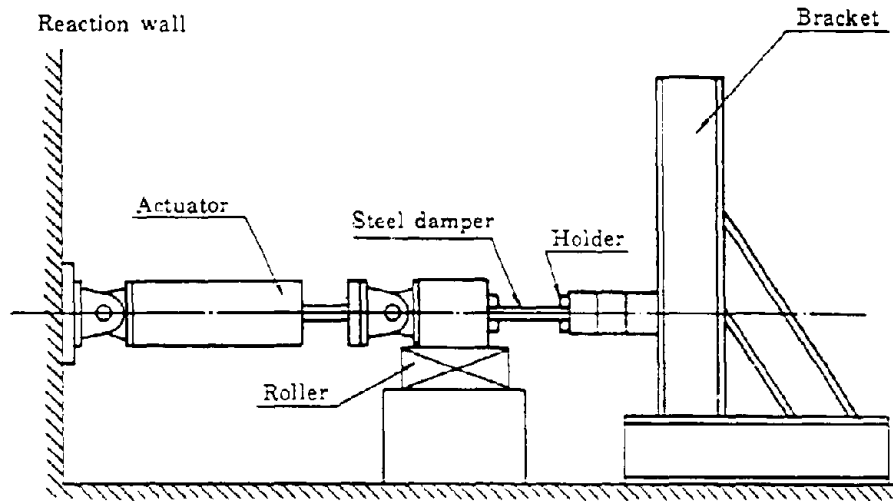


Figure 2 Testing Facilities

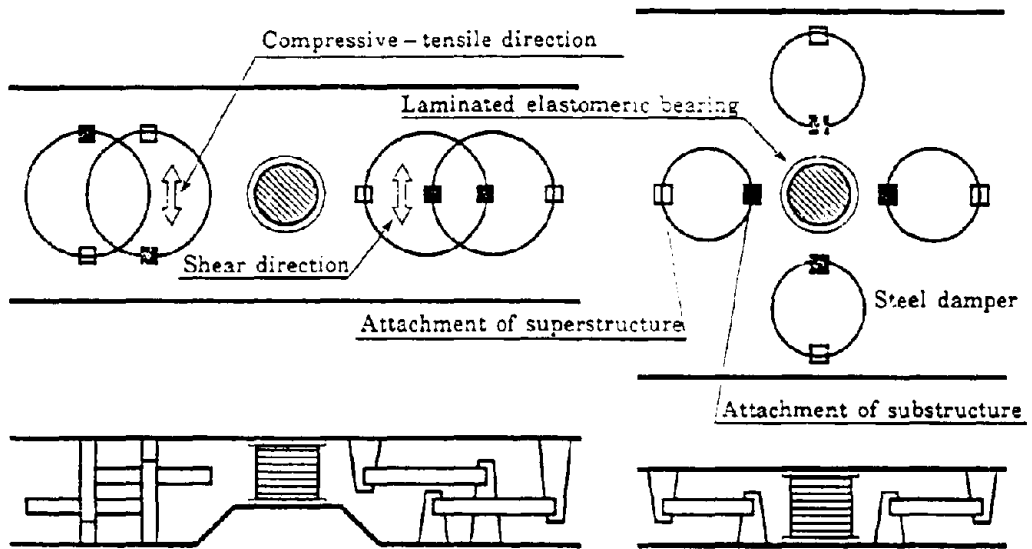


Figure 3 Configuration of Menshin Device

TEST RESULTS

Static loading tests The force - displacement hysteresis loop according to the loading direction are shown in Figure 4. For identical displacements, the force in the compressive - tensile direction is about three times larger than that in the shear direction.

The force - displacement hysteresis loop according to the damper width are shown in Figure 5. The wider the damper width, the larger the force is. The increment in force is proportional to the increase in width.

Effective damping ratio that were obtained from natural loops of the tests are shown in Figure 6. In all tests, the effective damping ratio increased as displacement increased. A comparison of effective damping ratios depending on the loading direction indicated that they were larger in the compressive - tensile direction than in the shear direction.

Dynamic loading tests The results of the dynamic loading tests using frequency and amplitude as test parameters are presented in Table 2. The force - displacement hysteresis loop corresponds to that of the static loading test.

With identical frequencies, the number of cycles before the occurrence of failure decreased as the amplitude increased. Loading with the same amplitude but with different frequencies failed the damper after a comparable number of cycles.

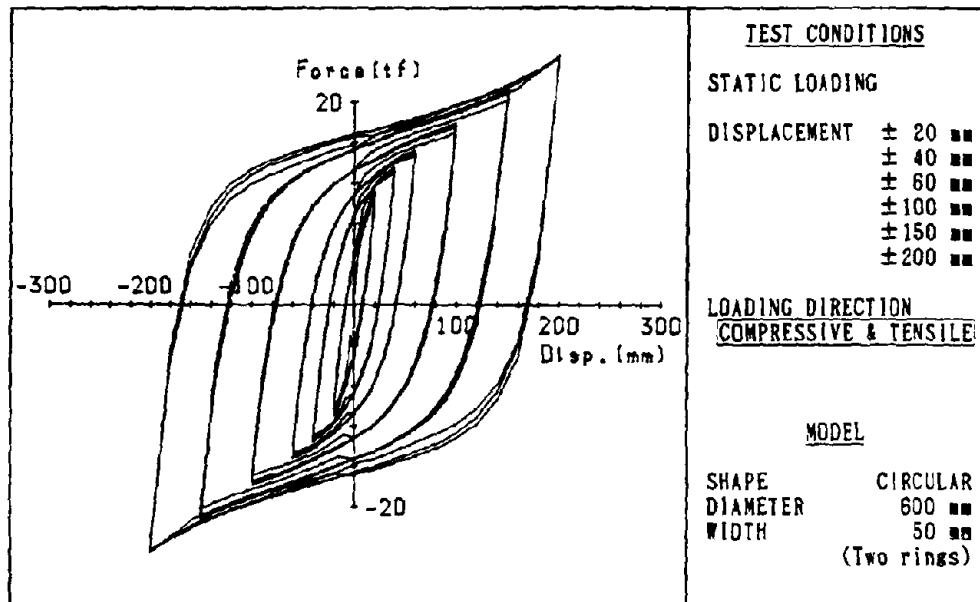
A comparison between the force in the shear direction and that in the compressive - tensile direction revealed that the former withstood a larger number of cycles before failure.

The amount of cumulative energy before failure took place was unaffected by the frequency, velocity and amplitude in any given loading direction.

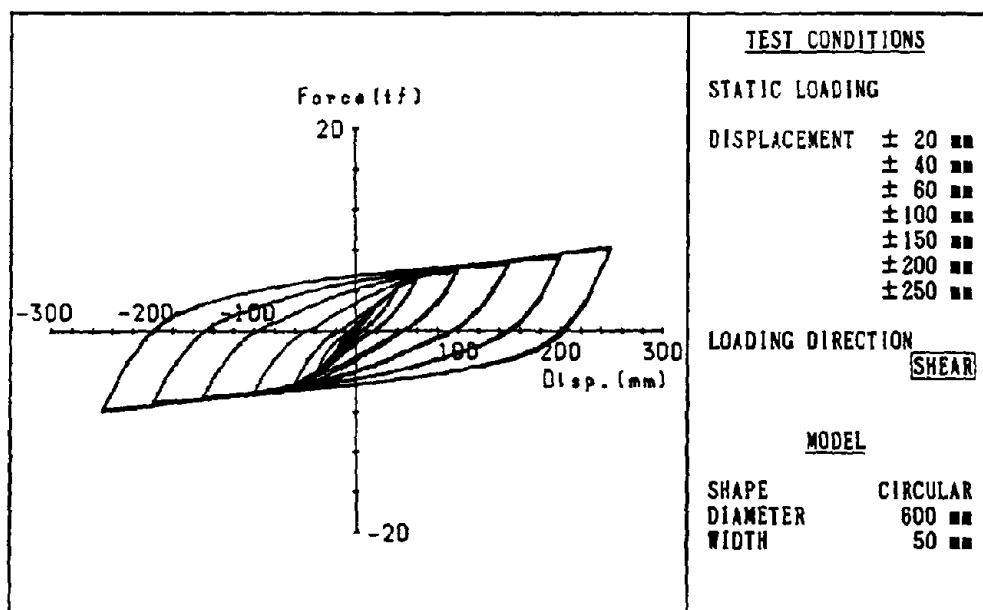
CONCLUSIONS

We carried out a number of characteristic tests on steel dampers that we had developed. The following conclusions were obtained.

- (a) The developed steel dampers are made of stainless steel. They are resistant to rust and have strength and elongation equal to or higher than that of iron. The steel dampers have a fairly good damping capacity.
- (b) The stiffness of a steel damper can be freely adjusted by changing its width. In addition, design displacement can be adjusted by changing the damper's diameter.
- (c) Steel dampers depend only slightly on frequency, velocity and the environment. Therefore, they are relatively easy to design.
- (d) The failure of steel dampers can be evaluated by interpreting it as the amount of cumulative energy obtained from hysteresis loops.

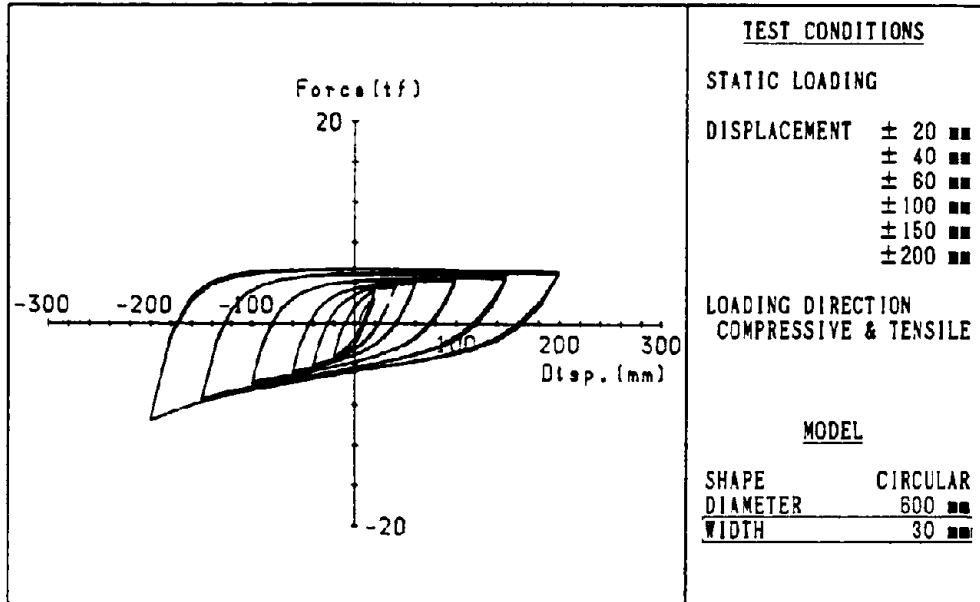


(a) Compressive - Tensile Direction

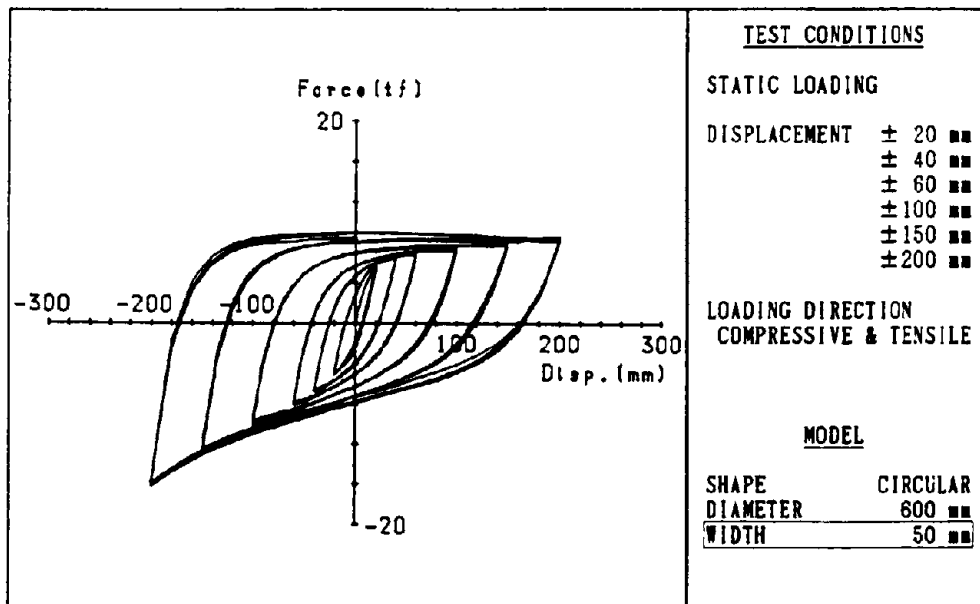


(b) Shear Direction

Figure 4 Force - Displacement Hysteresis Loop
(Comparison of Loading Direction)

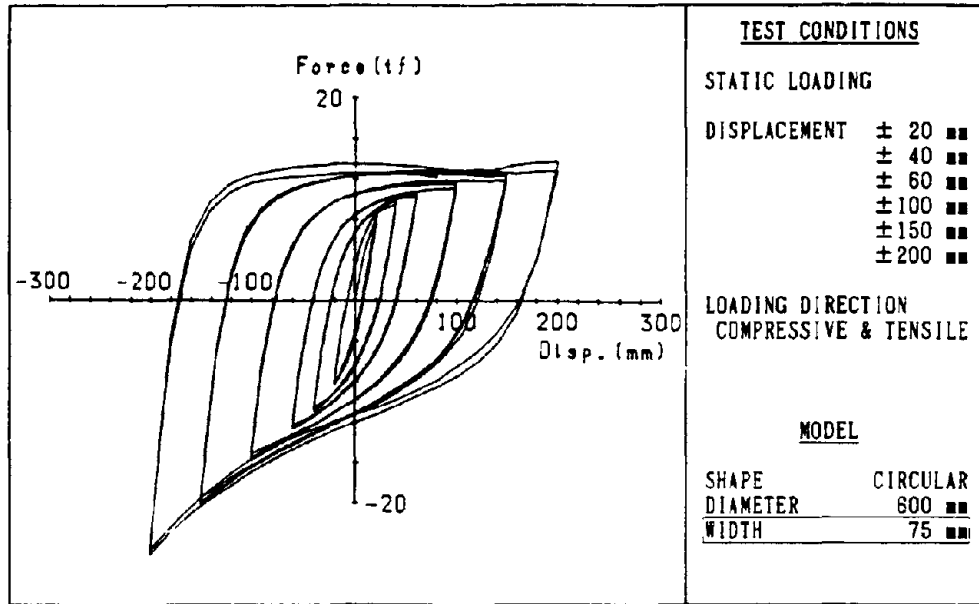


(a) 30 mm



(b) 50 mm

Figure 5 Force - Displacement Hysteresis Loop
(Comparison of Damper Width)



(c) 75 ■■

Figure 5 Force - Displacement Hysteresis Loop
(Comparison of Damper Width)

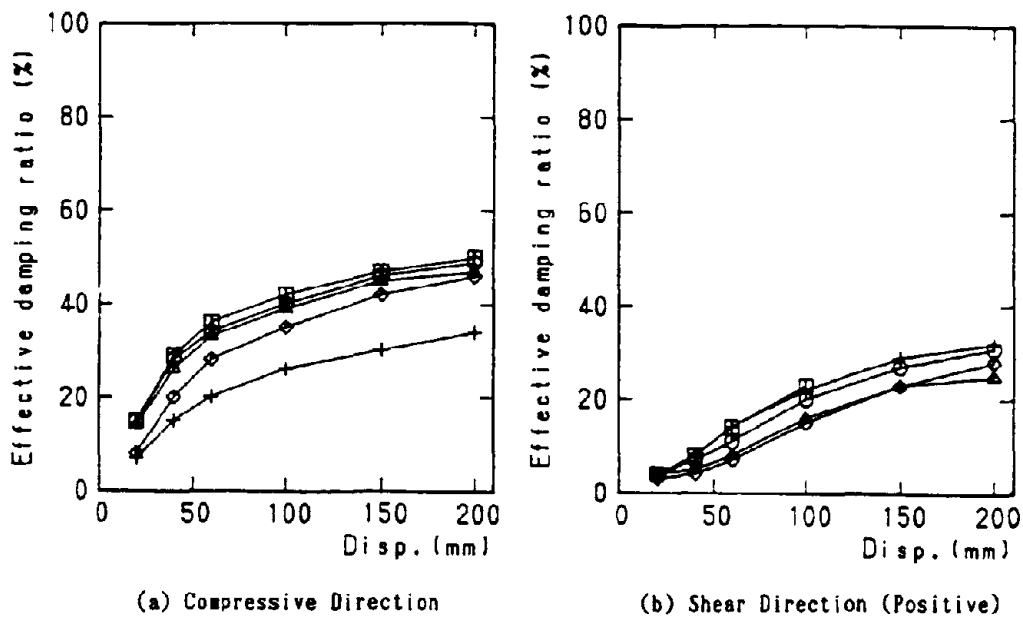


Figure 8 Comparison of Effective Damping Ratio

Table 2 Dynamic Test Results

(a) Circular Type (D=800, W=30)

Test name	Freq. (Hz)	Amplitude (mm)	Failure cycle (count)	Hysteresis area (tf·mm)	Accumulated energy (tf·mm)
80-TC1	1	40	498	200	99,600
80-TC2	0.5	40	579	170	98,430
80-TC3	0.5	90	121	770	93,170
80-TC4	0.2	90	125	700	87,500
80-TC5	0.2	130	67	1,240	83,080
80-SS1	1	40	10,000*	20	200,000
80-SS2	0.5	40	10,000*	20	200,000
80-SS3	0.5	90	1,120	190	212,800
80-SS4	0.2	90	1,320	160	211,200
80-SS5	0.2	130	579	370	214,230

(b) Circular Type (D=600, W=50)

Test name	Freq. (Hz)	Amplitude (mm)	Failure cycle (count)	Hysteresis area (tf·mm)	Accumulated energy (tf·mm)
60-TC1	1	20	520	150	78,000
60-TC2	1	40	160	450	72,000
60-TC3	0.5	40	190	430	81,700
60-TC4	0.5	60	105	910	95,550
60-TC5	0.2	60	110	890	97,900
60-SS1	1	20	1,000*	10	10,000
60-SS2	1	40	1,000*	70	70,000
60-SS3	0.5	40	1,000*	70	70,000
60-SS4	0.5	60	1,000*	230	230,000
60-SS5	0.2	60	500*	220	115,000

(c) Oval Type

Test name	Freq. (Hz)	Amplitude (mm)	Failure cycle (count)	Hysteresis area (tf·mm)	Accumulated energy (tf·mm)
L-TC1	0.5	60	360	420	151,200
L-SS1	0.5	60	1,000*	280	280,000

*Not failure until that count.

DYNAMIC LOADING TESTS AT PWRI

Testing Methods The test parameters used at the Public Works Research Institute (PWRI) are presented in Table 3. The testing facilities are shown in Photos 1 and 2.

The steel damper was subjected to ten cycles at each displacement with a fixed frequency of 0.5 Hz and an amplitude of 50, 100 and 150 mm. Since the steel damper does not shoulder vertical forces, the test was performed so as to avoid applying external forces in the vertical direction to the damper.

In addition, endurance tests of the steel dampers, steel dampers were subjected to 40 cycles with a frequency of 0.5 Hz and an amplitude of 100 mm, and then subjected to tests of the same amplitude and frequency for three hours.

Table 3 Test Parameter for Dynamic Loading Tests at PWRI

TEST No.	SHAPE	FREQ. (Hz)	DISP. (mm)
1	CIRCULAR	0.5	50
2		0.5	100
3		0.5	150
4	OVAL	0.5	50
5		0.5	100
6		0.5	150
40-1	CIRCULAR	0.5	100
40-2		0.5	100

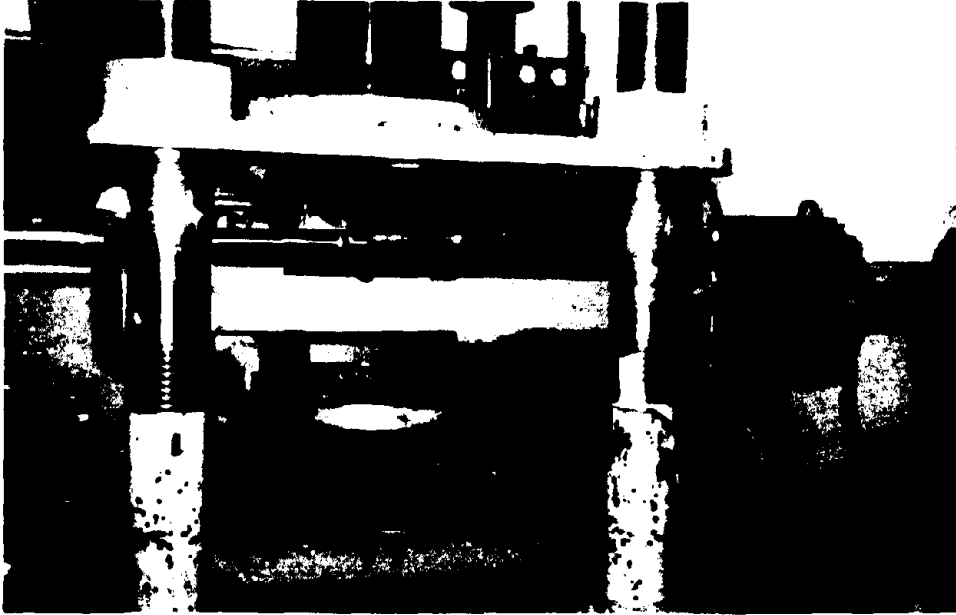


Photo 1 Testing Facilities for Dynamic Loading Tests at PWRI

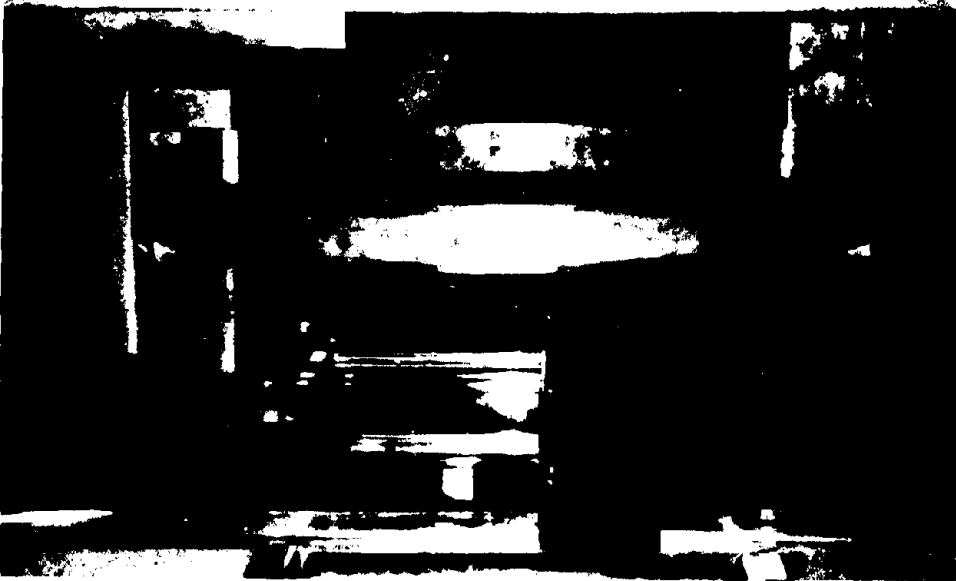
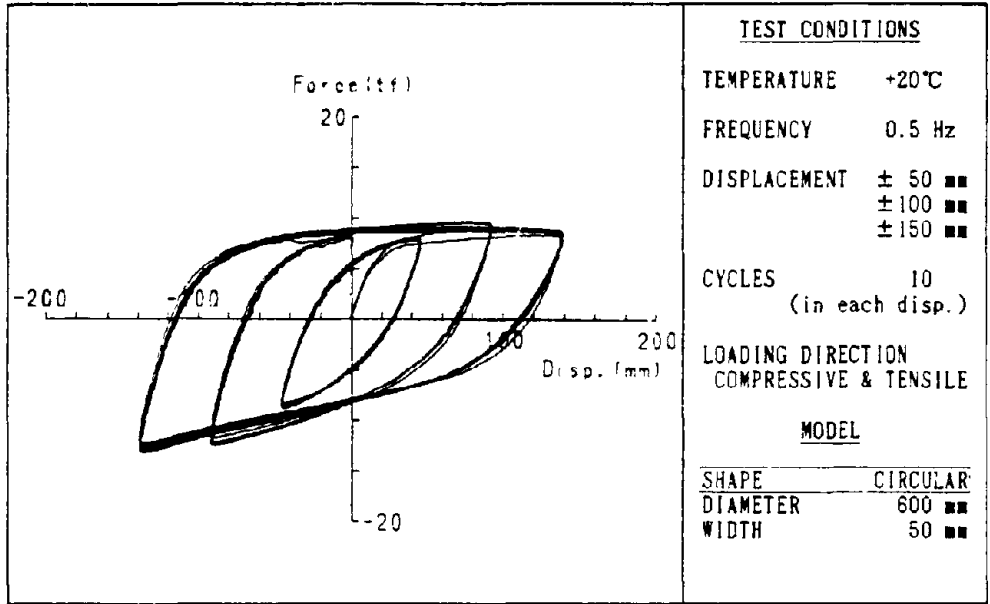


Photo 2 Testing Facilities for Dynamic Loading Tests at PWRI

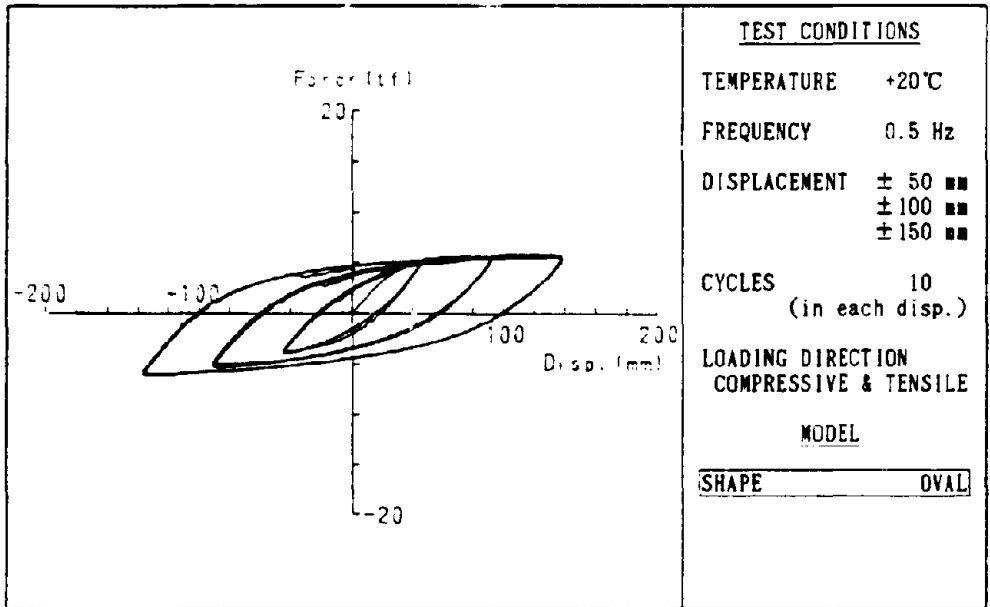
Test Results The results of the dynamic loading tests at PWRI are presented in Table 4. Test No.1 to 3 denote circular steel dampers and No.4 to 6 are oval steel dampers. Examples of the force - displacement hysteresis loop are shown in Figure 7. The steel dampers revealed a large damping capacity due to plastic deformation. The effective damping ratio was in the neighborhood of 27% to 40%. The effective stiffness tended to decrease as displacement increased, where as the effective damping ratio increased as displacement increased.

Table 4 Results of Dynamic Loading Tests at PWRI

Test No.	Freq. (Hz)	Lateral Disp. (mm)	Test results								
			Lateral Disp. (mm)	Shear characteristics							
				Effective stiffness (tf/mm)				Effective damping ratio(%)			
				Cycle1	Cycle3	Cyc.10	Mean (C4-C10)	Cycle1	Cycle3	Cyc.10	Mean (C4-C10)
1	0.5	± 50	45.8	1.77	1.83	1.82	1.83	28.0	27.6	27.2	27.4
				0.97	1.00	0.99	1.0	1.02	1.01	0.99	1.0
2	0.5	± 100	92.3	1.13	1.20	1.19	1.20	37.4	36.9	36.1	36.5
				0.95	1.00	0.99	1.0	1.03	1.01	0.99	1.0
3	0.5	± 150	139.1	0.76	0.80	0.77	0.79	40.4	39.9	39.1	39.5
				0.96	1.01	0.97	1.0	1.02	1.01	0.99	1.0
4	0.5	± 50	45.7	0.98	1.02	1.01	1.01	19.0	19.0	17.6	18.1
				0.97	1.00	1.00	1.0	1.05	1.05	0.97	1.0
5	0.5	± 100	91.5	0.59	0.60	0.59	0.60	31.9	30.7	29.8	30.1
				0.98	1.00	0.99	1.0	1.06	1.02	0.99	1.0
6	0.5	± 150	137.6	0.43	0.43	0.42	0.43	37.0	36.7	36.6	36.7
				1.01	1.01	0.99	1.0	1.01	1.00	1.00	1.0



(a) Circular Type



(b) Oval Type

Figure 7 Force - Displacement Hysteresis Loop
(Dynamic Loading Tests at PWRI)

CONCLUSIONS

The following conclusions are led from the results of the series of tests at PWRI.

- (a) Effective damping ratios of the circular steel damper are 27% with a displacement of 50 mm and 40% with a displacement of 150 mm. The effective damping ratio tended to increase as displacement increased.
- (b) The effective stiffness of a circular steel damper tends to decrease as displacement increases.
- (c) Both the effective stiffness and effective damping ratio of an oval steel damper are smaller than those of a circular steel damper.
- (d) The hysteresis loop of a circular steel damper is asymmetrical with respect to positive and negative fluctuations, while that of an oval steel damper still indicates the behavior of symmetrical curve about positive and negative values even when the displacement is the same.

ACKNOWLEDGEMENTS

Development of Steel Damper for Menshin Bridges (part 7) was made as a part of the joint research program on "Development of Menshin Systems of Highway Bridges" between PWRI and Nishimatsu Construction. Grateful acknowledgements are made to Dr. K. Kawashima, Mr. K. Hasegawa, Mr. S. Unjo and Mr. H. Nagashima of the Earthquake Engineering Division of PWRI for their cooperation.

DEVELOPMENT OF VISCOUS DAMPER FOR MENSIN BRIDGES

Kazuhiko KAWASHIMA¹, Jiroh ISEKI², Ikuo SHIMODA¹ and Yutaka MAKIGUCHI¹

¹Head, Earthquake Engineering Division, Public Works Research Institute

²Manager, Technical Development Department 2, Oiles Corporation

³Staff Manager, Technical Development Department 2, Oiles Corporation

⁴Staff Manager, Technical Development Department 2, Oiles Corporation

SUMMARY

This paper discusses the development of a viscous damper for menshin highway bridges that utilizes the flow resistance of a highly viscous material. The viscous damper functions both as an energy absorber and as a reinforcement device that prevents the superstructure from sliding off the bridge pier. In February 1991, the dynamic loading tests of the development viscous damper were carried out at the Public Works Research Institute (PWRI) to verify its fundamental properties and durability. A series of these tests revealed that the damping force of this viscous damper is proportional to the 4.3rd power of the relative velocity between the superstructure and the substructure. It was also proved that the viscous damper provides damping performance and durability suitable for menshin bridges.

INTRODUCTION

Viscous dampers were developed in Japan in the 1960's with the original object of dispersing the horizontal force that acts on multi-span continuous bridges during earthquakes. These viscous dampers were intended to function as an earthquake stopper, not as a Menshin device. Since then, such earthquake-stopper type viscous dampers have been applied widely to highway bridges and railway bridges. The main purpose of these conventional viscous dampers is to transfer the inertial force of the superstructure to the substructure during earthquakes. They are not expected to exhibit particularly good energy absorption. Conventional viscous dampers thus use highly viscous materials such as hydrocarbon polymer, butane polymer, and polyolefin polymer. However, since hydrocarbon polymer and butane polymer do not flow at room temperature, they are inappropriate for use as viscous materials for menshin devices. On the other hand, although polyolefin polymer has higher flowability than other two polymers, its viscosity is affected by temperature changes. For these reasons, a new viscous damper was developed using silicone oil as a viscous material, which also has good flowability and comparatively smaller variation in viscosity due to temperature changes. This material is used to ensure uniform deformation and stable damping properties, both of which are essential for menshin bridges.

As shown in Figure 2, the new viscous damper consists of a steel movable post that is secured to the superstructure, a top cover that is fastened to the steel movable post and seals the viscous materials together with a rubber seal, and a rubber seal that encloses the viscous material and an external steel box that is embedded and clamped in the substructure. The external box is fully packed with silicone oil, and a pressure regulating tank installed at the bottom end of the steel movable post is designed to stabilize the external box while the pressure of the silicone oil is floating.

- The characteristics of the new viscous damper are as follows:
- 1) The resistance force of the damper is basically dependent only upon the relative velocity between the superstructure and the substructure, and increases as the velocity increases. In other words, the resistance force rarely appears against long-term loads, such as a thermal load, even if the displacement caused by these loads is large.
 - 2) The damper also possesses the functions of a reinforcement device.
 - 3) There are no design restrictions for displacement, except for the dimensional restrictions of the substructures.
 - 4) The secular change in properties of the viscous material is minimal; stable damping performance is assured for long-term service.

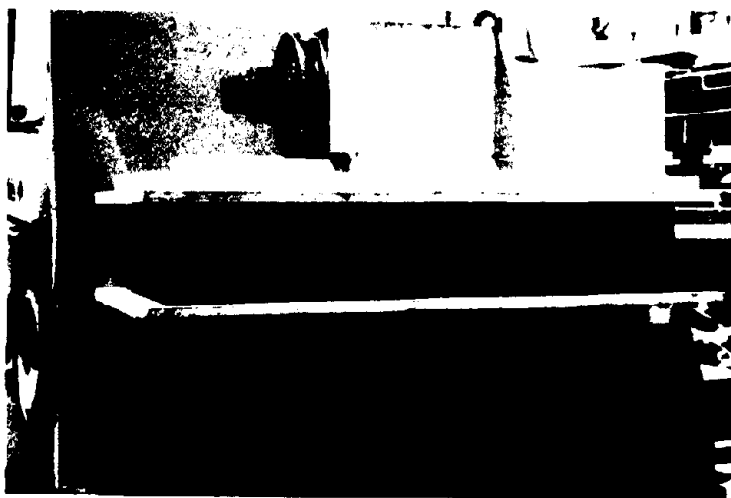


Figure 1 Viscous Damper

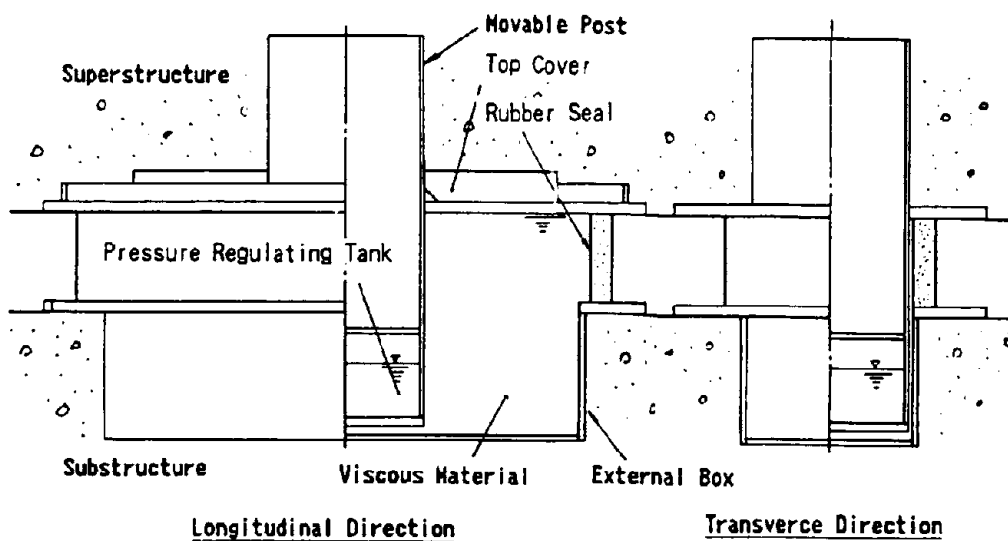


Figure 2 Details of a Typical Viscous Damper

FUNDAMENTAL PROPERTIES OF VISCOUS DAMPERS

Properties of Viscous Materials Generally, the viscosity-temperature characteristic of a viscous material is expressed by the following equation :

$$\eta \propto e^{-ct} \tag{1}$$

Where

- η : rotational viscosity (poise)
- e : natural logarithm
- c : constant determined by a viscous material
- t : temperature (°C)

As is clear from equation (1), the larger c is, the more the viscosity of the viscous material is liable to be influenced by temperature changes. Table 1 shows c-values and rotational viscosity at -10°C and +20°C of various viscous materials obtained in past tests.

Table 1 C-values and rotational viscosity of viscous materials

Viscous Materials	c	Rotational viscosity (Poise)		Touch
		-10°C	+20°C	
Hydrocarbon polymer	0.065	70,300	10,000	Solid asphalt
Butane polymer	0.043	36,300	10,000	Solid asphalt
Polyolefin polymer	0.066	7,200	1,000	Starch syrup
Silicone oil	0.023	400	200	Salad oil

As is evident from the table, silicone oil, which is used in the new viscous damper, is excellent in both flowability and stability to temperature changes.

Damping Force of the Viscous Damper Generally, the damping force of a viscous damper is expressed by the following equation :

$$F = k_1 \times k_2 \times k_3 \times V^d \tag{2}$$

Where

- F : damping force of a viscous damper (t·f)
- k_1 : constant determined by the type of viscous material
- k_2 : constant determined by the shape of a damper
- k_3 : constant regarding temperature characteristic ($= e^{-ct}$)
- V : relative velocity (cm/sec)
- d : constant determined by the type of viscous material

k_1 , k_2 and d are unknown constants whose values are difficult to obtain theoretically. These constants were thus estimated from the results of past element tests performed on a horizontal-force-dispersed viscous damper that was applied to the prestressed concrete bridge on the Yoshima Bridge between Honshu and Shikoku. The viscous damper used polyolefin polymer. Figure 3 shows a schematic of the viscous damper used for the element tests. The longitudinal width of the steel movable post of the test viscous damper is variable three stages of 38 cm, 58 cm and 78 cm. Figure 4 shows a typical relationship between the damping force and the velocity of the viscous damper used in the element tests. The element tests produced the following numerals for each constant :

$$k_1 : 3.5 \times 10^{-4}$$

$$k_2 : (0.91 \ell \times 1.0) \times (S/S_0)$$

$$k_1 : e^{-0.0066t}$$

$$d : 0.85$$

Where

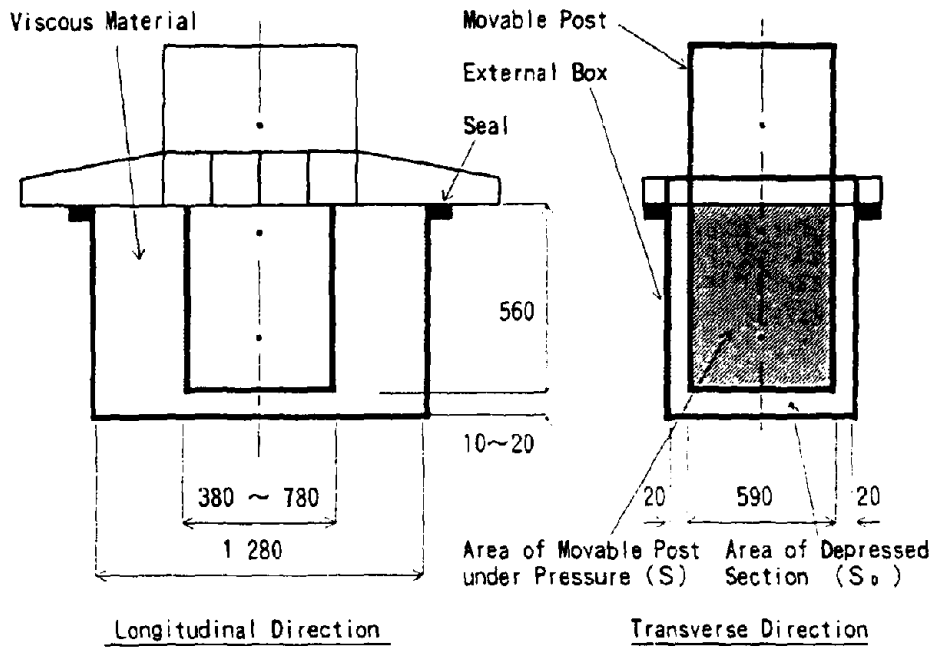
- ℓ : longitudinal width of the steel movable post (cm)
- S : area of the steel movable post under pressure (cm²)
- S₀ : area of the depressed section (cm²)

(see Figure 3). From these results, assuming that

1. The shape constant, k_2 , is common regardless of the viscous material to be used,
 2. $k_1 \times k_2 \times k_3$ at -20°C is proportional to the rotational viscosity at the same temperature, and
 3. The empirical judgment determines $d = 0.5$,
- the equation for the damping force (F) of the viscous damper with silicone oil can be presumed as follows :

$$F = 6.75 \times 10^{-1} \cdot (0.91 \ell^{-1.0}) \cdot (S/S_0) \cdot e^{-0.0066t} \cdot \dot{V}^{0.5} \quad (3)$$

**Reproduced from
best available copy**



(mm)

Figure 3 Schematic Drawing of a Viscous Damper for Element Tests

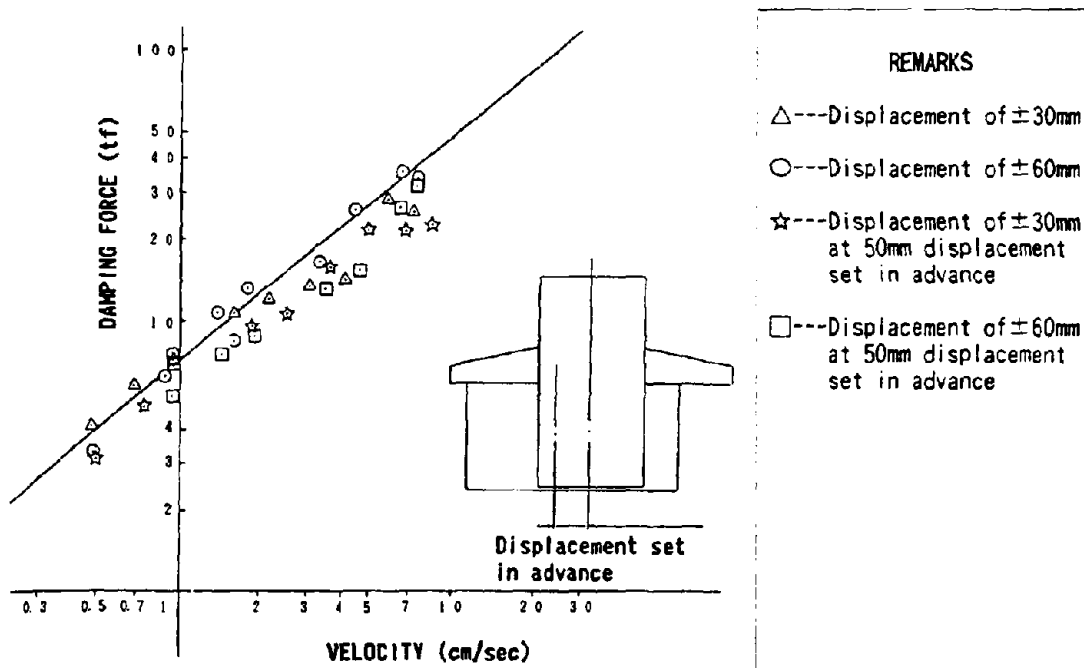


Figure 4 Relationship between Damping Force and Velocity of a Viscous Damper with Polyolefin Polymer

DYNAMIC LOADING TESTS AT PWRI

Summary of Dynamic Loading Tests To verify the dynamic properties and durability of viscous dampers, six series of dynamic loading tests were performed as detailed below. All of the tests were carried out in the room controlled at a constant temperature of +20 °C. The large-stroke actuator having the capacities of maximum excitation ± 125 tf (dynamic), maximum stroke ± 500 mm, and maximum velocity ± 100 cm/sec owned by PWRI was used.

Test Viscous Damper Figure 5 and 6 shows the structure of the test viscous damper and the dynamic loading tests at PWRI, respectively. The movable post and the external box of the test viscous damper are all made of steel plates 10 mm thick. Neoprene rubber, which has a high degree of resistance to oil, is used as seal rubber. The viscous material used is silicone oil, whose rotational viscosity at +20 °C is 200 poise.

Test Conditions In the series 1 tests, the test object is repeatedly loaded 10 times each at five different velocities of 10, 20, 30, 40 and 50 cm/sec, with a vibration frequency 1.0 Hz. In the series 2 and series 3 tests, the test object is excited in the same manner as in the series 1 tests, with two vibration frequencies of 0.8 Hz and 0.5 Hz. In the series 4 tests, ten cyclic loads are applied each under four different displacements of ± 20 , 50, 100, and 200 mm at a velocity of 10 cm/sec. In the series 5 tests, the test object is loaded repeatedly 10 times each at five different vibration frequencies of 0.1, 0.2, 0.3, 0.4, and 0.5 Hz under displacements of ± 50 mm. The series 6 tests determine durability; a total of 80 cyclic loads are applied under a vibration frequency of 1.0 Hz and a displacement of ± 50 mm between one three-hour pause. The excitation wave is sinusoidal in all cases.

Test Results Figures 8 to 13 show the test results of series 1 to 6, and Figures 14 and 15 show force-displacement hysteresis loops of series 3 and 4 tests. The damping force in the figures is the sectional strength of the axis of ordinate of the force-displacement hysteresis loop shown in Figure 7. And, the absorbed energy denotes an area encircled with the hysteresis loop of one cycle.

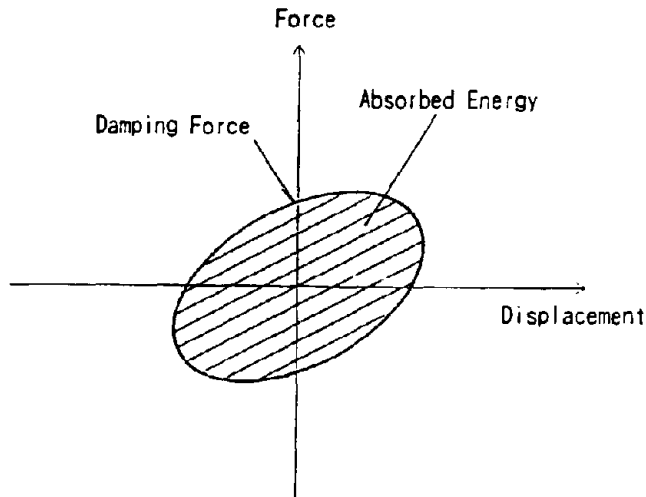


Figure 7 Typical Force-Displacement Hysteresis Loop

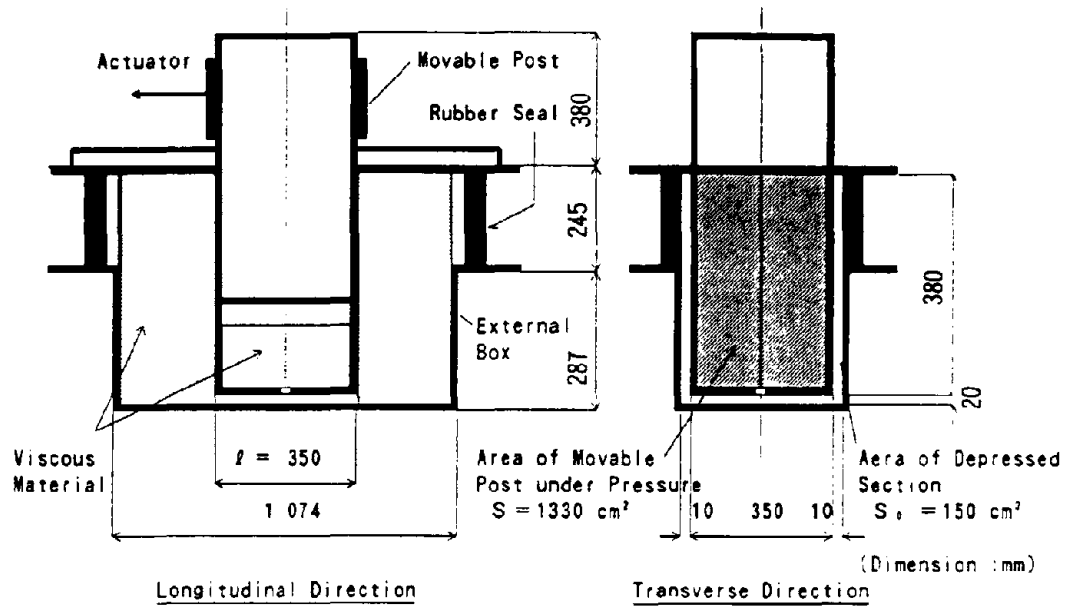


Figure 5 Schematic Drawing of the Viscous Damper for Dynamic Loading Tests at PWRI

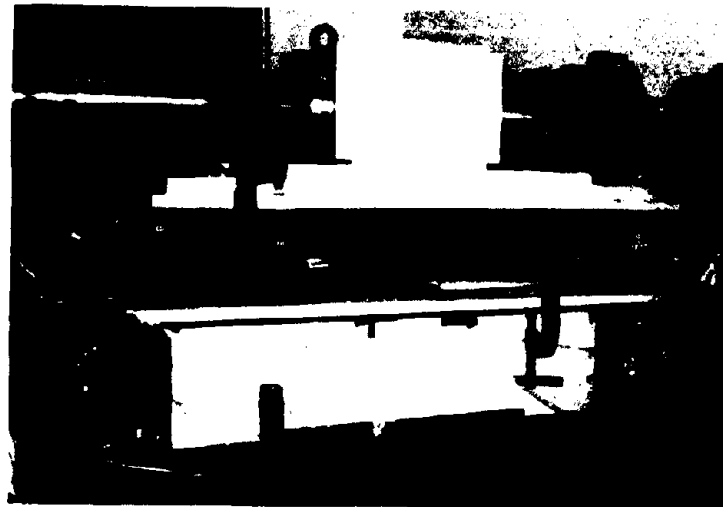
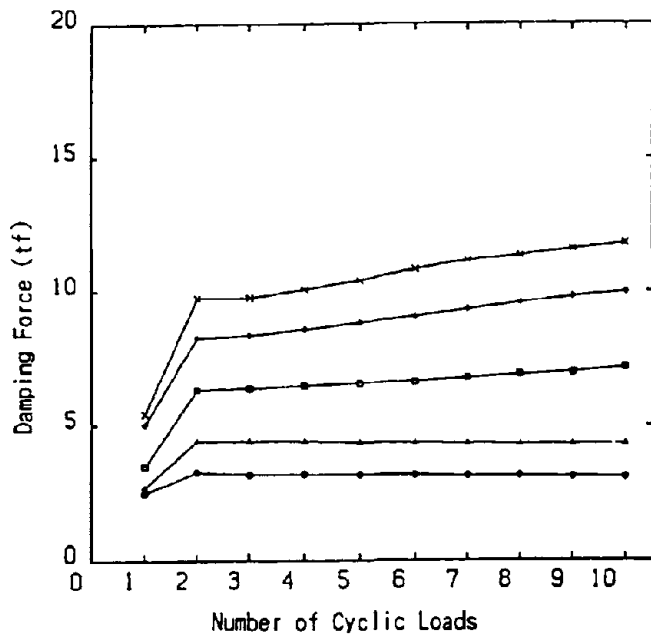


Figure 6 Dynamic Loading Tests at PWRI



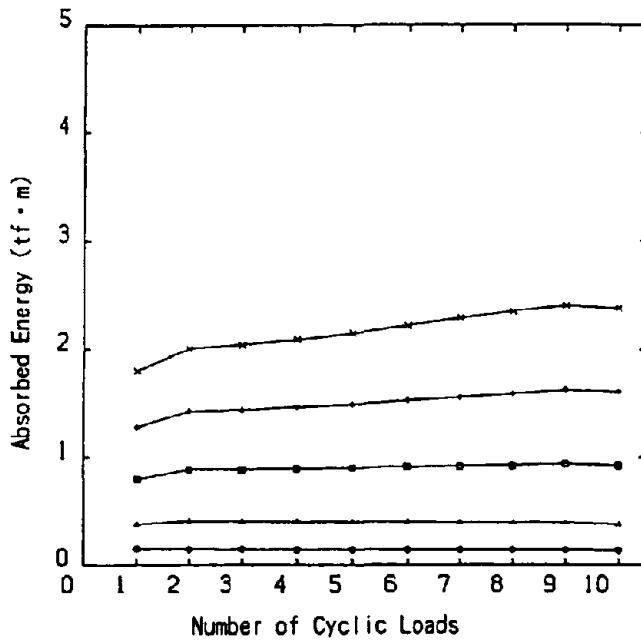
Test Conditions and Remarks

Frequency : 1.0 Hz

Velocity :

- --- 10 cm/sec
- △ --- 20 cm/sec
- --- 30 cm/sec
- ◇ --- 40 cm/sec
- × --- 50 cm/sec

(a) Relationship between Damping Force and Velocity at Frequency of 1.0 Hz



Test Conditions and Remarks

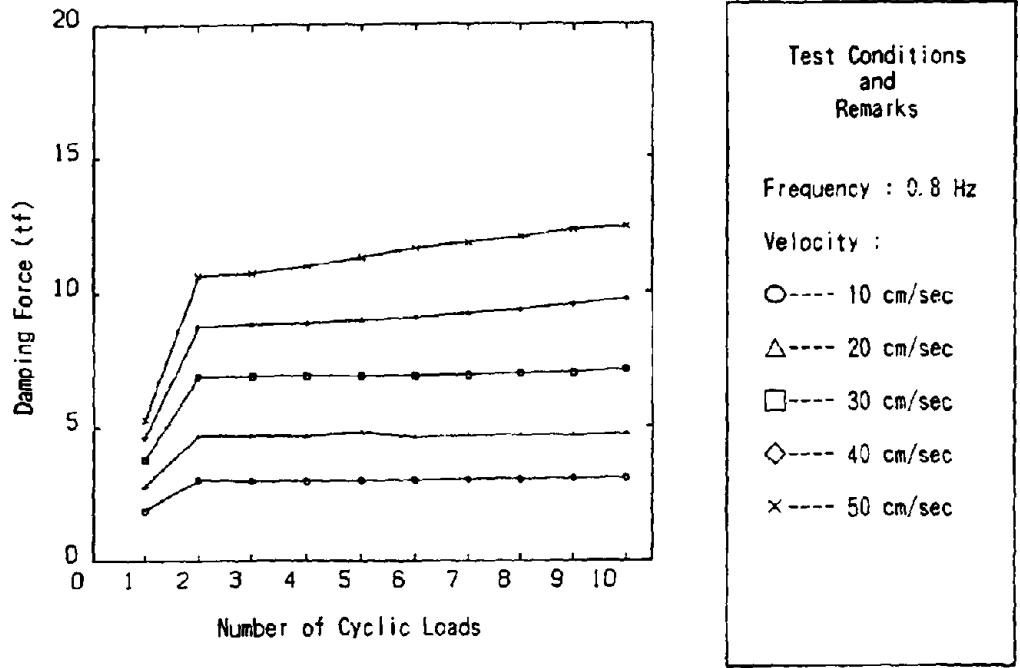
Frequency : 1.0 Hz

Velocity :

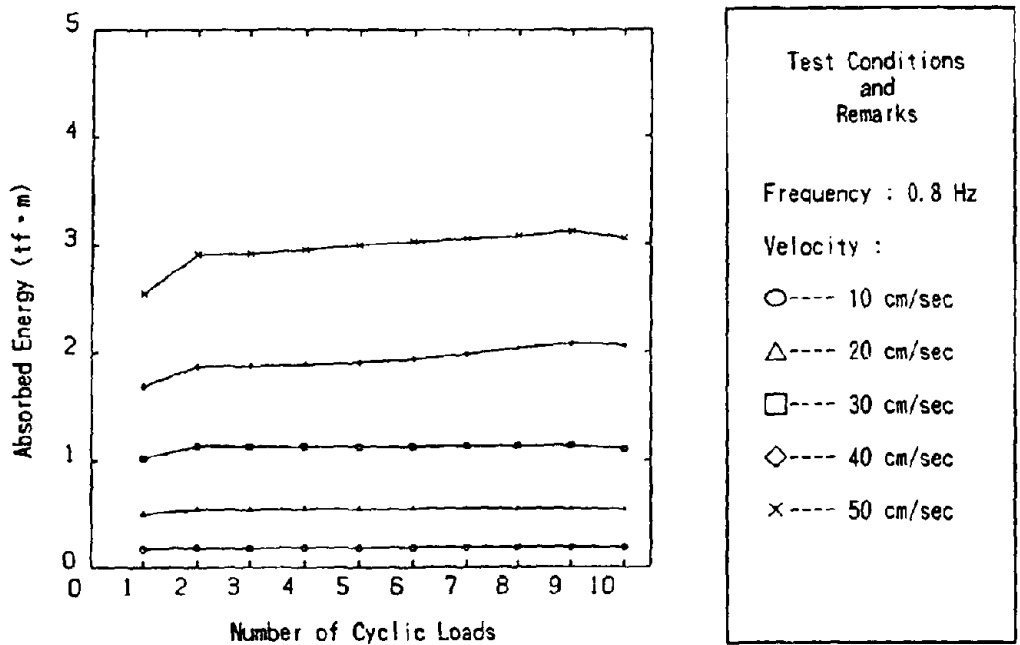
- --- 10 cm/sec
- △ --- 20 cm/sec
- --- 30 cm/sec
- ◇ --- 40 cm/sec
- × --- 50 cm/sec

(b) Relationship between Absorbed Energy and Velocity at Frequency of 1.0 Hz

Figure 8 Test Results of Series 1

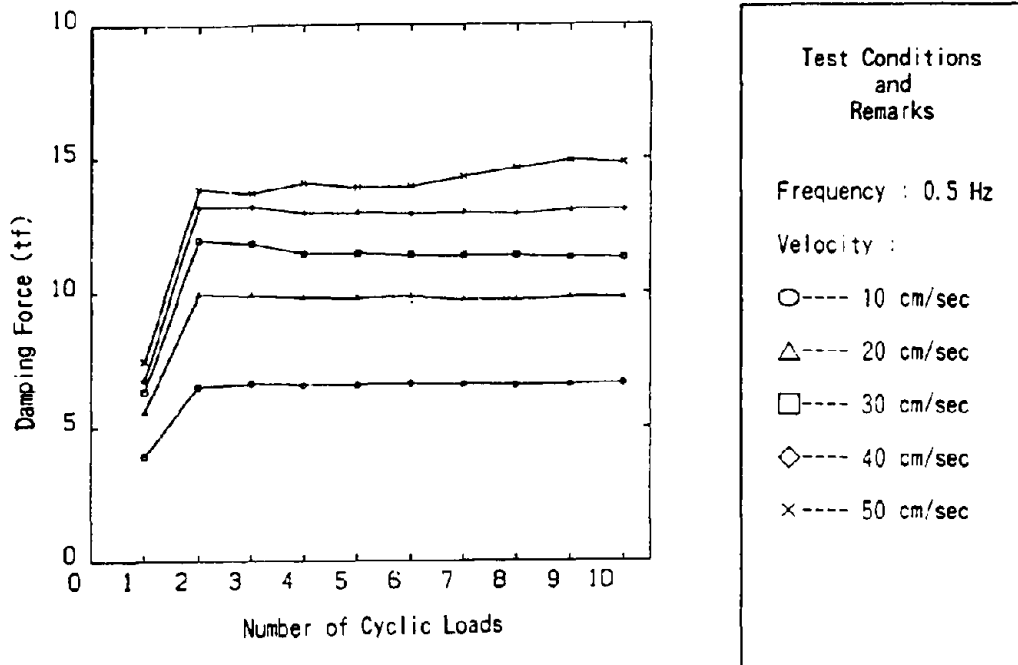


(a) Relationship between Damping Force and Velocity at Frequency of 0.8 Hz

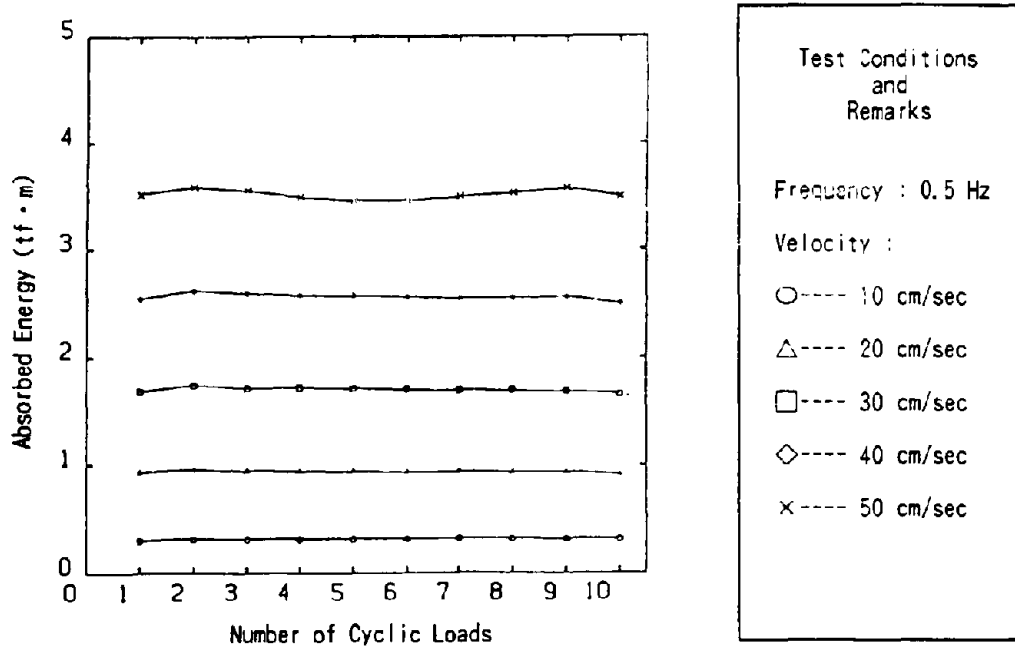


(b) Relationship between Absorbed Energy and Velocity at Frequency of 0.8 Hz

Figure 9 Test Results of Series 2

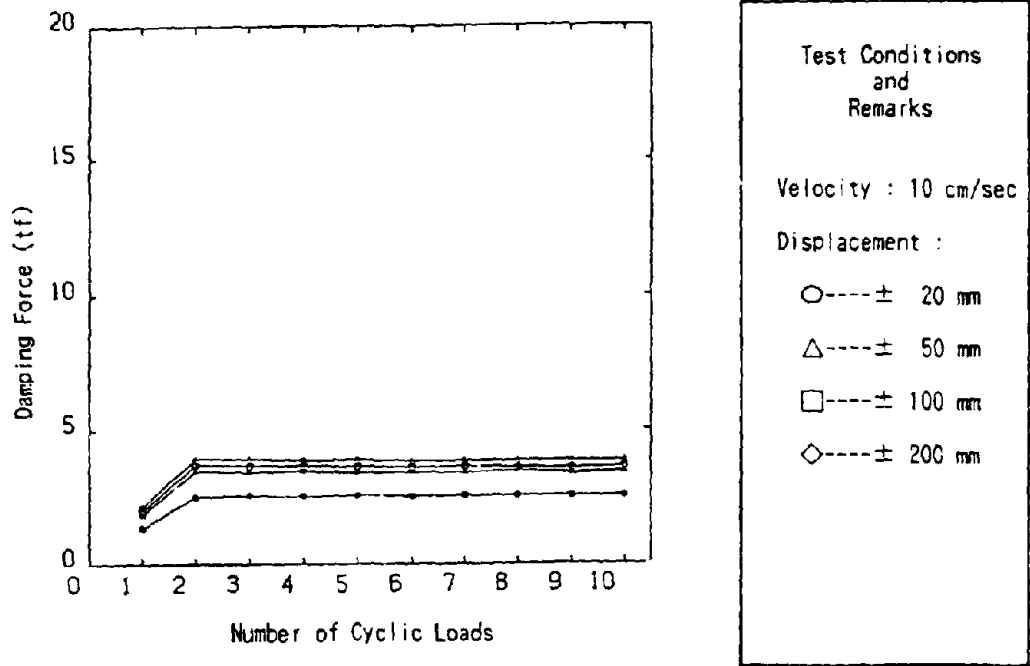


(a) Relationship between Damping Force and Velocity at Frequency of 0.5 Hz

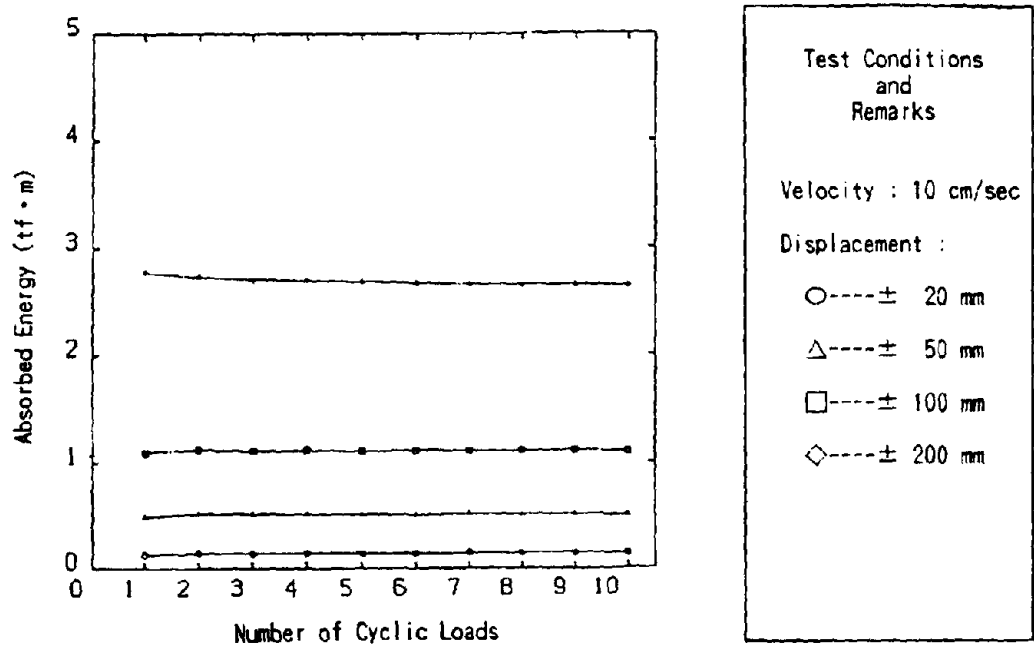


(b) Relationship between Absorbed Energy and Velocity at Frequency of 0.5 Hz

Figure 10 Test Results of Series 3

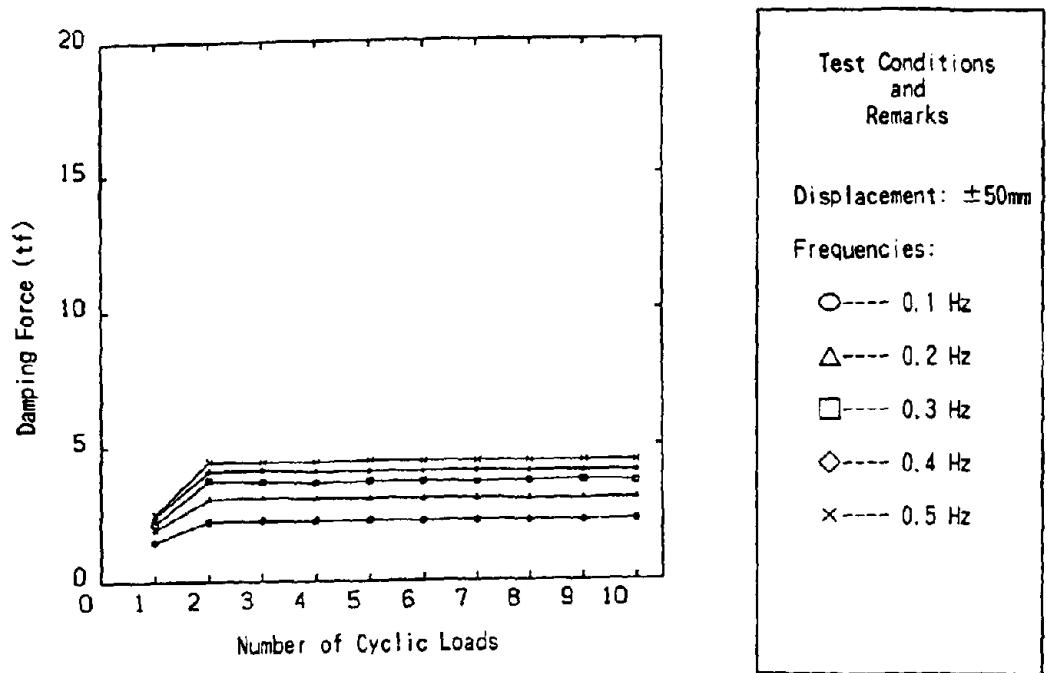


(a) Relationship between Damping Force and Displacement at Velocity of 10 cm/sec

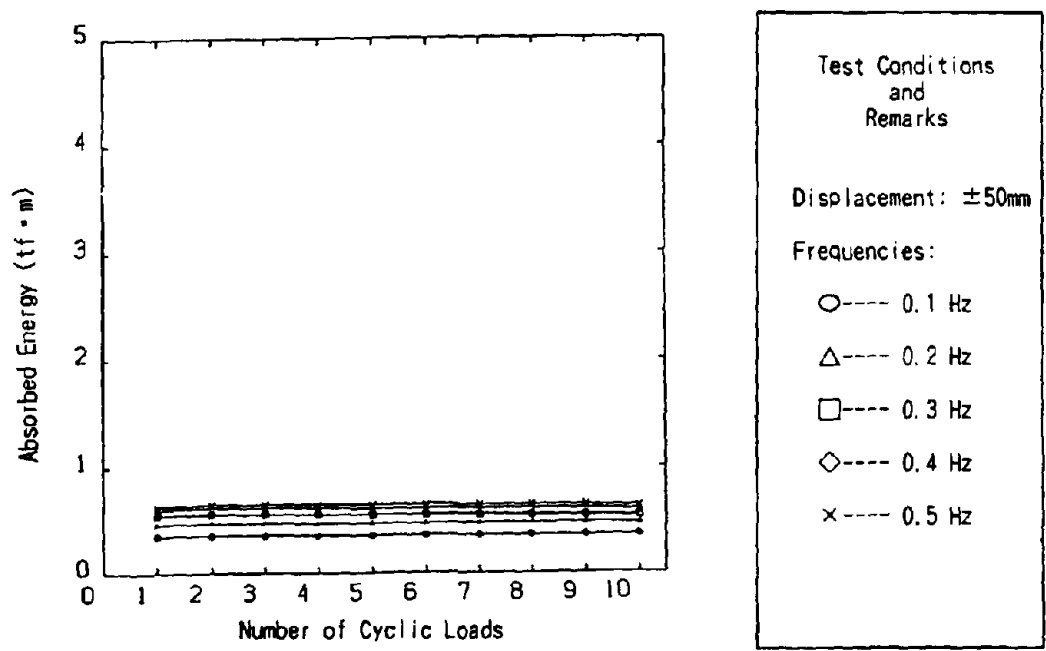


(b) Relationship between Absorbed Energy and Displacement at Velocity of 10 cm/sec

Figure 11 Test Results of Series 4

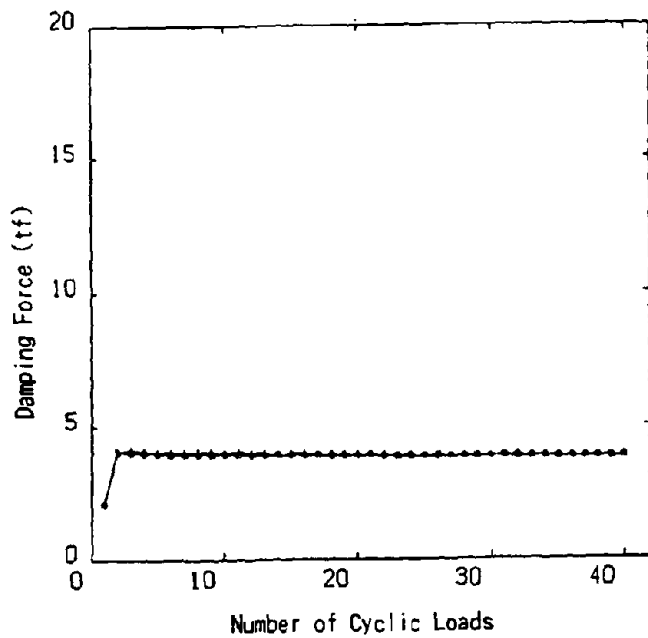


(a) Relationship between Damping Force and Frequency at Displacement of $\pm 50\text{mm}$



(b) Relationship between Absorbed Energy and Frequency at Displacement of $\pm 50\text{mm}$

Figure 12 Test Results of Series 5



Test Conditions and Remarks

Frequency : 1.0 Hz

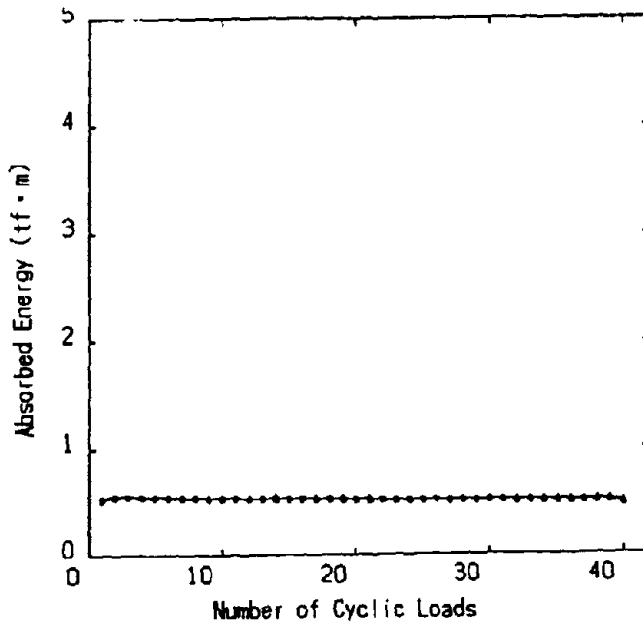
Displacement: $\pm 50\text{mm}$

Number of Cyclic Loads

○---First 40 times

△---Last 40 times after three-hour pause

(a) Stability of Damping Force for a Total of 80 Cycle Loads



Test Conditions and Remarks

Frequency : 1.0 Hz

Displacement: $\pm 50\text{mm}$

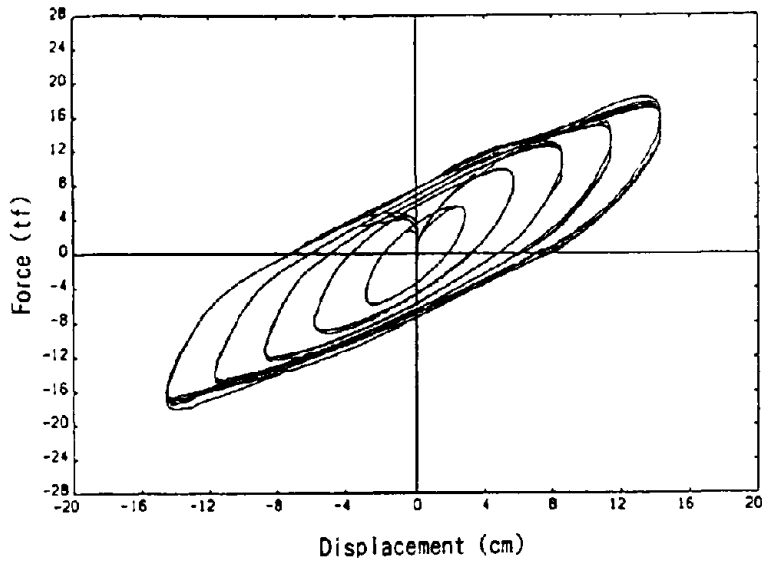
Number of Cyclic Loads

○---First 40 times

△---Last 40 times after three-hour pause

(b) Stability of Absorbed Energy for a Total 80 Cycle Loads

Figure 13 Test Results of Series 6



Test Conditions and Remarks

Frequency : 0.5 Hz

Displacement(Velocity)

± 29 mm (9 cm/s)

± 58 mm (18 cm/s)

± 87 mm (27 cm/s)

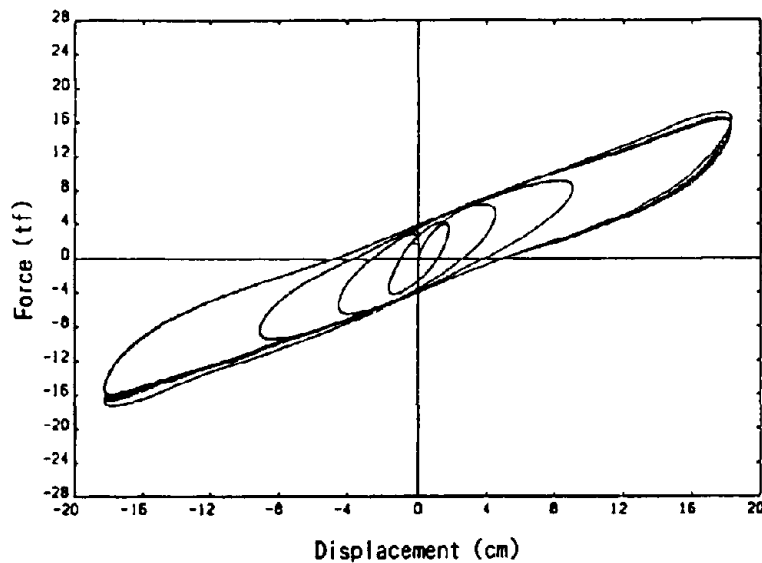
± 116 mm (37 cm/s)

± 145 mm (46 cm/s)

Number of Cyclic Loads

10 times each

Figure 14 Force-Displacement Hysteresis Loops (Series 3)



Test Conditions and Remarks

Velocity : 10 cm/sec

Displacement:

± 18 mm

± 46 mm

± 92 mm

± 184 mm

Number of Cyclic Loads

10 times each

Figure 15 Force-Displacement Hysteresis Loops (Series 4)

Discussions Theoretically the damping force of viscous dampers is dependent on vibrational velocity only ; it is not influenced by displacement, vibration frequency, or the number of cyclic loads. In practice however, many factors other than vibrational velocity, such as pressure changes in viscous material due to changes in displacement or vibration frequency, or temperature rise as a result of repeating loading, may have an influence on the damping force. The main purpose of the series of dynamic loading tests was to confirm the relationship between the damping force of dampers and the vibrational velocity. The test also verified the effect factors other than the vibrational velocity have on dampers.

As evidenced in Figure 8 to 12, the damping force and absorbed energy with respect to the number of cyclic loads are both very stable except for the first cycle. The reason that the damping force and absorbed energy in the first cycle are small is that they are calculated from the hysteresis loop that is plotted when they are stationary. The results in the first cycle are therefore meaningless data. On the basis of a mean value from the 4th cycle to the 10th cycle as the reference value, the maximum dispersion of the characteristic value in ten cyclic loads is around 10%.

Sinusoidal waves were used for excitation in the tests. The following interrelation is established among maximum vibrational velocity, vibration frequency, and displacement :

$$v = 2 \cdot \pi \cdot f \cdot u \quad (4)$$

where

v : maximum vibrational velocity (cm/sec)
f : vibration frequency (Hz)
u : displacement (cm)

From the equation, it is clear that changing vibration frequency under a fixed vibrational velocity also changes the displacement. It is impossible to study the relationship between the damping force and vibration frequency or the relationship between the damping force and displacement independently. However, as discussed previously, the damping force under discussion is a reaction force at zero displacement, where vibrational velocity is maximum. The damping force here is inherently independent of displacement. It is the vibration frequency that can have some influence on the damping force.

Figure 16 shows the relationship between the damping force and vibrational velocity with vibration frequency as parameter. The figure demonstrates that vibration frequencies of 1.0 Hz (series 1) and 0.8 Hz (series 2) produced relationships in good agreement with the damping force and vibrational velocity, whereas a vibration frequency of 0.5 Hz (series 3) produced a decreasing slope of damping force against vibrational velocity compared with the other two cases with vibrational frequencies of 1.0 Hz and 0.8 Hz. The probable reasons for this are as follows.

In the series 1 and 2 tests, rotation at the hinged section of the actuator did not take place smoothly, and thus the frictional force was added to the reaction force and recorded. On the other hand, the series 3 tests were carried out after improving the hinged section, resulting in smaller values compared with the other two series of tests. The data of 1.0 Hz and 0.8 Hz are therefore less reliable. We will continue to test the effect of changing the vibration frequency.

Figure 13 shows the test results when the test viscous damper was excited by a total of 80 cycle loads, 40 each before and after the three-hour pause, under a vibration frequency of 1.0 Hz and a displacement of ± 50 mm. The figure plots the results of 40 cyclic loads over those of the other 40 cyclic loads after the pause. Both are in complete agreement. From the results, it can be postulated that the viscous damper has sufficient durability with regards to dynamic behavior.

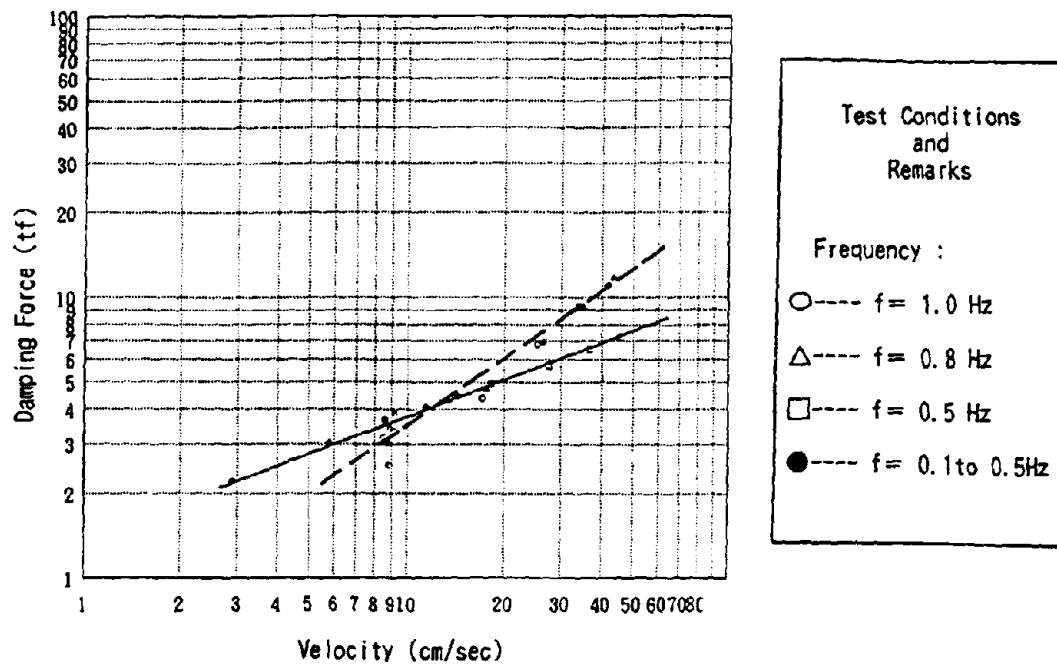


Figure 16 Relationship between Damping Force and Velocity

If the test results at 0.5 Hz are regarded as positive (plotted in solid lines in Figure 16), the relationship between damping force and velocity can be expressed by the following equation :

$$F = A \cdot V^4 = 1.1 \times v^{0.48} \quad (5)$$

where

F : damping force (tf)

A : constant

v : velocity (cm/sec)

This equation is compared with the theoretical equation (3). Substituting the constants of the test viscous damper $\ell = 35 \text{ cm}$, $S = 1330 \text{ cm}^2$, $S_0 = 150 \text{ cm}^2$, and $t = 20 \text{ }^\circ\text{C}$ in equation (3) produces the following equation :

$$F = 1.07 \times V^{0.5} \quad (6)$$

Substitution in equations (5) and (6) of $v = 50 \text{ cm/sec}$ gives $F = 7.2 \text{ tf}$ in equation (5) and $F = 7.5 \text{ tf}$ in equation (6), a difference of about 5 %. Equation (3) is thus sufficiently accurate.

CONCLUSIONS

The following conclusions were reached in the above-discussed considerations and tests.

a) The damping force of viscous dampers can be expressed by the following equation : (See equation (3) for symbol notations.)

$$F = 6.75 \times 10^{-4} \times (10.91 \ell + 1.0) \times (S/S_0) \times e \times v^{0.18} \quad (7)$$

- b) The properties of viscous dampers are very stable against cyclic dynamic loads.
- c) Viscous dampers are durable in a number of earthquakes to which bridges may be subjected during their serviceable period.

Experiments will continue on the effect differences in the vibration frequency, temperature, and configuration. These effects could not be verified throughly in these tests. We hope to reach a conclusion within this year.

ACKNOWLEDGEMENTS

The development of the viscous damper was made as part of a joint research program on "Development of Menshin Systems for Highway Bridges" between PWRI and Oiles Corporation. Grateful acknowledgement is made to Mr. K. Hasegawa, Mr. S. Unjo, and Mr. H. Nagashima of the Earthquake Engineering Division of PWRI for their cooperation.

REFERENCES

1. Machida et al., "Distribution and Damping of Horizontal Force in Bridge Structures at Earthquake," Joint sealing and bearing Systems for Concrete Structures, Volume 2, American Concrete Institute, 1187 - 1224 (1981)
2. PWRI and 29 Private Firms, "Development of Menshin Systems for Highway Bridges - Report No.1," PWRI Joint Research Report No.44, March 1990 (in Japanese)

DEVELOPMENT OF FINGER JOINT MOVABLE IN HORIZONTAL DIRECTIONS -FOR MENSIN BRIDGES

Teruo KIMISHIMA¹, Takashi HARADA² and Daisuke OZAKI³

¹ Steel Structural Department, Nippon Chuzo Co.,Ltd., Kawasaki, Kanagawa, Japan

² Steel Structural Department, Nippon Chuzo Co.,Ltd., Kawasaki, Kanagawa, Japan

³ Civil Engineering Division, Taisei Corporation, Shinjuku, Tokyo, Japan

SUMMARY

Multi-directional expansion joint for Menshin bridges, which would accommodate the relative displacement in any horizontal direction, was developed through the application of Menshin structural systems to bridges. Applicability of these devices to Menshin bridges was confirmed through laboratory tests using full-scale models.

INTRODUCTION

Application of expansion joint which allows relative movement between deck and abutment in only longitudinal direction cannot be adopted to Menshin bridge. For application to Menshin bridge, it is of great importance to develop the expansion joint movable in any horizontal directions. Menshin design is being introduced in Japan for highway bridge. Because it is the primary purpose to absorb deck movement associated with temperature change, expansion joints capable for absorbing relative movement in longitudinal direction have been developed. From this reason, the Menshin bridges recently designed and constructed in Japan have a stopper for preventing relative deck movement in transverse direction. However, it is effective to adopt Menshin design not only in transverse direction but in longitudinal direction, and development of expansion joint capable for absorbing relative movement in two horizontal directions is a key importance. For the purpose of this requirement, an expansion joint capable of accommodating relative movement of superstructure in any horizontal directions was developed. This paper represents applicability of the expansion joint which is being developed for aiming to apply to Menshin bridge.

STRUCTURE OF EXPANSION JOINT

Outline of Expansion Joint In addition to the movability in any horizontal directions, the requirements for expansion joints are :

- (1) Durability
- (2) Simplicity of structure to facilitate maintenance.
- (3) Applicability to road surface with various transverse gradient.
- (4) Simplicity of structure to facilitate manufacturing and installation.

Because finger joints which have often been used in Japan satisfy the four requirement, it was aimed to modify the finger joints so that they can move in

transverse direction as well. The expansion joint developed is presented in Figs. 1 and 2. It should be noted that seismic effect is not generally considered for determining clearance of expansion joint. In the development, it was aimed to develop the finger joints which accommodate the clearance required to absorb relative deck movement during on destructive earthquake such as the 1923 Kanto Earthquake. Because finger plate connected to deck (designated herein as "superstructure finger joint") as shown in Fig. 1 becomes excessively long to provide the capability for accommodating such long relative deck movement, it was decided to simply support the superstructure finger plate at a pivot bearing and substructure finger plate. Although the superstructure finger plate is generally fixed to deck in a cantilever form, this type of connection was avoided so as to reduce the thickness of superstructure finger plate. The substructure finger plate is placed on a support beam so that movement of the substructure finger plate relative to the support beam can be developed in transverse direction as shown in Figs. 1 and 2. For reducing friction force at the sliding surface, a teflon plate and stainless plate are attached on bottom of the substructure finger plate and upper surface of the support beam, respectively. Because four sheets of the teflon plate have an area of 560cm², stress at the sliding surface becomes 3kgf/cm² for the design vertical load of 1.6tf at a set of block.

A clearance of 60 mm was provided between the substructure finger plate and the parapet of abutment and it was filled with sealing rubber for waterproofing. This sealing rubber is so flexible that it does not hinder the movement of the substructure finger plate in transverse direction. The flanges of the support beam were sandwiched by a guide block to prevent lifting and longitudinal movement of the substructure finger plate against wheel loads. Gutters were installed against leakage of waters from the girder clearance.

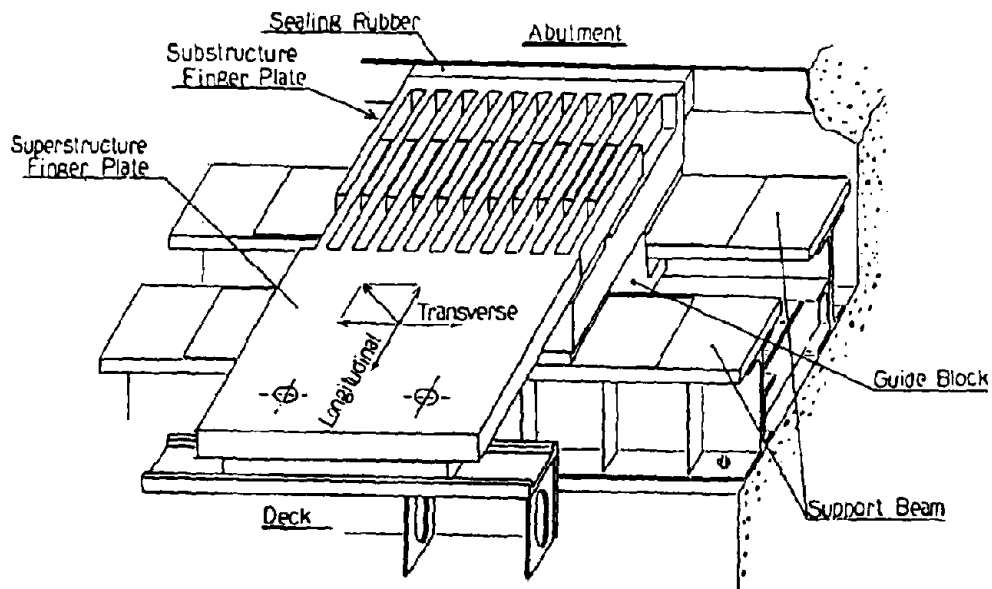


Fig. 1 Structural Outline (Showing 1 Block of Finger Plate)

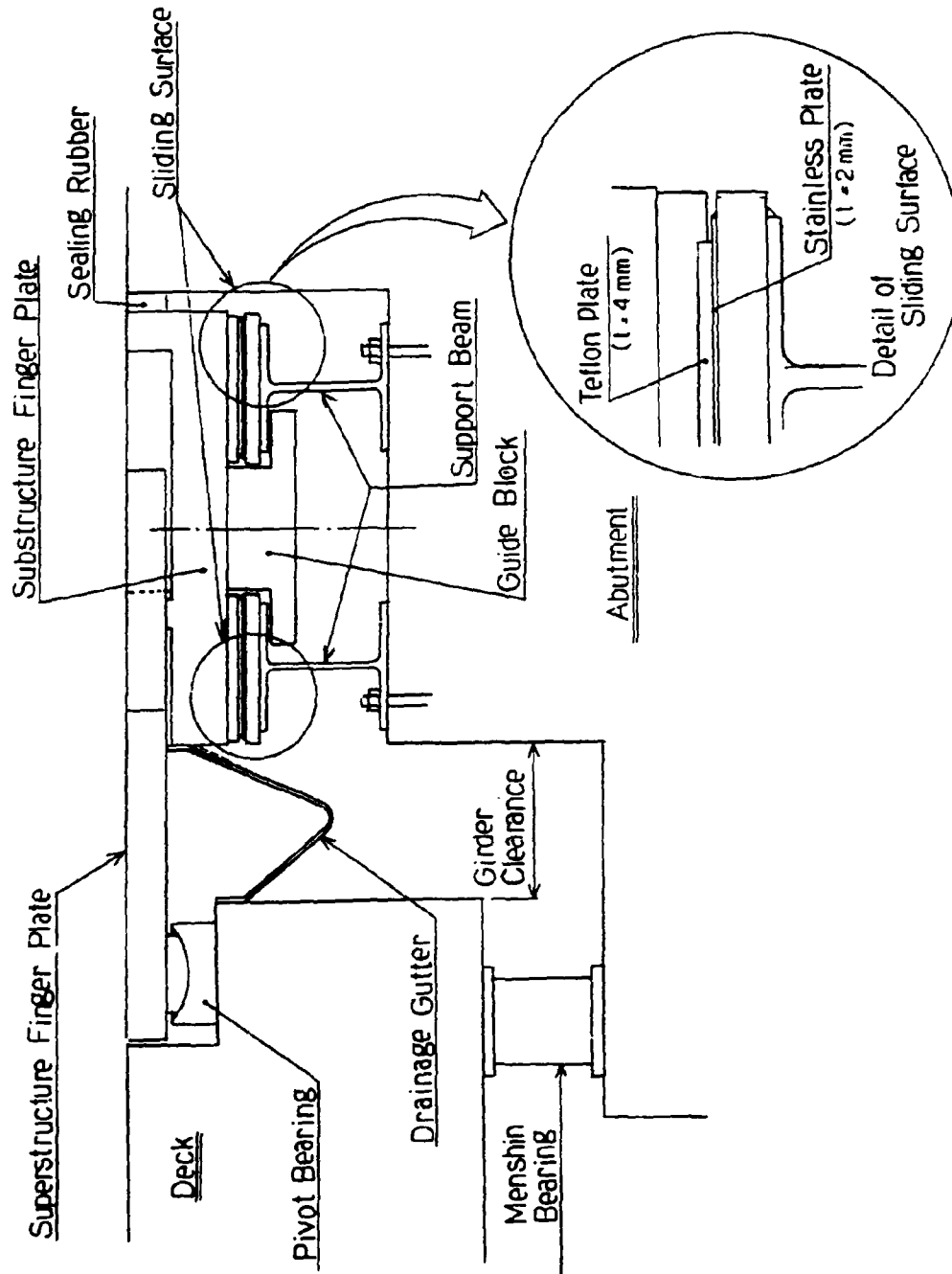


Fig. 2 Cross-Section

LABORATORY TEST ON EXPANSION JOINT

Excitation tests were conducted on the expansion joint model to evaluate applicability of the device subjected to ground motion in any horizontal directions.

Test Model The maximum displacement of a superstructure as shown in Fig. 3 and Table 1 was computed by a dynamic response analysis, and it was used as the movement for design of the expansion joint model. The fundamental natural period of the bridge is 1.26 second. The super and substructure finger plates in the designed expansion joint model were divided into several blocks along transverse direction for manufacturing and installation. The full-scale test model which is a part of the actual expansion joint model is shown in Fig. 4. This consists of two block.

Test Method The test model was placed on a shaking table as shown in Fig. 5 and Photo 1. A series of sinusoidal excitation tests with amplitude and frequency as shown in Table 2 and ground motion excitation tests with an input ground displacement as shown in Fig. 6 were made. Excitation was made for the three directions, i.e., in longitudinal, transverse and 45 degree from the longitudinal direction.

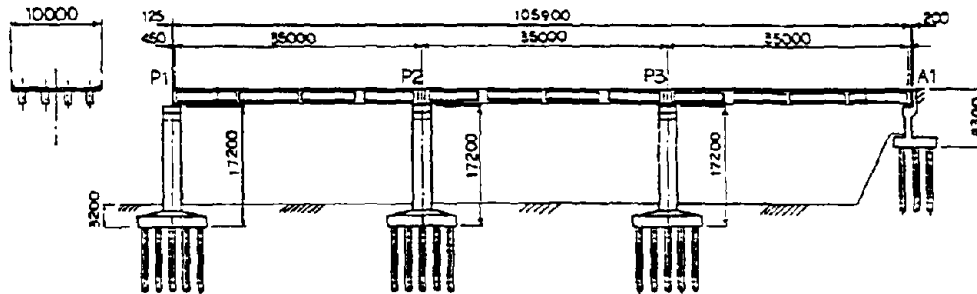


Fig. 3 Menshin Bridge for which The Expansion Joint was designed

Table 1 Dead Load of Superstructure

Unit : t f

	P1	P2	P3	A2	total
Dead Load Reaction Force	3 0 5	7 7 7	7 7 7	3 0 5	2 1 6 4

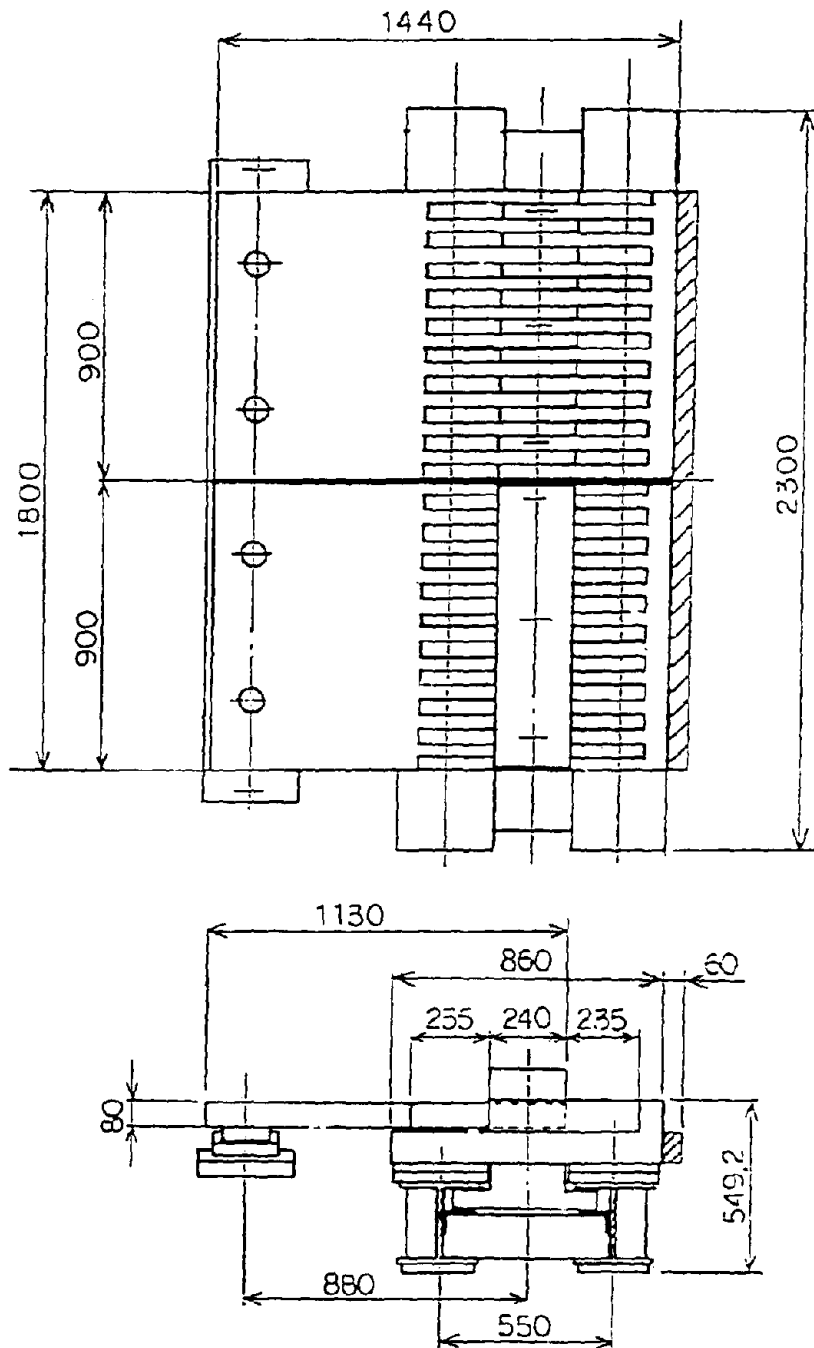


Fig. 4 Test Model



Photo 1 Test Model

Table 2 Sinusoidal Excitation Tests

Case No.	1	2	3
Frequency (Hz)	0.1	0.4	0.8
Displacement (mm)	± 180	± 180	± 100
Maximum Velocity (cm/s)	11.3	45.2	50.3
Duration (sec)	60	60	60

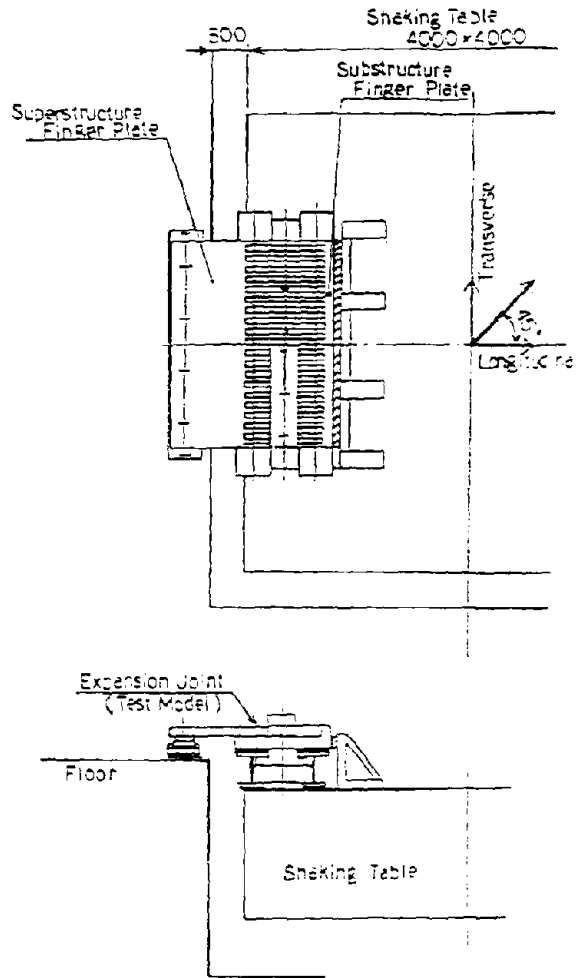


Fig. 5 Expansion Joint Model set up on Shaking Table

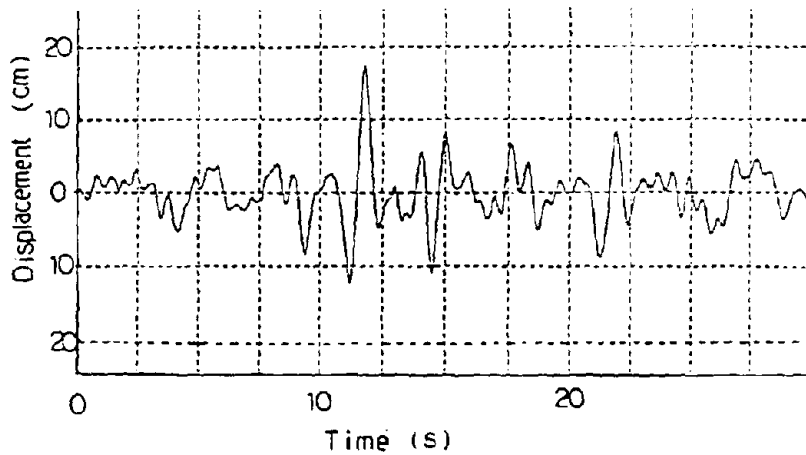


Fig. 6 Response Displacement computed for A Bridge presented in Fig. 3, which was used as Input Motion to Excitation Test

TEST RESULTS

Increase Surface Temperature at Sliding Face Temperature at sliding surface between the teflon and stainless steel plates increased as high as 8°C from the original temperature of 22°C during the extreme sinusoidal excitation tests with amplitude of 100mm and frequency of 0.8Hz for 60 seconds. Because teflon plates can move smoothly from -200°C to +260°C, such amount of temperature increase at the sliding surface would cause no problems for practical use.

Resistant Force of Expansion Joint under Excitation Tests The resistant forces of the expansion joint under Case 2 (refer to Table 2) are shown in Figs. 7, 8 and 9. It is seen in these figures that the resistant forces show the force vs. time relation typically observed for a system with coulomb friction. The resistant forces have several spikes, and this represents the effect of collision developed between the superstructure finger plate and the substructure finger plate.

Dependence of resistant forces on loading velocity is shown in Figs 10, 11 and 12. It is apparent from these figures that while the impact force increases as the loading velocity increases, the friction force is independent of the loading velocity. The impact force and friction force developed during the ground motion excitation test are shown in Table 3. Results by ground motion excitation tests which will be described later are also shown in Table 3.

In longitudinal excitation, the maximum resistant force was about 780kgf. This is developed by friction between the superstructure finger plate and the substructure finger plate. Because the vertical load developed at this sliding surface is 510kgf and is smaller than the vertical load developed at the sliding surface between the teflon plates and stainless plates, the resistant force in longitudinal direction is about 40% of the resistant force in transverse direction.

Friction coefficient for transvers excitation is about 0.2. Although this value is rather higher for dynamic loading with velocity from 11.3cm/s to 50.3cm/s for loading force of 3kgf/cm², it is not exceptionally high from the test results for friction between teflon and stainless steel.⁴⁾

The resistant forces developed during the 45° sinusoidal excitation were almost equal to or larger than those developed during the sinusoidal excitation in either longitudinal or transvers direction. On the other hand, the resistant forces developed during the 45° ground motion excitation were smaller than those developed during the ground motion excitation in either longitudinal or transvers direction. The reason for these is now being examined.

The resistant force of the expansion joint under ground motion excitation are shown in Figs. 13, 14 and 15. The friction forces shown during the ground motion excitation are almost equal to the friction force under sinusoidal excitation, so the friction force is independent of excitation methods.

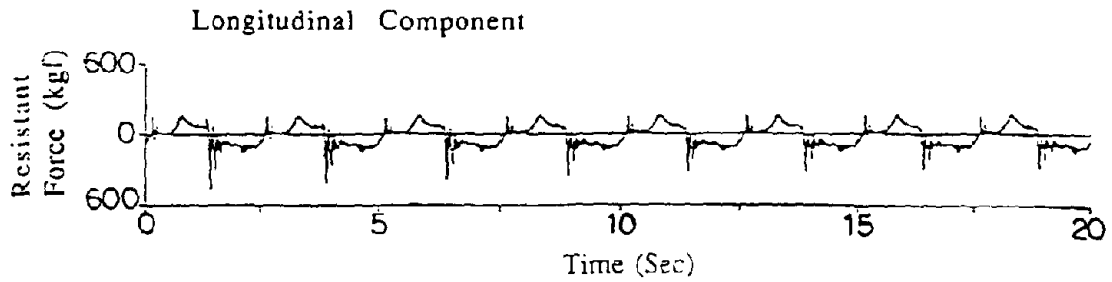


Fig. 7 Excitation in Longitudinal Direction

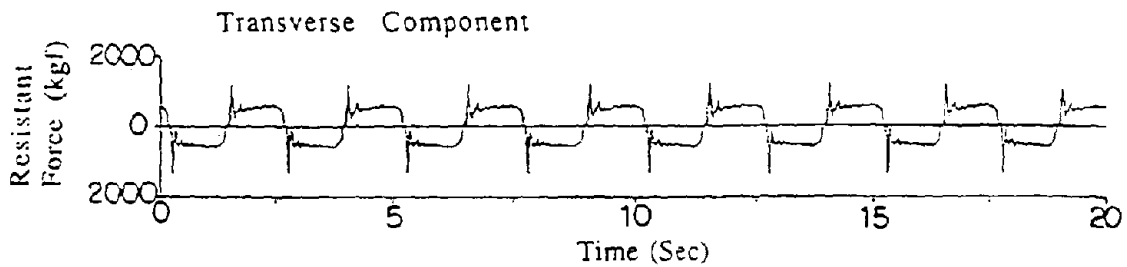


Fig. 8 Excitation in Transverse Direction

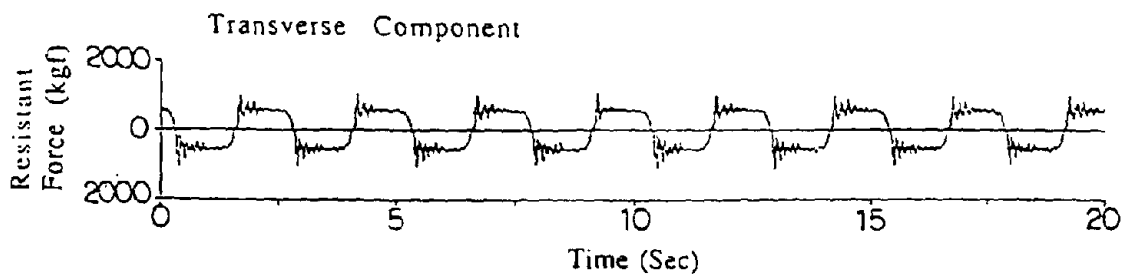
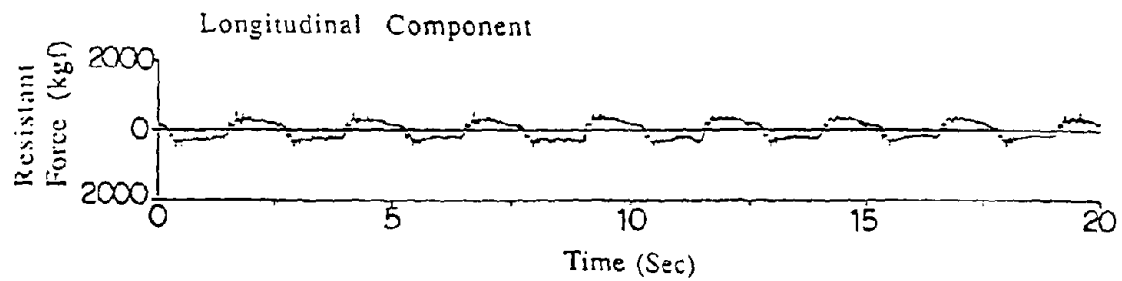


Fig. 9 Excitation in 45° Degree from The Longitudinal Direction

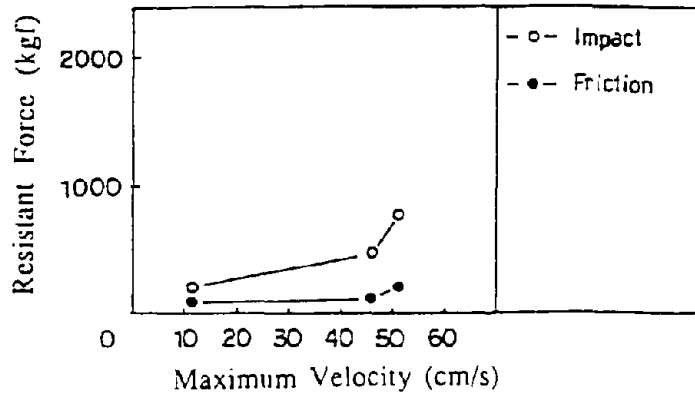


Fig. 10 Excitation in Longitudinal Direction

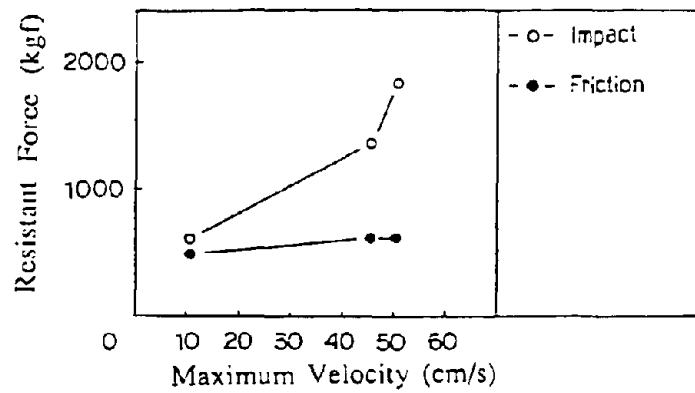


Fig. 11 Excitation in Transverse Direction

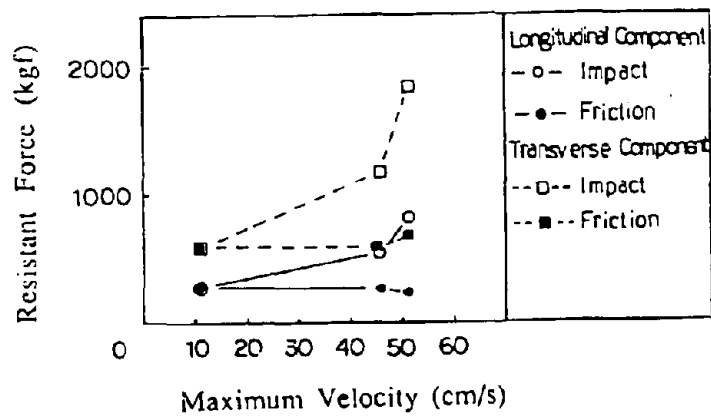


Fig. 12 Excitation in 45° Degree from The Longitudinal Direction

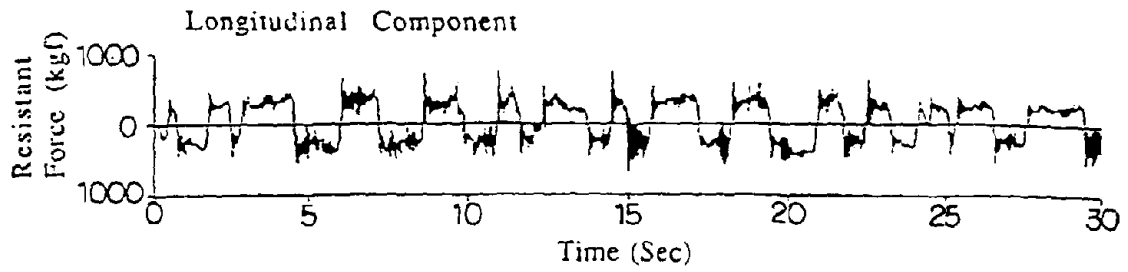


Fig. 13 Excitation in Longitudinal Direction

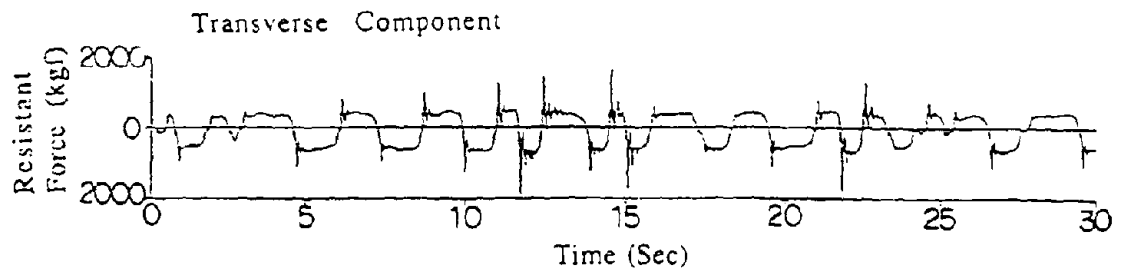


Fig. 14 Excitation in Transverse Direction

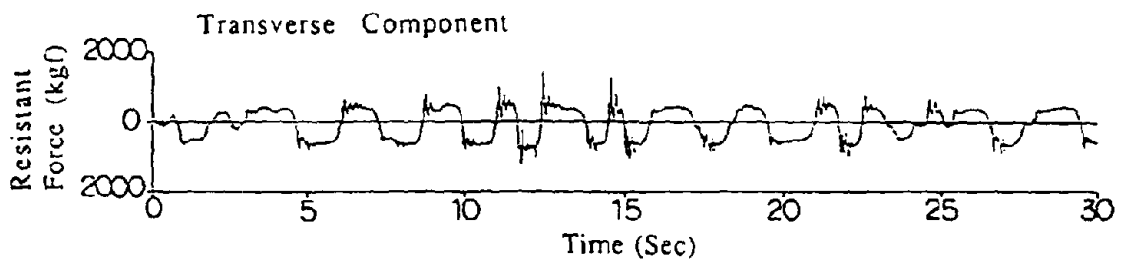
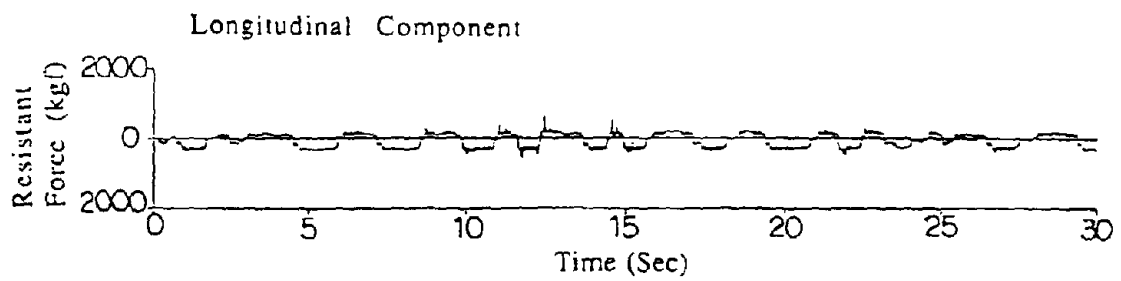


Fig. 15 Excitation in 45° Degree from The Longitudinal Direction

Table 3 Resistant Force of Expansion Joint under Excitation Tests
(for 2 Blocks of Finger Plates)

Direction	Sinusoidal Excitation			Ground Motion Excitation		Remark
	Case No.	Impact Force maximum(kgf)	Friction Force average(kgf)	Impact Force maximum(kgf)	Friction Force average(kgf)	
Longitudinal	1	195	88	740	263	Longitudinal Component
	2	488	122			
	3	780	195			
Transverse	1	610	488	1880	558	Transverse Component
	2	1366	610			
	3	1829	585			
45 degree from the Longitudinal Direction	1	293	268	621	221	upper; Longitudinal Component lower; Transverse Component
		610	585			
	2	537	244	1439	484	
		1195	595			
	3	829	220			
		1854	683			

APPLICATION OF TEST RESULTS TO A PROTOTYPE BRIDGE

Base on the test results presented in Table 3, actual resistant force was evaluated to a prototype bridge shown in Fig. 3. Because 10 block of expansion joint are required in the bridge, the resistant force becomes 5 times larger as shown in Table 4 than presented in Table 3. For transverse movement, the anticipated resistant force is about 18.8tf, and this is only 0.8% of the total deck weight.

Table 4 Resistant Force of Expansion Joint for A Bridge shown in Fig. 3

Direction	Resistant Force (tf)	Remark
Longitudinal	$0.74 \times 5 \times 2 \text{set} = 7.4$	Longitudinal Component
Transverse	$1.88 \times 5 \times 2 \text{set} = 18.8$	Transverse Component
45 degree from	$0.62 \times 5 \times 2 \text{set} = 6.2$	Longitudinal Component
the Longitudinal	$1.44 \times 5 \times 2 \text{set} = 14.4$	Transverse Component

CONCLUSIONS

From the studies presented herein, the following conclusions may be deduced:

- 1). Only small increase of temperature about 8°C in extreme loading conditions occurred in the excitation tests. Because teflon plate works in wide range of temperature from -200°C to +260°C, such an increase of temperature at sliding surface would cause no practical problem.
- 2). The resistant forces are developed by impact force as well as friction force. The impact force increases as the loading velocity increases, while the friction force is independent of loading velocity. The coefficient of friction in the tests is about 0.2.
- 3). Based on an application to a prototype bridge, anticipated resistant force of the expansion joint was estimated as about 0.8% of the total weight of the deck. The resistant forces developed by the expansion joint are so small that they could be ignored in the design of Menshin bridges.
- 4). For further improving the expansion joint, development of the materials reducing noise by live load as well as the impact force during an earthquake is required. And development of drainage equipment is also important.

ACKNOWLEDGEMENT

The studies reported here were conducted as a part of the joint research project on "Development of Menshin Systems of Highway Bridges" between the Public Works Research Institute (PWRI) of the Ministry of Construction and 28 private firms in Japan. The authors would like to acknowledge their debt to Dr.K.Kawashima, Mr.K.Hasegawa, Mr.S.Unjo, and Mr.H.Nagashima of the PWRI for their advice concerning the basic requirement for the expansion joint and direction of the development.

REFERENCES

1. PWRI and 29 Private Firms : "Development of Menshin Systems of Highway Bridges Report NO.1-", PWRI Joint Research Reports NO.44, March 1990(in Japanese)
2. PWRI and 28 Private Firms : "Development of Menshin Systems of Highway Bridges Report NO.2-", PWRI Joint Research Reports NO.60, July 1991(in Japanese)
3. Technology Research Center for National Land Development : "Guideline on Design of Menshin Highway Bridges (Draft) ", March 1989 (in Japanese)
4. Technical Report in Taisei Corp.: "Base Isolation System with Sliding Bearings",June 1987(in Japanese)

DEVELOPMENT OF HIGH DAMPING RUBBER BEARING FOR MENSHPIN BRIDGES (PART 1)

Yoji SUIZU¹ and Chiaki SUDOH²

¹BRIDGESTONE CORPORATION, Kodaira-shi, Tokyo, Japan

²BRIDGESTONE CORPORATION, Totsuka-ku, Yokohama, Japan

SUMMARY

A new high damping rubber material which is more suitable for Menshin devices for highway bridges was developed. This material has 1.5 times higher shear modulus than that of the ones already developed for the Menshin device for buildings. In addition to some fundamental properties of the material in itself, the various properties necessary of the Menshin device for highway bridge obtained by some experiments using its scale model are reported here.

INTRODUCTION

The high damping laminated rubber bearing is basically a maintenance-free and isotropic Menshin device, which can show all functions required as a Menshin device, namely vertical load-bearing, horizontal restoring force and energy damping, by its simple structure (Ref.1). These are the excellent characteristics for the Menshin devices for bridges, and are recently being studied and applied to some bridges in our country (Ref.2).

In the case of the Menshin system for bridges, the higher horizontal effective stiffness of the Menshin device is more desirable in comparison with the one in the case of buildings. The reason is as follows: In bridges, the relative displacement between superstructure and substructure caused by an earthquake should be restricted, because there is a limitation of the capacity of expansion joint, and excessive displacement causes the falling-off of the superstructure. On the other hand, the effective stiffness of all the system of bridge becomes lower owing to adding the stiffness of the substructure compared with the one in building with rigid substructure, and this fact means that the Menshin device would be larger in order to restrict the displacement, if we use the same material as the devices for buildings.

We have developed a new high damping rubber material having 1.5 times higher shear modulus in comparison with the one for the buildings. Furthermore, we tested some specific properties (property of horizontal restoring force under the pre-displacement, stability for a large displacement, stability for cyclic horizontal loading, and so on) required for the Menshin bearings of the bridges by using a scale model of a Menshin bearing and obtained many good results (Refs.3 and 4).

PHYSICAL PROPERTIES OF RUBBER MATERIAL

Testing Method Some fundamental physical properties are tested on using some testing devices shown in Photo 1. The test is carried out by using the dumbbell type of specimens shown in Fig.1 and also according to JIS K 6301 (Ref.5)

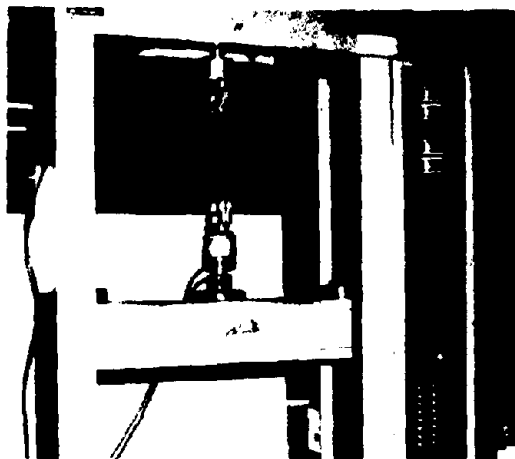


Photo 1 Tensile Testing Facilities

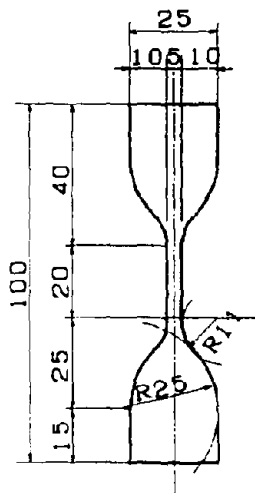


Fig.1 Dumbbell Type Test Piece (JIS K 6301)

Test Result A summary of the physical properties of the new material is shown in Table 1. In order to compare with these results, those of the existing high damping material are also shown in Table 1.

Table 1 The Fundamental Physical Properties

Test Items (JIS K 6301)	Test results	
	DEVELOPED	EXISTING
Hardness [degree]	79	68 ± 5
Tensile strength [kgf/cm ²]	122	min. 90
Ultimate elongation [%]	668	min. 650
Tensile stress(300%) [kgf/cm ²]	61	37 ± 6

Conclusions This new material has a higher modulus and an equal ultimate elongation in comparison with the existing high damping material.

FUNDAMENTAL PROPERTIES OF HIGH DAMPING LAMINATED RUBBER BEARING

Testing Devices and Models The test on the properties as the laminated rubber bearing was carried out at our laboratory by using the bi-directional actuator on its scale models, the outlines and capacities of the actuator are shown in Fig.2 and Table 2, respectively. Testing specimens shown Fig.3 are the 1/5 reduced scale model of a 700tonf bearing-load class high damping rubber bearing which is designed actually for the 6 spans continuous PC box girder bridge in Japan (Ref.2).

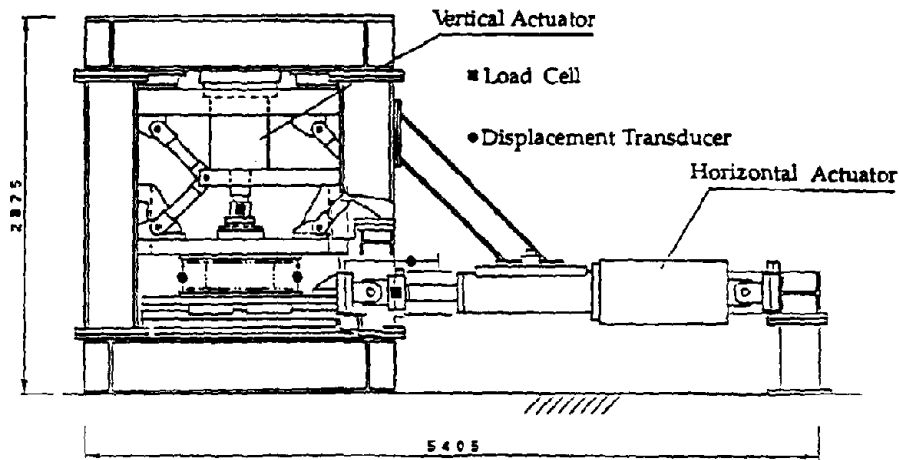


Fig.2 Bi-directional Actuator

Table 2 Main Capacities of The Bi-directional Actuator

Direction	Load	Stroke	Frequency
Vertical	Comp. 100 tonf Tens. 30 tonf	± 100 mm	0.01 ~ 5 Hz
Horizontal	± 20 tonf	± 300 mm	0.01 ~ 5 Hz

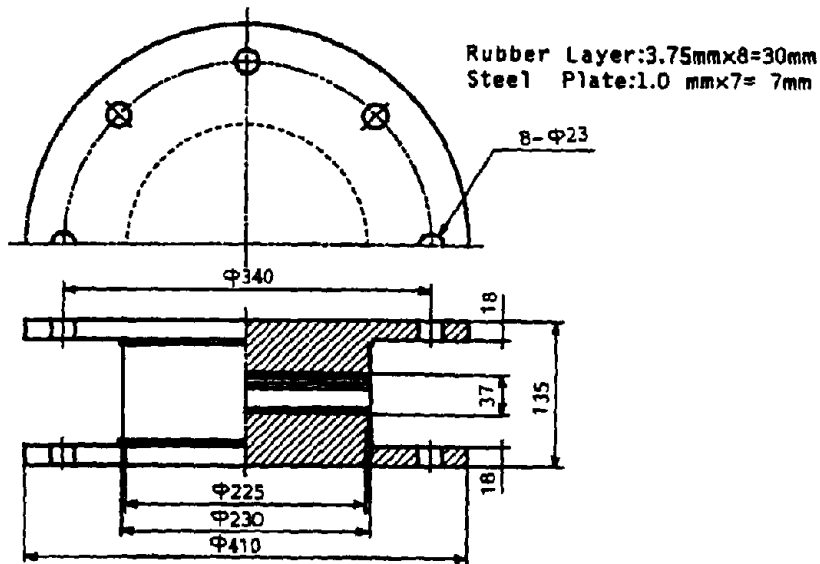


Fig.3 1/5 Reduced Scale Model

Definition of Horizontal Restoring Force Property The horizontal restoring force property of the high damping rubber bearing is expressed by effective stiffness K_{ee} and effective damping ratio h_{ee} , both of which are calculated from hysteresis curve obtained in a horizontal loading test, which is as follows:

In Fig.4, if the load in maximum displacement X_m is expressed as F_m , effective stiffness K_{ee} can be obtained from the following equation:

$$K_{ee} = F_m / X_m \quad (1)$$

When the apexes of the rectangle circumscribed with the hysteresis curve are assigned to A, B, C and D, the area of a triangle ABC is W and the area surrounded by the hysteresis curve is ΔW , the effective damping ratio h_{ee} is expressed in the following equation:

$$h_{ee} = \Delta W / (\pi W) \quad (2)$$

And, the effective stiffness K_{ee} has the following relation to the shear modulus of elastomeric materials G , which is rather frequently used for a specific property.

$$K_{ee} = A G / \Sigma t_e \quad (3)$$

where, A is the bearing area, and Σt_e is total thickness of the elastomeric materials used for the bearing.

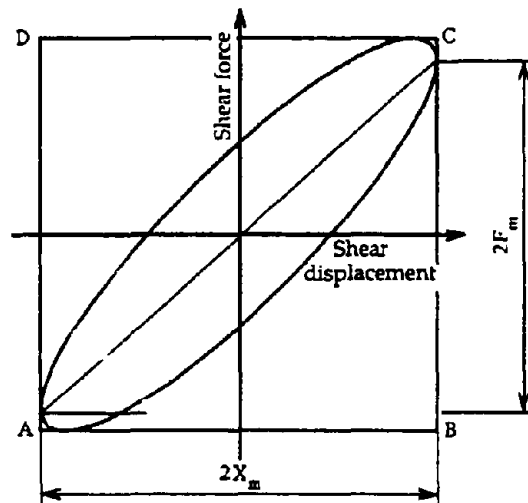


Fig.4 Definition of Effective Stiffness & Damping Ratio

Fundamental Horizontal Restoring Force Property (Strain Dependency) Restoring force properties at each shear strain which are one of the fundamental data for design of the Menshin device made of the high damping rubber was measured. Fig.5 and Fig.6 show the actual hysteresis curves obtained by horizontal loading tests, Fig.5 shows the ones of the "1st series" which is the first experience of each displacement to the specimen and Fig.6 shows the ones of the "2nd series" which is the repeated experience of each displacement after the first experience of the maximum displacement.

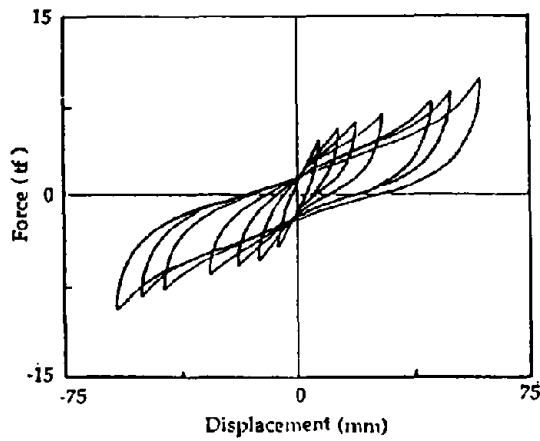


Fig.5 Hysteresis Curve (1st Series)

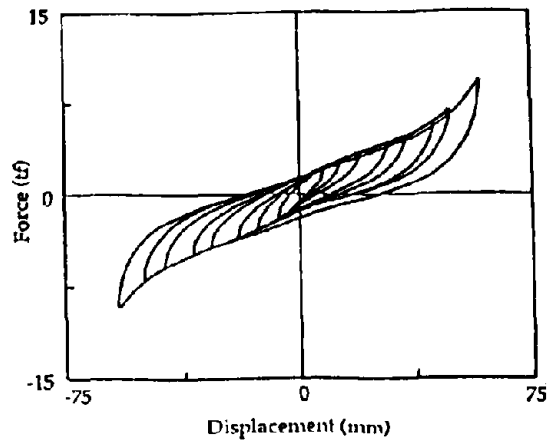


Fig.6 Hysteresis Curve (2nd Series)

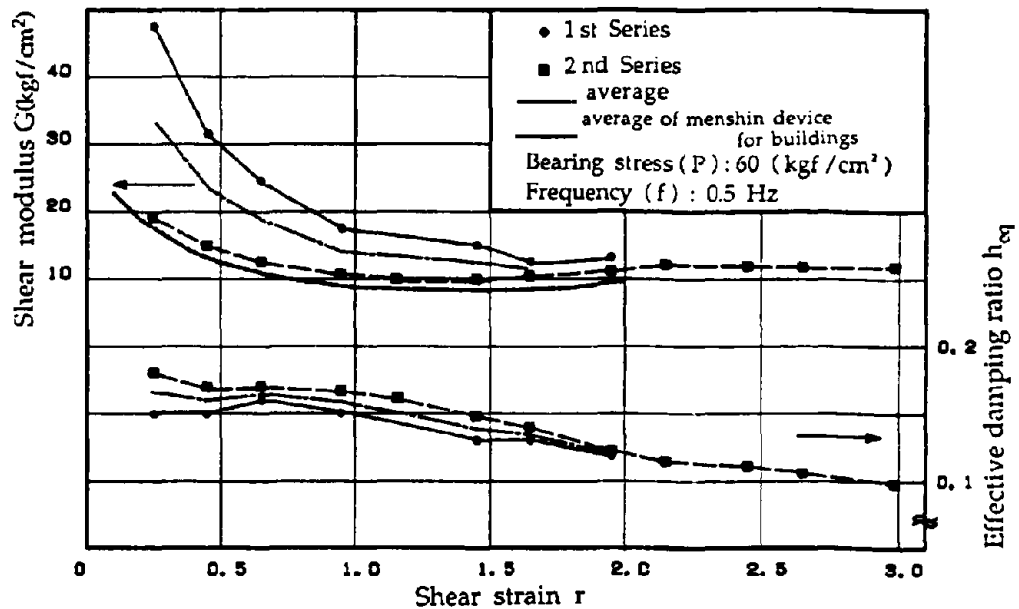


Fig.7 Influence of Strain & Strain Experience on Horizontal Restoring Force

Fig.7 shows both the shear modulus and effective damping ratio to the shear strain. The features of the result are as follows:

- (1) Shear modulus was larger at the smaller strain, decreasing downward as the strain increased, and showed nearly a constant value (12-13kgf/cm²) at a strain over 120%.
- (2) Effective damping ratio tended to decrease downward a little according to the increase in the strain, and showed nearly a constant value (15%) in the above-mentioned region.
- (3) A stable restoring force was obtained at larger strain over 200%.

(4) This material was subjected to the effect of its career in experienced strain, similarly the existing other high damping rubber materials. It was observed in the shear modulus by their reduction after the large strain experience, especially significant in the lower strain region, but was about 30% at such a higher (about 120%) region as used as a design displacement for earthquakes. Regarding effective damping, such variations were small and rather tended to increase.

Influence of Frequency of the Horizontal Loading To inspect the response to a wide range of oscillational components occurring during an earthquake, horizontal restoring force and damping under various frequency were measured. Fig.8 shows the results.

As the frequency increased, both shear modulus and effective damping ratio tended to increase. By a comparison at 0.01Hz with at 1.0Hz in 100% strain, both increase of about 30% in shear modulus and about 10% in the effective damping ratio were shown.

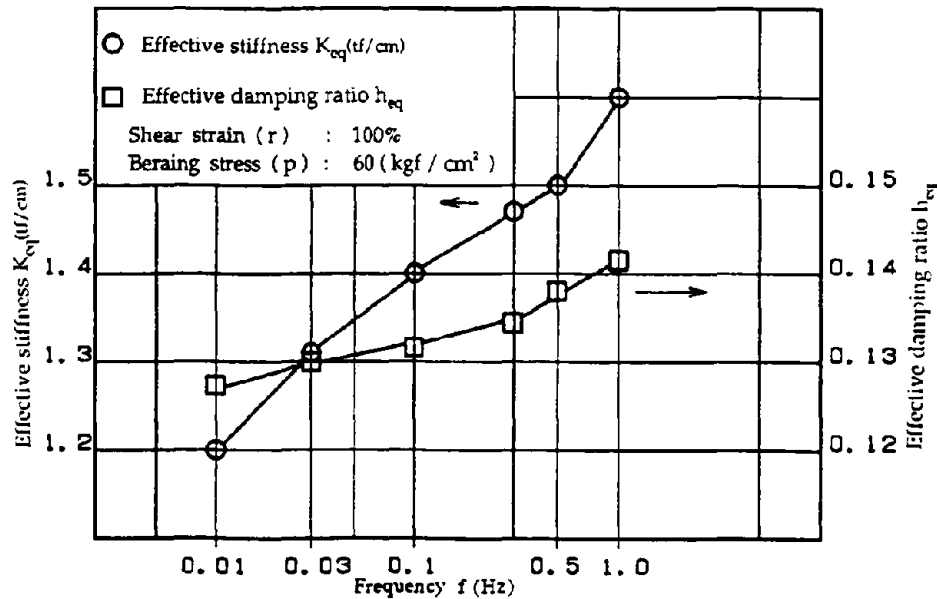


Fig.8 Influence of Excitation Frequency on Horizontal Restoring Force

Influence of Bearing Stress As the bearing stress subjected to the Menshin device varies, horizontal restoring force at various bearing stress conditions were measured. The results is shown in Fig.9.

As a result of horizontal loading test under 20 - 100 kgf/cm² of the bearing stress, both the shear modulus and effective damping ratio did not show any significant change.

Influence of Pre-displacement As a specific condition to the Menshin device for bridges, there is a static pre-displacement caused by expansion of the span on varying temperature and the others. the restoring force property under such a pre-displacement was tested, and the result is shown in Fig.10. The pre-displacement (50% in shear strain) was held for 6 hours before excitations.

At the lower shear strain region below 50%, in comparison with under no pre-displacement, the shear modulus was lower by 25-35%, and the effective damping ratio was higher by 10-15%. On the other hand, at the higher shear strain region above 100%, both properties were nearly consistent with under no pre-displacement.

Durability to Cyclic Loading The durability to 200 times cyclic loading was tested. The number of 200 times was defined as the number of the main excitation of a large-scale earthquake (assumed 0.5Hz, 150% in shear strain, 20cycles) multiplied by ten. Fig.11 shows the result.

After the 200 times of cyclic loading, both the effective stiffness and effective damping ratio showed a tendency to drop, but no damage and no unstable change in their properties could be found. The reduction from the first loading to the 200th one was about 40% in effective stiffness and about 30% in effective damping ratio, and that for the one after first 20 times of loadings was about 20% and about 12%, respectively.

Vertical Stiffness The vertical stiffness of the high damping rubber bearings was tested both with and without pre-displacement. Fig.12 shows the result.

The vertical stiffness at an amplitude of bearing stress of between 0 and 80 kgf/cm² was lower by about 10-20% than that between 40 and 80 kgf/cm². And the pre-displacement lowered it about 20% compared with under no pre-displacement.

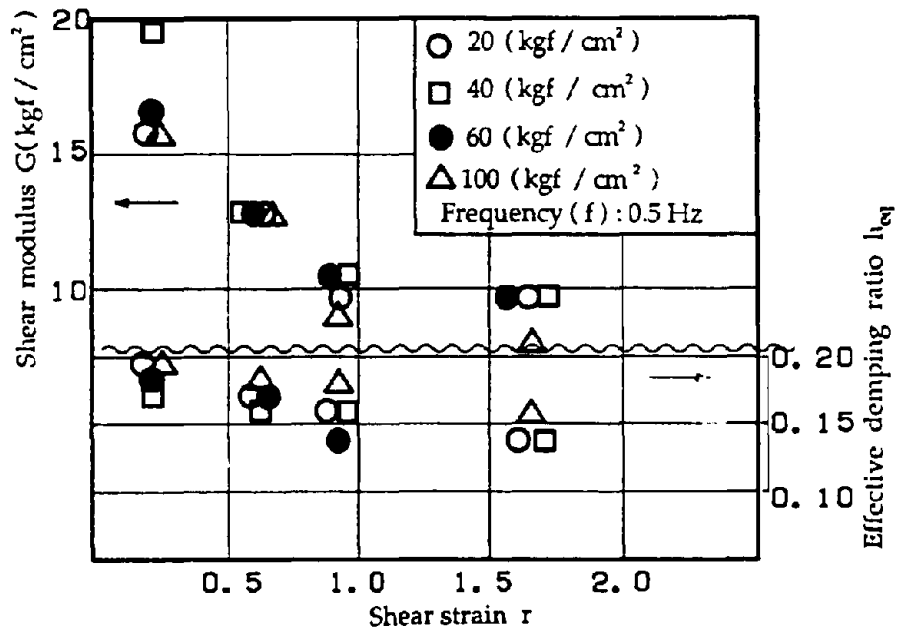


Fig.9 Influence of Bearing Stress on Horizontal Restoring Force

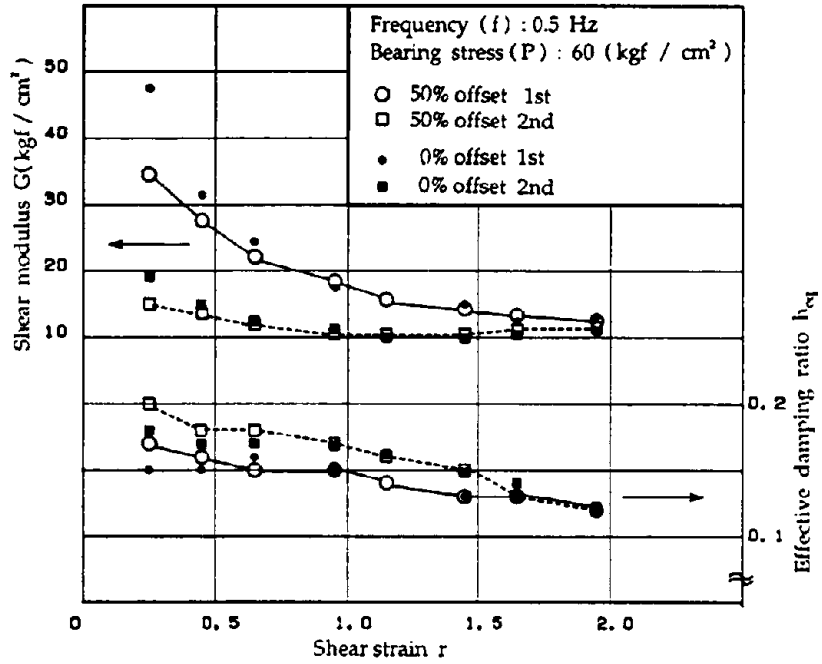


Fig.10 Influence of Pre-displacement on Horizontal Restoring Force

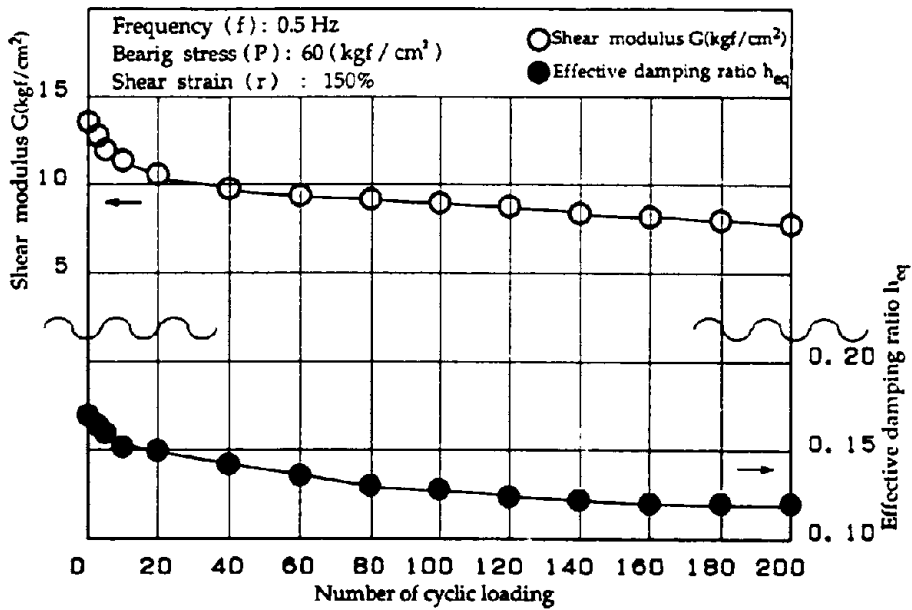


Fig.11 Durability to Cyclic loading on Horizontal Restoring Force

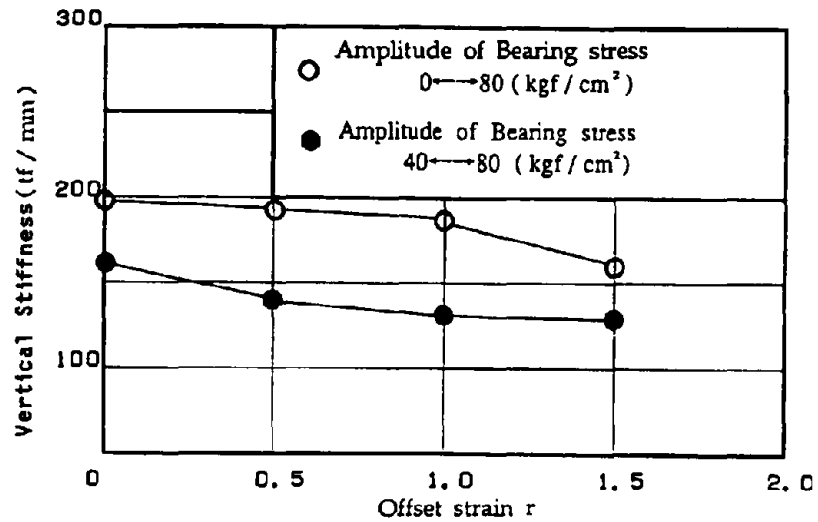


Fig.12 Influence of Pre-displacement on Vertical Stiffness

DYNAMIC LOADING TESTS AT PWRI (Public Work Research Institute)

In the Joint Research Program between PWRI and private corporations, PWRI carried out a dynamic loading tests under a common testing condition using the scale models of the Menshin devices developed by each of the companies, and measured some fundamental properties of the devices and their stabilities.

Testing Method Table 3 shows the testing conditions. The models used were made using the same specifications as the ones used in our laboratory above described (Refer to Fig.3).

Table 3 Testing conditions

Series No.	Bearing stress [kgf/cm ²]	Frequency [Hz]	Pre-strain [%]	Strain [%]	Cycles	Model state
1	80	0.1	0	25,50,100,150,200	10	1st
2	80	0.1	0	25,50,100,150,200	10	2nd
3	80	1.0	0	25,50,100,150	10	3rd
4	80	0.1	50	25,50,100,150	10	4th
5	60	0.5	0	150	40	1st
6	60	0.5	0	150	40	2nd

Stability to the Cyclic Loadings (Series 1 and 2) The aim of this test is to estimate whether the change in the horizontal restoring force and damping in the case of repeating the displacement is stable or divergent. Fig.13 and Fig.14 shows the result of the Series 1 and the Series 2, respectively.

In the first strain (Series 1), both the shear modulus and the effective damping ratio decreased downward by about 10-30% for each loading. However, 2/3 of these reductions occurred during the first three cycles, so these changes can be said to be stable. On the other hand, the above-mentioned changes could scarcely be observed after once experienced a 200% strain (Series 2).

Strain Dependency and Influence of the Strain Experience (Series 1 and 2) The dependency on the shear strain and the influence of the experience of large shear strain for the horizontal restoring force properties were tested. The result is shown in Fig.15

Both shear modulus and the effective damping ratio tended to drop as the shear strain increased, and after experiencing a large strain the modulus also dropped but the damping ratio increased. This result was consistent with both value and tendency obtained at our laboratory mentioned previously, showing good reproductivity.

Influence of Frequency (Series 2 and 3) The influence of the frequency of horizontal loading on the horizontal restoring force properties was tested, at 0.1Hz and 1.0Hz. The result is also shown in Fig.15

Both shear modulus and effective damping ratio increased as the frequency increased, which is consistent with the test results and tendency obtained at our laboratory described above.

When comparing the shear modulus and effective damping ratio with 100% strain at 0.1Hz with ones at 1.0Hz, both were found to be about 10% larger at 1.0Hz. However, such changes were thought to have no special interference with the design for the Menshin devices.

Influence of Pre-displacement (Series 2 and 4) The influence of the pre-displacement supposed to be objected to Menshin devices for bridges on the horizontal restoring force properties were tested. Fig.16 shows the result.

The trends of the changes of the shear modulus and effective damping ratio against the shear strain or repeating cycles were equal to the ones in the case of no pre-displacement. The difference between with and without pre-displacement was about 3% in shear modulus and about 4% in effective damping ratio, respectively.

Durability to Cyclic Loading (Series 5 and 6) It was tested whether the device had a sufficiently stable horizontal restoring force property against the main excitation of a large-scale earthquake by the horizontal loading of the twice numbers (40cycles) as supposed. Fig.17 shows the result.

As numbers of repeating cycle increased, both the shear modulus and effective damping ratio showed a tendency to drop like the other above described tests, and its reduction at the beginning of the test was predominant.

In a test restarted after testing of 40 cycles and resting for 3 hours (Series 6), the first (41 in total) obtained values of both shear modulus and effective damping ratio were found to recover nearly to an average one of from 4 to 10 cycles in the first test (Series 5).

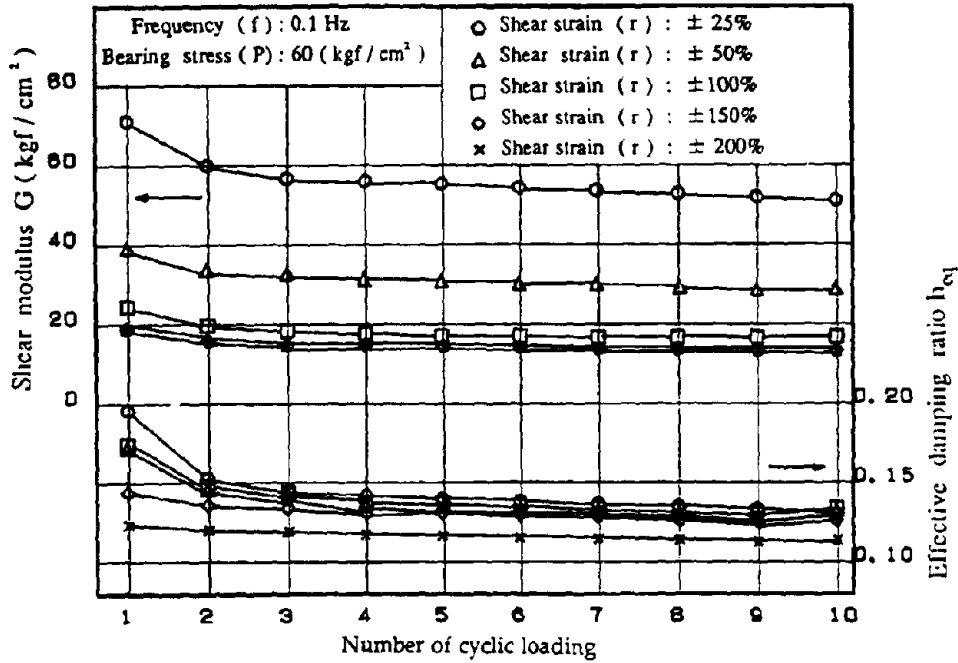


Fig.13 Stability to the Cyclic Loadings of Hor. Restoring Force (1st Series)
[Testing Series 1]

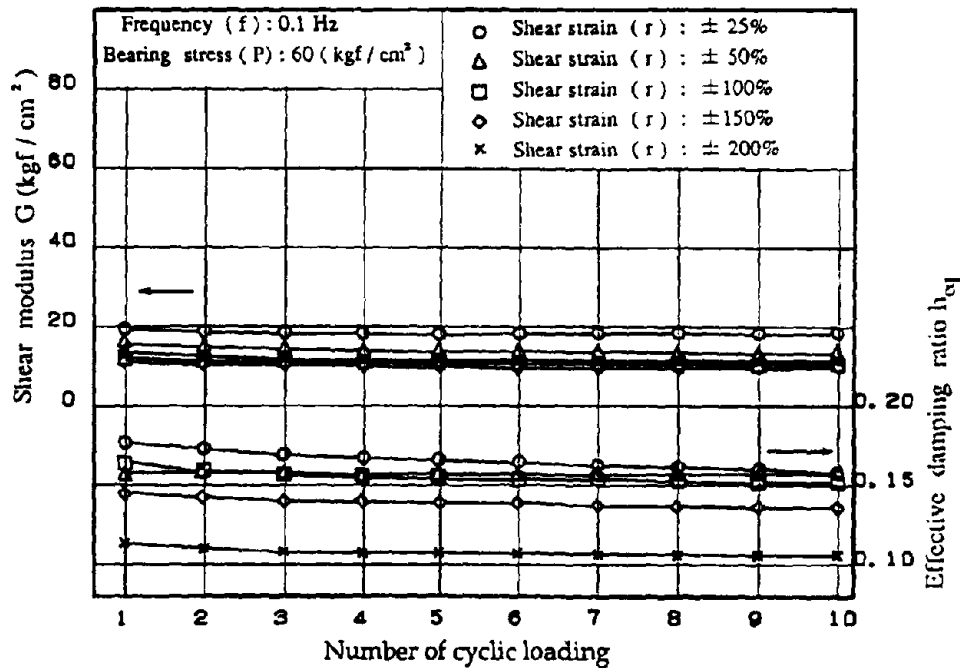


Fig.14 Stability to the Cyclic Loadings of Hor. Restoring Force (2nd Series)
[Testing Series 2]

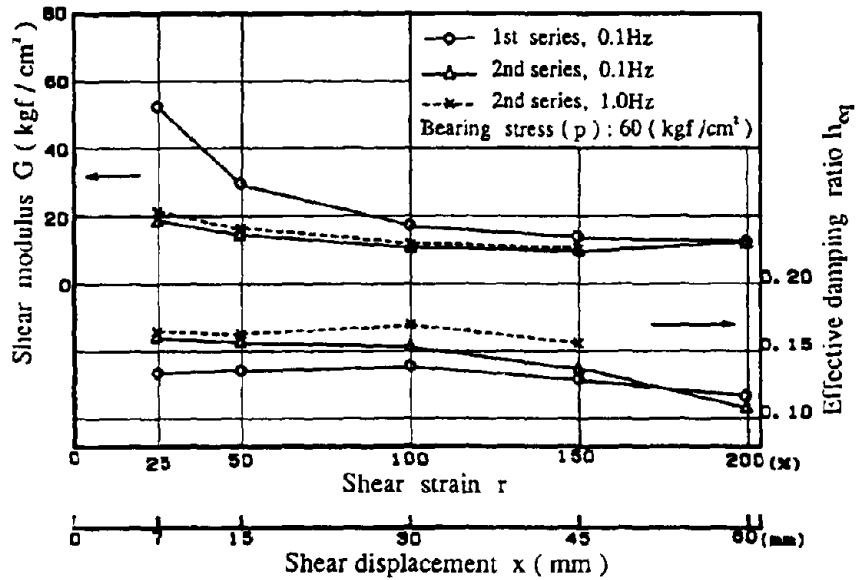


Fig.15 Influence of Strain, Strain Experience & Frequency on Horizontal Restoring Force [Testing Series 1,2 & 3]

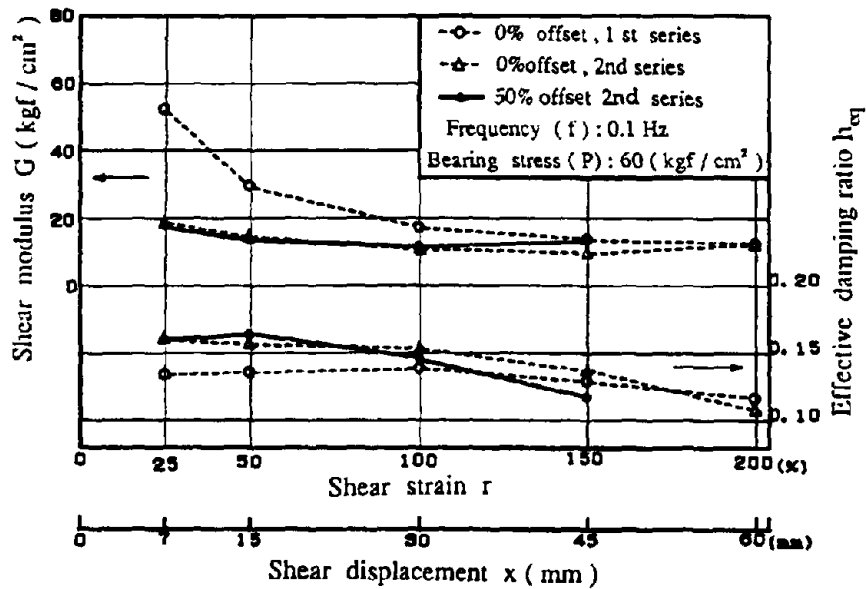


Fig.16 Influence of Pre-displacement on Horizontal Restoring Force [Testing Series 2 & 4]

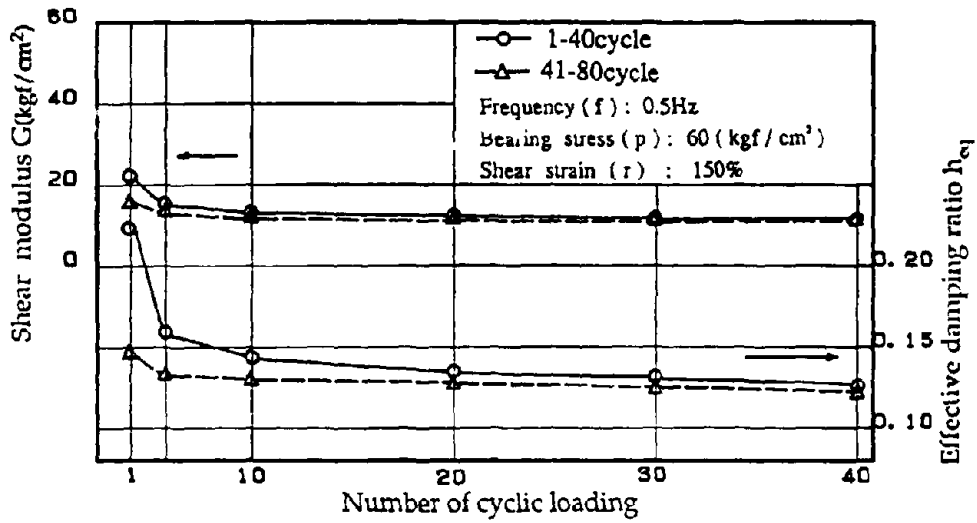


Fig.17 Durability to Cyclic Loading on Horizontal Restoring Force
 [Testing Series 5 & 6]

CONCLUSIONS

By the fundamental tests carried out at our laboratory and the dynamic loading tests at PWRI, new high damping rubber bearing developed here was confirmed to have about 1.5 times higher horizontal stiffness in the strain range from 100 to 200%, and have nearly equal damping property (about 15% in effective damping ratio), in comparison with the existing high damping material developed for Menshin buildings. Furthermore, it was determined as a result of these tests that this bearing functions stably for some requirements for the Menshin device for bridges. Conclusions are summarized as follows:

- (1) The effective stiffness is high during low shear strain, but is low during high shear strain, and that is nearly constant (12-13 kgf/cm²) at a strain over about 120%. The effective damping ratio shows a low strain dependency (about 15%). And this material shows no damage and stable horizontal restoring force property at large displacement up to 300% in shear strain.
- (2) As numbers of cyclic loading increase, both effective stiffness and effective damping ratio decrease, but they are almost stabilized during the third loading. After loading 40-200 times at a strain of 150%, this material shows no damage and no divergent tendency of reducing properties.
- (3) As the frequency becomes higher, both effective stiffness and effective damping ratio tend to increase. At 0.01Hz and 1.0Hz at a strain of over 100%, the stiffness and damping ratio shows an increase of 30% and 10%, respectively.
- (4) The horizontal restoring force properties are scarcely influenced by the change of the bearing stress (20-100 kgf/cm²) or the pre-displacement (50%), which are the specific requirements for the Menshin bearings of bridges.

ACKNOWLEDGMENTS

The development of the High Damping Rubber Bearing (Part 1) was made as a part of the Joint Research Program on "Development of Menshin System of Highway Bridges" between PWRI and Bridgestone Corporation. The authors are very grateful to Dr. K. Kawashima, Mr. K. Hasegawa, Mr. S. Unjo and Mr. H. Nagashima of the Earthquake Engineering Division of PWRI for their cooperation.

REFERENCES

1. Suizu, Y., "High Damping Rubber Bearing", "The 43th annual scientific lecture of the Japan Society of Civil Engineers, 1988 (in Japanese)
2. Ikeda, T., Kumakura, K., Ozeki, K. and Abe, N., "Design of Karasuyama No.1 Bridge (Base Isolated Bridge)", Bridge and Foundation Engineering, Kensetsu Tosho Co., Ltd. Japan, Vol.25 No.6, 1991 (in Japanese)
3. P.W.R.I., "The Report of The Joint Research Program on Development of Menshin System of Highway Bridges (No.1)", P.W.R.I. Joint Research Report No.44, 1990 (in Japanese)
4. P.W.R.I., "The Report of The Joint Research Program on Development of Menshin System of Highway Bridges (No.2)", P.W.R.I. Joint Research Report No.60, 1991 (in Japanese)
5. JIS, "Physical Testing Methods for Vulcanized Rubber", Japanese Standards Association, JIS K 6301, 1975 (in Japanese)

DEVELOPMENT OF HIGH DAMPING RUBBER BEARING FOR MENSIN BRIDGES (Part 2)

Kazuhiko KAWASHIMA¹, Masahiro KOSHITDGE¹, Kazuo ENDO², Chikafumi YAMADA² and Tatu NISHIMOTO²

¹Public Works Research Institute, Ministry of Construction,
Tsukuba-shi, Ibaraki, Japan

²The Yokohama Rubber Co., Ltd., Hiratsuka-shi, Kanagawa, Japan

SUMMARY

This paper describes fundamental properties and dynamic loading test results of high damping rubber bearings for Menshin bridges which have been developed taking part in the joint research program between Public Works Research Institute (hereinafter called "PWRI") and The Yokohama Rubber Co., Ltd. (hereinafter called "YRC"). Through a series of tests performed, factors which significantly influence the properties of high damping rubber bearings became apparent. An effective damping ratio of 15% or over could be obtained under the assumed largest earthquake.

INTRODUCTION

Japan is one of the most earthquake pronoun countries, and careful consideration for earthquake resistance should be required when designing bridges. Because earthquake damage of highway bridges yeilds serious traffic disaster, suitable earthquake resistance must be provided. In view of the above background, YRC has developed a high damping rubber bearing for Menshin bridges taking part in the joint research program with PWRI. The properties and characteristics of a high damping rubber bearing developed were confirmed by a series of dynamic loading tests.

This paper describes dynamic loading tests and fundamental properties of high damping rubber bearings developed for Menshin bridges. The high damping rubber bearings developed have suitable stiffness and excellent high damping properties. The properties are not seriously affected by a change of vertical load or lateral load frequencies, and are hardly affected by pre-set displacement. (Ref.1,2)

FUNDAMENTAL PROPERTIES OF HIGH DAMPING RUBBER BEARINGS

Physical Properties of Rubber In order to evaluate the physical properties of rubber, the physical tests were carried out in accordance with JIS K-6301 (Ref.3). Dumbbell specimens as shown in Fig. 1 were used for the tests. The summary of test results is shown in Table 1.

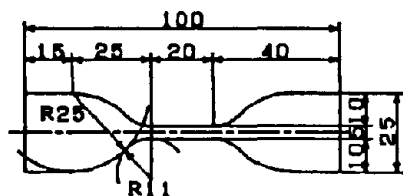


Figure 1 Dumbbell specimen

Table 1 Summary of physical properties

Tensile strength	210kgf/cm ²
Elongation	680%
Tensile stress at 100% strain	20.0kgf/cm ²
Hardness (IRHD)	68

Effect of temperature change on the dynamic properties of rubber was investigated by varying the temperatures as -10°C , $+20^{\circ}\text{C}$ and $+40^{\circ}\text{C}$. Specimens of $25\text{mm} \times 25\text{mm} \times 4.8\text{mm}$ were dynamically loaded as shown in Fig. 2 at a frequency of 0.5Hz with shear strain of 100% for ten cycles for each temperature condition. From the force-displacement hysteresis loops, the shear modulus G_{eq} and the effective damping ratio h_{eq} were defined as

$$G_{eq} = (K_{eq} \times t_r) / A_r \quad (1)$$

$$h_{eq} = \Delta W / (2\pi W_e) \quad (2)$$

where K_{eq} is effective stiffness defined by $(F_{max} - F_{min}) / (U_{max} - U_{min})$. A_r and t_r are effective area and thickness of rubber respectively, and ΔW and W_e are energy dissipation and elastic energy per cycle as shown in Fig. 3. The test results are presented in Table 2, in which the averaged G_{eq} and h_{eq} over 4th to 10th cycle loading are presented. A remarkable advantage of the high damping rubber developed is large elongation capability of 680% at break, high shear stiffness and excellent damping characteristics. As temperature decreases, both G_{eq} and h_{eq} increase. Compared with the values at 20°C , G_{eq} and h_{eq} become larger by 27% and 28% , respectively, at -10°C .

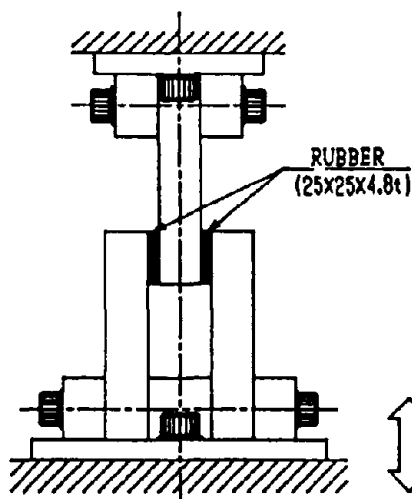


Figure 2 Specimen for dynamic properties test

Table 2 Results of dynamic properties test

Temperature	G_{90} (kg/cm ²)	h_{90} (%)
-10°C	12.1	21.9
20°C	9.5	17.3
40°C	8.3	16.3

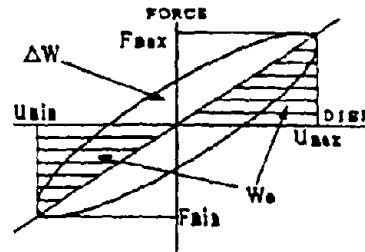


Figure 3 Hysteresis loops of rubber

Fundamental Properties of Laminated High Damping Rubber Bearings In order to study the fundamental properties of laminated high damping rubber bearings, a dynamic loading test was performed on the 1/3 scaled model. A three-span continuous steel girder bridge with width of 10m and the deck length of 100m was assumed to design the prototype. Fundamental natural period and model damping ratio were assumed as 1.6 seconds and 0.15, respectively. Reaction force was assumed as 100tf in the prototype. Fig. 4 shows the 1/3 scaled model. It is made by laminating rubber sheets with 176.5mm diameter and 3.2mm thick and 1.2mm thick steel plates one after another to form 15 rubber layers. The testing condition is presented in Table 3. In the series A tested was the dynamic properties of 1/3 scaled model for shear strain from 25% to 200%. Loading was made twice at an interval of 24 hours so as to investigate the effect of amplitude change and loading hysteresis. In the series B tested was the effect of loading frequency. The specimen was subjected to cyclic loading by varying the frequency. In the series C tested was the effect of compressive stress.

Table 3 Testing methods for laminated high damping rubber bearings

Series	Bearing stress kgf/cm ²	Frequency Hz	Strain %	Cycles	Model
A	60	0.5	25 50 100 150 200	10×2	a
B	60	0.01 0.1 0.5 1.0	25 50 100 150	10	b
C	30 60 80 100	0.5	25 50 100 150	10	c

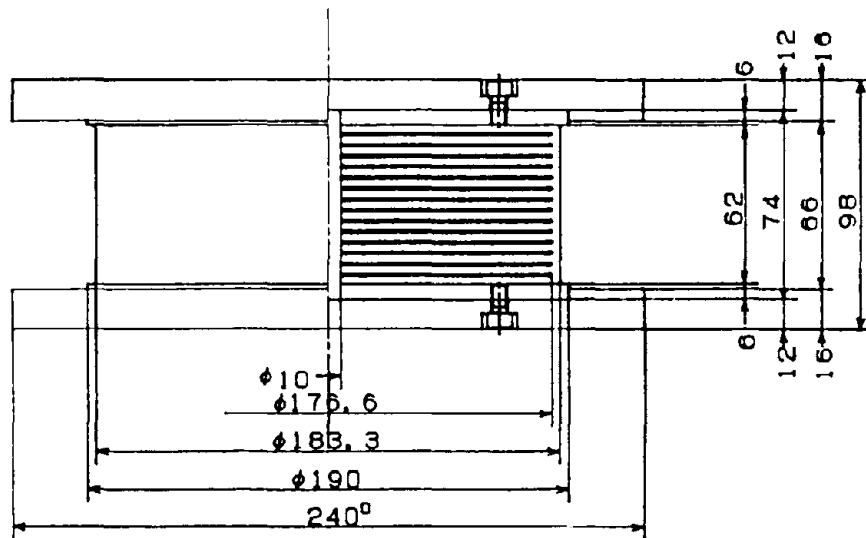


Figure 4 1/3 scaled model of laminated high damping rubber bearing



Photo 1 Bi-axial dynamic loading tester

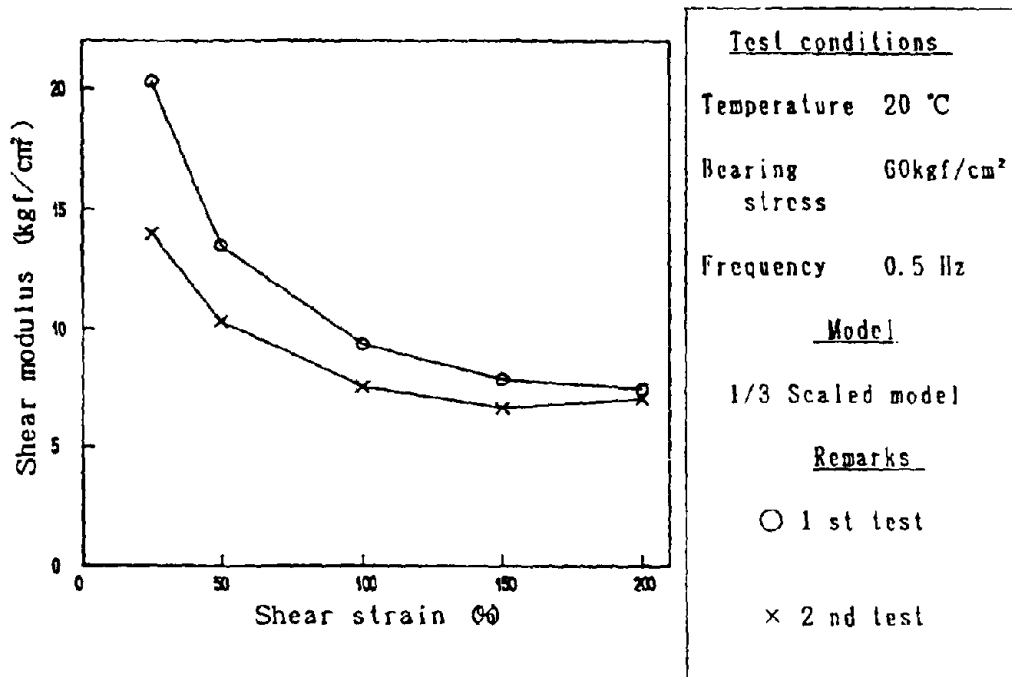


Figure 5 Effect of loading amplitude on the shear modulus

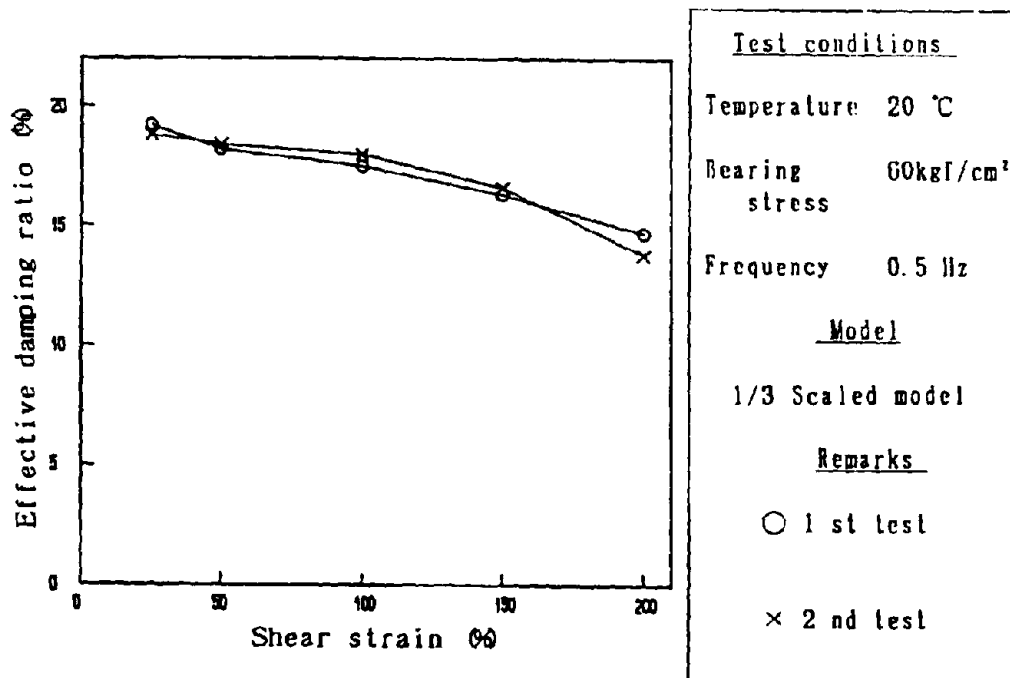


Figure 6 Effect of loading amplitude on the damping ratio

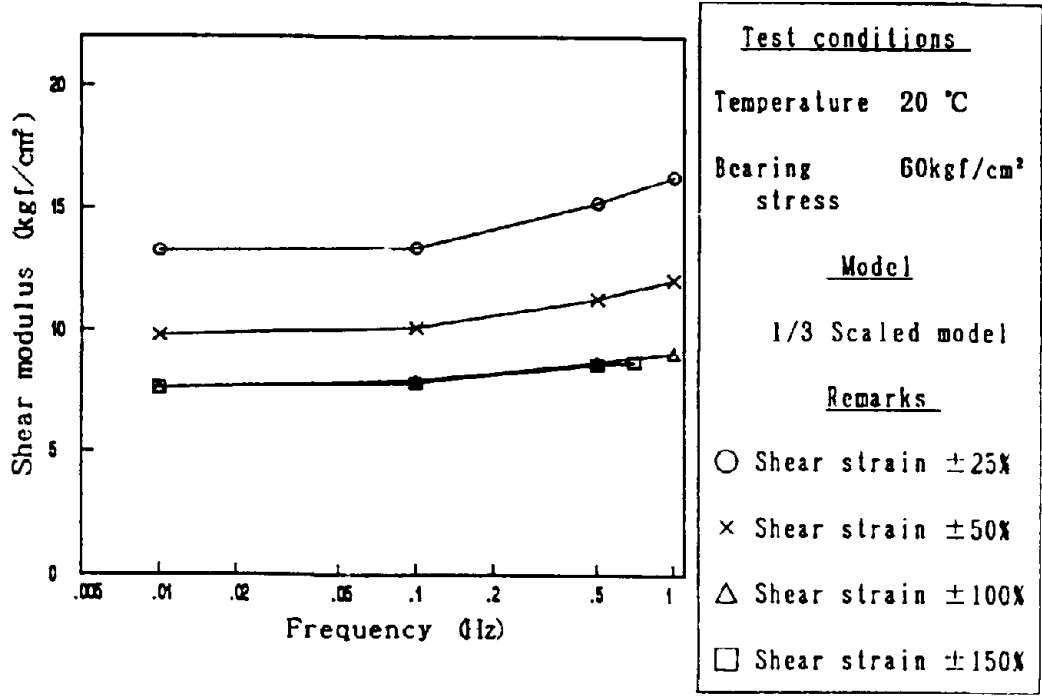


Figure 7 Effect of loading frequency on the shear modulus

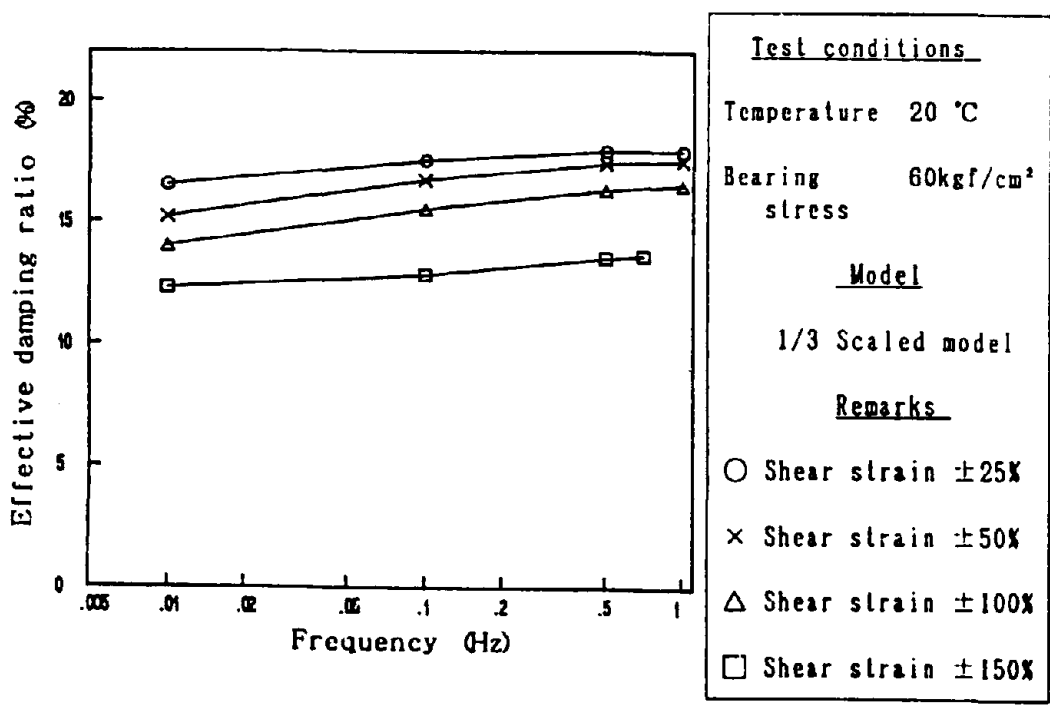


Figure 8 Effect of loading frequency on the damping ratio

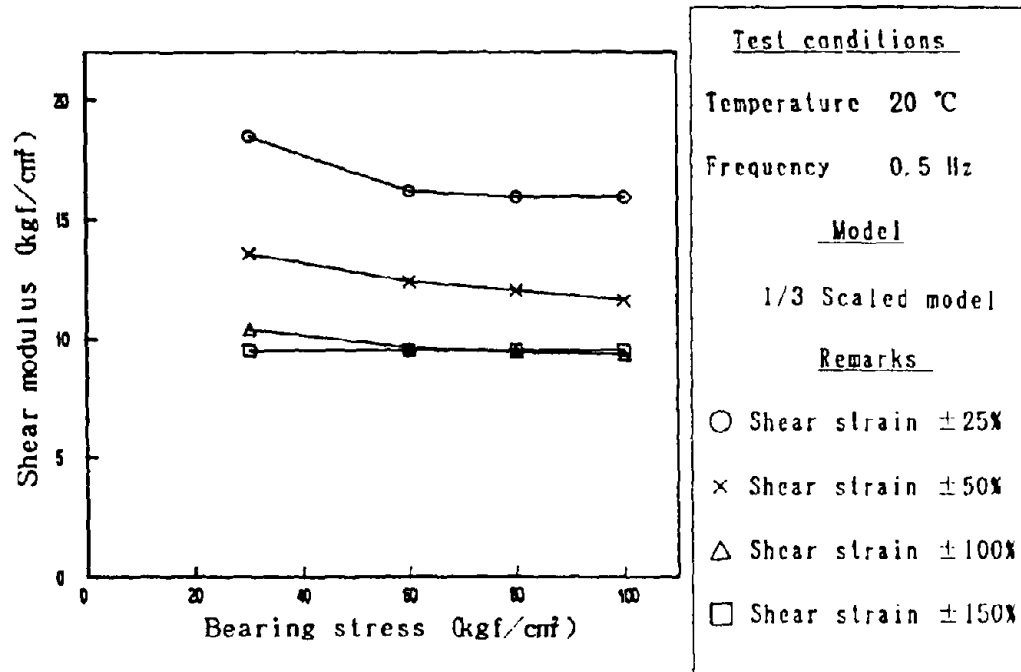


Figure 9 Effect of bearing stress on the shear modulus

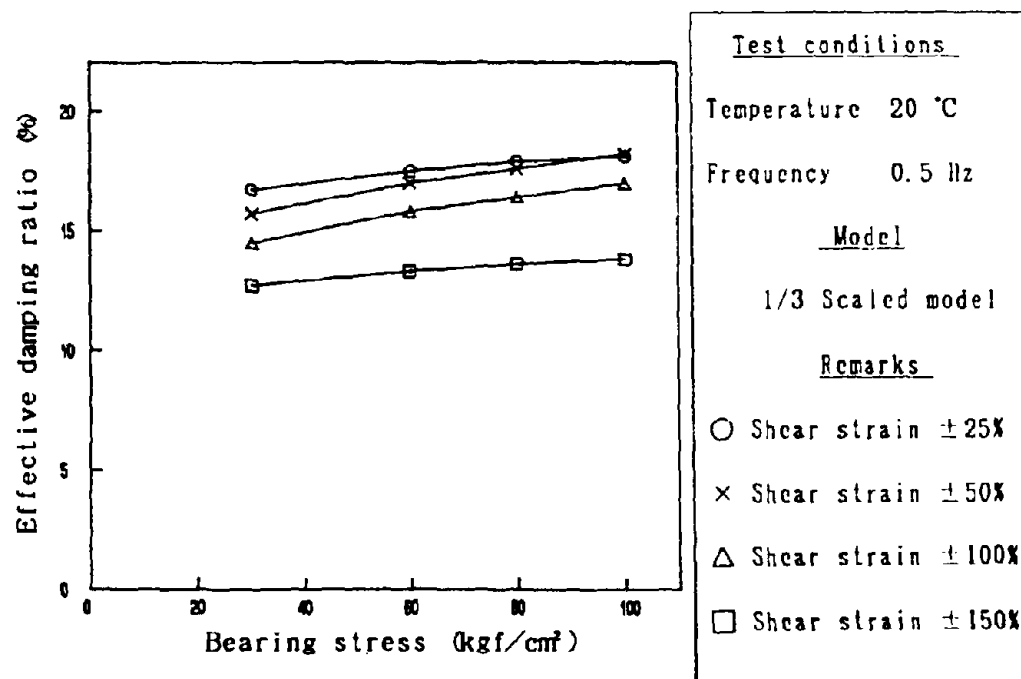


Figure 10 Effect of bearing stress on the damping ratio

Figs. 5~10 show the G_{eq} and h_{eq} obtained by taking average over 4th to 10th loading cycle. It is understood that as shear strain increases, both G_{eq} and h_{eq} tend to reduce. It is also certain that G_{eq} is significantly affected by loading history while h_{eq} is scarcely effected. From Figs. 7 and 8, as frequency increases, both the G_{eq} and h_{eq} increase. Taking 0.5Hz at 100% shear strain as the reference, G_{eq} becomes -9% at 0.1Hz and +5% at 1.0Hz, and h_{eq} -5% at 0.1Hz and +1% at 1.0Hz. From Figs. 9 and 10, it is understood that as bearing stress increases, G_{eq} decreases while h_{eq} increases. Taking 60kgf/cm² at 100% shear strain as the reference, G_{eq} becomes +8% at 30kgf/cm² and -3% at 100kgf/cm², while h_{eq} -8% at 30kgf/cm² and +8% at 100kgf/cm².

DYNAMIC LOADING TEST AT PWRI

Testing Method Fig. 11 illustrates the 2/3 scaled test model, which is made by laminating 353.3mm diameter, 6.33mm thick rubber sheets and 2.2mm thick steel plates one after another to form 15 rubber layers (95mm in total) and 14 steel plate layers (30.8mm in total), respectively. Table 4 shows a testing method and Photo 2 indicates the deformation of the model under testing. The test was made in a room controlled at a constant temperature of +20 °C. Series 1 through 4 were continuously tested to evaluate fundamental properties of the model. Series 40-1 and 40-2 were tested at a interval of 3 hours to evaluate endurance of cyclic deformations, using a different model with the same scale.

Table 4 Testing methods

Series No.	Bearing stress kgf/cm ²	Frequency Hz	Pre-strain %	Strain ± %	Number of cycles	Model used
1	60	0.1	0	25 100 150 200	10	No. 1
2	60	0.1	0	25 100 150 200	10	
3	60	1.0	0	25 100	10	
4	60	0.1	50	25 100 150	10	
40-1	60	0.5	0	150	40	No. 2
40-2	60	0.5	0	150	40	

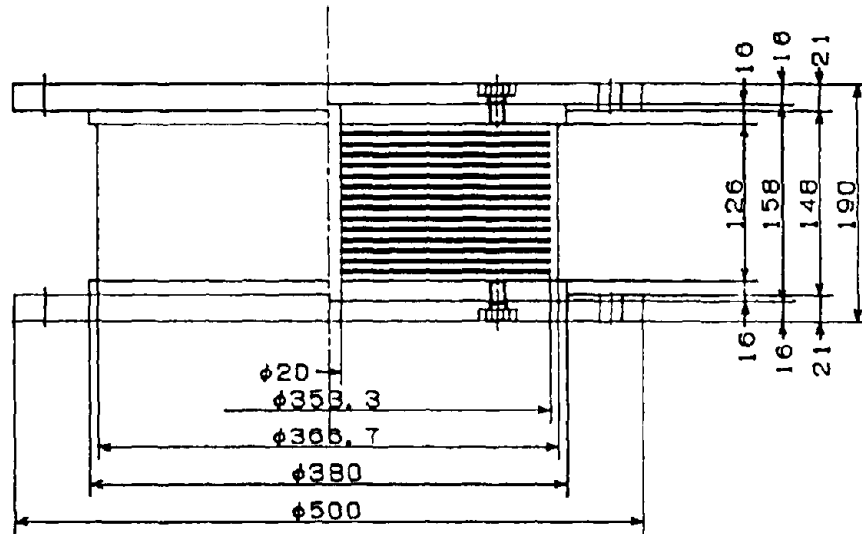


Figure 11 2/3 scaled model of laminated high damping rubber bearing

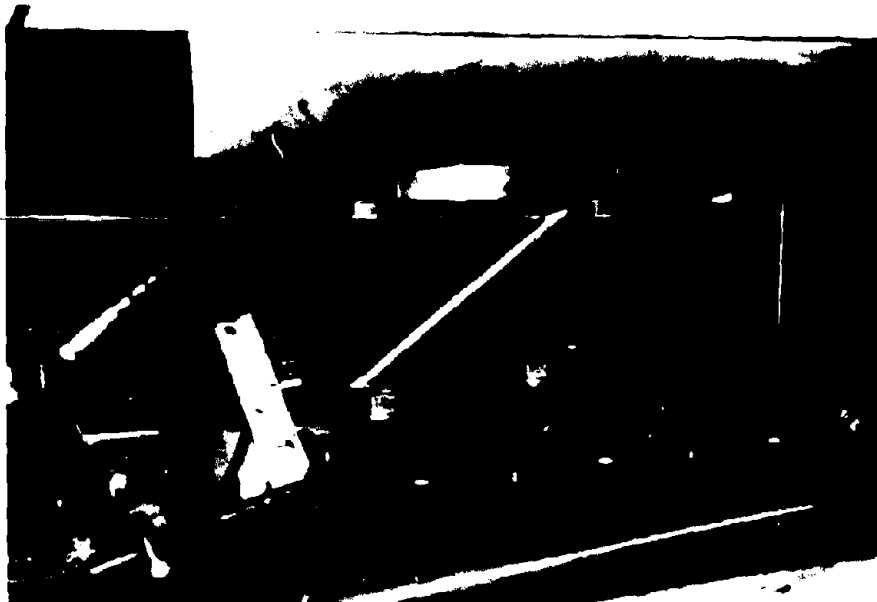


Photo 2 Dynamic loading test conducted at PWRI

Test Results Fig. 12 shows the force-displacement hysteresis loops in series 1, in which no pre-strain was given to the model in advance. Fig. 13 shows the force-displacement hysteresis loops in series 2, which was made after series 1 causing 200% strain as maximum. Figs. 14 and 15 show $G_{e,q}$ and $h_{e,q}$ vs. shear strain relation for series 1 to 4. Table 5 shows the test results for $G_{e,q}$ and $h_{e,q}$ which are average over 4th to 10th cycle. From the test results of series 40-1 and 40-2, Figs. 16 and 17 show the effect of loading cycle on the shear modulus and damping ratio. It may be pointed out from these results :

(a)Effect of Stress/Strain Experience on the Shear Properties From Figs. 12 and 13, it is certain that shear stiffness tend to decrease as number of cyclic loading increases. In particular, a remarkable reduction observed at the 1st and 2nd cycles. Taking the average over 4th to 10th cycle at 100% shear strain as the reference, $G_{e,q}$ is larger by 25% and 6% at 1st and 3rd cycle, respectively, and $h_{e,q}$ is also larger by 10% and 1% at 1st and 3rd cycle, respectively. It is certain that reduction of $h_{e,q}$ is smaller than the reduction of $G_{e,q}$. The decreasing ratio of $G_{e,q}$ and $h_{e,q}$ in series 2 is half of that in series 1.

(b)Effect of Amplitude on the Shear Properties $G_{e,q}$ and $h_{e,q}$ tend to decrease as shear strain increases. Taking 100% shear strain as the reference, $G_{e,q}$ becomes double and $h_{e,q}$ grows approximately 15% at 25% shear strain. $G_{e,q}$ becomes 1.7 times larger and $h_{e,q}$ 1.1 times at the same 25% shear strain in series 2 followed by the series 1, in which loading as large as 200% strain was made. $G_{e,q}$ in series 2 is smaller by approximately 20% than that of series 1 at 100% shear strain, and by 3% at 200% shear strain. Changes are hardly seen in $h_{e,q}$ in the range below 150% shear strain, and $h_{e,q}$ in series 2 is smaller than that of series 1 by approximately 8% at 200% shear strain.

(c)Effect of Frequency on the Shear Properties Effect of frequency can be estimated by comparing series 2 with series 3. As frequency decreases, both $G_{e,q}$ and $h_{e,q}$ tend to reduce. Taking 1 Hz at 100% shear strain as the reference, $G_{e,q}$ and $h_{e,q}$ decrease by 3% and 12%, respectively, at 0.1Hz.

(d)Effect of Pre-strain on the Shear Properties Effect of pre-strain can be estimated by comparing series 2 with series 4. Taking 0% pre-strain as the reference, changes are hardly seen in $G_{e,q}$ and $h_{e,q}$ at 50 and 100% shear strains when 50% pre-strain is applied, while $G_{e,q}$ is larger by 10% and $h_{e,q}$ is smaller by 10% at 150% shear strain.

(e)Effect of Number of Loading Cycle on the Shear Properties Cyclic loading with 40 cycles was made twice. Figs. 16 and 17 indicate that $G_{e,q}$ and $h_{e,q}$ decrease as the number of loading cycle increase. When the average obtained from 4th to 10th loading cycle is taken as the reference, $G_{e,q}$ decreases by 12 to 15% and $h_{e,q}$ decreases by 6 to 10% at 40th cycle. Because a surface temperature increased (20 °C at start and 30.6°C at end), it is considered that the increase of surface temperature greatly affected $G_{e,q}$ and $h_{e,q}$. When the test was resumed after 3 hours, it was seen that the decreased $G_{e,q}$ and $h_{e,q}$ recovered to 84% of the original values as shown in Figs. 16 and 17. Comparing the average value obtained from 4th to 10th loading cycle, $G_{e,q}$ at the 1st and 2nd test is 9.1kgf/cm² and 8.6kgf/cm², respectively, and $h_{e,q}$ at the 1st and 2nd test is 15.9% and 14.6%, respectively. Therefore variation between the 1st test and the 2nd test may be small.

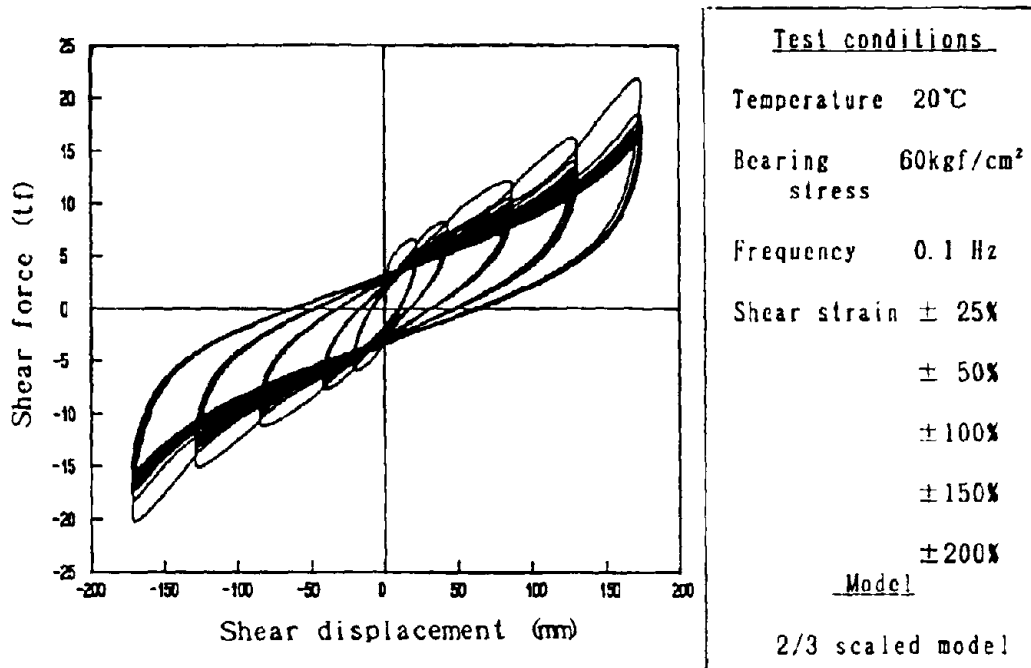


Figure 12 Force-Displacement hysteresis loops of series 1 conducted at PWRI

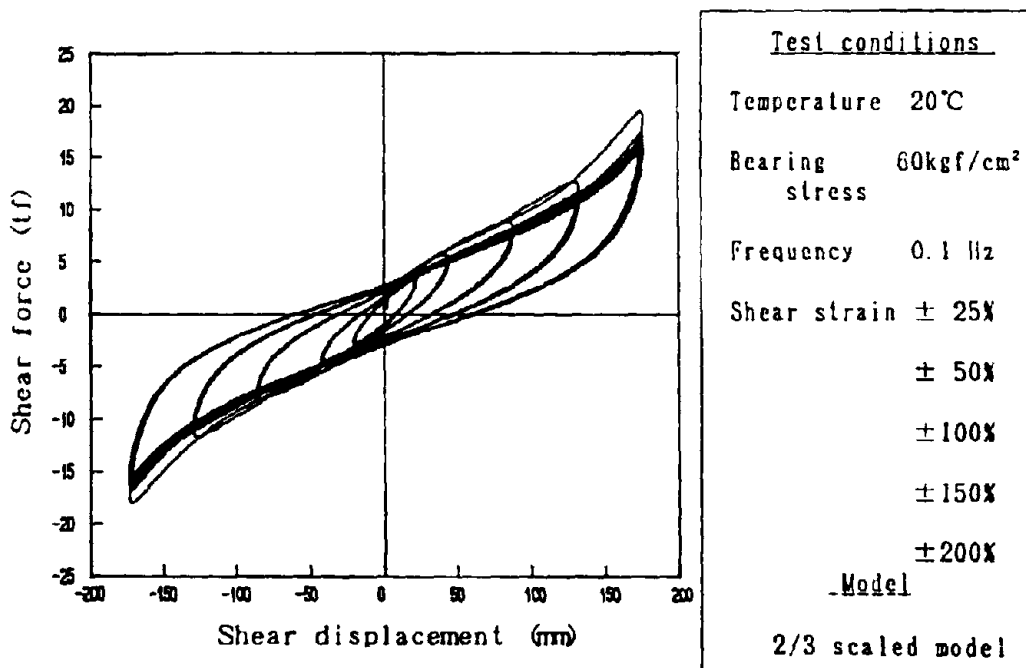


Figure 13 Force-Displacement hysteresis loops of series 2 conducted at PWRI

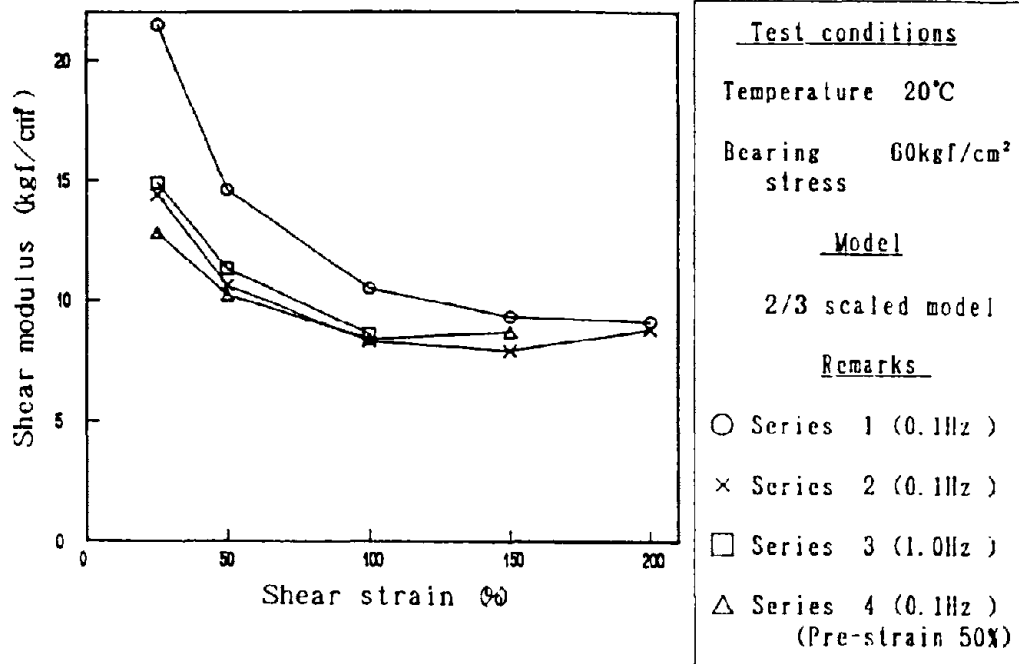


Figure 14 Effect of loading amplitude on the shear modulus conducted at PWRI

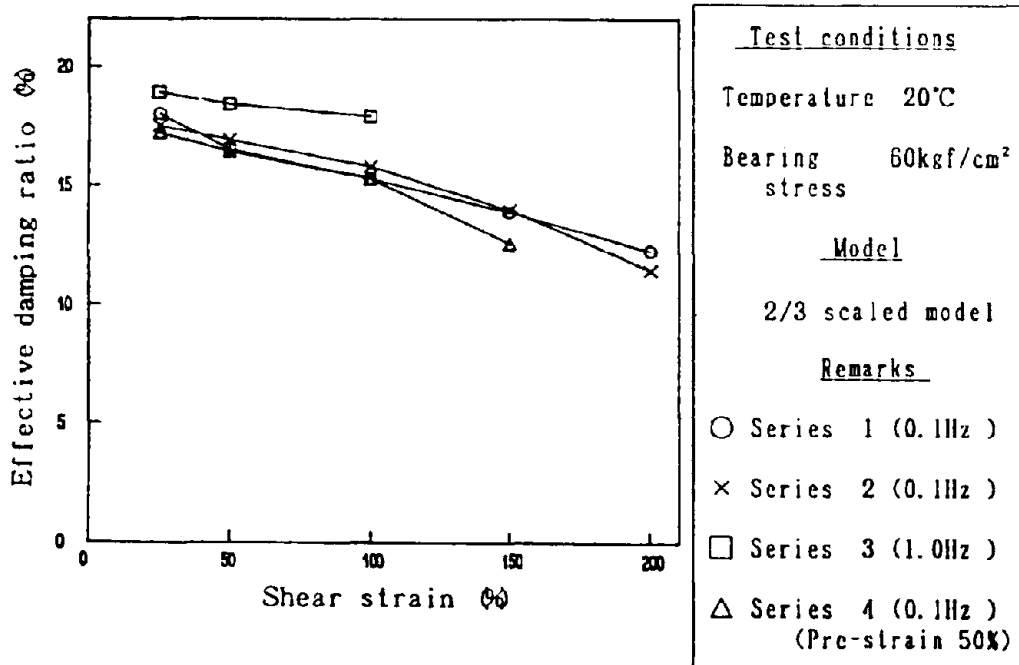


Figure 15 Effect of loading amplitude on the damping ratio conducted at PWRI

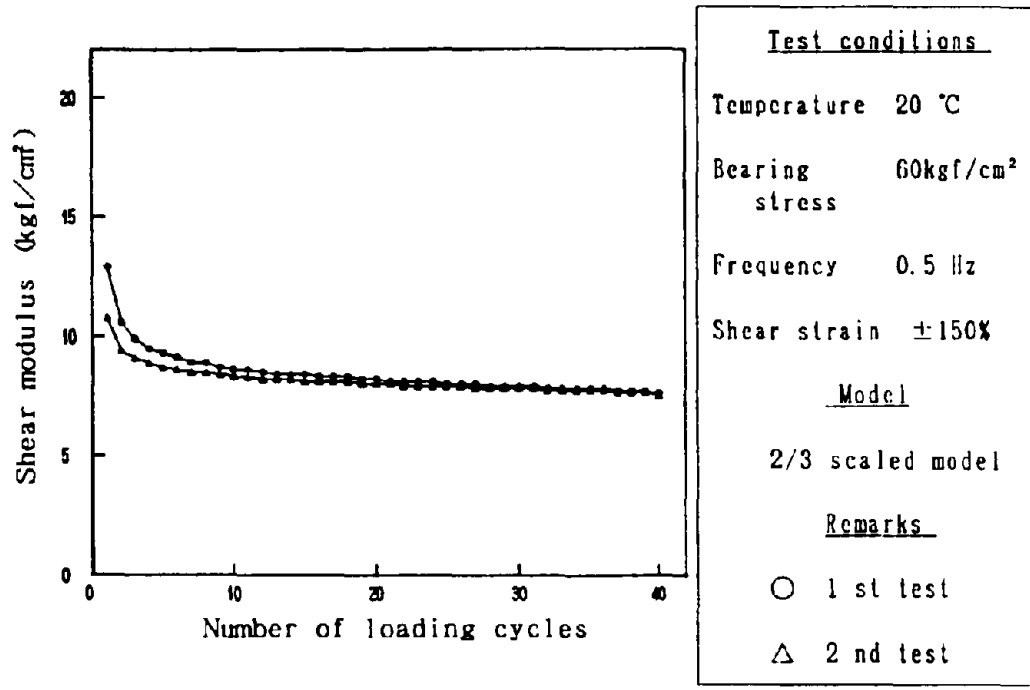


Figure 16 Effect of number of loading cycle on the shear modulus conducted at PWRI

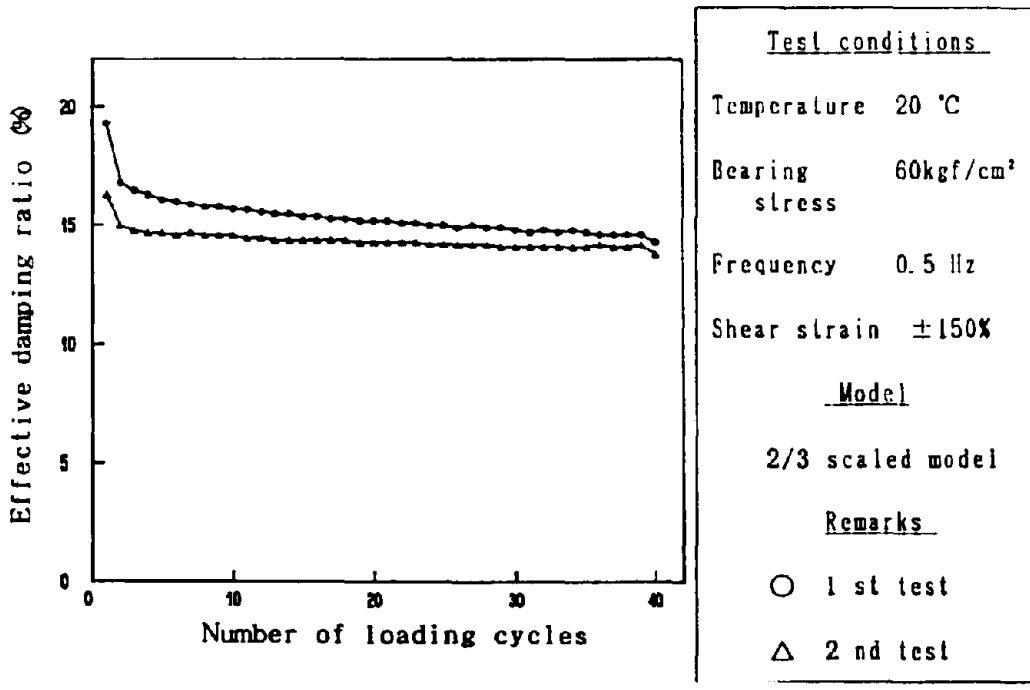


Figure 17 Effect of number of loading cycle on the damping ratio conducted at PWRI

Table 5 Results of dynamic loading test conducted at PWRI

Series No.	Frequency Hz	Shear strain %	Shear modulus kgf/cm ²	Damping ratio %
1	0.1	25	21.5	18.0
		50	14.6	16.5
		100	10.5	15.3
		150	9.3	14.8
		200	9.1	12.3
2	0.1	25	14.4	17.5
		50	10.6	16.9
		100	8.3	15.8
		150	7.8	14.0
		200	8.8	11.5
3	1.0	25	14.9	18.9
		50	11.3	18.4
		100	8.6	17.9
4	0.1	50 ± 25	12.8	17.2
		50 ± 50	10.2	16.4
		50 ± 100	8.4	15.3
		50 ± 150	8.7	12.6
		40-1	0.5	150
40-2	0.5	150	8.6	14.6

CONCLUSION

Following conclusions were derived from the dynamic loading tests conducted at the Public Works Research Institute:

- (1) Effective damping ratio h_{eq} of high damping rubber bearings developed is 14 to 16% at 150% shear strain.
- (2) Effective shear modulus G_{eq} at 150% shear strain is 8 to 9 kgf/cm².
- (3) Shear stiffness and damping ratio are affected by cyclic loading hysteresis, loading frequency, pre-set displacement and loading amplitude. However, the effect of loading frequency and pre-set displacement are comparatively small.
- (4) Although cyclic loading with 40 cycles was made twice for studying durability at $\pm 150\%$ shear strain, any abnormality was not visually observed.

ACKNOWLEDGEMENTS

The development of the high damping rubber bearing (Part 2) was made taking part in the joint research program on "Development of Menshin Systems of Highway Bridges" between PWRI and YRC. Grateful acknowledgement is made to Messrs. K.Hasegawa, S. Unjo and H. Nagashima of the Earthquake Engineering Division of PWRI for their cooperation.

REFERENCES

1. P.W.R.I., "The Report of The Joint Research Program on Development of Menshin System of Highway Bridges(No.1), P.W.R.I. Joint Research Report No.44, (1990)
2. P.W.R.I., "The Report of The Joint Research Program on Development of Menshin System of Highway Bridges(No.2), P.W.R.I. Joint Research Report No.60, (1991)
3. JIS, "Physical Testing Methods for Vulcanized Rubber", Japanese Standards Association, JIS K 6301, 1975 (in Japanese)

DEVELOPMENT OF HIGH DAMPING RUBBER BEARING FOR MENSIN BRIDGES(Part 3)

Ichiro Nishikawa¹ ,Naoki Katoh¹ ,Masaji Itoh² and Yoshitaka Muramatsu²

1)Rubber Molding Section, Showa Electric Wire & Cable Co.,Ltd.
Sagamihara-shi,Kanagawa,Japan

2)Research and Development Section, Showa Electric Wire & Cable Co.,Ltd.
Sagamihara-shi,Kanagawa,Japan

SUMMARY

This paper describes the results of property tests of rubber materials and dynamic loading tests of model specimens. The dynamic loading tests indicated that the high damping rubber bearing developed has more than 10 % of effective damping ratio under all experimental conditions, in spite of some changes of shear modulus G_{e0} and effective damping ratio h_{e0} due to shear-strain, frequency, and other factors.

INTRODUCTION

Various base-isolation devices have been used for buildings in order to reduce earthquake damage in Japan. For highway bridges, Menshin devices are expected to be used in the future. In highway bridges, since requirements different from base-isolation bearings for buildings are required, base-isolation bearings for highway bridges are now being developed in the joint research program between Public Works Research Institute (hereinafter PWRI) and 26 companies. As a part of this joint research, a high damping rubber bearing (hereinafter HDRB) is now being developed. This paper presents outline of the device being developed based on a series of loading tests.

FUNDAMENTAL PROPERTIES OF HDRB

Physical Properties of Rubber Physical property tests were carried out for three types of rubbers A, B, and C, conforming to JIS K 6301. Test results obtained using dumbbell specimens shown in Fig. 1 are presented in Table 1. Dynamic properties of rubbers were also measured at -20, 23, and 40 °C in order to examine the effect of temperature change on the hysteresis loss. Dumbbell specimens in Fig. 1 were subjected to dynamic loading as shown in Photo 1. They were stretched at a strain rate of 200 mm/min. up to 100% strain and then returned to the original test configuration at the same rate. This test was made 5 cycles at each temperature. Hysteresis loss was defined as shown in Fig. 2. as

$$\text{hysteresis loss} = \frac{\text{area OABCO}}{\text{area OABDO}} \quad (1)$$

The hysteresis loss determined by eq. (1) for the 5 loading cycle is shown in Table 2.

Table 1 shows that ultimate elongations and tensile strengths of the three rubbers are almost same, although the tensile strength of rubber A is a little bit larger than others, and judging from values of hardness and modulus, rubber A is hardest, followed by B and C. Table 2 shows that rubber C has the largest hysteresis loss, followed by B and A, and hysteresis losses of the three rubbers decrease with increasing temperature with little difference between 23 °C and 40 °C but have 20 ~30% larger values at -20°C than at 23 °C. Dependence of the

hysteresis loss on the temperature is a little larger in rubber C.

Table 1 Summary of Physical Properties of Rubbers

Rubbers	A	B	C
Hardness (JIS-A)	48	48	44
100% Modulus (kgf/cm ²)	13	12	11
200% Modulus (kgf/cm ²)	31	25	19
Tensile Strength (kgf/cm ²)	150	110	110
Ultimate Elongation (%)	680	650	660

Table 2 Effect of Temperature Change on Hysteresis Loss

Temperature (°C)	Hysteresis Loss		
	A	B	C
-20	0.40	0.50	0.59
23	0.28	0.38	0.44
40	0.26	0.35	0.40

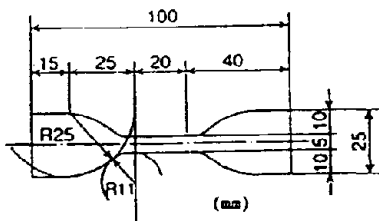


Figure 1 Dumbbell Specimen

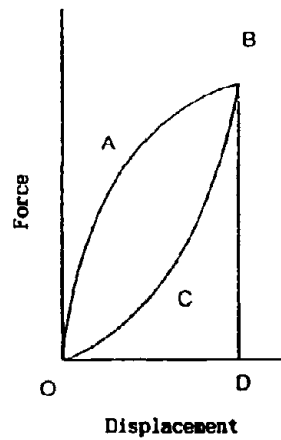


Figure 2 Hysteresis Loop of Rubber

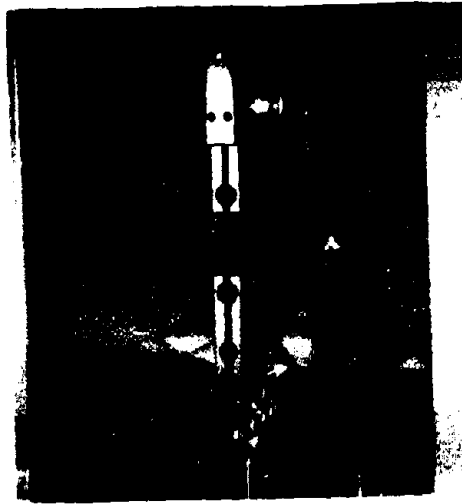


Photo 1 Testing Device for Hysteresis Loop Measurement

Fundamental Dynamic Properties of Small-scaled HDRB Three HDRB models as shown in Fig.3. were fabricated using the three rubbers, and each model was subjected to the dynamic loading test under various conditions listed in Table 3 with the testing device as shown in Photo 2.

High Damping Rubber : 14 layers (2.5mm plate)
 Inner Steel Plate : 13 layers (1.2mm plate)

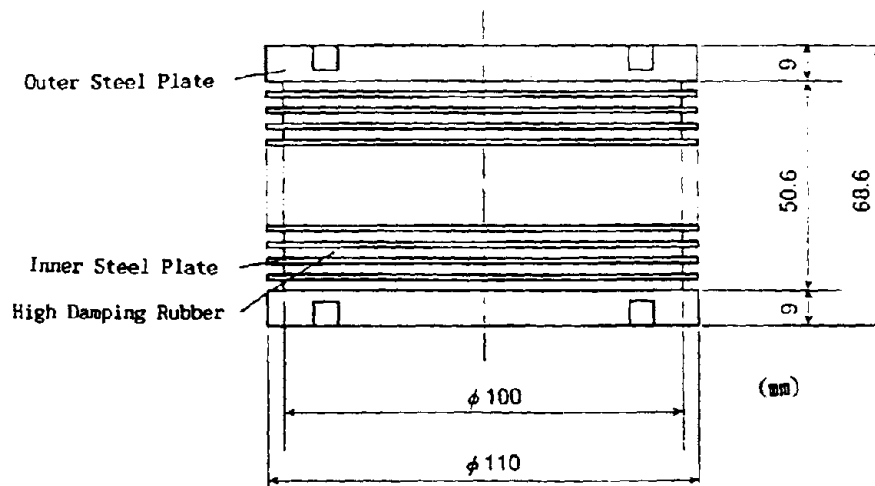


Figure 3 Small-scaled Model of HDRB

Table 3 Testing Methods of the Dynamic Loading Test

Series No.	Bearing Stress (kgf/cm ²)	Frequency (Hz)	Strain (%)	Cycles
1	0	0.1	+/-100	10
2	0	0.5	+/- 50	10
3	0	0.5	+/-100	10
4	0	0.5	+/-150	10
5	0	0.5	+/-200	10
6	0	1.0	+/-100	10

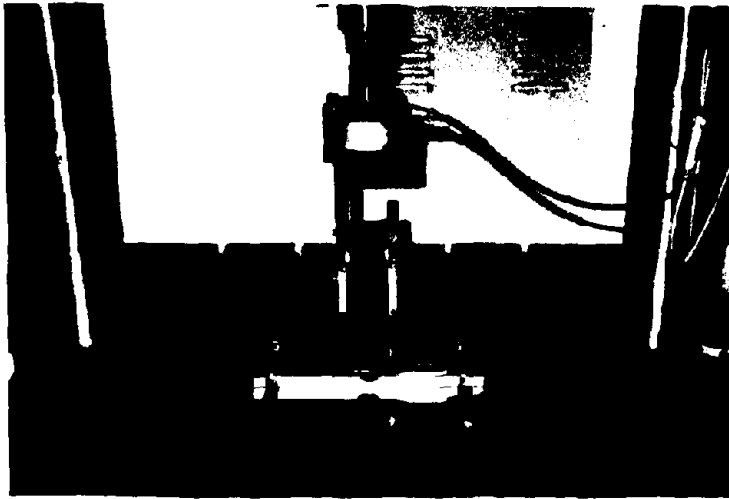


Photo 2 Testing Device for Small-scaled Model (Surbo Pulser type EHF-V5)

Fig 4 shows force~displacement hysteresis of the three specimens for series No.2~5 in Table 3. From these force~displacement hysteresis as shown in Fig.5. effective stiffness $K_{e,q}$ and effective damping ratio $h_{e,q}$ are defined as.

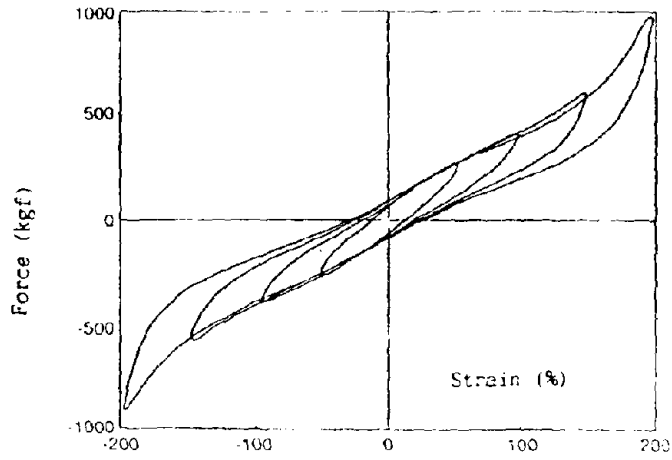
$$K_{e,q} = (F_{max} - F_{min}) / (U_{max} - U_{min}) \quad (2)$$

$$h_{e,q} = \frac{\Delta W}{2\pi W_e} \quad (3)$$

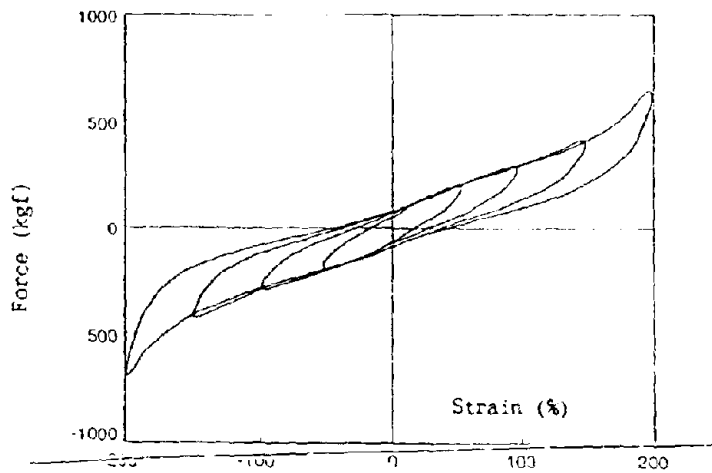
where, ΔW is an area surrounded by the hysteresis loop, and W_e is an elastic energy. Shear modulus $G_{e,q}$ is defined as.

$$G_{e,q} = \frac{K_{e,q} \times T_r}{A_r} \quad (4)$$

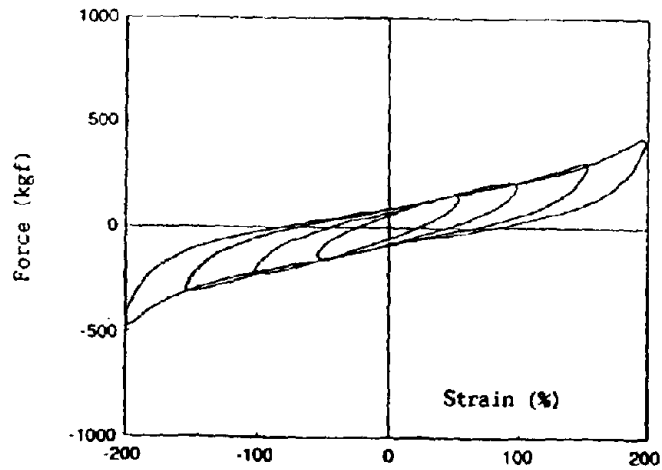
where, A_r is an effective area of rubber, and T_r is rubber thickness. Table 4 shows $K_{e,q}$ and $h_{e,q}$ for the three specimens.



(a) Rubber A



(b) Rubber B



(c) Rubber C

Figure 4 Force ~ Displacement Hysteresis Loops of Small-scaled HDRB

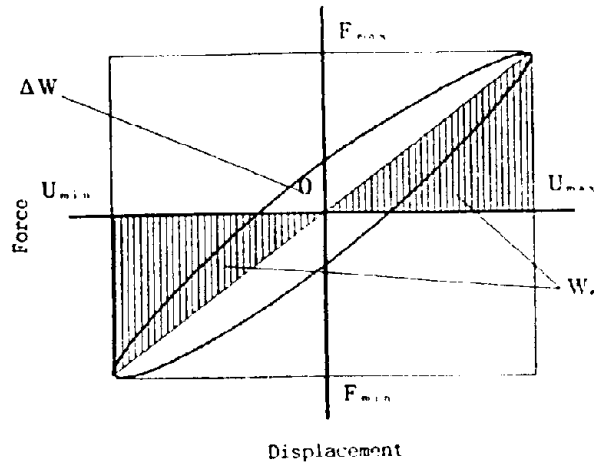


Figure 5 Hysteresis Loop of HDRB

Table 4 Effective Stiffness K_{eff} and Effective Damping Ratio h_{eff} of Small-scaled HDRB

Rubber	Strain (%)	Effective Stiffness (kgf/mm)			Effective Damping Ratio (%)		
		Frequency (Hz)			Frequency (Hz)		
		0.1	0.5	1.0	0.1	0.5	1.0
A	+/- 50	-	14.5	-	-	12.3	-
	+/-100	12.4	11.7	11.7	9.0	10.9	10.3
	+/-150	-	11.3	-	-	9.1	-
	+/-200	-	11.5	-	-	7.4	-
B	+/- 50	-	10.6	-	-	15.4	-
	+/-100	12.5	8.6	8.5	11.0	14.2	13.6
	+/-150	-	8.0	-	-	12.3	-
	+/-200	-	9.8	-	-	9.0	-
C	+/- 50	-	7.9	-	-	19.6	-
	+/-100	9.1	6.2	6.1	13.9	18.4	18.8
	+/-150	-	5.9	-	-	16.4	-
	+/-200	-	6.6	-	-	12.7	-

In comparing the three specimens, both K_{eff} and h_{eff} decrease with increasing shear-strain. However, K_{eff} at 200 % shear-strain is a little larger than at 150 % shear-strain. This increase is considered due to the generation of hardening phenomenon in the hysteresis loop near 200% shear-strain. As a whole, rubber A has the largest K_{eff} , followed by B and C. On the other hand, rubber C has the largest h_{eff} , followed by B and A. All these have the same tendency with test results on physical properties shown in Table 1 and 2.

At 100 % shear-strain, in frequency dependence of K_{eq} and h_{eq} , K_{eq} at 0.1 Hz is larger than at any other frequencies, and h_{eq} at 0.1 Hz is smaller than at any frequencies.

From above results, the properties of the three rubbers are summarized as follows. Although rubber C is considered to be the most desirable in a high damping aspect, because of its large h_{eq} , but it is too soft and its h_{eq} is greatly dependent on frequency, shear-strain and temperature. On the other hand, rubber A has smaller h_{eq} than any other rubbers. Therefore, though rubber B has a little smaller h_{eq} than rubber A, since other properties of rubber B are relatively better, rubber B has been chosen for the dynamic loading test at PWRI.

DYNAMIC LOADING TEST AT PWRI

Test Methods Laminated HDRB was fabricated with rubber B. The HDRB model 300 mm in diameter was made by laminating 24 \times 5.0 mm rubber plates and 23 \times 2.3 mm steel plates, as shown in Fig.6. Table 5 and Photo 3 show loading condition of the dynamic loading tests. The tests were conducted in a room kept at 20°C, using a single model for series 1 ~ 4 in order to evaluate fundamental properties. A different model was used for series 5 ~ 6 to evaluate durability of the HDRB.

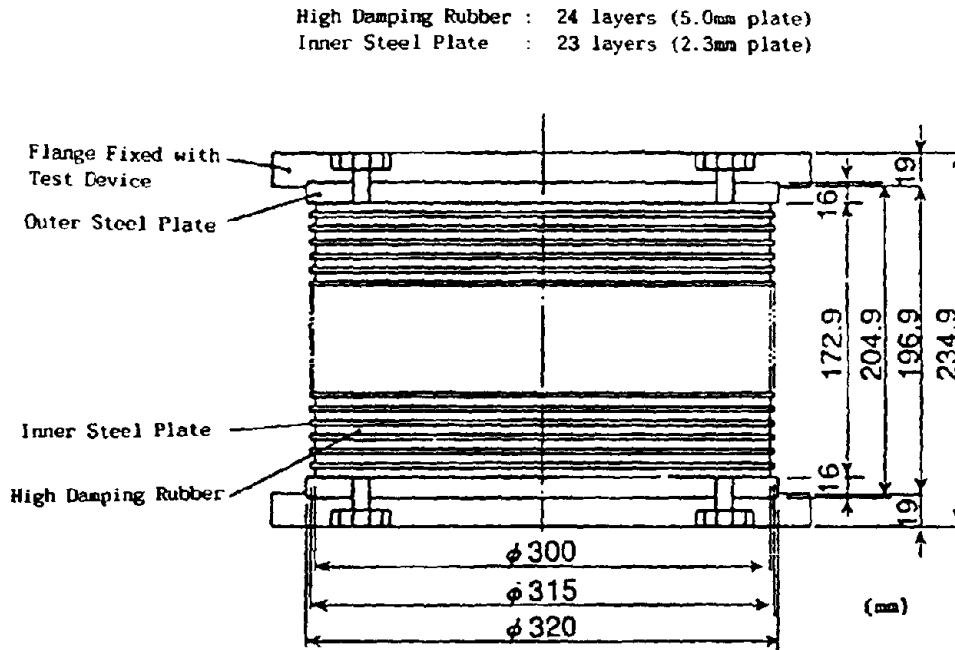


Figure 6 Model of HDRB

Table 5 Test Condition of the Cyclic Loading Tests at PWRI

Series No.	Bearing Stress (kgf/cm ²)	Frequency (Hz)	Pre-strain (%)	Strain (%)	Cycles for Each Strain	Model Used
1	60	0.1	0	25,50,100,150,200	10	No.1
2	60	0.1	0	25,50,100,150,200	10	
3	60	1.0	0	25,50,100,150	10	
4	60	0.1	50	25,50,100,150	10	
5	60	0.5	0	150	40	No.2
6	60	0.5	0	150	40	



photo 3 Dynamic Loading Test at PWRI

Test Results Figs.7 and 8 show examples of typical force-displacement hysteresis loops. Shear modulus $G_{e,s}$ and effective damping ratio $h_{e,s}$ were obtained by Eq.(3) and (4). $G_{e,s}$ and $h_{e,s}$ were obtained for each cycle, but Table 6 shows the values at cycles 1,3 and 10 in series 1 ~4 and the values at cycles 1,10 and 40 in series 5 ~6. Figs. 9 and 10 show relationships of $G_{e,s}$ vs number of cycles and $h_{e,s}$ vs. number of cycles for various strains from 25 % to 200 %. Figs. 11 and 12 show relationships of $G_{e,s}$ vs. shear-strain and $h_{e,s}$ vs. shear-strain from 25 % to 200 % for series 1 and 2. Furthermore, Figs. 13 and 14 show relationships of $G_{e,s}$ vs. number of cycles and $h_{e,s}$ vs. number of cycles for series 5 and 6.

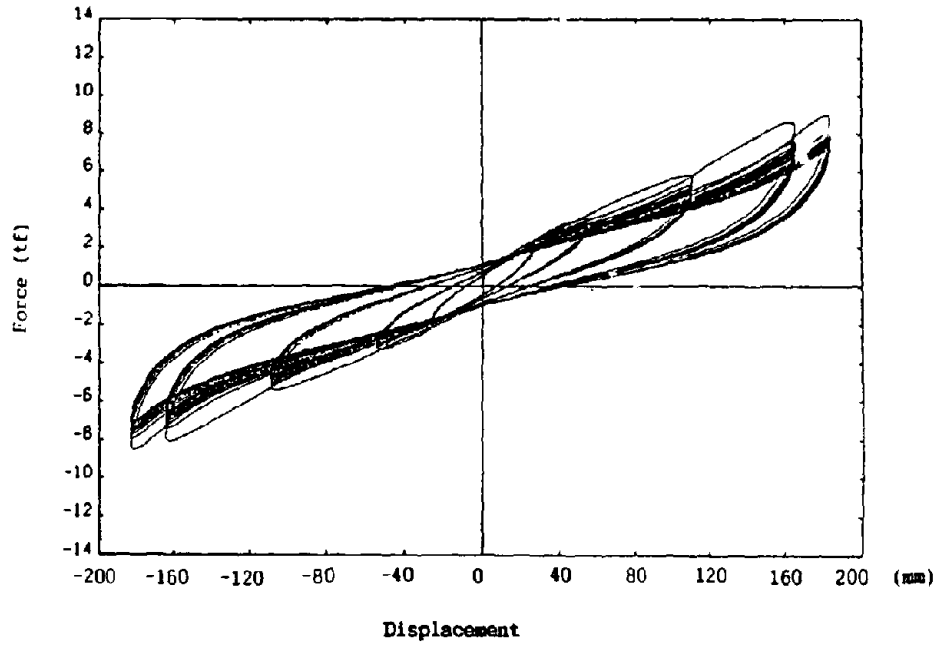


Figure 7 Force ~Displacement Hysteresis Loop of HDRB (Series No.1)

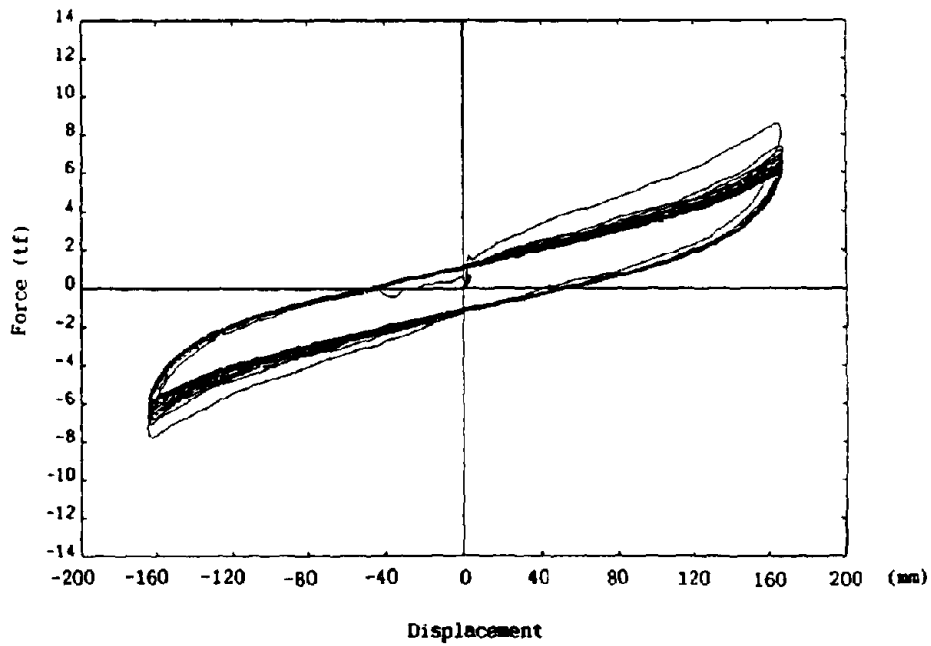


Figure 8 Force ~Displacement Hysteresis Loop of HDRB (Series No.5)

Table 6 Test Results of the Cyclic Loading Test at PWRI

Series No.	Strain (%)	Shear Modulus $G_{s,c}$ (kgf/cm ²)			Effective Damping Ratio $h_{s,c}$ (%)		
		cycle			cycle		
		1st	3rd	10th	1st	3rd	10th
1	+/- 25	13.9	12.9	12.4	14.1	13.1	12.8
	+/- 50	10.7	9.8	9.4	12.9	12.2	12.1
	+/-100	8.8	7.8	7.4	12.4	11.5	11.4
	+/-150	8.7	7.5	6.8	11.2	10.5	10.6
	+/-200	8.2	7.2	6.6	10.4	10.1	10.3
2	+/- 25	9.5	9.3	9.2	15.4	14.6	14.1
	+/- 50	7.9	7.5	7.3	13.7	13.5	13.3
	+/-100	6.6	6.1	5.9	13.2	12.7	12.5
	+/-150	6.8	6.2	5.9	11.5	11.1	11.0
	+/-200	7.2	6.6	6.2	10.4	10.0	10.1
3	+/- 25	11.6	10.8	10.3	16.3	15.4	14.4
	+/- 50	8.9	8.0	7.7	16.3	15.5	14.3
	+/-100	7.0	6.0	5.7	16.8	15.6	14.1
4	50+/- 25	9.1	8.8	8.7	16.8	15.6	15.0
	50+/- 50	7.8	7.3	7.1	14.5	14.8	14.7
	50+/-100	7.3	6.6	6.4	13.0	12.7	12.7
	50+/-150	7.4	6.8	6.5	11.7	11.5	11.8
		cycle			cycle		
		1st	10th	40th	1st	10th	40th
5	+/-150	9.7	7.0	6.2	13.7	11.9	11.0
6	+/-150	8.4	6.7	6.1	12.4	11.3	10.7

The following results were obtained for shear modulus $G_{s,c}$ and effective damping ratio $h_{s,c}$ from Table 6 and Figs. 9~14.

(a) Effect of Cycles

$G_{s,c}$ and $h_{s,c}$ at 0.1Hz (series 1) decrease up to 3 cycles as number of loading cycle increases, and then they approach to a certain value. However, at 1Hz (series 3), $h_{s,c}$ still decreases up to 10 cycles.

(b) Effect of Strain

$G_{s,c}$ and $h_{s,c}$ decrease with increasing shear-strain, as shown in Figs. 9~12. Although $G_{s,c}$ decreases greatly from 25% to 100% shear-strain, it slightly decreases over 100% shear-strain. $h_{s,c}$ gradually decreases as shear-strain increases from 25% to 200%.

(c) Effect of Repeated Loading

As shown in Figs 11 and 12, $G_{s,c}$ and $h_{s,c}$ for 2nd loading (series 2) are smaller than those for 1st loading (series 1). The difference of $G_{s,c}$ and $h_{s,c}$ between the 1st and 2nd loading decreases with increasing shear-strain, being almost negligible at 200% shear-strain.

(d) Effect of Frequency

Comparing series 2 with series 3 presented in Table 6, $G_{s,c}$ and $h_{s,c}$ slightly decrease with increasing frequency.

(e) Effect of Pre-strain

Comparing series 2 with series 4 presented in Table 6, $G_{s,c}$ and $h_{s,c}$ do not affected by whether pre-strain is presented or not.

(f) Reliability of Long-term Cyclic Loading

As shown in Figs. 13 and 14, $G_{s,c}$ and $h_{s,c}$ during 2nd loading are slightly smaller than those during 1st loading. Table 6 also indicates that they approach to a certain value after 10 cycles.

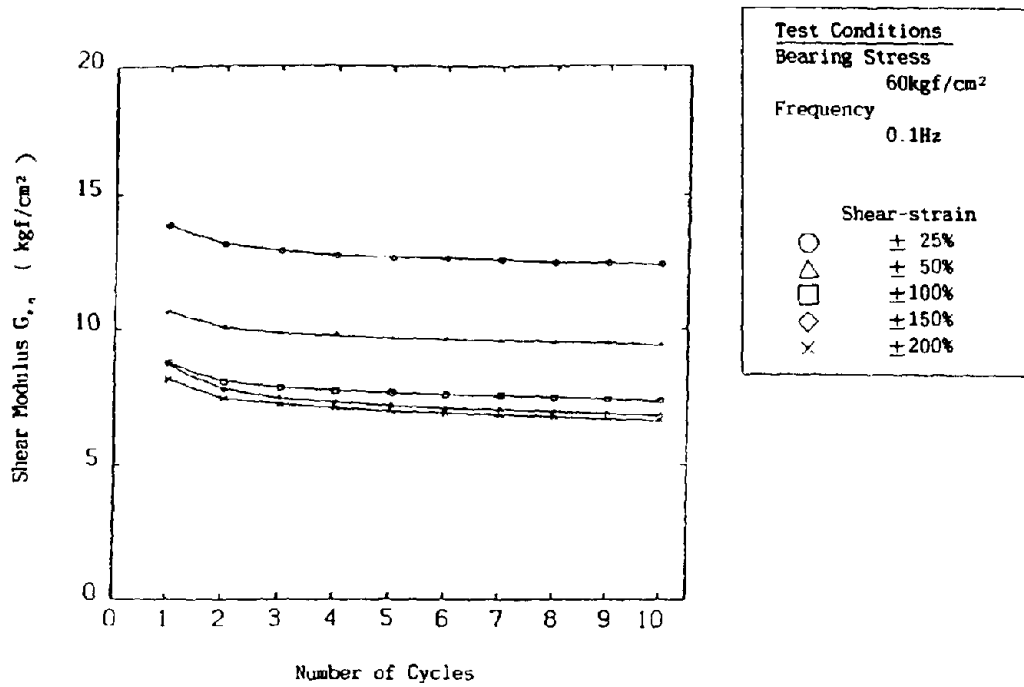


Figure 9 Effect of Shear-strain on Shear Modulus

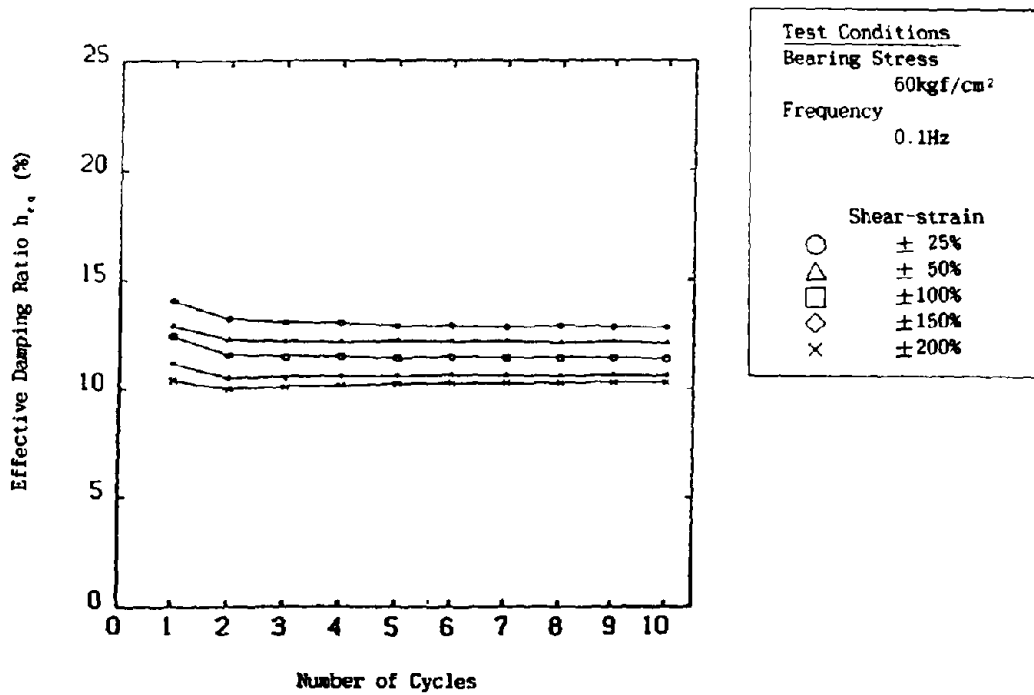


Figure 10 Effect of Shear-strain on Effective Damping Ratio

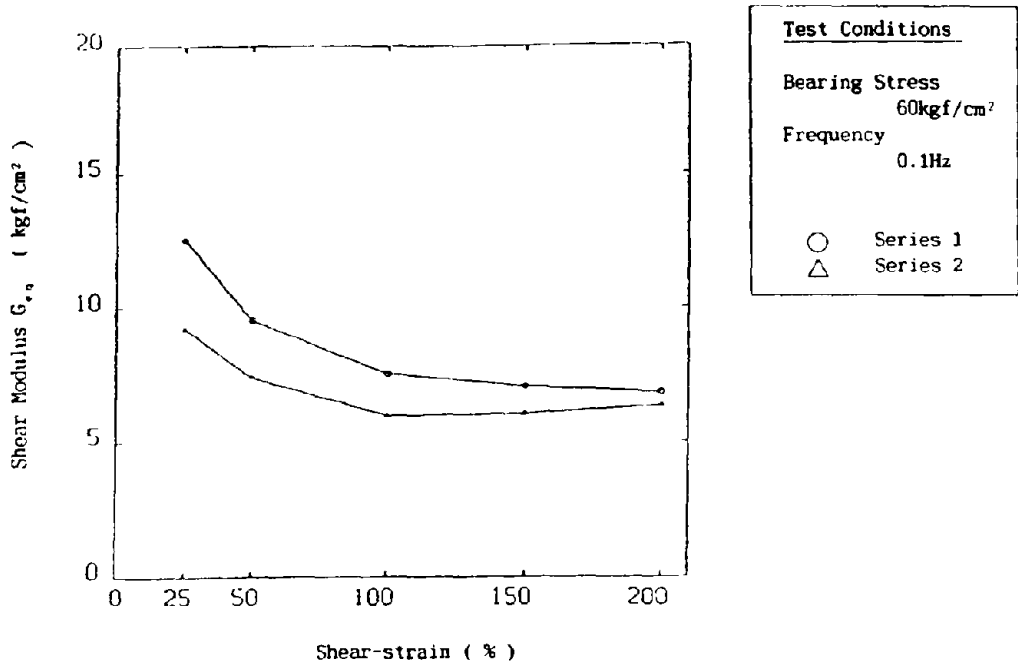


Figure 11 Difference in Shear Modulus between 1st and 2nd Loading

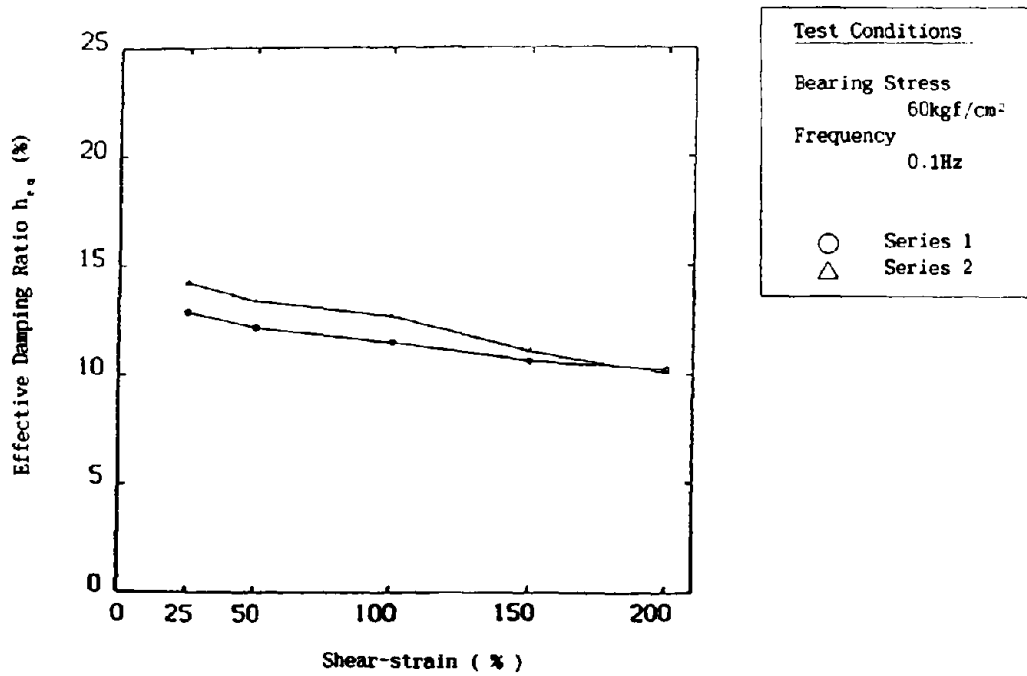


Figure 12 Difference in Effective Damping Ratio between 1st and 2nd Loading

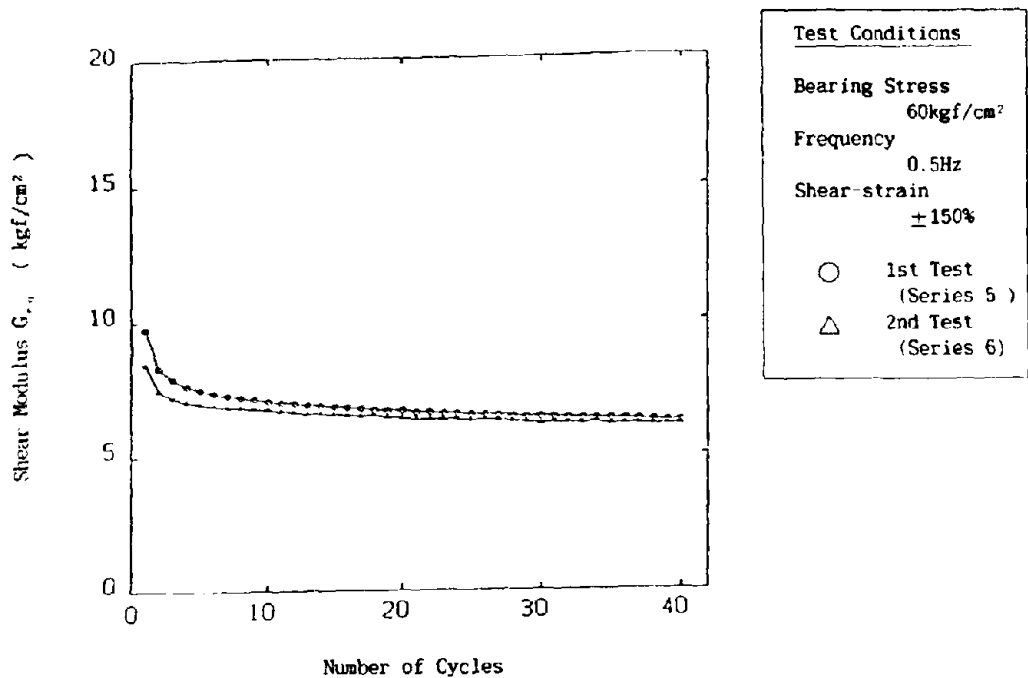


Figure 13 Shear Modulus vs. Number of Cycles

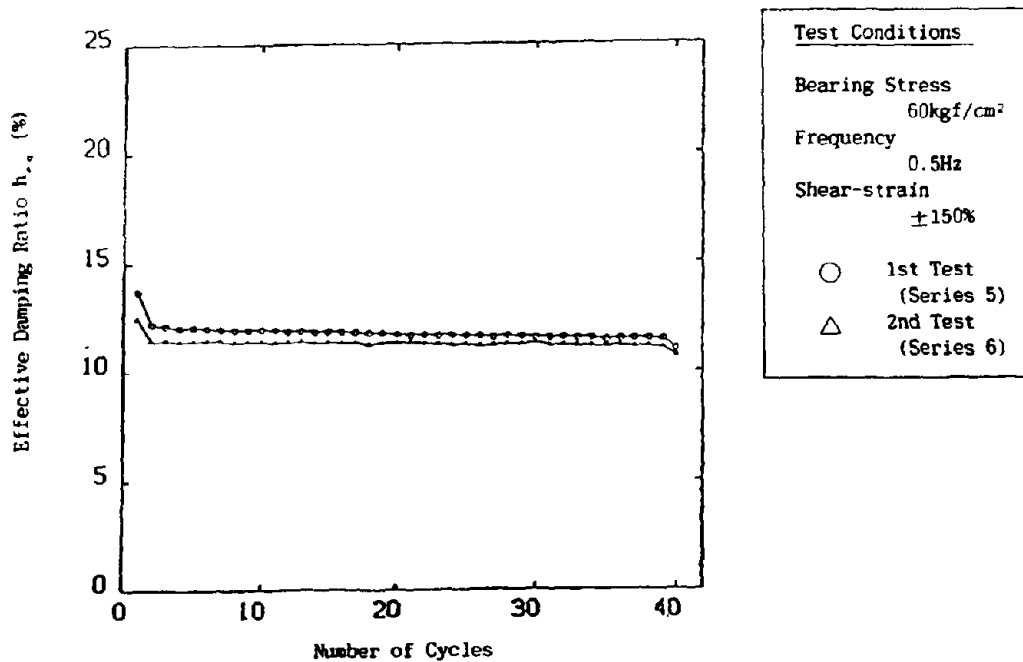


Figure 14 Effective Damping Ratio vs. Number of Cycles

CONCLUSION

From the results presented here, the following conclusions were obtained.

- (1) Effective damping ratio $h_{e,q}$ was within 10~15%.
- (2) Dependence of $G_{e,q}$ and $h_{e,q}$ on loading cycle, shear-strain, frequency and pre-strain was investigated. As a result, it was found that frequency and pre-strain dependence of $G_{e,q}$ and $h_{e,q}$ was less sensitive.
- (3) For studying the durability, 40 times loading with shear-strain of 150% was made twice leaving 3 hours between the two tests. It was found that $G_{e,q}$ and $h_{e,q}$ of the second test were almost the same with those of the first test. No visible failure was developed during the two tests.

ACKNOWLEDGEMENT

The development of the High Damping Rubber Bearing (Part 3) was made as a part of the joint research program on "Development of Menshin Systems of Highway Bridges" between PWRI and Showa Electric Wire and Cable Co., Ltd. Grateful acknowledgement is made to Dr. K. Kawashima, Mr. K. Hasegawa, Mr. S. Unjo and Mr. H. Nagashima of the Earthquake Engineering Division of PWRI for their cooperation.

FINITE ELEMENT ANALYSIS OF ELASTOMERIC ISOLATION BEARINGS FOR DIFFERENT CONNECTION DETAILS

Ian G. Buckle and He Liu
Department of Civil Engineering
State University of New York at Buffalo

INTRODUCTION

Elastomeric bearings are widely used for the seismic isolation of bridges and buildings, not only in the United States, but around the world. In most cases the elastomer is natural rubber which may be compounded to enhance its damping properties or the bearing itself may enclose a lead core for the same purpose, i.e. to increase hysteretic energy dissipation during cyclic shear deformations.

Of interest to designers is the mechanical attachment of these bearings to the superstructure above and the substructure below. To avoid the development of high tensile stresses in the elastomer (during periods of high shear strain) shear-only connections have been preferred. These may take the form of a set of dowels or pins which are fixed to the masonry and sole plates and engage in preformed holes in the outer shims of the bearing. Under these circumstances these two particular shims are thickened to accommodate the bearing stresses. Thicknesses up to 1" are commonly specified for this purpose.

However, a shear-only connection has two disadvantages. Since transfer of tension into the bearing is prevented, the connection cannot be used to resist uplift or inhibit roll-over should the bearing be subject to extreme loads (those in excess of the design loads).

For this reason, bolted connections have been proposed and used in some instances in Japan. Nevertheless the concern remains as to the added demand such a connection places on the elastomer and the bond between the elastomer and internal steel laminates during combined compression and shear loads.

This paper describes some preliminary work done using a nonlinear finite element computer program, to study the effect of different end conditions on internal stress and strain states in elastomeric bearings at high shear strain. The purpose is to give some insight into the above issues.

FINITE ELEMENT ANALYSIS

A nonlinear finite element computer program, ADINA [1], was used for the displacement and stress analysis in this study. Many different analysis options are available in ADINA and in this instance the behavior of multilayer elastomeric bearings under monotonically increasing compressive and shear loads was investigated.

This displacement-based finite element method can solve nonlinear problems involving almost incompressible materials. However, the number of elements required to obtain acceptable accuracy is usually much greater than in a comparable problem involving compressible materials. A displacement-pressure finite element formulation has been introduced in ADINA to explicitly replace the pressure computed from the displacement field by a separately interpolated pressure function. The formulations in ADINA permit geometrical and material nonlinearity in compressible and almost incompressible solids. Incremental nonlinear analysis including contact boundary conditions may also be performed.

A modified Mooney-Rivlin [2] material description was chosen to characterize rubber undergoing large displacements and large strains. Conventional Mooney-Rivlin materials assume the material to be totally incompressible; but for an almost incompressible material like rubber, a better assumption is that the bulk modulus is several thousand times as large as the shear modulus [3, 4, 5]. A hydrostatic work term is also added into the strain energy function.

To reduce the computational effort, the bearings studied in this paper were assumed to be infinitely long strips, so that two-dimensional plane strain elements could be used in the calculation. Since theoretical and numerical analysis show that a displacement pressure element with nine nodes and three pressure variables exhibits the best pressure approximation [6], a plane strain finite element with these degrees of freedom was chosen.

To prevent material overlapping at free surfaces during large deformations, contact boundary elements were used [7]. In the region of contact, surface tractions were evaluated from the externally applied forces, the nodal point forces and Coulomb's law of friction. Surface tractions between nodal points were employed to decide whether a nodal point is in sticking or sliding contact, or is releasing (surface separation).

ISOLATION BEARING EXAMPLES

In this study, six elastomeric bearings were studied using ADINA to determine the influence of end connection details on bearing deformations and stresses. These six bearings were all 6 inches in overall width and comprised 4 internal, 1/2 inch thick, rubber layers for a total rubber thickness of 2 inches. For the purpose of this study, a 1" wide slice of each bearing was analyzed using the plane strain assumption. The six bearings were characterized by 3 different connection types and 2 different end plate thicknesses. Details are shown in Table 1 and Figure 1. Material properties for the elastomer (natural rubber) and steel are summarized in Table 2.

In all cases, the compressive load was maintained constant at 0.5 ksi (total load = 3 kips) while the shear deformation was increased until convergence could no longer be obtained. The maximum applied shear strain ranged from 1.5 to 2.3 .

Group No.	Bearing No.	Connection Type	Width * Height (in*in)	No. of Internal Rubber Layers	Thickness of Rubber Layers	Thickness of Steel Shims (in)	Thickness of Steel End Plates (in)
1	D-1	doweled	6*4.625	4	0.5	0.125	1.0
	B-1	bolted	6*4.625	4	0.5	0.125	1.0
	F-1	fixed	6*4.625	4	0.5	0.125	1.0
2	D-2	doweled	6*3.125	4	0.5	0.125	0.25
	B-2	bolted	6*3.125	4	0.5	0.125	0.25
	F-2	fixed	6*3.125	4	0.5	0.125	0.25

Note: D = doweled connection
 B = bolted connection
 F = fully fixed connection

TABLE 1: DIMENSIONS AND INTERNAL CONSTRUCTION DETAILS OF EXAMPLE BEARINGS

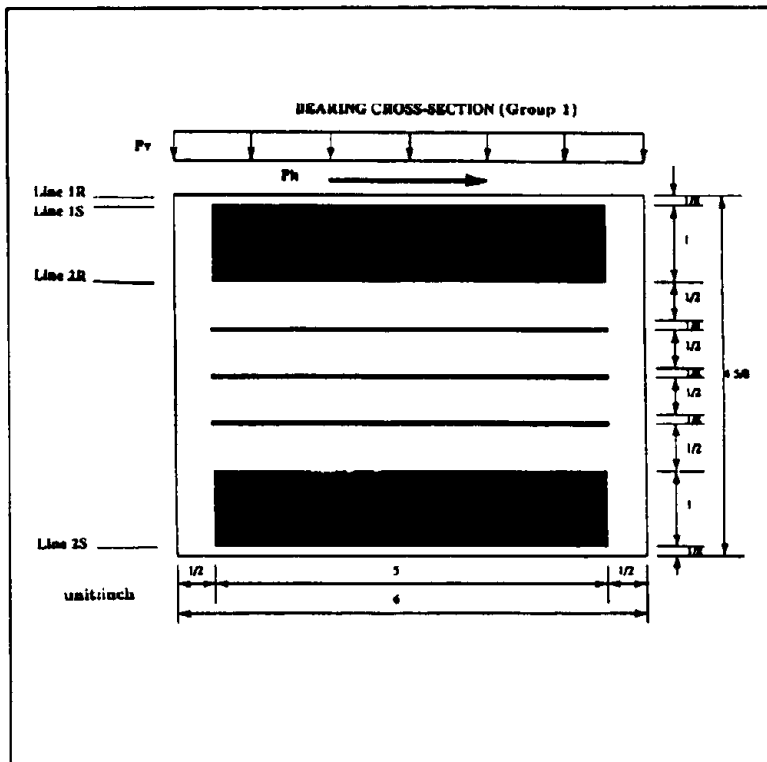
Material	Shear Modulus (ksi)	Young's Modulus (ksi)	Bulk Modulus (ksi)
Rubber	0.136	0.408	204.21

(a) Rubber Properties

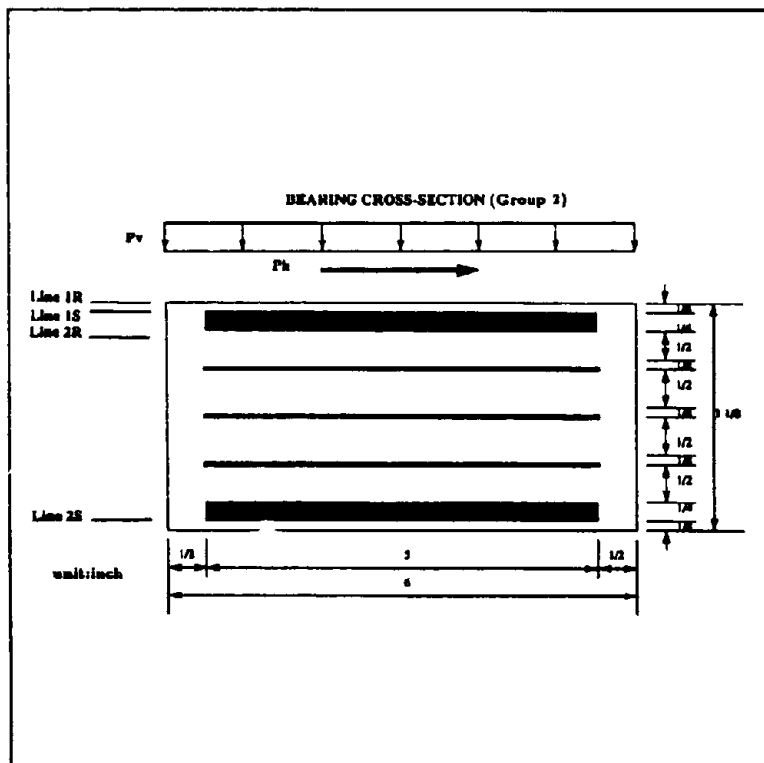
Material	Young's Modulus (ksi)	Yield Stress (ksi)	Strain Hardening Modulus (ksi)
Steel	30,000	44	300

(b) Steel Properties

TABLE 2: MATERIAL PROPERTIES ASSUMED FOR EXAMPLE BEARINGS



(a)



(b)

FIG. 1 DIMENSIONS OF BEARINGS

ADINA MODEL OF BEARINGS

As shown in Figure 2, the finite element mesh for the ADINA model of these bearings comprised 204, 9-node elements (134 rubber elements and 70 steel elements). The sole plate (that plate which is fixed to the superstructure) was modelled as a 1" thick plate which was free to move both horizontally and vertically but not rotate. The masonry plate (that which is fixed to the substructure) was represented by a fixed boundary and contact surface as appropriate; this boundary was constrained against translation and rotation.

Contact boundary elements used a Coulomb friction law with a 0.7 coefficient of friction. These elements were used on the upper and lower surfaces to permit the separation of the bearing from external plates as necessary (see for example the doweled connections in Figure 2(a)) and also on selected vertical surfaces to prevent material overlapping at high shear deformations.

Material properties have been listed in Table 2. The corresponding Mooney-Rivlin constants for the elastomer were $C_1 = 0.0424$ ksi and $C_2 = 0.0256$ ksi .

RESULTS

As noted above, the finite element method was applied in this study to multilayer elastomeric bearings under large shear deformation. This study was conducted to determine the characteristics of, and the stress distributions in, multilayer elastomeric bearings while at large shear strains. In this section, results relating to the following issues are briefly presented: bearing deformations, shear stiffness and stress distributions in the outer rubber layers. In each case the effect of end connection type is illustrated. Finally some data on bolt forces (in the bolted connection detail) are presented.

Bearing Deformations

One of the main benefits of the finite element method is that it provides estimates of the performance of multilayer elastomeric bearings under extreme loads and deformation. Each bearing in the present study was first loaded in compression and then deformed in shear. Figure 3(a,b,d) shows the deformed finite element meshes of the three Group 1 bearings at approximate compressive and shear strains of 10% and 150%, respectively. For comparative purposes Figure 3(c) shows bearing B-1 at 230% shear strain. It is seen that as the combined compressive and shear deformations increase, the principal strain distribution changes markedly. The maximum compressive strain in the elastomer appears to be in the upper left and lower right corners of the bearings whereas the maximum tensile strains appear to be in the opposite corners. It will also be seen that whereas the end plates remain largely unaffected, the internal shims are significantly deformed in flexure as the shear load is applied. High flexural stresses are to be expected in these shims. The effect of end connection type is seen by comparing Figure 3(a) with 3(b). The separation of the contact surfaces in Figure 3(a) is clearly

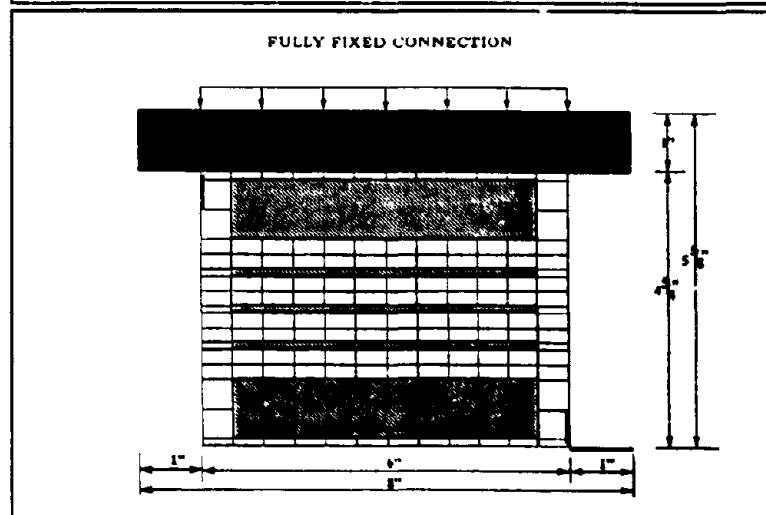
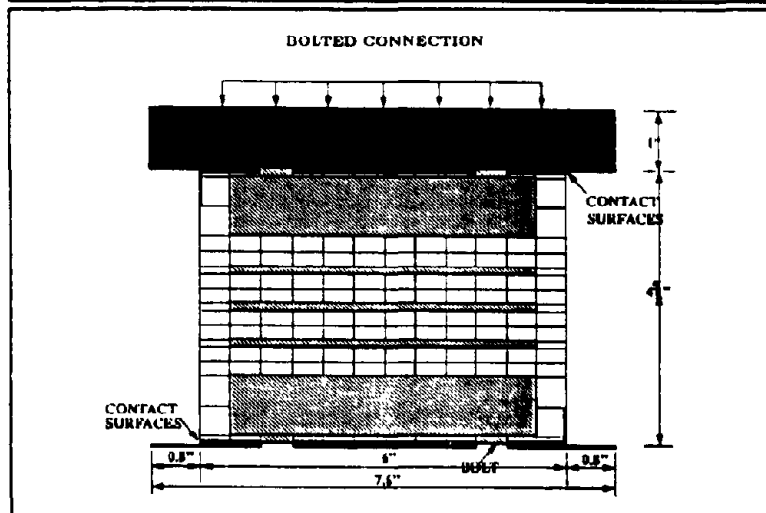
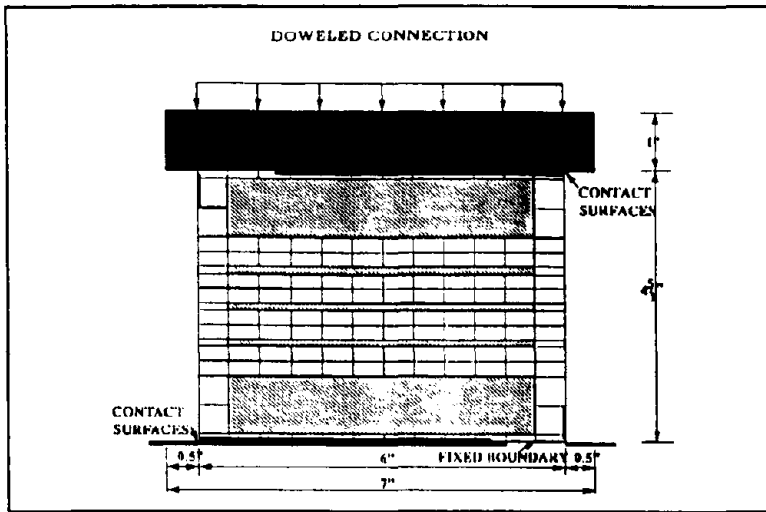


FIG. 2 FINITE ELEMENT MESHES FOR EXAMPLE BEARINGS SHOWING 3 END CONDITIONS

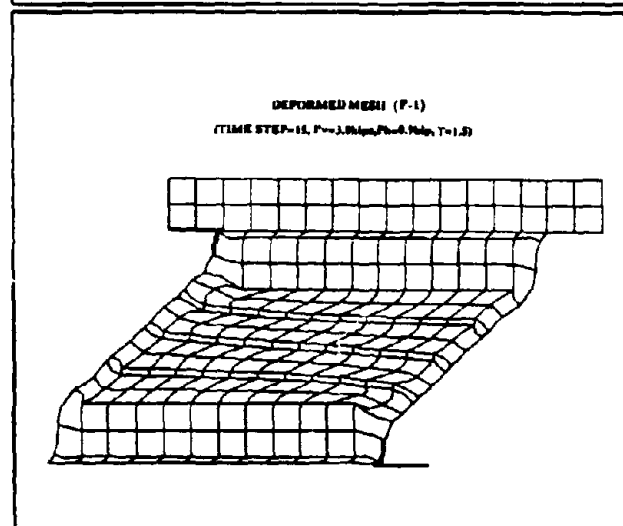
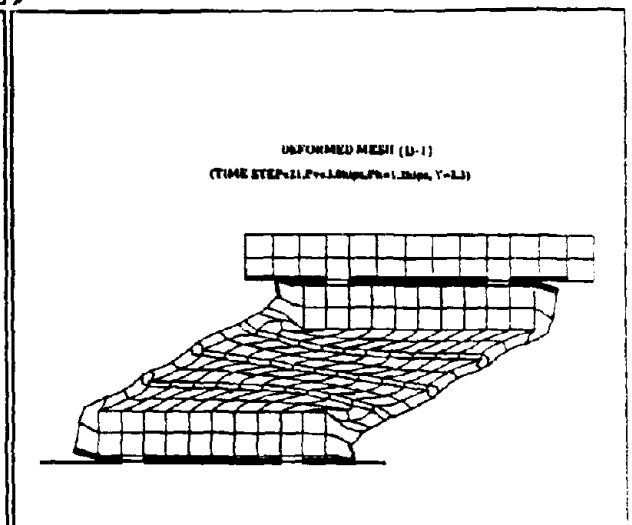
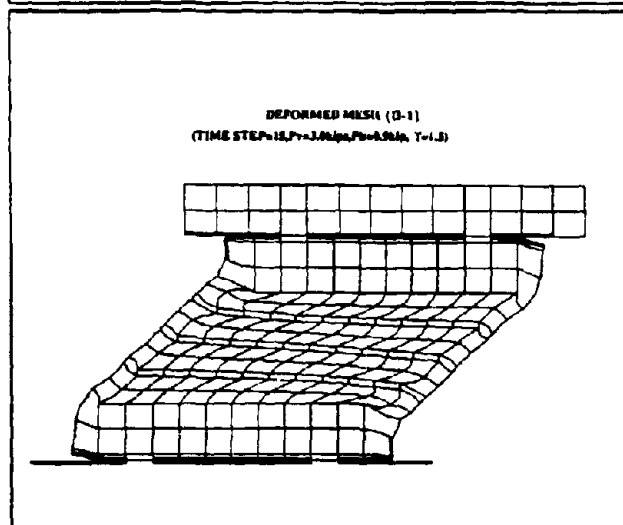
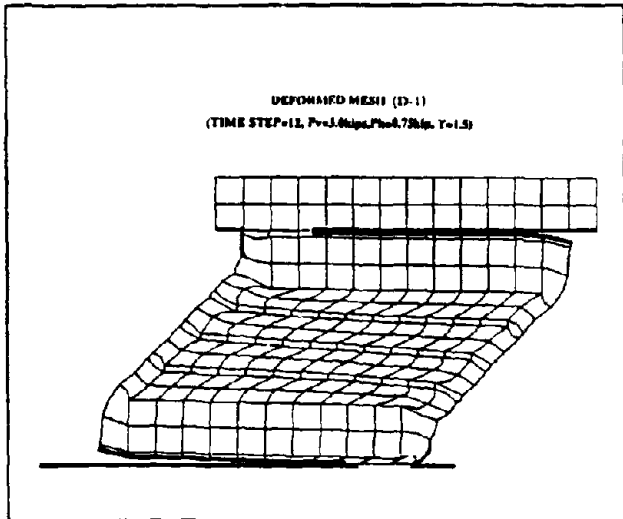


FIG. 3 GROUP 1 BEARING DEFORMATIONS SHOWING EFFECT OF DIFFERENT END CONDITIONS AT $\gamma=1.5$ AND 2.3

evident due to the lifting (tilting) of the bearing end plate. This action is suppressed when bolted connections are used, and the only separation evident in Figures 3(b) and (c) is in the side cover rubber layers. In the fully fixed case, even the separation in these cover layers is prevented (Figure 3(d)).

Shear Stiffness

Figure 4(a) compares the shear properties of the bearings for the different end conditions. As shown in these force-displacement plots, all six bearings show the same linear behavior at strains less than 50%, but that nonlinearities and differences in stiffness occur and become more pronounced at higher shear strains. The bearings with the bolted connection show the higher shear stiffness while those with doweled connections show the lower shear stiffness. When the shear strain approaches 100%, the slope of the force-displacement curve in doweled condition (D-1, D-2) appears to start decreasing while the shear stiffnesses in the bolted (B-1, B-2) and fixed conditions (F-1, F-2) remains constant. At about 175%, even these bearings begin to show a decrease in shear stiffness and may even approach zero at 300%. This is in contrast to observations made in practice on the bolted bearings where stiffening effects have been reported at very high shear strains. However, it should be remembered that in these analyses the rubber is modelled as a nonlinear elastic material with no hysteretic properties. Real rubber properties at high shear strain are not included and it is felt that the softening seen here is due to a critical or buckling load state being approached at these high shear strains. (At 300% shear strain, the top plate has been displaced 6 inches and totally overhangs the 5 inch bottom plate – i.e. the area of the effective column is now negative.)

There are generally three limit states in the design of isolation bearings, of which two are stability-related deformation modes. The first of these is the stability of the bearing against buckling and the corresponding reduction in lateral stiffness. This phenomena may account for the softening of the fixed and bolted bearings as just discussed. The second is the stability of the bearing against overturning which may become critical under a combination of low compressive load and high shear force. This behavior is characteristic of doweled bearings as illustrated in Figure 5(a). This figure shows a bearing deformed laterally by shear forces (V) while carrying an axial load (P). If overturning is imminent, the axial forces act at the extreme edges of the upper and lower shims or dowel plates. Figure 5(b) shows the possible shear force-displacement diagram for typical linear and nonlinear bearings and illustrates the limiting effects of overturning [8]. It is seen in Figure 4(a) that, when the nominal shear strain is over 150%, the bearings with doweled connections show a tendency to lose shear stiffness rapidly. Rollover effects are beginning to control the behavior at these shear strains and this is illustrated in Figure 4(b). Since it was not possible to use ADINA to compute the shear-displacement curve through the negative stiffness region, the theoretical rollover curves of Figure 5(b) are laid over those of Figure 4(a), and the result shown in Figure 4(b) is obtained. The match between these curves suggests that the onset of rollover in the doweled bearings is imminent. These curves also show the restraint provided against rollover by bolted or fully-fixed connections.

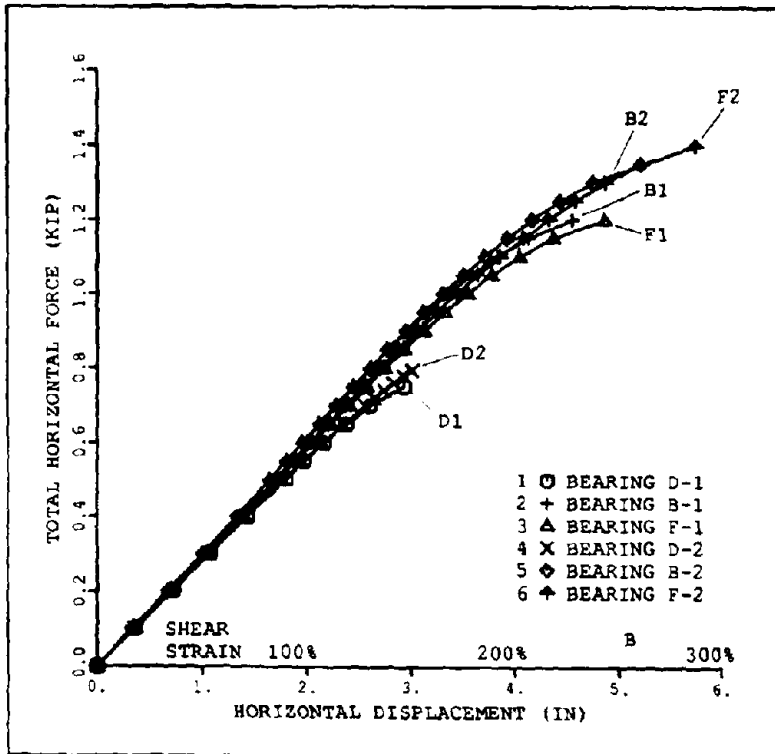


FIG. 4(a) TOTAL FORCE-DISPLACEMENT RESPONSE FOR BEARINGS WITH DIFFERENT END CONDITIONS

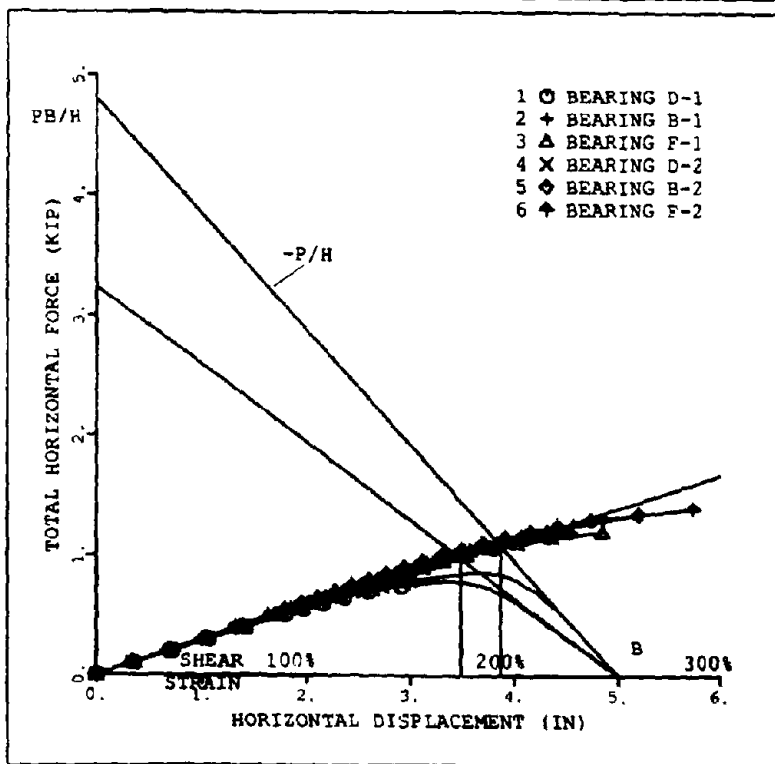
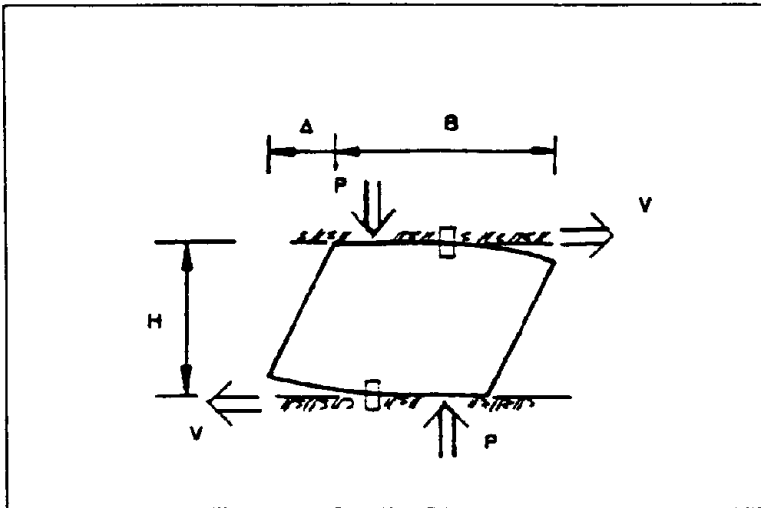
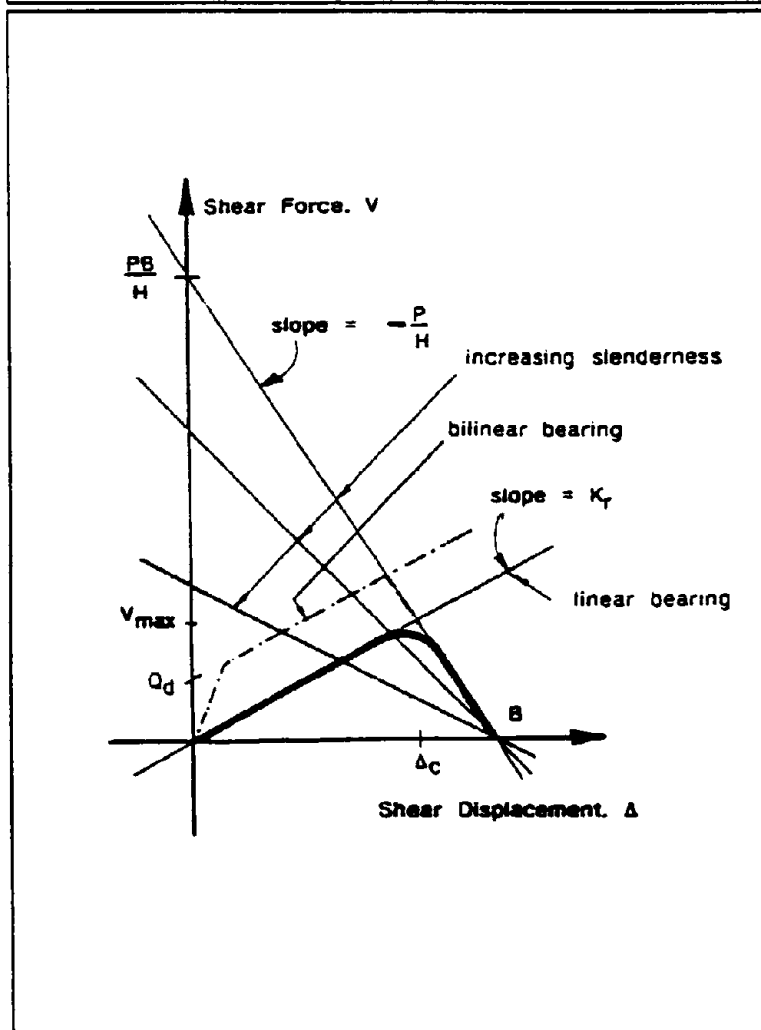


FIG. 4(b) ROLLOVER CURVES FOR BEARINGS WITH DOWEL CONNECTIONS



(a)



(b)

FIG. 5 ROLLOVER

Stress Distribution in the Outermost Rubber Layers

Stress distributions in the elastomer at a nominal shear strain of 150% are compared along line 2R (see Figure 1(a)) in Figure 6. Three stress components are plotted. These are the vertical compressive stress, σ_{xx} , the horizontal tensile stress, σ_{yy} , and the shear stress, σ_{xy} .

In every instance the stresses for the doweled end connection are less than either of the other two cases. Although this trend is consistent with the physical release that the dowel connection provides, the amount of relief is actually very small. In other words the maximum axial stress in the elastomer in the outer layer is relatively insensitive to the connection detail. Even when the thickness of the end plate is reduced from 1 inch to 1/4 inch the changes in axial stresses are small (Figure 7). One conclusion from this limited study is that the use of dowel connections to protect the elastomer from high tensile stresses (and perhaps cavitation) during large shear deformations is of marginal value. It should however be noted that the stresses in the top and bottom cover layers are not so insensitive to the type of connection. Here the doweled and bolted connections completely relieve all tension, but the fully fixed detail requires significant tensile stresses to be transmitted. In this study these stresses peaked at about 0.6 ksi (about twice the elastic modulus of the elastomer).

Internal Forces in the Bolts

Axial and shear stresses in the two bolts shown in Figure 2(b) were computed and these are plotted in Figure 8. Three stress points are plotted in each bolt on line 1S (Figure 1(a)). From these values it is clear that each bolt, in addition to compression and shear, is subject to flexure. Both actions are defined in Figure 8(c) and may be found by integrating the stresses shown in Figures 8(a) and (b). A summary of these actions is given in Table 3 for the case of the 1 inch thick end plate. The results for the thinner plate are not significantly different to those in Table 3.

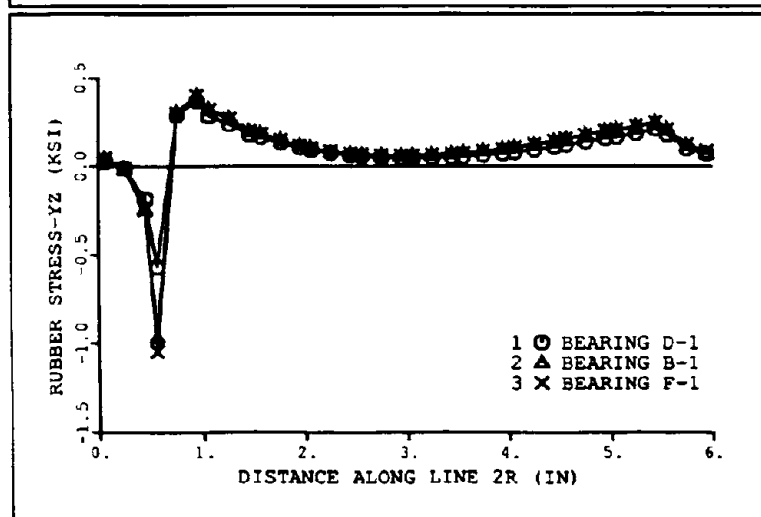
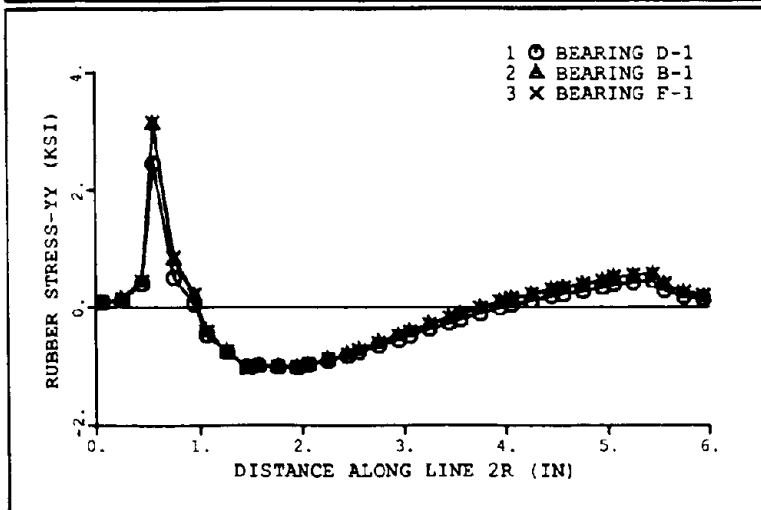
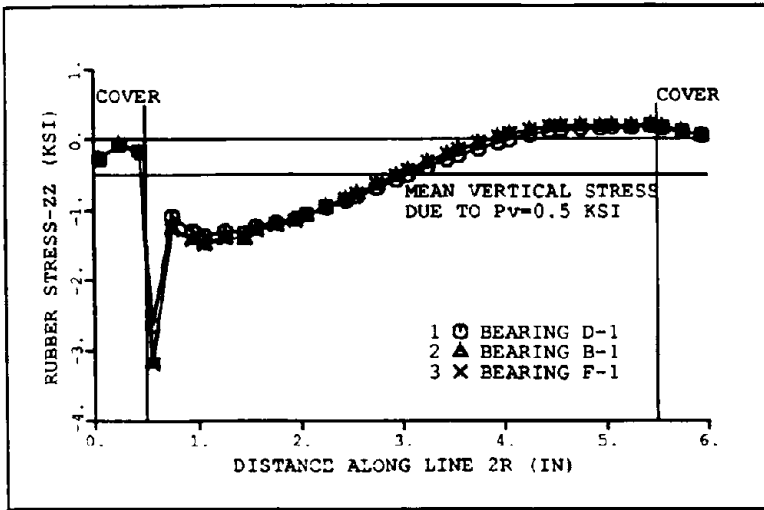
It is seen that between 80 and 85% of the axial load is carried by the bolts at this shear strain; the remainder of P_v is carried by the steel to rubber contact surfaces. This relatively high proportion is due to the high compressive stiffness of this confined layer of thin cover rubber.

By contrast, almost all of the shear is carried by the bolts but this is not surprising since the shear stiffness of the cover rubber is virtually negligible when compared to that of the bolts.

Overall equilibrium of the bearings, using the bolt forces in Table 3, can be readily confirmed as follows:

$$\text{Overturning moment on bearing} = P_v \cdot \Delta + Qh$$

$$\text{Restoring moment on bearing} = 0.5(N_{11} + N_{12} + N_{21} + N_{22})b + (M_{11} + M_{12} + M_{21} + M_{22})$$

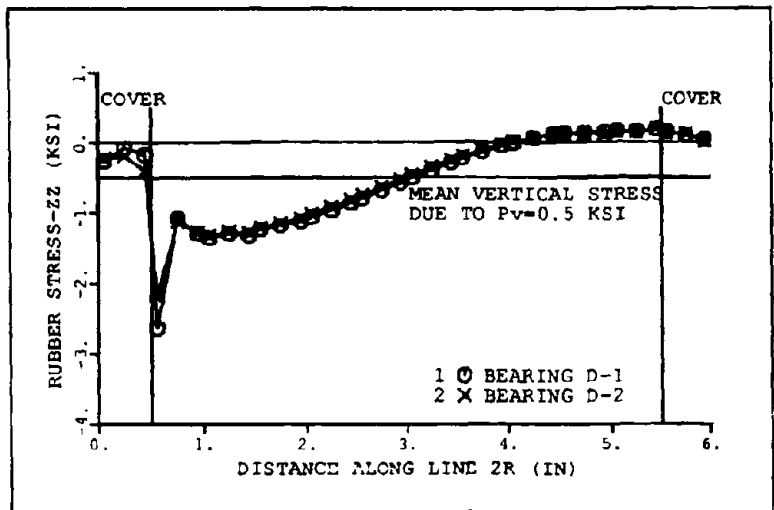


(a)

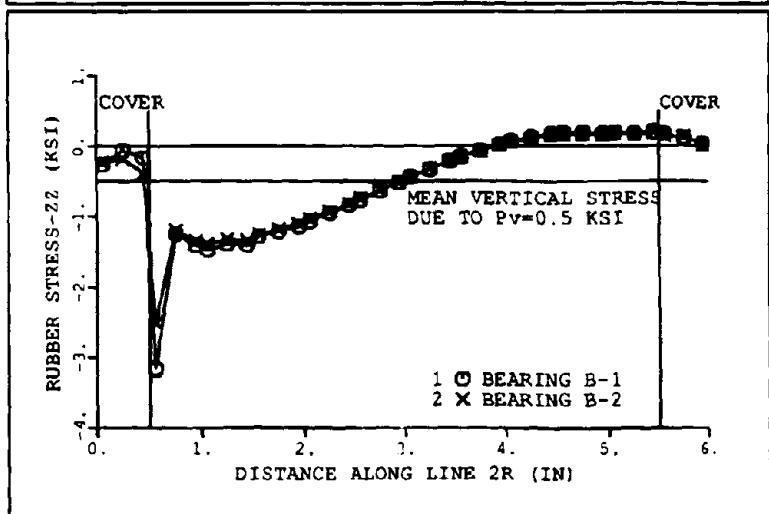
(b)

(c)

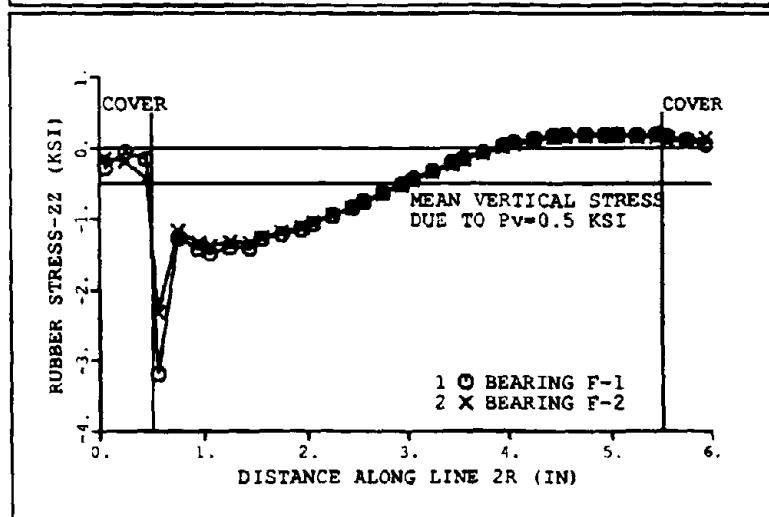
**FIG. 6 STRESS DISTRIBUTION IN
OUTERMOST RUBBER LAYER
FOR GROUP 1 BEARINGS AT
Y=1.5 SHOWING EFFECT OF
DIFFERENT END CONDITIONS**



(a)

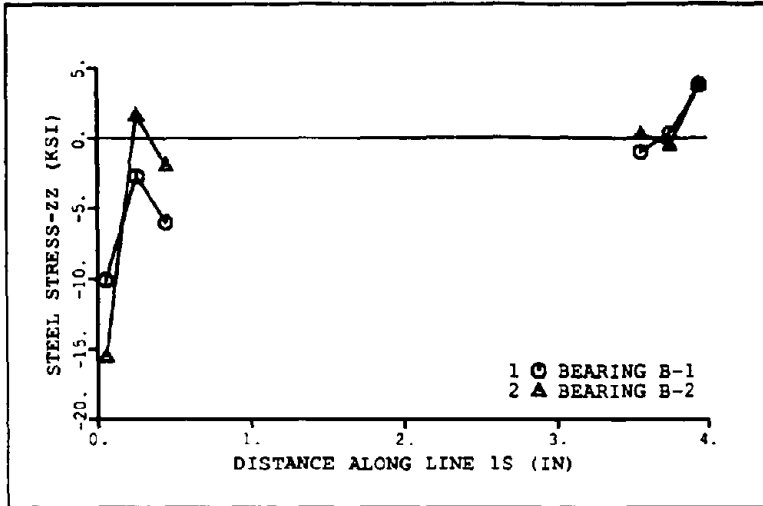


(b)

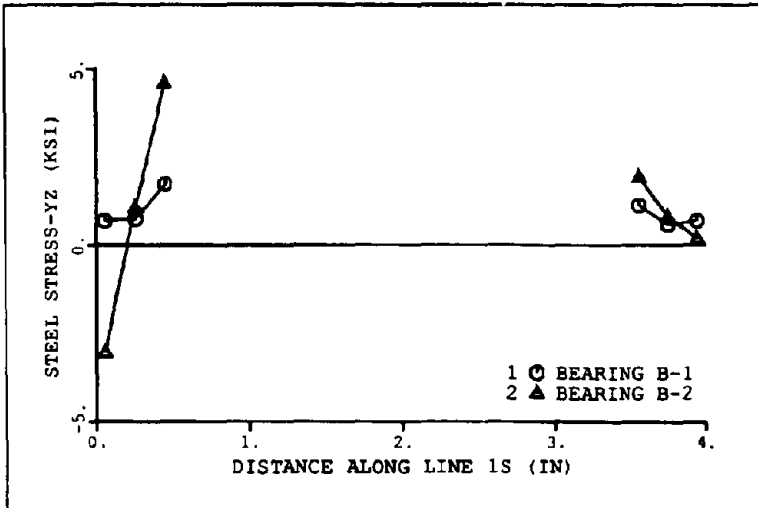


(c)

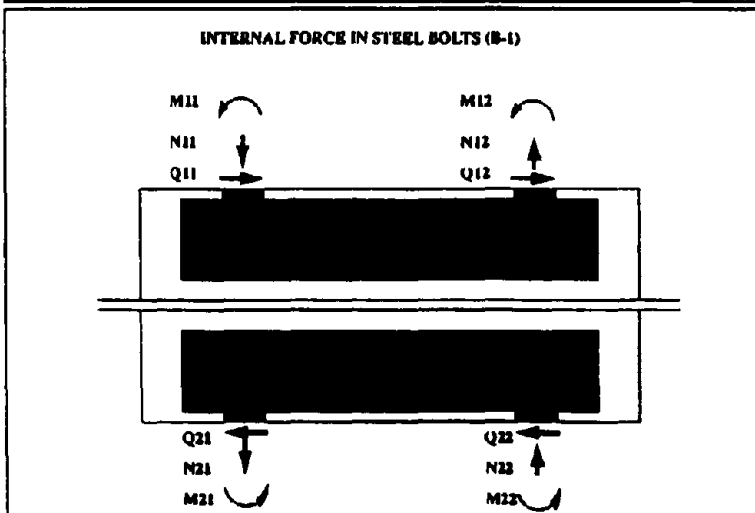
FIG. 7 VERTICAL STRESS DISTRIBUTION IN OUTERMOST RUBBER LAYER FOR DIFFERENT END PLATE THICKNESSES AND DIFFERENT END CONDITIONS



(a)



(b)



(c)

FIG. 8 BOLT STRESSES AND ACTIONS FOR DIFFERENT END PLATE THICKNESS FOR BOLTED CONNECTIONS

(a) Axial Forces (B-1)

Line #1	N_{11} (kip)	N_{12} (kip)	$N_1 = N_{11} + N_{12}$ (kip)	P_v (kip)	N_1/P_v (%)
1	-2.848	0.468	-2.38	-3.0	80
2	0.387	-2.896	-2.509	-3.0	84

(b) Shear Forces (B-1)

Line #1	Q_{11} (kip)	Q_{12} (kip)	$Q_1 = Q_{11} + Q_{12}$ (kip)	P_h (kip)	Q_1/P_h (%)
1	0.505	0.385	0.89	0.9	99
2	0.284	0.604	0.888	0.9	99

(c) Moments (B-1)

Line #1	M_{11} (kip.ins)	M_{12} (kip.ins)	$M_1 = M_{11} + M_{12}$ (kip.ins)
1	0.103	0.119	0.222
2	0.156	0.146	0.302

(B-1, $P_v = 3.0$ kips, $P_h = 0.9$ kip, $\gamma = 1.5$)

TABLE 3: INTERNAL FORCES IN STEEL BOLTS

Where

P_v	= total compressive load = 3.0 kips
Q	= total horizontal shear = 0.9 kips
Δ	= horizontal displacement = 3 inches for $Q = 0.9$ kips
b	= distance between bolts = 4 inches
N_{ii}	= bolt axial forces as defined in Figure 8(c)
M_{ii}	= bolt moments as defined in Figure 8(c)

Using the values for bolt forces given in Table 3:

Overturning moment on bearing at 150% shear strain	= 13.61 kip.ins
Restoring moment calculated from bolt actions	= 13.74 kip.ins

The slight numerical difference between these two moments could be due to the calculation of bolt actions from a very coarse finite element mesh (only one element was used across the full width of each bolt).

CONCLUSIONS

A bolted connection gives rise to virtually the same behavior as a fully fixed connection and essentially prevents rollover from occurring. The reason for using doweled connections is to reduce the tensile stresses in the elastomer when at high shear strain. In practice, the results presented above show minimal difference in tensile stresses within the bearing between bolted and doweled conditions. Additional case studies should be investigated to determine if this is generally true. The advantage of being able to use a bolted connection is increased resistance to rollover and a measure of uplift restraint against extreme overturning loads. If there is no significant difference in internal stresses the bolted connection may become the connection of choice.

REFERENCES

1. ----, "Automatic Dynamic Incremental Nonlinear Analysis -- IN," ADINA Users Manual, Report ARD 90-4, ADINA R&D, Inc., September, 1990.
2. Rivlin, R.S., "Large Elastic Deformations of Isotropic Materials IV, Further Developments of the General Theory," Phil. Trans. A241, 1948.
3. Penn, R.W., "Volume Changes Accompanying the Extension of Rubber," Trans. Soc. Rheology 14, 1970.
4. Ogden, R.W., "Volume Changes Associated with the Deformation of Rubber-like Solids," J. Mech. Phys. Solids 24, 1976.
5. Treloar, L.R.G., "Dilation of Rubber on Extension," Polymer 19, 1978.

6. Bathe, K.J., "Nonlinear Finite Element Analysis and ADINA," Proc. 6th ADINA Conference, Massachusetts Institute of Technology, Cambridge, June 1987.
7. Bathe, K.J. and Chaudhary, A., "A Solution Method for Planar and Axisymmetric Contact Problems," Intl. J. for Numerical Methods in Engineering, Vol. 21, 1985.
8. Buckle, I.G. and Kelly, J.M., "Properties of Slender Elastomeric Isolation Bearings during Shake Table Studies of a Large Scale Model Bridge Deck," American Concrete Institute, Special Publication SP-94, 1986, pp. 247-269.

FINITE ELEMENT ANALYSIS OF ELASTOMERIC BEARINGS

by

R. Shepherd* and L. J. Billings**

ABSTRACT

An awareness of the limited understanding of the mechanics of elastomeric bearings under large compression and shear loads, coupled with the availability of advanced computer codes, prompted a study using finite element techniques. The analytical results obtained are compared with those obtained using existing simplistic design considerations and with experimental results of previous tests. The verification that a representative and reliable computer model can be used to study elastomeric bearings allows hitherto incompletely understood aspects of the behavior of bridge bearings at high strains to be studied.

INTRODUCTION

The principle of isolating a structural system from ground vibrations has been understood for many years, and many successful implementations exist in which bridges or buildings are mounted on resilient bearings. However, it is only in the last 15 years that designers have developed sufficient confidence to incorporate isolation as the primary means of protecting structures from earthquake-generated strong ground motion.

The concept of seismic isolation is simple and not new. A United States patent for an earthquake-proof building was granted in 1906 [1]. Bechtold's concept involved a building supported on a rigid base plate riding freely on a mass of hard spherical bodies. Many similar proposals were made in the following years. All involved the provision of flexible support so that the system is detuned from the excitation. Developments included restricting the motion between the supported structures and the surrounding ground to an acceptable level by the provision of adequate energy dissipation and, in the case of wind or other relatively minor lateral loads, by incorporation of initial stiffness under service load conditions.

As with many engineering innovations, successful application of the concept was delayed by difficulty in developing reliable and predictable devices which would not only possess the necessary characteristics at the time of construction, but would preserve these properties throughout the expected life of the structure. Greater understanding of the nature of strong seismic ground movements, and the ability to model structural systems using computers, undoubtedly have benefitted the design process, but the most significant recent advances have been prompted by the development of a range of viable isolator devices. These include various combinations of simple rubber blocks, steel torsional and flexural beams, lead extrusion elements and steel plates interlayered with elastomeric materials [2].

* Professor and ** Graduate Student, University of California, Irvine

One of the most promising of these devices appears to be the laminated steel/elastomer bearing. By sandwiching a series of relatively thin slices of elastomer between horizontal steel shims, a composite block can be formed possessing the desirable properties of large vertical stiffness and large horizontal flexibility.

The design of laminated bearings is still at the stage of progressive refinement. Elementary considerations in typical use necessarily reflect a very conservative approach, as the behavior of these bearings at high strains is imperfectly understood. Current practice in the United States involves verification testing of a proportion, as high as ten percent, of the isolators manufactured for use in a given project. The tested units are then discarded. In Japan, typically each isolator is tested before installation. The object in both cases is to verify the integrity of the units in the light of the use of a somewhat simplistic design process, and the undoubted difficulty in assuring quality control of the complex production process.

FINITE ELEMENT MODELLING

The mathematical model widely used currently to predict the behavior of elastomeric bearings is based on simple small strain elastic theory. Stress is assumed linear with respect to strain and the vertical stiffness k_v may be expressed as:

$$k_v = \frac{P}{\delta} = \frac{E_c A}{n t} \quad (1)$$

where P is the vertical load, δ the vertical displacement, A the cross sectional area of the bearing, n the number of elastomeric layers, t the thickness of each layer and E_c an equivalent compression modulus of the elastomer.

A similar approach leads to the horizontal stiffness k_h being expressed as:

$$k_h = \frac{F}{\Delta} = \frac{G A}{n t} \quad (2)$$

where F is the horizontal load, Δ the horizontal displacement, and G the shear modulus of the elastomer.

Modifications of these expressions for bearings with many layers have been suggested [3]. Clearly the equations do not reflect the observed non-linear behavior of the elastomer, nor do they provide any information of the internal stresses and strains within the bearing. If an improved understanding of the actual behavior of multi-layered isolators is to be developed, a more realistic mathematical model is needed.

One approach utilizes finite elements to represent the elastomer and the steel shims. The most significant problem is representing the elastomer and its material properties. It is difficult to determine the material properties experimentally and the analyses are sensitive to the value of input constants. The number of elements used to represent the continuum accurately is

important. Many elements are needed where the stress concentrations are high, but this may not be known until after the analysis. Adaptive mesh and rezoning techniques based on previous results are justified. Many bearings with large numbers of layers, some with thirty-two laminates, are now being used. In such cases, the total number of elements may well be of the order of several thousand, and the use of a very large capacity computer is necessary.

A bearing chosen for finite element analysis is shown in Figure 1. This low shape factor bearing was tested at U. C. Berkeley [4,5]. Test results for the bearing under compression are shown in Figure 2 and for 500 psi compression plus shear in Figure 3.

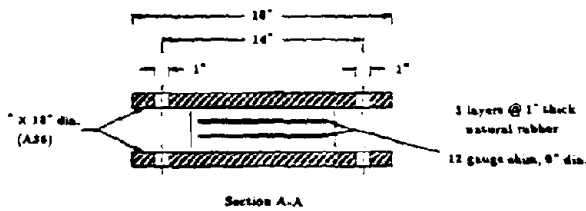


Figure 1. Test Bearing Design: Bolted Connections [4]

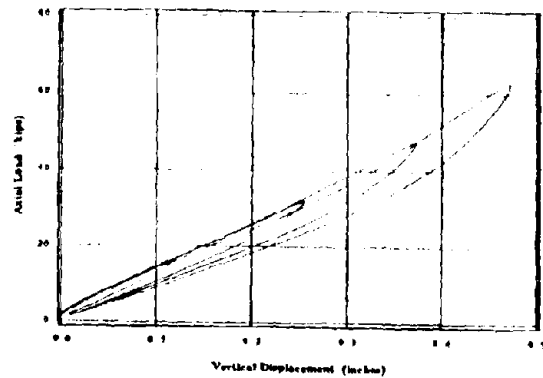


Figure 2. Experimental Results for Vertical Loading [4]

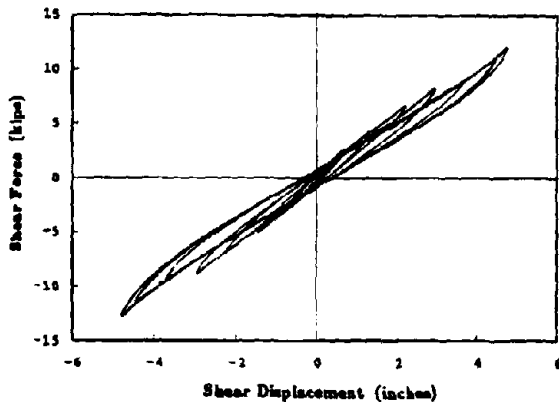


Figure 3. Experimental results for shear tests under 500 psi compression[4]

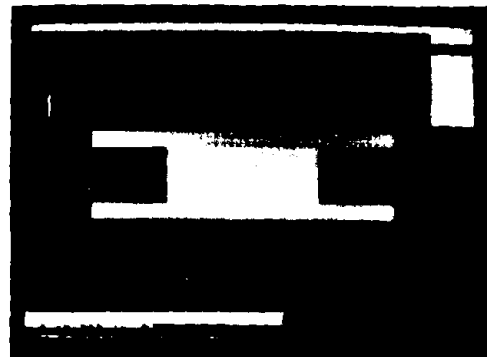


Figure 4. Finite element mesh of bearing tested at UC Berkeley

Finite element analyses were undertaken for the above bearing using the code MARC. The geometry and mesh are shown in Figure 4. The top plate of the bearing was bolted, therefore the boundary conditions are for the two end plates to remain parallel and the base plate to remain fixed. 8-noded plane strain elements were used for a total of 440 elements and 1477 nodes. The analysis was run on U.C. Irvine's CONVEX C240.

The rubber is represented in the code using a potential function $W(I_1, I_2)$ studied by James, Green and Simpson [6] viz:

$$W(I_1, I_2) = C_{10}(I_1 - 3) + C_{01}(I_2 - 3) + C_{11}(I_1 - 3) + C_{20}(I_1 - 3)^2 + C_{30}(I_1 - 3)^3 \quad (3)$$

where I_1 , I_2 and I_3 are strain invariants defined by,

$$I_1 = \lambda_1^2 + \lambda_2^2 + \lambda_3^2 \quad (4)$$

$$I_2 = \lambda_1^2 \lambda_2^2 + \lambda_2^2 \lambda_3^2 + \lambda_3^2 \lambda_1^2$$

$$I_3 = \lambda_1^2 \lambda_2^2 \lambda_3^2$$

and λ_1 , λ_2 , and λ_3 are the principle extension ratios. The condition of incompressibility requires that,

$$I_3 = \lambda_1^2 \lambda_2^2 \lambda_3^2 = 1 \quad (5)$$

and hence I_3 is not a function of the strain. Thus, the potential function W can be expressed as a function of I_1 and I_2 [7].

The MARC code requires the five constants, C_{10} , C_{01} , C_{11} , C_{20} , and C_{30} , as input. The material is then modeled as nonlinear elastic. The problem of assigning values to the constants has been recognized and some unique options have been discussed such as setting C_{01} and C_{11} to zero and assigning values to C_{10} , C_{20} , and C_{30} [8]. The difficulty lies in justifying the assigned values. Assistance from the Malaysian Rubber Producers' Research Association (MRPRA) in Herford, England was sought regarding the above constants. On the basis of advice received, elastomeric materials used in isolation bearings typically exhibit hysteresis, therefore, it is justifiable to use simplified forms of the potential function W . It was suggested to use the simplest of all options and set $C_{01} = C_{11} = C_{20} = C_{30} = 0.0$, and fit C_{10} from MRPRA's test data. Taking only the first term yields the Neo-Hookean material model,

$$W(I_1) = C_{10}(I_1 - 3) \quad (6)$$

C_{10} was chosen as 65.3 psi and assigned to all elements representing the elastomer.

The material properties assigned to the elements representing the steel were allocated a high yield stress of 100,000 psi to prevent yielding in the steel shims.

50 psi vertical load was applied in 10 increments for a total compressive load of 500 psi. A horizontal load of 3.144 psi was applied in the next 50 increments for a total horizontal shear of 157.2 psi. This loading condition is the three dimensional equivalent of 10.0 kips horizontal force with 31.8 kips vertical load as was applied in the experiment. The loading histories are shown in Figures 5 and 6. It was noted that there was a slightly nonlinear response of vertical displacement with increasing horizontal displacement.

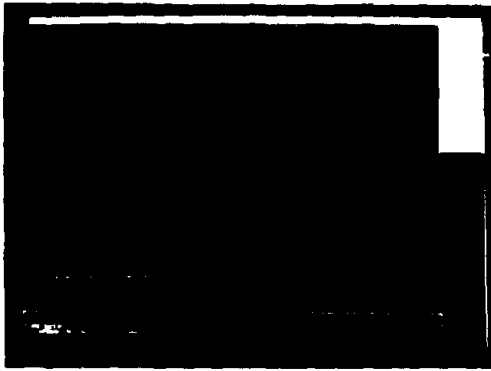


Figure 5. Load Increment versus Vertical Displacement

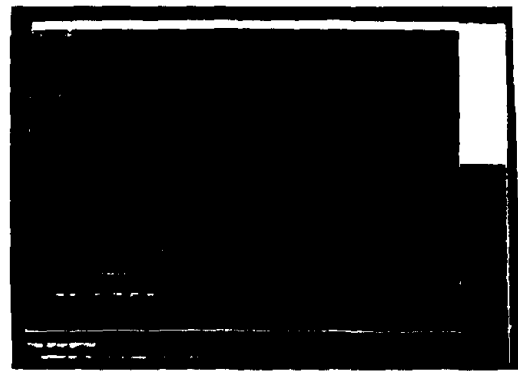


Figure 6. Load Increment versus Horizontal Displacement

COMPARISON OF RESULTS

Comparison of the F.E.M.'s displacement of 0.123-inch for the top plate shown in Figure 5 with the experimental results shown in Figure 2, reveals that the finite element model gives a stiffer response.

The horizontal displacement under both compression and shear is shown in Figure 7. Contact between the elastomer and lower steel plate was allowed for in the analysis and occurs at the lower right and upper left corners of the bearing. The finite element model's horizontal displacement of 4.15-inch compares favorably with the experimental results in Figure 3 for horizontal displacement from U.C. Berkeley [5]. The hysteretic effects of the rubber were not modeled and hence were not expected to be replicated.

The maximum stress in the steel plate under compression is 6300 psi as shown in Figure 8. This was compared with the value determined using the formula below for internal stress in the steel shims [9]:

$$\sigma_{s, \max} = \left(\frac{t_1 + t_2}{2t_s} \right) \left(\frac{1.5}{1 + 1/S^2} \right) \bar{\sigma}_c \quad (7)$$

where t_1 and t_2 are the thickness of the elastomeric layers on each side of the steel shim, t_s is the thickness of the steel shim, S is the bearing's shape factor, and $\bar{\sigma}_c$ is the compressive stress. Application of this expression to the particular bearing examined yields a maximum stress of 6810 psi which is within 8% of the F.E.M. value.

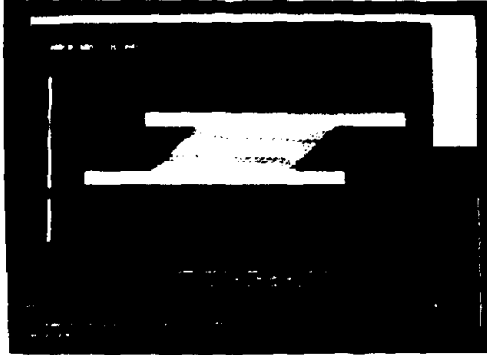


Figure 7. Horizontal Displacement under 500 psi Compression and 157 psi Shear

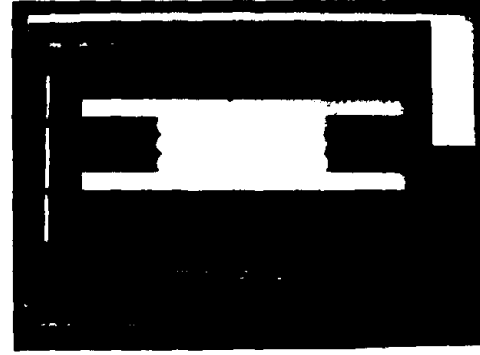


Figure 8. σ_{xx} in Steel Plates under 500 psi Compression

The shear strain under compression is shown in Figure 9. The maximum value of 0.86 occurs at the edge of the rubber-steel interface. Its value was compared with that calculated using an expression for maximum shear strain γ_c at the rubber-steel interface, γ_c [6]:

$$\gamma_c = 6.5\bar{\epsilon}_c \quad (8)$$

where $\bar{\epsilon}_c$ is the compressive strain. The above expression yields a value of $\gamma_c = 1.17$ which, when compared to the F.E.M. value, provides agreement within about 25%. However, the strain value improved towards the theoretical value as the F.E.M. model was meshed more finely in the region of maximum shear strain.

Ongoing work includes modelling the circular bearing in three dimensions and comparing the results to these two dimensional results. Once the above bearing is adequately represented, the next goal is to model larger bearings with more layers and higher shape factors.

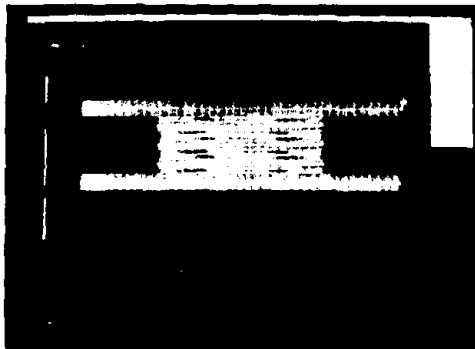


Figure 9. Maximum Shear Strain under 500 psi Compression

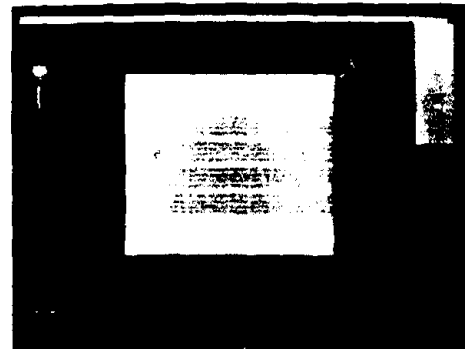


Figure 10. Finite Element Mesh of NCEER Bearing

JOINT RESEARCH WITH NCEER

In cooperation with the National Center of Earthquake Engineering Research at the State University of New York at Buffalo, a bearing was analyzed using MARC with 8-noded plane strain elements shown in Figure 10. The identical bearing was analyzed at SUNY using ADINA. Results for vertical displacement are shown in Figure 11 and the internal stress in the steel shims in Figure 12. The stress results were compared with those obtained using the formula for $\sigma_{x,max}$ above showing a 3% agreement. Recent results have compared favorably with the ADINA results and are currently being reviewed more extensively.

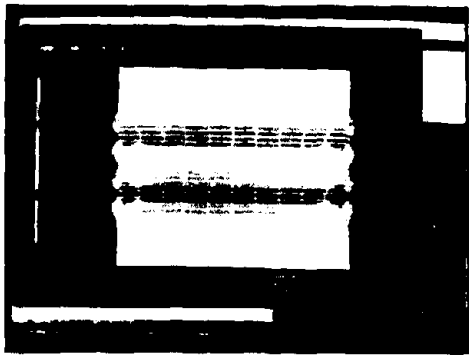


Figure 11. Vertical Displacement under 500 psi Compression

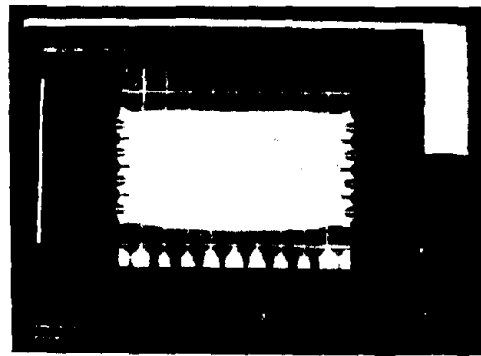


Figure 12. σ_{xx} in Steel Plates under 500 psi Compression

CONCLUSION

Some aspects of the behavior of elastomeric bearings at high strains are beginning to be understood better with the aid of finite element analysis. Specifically, the distribution of stress at the steel rubber interface, the bearing's axial stiffness, especially when combined with shear loads, and the horizontal stiffness are becoming more clearly understood. As the work progresses, some questions are answered but many more questions arise such as how the onset of rollout may be predicted, how the cover rubber's effects may be evaluated, and how boundary conditions represented by the top and bottom plates being connected by bolts or dowels influence the tension in the rubber. It is planned to address these aspects in ongoing work.

ACKNOWLEDGEMENTS

The continuing interest and assistance of Ian G. Buckle and Helen Liu of the National Center for Earthquake Engineering Research and of Alan Muir and Hamid Ahmadi of the Malaysian Rubber Producers' Research Association is recorded with gratitude.

REFERENCES

1. Bechtold, Jacob. "Earthquake-Proof Building", U.S. Patent No. 845,046 1907.
2. Buckle, I. and Mayes, R. "Seismic Isolation: History, Application and Performance", Earthquake Spectra, Vol. 6, No. 2, 1990, pp. 161-201.
3. Kelly, J., Aiken, I., & Tajirian, F. "Mechanics of High Shape Factor Elastomeric Seismic Isolation Bearings", Report UCB/EERC 90-01, University of California, Berkeley, 1990.
4. Aiken, I., Kelly, J., and Tajirian, F. "Mechanics of Low Shape Factor Elastomeric Seismic Isolation Bearings", Report No. UCB/EERC-89/13, University of California, Berkeley, November 1989.
5. Tajirian, F., Aiken, I., and Kelly, J. "Seismic Isolation for Advanced Nuclear Power Stations", Earthquake Spectra, Special Vol. 6, No. 2, California: Earthquake Engineering Research Institute, El Cerrito, 1990.
6. James, A., Green, A., and Simpson, G. Journal of Applied Polymeric Science: 19, 2033, 1975.
7. Treloar, L. The Physics of Rubber Elasticity, Oxford: Clarendon Press, 3rd ed., 1975.
8. Yeoh, O. "Characterization of Elastic Properties of Carbon-Black-Filled Rubber Vulcanizates", presented at a meeting of the Rubber Division, American Chemical Society, Las Vegas, Nevada, May 29-June 1, 1990.
9. Stanton, J. and Roeder, C. "Elastomeric Bearings Design, Construction, and Materials", National Cooperative Highway Research Program (NCHRP) Report No. 248. Washington, D.C.: Transportation Research Board. August, 1982.

DEVELOPMENT OF ROLLER-TYPE BEARING FOR MENSHPIN BRIDGES

by ¹Tatsumasa TAKAKU, ¹Masahiro SHIMADA,
²Naoyoshi TSUMURA and ³Shinichi IZUMA

¹Bridge Construction and Engineering Department,
NKK Corporation, Tsurumi-ku, Yokohama, Japan
²Engineering Research Center, NKK Corporation,
Kawasaki-ku, Kawasaki, Japan
³Engineering Design Department, Japan Casting Co.Ltd
Kawasaki-ku, Kawasaki, Japan

SUMMARY

A new type of Menshin bearing has been developed for seismic isolation of bridge structures by the NKK (Nippon Kokan) Group. The new system is composed of R+HDR (Roller-type bearing with High Damping Rubber).

The past broad experience of casting and shoe-making technology provides complete proof of the bearing mechanism by installing the conventional roller. HDR is only subjected to the lateral forces, free from the vertical bearing loads. It is tested in state of material, then with the total system and verified to have enough energy absorbing capacity of about 12 % damping ratios.

Extensive tests have been conducted on the new system for: (a) fundamental mechanical properties (b) response characteristics due to cyclic loading. Mainly, the experimental results are presented. Prototypes of R+HDR are made for testing. The configuration and general features of R+HDR are detailed.

INTRODUCTION

Based upon the recent developments in material, design, and fabrication technology, seismic isolation systems have become reliable and practical. The idea itself is not new, but its practical use is new. In Japan, seismic isolation systems have been tried in the Miyagawa Bridge at Shizuoka in 1991, and now several trials are planned, some of them are under construction.

The NKK Group (NKK Corporation + Japan Casting Co.Ltd) has originated the new R+HDR. It is combined with conventional bridge shoes to constitute seismic isolation systems, installing high performance damping rubber inside.

The advantage of the new configuration is its easy application to existing bridges as well as to new projects. For existing bridges, seismic isolation is an effective solution to the problem of old substructures and superstructures due to the force reduction. An alternative solution can be achieved by the replacement of the existing bearings with Menshin bearings. R+HDR consists of conventional shoes plus isolation systems. Use of conventional roller-type bearings provides complete guarantee of bearing mechanism and the best fit for the existing position without any differences in sizes. Small differences in height are adjusted for by using tapered steel spacer plates to maintain alignment and elevation.

Most bridges have bearings to accommodate thermal movements. In the case of roller-type bearings, they allow movement only in the longitudinal direction. In transverse direction side blocks restrict against external forces. In turn, seismic isolation is limited only to the longitudinal direction of bridge layout. Commonly, substructures have weak axes in longitudinal direction against overturning. Therefore, even if the effects are not limited in all directions, R+HDR will be a practical solution, on-site.

FUNDAMENTAL PROPERTIES OF HIGH DAMPING RUBBER MATERIAL

Physical properties of rubber

Table 1 summarizes the specification of rubber used.

Response of HDR and damping quality

Fig.1 shows the specimen of HDR material used for dynamic shear test to get response of HDR and damping quality. Testing conditions are as follows;

strain amplitude : $\pm 10 \sim 200$ %
frequency of cyclic loading : 0.5 Hz
temperature at testing : room temperature.

Results are shown in Table 2 and Fig.2. Based on the measured data, shear modulus G_{eq} is calculated by the following formula;

$$G_{eq} = \frac{K \cdot h}{A} \quad (1)$$

where

K : Measured effective stiffness
h : Height of specimen
A : Cross sectional area of specimen

Influence of temperature change

Dynamic test (Fig.3) have been conducted under the following conditions;

shear strain amplitude : ± 100 %
frequency of cyclic loading : 0.5 Hz
temperature at testing : -10, 20, 40°C

Results are summarized in Table 3.

MENSHIN BEARINGS : R+HDR

With vast experience in bridge shoe making and extensive testing of HDR, the NKK group originated R+HDR. Prototypes of R+HDR have been made for testing. Its configuration and general features are described.

Design criteria of prototype

Assuming 3 continuous plate girder bridge of about 100 m in total length, design criteria for Menshin bearing are described in Table 4.

Configuration and features

A prototype of R+HDR is detailed in Fig.4. Thickness of rubber has been determined so as to be 150 % of shear strain when maximum allowable design movement is reached. Two types of rubber, a) solid type, b) laminated type, have been prepared for testing. The laminated one is expected to support earthquake force in transverse direction of bridge.

LABORATORY TESTS

Cyclic loading tests have been conducted for determining mechanical properties of the isolators. Laboratory tests are done to evaluate effective stiffness and effective damping ratios of the isolators.

Experimental work has been done twice, first at NKK, then at PWRI (Public Works Research Institute) based on the Joint Research Program between PWRI and NKK Group.

- a) Static loading tests at NKK : fundamental tests for full scale model of roller-type bearing, HDR elements and R+HDR, with an actuator of rather low frequency range.
- b) Dynamic loading tests at PWRI : formal tests for R+HDR due to Joint Research Program between PWRI and each industry, with an actuator of rather high frequency range.

In principle, both testing methods for R+HDR were similar to each other. The experimental results are reported based upon both data.

Testing methods

The test rig for R+HDR shown in Fig.5 is used in NKK Laboratory. A HDR model is laterally displaced, while sustaining an axial load. Lateral displacement is given by a side actuator and vertical force, equivalent to dead load (30.5 tf), is applied to the bearings by means of the load-transfer beam accommodated. During testing, lateral movement, lateral reaction, vertical force, lift-up displacement of upper bearing, and temperature change of rubber have been measured.

For several cases, increasing amplitudes of shear strain $\pm 25 \sim 200\%$ (cyclic displacement $\pm 21 \sim 185$ mm), with 10 times laterally loading repeated, load-deformation curves have been drawn in Fig.6.

The hysteretic curve (Fig.6) tested gives effective stiffness and effective damping ratios of the isolators.

$$K_{eq} = \frac{P_{max} - P_{min}}{\delta_{max} - \delta_{min}} \quad (2)$$

$$h_{eq} = \frac{\Delta W}{2\pi W} \quad (3)$$

where, P_{max} , P_{min} , δ_{max} , δ_{min} are maximum and minimum values of load and displacement respectively, as a result of hysteretic behavior of model tested. ΔW is area of a closed loop hysteresis. Then, W is calculated by the following formula;

$$W = \frac{1}{8} (P_{max} - P_{min}) * (\delta_{max} - \delta_{min}) \quad (4)$$

Effective stiffness is converted to a form of shear modulus G_{eq} by equation (1).

Shear modulus and effective damping ratio

Fig.7 and Fig.8 illustrate shear modulus and effective damping ratio as a result of solid type R+HDR, obtained from the static loading tests at NKK. When 150 % straining, R+HDR is; $G_{eq} = 7.5$ kgf/cm², $h_{eq} = 9.8$ %. Results of the static loading for HDR elements and the dynamic shear test using specimens of HDR material are also shown in Fig.7 and Fig.8.

No big difference exists between test results of R+HDR, and HDR separated when compared with both data. In turn, it can be observed that no influence of the rollers is recognized in the behavior of isolator systems. In the case of R+HDR tests, compared with the dynamic shear tests, shear modulus goes up slightly, conversely, the effective damping ratios goes down. These different phenomena result from the varying behavior of HDR;

- a) Shear modulus depends upon shape of rubber and history of loading.
- b) Effective damping ratio depends upon frequency of loading.

In Fig.9 and Fig.10, no big difference has been recognized between solid type and laminated type HDR. Consequently, HDR can be safely designed based upon the solid type data, even when laminated type HDR is used in case where stiffness in transverse direction required.

When removing HDR from the isolators, horizontal reaction against the roller is recorded to be less than 200 kgf, which indicates that the coefficient of friction must be less than 0.01, and the basic performance of the isolators only depends on the properties of HDR.

Effects of loading velocity, loading history and pre-strain

The comparative test results between NKK and PWRI are shown in Fig.11 and Fig.12, where the dotted line indicates the results of the static test at NKK. With cyclic loading of 1Hz, dynamic effects are observed as $G_{eq} = 8.3$ kgf/cm², $h_{eq} = 10.4$ %; which are larger than that of static loading. Accordingly, shear modulus is very sensitive to the history of cyclic loading and large decrease in modulus has been observed within a small range of shear strain. After subjected to cyclic loading, shear modulus of HDR remains unchanged without any effects from loading frequency and pre-straining.

No change of effective damping ratio has been observed, when 0.1 Hz cyclic loading, then static loading, regardless of the existence of pre-straining and the history of cyclic loading. When 1.0 Hz cyclic loading, effective damping ratio increases in number within wide range of shear strain. Fig.13 shows the influence of loading velocity on the quality of HDR, with 150 % shear strain. Small range bias is recognized to some extents due to loading velocity. It is conservatively estimated that effective damping ratio shall be approximately 12%, at the

range of cyclic loading frequency beyond 0.5Hz, taking sensitive influence of cyclic loading into consideration.

Characteristic at earthquake

Fig.14 shows dynamic behavior of Menshin bearings R+HDR when subjected to strong seismic motion equivalent to a large-scale earthquake at PWRI. Strong forces are defined as follows;

displacement amplitude : 126 mm (shear strain : 150 %)
frequency of loading : 0.5 Hz
cyclic number of loading : 40 times.

Both G_{eq} and h_{eq} decrease in quality with an increase in loading cycles, as low as 19 % and 17 % each, compared with average values of 4-10 cycles loading, when temperature of HDR is recorded to be 7°C change up.

In spite of the fact that these qualities of HDR lessen to considerable points due to cyclic loading so as to take the vulnerable effects into consideration for design analysis, it is still considered to be safe in practical use.

CONCLUSIONS

A set of R+HDR seismic isolators was tested. Its basic behavior and performance have been obtained as a result of tests and analysis.

- 1) Response mechanism of R+HDR due to seismic motion depends mainly upon the HDR only, independently from the roller movement with small friction. Therefore the performance of the isolator can be securely obtained by the independent tests of rubber materials.
- 2) No difference is recognized in quality between solid and laminated types of HDR. It can safely be said that HDR is designed on the basis of solid type testing data.
- 3) As a result of tests, shear modulus and effective damping ratio are;

$$G_{eq} = 8 \text{ kgf/cm}^2, \quad h_{eq} = 12 \%$$

Effective damping ratio was lower than that of planning prior to tests (at the first stage of planning, $G_{eq} = 8 \text{ kgf/cm}^2$, $h_{eq} = 15 \%$). In reality, no serious discrepancy occurs in practical use for design.

- 4) No roller lift-up and slip phenomena have been observed due to strong seismic motion. In turn, cyclic load-deformation hysteretic behavior of HDR still remains in linear motion even when subjected to a strong earthquake.

From these results, we have verified that the mechanical properties and the earthquake response characteristics of the newly developed R+HDR are useful for seismic isolation systems both for existing bridges as well as for new construction. Further study will be required to formulate the design methods of R+HDR, by normalizing the non-linear behavior of oscillation amplitude and frequency.

ACKNOWLEDGEMENTS

The development of the roller-type bearing (R+HDR) for Menshin Bridges has been conducted extensively as a part of the joint research program on "Development of Menshin Systems of Highway Bridges" between Public Works Research Institute (PWRI) and the NKK Group. Grateful acknowledgement is made to Dr.K.Kawashima, Mr.K.Hasegawa, Mr.S.Unjo and Mr.H.Nagashima of the Earthquake Engineering Division of PWRI for their cooperation.

REFERENCE

1. Buckle, I.G. and Mayes, R.L., "Seismic Isolation: History, Application and Performance --- A World View", Special Volume on Seismic Isolation, Earthquake Spectra, Earthquake Engineering Research Institute, 1990.

Table 1 Summary of physical properties of rubber

Type of testing	Specimen	Testing condition	Physical properties
Tension test	No.3 type dumbbell specimen	Room temperature 23°C Tensile velocity 500 mm/min	Tensile strength 210 kgf/cm ² Elongation at breaking point 680% 100% modulus 20 kgf/cm ²
Tear test	A-type	Ditto	Tearing strength 122 kgf/cm ²
Hardness test	6 specimens accumulated with 2mm thickness each	Room temperature 23°C	Hardness 68°

Table 2 Testing result of HDR specimens

Strain amplitude γ (%)	(measured) Shear modulus G_{eq} (kgf/cm ²)	(modified) Shear modulus G' (kgf/cm ²)	Effective damping ratio h_{eq}
10	19.35	20.82	0.215
20	14.88	16.00	0.201
50	9.77	10.51	0.186
100	7.41	7.95	0.163
150	6.87	7.39	0.136
200	7.69	8.27	0.104

$G' = (1+1/3 (h/a)^2) G_{eq}$
 h : height of specimen, a : length of specimen.

Table 3 Influence of temperature change on HDR

temperature	G_{eq}/G	h_{eq}/h
-10°C	1.33	1.26
40°C	0.87	0.96

remarks G, h : values at 20°C.

Table 4 Design criteria for R+HDR

Total reaction	R	59.0 tf
Reaction due to dead load	Rd	30.5 tf
Effective stiffness	K_B	123 tf/m ($G_{eq}=8.0$ kgf/cm ² assumed)
Damping ratio	h_B	0.15 ($h_{eq}=0.15$ assumed)
Natural period of bridge	T	1.0 sec
Design lateral force coefficient	K_{bc}	0.5 ($1.0 \cdot 1.0 \cdot 0.7 \cdot 0.714 \cdot 1.0$)
Allowable design movement	U_B	125 mm

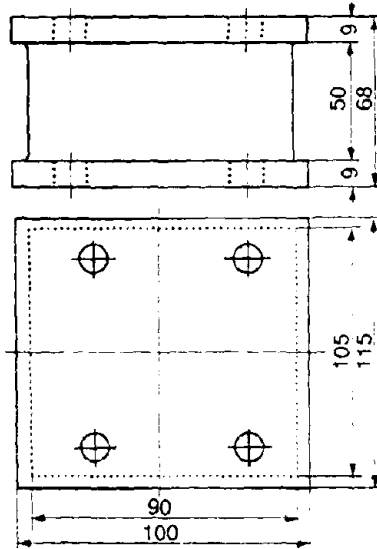


Fig. 1 Specimen of HDR material used for dynamic shear test

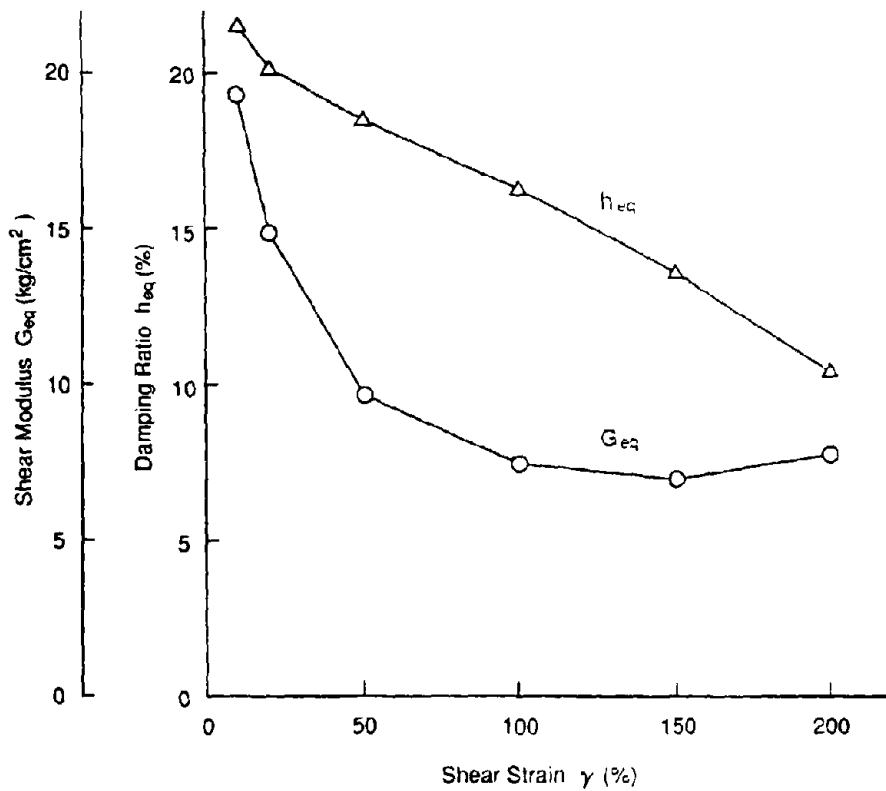


Fig. 2 Results of dynamic shear test using specimens of HDR material

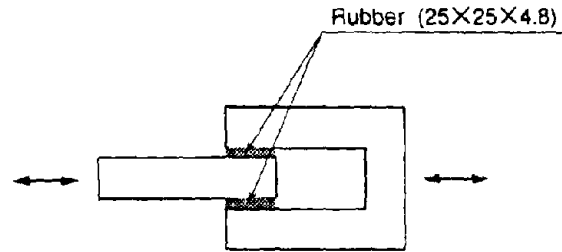
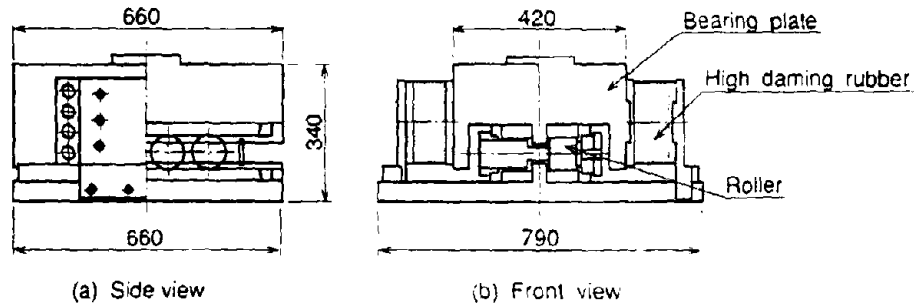
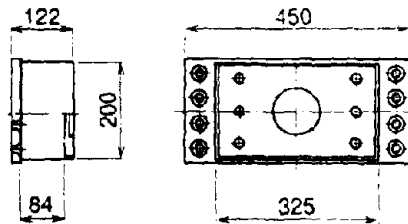


Fig. 3 Dynamic test for evaluating influence of temperature change on HDR characteristics

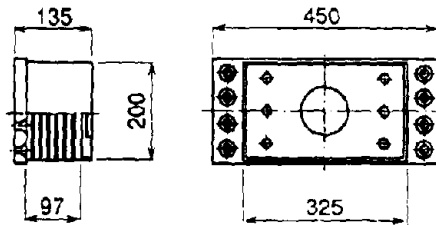


(a) Side view

(b) Front view



(c) HDR element (Solid type)



(d) HDR element (Laminated type)

Fig. 4 Full scale model of R+HDR

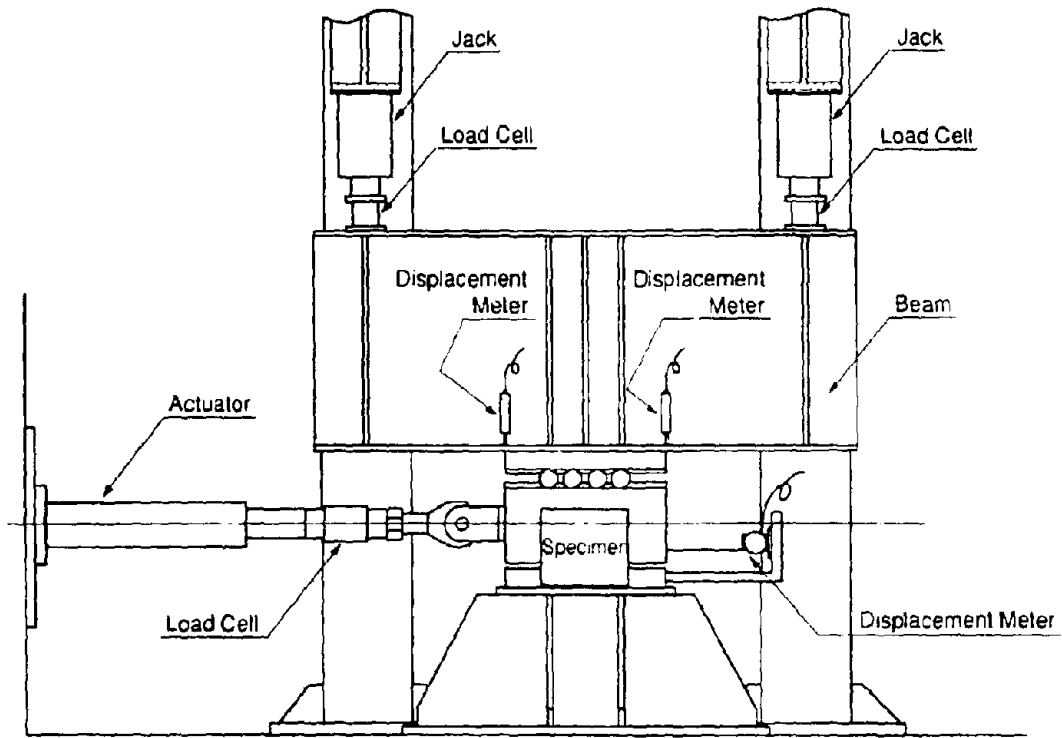


Fig. 5 Test rig for R+HDR

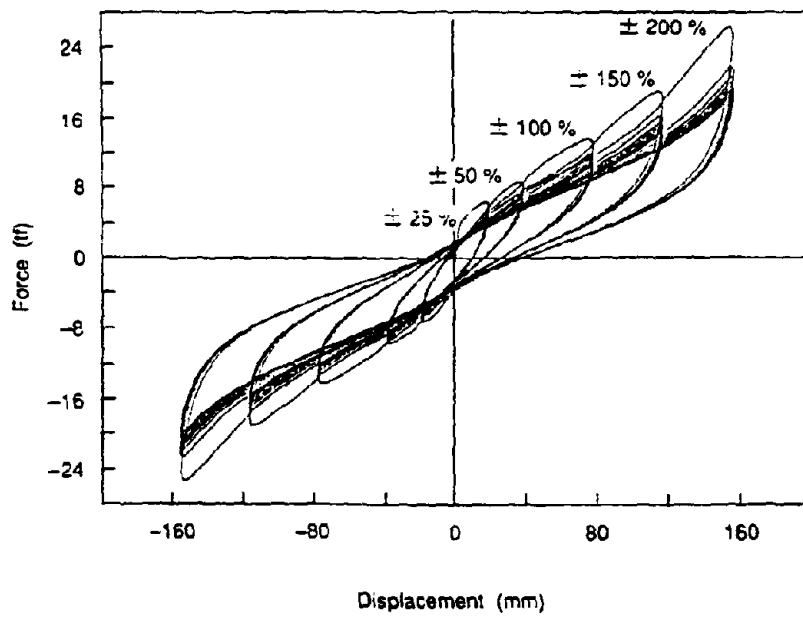


Fig. 6 Hysteretic curves of R+HDR

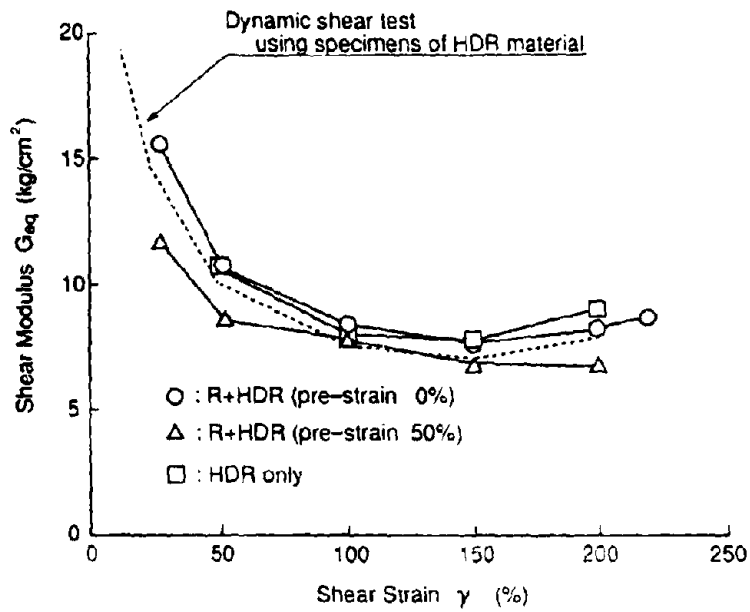


Fig. 7 Shear modulus measured in static loading tests

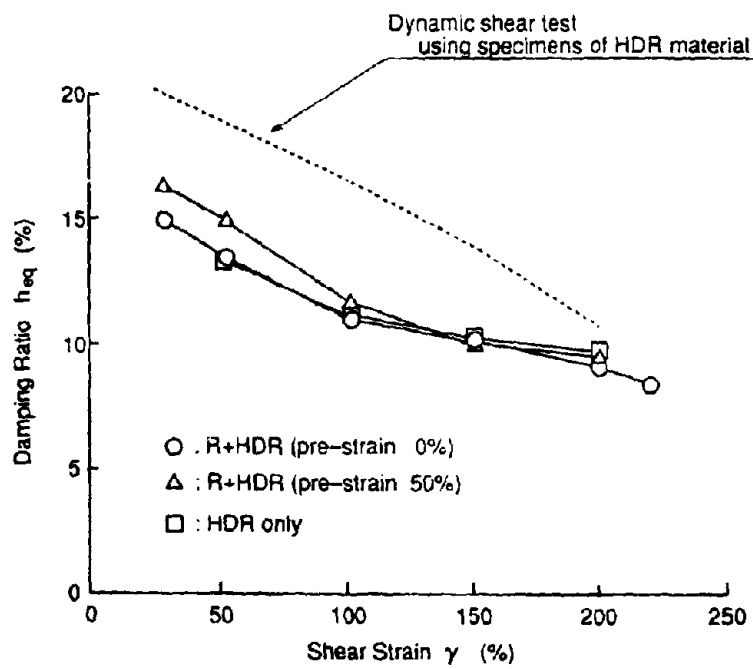


Fig. 8 Effective damping ratios measured in static loading tests

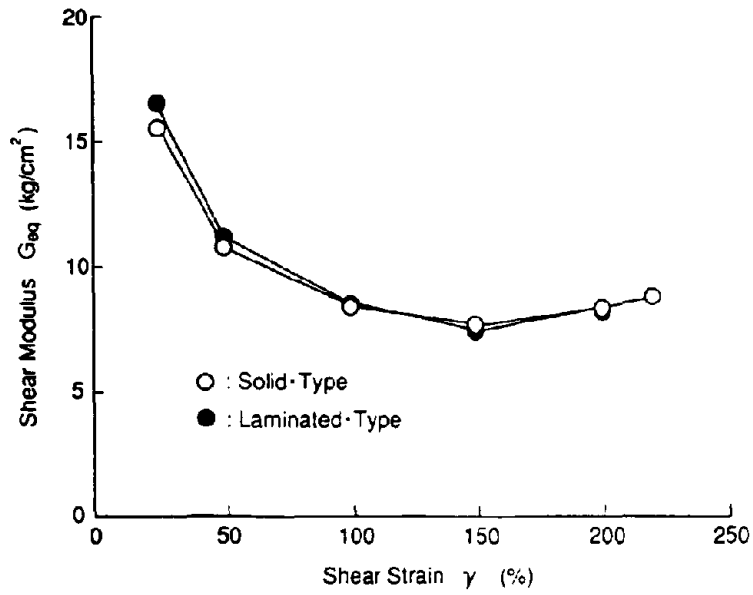


Fig. 9 Comparison of shear modulus between solid type HDR and laminated type HDR

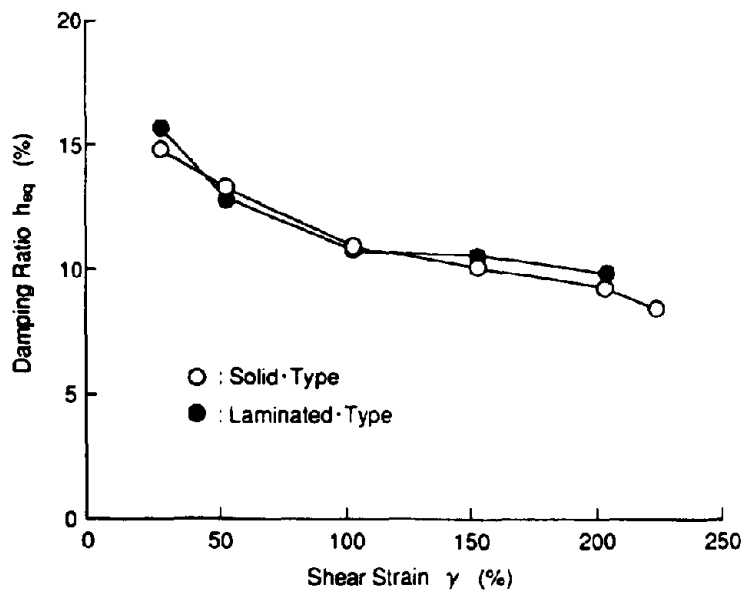


Fig. 10 Comparison of effective damping ratios between solid type HDR and laminated type HDR

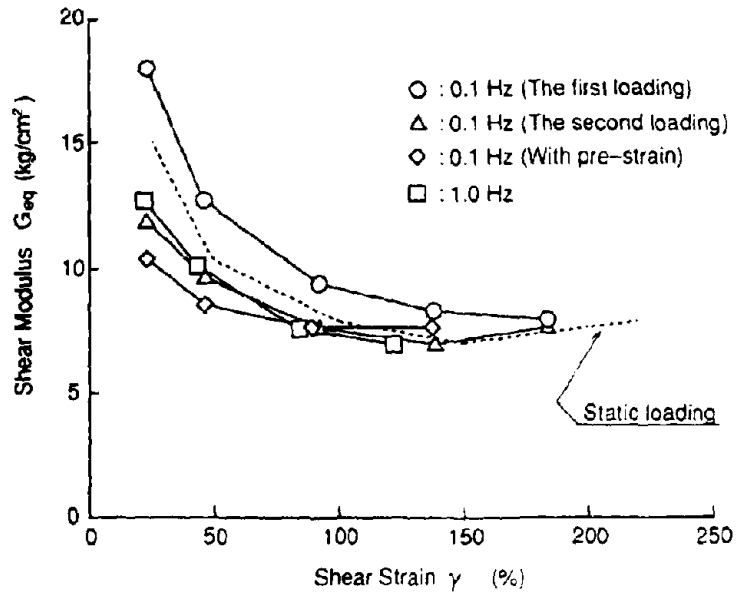


Fig. 11 Measured shear modulus of R+HDR

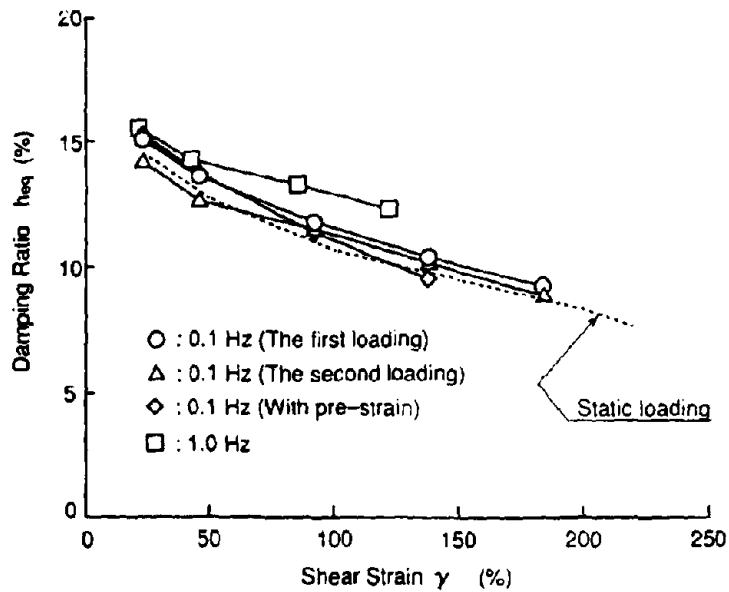


Fig. 12 Measured effective damping ratios of R+HDR

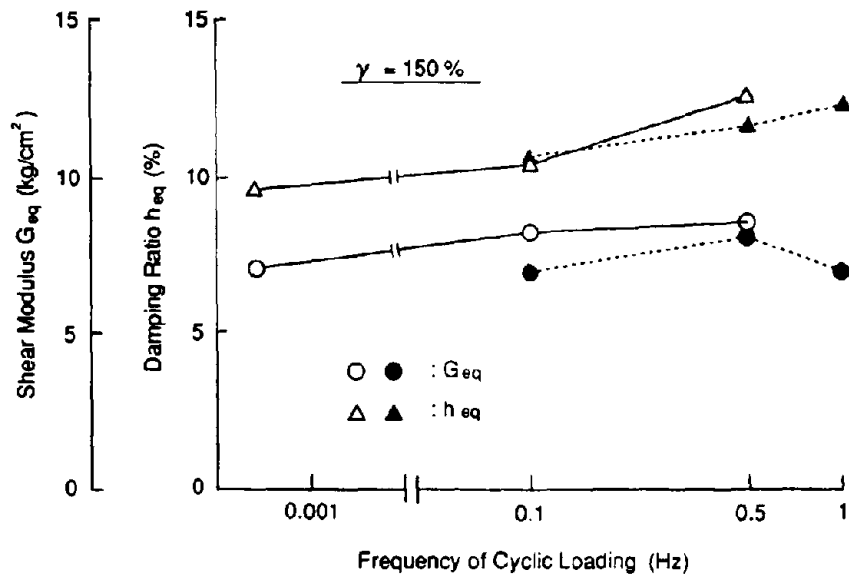


Fig. 13 Influence of frequency of cyclic loading on HDR characteristics

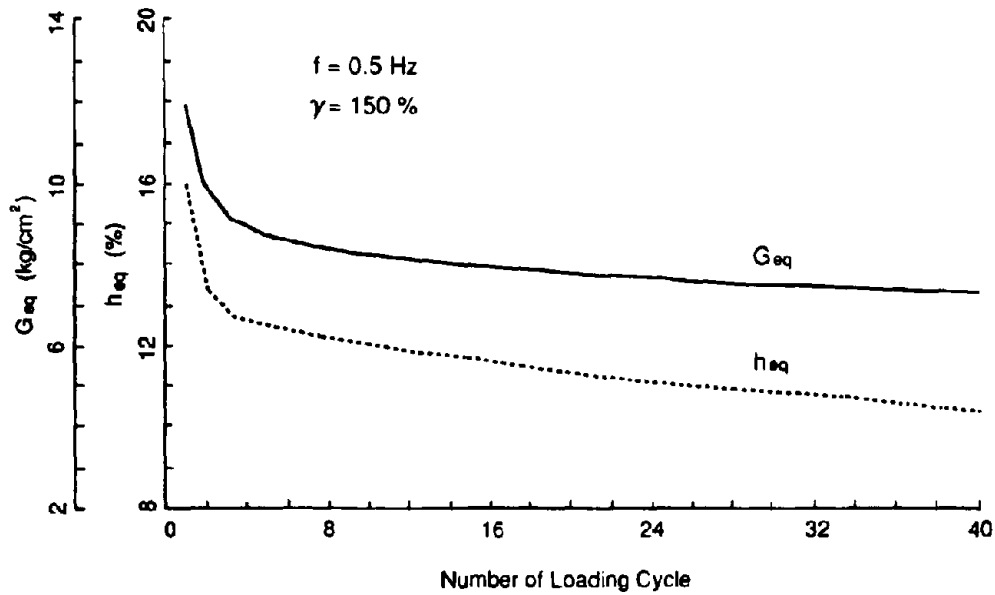


Fig. 14 Behavior of R+HDR under strong seismic motion

SLIDING ISOLATION SYSTEMS FOR BRIDGES

M. C. CONSTANTINOU

Department of Civil Engineering
State University of New York at Buffalo
Buffalo, New York 14260, USA

SUMMARY

The paper presents a summary of the work on sliding seismic isolation system for bridges at the State University of New York at Buffalo. Furthermore, the paper describes a major forthcoming application of sliding isolation bearings in three bridges.

INTRODUCTION

Seismic isolation systems are typified by use of either elastomeric or sliding bearings. Elastomeric systems reduce the fundamental frequency of the isolated structure so that the isolation effect is produced by primarily deflecting rather than absorbing the earthquake energy. This results in in-phase response with low accelerations and large bearing displacements. Reduction of bearing displacements is accomplished by use of energy dissipating devices like mild steel devices and lead-rubber bearings (Ref. 1). The introduction of significant damping may create out-of-phase response and large response acceleration in flexible, tall structures. In bridges, which have squat and stiff superstructures, this behavior does not occur and a significant isolation effect may be produced with both low acceleration and displacement response. Hence, elastomeric bearings/mild steel devices and lead-rubber bearings found wide application in bridge isolation in New Zealand, United States and elsewhere (Ref. 1).

Sliding isolation systems limit the transfer of force across the isolation interface, absorb earthquake energy and produce the isolation effect. They are characterized by insensitivity to the frequency content of earthquake excitation, stability, and low bearing displacements. The insensitivity to the frequency content of input motion results from the tendency of sliding isolation systems to reduce and spread the earthquake energy over a wide range of frequencies. Sliding isolation systems have found several applications in Japan and Italy where they have been used for longitudinal isolation of bridge decks (Ref. 1).

Research on sliding isolation systems at the State University of New York, Buffalo started in 1988. The work concentrated first on:

- (a) Determination of the frictional properties of Teflon-steel interfaces under conditions of interest in seismic isolation (Refs. 2-5),
- (b) Development, calibration and verification of models of friction for sliding isolation bearings (Refs. 4,6),
- (c) Shake table testing of large scale isolated model structures (Refs. 7-10),

- (d) Development of analytical techniques to provide interpretation of the experimental results (Refs. 7-13), and
- (e) Development of a computer code for the dynamic nonlinear analysis of isolated structures (Refs. 14-16).

The results of this work convinced the researchers at Buffalo on the potential of sliding systems and the research was directed towards the study and development of sliding isolation systems for bridges. This paper presents a summary of this work. In particular, the following are described:

- (a) Frictional properties of sliding bearings,
- (b) Restoring force devices for bridges,
- (c) Shake table test results of isolated bridge decks with (i) spherical sliding bearings and (ii) flat sliding bearings and displacement control devices, and
- (d) A major forthcoming application of sliding isolation bearings in three bridges.

FRICTIONAL PROPERTIES OF SLIDING BEARINGS

Sliding isolation systems utilize in some form or another Teflon or Teflon based materials in contact with polished metals as the sliding interface. The frictional properties of these interfaces were assessed in an experimental program. Tests were conducted under the following conditions:

- (a) Unfilled and glass filled Teflon at compositions of 15% and 25% by weight and woven Teflon were tested in contact with polished stainless steel of roughness in the range of 0.03 to 0.04 μm AA (or CLA scale),
- (b) Bearing pressure was varied between 500 and 10,000 psi (3.5 to 69 MPa),
- (c) Velocity of sliding was varied between 0.1 in/sec and 20 in/sec (2.5 to 508 mm/sec), and
- (d) Load on the specimens was maintained prior to testing from a few minutes to 594 days.

The tests revealed that

- (a) The coefficient of sliding friction depends primarily on the type of interface (Teflon composition and roughness of stainless steel), velocity of sliding and bearing pressure. In particular, the coefficient of sliding friction drops with increasing pressure and increases with increasing velocity of sliding. Figure 1 shows recorded values of the sliding coefficient of friction of unfilled Teflon in contact with stainless steel. The effects of pressure and velocity of sliding are evident. In general, the variation with velocity of sliding follows the relation

$$\mu_s = f_{\max} - (f_{\max} - f_{\min}) \exp(-a|V|) \quad (1)$$

in which f_{\max} and f_{\min} are respectively the maximum and minimum values of the coefficient of sliding friction and a is a parameter that controls the variation of μ_s with velocity, V . Values of parameters f_{\max} , f_{\min} and a have been reported in Refs. 2,4, and 5.

- (b) The static (or breakaway) value of the coefficient of friction (which occurs at initiation of sliding) is larger than f_{\min} but always less than f_{\max} . In general, the transmission of force through the sliding interface is controlled by the value f_{\max} .
- (c) Dwell of load has no effect on the frictional properties.

A model of friction of Teflon-steel interfaces was developed (Refs. 4,6). The model accounts for bidirectional motion, velocity of sliding and bearing pressure effects. Verification tests with bidirectional high velocity motion were conducted (Ref. 6) and a sample of results is shown in Figure 2. The motion at the sliding interface was the recorded ground motion during the 1985 Mexico City earthquake (compressed in time by a factor of 2). The recorded loops of force vs displacement in the two orthogonal directions compare very well with the analytical prediction. The analytical model was based on the implementation of eq. 1 in a model of viscoplasticity (Refs. 4,6).

RESTORING FORCE DEVICES

Restoring force devices are important elements in sliding isolation systems. Their function consists of

- (a) Re-centering the structure during earthquake excitation,
- (b) Providing additional energy dissipation if necessary,
- (c) Providing rigidity under service loads, and
- (d) Counteracting the effects of accidental inclination at the sliding bearings.

The accidental inclination of sliding bearings in a single direction may have important consequences in systems without or with very weak restoring force capability. Experiments performed at the State University of New York at Buffalo with sliding bearings inclined at an angle of only 0.4 degrees resulted in excessive displacements in the direction of inclination (Refs. 8,10). The problem was alleviated by the introduction of sufficiently strong restoring force.

The researchers at Buffalo experimented with a variety of restoring force devices. Of these, two have been used in shake table tests and will be briefly described herein.

Sliding Bearings with Spherical Surface

The sliding surface in these bearings has a spherical shape so that restoring force is provided by the weight of the structure during rising along the spherical surface. The bearing carries the trade name Friction Pendulum System or FPS (Refs. 7,9,17).

Figure 3 shows the construction of a FPS bearing used in shake table tests. The lateral force-displacement relation of this bearing is given by

$$F = \left(\frac{W}{R}\right) u + \mu_s W \operatorname{sgn}(\dot{u}) \quad (2)$$

in which W is the weight carried by the bearing, R is its radius of curvature, μ_s is the coefficient of sliding friction at the interface and u is the displacement. The quantity W/R represents the stiffness of the bearing. Accordingly, the period of vibration of a rigid structure on such bearings is

$$T = 2\pi \left(\frac{R}{g}\right)^{1/2} \quad (3)$$

which is independent of the mass of the structure. The bearing provides rigidity to forces up to the static value of the coefficient of friction times the weight.

Displacement Control Device

A displacement control device (or DCD) for use in sliding isolation systems has been described in Ref. 18. It is schematically shown in Figure 4. It consists of frictional and spring assemblies connected in series. The frictional assembly provides an adjustable characteristic strength, F_f , to the device. The device is rigid for forces below this limit. For forces exceeding the characteristic strength, the spring assembly is activated. The output of the device is a bilinear force-displacement loop with very large initial and unloading stiffness as shown in the experimental loop of Figure 5.

The installation of the device in a two-span bridge is illustrated in Figure 6. The deck is supported by multi-directional sliding bearings and displacement control devices are installed at the two abutments. The installation is such that rigidity for service loads is provided in the longitudinal direction at one abutment, while the other side is allowed to expand and accommodate thermal movement.

The group at Buffalo is currently experimenting with restoring force devices in the form of wire rope springs and liquid spring-dampers.

SHAKE TABLE TESTING

Shake table tests of a 51 Kip (227 kN), quarter scale model bridge deck were conducted. The model deck was supported by four sliding bearings of either the flat shape together with displacement control devices or of the spherical shape. A summary of the experimental results is presented below.

Sliding Disc Bearing and Displacement Control Device

A sliding disc bearing consists of a Teflon-stainless steel sliding interface with an Adiprene (Urethane rubber) supporting disc to provide rotational capability. An illustration of the bearing is shown in Figure 7. In the tests, various materials at the sliding interface were used under a variety of bearing pressures so that different frictional properties were produced.

In a set of tests the frictional properties of the sliding bearings followed the law of eq. 1 with $f_{\max} = 0.12$ and $f_{\min} = 0.06$. One displacement control device with spring stiffness $K=3.85$ kip/in (0.67 kN/mm) and characteristic strength over weight of deck ratio, F_f/W , equal to about 0.05 was used. In selected tests a larger ratio (up to 0.07) was used to demonstrate the importance of friction in long period excitation. The spring stiffness in the displacement control device gave a period of free vibration (in the absence of friction) equal to 1.16 secs (or 2.33 secs in prototype scale).

Table 1 presents a summary of the experimental results. The earthquake excitation consisted of historic records some of which have been scaled up in acceleration to create severe excitation. Two of the motions, the Japanese Hachinohe and Mexico City records, are of long period. In particular, the Mexico City motion is essentially a sine wave at a period almost equal to the free vibration period of the isolated model.

The results of Table 1 demonstrate a very effective isolation system. The deck acceleration is maintained at about 0.2g for earthquake motions of significantly different content in frequency and peak ground acceleration. The differences in the various earthquake excitations are accommodated by different movement in the sliding bearings. This is a characteristic of sliding isolation systems (Ref. 8). It should be noted that the deck displacements are very low and in general less than 1 in. (25 mm) or 4 in. (100 mm) in the prototype scale.

Of interest is the sequence of tests with the Mexico City motion in which the model is driven at resonance. Despite this, the isolated deck responds with small displacement amplitude without amplifying the ground acceleration. A minor increase of the characteristic strength of the displacement control device from 0.05 to 0.057 of the deck weight resulted in reduction of displacements to about half with a simultaneous decrease in the acceleration. This remarkable property may play a significant role in the case of isolated bridges in which after construction a determination is made that strong long period earthquakes may occur at the site. The characteristic strength of the displacement control devices may be easily adjusted in the field to values appropriate for the anticipated excitation.

Analytical techniques for accurate calculation of the dynamic response of sliding isolated structures are available (Refs. 7,10). Such techniques were

employed in the analysis of the response of the model bridge and results are shown in Figure 8 for the case of the test with the Pacoima Dam motion. The figures compare experimental and analytical results on the time history of deck displacement and loop of base shear versus deck displacement. The base shear is the combined force from the sliding bearings and displacement control device. Evidently, the analytical results are in very good agreement with the experimental results.

Bearings with Spherical Sliding Surface (FPS)

The same model bridge was tested with four spherical sliding bearings having the construction of Figure 3. The bearing material was a form of woven Teflon with frictional properties $f_{\max} = 0.11$ and $f_{\min} = 0.03$. The period of the isolated deck is given by eq. 2 as 1 sec (or 2 sec in prototype scale). Accordingly, the primary difference between the two systems has been the total frictional force at the isolation interface: 0.11 times the weight in the FPS system and about 0.17 times the weight in the system with displacement control devices (0.12 from sliding bearings plus about 0.05 from DCD).

A summary of the experimental results is presented in Table 2. In comparing with the higher friction displacement control device system, we observe higher deck displacement and lower permanent displacement for all motions. The deck acceleration is lower in the weaker motions and slightly larger in the strongest motions.

These experimental results and other results obtained in tests of building models (Refs. 2-10) lead to the following conclusions:

- (a) Sliding isolation systems may be designed with conventional means to deliver a coefficient of friction at high velocity of sliding, f_{\max} , in the range of 0.06 to about 0.18,
- (b) Higher friction values are appropriate for strong earthquake excitation and long period excitation, and
- (c) Reliable analytical techniques are available for the prediction of seismic response of sliding isolated structures.

FORTHCOMING APPLICATION OF SLIDING ISOLATION BEARINGS IN BRIDGES

The analytical and experimental results obtained for sliding isolation systems gave sufficient confidence to the researchers at Buffalo to propose a sliding isolation system for three similar bridges over the Corinth Canal in Greece (Ref. 19). The bridges are located within a few kilometers of several known faults. The seismicity of the area is characterized by the design-basis-earthquake having a peak ground acceleration of 0.27g and containing significant long period components.

The developed design calls for concrete box-girder structures with a free span of about 150m as shown in Figure 9. Each bridge is supported by two rows of heavily-loaded bearings at two central supports and two rows of lightly-loaded

bearings at the abutments. The structure between abutment and central support represents the counter-weight. It is to be filled with about 3.8m of gravel so that a sufficient compression force is maintained on the abutment bearings, under all possible loading combinations of the completed bridge. The dead load of the structure above the bearing level is 196 500 kN. Each of the central location bearings is subjected to an axial load of 20 465 kN as a result of dead, live and thermal loading combinations, and to a load of 17 900 kN due to dead load only.

Bearings with a spherical sliding surface (FPS) were selected, owing to their:

- (a) relatively small size under the heavy axial load of 20 500 kN and
- (b) anticipated satisfactory performance under seismic loading rich in long-period components.

Figure 10 shows the design details of the most heavily loaded FPS bearing. Its size, 813 mm x 813 mm, is considerably smaller than what would be required for (circular) elastomeric bearings (diameter in the range of 1375 to 1950 mm). The concave spherical surface of the FPS bearings has a radius of curvature $R = 994$ mm, and the coefficient of friction at the sliding interface has a value of 0.06 at high velocity of sliding. The displacement capacity of the bearing is 150 mm.

The design of the isolation system was based on dynamic nonlinear analyses which demonstrated a reduction of internal forces and displacements by a factor of 2.5 in comparison to the conventionally built bridge for the design-basis-earthquake. Dynamic bearing displacements were 85 mm with a permanent displacement of 2 mm.

Construction of the bridges is expected to start in 1992.

ACKNOWLEDGEMENTS

The work on sliding isolation systems at the State University of New York at Buffalo is supported by the National Center for Earthquake Engineering Research, the National Science Foundation, Watson Bowman Acme Corp., Earthquake Protection Systems, Inc., GERB Vibration Control and Taisei Corporation.

REFERENCES

1. Buckle, I.G. and Mayes, R.L. "Seismic Isolation-History, Application, and Performance - A World View", *Earthquake Spectra*, Vol. 6, No. 2, pp. 161-201, 1990.
2. Mokha, A.S., Constantinou, M.C. and Reinhorn, A.M. "Teflon Bearings in Aseismic Base Isolation: Experimental Studies and Mathematical Modeling," Report No. NCEER-88-0038, National Center for Earthquake Engineering Research, Buffalo, New York, 1988.
3. Mokha, A.S., Constantinou, M.C. and Reinhorn, A.M. "Teflon Bearings in Base Isolation. I: Testing," *J. Structural Engineering*, ASCE, Vol. 116, No. 2, pp. 438-454, 1990.

4. Constantinou, M.C., Mokha, A. and Reinhorn, A.M. "Teflon Bearings in Base Isolation II: Modeling," J. Structural Engineering, ASCE, Vol. 116 (2), pp. 455-474, 1990.
5. Mokha, A., Constantinou, M.C. and Reinhorn, A.M. "Further Results on Frictional Properties of Teflon Bearings", J. Structural Engineering, ASCE, Vol. 117(2), pp. 622-626, 1991.
6. Mokha, A.S., Constantinou, M.C. and Reinhorn, A.M. "Verification of Friction Model of Teflon Bearings under Triaxial Load," submitted for review, 1991.
7. Mokha, A.S., Constantinou, M.C., Reinhorn, A.M. and Zayas, V. "Experimental Study of Friction Pendulum Isolation System." J. Structural Engineering, ASCE, Vol. 117, No. 4, pp. 1203-1219, 1991.
8. Constantinou, M.C., Mokha, A. and Reinhorn, A.M. "Study of a Sliding Bearing and Helical Steel Spring Isolation System." J. Structural Engineering, ASCE, Vol. 117, No. 4, pp. 1259-1277, 1991.
9. Mokha, A.S., Constantinou, M.C. and Reinhorn, A.M. "Experimental Study and Analytical Prediction of Earthquake Response of a Sliding Isolation System with a Spherical Surface," Report No. NCEER-90-0020, National Center for Earthquake Engineering Research, Buffalo, New York, 1990.
10. Constantinou, M.C. Mokha, A.S. and Reinhorn, A.M. "Experimental and Analytical Study of a Combined Sliding Disc Bearing and Helical Steel Spring Isolation System," Report No. NCEER-90-0019, National Center for Earthquake Engineering Research, Buffalo, New York, 1990.
11. Makris, N. and Constantinou, M.C. "Fractional Derivative Maxwell Model for Viscous Dampers," J. Structural Engineering, ASCE, Vol. 117 (9), pp. 2708-2724, 1991.
12. Makris, N. and Constantinou, M.C. "Viscous Dampers: Testing, Modeling and Application in Vibration and Seismic Isolation," Report No. NCEER-90-0028, National Center for Earthquake Engineering Research, Buffalo, New York, 1990.
13. Constantinou, M.C. and Papageorgiou, A.S. "Stochastic Response of Practical Sliding Isolation Systems," Probabilistic Engineering Mechanics, Vol. 5 (1), pp. 27-34, 1990.
14. Nagarajaiah, S., Reinhorn, A.M. and Constantinou, M.C. "3D-BASIS. Nonlinear Dynamic Analysis of Three-Dimensional Base Isolated Structures: Part II," Report No. NCEER-91-0005, National Center for Earthquake Engineering Research, Buffalo, New York, 1990.
15. Nagarajaiah, S., Reinhorn, A.M. and Constantinou M.C. "Nonlinear Dynamic Analysis of 3-D-Base-Isolated Structures," J. Structural Engineering, ASCE, Vol. 117 (7), pp. 2035-2054, 1991.
16. Tsopelas, P., Nagarajaiah, S., Constantinou, M.C. and Reinhorn, A.M. "3D-BASIS-M. Nonlinear Dynamic Analysis of Multiple Building Base Isolated Structures," Report No. NCEER-91-0014, National Center for Earthquake Engineering Research, Buffalo, New York, 1991.

17. Zayas, V., Low, S.S. and Mahin, S.A. "The FPS Earthquake Resisting System, Experimental Report." Report No. UCB/EERC-87/01, Earthquake Engineering Research Center, University of California, Berkeley, CA, 1987.
18. Constantinou, M.C., Reinhorn, A.M., Mokha, A. and Watson, R. "Displacement Control Device for Base-Isolated Bridges," Earthquake Spectra, Vol. 7(2), pp. 179-200, 1991.
19. Constantinou, M.C. and Gazetas, G. "Forthcoming Applications of Seismic Isolation in Greece," 1991 Post-SMIRT Conference Seminar on Seismic Isolation of Nuclear and Non-Nuclear Structures, Nara, Japan, 1991.

Table 1 - Summary of Experimental Results in System with Displacement Control Device (1 in. = 25.4 mm)

Excitation	Pk. Table Accel. (g)	$\frac{F_f}{W}$	Pk. Deck Displ. (in)	Pk. Deck Accel. (g)	Permanent Displacement (in)
1952 TAFT N21E	0.544	0.056	0.337	0.187	0.002
1952 TAFT N21E	0.747	0.052	0.657	0.207	0.029
1940 EL CENTRO S00E	0.330	0.052	0.214	0.175	0.103
1940 EL CENTRO S00E	0.747	0.054	0.913	0.221	0.130
1968 HACHINOHE NS	0.304	0.051	0.270	0.167	0.172
1968 HACHINOHE NS	0.445	0.052	0.661	0.205	0.041
1978 MIYAGIKEN-OKI EW	0.521	0.054	0.252	0.186	0.060
1978 MIYAGIKEN-OKI EW	0.662	0.052	0.691	0.210	0.038
1971 PACOIMA DAM S74W	1.070	0.052	0.847	0.215	0.008
1985 MEXICO CITY N90W	0.174	0.044	0.295	0.156	0.026
1985 MEXICO CITY N90W	0.203	0.050	0.913	0.205	0.032
1985 MEXICO CITY N90W	0.209	0.057	0.540	0.190	0
1985 MEXICO CITY N90W	0.209	0.065	0.430	0.190	0.013

F_f = Characteristic Strength of Displacement Control Device

Table 2 - Summary of Experimental Results in System with Spherical Sliding Surface - FPS (1 in. = 25.4 mm).

Excitation	Pk. Table Accel. (g)	Pk. Deck Displ. (in)	Pk. Deck Accel. (g)	Permanent Displacement (in)
1952 TAFT N21E	0.495	0.780	0.157	0.005
1952 TAFT N21E	0.670	1.286	0.217	0.000
1940 EL CENTRO S00E	0.293	0.326	0.118	0.027
1940 EL CENTRO S00E	0.634	1.464	0.221	0.007
1968 HACHINOHE NS	0.233	0.478	0.132	0.005
1968 HACHINOHE NS	0.358	1.078	0.184	0.000
1978 MIYAGIKEN-OKI EW	0.451	0.413	0.125	0.002
1978 MIYAGIKEN-OKI EW	0.556	0.880	0.170	0.000
1971 PACOIMA DAM S74W	1.190	1.380	0.239	0.002

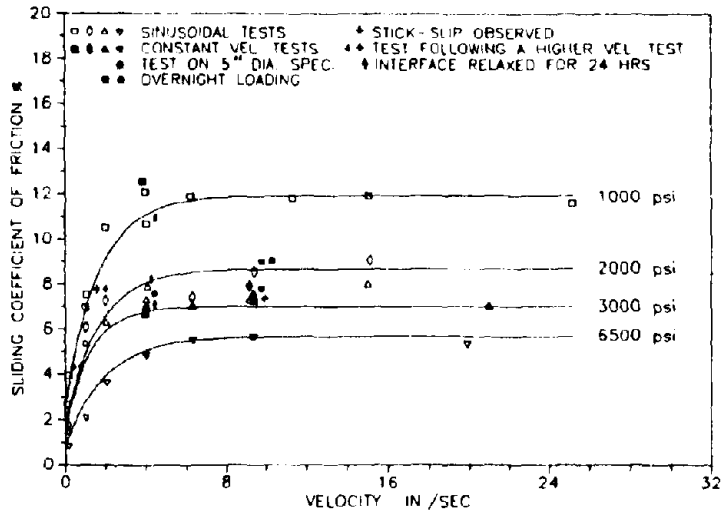


Fig. 1 - Coefficient of Sliding Friction of Unfilled Teflon in Contact with Polished Stainless Steel (1 in = 24.5 mm, 1000 psi = 6.9 MPa).

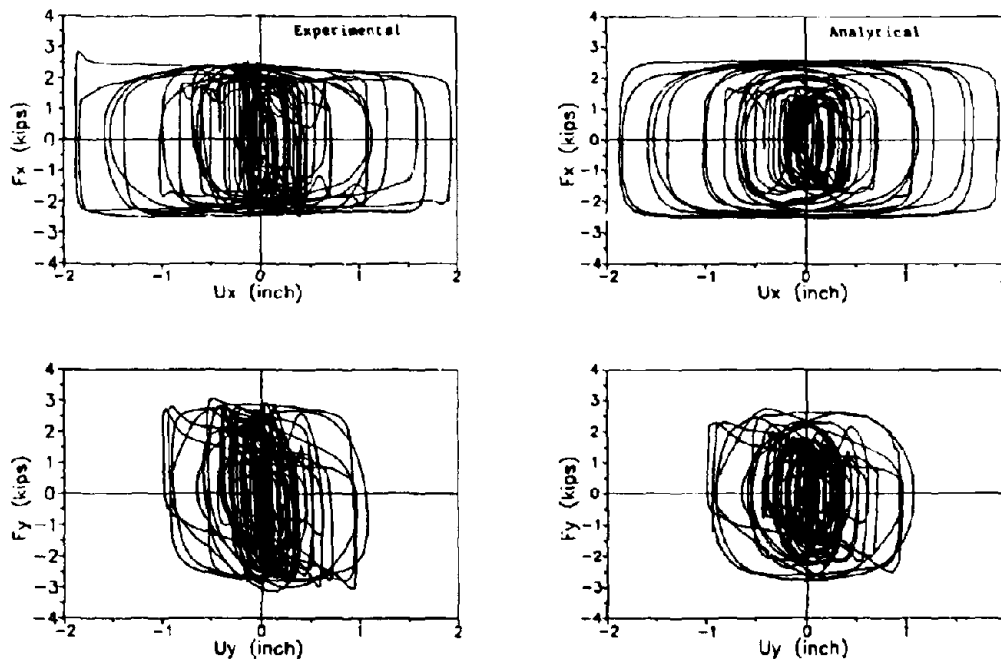


Fig. 2 - Comparison of Analytical and Experimental Force-Displacement Loops of Sliding Bearing Subjected to Bi-directional Motion (1 in. = 25.4 mm, 1 kip = 4.46 kN).

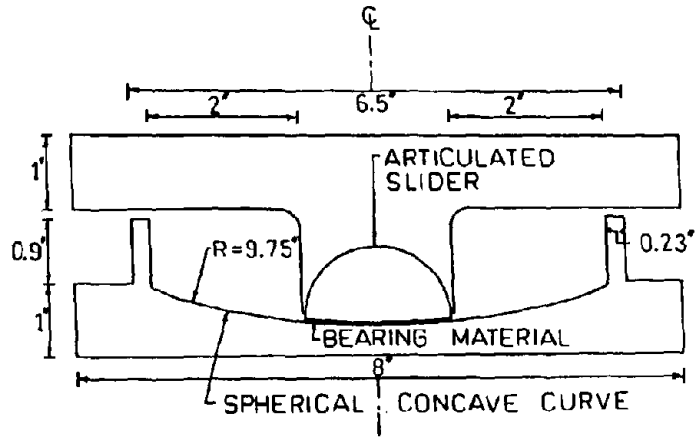


Fig. 3 - Bearing with Spherical Sliding Surface - FPS (1 in. = 25.4 mm).

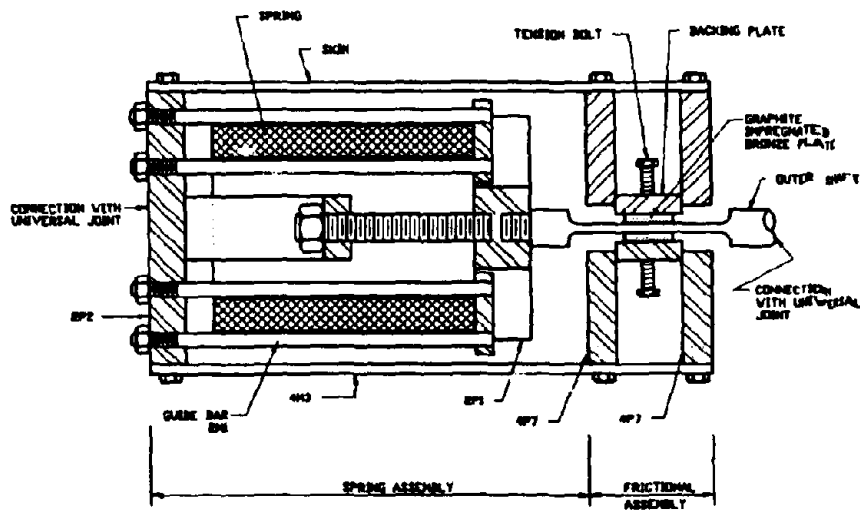


Fig. 4 - Construction of Displacement Control Device.

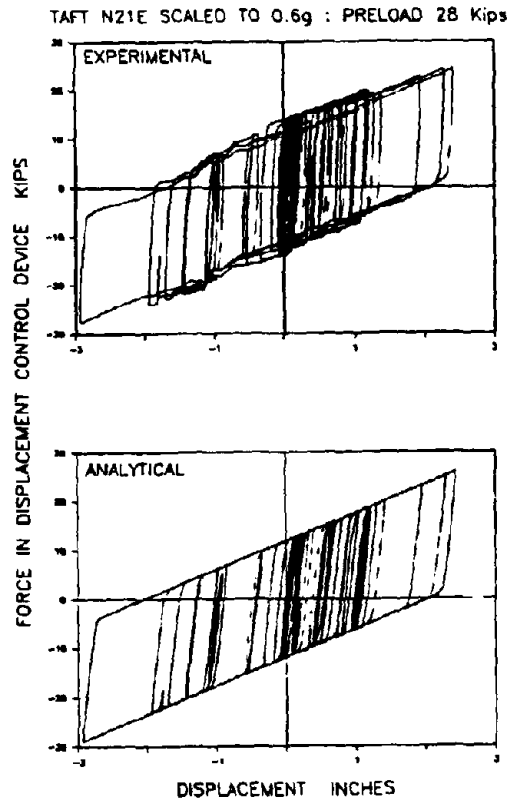


Fig. 5 - Force-Displacement Loop of Displacement Control Device (1 in. = 25.4 mm, 1 kip = 4.46 kN).

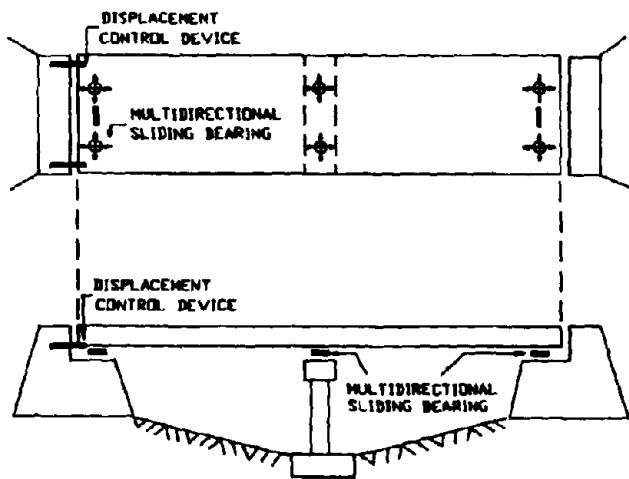


Fig. 6 - Isolated Two Span Bridge with Displacement Control Devices.

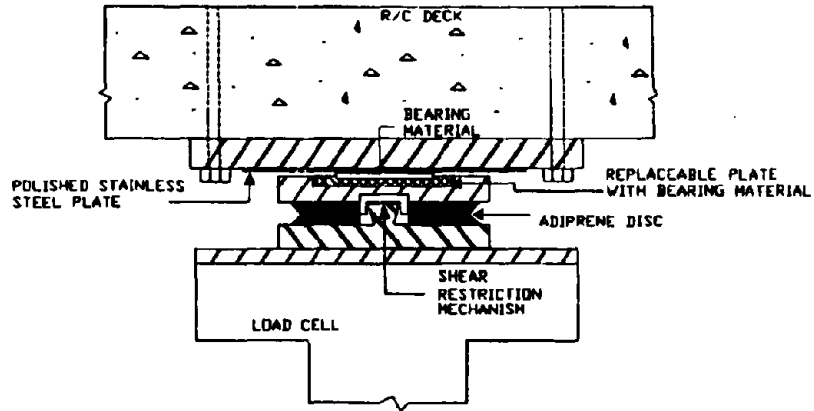


Fig. 7 - Construction of Sliding Disc Bearing.

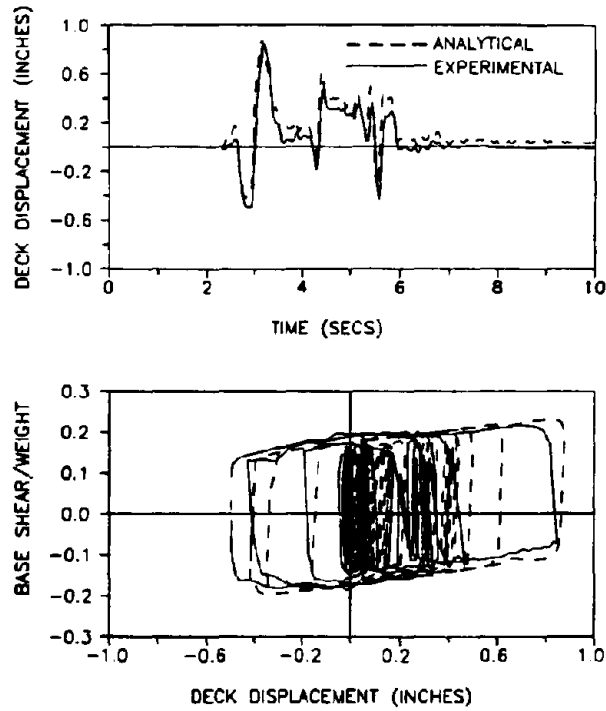


Fig. 8 - Comparison of Analytical and Experimental Response of Isolated Bridge Deck for Pacoima Dam Input (1 in. = 25.4 mm).

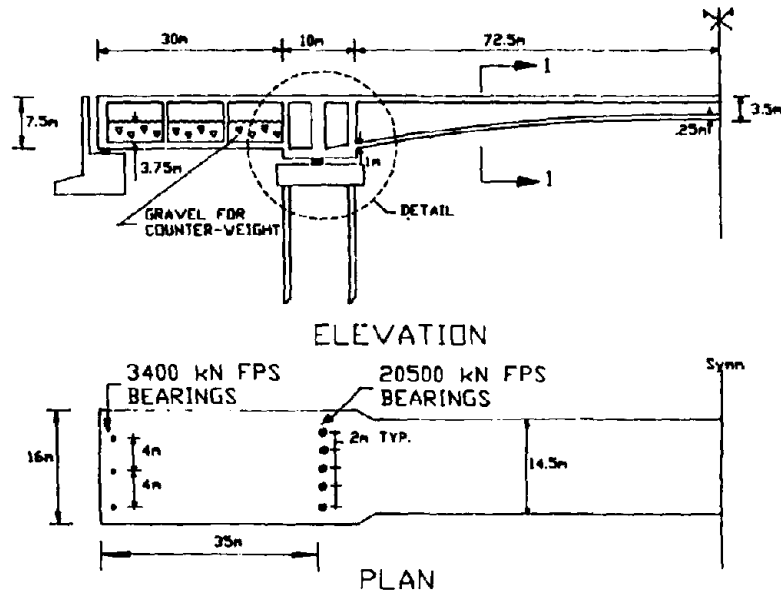


Fig 9 - Plan and Elevation of Seismic Isolated Corinth Canal Bridge.

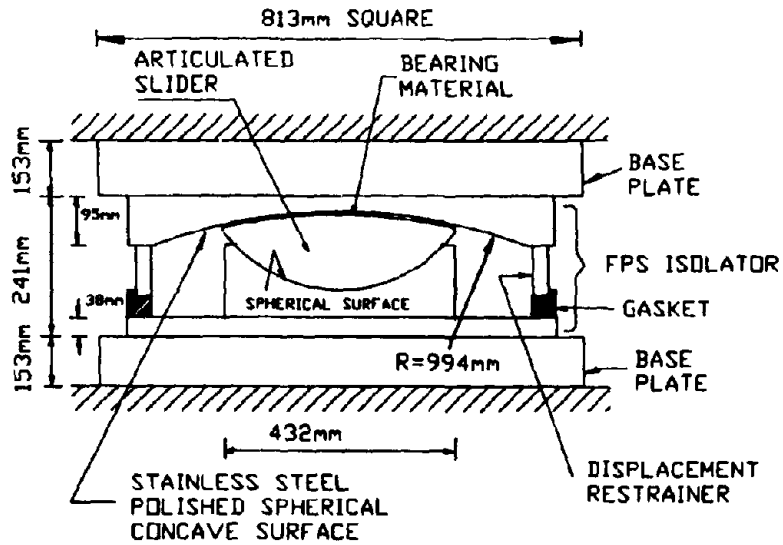


Fig 10 - Construction of 20 500 kN Spherical Sliding Bearing.

CERTIFICATION TEST OF MENSIN DEVICES

Kazuhiko KAWASHIMA¹, Kinji HASEGAWA², Hiroyuki NAGASHIMA³,
Yutaka MAKIGUCHI⁴, Yoji SUIZU⁵

¹Public Works Research Institute, Ministry of Construction

²Ditto

³Ditto

⁴Oiles Corporation

⁵Bridgestone Corporation

SUMMARY

This paper describes the performance characteristics required for menshin devices which are used in highway bridges, and also proposes testing and evaluation procedures for certifying the performance. The proposed certification tests intend to verify that the design performance of menshin devices is maintained stable under static, dynamic and any other loaded conditions to which menshin devices are presumably subjected during their service period. Certification test items are largely classified into dynamic characteristic, static characteristic and when a menshin device is placed under its ultimate state. Specifically with respect to the certification of dynamic characteristic, seven items including the stability to cyclic live loads, the stability to the change in vibration frequency and the stability to temperature changes are tested. The definition of "index" to evaluate respective degree of stability and permissible index value are also proposed.

CLASSIFICATION OF MENSIN DEVICES AND BASIC DYNAMIC CHARACTERISTIC

Classification of Menshin Devices Menshin devices are grouped three general classifications depending on the mechanism of damping force development; displacement dependent, frictional force dependent, and velocity dependent menshin devices. Table 1 compiles the classifications and representative menshin devices.

Table 1 Classifications and Representative Menshin Devices

Classifications	Representative Menshin Devices
Displacement Dependent Menshin Device	Lead Rubber Bearing High Damping Rubber Bearing Steel Damper
Frictional Force Dependent Menshin Device	Friction Damper
Velocity Dependent Menshin Device	Viscous Damper

Basic Dynamic Characteristic The following factors are verified on three types of menshin devices shown in Table 1.

a) Displacement dependent menshin device

The effective stiffness and effective damping ratio, which are defined by equations (1) and (2). of the displacement dependent menshin device are verified.

$$K_B = \frac{F_{max} - F_{min}}{U_{max} - U_{min}} \quad (1)$$

$$h_B = \frac{\Delta W}{2 \pi \times W} \quad (2)$$

Where

- K_B : effective stiffness of menshin device
- h_B : effective damping ratio of menshin device
- F_{max} , F_{min} : force at maximum and minimum displacement
- U_{max} , U_{min} : maximum displacement, minimum displacement
- ΔW : area enclosed by a one-cycle hysteresis loop
- W : area shown in Figure 1

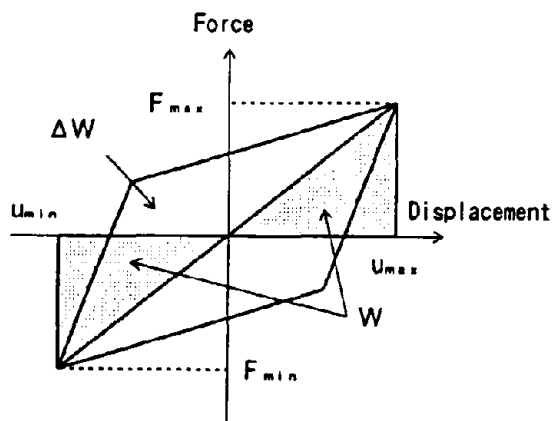


Fig.1 Force-Displacement Hysteresis Loop

b) Friction force dependent menshin device

The coefficient of friction, which is defined in equation (3), of the frictional force dependent menshin device is verified, in addition to the effective stiffness and effective damping ratio which are defined in equations (1) and (2) above.

$$\mu = \frac{F_0}{R} \quad (3)$$

Where

- μ : coefficient of friction
- F_0 : sectional load at zero displacement in the force-displacement hysteresis loop
- R : vertical load

c) Velocity dependent menshin device

The coefficient of viscosity, which is defined in equation (4), of the velocity dependent menshin device is verified, in addition to the effective stiffness and effective damping ratio which are defined in equations (1) and (2).

$$(4) \quad C = \frac{F_0}{V}$$

Where

- C : coefficient of viscosity
- F₀ : sectional load at zero displacement is the force-displacement hysteresis loop
- V : velocity

STABILITY TO DYNAMIC CHARACTERISTICS

Properties to be tested for Certification Stability with regard to each of (a) thru (g) below is verified to predefined characteristic values for menshin devices.

- (a) The influence of cyclic loads
- (b) The influence of hysteresis experience
- (c) The influence of changes in vertical load
- (d) The influence of changes in vibration frequency
- (e) The influence of static pre-displacement
- (f) The influence of loading direction
- (g) The influence of changes in temperature

Method of certification

(a) The influence of cyclic loads.

The application of continuous and repeated loads changes the effective stiffness or damping ratio of some menshin devices. Here it was postulated that the number of principal motions in an earthquake is ten, and verification was made as to whether menshin devices would be brought back to a stabilized condition at an early time and with a small scatter of the characteristic value under such repeated loads.

1) Test method

The displacement dependent menshin device and the frictional force dependent menshin device are loaded ten times continuously to 1/8, 1/4, 1/2 and 1.0 times the design displacement at a temperature of +20°C, bearing a stress of 60 kgf/cm² and a vibration frequency of 0.5 Hz, while the vibration velocity dependent menshin device is subjected to a cyclic load ten times in five steps of vibration velocities of 10 cm/sec, 25 cm/sec, 50 cm/sec, 75 cm/sec, and 100 cm/sec at the temperature of +20 °C, bearing a stress of 60 kgf/cm² and a vibration frequency of 0.5 Hz.

2) Verification method

The stability index which is defined in equation (5) satisfies equation (6) in terms of all displacements and all vibration velocities.

$$R_j = \frac{|\bar{L} - L_j|}{\bar{L}} \quad (5)$$

$$\left. \begin{aligned} R_j &\leq 0.30 \text{ (Where, } j = 1, 2, 3) \\ R_j &\leq 0.05 \text{ (Where, } j = 4, 5, \dots 10) \end{aligned} \right\} \quad (6)$$

Where

- \bar{R}_j : the stability index with regard to cycle loads
- \bar{L} : the reference characteristic value, mean characteristic value from the 4th to 10th loading
- L_j : the characteristic value of the j-th loading

(b) The influence of hysteresis experience.

Some menshin devices show change to the characteristic value of the 2nd loading when

composed to that of the 1st loading if the loading to a certain displacement is applied again after a lapse of reasonable time. Here a series of loading which makes the design displacement the greatest is defined as the "1st series", and this "1st series" is applied twice (the 2nd series) to verify that the change between the 1st series and the 2nd series is small.

1) Test method

Loading as specified in (a)-1) is defined as the 1st series and this 1st series is repeated once (the second loading is repeated under the same conditions and same procedure as the first loading).

2) Verification method

The stability index which is defined in equation (7) satisfies equation (8).

$$R_R = \frac{|\bar{L}_1 - \bar{L}_2|}{\bar{L}_1} \quad (7)$$

$$R_R = \leq 0.30 \quad (8)$$

Where

R_R : stability index with regard to hysteresis experience

\bar{L}_1, \bar{L}_2 : reference characteristic value of the 1st series and the 2nd series, respectively (mean characteristic value from the 4th to 10th loading)

(c) The influence of changes in vertical load.

1) Test method

Each menshin device is loaded ten times continuously to the design displacement at a temperature of +20 °C, and bearing stress of 40, 60, 80 kgf/cm² and a vibration frequency of 0.5 Hz.

2) Verification method

The stability index which is defined in equation (9) satisfies equation (10).

$$R_V = \frac{|\bar{L}_{60} - \bar{L}_V|}{\bar{L}_{60}} \quad (9)$$

$$R_V = \leq 0.15 \quad (10)$$

Where

R_V : the stability index with regard to changes in vertical load

\bar{L}_{60} : the reference characteristic value at a bearing stress of 60 kgf/cm²

\bar{L}_V : the reference characteristic value at a bearing stress of 40 kgf/cm² or 80 kgf/cm²

(d) The influence of changes in vibration frequency.

1) Test method

Each menshin device is loaded ten times continuously to the design displacement at a temperature of +20 °C, and a bearing stress of 60 kgf/cm² and vibration frequencies of 0.1, 0.5 and 1.0 Hz.

2) Verification method

The stability index which is defined in equation (11) satisfies equation (12).

$$R_1 = \frac{|\bar{L}_{0.5} - \bar{L}_V|}{\bar{L}_{0.5}} \quad (11)$$

$$R_1 = \leq 0.2 \quad (12)$$

Where

R_1 : the stability index with regard to changes in vibration frequency

$\bar{L}_{0.5}$: the reference characteristic value at vibration frequency 0.5 Hz

L_r : the reference characteristic value at vibration frequency 0.1 Hz or 1.0 Hz

(e) The influence of static pre-displacement.

1) Test method

Each menshin device is loaded ten times continuously to 1/2 of the design displacement at a temperature of +20°C, a bearing stress of 60 kgf/cm² and a vibration frequency of 0.5 Hz by placing the device under static pre-displacement equivalent to 0 and 1/4 of the design displacement.

2) verification method

The stability index which is defined in equation (13) satisfies equation (14).

$$R_u = \frac{|\bar{L}_u - \bar{L}_0|}{\bar{L}_0} \quad (13)$$

$$R_u = \leq 0.2 \quad (14)$$

Where

R_u : the stability index with regard to static pre-displacement

\bar{L}_0 : the reference characteristic value when the static pre-displacement is zero

\bar{L}_u : the reference characteristic value when the static pre-displacement is 1/4 of the design displacement

(f) The influence of loading directions.

1) Test method

Each menshin device is loaded ten times continuously to the design displacement at a temperature of +20 °C, a bearing stress of 60 kgf/cm², a vibration frequency of 0.5 Hz and in the directions of 45 and 90 degrees to the reference axis.

2) Verification method

The stability index which is defined in equation (15) satisfies equation (16).

$$R_D = \frac{|\bar{L}_D - \bar{L}_0|}{\bar{L}_0} \quad (15)$$

$$R_D = \leq 0.05 \quad (16)$$

Where

R_D : the stability index with regard to loading direction

\bar{L}_0 : the reference characteristic value in the direction of reference axis

\bar{L}_D : the reference characteristic value in the direction of 45 or 90 degrees to the reference axis

(g) The influence of changes in temperature.

1) Test method

Each menshin device is loaded ten times continuously to the design displacement at a bearing stress of 60 kgf/cm², a vibration frequency of 0.5 Hz and temperatures of -10°C, +20 °C and +40°C.

2) Verification method

The stability index which is defined in equation (17) satisfies equation (18).

$$R_T = \frac{|\bar{L}_{20} - \bar{L}_T|}{\bar{L}_{20}} \quad (17)$$

$$R_T = \leq 0.20 \quad (18)$$

Where

R_T : the stability index with regard to temperature changes

\bar{L}_{20} : the reference characteristic value at +20°C

L_T : the reference characteristic value at -20°C or 40°C

STATIC CHARACTERISTICS OF MENSIN DEVICES

This paper proposes a testing method on the reaction force characteristics of menshin devices with regard to slowly applied loads such as found during temperature changes.

Reaction force characteristics due to a slowly applied load The displacement velocity of a menshin device due to a slowly applied load such as found during temperature changes is approximately 0.0001 to 0.0005 mm/sec. It is however normally difficult to do tests at this low speed. Thus a reasonable displacement velocity of 1.0 mm/sec is used to estimate the reaction force of a menshin device as follows.

1) Test method

Under a condition in which a menshin device is loaded with a 60 kgf/cm^2 bearing stress, force is applied at a velocity of 1.0 mm/sec until a half of the static design displacement takes place and then the menshin device is left as it is for six hours. After a lapse of six hours, the same procedure is repeated until the full static design displacement is obtained. Then the menshin device is left as it is for another six hours. The reaction force relief at each displacement as shown in Figure 2 takes place during these six-hour periods. A curve obtained by connecting O, A and B points in the figure is specified as the reaction force characteristic against slowly applied load.

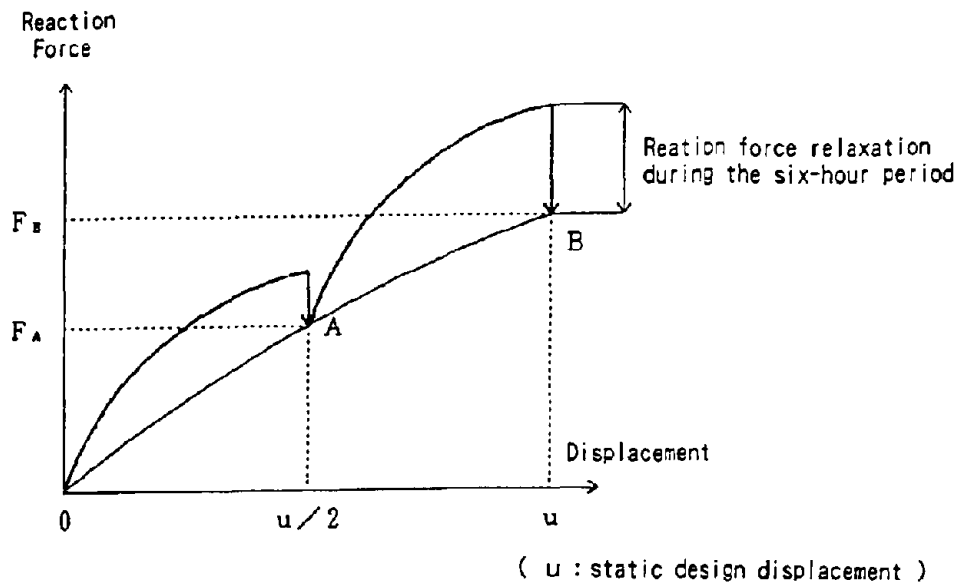


Fig. 2 Reaction Force Characteristic against a long-period loading

2) Calculation of the reacting force against long-period loading

It is assumed that the relationship between the reaction force and the displacement can be expressed by equation (19).

$$F = a \cdot u^b \quad (19)$$

Where

- F : the reaction force against long-period loading (tf)
- u : the static design displacement (cm)
- a, b: the constants expressed by equations (20) and (21)

$$a = \frac{\text{Log } F_A \times \text{Log } u - \text{Log } F_B \times \text{Log } (u/2)}{\text{Log } \left(\frac{u}{u/2} \right)} \quad (20)$$

$$b = \frac{\text{Log } (F_B / F_A)}{\text{Log } \left(\frac{u}{u/2} \right)} \quad (21)$$

ULTIMATE STRENGTH OF MENSIN DEVICES

Durability

1) Test method

A 40-time repeated loading to the design displacement at a temperature of +20°C, a bearing stress of 60 kgf/cm² and a vibration frequency of 0.5 Hz is specified as one-series of the test. This test is performed twice within a three-hour stopping time.

Because one large earthquake is expected to rock 20 times, in order give allowance for the estimated reciprocation, a number of cyclic loads twice as large, i.e., 40 times, is adopted. The reason that one-series of testing is repeated twice is to take into consideration of the influences of aftershocks.

2) Verification method

The menshin device that has undergone excitation should be free of any significant damage. Moreover, the characteristic values of the menshin device after being excited should be within ±50% of those values before excitation.

Large deformation controllability This test is performed to verify that menshin devices, even if subjected to earthquakes larger than those postulated by the design, are not susceptible fracture or other marked damage.

1) Test method

Two loads are applied continuously at 1.5 times larger the design displacement at a temperature of +20 °C, a bearing stress of 60 kgf/cm² and a vibration frequency of 0.5 Hz.

2) Verification method

The menshin device that has undergone excitation should be free from fracture and significant damage.

CONCLUSIONS

The testing and evaluation procedures considered necessary to certify the performance characteristics required for menshin devices which are used in highway bridges were proposed. Some of the proposed properties tested items were applied to the performance verification tests of nine types of menshin devices which had been developed as part of a joint research program on "Development of Menshin Systems for Highway Bridges" between PWRI and 28 private firms and their practicability has been verified. However, opinions prevail that some of the target stability index values for the dynamic characteristics proposed herein are too stringent from a viewpoint of those in charge of the development of menshin devices. This area remains unresolved and is left for further studies.

ACKNOWLEDGEMENT

This study was made as part of a joint research program on the Development of Menshin

Systems for highway Bridges between PWRI and 28 private firms.

REFERENCE

1. PWRI and 28 private firms, "Development of Menshin Systems for Highway Bridges - Report No.1", PWRI Joint Research Report No.44, March 1990 (in Japanese)

INVESTIGATION OF FRICTION PENDULUM SYSTEMS

by

Stephen A. Mahin
Nishkian Professor of Structural Engineering
University of California at Berkeley

INTRODUCTION

Increasing attention has been placed in recent years on the possibility of base isolating bridges, both in terms of new construction and retrofit of existing seismically deficient structures. Isolators must be durable under traffic and environmental conditions, able to sustain large loads under substantial lateral displacements, capable of dependably and repetitively achieving their specified restoring force characteristics, and hopefully, easy to design. The applicability of a number of different types isolators has been recently investigated. In this paper, some of the attributes of Friction Pendulum System (FPS) connections will be reviewed and the application of these devices to bridge structures will be discussed.

Friction bearing systems have been long used in bridge construction to accommodate motions due to thermal expansion and foundation settlement. A variety of seismic isolation systems has been developed along similar lines; typically, a teflon bearing slides along a flat stainless steel plate. This system is inherently able to sustain large loads and displacements, is able to dissipate dependably large amounts of hysteretic energy, and utilizes technology long employed in bridge construction. However, post-earthquake residual displacements are potentially large resulting in disruption of operation while the bridge is re-centered. Supplemental stiffening elements are usually added to such systems in order to reduce residual displacements. The design of such restoring force systems is often troublesome and their implementation complex.

FEATURES OF THE FRICTION PENDULUM SYSTEM

The Friction Pendulum System offers a simple solution to these problems. Figure 1 schematically shows a cross section through a FPS connection. The sliding surface is spherical in shape, rather than flat, and the bearing material is supported by an articulated slider that conforms to the concavity of the sliding surface. Various bearing materials are available that can provide effective dynamic friction coefficients ranging between roughly 2% to 10% and greater.

This simple device provides ideal bilinear restoring force characteristics as shown in Fig. 2. When activated, friction provides a restoring force proportional to the supported weight ($R = \mu W$). The spherical shape of the sliding surface raises the structure in a pendulum motion resulting in an additional restoring force which increases as the structure is displaced away from its original position. This latter term is proportional to the weight of the supported structure and the lateral displacement, δ , and inversely proportional to the radius of curvature, r , of the spherical surface. Thus, the total restoring force is given by:

$$R = \mu W + W\delta/r \quad (1)$$

This relation results in a number of desirable response characteristics. For example, the activated period of a (rigid) structure supported on FPS connections will not depend on the weight of the structure, but rather be governed by the relations for a pendulum. That is, $T_c = 2\pi\sqrt{r/g}$, where g is the gravitational constant. This makes the inelastic response of the system relatively insensitive to variations in the supported mass. The dependence of the restoring force on the supported weight also results in the center of mass coinciding with both the centers of strength and stiffness of the activated structure. Thus, the activated system has little tendency to twist about a vertical axis.

The restoring force characteristics are reliably predicted by Eq. 1 (see Fig. 3). moreover, they can be easily altered in design by simply changing r or μ as desired.

It can be noted that a pin connection is provided within the connection. This allows the connections to be used alternatively at the top or bottoms of columns or piers in situations where moment transfer is not required or desirable. The pin connection makes the devices insensitive to rotations associated with thermal movements, load distributions, foundation deflections and so on. A pin connection at one end of a column may not be desirable if a stiffer structure is needed or if the column size needs to be limited. In such cases, the FPS connection can be inobtrusively placed at the mid-height of the column or pier at its point of inflection. This will result in increased lateral stiffness and lower moment demands for the same design base shear.

As indicated in Fig. 1 the FPS connectors are compact in size. Their diameters can be selected to accommodate the required lateral seismic displacements. The height of the connection can be as little as 4 inches (100 mm) since the vertical displacements needed by the pendulum motions are actually quite small. This makes the connections particularly suitable where aesthetic or retrofit considerations limit the size of the isolator.

Another feature that differs in the devices relative to conventional bridge bearings is that the bearing materials utilized allow much higher bearing stresses. These usually range from 15 to 25 ksi (1 to 1.7 tf/cm²), resulting in bearing areas considerably smaller than required with elastomeric isolators or conventional pot or spherical bearings. As schematically indicated in Fig. 1, displacement restraints can be built directly into the connections. Thus, the FPS connection provide the required isolation, restoring force and displacement restraint in a compact, self contained package. It is interesting, and important, to note that the devices can operate either with the concave surface facing up (as in Fig. 1) or down.

EXPERIMENTAL VERIFICATION

Numerous static and dynamic tests have been carried out to verify the operation of FPS connections [1 and 2]. Results for individual connectors (e.g., see Fig. 3) reflect the ideal bilinear hysteretic behavior desired for seismic response. This behavior simplifies nonlinear analysis of structures supported on the connectors. More than a hundred shaking table tests have been completed on various multilevel structures. In these, the isolators have been placed at the top of the columns in the lower level. No special framing was provided at the base of the connections to rotationally restrain the connections. In these tests a variety of ground motions were considered and structures with different weights, periods, height to width ratios, and stiffness and mass eccentricities were examined. Cases resulting in impact of the isolators against displacement restrainers, and uplift (and subsequent recontact) of the bearings from the sliding surfaces were included. The FPS

supported structures all performed according to expectations and experimental results could be accurately predicted using conventional nonlinear analysis programs.

The tests indicated that the FPS connectors substantially reduced the forces developed in the supported system. The connections absorbed increasing proportions of the total lateral displacement as the period of the supported system decreased. For structures with periods greater than the predominant period of the ground motion, the total lateral displacement virtually equalled the elastic displacement of the structure computed considering the initial elastic period of the structure and conventional damping values associated with non-isolated structures. In the short period range displacements of the FPS supported structures exceeded those of comparable elastic systems. This behavior can be seen by referring to Fig. 4 in which the maximum total and connector displacements are plotted for different structural periods on the same graph as the elastic response spectrum for the ground excitation used. This behavior is expected considering the observation by Newmark [3] and others that the displacement of elastic and inelastic systems are nearly equal in the moderate and long period ranges, and that conservation of energy may be used to predict the increased displacements in the short period range. The nearly ideal bilinear hysteretic response characteristics of FPS supported systems lends itself to simplified analysis and design utilizing Newmark's procedures.

In addition, the easily predicted bilinear restoring force characteristics simply nonlinear analysis. Fig. 5 compares the experimental and analytical results for one shaking table test. The results are in excellent agreement.

IMPLEMENTATIONS

FPS connectors have thus far not been installed in bridge structures. However, they are being considered in feasibility studies for the design and retrofit of several bridges in California. In addition, FPS connectors have been installed in other types of structures, such as a four story apartment building in San Francisco's Marina District [4] and an elevated liquid storage tank.

TORSIONAL RESPONSE OF ECCENTRIC STRUCTURES

As indicated above, one of the unique features of the FPS system is that the centers of mass, stiffness and strength all coincide once the connectors are activated. Structures with significant mass and stiffness eccentricities in the elastic range are generally prone to severe torsional motions. It is often difficult to tailor the distribution and properties of elastomeric bearings to correct for these performance deficiencies. The FPS system does so automatically, generally with a substantial reduction in torsional response.

For example, consider Fig. 6 in which experimental shaking table data for a FPS isolated structure is plotted against analytical simulations for identical non-isolated structures. In these structures, a variety of eccentricities were introduced by moving the center of mass and modifying member properties to shift the center of elastic stiffness. It can be seen in Fig. 6 that the FPS connectors reduced the torsional motion of the structure relative to the non-isolated structure by 80%, 85% and 89% for eccentricities of 10%, 20% and 30% of the shaking table model's maximum dimension. Eccentricities represent the horizontal distance between the center of elastic stiffness and center of mass. D_t in the figure represents the difference between the displacement at the corner of the structure and at its geometric center, D . This results in very significant reductions in torsional response.

Torsion introduced by "accidental" variations in connector properties have also been investigated. It has been shown [2] that, by introducing a 20% error in the friction coefficients in the FPS connections supporting one half of a structure, increases in corner seismic response are less than 5% of the displacement at the center. This increase is less than half that which would have occurred in a non-isolated structure with a 5% accidental mass eccentricity. Thus, the FPS characteristics tend to attenuate accidental torsional effects associated with structural as well as isolator induced eccentricities.

DISPLACEMENT RESTRAINT EFFECTS

A major concern in seismic design of isolated structures is the effect of unexpectedly large displacements in the isolators. A series of shaking table studies were also carried out to assess this behavior for FPS connections. In these tests the isolated structure was subjected to unusually intense ground motions. As in the previous tests, the structure was supported by columns, fixed at their base and with FPS connectors at the top. A restraining ring in the FPS connector (Fig. 1) limited lateral displacement in the connector.

When the restrainer ring limited connector displacement, a very brief increase in structural load occurred resulting in increased deformations in the supported structure. Figure 7 shows the results of an experimentally verified series of analyses. The ductility demand on the supported structure is plotted as a function of the ratio of the displacement required in a ideal system without a displacement restraint to the limiting displacement provided by the restrainer ring. In Fig. 7 it can be seen that the increases in ductility demand are negligible until the required displacements exceed the limiting displacements by a factor of two. In this case the ductility demands are similar to those that would have been required had the FPS isolators not been present at all.

The velocity and momentum of the structure is decreased by the FPS connectors at the point of impact so the impulse provided by the impact is small. In addition, positioning the connectors at the top of columns lessens the effect of the impact. It would appear that it is prudent to provide ductile detailing in FPS supported structures, but that it is not necessary to increase the strength of the structure to resist the effects of displacement restraint.

CONCLUDING REMARKS

FPS connections provide an alternative form of isolation that should prove useful in the design and retrofit of bridge structures. Their compact size, easily controlled bilinear hysteretic characteristics, and use of proven bridge bearing technologies make them particularly attractive. Simplified design procedures based on methods suggested by Newmark provide a quick and reliable means of preliminary design. There beneficial behavior under conditions of mass or stiffness eccentricities may be utilized in bridge construction. Additional research is needed to study in depth the applicability of FPS and other types of connections to bridge structures.

ACKNOWLEDGEMENTS

The author is especially grateful for the joint funding for the research described herein by Earthquake Protections Systems and the U.S. National Science Foundation. The

FPS connector is a patented product of Earthquake Protection Systems of San Francisco, and licensed in Japan and Taiwan to Oiles Corporation.

REFERENCES

1. Zayas, V., Low, S. and Mahin, S., "The FPS Earthquake Resisting System: Experimental Report," *Report No. UCB/EERC-87/01*, Earthquake Engineering Research Center, University of California, Berkeley, June 1987.
2. Zayas, V., Low, S., Bozzo, L. and Mahin, S., "Feasibility and Performance Studies on Improving the Earthquake Resistance of New and Existing Buildings using the Friction Pendulum System," *Report No. UCB/EERC-89/09*, Earthquake Engineering Research Center, University of California, Berkeley, Sept. 1989.
3. Newmark, N. and Rosenbleuth, E., *Fundamentals of Earthquake Engineering*, Prentice Hall, 1971.
4. "New Seismic Isolators and Seismic Retrofit," *Civil Engineering*, ASCE, October 1991.

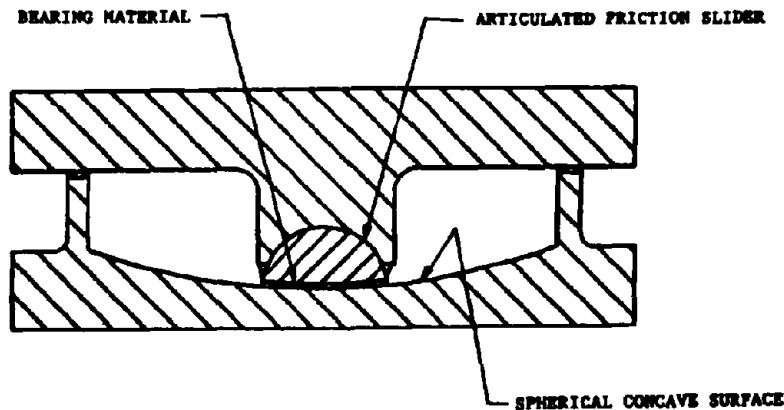


Fig. 1 Schematic of a FPS Connection

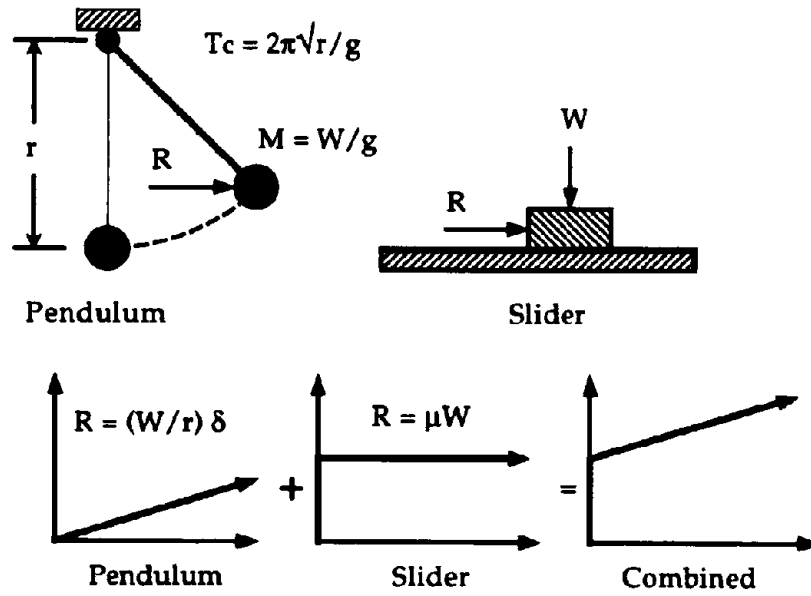


Fig. 2 Pendulum and Friction Action Resulting in Bilinear Restoring Force Characteristics

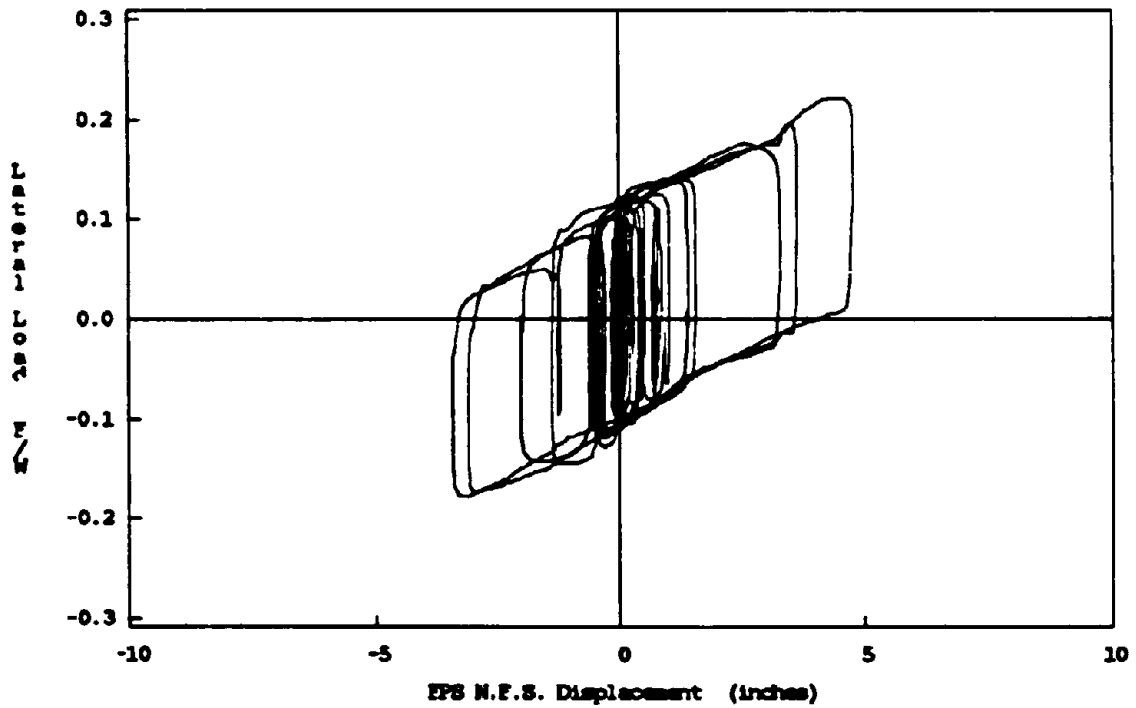


Fig. 3 Typical Hysteresis Loops for a FPS Connector

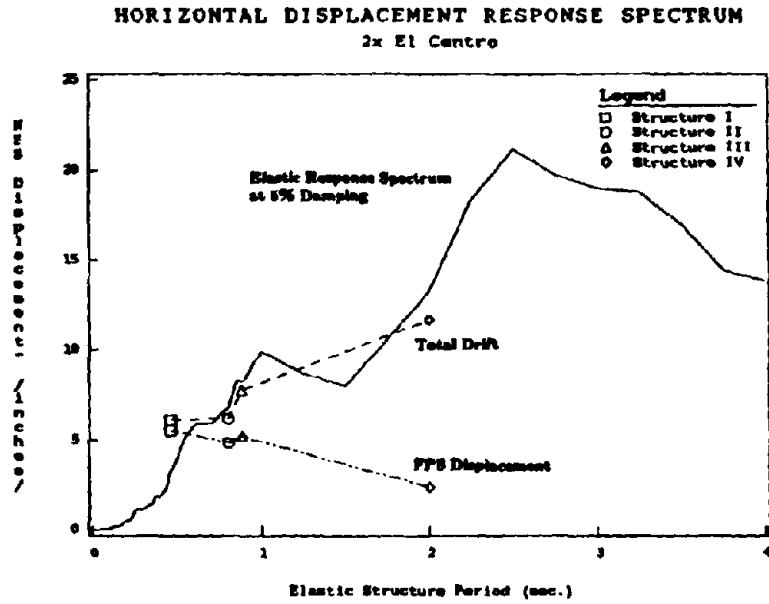


Fig. 4 Comparison of Inelastic Response of FPS Supported Structure with Elastic Response Spectrum

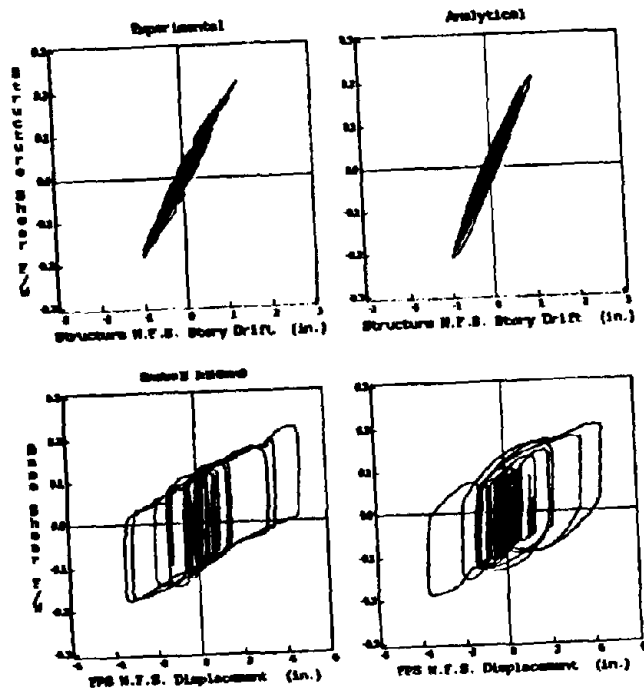


Fig. 5 Comparison of Experimental and Analytical Results for Two Level FPS Supported Structure

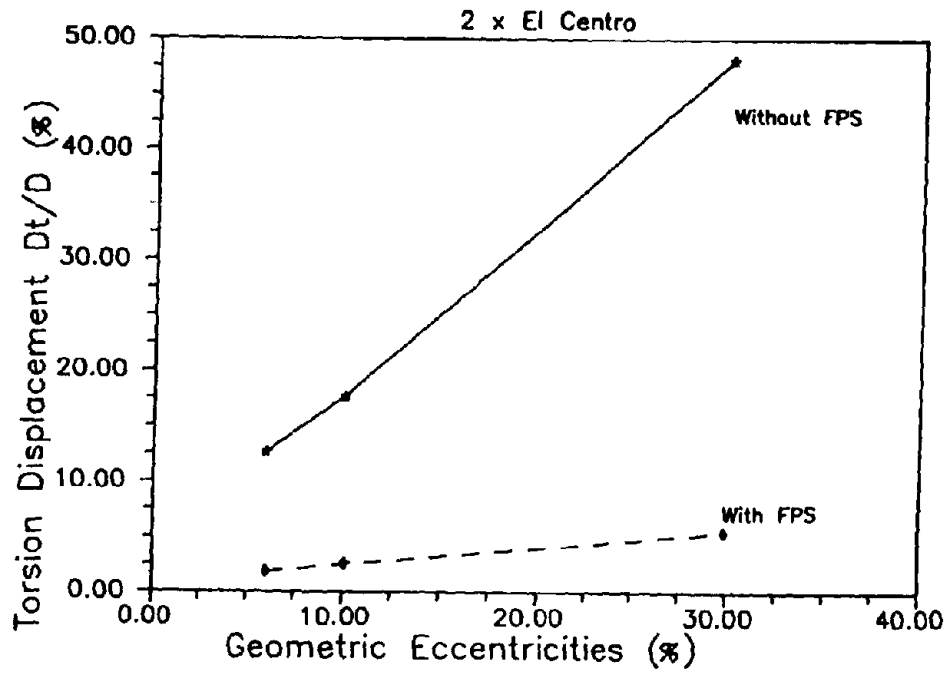


Fig. 6 Variation of Response with Increase in Torsional Eccentricities

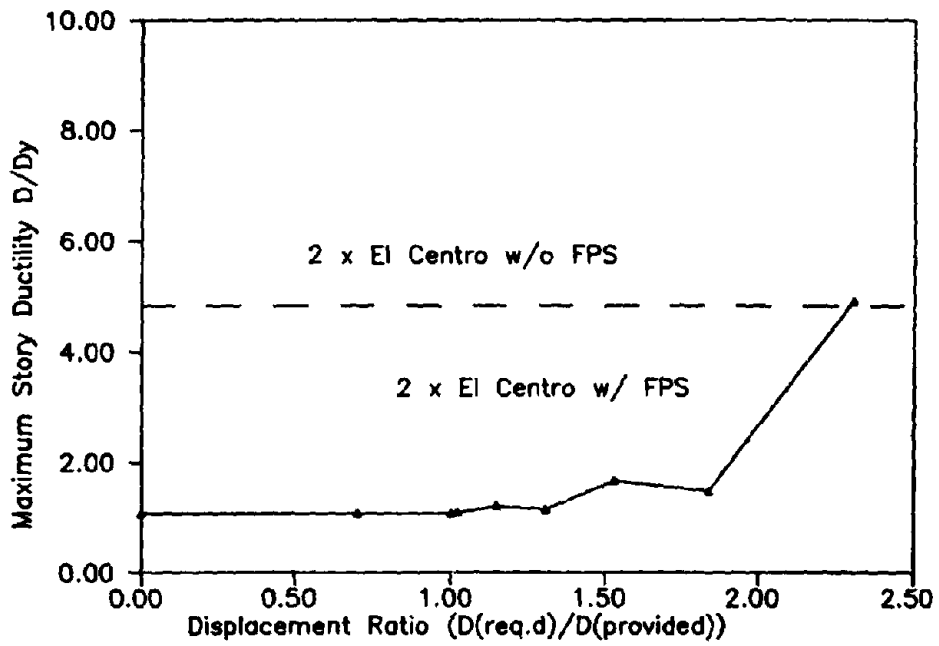


Fig.7 Comparison of Ductility Demands With and Without Displacement Restraint

LATERAL LOADING TESTS OF KNOCK-OFF MECHANISM FOR MENSHIN BRIDGES

Toshio KIKUCHI and Yozo GOTO

Technical Research Institute, Obayashi Corporation, Kiyose-shi, Tokyo, Japan

SUMMARY

Experiments with 1/2 scale models were performed on the knock-off device, which absorbs bridge girder displacement by transforming one section of the bridge abutment towards the backfill earth when the Menshin designed bridge girder collide with the abutment during a major earthquake. In the experiments, both resistance, as well as damage to the backfill earth and pavement when the knock-off device slides due to girder collisions were investigated, and necessary information for a rational design of the knock-off device was obtained.

INTRODUCTION

The girder response displacement of Menshin designed bridges becomes greater than that of non-Menshin designed bridges. For that reason, it is necessary to leave a large interval of space between the girder and the abutment, as well as between the girders themselves, and to incorporate an expansion device with a large capacity of expansion. Incidentally, this kind of expansion device is not just expensive, it results in the loss of stability of automobiles, harm to the surrounding environment from noise and vibration, and traffic stoppage due to frequent damage and its repair work.

Therefore, if the large and expensive expansion device is used in a bridge for major earthquakes which occur in such a small probability of occurrences as once or twice during its lifespan, but if such an earthquake should actually occur and the expansion device is damaged, allowing the girder to collide with the abutment or to collide among themselves, then it would be reasonable to think that it can be designed so that one section of the girder or abutment is allowed to move and is damaged within a predetermined range for ease of repair when a major earthquake hits the bridge. As one example of this ingenuity, the knock-off device has actually been applied in New Zealand as shown in Fig. 1 (Ref. 1). In this case, when the girder collides with the abutment during major earthquake, the knock-off element built on the abutment crest detaches to the backfill earth, so structural damage to the abutment and girders from collision is avoided and repairs can made easily.

There are no cases in which this kind of device has been used in Japan and no design method has yet been established. Japan, which has more traffic than New

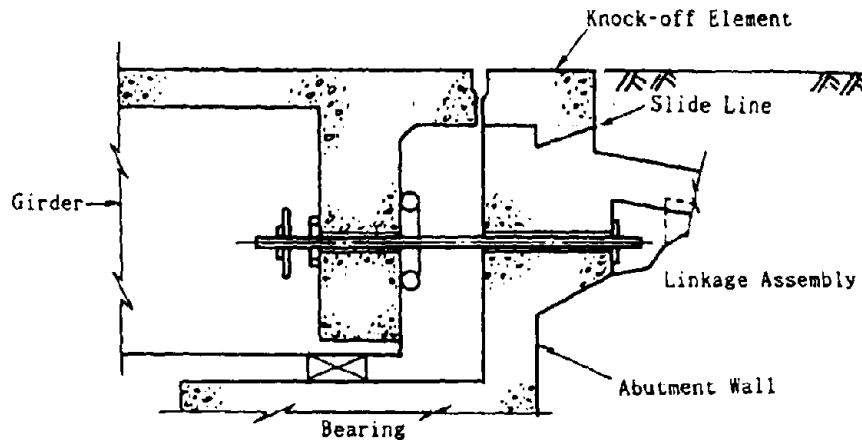


Fig. 1 Knock-off Device (Moonshine Bridge in New Zealand)

Zealand and which is likely to experience an earthquake with a great magnitude causing response displacement large, needs to develop a knock-off device, confirm its function, and establish a design method taking into consideration both the concept developed in New Zealand (Ref. 2) and the domestic circumstances of Japan.

Therefore, this research consisted of producing knock-off models of a scale 1/2 that of the actual structures including backfill earth as well as asphalt pavement, and performing tests on them under both static and dynamic loads applied with an actuator.

EXPERIMENTAL METHODS

Loading System A rough outline of the test device is shown in Fig. 2. The bridge abutment ① and the backfill soil ② are loaded onto the test table ③ and then the girder ④ is fixed to the reaction wall. The test table is supported by a hydro-static pressure bearing ⑤ and the actuator ⑥ causes it to slide in a lateral direction. From the static and dynamic motion of the test table caused by the actuator, the knock-off element ⑦ and girder can be made to collide. A load cell is installed in the tip of the girder to enable measurements of the reaction during collision.

Model Configuration The size of the models is 1/2 that of the actual structures and the knock-off element of each model is made of reinforced concrete with a depth of 2 m, a width of 0.25 m and a height of approximately 0.25 m. The asphalt pavement model has the same strata as the actual structure and uses asphalt pavement material with a layer thickness 1/2 that of the actual structure. Fig. 3 shows details of the knock-off element and asphalt pavement models. The knock-off element models simulate cases in which the anchor dowel is present and others when it is not. In the New Zealand example, there is no anchor dowel, but when Japanese traffic conditions and expansion device installation conditions are considered it is thought that the anchor dowel becomes necessary (Ref. 3). The necessary section area for the anchor dowel is determined to be the section area that can resist the extraction force from the moment of overturn that is generated by wheel and brake loads as shown in Fig. 4.

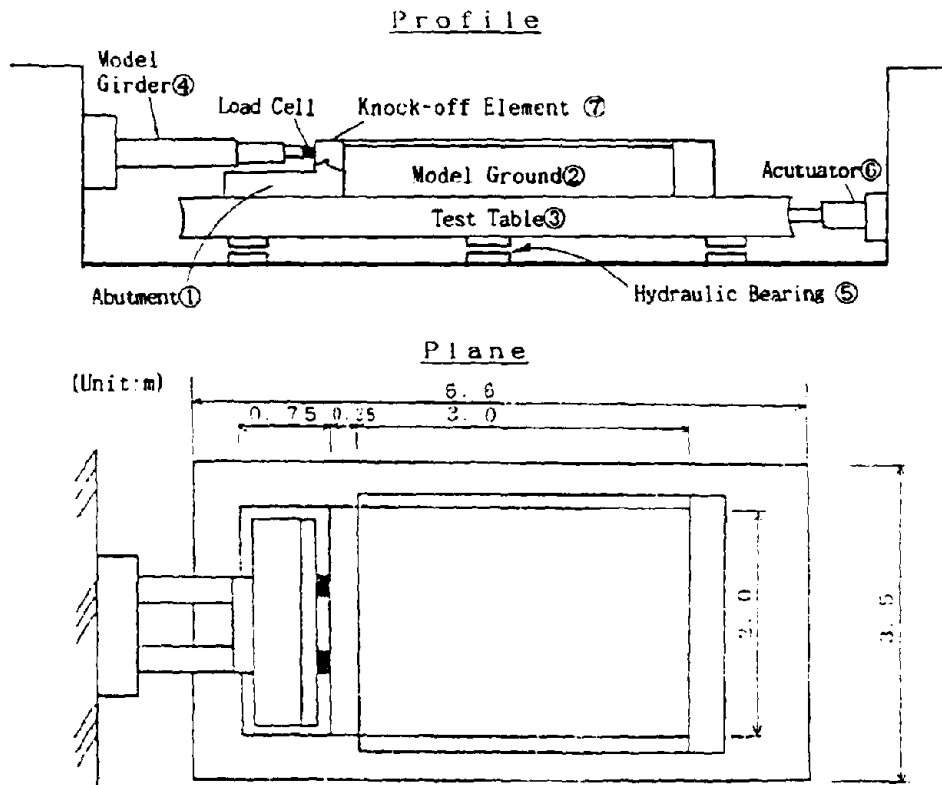


Fig. 2 Test Device

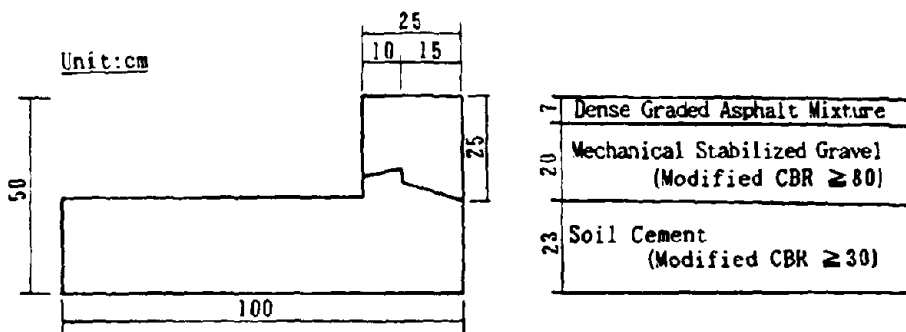
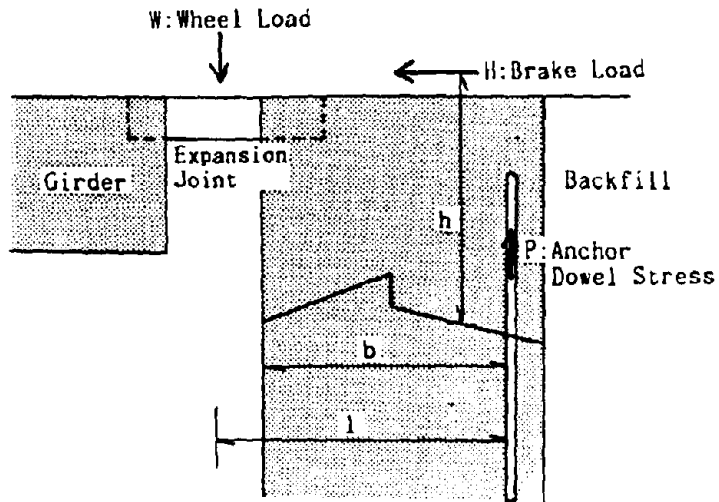


Fig. 3 Model of Knock-off Device and Asphalt Pavement



$$P b = W l + H h$$

Fig. 4 Design Load of Anchor Dowel

Table 1 Test Cases

Test No.	Model Type		Loading Speed			Backfill Condition			
	Without Anchor Dowel	With Anchor Dowel	Static	Dynamic (cm/sec)			Without Backfill	Dry Sand	Asphalt Pavement
				10	15	20			
1	○		○				○		
2		○	○				○		
3	○		○					○	
4	○			○				○	
5	○				○			○	
6	○					○		○	
7	○		○						○
8	○			○					○
9	○				○				○
10	○					○			○
11		○	○						○

Test Cases Six knock-off models were produced and a total of 12 different experiments were performed under different conditions. The test cases are shown in Table 1. The sliding resistance of the knock-off element was examined in the experiments without backfill earth. In the dry sand test, it was easy to analyze the generative mechanism of the resistance when the knock-off element slid towards the backfill by using material with known properties. The purpose of the experiments conducted without the anchor dowel was also to analyze the mechanism of resistance.

The purpose of the dynamic test was to study the effect of velocity when the knock-off element is pushed in to the backfill earth. The test velocity is set taking into consideration the normal earthquake response velocity of girders.

Measurements Items measured include the reaction at and after collision, horizontal, vertical, and rotational displacement of the knock-off element, as well as land surface displacement of the backfill earth and the pavement.

EXPERIMENTAL RESULTS

Displacement - Resistance Relationship The relationship at collision between the sliding resistance force of the knock-off element and the lateral displacement at the central position is shown in Figs. 5 - 7.

Fig. 5 depicts a backfill of dry sand with no anchor dowel. The maximum resistance is between 1.3 - 1.6 tons and the effect of the knock-off velocity is small. On the other hand, Fig. 6 shows the results when the surface of the backfill paved with asphalt, also with no anchor dowel. In the case of asphalt pavement, the maximum resistance increases between 5.6 - 24.4 tons and the effect of the velocity becomes prominent. When the resistance reaches the maximum value, the displacement with dry sand of Fig. 5 is from 0.5 to 1cm, but is almost twice this amount with asphalt pavement of Fig. 6. From these observations, it is understood that the effect of pavement on the knock-off device is great and that the effect of viscosity, a special property of asphalt, becomes strong on the generative mechanism of the resistance.

Fig. 7 compares the presence of the anchor dowel with the absence of it under the conditions of asphalt pavement. With the anchor dowel, the resistance increases substantially and the maximum displacement also increases, attaining a value of 4 cm. The anchor dowel, which does not break off even when the knock-off component starts sliding, bears the majority of the resistance after sliding while causing post-yield expansion and extraction. These experiments in which the reinforced section area for the area of the knock-off sliding surface is 0.08% while that for the section area of asphalt pavement is 0.28%, revealed that resistance when this amount of anchor dowel is present is almost equivalent to that of asphalt pavement.

Failure Mode Damage conditions with dry sand backfill are shown in Photo 1. It is understood that a slip line appeared on the surface of the sand at a position 75 - 100cm from the end section of the knock-off device and the area rose up, causing slip damage when the backfill earth was subjected to passive earth pressure. The angle of inclination for the lateral slip surface was 15 - 20 degrees. In the case of asphalt pavement as well, it was observed that the earth surface below the pavement surface caused slip damage. On the average, the inclination for that lateral slip surface was 30 degrees.

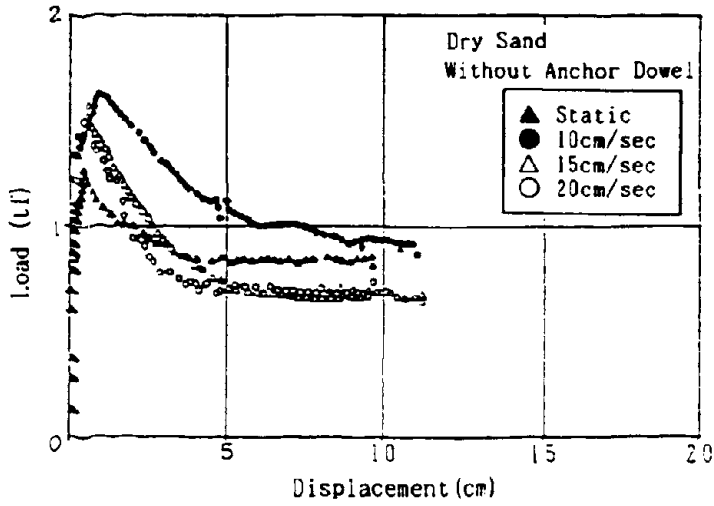


Fig. 5 Effect of Loading Speed

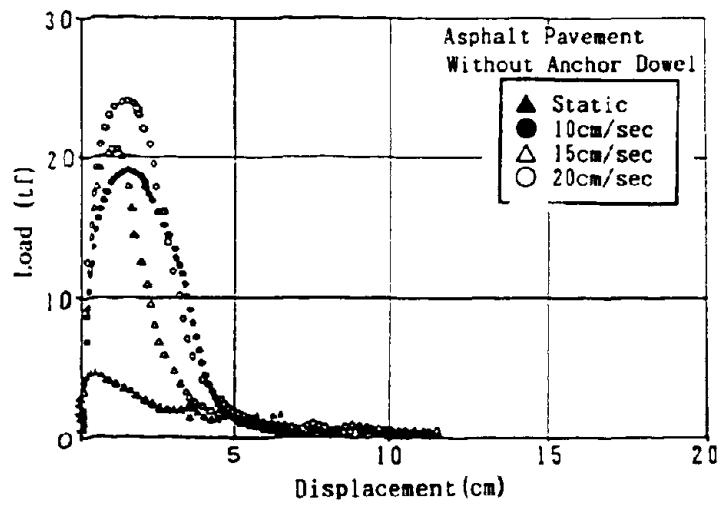


Fig. 6 Effect of Loading Speed

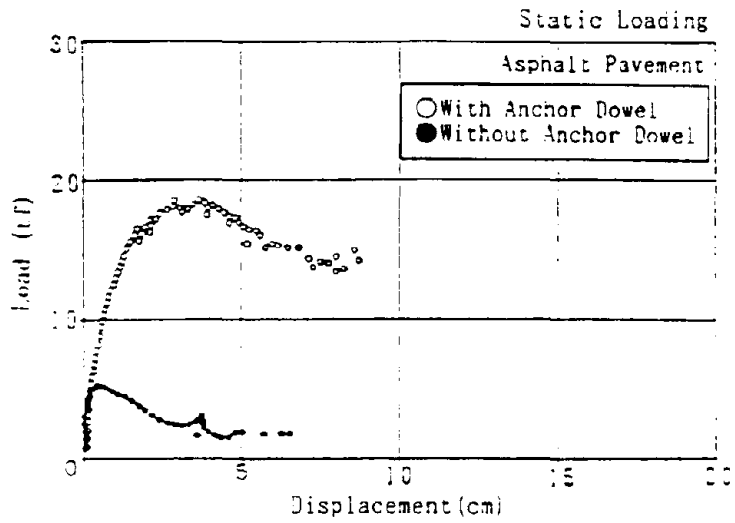


Fig. 7 With and Without Anchor Dowel



Photo 1 Rise up of Backfill Sand

Photos 2 and 3 show the damage features of the pavement surface when paved with asphalt. In Photo 2, the pavement surface in a vicinity of approximately 50 cm from the knock-off section bent and caused damage during static load. In Photo 3, the pavement peeled up and the knock-off section crept under the pavement causing damage during dynamic load. These damages were the same in each of the two cases of static load and the four cases of dynamic load.

It is thought that the difference in the form of damage between static load and dynamic load depends on the effect of the visco-elastic property of asphalt. Assuming that there may be high-speed run-away automobiles during or immediately following a major earthquake, it is not desirable for the pavement to rise up as shown in Photo 2, but is desirable that the form of damage be as shown in Photo 3.

Reparability Since major damage does not occur to the knock-off section when there is no anchor dowel, repair can be made by removing the damaged section of the pavement and repaving the area. Since the anchor dowel is not easily broken off when it is present, damage can occur when a fissure appears in the concrete from the root insertion section of the anchor dowel and the concrete peels. It is necessary to improve the design method of the anchor dowel by making a knock-off device with good reparability.

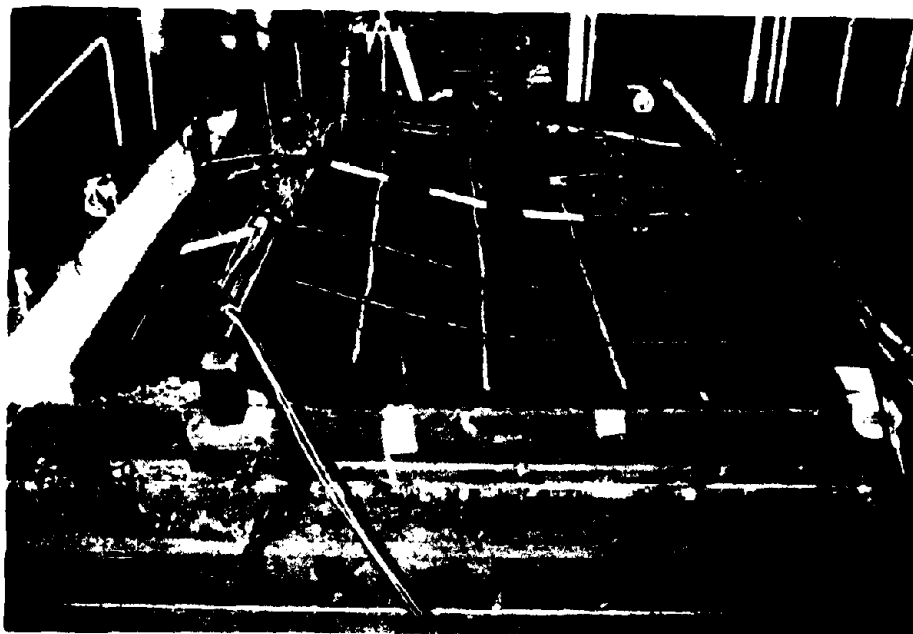


Photo 2 Deformation by Static Load

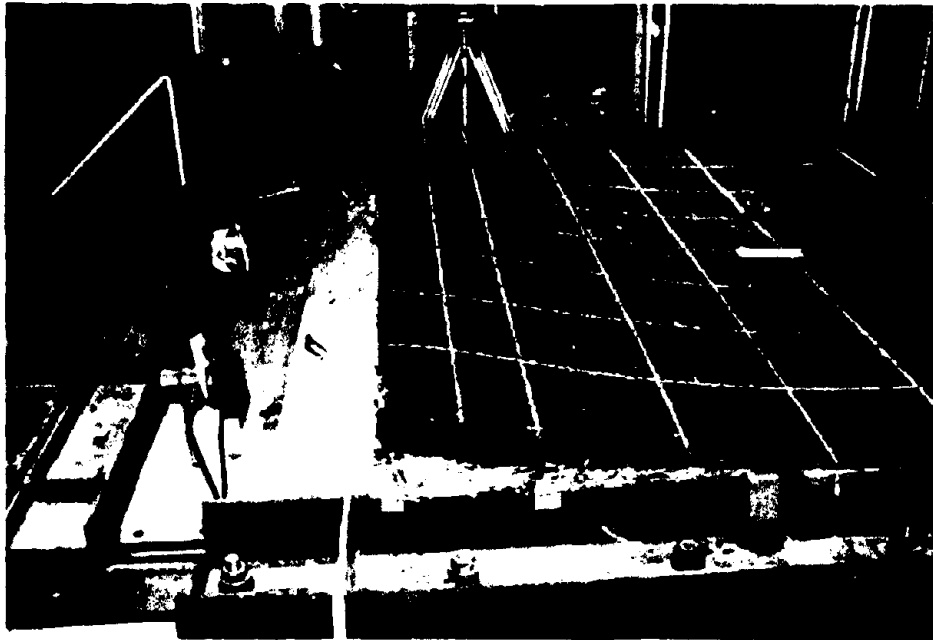


Photo 3 Deformation by Dynamic Load

NUMERICAL ANALYSIS

Analysis by Plastic Equilibrium Theory Resistance was calculated based on the plastic equilibrium theory in which friction and adhesion act on the slip surface of each analysis model considering the wedge-shaped soil block shown in Fig. 8. It is assumed that adhesion acts on the inside of the asphalt pavement. In addition, it is assumed that the resistance of the anchor dowel is from extraction. The material property values used in the analysis are shown in Table 2, and a comparison of the test values and analysis values is shown in Table 3. The static load test results can be virtually explained by this analysis, but there is a great disparity with the analysis values from the results of the dynamic load test, and it is understood that it is very important to correctly evaluate the dynamic material properties of asphalt pavement.

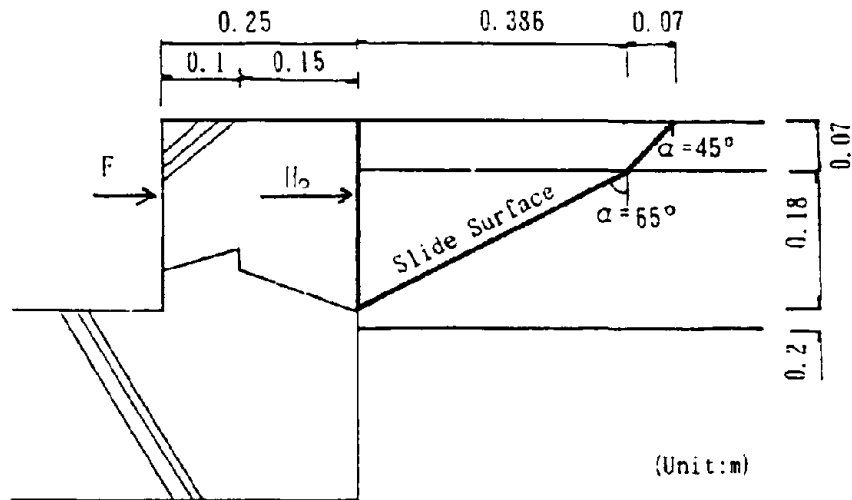


Fig. 8 Soil Wedge Model

Table 2 Material Constants

	Concrete	Dry Sand	Gravel	Asphalt Pavement
Unit Weight (tf/m ²)	2.4	1.52	2.1	1.03
Friction Angle	—	41.8°	40.0°	0°
Cohesion Force (tf/m ²)	—	0.	0.	15.

Table 3 Maximum Resistant Force (Static Loading)

Model Type	Backfill Condition	Experiment (tf)	Analysis (tf)
Without Anchor Dowel	Without Backfill	0.12	0.12
	Dry Sand	1.27	1.31
	Asphalt Pavement	5.57	4.78
With Anchor Dowel	Asphalt Pavement	19.0	7.92
Without Anchor Dowel	Asphalt Pavement	19.0~24.0	—
Dynamic Load			

CONCLUSION

(1) From the results of the model experiments, resistance when the knock-off element slides toward the backfill could be analyzed by using the plastic equilibrium theory, and it was made clear that resistance mainly arises from asphalt pavement and steel reinforcement. In particular, it is thought that the asphalt resistance with dynamic load reaches a level that is several times that of static load, and it is important to adequately estimate that resistance.

(2) From the results of the model experiments, it was made clear that the backfill material of the knock-off element causes wedge-shaped slip damage. In the case of static load, damage occurred when the surface of the asphalt pavement rose up and buckled, but in the case of dynamic load, the asphalt peeled up and the knock-off element crept under it. Improvement of the design so that the knock-off element normally creeps under the pavement is desirable to insure the driving safety of automobiles during and immediately following an earthquake.

(3) Repair of backfill material and pavement damaged in a wedge is relatively easy. Design improvements on anchor dowel are needed because it damages the concrete at the point where it is attached.

(4) In the future, analyses concerning test result values, asphalt properties, and the reduction effect from the absorption of energy from the knock-off procedure will be conducted and further development of the knock-off device and design methods used in Japanese highway bridges is planned.

ACKNOWLEDGEMENT

This study was made as a part of the joint research program on "Development of Menshin Systems of Highway Bridges" between PWRI and 28 private firms in Japan. Grateful acknowledgement is made to Dr. K. Kawashima, Mr. K. Hasegawa, Mr. K. Unjou and Mr. H. Nagashima of PWRI and members from 28 private firms for their valuable discussions on this research.

REFERENCES

1. Ministry of Works and Development of New Zealand : "Wellington - Kaitoke Motorway, Upper Hutt Bypass, Moonshine Bridge · Linkage Bolts and Abutment Steel work Details" As Built Drawing Code 7504 Sheet 21
2. A. G. Lanigan, R. L. Preston, R. W. Fisher and M. J. Stockwell : "Seismic Design of Bridges - Section 8 - Structural and Non Structural Details" Road Research Unit Bulletin 56, National Roads Board, Wellington, New Zealand, 1981
3. Technology Research Center for National Road Development : "Guidelines on the Design of Menshin Highway Bridges (Draft)", March 1989 (in Japanese)

DEVELOPMENT OF FALLING-OFF PREVENTION DEVICES FOR MENSHIN BRIDGES

Daisuke OZAKI¹ and Fumio MATSUMOTO²

¹ Civil Engineering Division, Taisei Corporation, Shinjuku-ku, Tokyo, Japan

² Technical Department, Tokyo Fabric Industry Co., Shinjuku-ku, Tokyo, Japan

SUMMARY

This report deals with the development of anchor bar type falling-off prevention devices for Menshin bridges equipped with shock absorber (laminated rubber) (Fig.1). The effectiveness of the falling-off prevention devices with absorbers in reducing the relative displacement between the super and substructures of Menshin bridges and the horizontal reaction force was demonstrated through numerical analysis on a bridge model. Clarifications were then made on the compression-reaction force properties of the falling-off prevention devices through element tests involving static compression loading on laminated rubber with round steel bars (anchor bars).

INTRODUCTION

Falling-off prevention devices, as restrainers for reducing the large inertia force and displacement of the superstructure during severe earthquakes, should desirably be installed not only at the ends of the girders but also at the support points in between to disperse the horizontal reaction force during earthquakes. That is to say, since a certain amount of relative displacement occurs at each support point on Menshin bridges or reaction force dispersion bridges, it is desirable to disperse the horizontal reaction force at each support point. They should also have a structural capability of accommodating the relative displacement between the super and substructures with flexibility so as not to impair the basic performance of the Menshin devices for support, restoration, damping and deformation. (Ref.1)

A shock absorber, as shown in Fig.1, made up of anchor bars and laminated rubber and capable of flexible accommodation of the horizontal forces was developed as a falling-off prevention device that can be installed on piers and abutments. The results of the numerical analysis on a bridge model and element tests on the device are reported below.

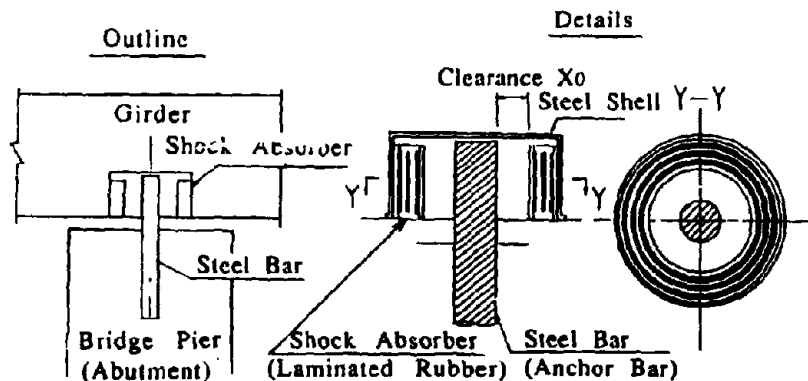


Fig. 1 Structural Outline of Falling-Off Prevention Device

NUMERICAL ANALYSIS

Analysis Conditions Non-linear time history response analysis was carried out on the two-dimensional bridge model shown in Fig.2 using seismic input along the direction of the longitudinal axis, for the purpose of demonstrating the effectiveness of the falling-off prevention devices equipped with shock absorber in reducing the relative displacement between the super and substructures of a Menshin bridge, as well as the horizontal reaction force, and to determine the spring stiffness of the absorber to be developed. The node weights, properties of the super and substructure members and spring stiffnesses are given in Tables 1, 2 and 3.

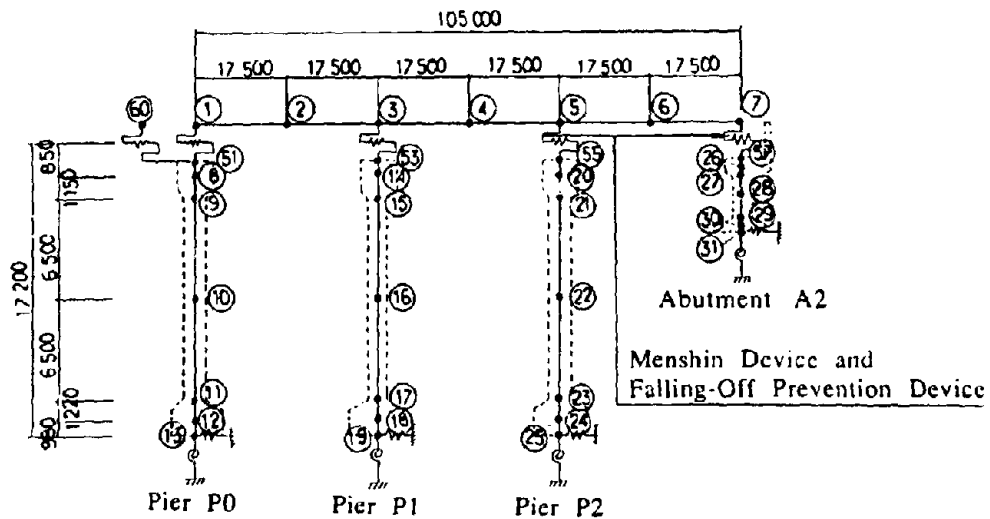


Fig. 2 Bridge Model (frame model)

Table 1 Weight of Node

Node	Weight (t f)	Node	Weight (t f)	Node	Weight (t f)
1	180.3	13	0.0	25	0.0
2	360.7	14	105.3	26	106.1
3	360.7	15	0.0	27	0.0
4	360.7	16	236.9	28	69.8
5	360.7	17	0.0	29	0.0
6	360.7	18	468.1	30	208.5
7	180.3	19	0.0	31	0.0
8	105.3	20	105.3	51	0.0
9	0.0	21	0.0	53	0.0
10	236.9	22	236.9	55	0.0
11	0.0	23	0.0	57	0.0
12	468.1	24	468.1	60	360.7

Table 2 Properties of Members in Super and Substructures

Member	Sectional Area (m ²)	Geometrical Moment of Inertia (m ⁴)	Young's Coefficient E (tf/m ²)	Poisson's Ratio ν	Damping Constant h
Girder	∞	∞	2.7E+6	0.167	5%
Pier	5.044	2.120	2.7E+6	0.167	5%
Abutment	8.553	0.205	2.7E+6	0.167	5%

Table 3 Ground Spring Stiffness

Member	Horizontal Spring (tf/m)	Rotational Spring (tf·m/rad)	Vertical spring (tf/m)	Damping Constant h
Pier	5.76E+5	4.58E+6	FIXEND	10%
Abutment	4.11E+5	1.37E+6	FIXEND	10%

The falling-off prevention devices were designed to come into operation under seismic motions which has a magnitude of the Kanto Earthquake or above. The seismic motion for such an earthquake had the acceleration response spectrum shown in Fig.3. Two simulated seismic waves were used for input seismic motions in the time history response analysis, one corresponding to that for the earthquake of the same magnitude as the Kanto Earthquake (input level for Menshin device design, Wave W1) and the other approximately 1.3 times that (input level for falling-off prevention device design Wave W2). The input accelerations of the simulated seismic waves are shown in Fig.4.

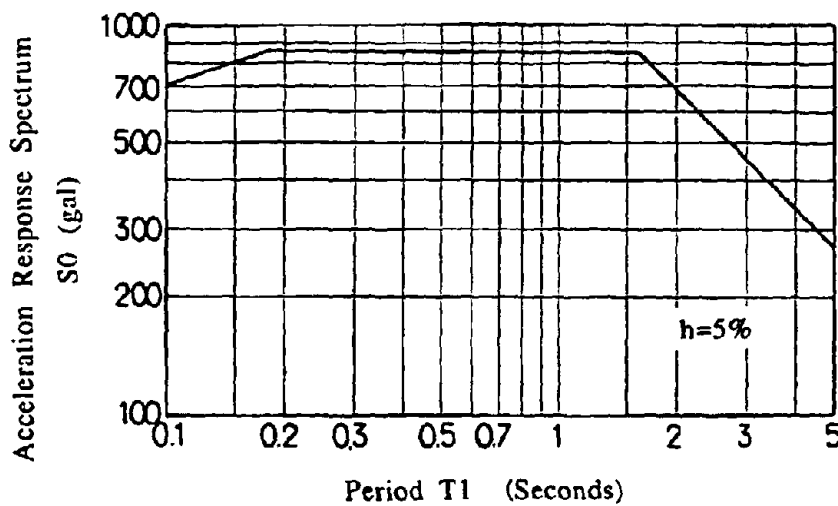
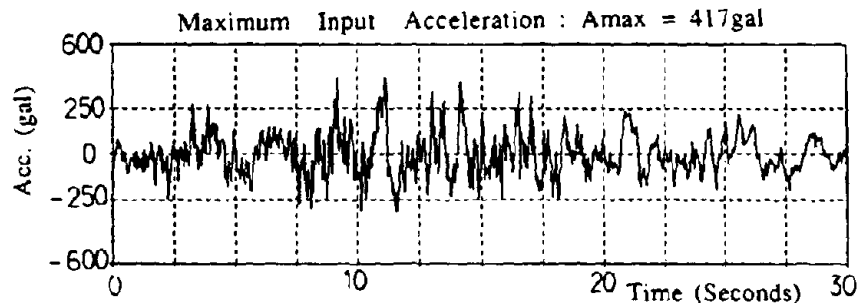
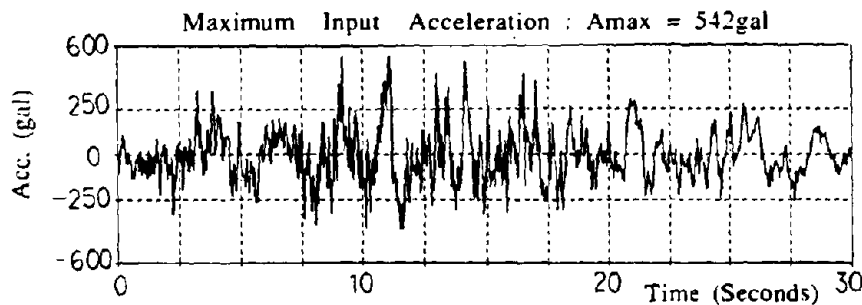


Fig. 3 Acceleration Response Spectrum (The same magnitude of the Kanto Earthquake)



(a) The same magnitude of the Kanto Earthquake
(Input Level for Menshin Device Design .Wave W1)



(b) The 1.3 times magnitude of the Kanto Earthquake
(Input Level for Falling-Off Prevention Device Design .Wave W2)

Fig. 4 Input Acceleration

Models of Menshin and Falling-Off Prevention Devices The Menshin devices were represented as non-linear spring members with bilinear hysteresis properties as shown in Fig.5 and Table 4, while spring members with their spring stiffness varying along the hysteresis loop as shown in Fig.6 and Table 5 and three cases were established for the falling-off prevention devices. (Case B was subdivided into 3 types.) The following conditions are required in establishing the models.

- (a) The clearance X_0 in the falling-off prevention devices (See Fig.1.) was made about the same as the maximum relative displacement of the bearings in the analysis at input level for the Menshin device design (Wave W1).
- (b) A rigid model (Case A) with an extremely large spring stiffness was used as a model of the conventional falling-off prevention device without the shock absorber.
- (c) Case B was used in investigating the optimum spring stiffness for the shock absorber with three different spring stiffnesses for Types ①, ② and ③.
- (d) Case C, corresponding to Case B Type ②, was established for investigations on how accurately the spring properties of the shock absorption materials needed to be represented.

The spring members of the Menshin and falling-off prevention devices were placed parallel to each other in the bearing models.

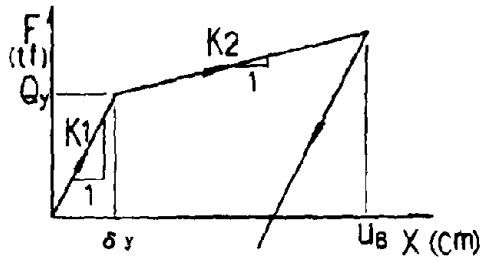


Fig. 5 Idealized Force-Displacement Loop of Menshin Device

Table 4 Physical Properties of Menshin Device

Item	P 0	P 1	P 2	A 2
K 1(tf/cm)	49.4	126.0	126.0	49.4
K 2(tf/cm)	10.2	26.4	26.4	10.2
Q _y (tf)	30.5	77.7	77.7	30.5
δ _y (cm)	0.62	0.62	0.62	0.62

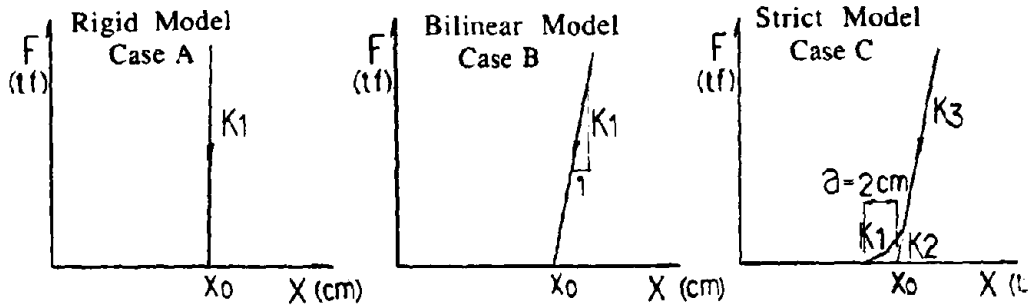


Fig. 6 Idealized Force-Displacement of Falling-off Prevention Device

Table 5 Physical Properties of Falling-off Prevention Device

Model Case	Item	P 0	P 1	P 2	A 2	
All Cases	x ₀ (cm)	15	15	15	17	
Case A	K 1(tf/cm)	10 000	25 000	25 000	10 000	
Case B	Type①	K 1(tf/cm)	33	83	83	33
	Type②	K 1(tf/cm)	100	250	250	100
	Type③	K 1(tf/cm)	300	750	750	300
Case C	K 1(tf/cm)	6	15	15	6	
	K 2(tf/cm)	30	75	75	30	
	K 3(tf/cm)	100	250	250	100	

Analysis Results The maximum horizontal displacements between the super and substructures are shown in Fig.7. The analysis results indicate that the falling-off prevention devices effectively reduce the maximum horizontal displacement. (Compare, for example, the maximum horizontal displacement of 21.7cm on Pier P1 without falling-off prevention device to that of 16.9cm with falling-off prevention device in Case B Type ②) There is no difference in the response between the bilinear model (Case B Type ②) and the strict model (Case C).

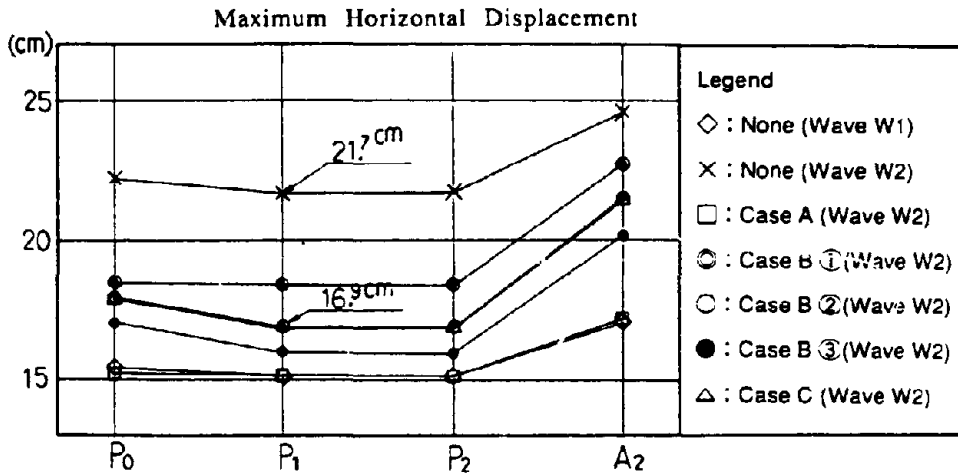


Fig. 7 Maximum Horizontal Displacement between Super and Substructures

The maximum horizontal forces in the falling-off prevention devices are shown in Fig.8. The analysis results indicate that the falling-off prevention devices equipped with shock absorber are particularly effective in reducing the maximum horizontal force. (Compare, for example, the maximum horizontal force of 2,023tf in the falling-off prevention device for Pier P1 in the rigid model (Case A) to that of 474tf in Case B Type ②) A large horizontal reaction force was generated at the Abutment A2 in the rigid model (Case A), creating unbalance reaction forces between the piers and the abutment. There is no difference in the behavior between the bilinear model (Case B Type ②) and the strict model (Case C).

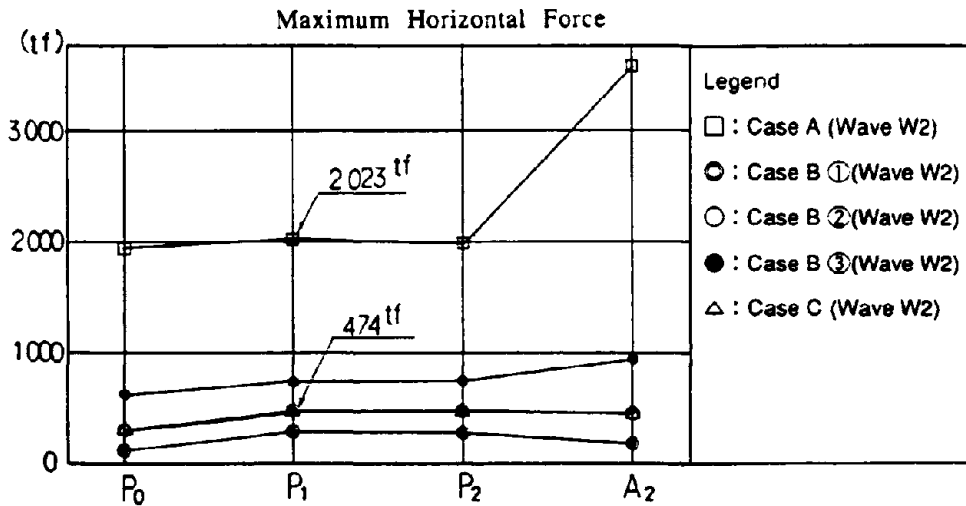


Fig. 8 Maximum Horizontal Force of Falling-Off Prevention Device

The time histories of the horizontal forces in the falling-off prevention device on Pier P1 are given in Fig.9. These figures show that the horizontal reaction force (impact force) acting on the falling-off prevention device decreases and the collision time increase as the spring stiffness of the shock absorber decreases. The falling-off prevention device came into operation twice in each analysis case in this occasion.

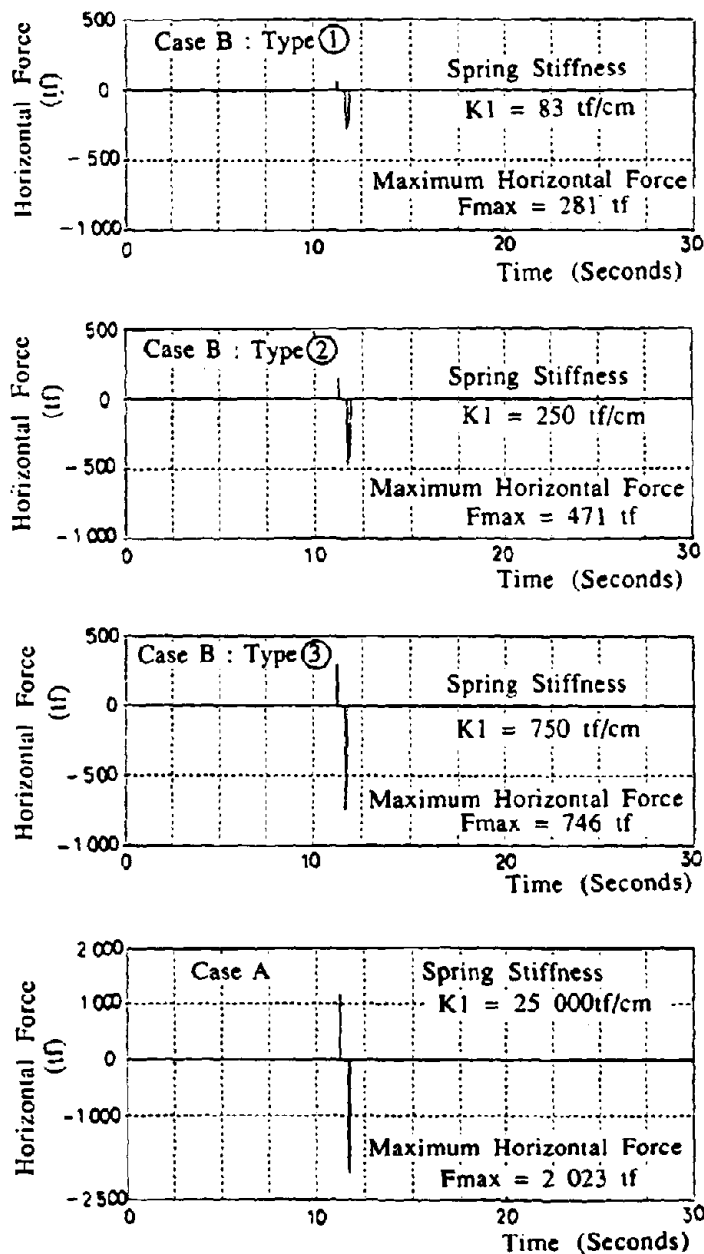


Fig. 9 Time History of Horizontal Force (Pier P1)

- The analysis results may be summarized as follows.
- (a) An extremely large maximum horizontal reaction force was found acting on the falling-off prevention devices in the rigid model (Case A), creating an imbalance in maximum reaction forces acting on each of the support points.
 - (b) The relative displacement between the super and substructures can be restrained to some extent and the horizontal reaction force acting on the falling-off prevention devices was reduced by using shock absorber with appropriate spring stiffness. In this occasion, appropriate spring stiffness value is about 150~500tf/cm at the pier and about 60~200tf/cm at the abutment.
 - (c) There was no difference in the analysis results between the bilinear model(Case B Type ②) and strict model(Case C).
 - (d) The horizontal reaction forces (impact force) acting on the falling-off prevention devices decrease and the collision time increase as the spring stiffness of the shock absorber decreases.

ELEMENT TEST

Outline Static compression loading tests on laminated rubber with round steel bars as shown in Fig.10 and Photograph 1 were carried out, for the purpose of clarifying the compression-reaction force properties of the anchor bar type falling-off prevention devices equipped with shock absorber, and investigating the methods for determining appropriate spring stiffnesses.

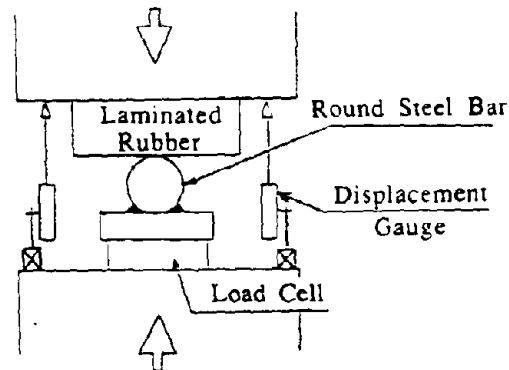


Fig. 10 Outline of Compression Test

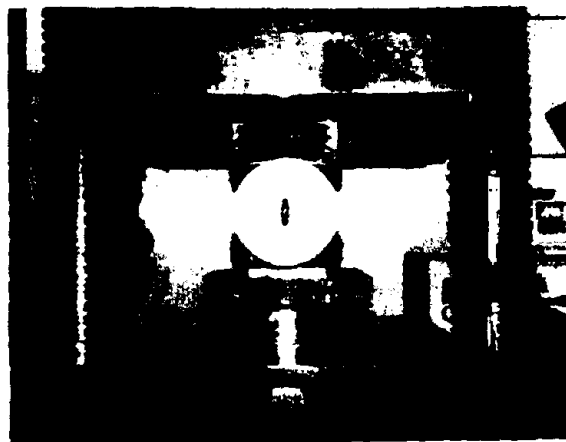


Photo 1 Compression Test

The materials and dimensions of the laminated rubber was determined by setting the development target for the spring stiffness at between 100 and 500 tf/cm, a level at which it was found that one could expect adequate shock absorption effect in the numerical analysis. The diameters of the round steel bars were set at 100, 150 and 200 mm, selected as size at which one could calculate the estimated maximum horizontal forces from the yield strengths. The cross-section of the test piece (laminated rubber) is shown in Fig.11, the material properties of the test piece and round steel bar in Table 6 and the dimensions of the test piece and the test cases in Table 7.

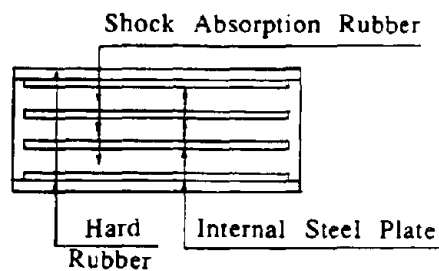


Fig. 11 Test Piece Cross-Section

Table 6 Material Properties of Test Piece

	Member	Material	Physical Properties
Test Piece	Shock Absorption Rubber	High Damping Rubber	$G = 6\text{kgf/cm}^2$ Hardness : 50 degrees
	Hard Rubber	Synthetic Rubber	$G = 150\text{kgf/cm}^2$ Hardness : 90 degrees
	Internal Steel Plate	Steel	$\sigma_y = 2400\text{kgf/cm}^2$
	Round Steel Bar	Steel	$\sigma_y = 2400\text{kgf/cm}^2$

Table 7 Test Piece Dimensions and Test Cases

Test Case	Rubber Layer Thickness (mm)	Number of Layers	Total Thickness (mm)
A - 1	12	2	50
A - 2	12	3	65
A - 3	12	4	80
B - 1	16	2	55
B - 2	16	3	80
B - 3	16	4	100
C - 1	20	2	65
C - 2	20	3	90
C - 3	20	4	115

Note: The test pieces are 200mm x 200mm.

Note: Round steel bars with diameters of 100, 150 and 200mm were used in all the tests.

Method of Determining Spring Stiffness The compression displacement-reaction force properties shown in Fig.12 were obtained in the test. The spring stiffness is determined from the gradient of the envelope drawn in the figure and the intersection of the envelope and the horizontal axis is then sought. The Intersection "a" of the envelope and the horizontal axis, which is thought to represent the amount of settlement before the spring stiffness of the laminated rubber reaches a constant level, corresponds to the value "a" (2cm) in the strict model shown in Fig.6 and is thought to be an important physical value in determining the clearance X_0 .

It was confirmed in the test that the envelope of the peak point under cyclic loading in which the load was gradually increased as shown in Fig.12 more or less coincided with the compression displacement-reaction force properties when the load was increased within a onetime loading.

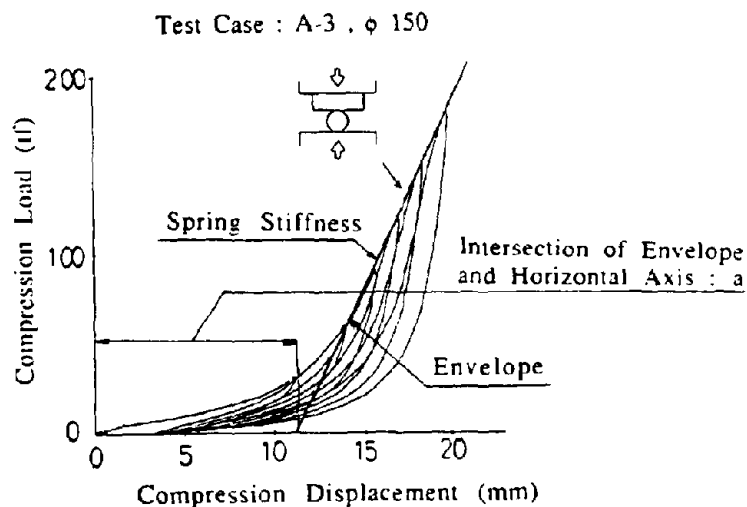


Fig. 12 Compression Displacement-Reaction Characteristics

Test Results The spring stiffnesses are given in Table 8 and Fig.13 and the Intersection "a" of the envelope and the horizontal axis in Table 9 and Fig.14, while the variation in the compression properties under the cyclic loading test in the range up to 150tf is shown in Fig.15. Since the values shown on the displacement gauge were returned to zero for the second and subsequent loadings, the residual displacement is not included in the values shown in the figure.

The test results may be summarized as follows.

- (a) When the same shock absorption material is used, the spring stiffness increases with the diameter of the round steel bar.
- (b) When the diameter of the round steel bar is maintained constant, the spring stiffness varies with the variation in the thickness of the shock absorption material.
- (c) The Intersection "a" between the envelope and the horizontal axis remains more or less constant so long as the same shock absorption material is used, regardless of the steel round bar diameter
- (d) The variation in the spring stiffness is greater in the second and subsequent loadings than in the first loading, but remains constant in the subsequent loadings.

Table 8 Spring Stiffness

Test Cases	Diameter of Round Bar		
	ϕ 100	ϕ 150	ϕ 200
A - 1	218	321	367
A - 2	231	300	321
A - 3	191	212	269
B - 1	202	273	295
B - 2	152	205	228
B - 3	142	164	191
C - 1	173	214	231
C - 2	149	180	207
C - 3	129	137	171

Table 9 Intersection of Envelope and Horizontal Axis : " a "

Test Cases	Diameter of Round Bar		
	ϕ 100	ϕ 150	ϕ 200
A - 1	7.2	7.4	7.2
A - 2	9.9	8.9	9.3
A - 3	11.9	10.9	10.6
B - 1	11.4	11.1	10.5
B - 2	14.9	14.4	13.3
B - 3	17.5	16.6	16.3
C - 1	16.6	17.6	16.0
C - 2	21.1	20.2	19.3
C - 3	25.3	23.9	23.0

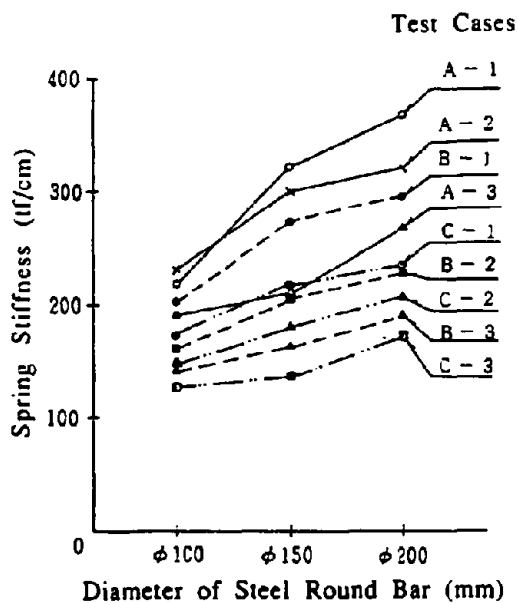


Fig. 13 Spring Stiffness

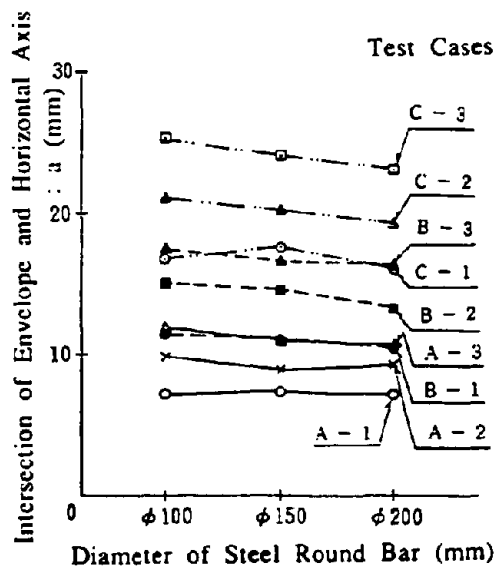


Fig. 14 Intersection of Envelope and Horizontal Axis : " a "

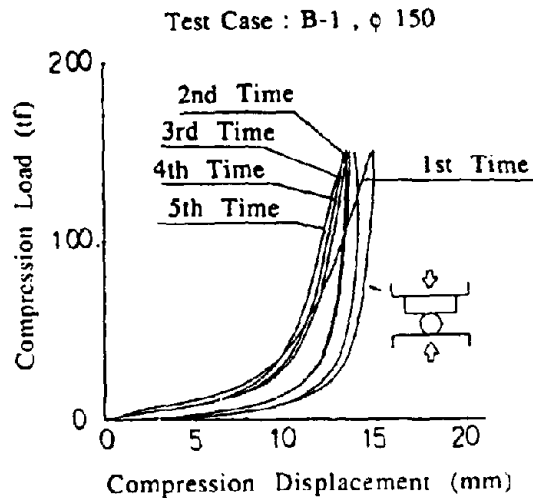


Fig. 15 Repetition Characteristics

CONCLUSIONS

The following conclusions were drawn from the numerical analysis and element test.

- (a) Effective reduction of the relative displacement between the super and substructures and the horizontal reaction force can be achieved through use of shock absorber with appropriate spring stiffness
- (b) The spring stiffness of the shock absorber was made as small as possible within the range that would effectively reduce the relative displacement between the super and substructures. This is desirable also from the point of view of reducing the impact force.
- (c) Regarding the reaction force displacement properties when compression loading is carried out on laminated rubber with a round steel bar, there is a certain amount of displacement (settlement) before the spring stiffness becomes constant. Accurate evaluation of this displacement is vital in determination of the clearance for the falling-off prevention device.

While it is thought to be profitable to apply the falling-off prevention devices to actual bridges, further studies will be needed on the following points in order to raise the reliability of the devices and to gain more detailed knowledge of their behavior during earthquakes.

- (a) Behavior of falling-off prevention devices during earthquakes taking into account the non-linearity of the bridge piers.
- (b) Proposal of experimental equations for calculation of spring stiffnesses.
- (c) Method of determining optimum dimensions of the shock absorption materials.

ACKNOWLEDGEMENT

The studies reported here were conducted as a part of the joint research project on "Development of Menshin Systems of Highway Bridges" between the Public Works Research Institute (PWRI) of the Ministry of Construction and 28 private firms in Japan. The authors would like to acknowledge their debt to Dr.K.Kawashima, Mr.K.Hasegawa, Mr.S.Unjo and Mr.H.Nagashima of the PWRI for their advice concerning the basic principles behind the falling-off prevention device and the direction of the development.

REFERENCES

1. K. Kawashima et al.: " Model Tests on Vibration Properties of Menshin Bridges" . Civil Engineering Technology Materials Vol. 30-10, Oct. 1988
2. PWRI and 29 Private Firms : " Development of Menshin Systems of Highway Bridges - Report NO.1-", PWRI Joint Research Reports No. 44, March 1990
3. PWRI and 28 Private Firms : " Development of Menshin Systems of Highway Bridges - Report NO.2-", PWRI Joint Research Reports No. 60, July 1991
4. Technology Research Center for National Land Development : " Guideline on the Design of Menshin Highway Bridges (Draft) " , March 1989 (in Japanese)

DESIGN CONCEPT OF FALLING-DOWN PREVENTION DEVICES FOR MENSJIN BRIDGES

Akio HAYASHI¹, Jiro IZEKI², Kazushige YOSHIKAWA³, Toshio KIKUCHI⁴,
Katsunori MATSUBARA⁵, Hiroshi KOYAMA⁶

- 1 Structural Engineer, Pacific Consultants Co., Ltd., Koto, Tokyo, Japan
- 2 Technical Engineer, Oilless Industry Co., Ltd., Fujisawa, Kanagawa, Japan
- 3 Structural Engineer, Pacific Consultants Co., Ltd., Koto, Tokyo, Japan
- 4 Research Engineer, Technical Research Institute, Ohbayashi Corporation, Kiyose, Tokyo, Japan
- 5 Research Engineer, Technical Research Institute, Hazama Corporation, Yono, Saitama, Japan
- 6 Steel Structures Division, Japan Casting Co., Ltd., Kawasaki, Kanagawa, Japan

SUMMARY

Using falling-down-prevention devices (FDPD) will allow bridges to sustain only minor damage when subjected to strong earthquake motion and will permit restoration later.

The mechanical properties we can use under present conditions involve three groups: visco-elastic, restoring force and friction, and hardening-elastic.

In this paper, the method of calculation for estimating the effectiveness of the device (FDPD) is presented. And the actual results of calculations using the three groups of mechanical properties are also presented. Bridges can be made more resistant to large earthquakes when the suitable mechanical properties have been selected in light of the particular condition of the bridge.

INTRODUCTION

Studies of bridges in real earthquake disasters show two definite patterns.

- 1) Substructure can support superstructure when sufficient seat length is prepared, even if the earthquake produces relative displacement greater than the movable length of the bearing.
- 2) Irregular collisions occur during an earthquake when the gap distance between the edge of a superstructure and the face of an opposing parapet wall of the abutment, or the edge of an adjoining superstructure is insufficient. It is difficult to estimate behavior after a collision has occurred. This phenomenon particularly happens when one superstructure is heavier than the other.

Both these patterns require sufficiently wide top surface of the substructure compared to peak response displacement of the superstructure. This is an important requirement for menshin bridges, because considerably large displacement is used in menshin bridges to reduce the inertia force. An effective measure to prevent the excessive displacement of the superstructure under an unpredictably severe earthquake is the installation of a device that can prevent excessive movement of superstructure.

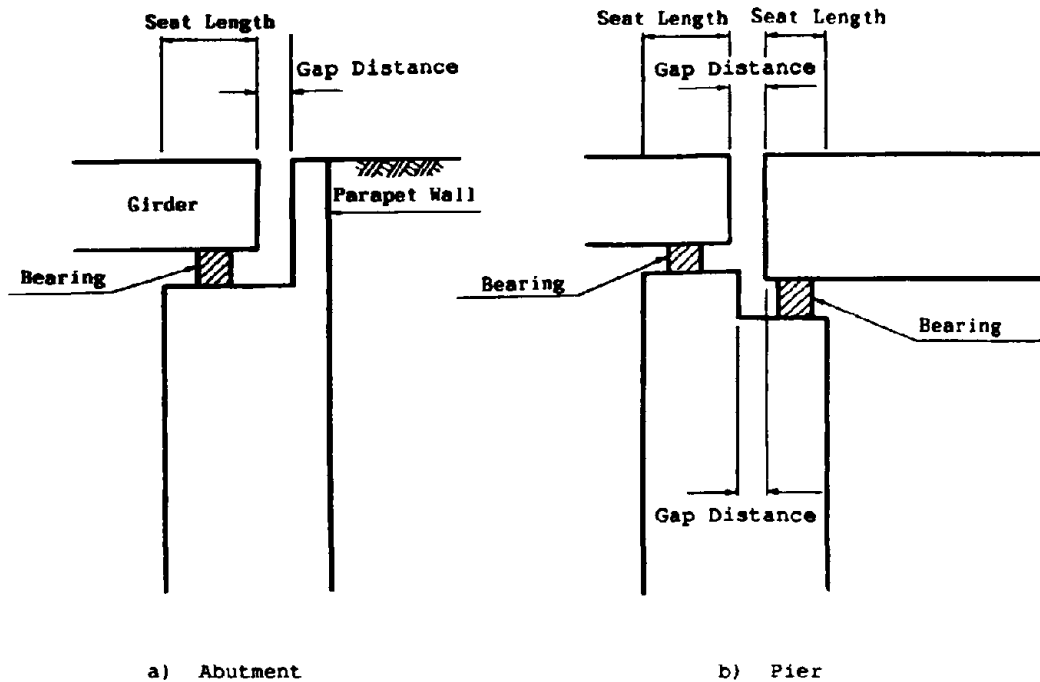


Fig. 1 Seat length and Gap distance

DESIGN CONCEPT

This study assumes that when the device by which we can prevent excessive displacement without significantly increasing the inertia force is prepared, collapse may not occur. This is the design concept of FDPD. The device calls for restoring force which starts to work when excessive displacement occurs, and calls for energy dissipation that can be obtained while the device works.

For designing FDPD, stiffness of the devices, amount of energy disipation, and the displacement over which FDPD works, have to be properly established. If the stiffness of FDPD is excessively high, it tends to cause large impacting force due to collision between FDPD and the deck. Although energy disipation is important to constrain the deck movement, it would work as "stopper" instead of energy dissipator. If the displacement where FDPD is initiated to work, which is designated hereinafter as gap distance X_s is too small, that would disturb smooth energy dissipation by menshin device.

Although precise study is required to determine the appropriate gap distance X_s , it was assumed here as the peak deck response displacement relative to the pier or the abutment when the bridge is subjected to design response spectrum as shown in Fig. 2. Because it is considered that FDPD is for preventing excessive relative deck movement when subjected to larger ground motion than assumed in the design, the effectiveness of FDPD was assumed here to be studied against a 1.5 times larger ground motion than that presented in Fig. 2. Fig. 3 represents the definition of gap distance X_s .

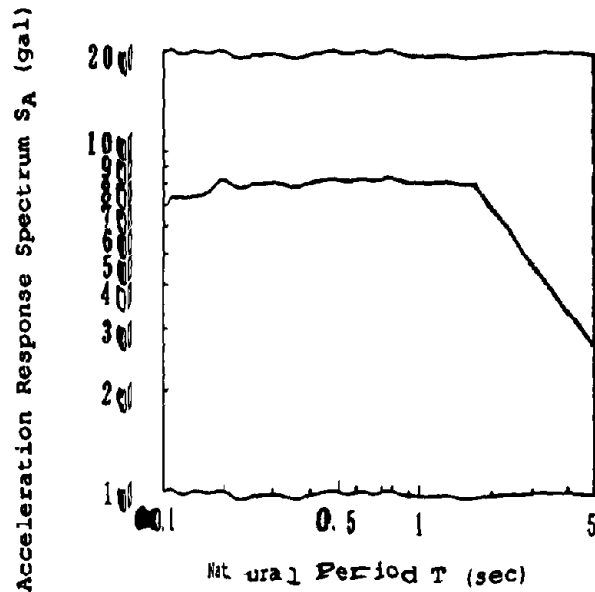


Fig. 2 Design Spectrum S_A

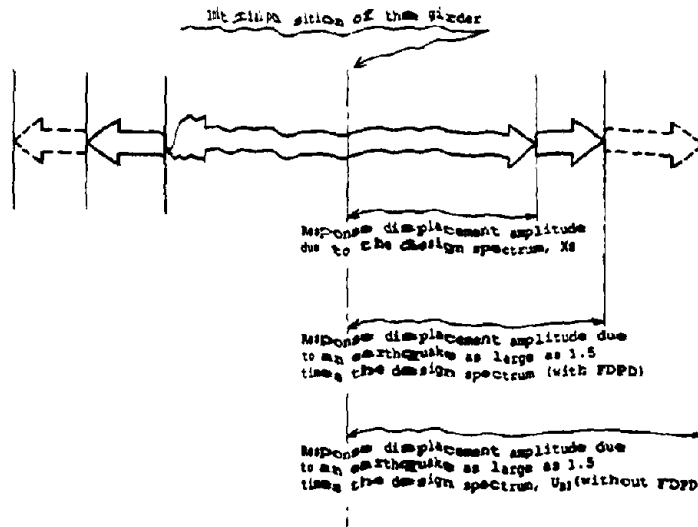


Fig. 3 Definition of gap distance X_s and relative deck movement U_1 and U_2 subjected to equal to or 1.5 times larger ground motion than design spectrum presented in Fig. 2

POSSIBLE FALLING-DOWN PREVENTION DEVICES

Although various types of FRPD have been developed, they may be classified into the following three groups based on their mechanical properties.

- 1) Visco-elastic type
- 2) Restoring Force and Friction type
- 3) Hardening-elastic type

Fig. 4, 5 and 6 show the reaction force versus relative displacement relationship for the three types of FDPD as well as typical devices for developing the reaction force. It should be noted in Fig. 6 that the reaction force versus relative displacement relationship is provided by strain hardening of rubber rings placed around a rod stopper, so energy dissipation is very small. Thus it is designated as "hardening-elastic". The reaction force of FDPD can be written as F_A .

a. Visco-elastic type

$$F_A = \text{SGN}(X) \cdot K_A |X - X_S| + C_A \dot{X} \quad (F_A \cdot X \geq 0, |X| \geq X_S) \quad (1)$$

where

F_A = reaction force
 X = displacement of superstructure
 \dot{X} = velocity of superstructure
 X_S = clearance of FDPD.

$$X_S = S_A \left(\frac{T_A}{2\pi} \right)^2 \quad (2)$$

S_A = design spectrum value shown Fig. 2

K_A = stiffness of spring

$$K_A = M \left(\frac{2\pi}{T_A} \right)^2 \quad (3)$$

M = deck mass

T_A = natural period of a system consisting of deck mass and spring of FDPD

C_A = damping coefficient of FDPD

$$C_A = 2h_A \cdot M \left(\frac{2\pi}{T_A} \right) \quad (4)$$

h_A = damping ratio of a system consisting of deck mass, spring and viscous element of FDPD

b. Restoring force and friction type

$$F_A = \text{SGN}(X) \cdot F_r + \text{SGN}(X) \cdot K_A |X - X_S| \quad (F_A \cdot X \geq 0, |X| \geq X_S) \quad (5)$$

where

F_A = reaction force
 F_r = friction force amplitude
 $F_r = W \cdot \mu$
 W = vertical reaction force
 μ = friction coefficient of FDPD $(F_A \cdot X \geq 0, |X| \geq X_S)$ (6)

c. Hardening-elastic type

$$F_A = \text{SGN}(X) \cdot R_A \left(\frac{|X - X_S|}{S_c} \right)^n \quad (7)$$

where

F_A = reaction force
 R_A = reaction force of rubber for compression strain of 100%
 $R_A = W \cdot C_K$
 W = deck weight
 C_K = coefficient for normalizing R_A (8)

S_t = total thickness of rubber
 $S_t = (U_{B3} - X_s) C_s$ (9)
 C_s = coefficient for normalizing S_t
 U_{B3} = peak deck displacement subjected to 1.5 times S_A without FDPD
 n = coefficient of hardening (4.8)

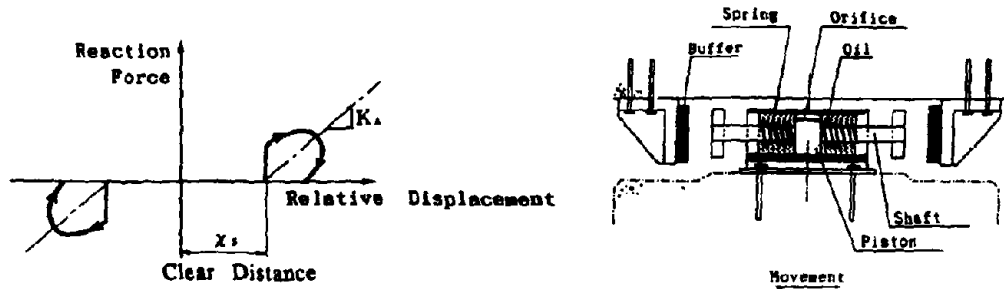


Fig. 4 Visco-elastic Type

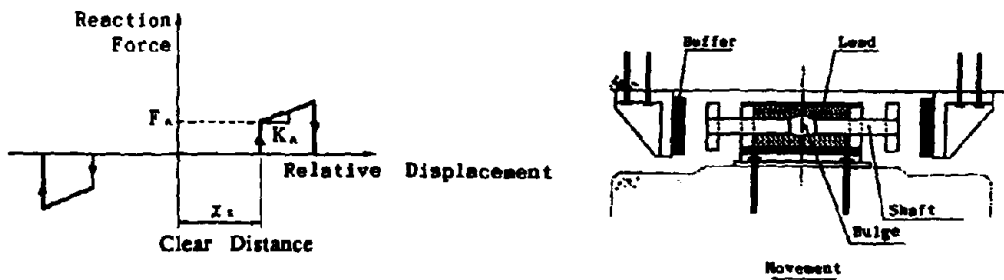


Fig. 5 Restoring Force and Friction Type

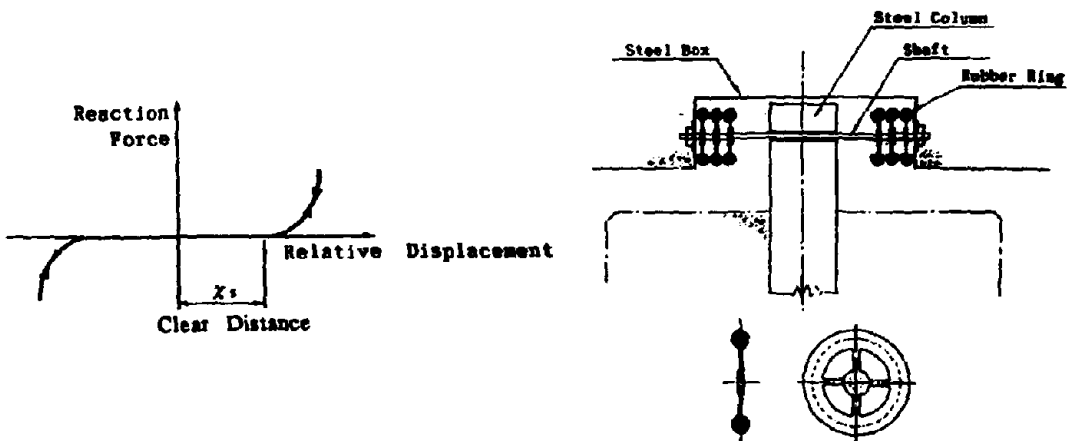


Fig. 6 Hardening-elastic Type

IDEALIZATION OF FDPD BY A SINGLE-DEGREE OF FREEDOM SYSTEM

For studying the effect of FDPD, only deck, menshin device and FDPD were idealized by a single-degree-of-freedom oscillator as shown in Fig 7. Foundation and pier were disregarded in this model for the sake of simplicity. The menshin device is idealized by a spring and a dash pot. Viscosity of dash pot is assumed to be estimated by the equivalent linear analysis. The equation of motion of a model presented in Fig 7 is:

$$M \cdot \ddot{X} + C_m \cdot \dot{X} + K_m \cdot X + F_A = M \cdot \ddot{e}(t) \tag{10}$$

where

- M = deck mass
 - C_m = damping coefficient of the menshin device
 - K_m = stiffness of the menshin device
 - F_A = reaction force of FDPD, given by Eq. (1) to (9)
 - $\ddot{e}(t)$ = ground motion, and was assumed similar as sinusoidal acceleration
- $$\ddot{e}(t) = 2 \cdot h_s \cdot S_A \cdot 1.5 \cdot \cos\left(\frac{2\pi}{T_s} t\right) \tag{11}$$
- T_s = natural period of the single degree of oscilator idealizing the deck and menshin device
 - h_s = damping ratio of the single degree of oscilator idealizing the deck and menshin device
 - S_A = design spectram shown in Fig. 2

Assuming the initial velocity \dot{x}_0 , as Eq. (12) can be solved through the direct integral method.

$$\dot{x}_0 = S_A \cdot 1.5 \left(\frac{T_s}{2\pi}\right) \tag{12}$$

In this paper, it is assumed that T_s = 2.0 second, h_s = 15%

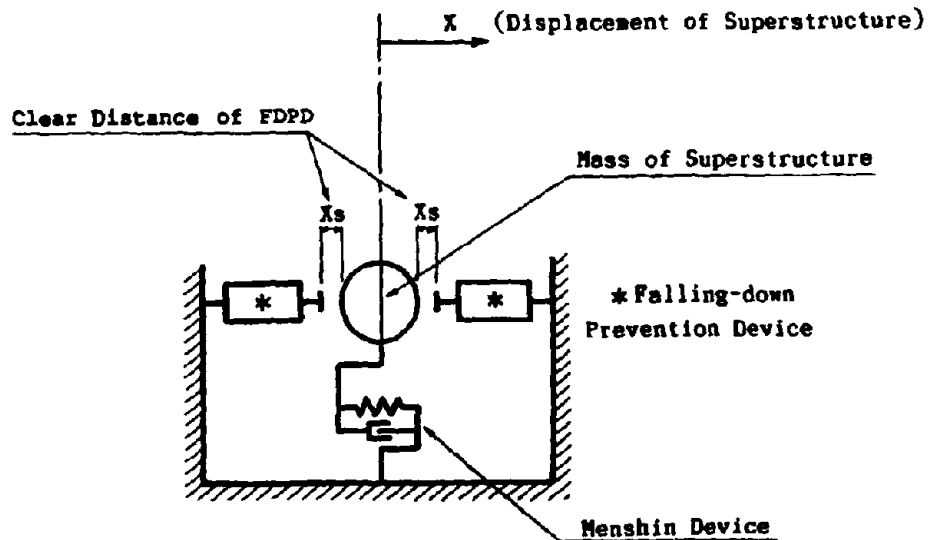


Fig. 7 Dynamic Analysis Model

PARAMETRIC STUDY

Results of dynamic response analysis for various devices are shown in Fig. 8 to 12.

Visco-elastic type Figure 8 shows calculation results for when the effective damping ratio (h_A) of the visco-elastic type is 15% and the spring stiffness (K_A) of the device varies from 0.5 to 3.5 times the stiffness of the menshin device.

This case is equivalent to FDPD consisting of a damper using oil or viscous material and a steel spring.

Calculations when the effective damping ratio (h_A) of the visco-elastic type is 2% and the spring stiffness (K_A) of the device changes in the same manner as above is shown in Fig. 9. This case is equivalent to FDPD consisting of a steel spring only, without a special device to produce a viscous effect.

Comparison between Fig. 8 and Fig. 9 reveals the following:

The superstructure stops with smaller displacements if a damper is used jointly.

A damper is indispensable if a practical effect is to be expected from the FDPD.

Restoring force and friction type The calculation results for when the coefficient of friction (μ) of the system is changed from 0.1 to 0.6 is shown in Fig. 10. This case is equivalent to when a friction damper is used.

Figure 11 shows the calculation results for when an elastic spring having a natural period (T_A) of 2.0 seconds is used in addition to the above. Comparison between Fig. 10 and 11 reveals no significant difference in effect. The elastic spring is provided for the purpose of giving the friction damper the ability to return to its original position. However, achieving this aim using the mechanism shown in Fig. 5 is more reasonable than using a spring.

Hardening-elastic type The calculation results using a coefficient of $C_s=1.0$ and a coefficient C_k of 0.25 to 2.0 is shown in Fig. 12. It is clear from the figure that this hardening-elastic type causes an abrupt increase in reaction force and has a very small buffering effect. When using the hardening-elastic type, therefore, it is desirable to devise means (for example, a friction bar) so that the reaction force is directly transferred to the ground behind the abutment instead of being transferred to the pier.

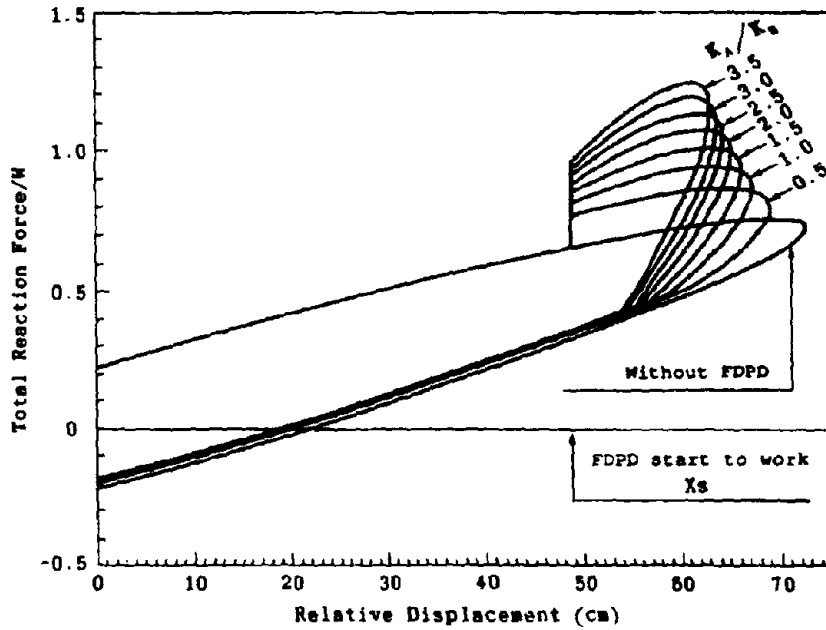


Fig. 8 . Effect of visco-elastic type (when a viscous element is provided)

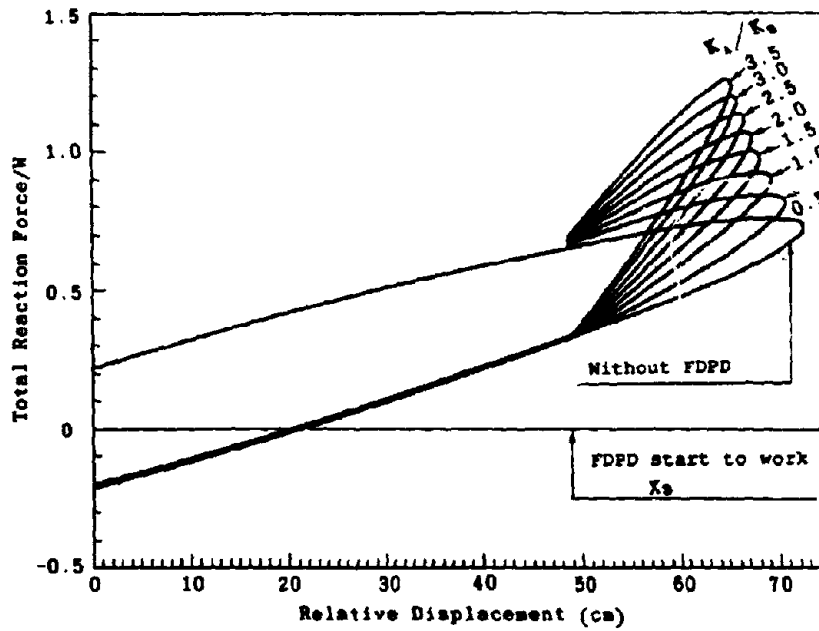


Fig. 9 Effect of visco-elastic type (when a viscous element is not specifically provided)

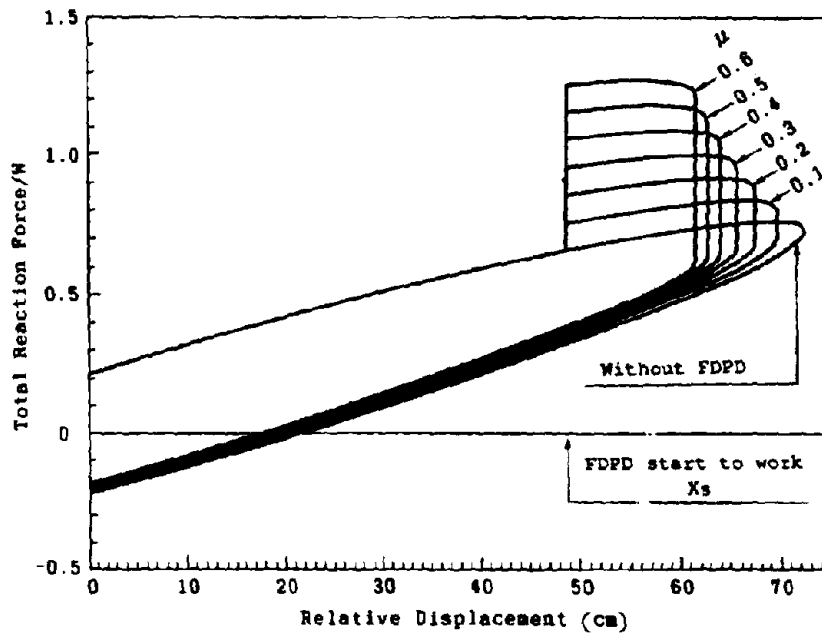


Fig. 10 Effect of restoring force and friction type (only friction elements are used)

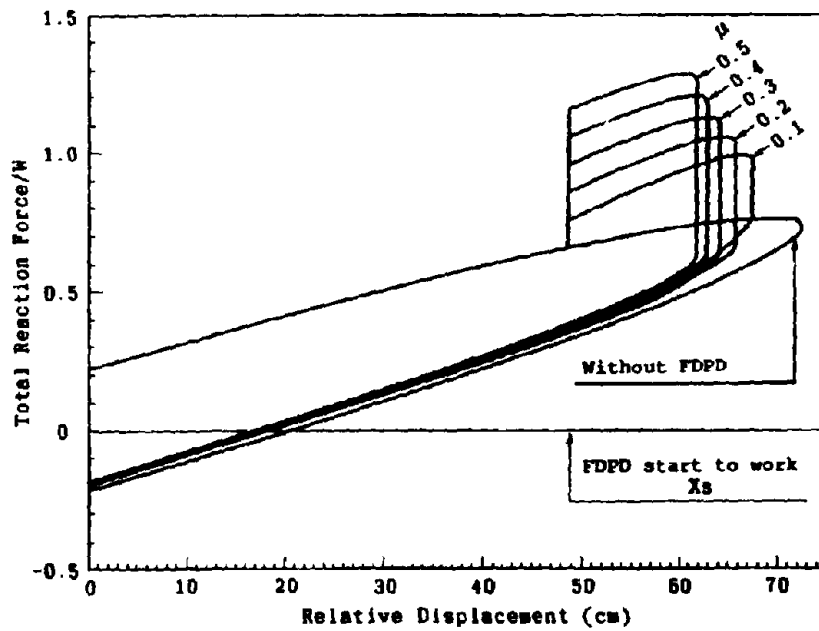


Fig. 11 Effect of restoring force and friction type (friction element and elastic spring element are used jointly)

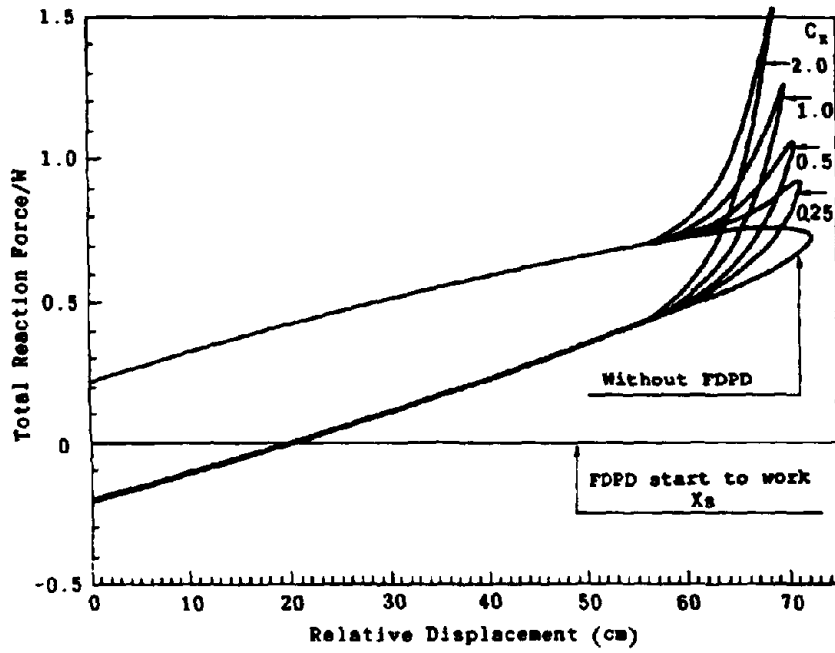


Fig. 12 Effect of hardening-elastic type

SHOCK ABSORBING EFFECT

Figure 13 shows the calculation results of the energy balance for each type of FDPD. These values were obtained to study the devices' shock absorbing effect, the most important characteristic among all other characteristics required for a FDPD. Figure 14 shows how the response velocity of the superstructure changes. These figures reveal that the device utilizing friction brings about a relatively good shock absorbing effect.

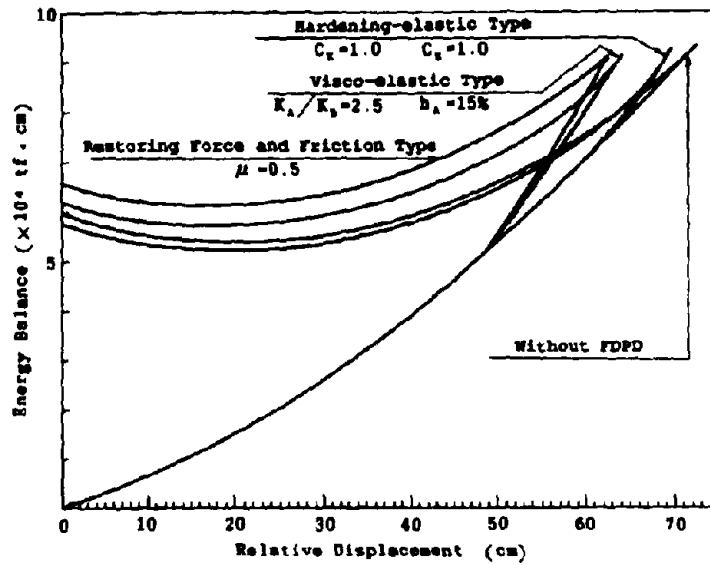


Fig. 13 Energy balance of menshin device and FDPD

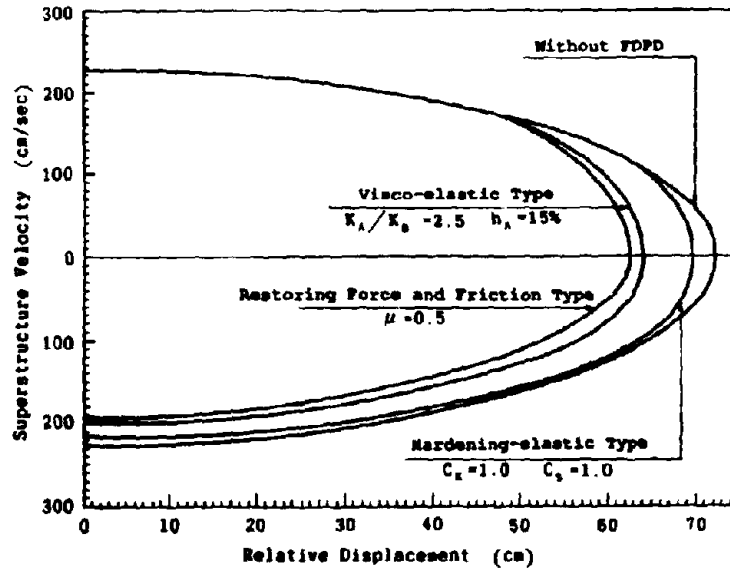


Fig. 14 Response velocity of the superstructure

CONCLUSIONS

It is important for falling-down prevention devices (FDPD) to provide appropriate stiffness and energy-dissipating capability for preventing an excessive impacting effect and excessive movement of girders, even if subjected to unexpectedly severe earthquake motion.

1. A practical design method was proposed by which a menshin bridge designer can evaluate the capability of FDPD, with regard to energy dissipation and displacement over which FDPD works.

2. If it is assumed that the resistant force of the pier in its ultimate state is 1.2 times the girder weight W , the upper limit of stiffness of FDPD should be 3.0 times the stiffness of the menshin device. The required distance to stop the movement after FDPD works is 15 cm at the lowest estimate.

3. The visco-elastic type and the restoring force and friction type bring about relatively good buffer action. The velocity of a girder when it returns to the point where FDPD starts to work decreases by approximately 20% for the visco-elastic type, 30% for the restoring force and friction type respectively.

4. The hardening-elastic type brings about relatively poor buffer action. The velocity of a girder when it returns to the point where the FDPD started to work decreases by approximately 3%.

The response spectrum assumed for the calculation of this paper is of an earthquake which may occur on medium-hard ground, so the results of this paper show only the general tendencies of the effects of FDPD. The benefit of using FDPD may be greater if the menshin bridge is located on softer ground than postulated. This is due to the fact that the required amount of seat length and gap distance may become large unexpectedly, according to accommodation to the bridge shape. Since the earthquake motion on soft ground contains large amounts of components of relatively long period, the eventual displacement of the girder may be rather large.

ACKNOWLEDGEMENTS

This study was made as a part of the joint research program on "Development of Menshin Systems of Highway Bridges" between PWRI and 28 private firms in Japan.

REFERENCES

1. Bridge committee of the New Zealand National Society for Earthquake Engineering, "Seismic Design of Bridges", Bulletin of the National Roads Board of New Zealand. (1981)
2. Skinner, R.I., Tyler, R.G., Heine, A.J., and Robinson, W.H., "Hysteretic Dampers for the Protection of Structures from Earthquakes", Bulletin of the New Zealand National Society for Earthquake Engineering Vol. 13, No. 1 (1980)

3. Testing of Isolated Bridges and Components

Effect of Dynamic Property of Menshin Devices and Stiffness of Substructures on Seismic Response of Menshin Bridges

T. Takeda, Y. Hishiki and H. Okamoto

Experiment and Analysis on Seismic Response of Menshin Bridges

K. Kawashima, K. Hasegawa and H. Nagashima

On-Line Earthquake Response Tests of High-Damping Rubber Bearings for Seismic Isolation

H. Iemura, Y. Yamada, W. Tanzo, Y. Uno and S. Nakamura

EFFECT OF DYNAMIC PROPERTY OF MENSHPIN DEVICES AND STIFFNESS OF SUBSTRUCTURES
ON SEISMIC RESPONSE OF MENSHPIN BRIDGES

Tetsuo TAKEDA¹, Yoshihiro HISHIKI² and Hiroyuki OKAMOTO²

¹ Civil Engineering Dept., Kajima Institute of Construction Technology, Tokyo, Japan

² Civil Engineering Design Div., Kajima Corporation, Tokyo, Japan

SUMMARY

Earthquake response analysis for a Menshin bridge was performed parametrizing the stiffness and damping ratio of Menshin bearings and the stiffness of the bridge's piers and foundation, and the effects of these factors on earthquake responses of the Menshin bridge were examined. As a result, it was confirmed that the stiffness and damping ratio of Menshin bearings greatly affected earthquake responses of the bridge, while the stiffness of the piers and foundation affected them only slightly. It was also confirmed that the sectional force of a pier can be increased by increasing the stiffness of Menshin bearings for the pier and the pier itself.

INTRODUCTION

In conducting studies on the application of Menshin (seismic isolation) devices to bridges or in designing Menshin bridges, it is important to understand the effects of dynamic properties of Menshin bearings and the stiffness of piers and foundations on earthquake responses of Menshin bridges.

This paper reports the results of analyses of a Menshin bridge, parametrizing the dynamic properties of Menshin bearings and the stiffness of piers and foundation, performed to investigate into the following:

- (1) Effect of the stiffness of the Menshin bearings and the substructure on earthquake responses of the Menshin bridge
- (2) Effect of the damping of the Menshin bearings on earthquake responses of the Menshin bridge

PARAMETRIC ANALYSIS

Analytical Model A five-span continuous prestressed concrete box-girder bridge as shown in Fig. 1 was analyzed.

As Menshin bearings, lead rubber bearings (LRB) were assumed.

Table 1 shows primary structural data of the bridge, and Table 2 shows specifications of the Menshin bearings. It was assumed that restoring force characteristics of the Menshin bearings could be modeled bilinearly, as shown in Fig. 2, and thus can be expressed by equivalent linear spring constant and equivalent damping ratio.

In the analysis, a multi-mass-spring model as shown in Fig. 3 was used.

Damping ratios for elements of the standard model are as follows:

Girder 3%
 Pier 5%
 Foundation 10%
 Menshin bearing 20%

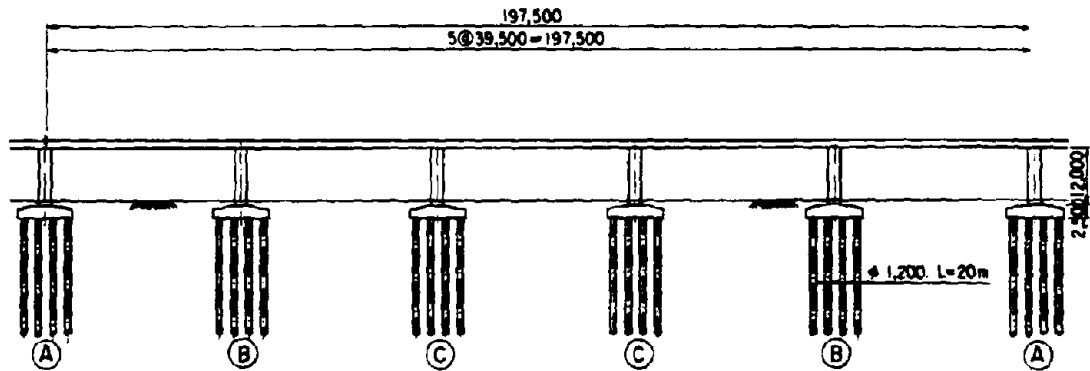


Fig. 1 Menshin Bridge for Analysis

Table 1 Structural Data

Type of Superstructure	5-span continuous prestressed concrete box-girder
Type of Substructure	Column-type reinforced concrete pier (rectangular cross section)
Type of Foundation	Cast-in-place concrete pile ($\phi 1200$)
Span	5 @ 39.5m = 197.5m
Effective Width	11.0m

Table 2 Data on Menshin Bearing

			Pier A	Pier B	Pier C	
Design Requirements	Weight of Superstructure		tf	5160		
	Reaction	Maximum (per bearing)	tf	270	715	645
		Deal Load (per bearing)	tf	200	580	510
	Displacement	Horizontal Displacement (ordinary)	mm	64.5	32.9	10.5
		Rotational Angle (ordinary)		1/300	1/600	1/600
	Number of bearings per pier		piece	2	2	2
	Stiffness of Pier K_p		tf/m	5430	10860	10860
Damping Factor of Pier h_p		%	5.0	5.0	5.0	
Configuration and Dimensions of Bearing	Shear Modulus of Rubber G_o		kgf/cm ²	8.0	8.0	8.0
	Plane Figure $A \times B$		cm	95 × 100	120 × 125	125 × 130
	Lead Plug $n \times \phi$		cm	2 × ϕ 14.4	4 × ϕ 16.0	4 × ϕ 14.9
	Thickness of Rubber t_r		cm	1.8 × 33 layers = 52.8	2.0 × 20 layers = 40.0	2.0 × 12 layers = 24.0
Dynamic Properties of Bearing		Initial Stiffness K_1	tf/m	2577	6200	10366
		Post-yield Stiffness K_2	tf/m	396	954	1595
		Yield Load Q	tf	50.8	125.5	108.0

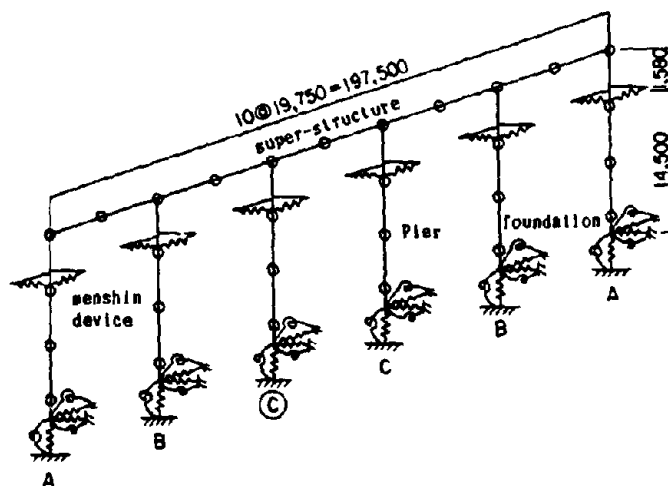


Fig. 2 Analytical Model

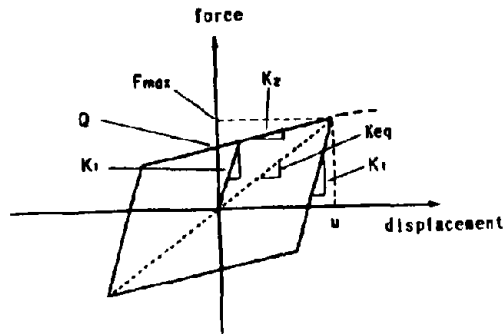


Fig. 3 Force-Displacement Relationship of Menshin Device

Analytical Method Seismic motions along the bridge axis were considered, and corresponding maximum response values were calculated by the response spectrum method.

Spectra based on the Specification for Highway Bridges in Japan, as shown in Fig. 4, were used as response spectrum curves.

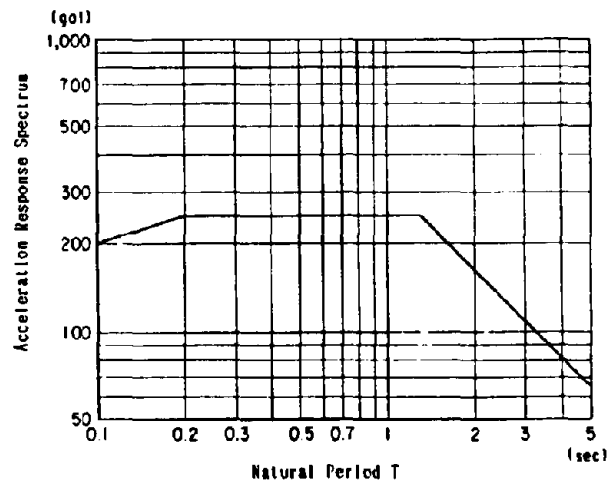


Fig. 4 Acceleration Response Spectrum

Modification of spectra to consider the effect of damping was made by multiplying the spectrum values shown in Fig. 4 by the following factor (C_D):

$$C_D = \frac{1.5}{40h_i + 1}$$

where h_i is the damping ratio for the i th mode. It was assumed that as shown in the following equation, the damping ratio could be expressed as a weighted average of damping ratios for elements with the amount of strain energy in each element, or a strain energy proportional damping ratio.

$$h_i = \frac{\sum_K h_k \cdot E_k (i)}{\sum_K E_k (i)}$$

where,

h_k : damping ratio for element K

$E_k(i)$: maximum strain energy in element K in the i th mode

Cases of Parametric Analysis Analyses were conducted for six cases. Parameters used in each case and the ranges of the parameters used are shown in Table 3.

Table 3 Analytical Cases

Case No.	Parameter	Range of Parameter
①	Stiffness of menshin bearing (for all piers)	Standard value times 0.5 ~ 4
②	Ditto (for only one pier)	Standard value times 1.5
③	Stiffness of pier and foundation (for all piers)	Standard value times 0.4 ~ 5
④	Stiffness of pier (for only one pier)	Standard value times 0.3 ~ 3
⑤	Stiffness of foundation (for a half of the bridge)	Infinity (fixed) or Standard value times 0.5
⑥	Damping factor of menshin bearing (for all piers)	10%, 20%, 30%

RESULTS AND DISCUSSION

Vibration Characteristics of Standard Model Table 4 shows modes of vibration caused by seismic motions in the bridge axis direction. The participation factors and effective mass ratios indicate that in the standard model, earthquake responses are governed almost exclusively by the primary mode responses shown in Fig. 5.

Table 4 Results of Eigen Value Analysis of Standard Model

Mode No.	natural period T (s)	participation factor	effective mass ratio (%)
1	1.5214	23.950	53.4
8	0.2126	9.383	8.2
10	0.2086	10.540	10.4
12	0.2046	7.172	4.8
18	0.0833	9.374	8.2
20	0.0820	10.120	9.5
22	0.0810	7.819	5.0

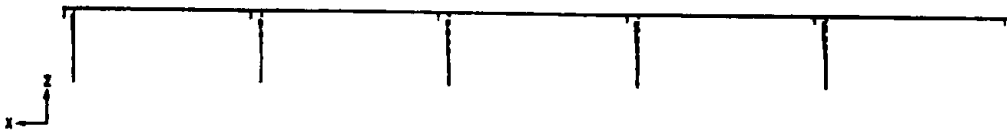


Fig. 5 First Vibration Mode of Basic Model

Results of Parametric Analysis (1) When the stiffness of the Menshin bearings for all piers were changed:

Fig. 6 and Fig. 7 show primary natural periods and primary-mode damping ratios for the bridge with stiffness 0.5 to 4.0 times as high as the standard level of stiffness of the Menshin bearings. Fig. 8 and Fig. 9 show horizontal displacements of the girder and bending moments at the bottom of the pier.

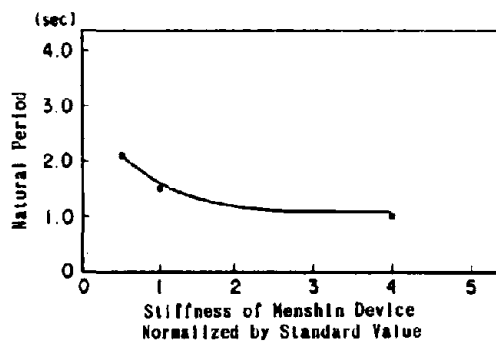


Fig. 6 Stiffness of Menshin Device vs. Natural Period

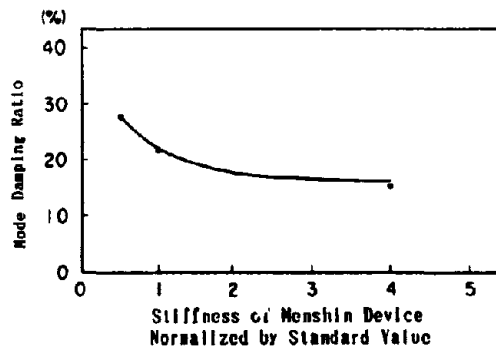


Fig. 7 Stiffness of Menshin Device vs. Mode Damping Ratio

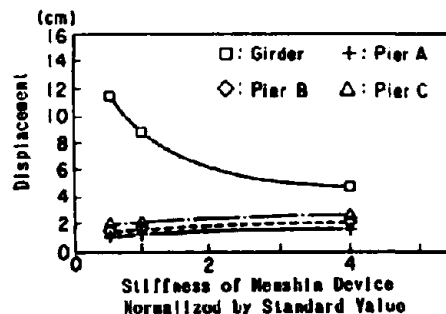


Fig. 8 Stiffness of Menshin Device vs. Displacement

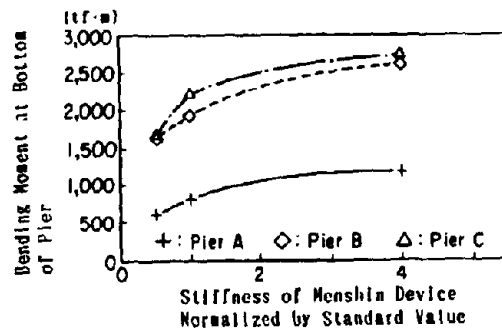


Fig. 9 Stiffness of Menshin Device vs. Bending Moment

These results indicate the following:

a) The natural period of the bridge changed considerably when the stiffness of the Menshin bearings became about 0.5 times as high as its standard level, but the natural period of the bridge remained almost the same even when the stiffness became about four times as high as the standard level.

b) Like the natural period, the mode damping ratio for the bridge tended to remain almost the same even when the stiffness of the Menshin bearings became about four times as high as its standard level.

c) When the stiffness of the Menshin bearings rose, the response displacement of the girder decreased. At the same time, however, displacement at the top of the pier increased and bending moments at the bottom of the pier rose.

From above, it was confirmed that the stiffness of the Menshin bearings affected not only the natural period of the bridge, but also the damping ratio, thus greatly affecting response displacements of the girder and bending moments at the bottom of the pier.

(2) When the stiffness of the Menshin bearings for only one pier was changed:

Fig. 10 and Fig. 11 show horizontal displacements of the girder and bending moments at the bottom of the pier when the stiffness of the Menshin bearings for only one pier (Pier C) increased to become 1.5 times as high as its standard level.

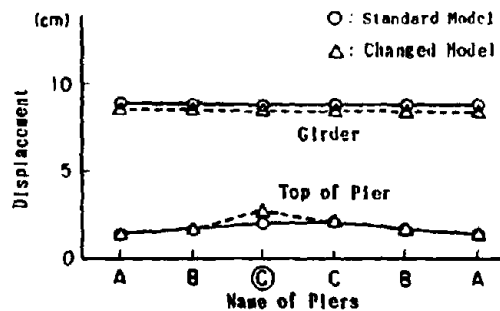


Fig. 10 Distribution of Displacement

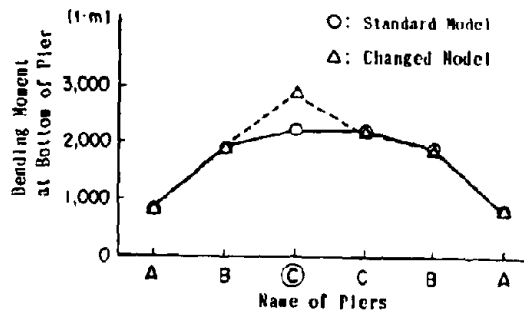


Fig.11 Distribution of Bending Moment

These results indicate that although the displacement of the superstructure decreased slightly in the whole region when the stiffness of the Menshin bearings for only one pier rose, only displacement at the top and bending moment at the bottom of the pier for which the stiffness of the Menshin bearings increased became greater.

(3) When the stiffness of all piers and foundations was changed:

Fig. 12 and Fig. 13 show the results of analysis where the standard levels of stiffness of all piers and foundations were changed by 0.4 to 5 times.

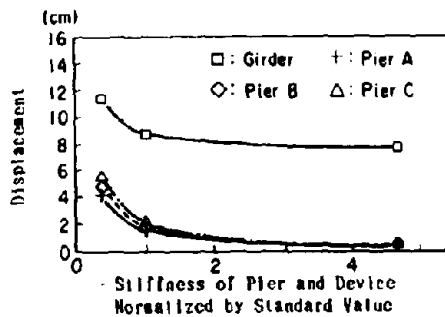


Fig. 12 Stiffness of Pier and Foundation vs. Displacement

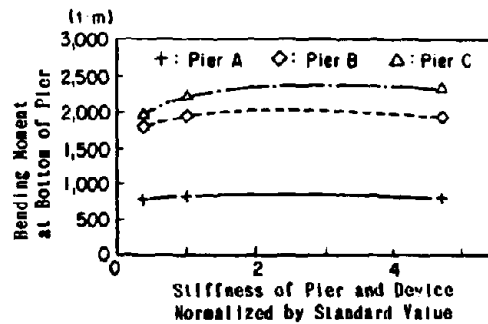


Fig. 13 Stiffness of Pier and Foundation vs. Bending Moment

Horizontal displacements of the girder and displacements at the top of the pier decreased as the stiffness of the piers and foundation increased, but the relative displacement of the bearings (displacement of the superstructure in relation to the top of the pier) did not change substantially. Therefore, it can be said that the influence of changes in the stiffness of the piers and foundation on earthquake responses of Menshin bridges is small.

(4) When the stiffness of only one pier was changed:

Fig. 14 and Fig. 15 show the results of analysis where the standard level of stiffness of only one pier (Pier C) was changed by 0.3 to 3 times.

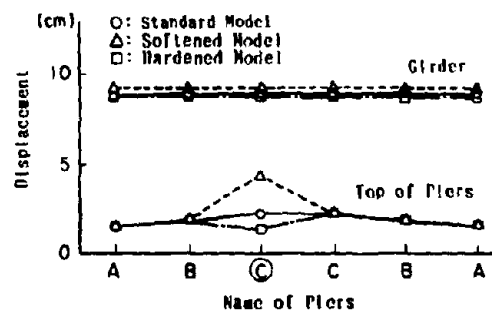


Fig. 14 Distribution of Displacement

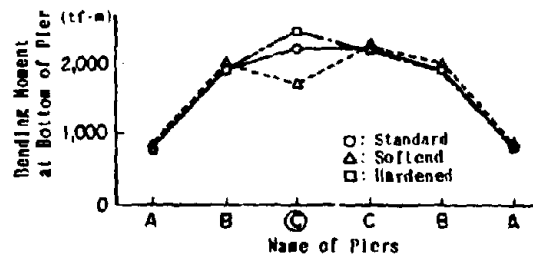


Fig. 15 Distribution of Bending Moment

The results obtained in this case were similar to the ones obtained when the stiffness of the Menshin bearings for only one pier was changed. When the stiffness of one pier rose, horizontal displacements of the girder invariably decreased and only the sectional force of the pier with increased stiffness became greater.

This case corresponds to a case where unequal piers exist. This should be taken into consideration when bridges having unequal height piers are designed.

(5) When the stiffness of only a half of the foundation was changed:

Fig. 16 and Fig. 17 show the results of analysis where the basic level of stiffness of the foundation for piers of only a half of the bridge was decreased to 1/2 and was fixed.

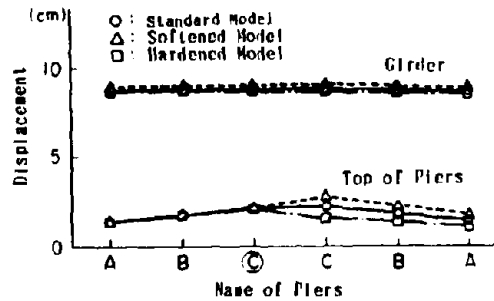


Fig. 16 Distribution of Displacement

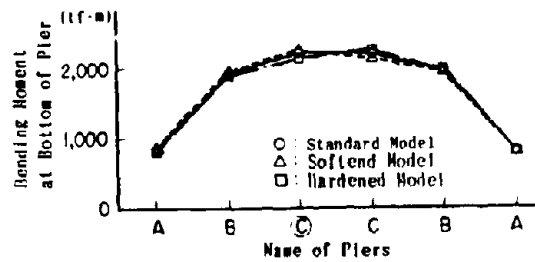


Fig. 17 Distribution of Bending Moment

In this case, no substantial changes in response displacement and response sectional force were indicated.

This case corresponds to a case where conditions of the bearing ground of a continuous bridge vary from place to place. It can be said, however, that in Menshin bridges, the influence of such conditions on earthquake responses is small.

(6) When damping ratios for Menshin bearings for all piers were changed:

Fig. 18 and Fig. 19 show the results of analysis where the damping ratio for the Menshin bearings was set at 10%, 20% and 30%.

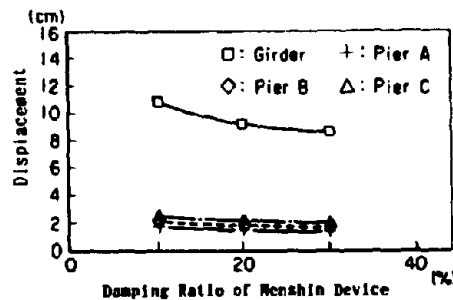


Fig. 18 Damping Ratio of Menshin Device vs. Displacement

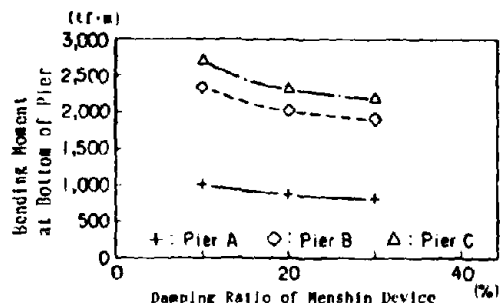


Fig. 19 Damping Ratio of Menshin Device vs. Bending Moment

It was confirmed that as the damping ratio for the Menshin bearings rose, response displacements and response sectional forces decreased as expected. However, as the damping ratio for the Menshin bearings rose, this tendency becomes weaker.

CONCLUSIONS

As a result of a series of analyses aimed at determining the effects of various factors, it was confirmed that the following items should be taken into consideration when a Menshin bridge is designed.

- (1) The stiffness of Menshin bearings affects not only the natural period, but also the mode damping ratio of a bridge. It also affects response displacements and response sectional forces considerably.
- (2) Changes in the stiffness of piers and foundations affect response displacement and response sectional forces only slightly.
- (3) If the stiffness of Menshin bearings for only one pier or the stiffness of only one pier increases, then the pier should be designed carefully because the sectional forces of the pier increases.
- (4) Changes in the stiffness of only a half of the bearing ground of a bridge affect earthquake responses only slightly.
- (5) The damping ratio for Menshin bearings greatly affects earthquake responses, and earthquake responses decrease as the damping ratio rises. The degree of this effect decreases as the damping ratio rises.

ACKNOWLEDGEMENTS

This study was made as a part of the joint research program on "Development of Menshin Systems of Highway Bridges" between Public Works Research Institute (PWRI) and 28 private firms in Japan.

Grateful acknowledgement is made to Dr. K. Kawashima, Mr. K. Hasegawa, Mr. K. Unjou, Mr. H. Nagashima of the Earthquake Engineering Division of PWRI.

EXPERIMENT AND ANALYSIS ON SEISMIC RESPONSE OF MENSHPIN BRIDGES

Kazuhiko KAWASHIMA, Kinji HASEGAWA and Hiroyuki NAGASHIMA

Earthquake Engineering Division, Public Works Research Institute

SUMMARY

To provide with realistic seismic response data of Menshin bridges, a series of shaking table tests were conducted at the Public Works Research Institute. Structural response characteristics were presented with emphasis on the effect of stopper and vertical excitation. Hysteretic behavior of Menshin bearings was studied by means of cyclic shear tests and a comparison with the seismic behavior during the excitation tests is presented. Analytical simulations are also presented for the excitation tests. Depending on the idealization of the nonlinear hysteretic behavior of the Menshin bearings, the equivalent linear analysis and the bilinear analysis were made. Analytical simulation for the effect of collision between the deck and the columns due to the stoppers was also presented.

INTRODUCTION

Seismic response of Menshin bridges subjected to significant earthquakes is of great interest for designing Menshin bridges in Japan. Because there have been so far no Menshin bridges which experienced significant earthquakes with the magnitude over 8, it is required to study their critical behavior carefully.

The most important issue in the structural response of Menshin bridges is the analytical idealization of the nonlinear hysteretic behavior of the Menshin bearings. Effect of stoppers which are provided to prevent excessive deck response is of another interest. When collision of deck with columns occurs, this would cause large impact force. Because bridges are subjected to large vertical excitation during destructive earthquakes, it is also important to study the response of Menshin bridges subjected to lateral and vertical excitations simultaneously.

For aiming to study the response of Menshin bridges, a series of excitation tests was made at the Public Works Research Institute. Two types of large scale model were used for the excitation tests. Analytical simulations by means of the equivalent linear analysis and bilinear analysis were made.

This paper shows structural response characteristic of Menshin bridges through shaking table tests and analytical simulation (Ref. 1,2,3).

STRUCTURAL RESPONSE OF MENSHPIN BRIDGES THROUGH SHAKING TABLE TESTS

Model and Test Procedure To provide a realistic seismic response data of a Menshin bridge, a series of shaking table tests were made at the Public Works Research Institute. A Menshin bridge model tested which is referred as "model 1" is a simple girder bridge supported by two columns placed on a shaking table as shown in Photo 1. The span length is 6 m and the deck weight is 39.8 tf. Two

types of Menshin bearing, i.e., lead rubber bearing (LRB) shown in Photo 2 and high damping rubber bearing (HDR) shown in Photo 3 were used. Two bearings were installed on each column, and totally four bearings supported the girder.



Photo 1 Setup of Shaking Table Test (Model 1)

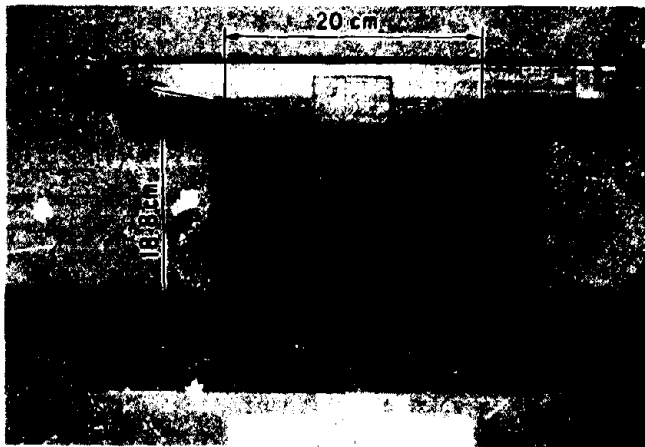


Photo 2 Lead Rubber Bearing

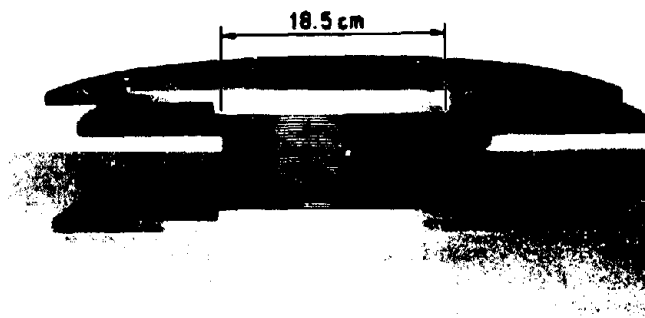


Photo 3 High Damping Rubber Bearing

The LRB (Ref. 4,5,6,7) was formed by laminating 20 layers of rubber with thickness of 5 mm and 19 steel plates with thickness of 2 mm, and the lead plug with diameter of 35 mm was pressed into at the center hole of the bearing. The HDR (Ref. 8) is composed of special rubber which is distinguished by damping characteristic from regular linear rubber. Therefore, the rubber itself would work as an energy dissipator as well as an isolator without any unique mechanism such as the lead plug, when it is subjected to shear deformation. The HDR was formed by vulcanizing 31 layers of the rubber with thickness of 2 mm, each layer of which was laminated between two steel plates with thickness of 0.6 mm. Both bearings are simple and compact as Menshin bearings for bridges so that they are very likely to be used in Menshin bridges.

Specific scale rule was not taken into consideration when the dimension of the model was decided, and the model was assumed as a small prototype. When the deck is supported by a fixed bearing at one end with the other end being supported by roller bearing, the fundamental natural period is about 1 sec. The stiffness of the Menshin bearings was designed to make the fundamental natural period about 2 sec, two times of regular one, so that the Menshin system performs effectively.

Excitation by sinusoidal motions and earthquake ground motions was made. Frequency as well as intensity was varied in the sinusoidal excitation to study the natural period of the model. Two ground motions which were recorded on the ground near the Kaihoku bridge during the Miyagi-ken-oki earthquake (M7.4) of 1978 and on the Hachiro-gata bank during the Nihon-kai-chubu earthquake (M7.7) of 1983 were used for the excitation. They are hereafter designated as a Kaihoku record and a Hachiro-gata record, respectively. The time of the Hachiro-gata record was reduced one half of the original. The intensity of the records was varied. Fig. 1 shows the response acceleration spectrum ratio (acceleration response/peak input acceleration) of the two records.

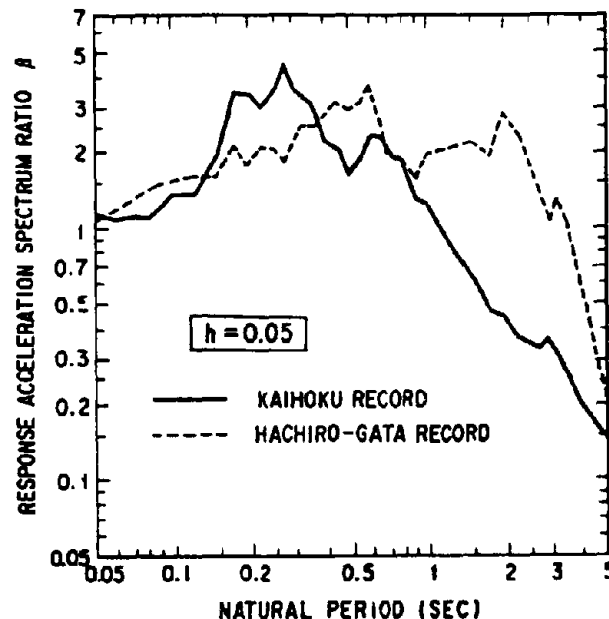


Fig.1 Response Acceleration Spectrum Ratio

Sinusoidal Excitation Figs. 2 and 3 show the resonance curve of acceleration and displacement. The fundamental natural frequency varied from 1.62 Hz to 0.67 Hz for the LRB model and from 1.95 Hz to 0.95 Hz for the HDR model by increasing the input acceleration from 0.01 g to 0.04 g. This clearly shows the shear-strain dependence of the stiffness of LRB and HDR. The fundamental natural frequency of the model supported by regular fix and roller bearings does not depend on the input acceleration.

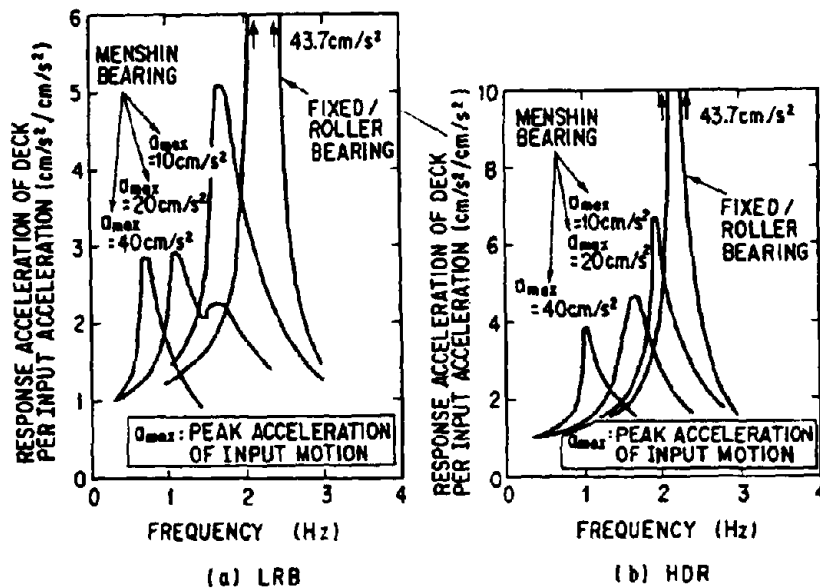


Fig.2 Amplification of Resonance Acceleration Curve

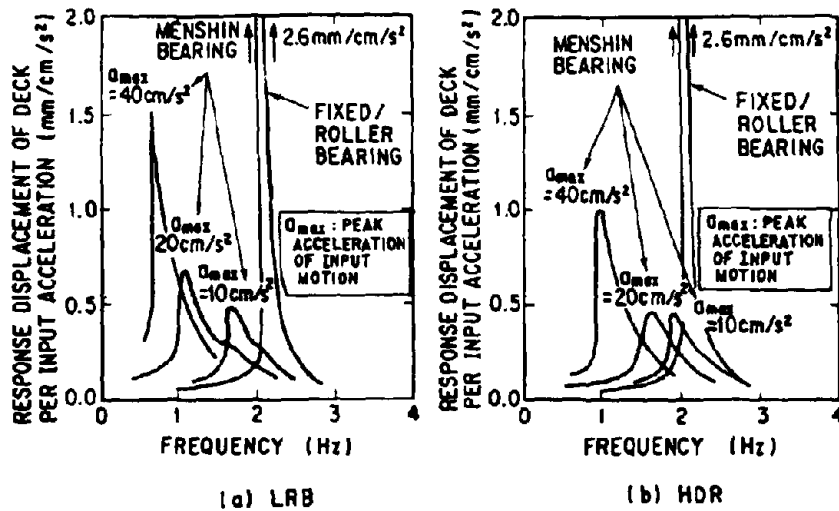


Fig.3 Amplification of Resonance Displacement Curve

Table 1 shows damping ratio by the half-power method with use of the resonance curves. The damping ratio is about 2 % for the model supported by the regular fix and roller bearings, and about 11 % and 9 % for the model supported by the LRB and the HDR, respectively, when subjected to the sinusoidal excitation with peak input acceleration of 0.04 g. It means that an increase of the damping ratio of 9 % and 5 % was made by adopting the LRB and the HDR, respectively.

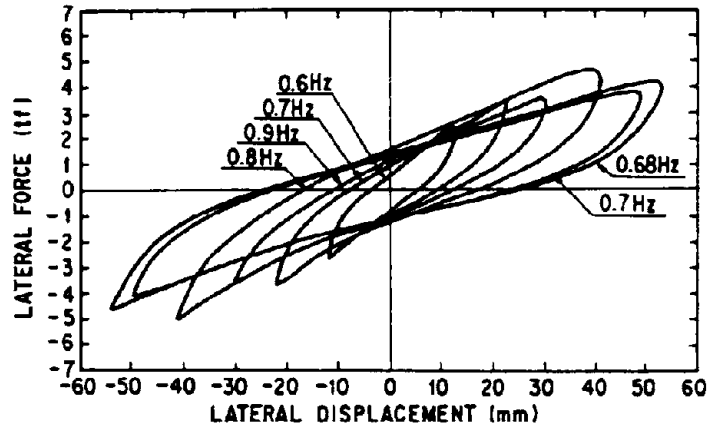
Table 1 Equivalent Viscous Damping Ratio by Half-Power Method

BEARING \ INPUT INTENSITY	INPUT INTENSITY		
	10 (cm/s ²)	20 (cm/s ²)	30 (cm/s ²)
LRB	0.08	0.092	0.113
HDR	0.064	0.087	0.092
FIXED/MOVABLE BEARING	0.02		

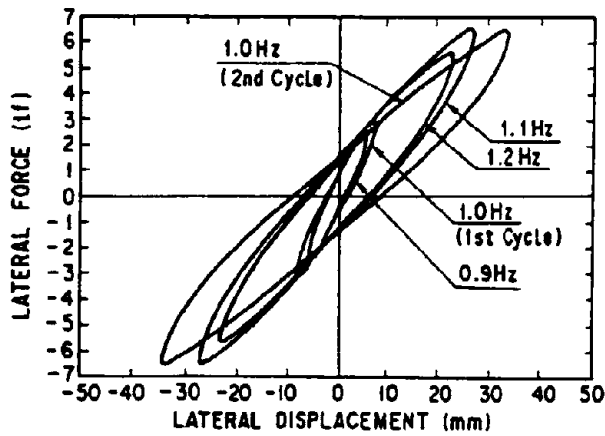
The hysteresis loops of shear force vs. shear deformation of the bearings are shown in Fig. 4. The hysteresis loops of the LRB look bilinear shape, especially in small amplitude, while the HDR is featured by the spindle-like shape. The lead plug of the LRB, which gives high initial stiffness, produces the bilinear shape. On the other hand, the HDR does not create high stiffness in small deformation and does not form the bilinear shape.

Figs. 5 and 6 show the dependency of the equivalent stiffness and the equivalent damping ratio on the deformation acquired from the sinusoidal excitation tests. The equivalent stiffness is defined as gradient of a line connecting the two points at the maximum and minimum displacement of a hysteresis loop, and the equivalent damping ratio is defined as a value proportional to the ratio of damping energy loss per cycle to strain energy stored at maximum displacement as shown in Fig. 7. An empirical equation for the equivalent stiffness k_e was obtained as shown in Fig. 5. Though the equivalent damping ratio is scattered, compared with the equivalent stiffness k_e , the damping ratio h_e may be considered 0.16 for the LRB and 0.13 for HDR in the range of the shear deformation from 1 to 50 mm.

The equivalent stiffness and the equivalent damping ratio from the cyclic shear loading tests of the bearing alone, which were conducted prior to the shaking table tests, are also shown in Figs. 5 and 6 for comparison. In the cyclic shear loading tests, alternating shear deformation was repeatedly applied to the bearings under constant vertical force corresponding to the dead weight of the deck. The equivalent stiffness and equivalent damping ratio estimated from the sinusoidal excitation tests are in good agreement with the result of the cyclic shear loading tests of the bearing alone so that it can be deduced that the test method, a shaking table test or a cyclic shear loading test, does not affect the equivalent stiffness and the equivalent damping ratio of a Menshin bearing.



(a) LRB



(b) HDR

Fig.4 Hysteresis of Lateral Force vs. Lateral Displacement

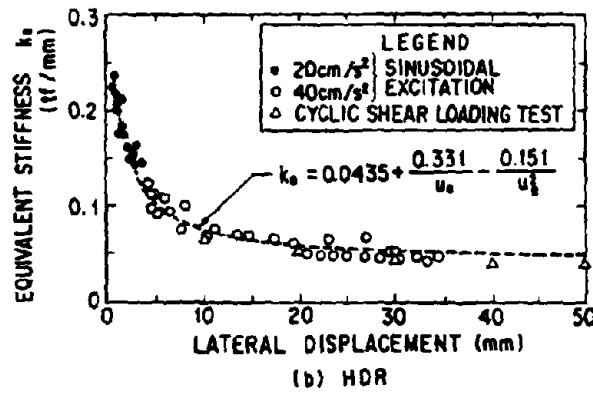
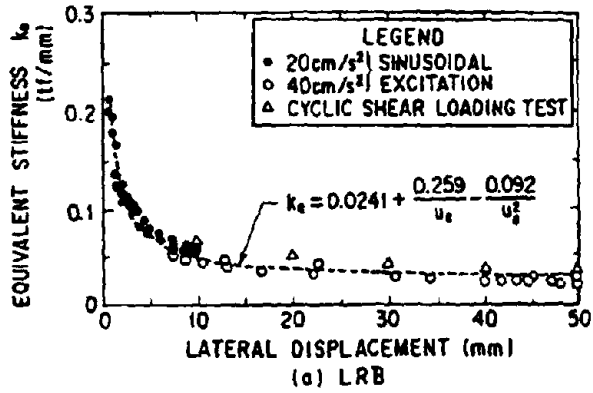


Fig.5 Equivalent Stiffness

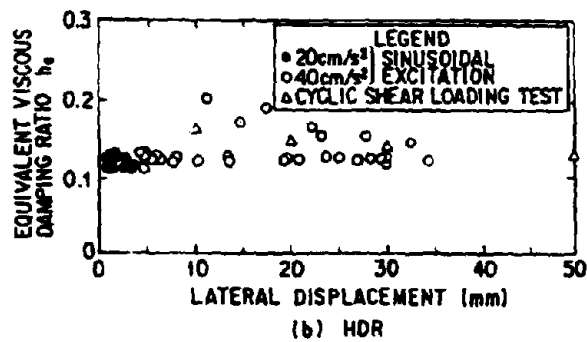
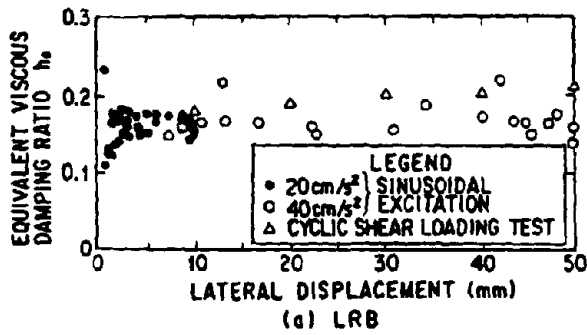


Fig.6 Equivalent Viscous Damping Ratio

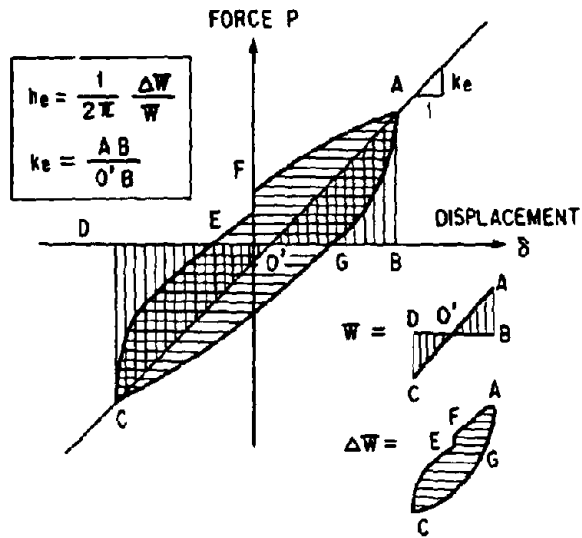


Fig.7 Definition of Equivalent Stiffness k_e and Equivalent Viscous Damping Ratio h_e .

Ground Motion Excitation Figs. 8 and 9 show how the peak deck response acceleration and displacement increase with the peak input acceleration. The effect of Menshin system can be apparently observed in Fig. 8, where the acceleration of the regular bridge amounts to more than two times acceleration of the Menshin bridge under the same input motion.

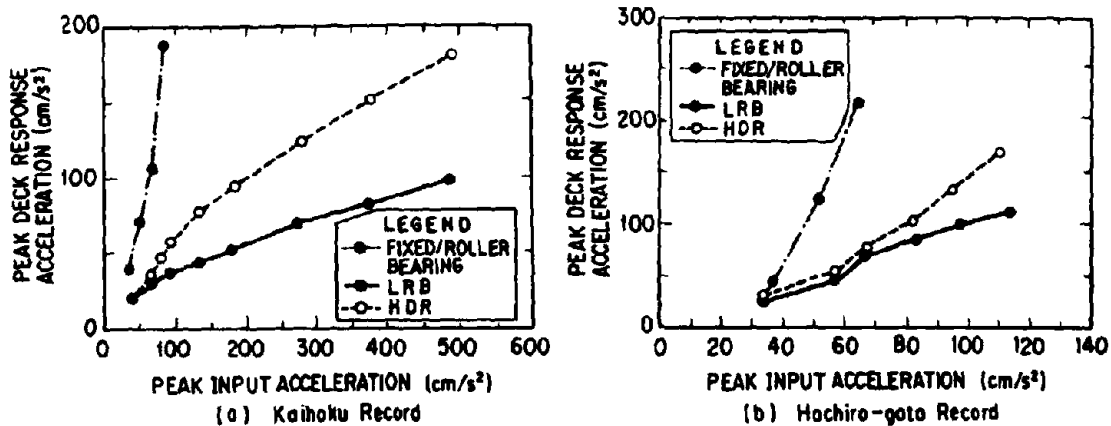


Fig.8 Peak Deck Response Acceleration

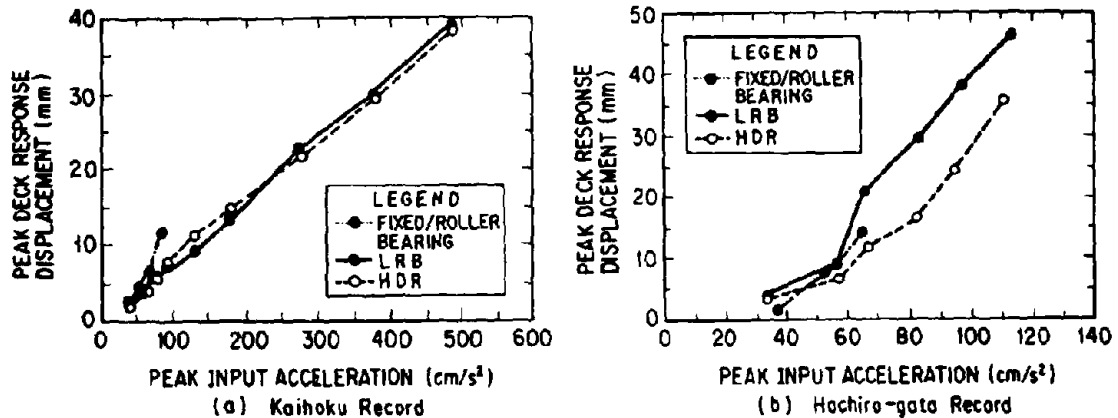


Fig.9 Peak Deck Response Displacement

EFFECT OF STOPPER AND VERTICAL EXCITATION

Tested Model For aiming to study effect of stopper and vertical excitation, another series of excitation tests were made. The columns and the Menshin bearings were replaced with new ones. The column was designed to have higher stiffness than an actual column since a flexible column could soften impact force due to collision developed at a stopper. The Menshin bearings, the lead rubber bearing and the high damping rubber bearing, were designed to make the fundamental natural period of the model about 0.6 sec. Photo 4 shows the Menshin bridge studied for the effect of stopper and vertical excitation. To distinguish the model with the one presented in Photo 1, it is referred as "model 2".



Photo 4 Setup of Shaking Table Test (Model 2)

The LRB was fabricated by vulcanizing 12 layers of rubber with thickness and diameter of 5 mm and 320 mm, respectively. They were laminated with 13 steel plates with thickness of 2 mm. The total thickness of rubber is 60 mm, and the total thickness of the entire bearing after fabrication is 110mm. The diameter of the lead plug is 40 mm. The HDR was fabricated by vulcanizing 16 layers of high damping rubber with thickness of 1.3 mm, and by laminating with steel plates with thickness of 3 mm.

Two stoppers which prevent excessive relative displacement between the deck and the columns were provided with the top of the each column as shown in Photo 5. A rubber was placed on the stopper to lessen the impact force of collision. Although the gap space of the stopper at both columns was adjusted to equalize each other as much as possible, it is noted that collision did not always take place simultaneously at each stopper.

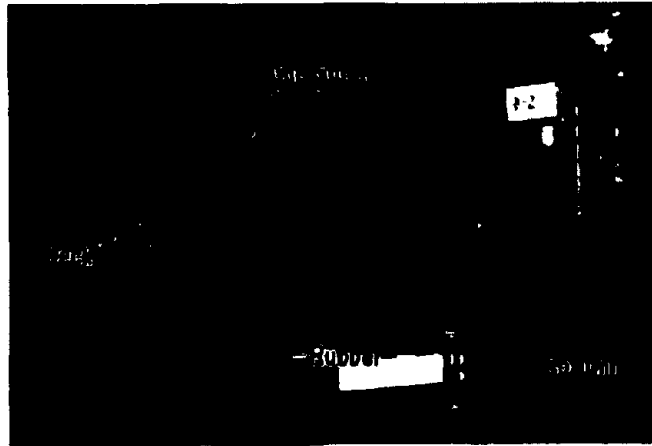


Photo 5 Stopper

Excitation was made either in longitudinal direction or in longitudinal and vertical direction. The horizontal and vertical components of the Kaihoku record and the Hachiro-gata record were used for the excitation. Ratio of acceleration intensity between horizontal and vertical components was assumed the same with the original records.

Effect of Collision and Vertical Excitation Fig. 10 shows the response of the model when the stoppers are not provided, and Fig. 11 shows the response when the stoppers with the gap space of 2 cm each were provided. Collisions, which took place when the stoppers of 2 cm gap was provided, developed greater acceleration at the deck and the columns.

Fig. 12 shows the hysteresis loops of the LRB for the tests shown in Figs. 10 and 11. Since the shear force computed by multiplying the acceleration developed at the deck by the mass of the deck is presented in Fig. 12, it should be noted that the shear force represents the total force transmitted to the columns through only the bearings when not colliding, and through both bearings and stoppers when colliding. The shear force jumped up significantly due to the collision.

Figs. 13 and 14 show the peak input acceleration vs. the peak deck response. It is seen in Figs. 13 and 14 that when the collision did not take place at the stoppers, the response displacement and acceleration of the deck are almost proportioned to the input acceleration. However, when the collision took place at the stoppers, the displacement of the deck is controlled by the stoppers within a little bit more than the gap space as shown in Fig. 13 (b). The acceleration of the deck is raised by the collision as shown in Fig. 14 (b). For example, the acceleration amounts to 0.69 g and 0.83 g for the gap of 3 cm and 2 cm, respectively, contrasted to 0.59 g without stoppers, under the excitation

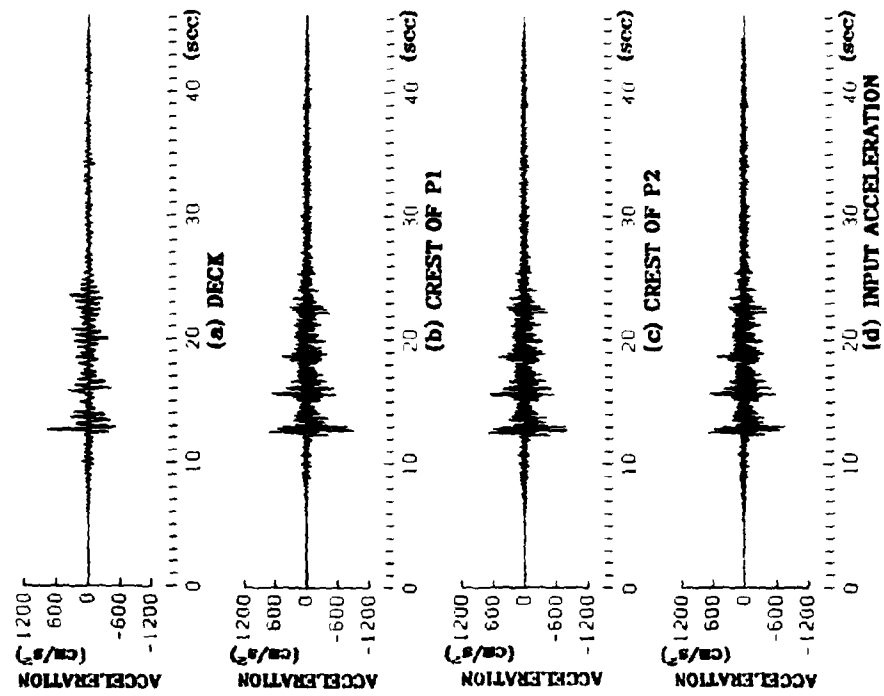


Fig.10 Response When Stopper Is Not Provided

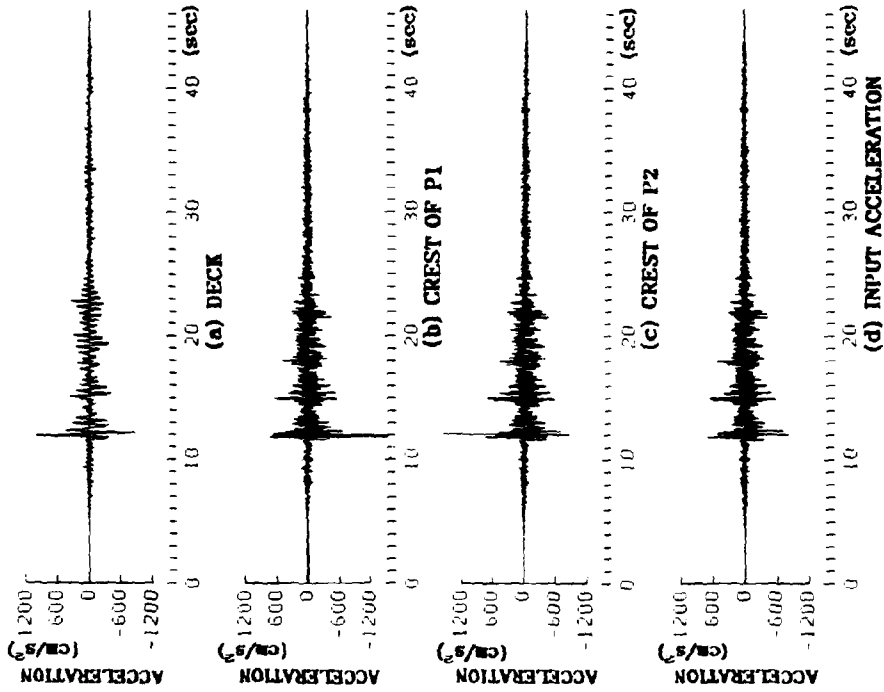


Fig.11 Response When Stopper with 2cm Gap Is Provided

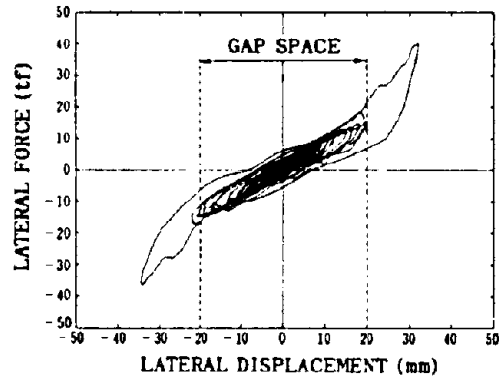
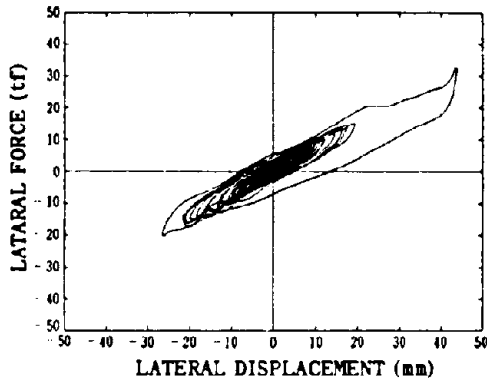


Fig.12 Hysteresis of Lateral Force vs. Lateral Displacement

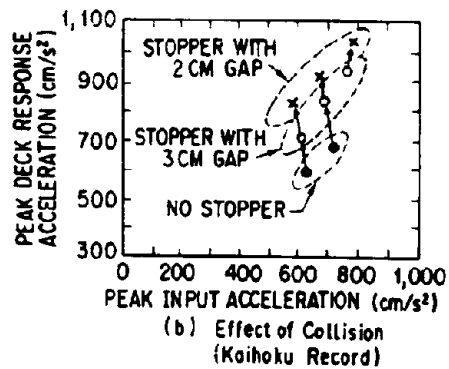
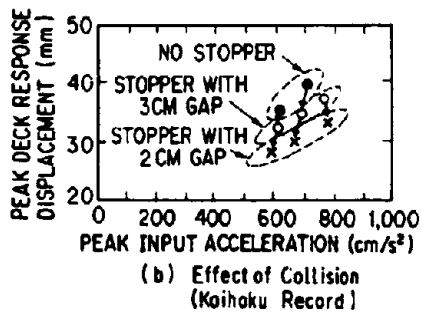
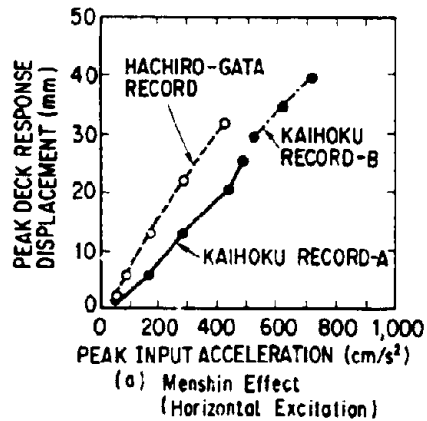
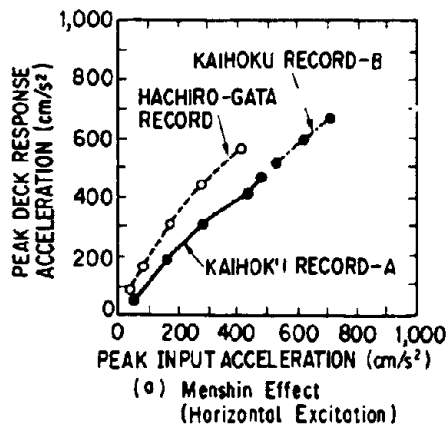


Fig.13 Effect of Stopper for Deck Response Displacement

Fig.14 Effect of Stopper for Deck Response Acceleration

of 0.6 g acceleration. This means that the seismic lateral force transmitted to the columns is increased by 1.2 times and 1.4 times for the gap of 3 and 2 cm, respectively, due to the collision.

Fig. 15 shows the effect of vertical excitation in terms of peak deck response. Although some effects of simultaneous excitation which was presumably caused by changes of the equivalent stiffness of the LRB due to variation of vertical force are seen, they are practically small.

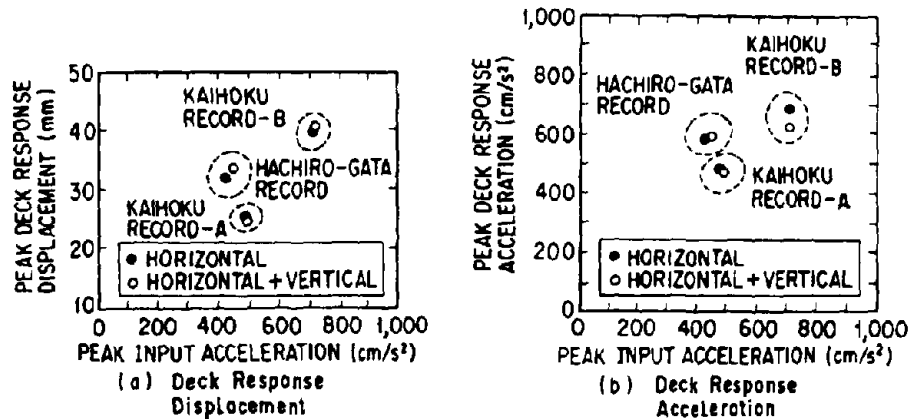


Fig.15 Effect of Vertical Excitation

Deck response when the HDR was adopted is basically analogous to that for the LRB, and so they are not presented here.

ANALYTICAL SIMULATION BY EQUIVALENT LINEAR ANALYSIS

Because the equivalent stiffness and the equivalent damping ratio of Menshin bearing depend on the displacement developed in it as shown in Figs. 5 and 6, they have to be evaluated for a specific response displacement u_e in the equivalent linear analysis. Therefore the response displacement u_e was assumed to be specified in the form of

$$u_e = c \cdot u_{max} \quad (1)$$

where u_{max} is the peak displacement of the Menshin bearing, and c is a coefficient ($0 \leq c \leq 1.0$) representing the intensity of the specific response displacement. The coefficient c was assigned as 0.7 and 1.0. Because the purpose of this study is to clarify the coefficient c , a simplification was introduced in the calculation, i.e., since the peak displacement u_{max} is unknown before the analysis, the iteration of analysis is inevitable in the equivalent linear analysis. However, since the peak displacement obtained from the tests should be the right peak displacement, it was used in Eq. (1) instead of the iteration.

Mode damping ratio of the entire bridge model with Menshin bearings was computed by the proportional-to-strain-energy damping computing method (Ref. 9). The method is to estimate the damping ratio for each mode shape of an entire structure as the weighted average of damping ratio of each element with

proportion to its strain energy as

$$h_i = \frac{\sum_{j=1}^n \phi_{ij}^T \cdot h_j \cdot k_j \cdot \phi_{ij}}{\phi_i^T \cdot K \cdot \phi_i} \quad (2)$$

where h_i is the damping ratio of i -th mode, ϕ_i is an i -th mode vector for j -th structural element, h_j is the damping ratio of j -th element, K_j is the stiffness matrix of j -th element, ϕ_j is i -th mode vector, K is stiffness matrix of the entire structure and n is the number of elements.

The model 1 supported by the LRB was analyzed. Table 2 shows the fundamental natural period and the mode damping ratio for the fundamental natural mode. Damping ratio of the columns was assumed as 0.2 %, which was estimated from the shaking table test results of the bridge model supported by the regular fix and roller bearings. It is seen in Table 2 that difference of the fundamental natural period and the mode damping ratio between for $c = 0.7$ and $c = 1.0$ is up to only 7 % and 2 % at most, respectively. This means that the fundamental natural period and the mode damping ratio are less sensitive on the coefficient c .

Table 2 Natural Period and Damping Ratio

(a) Natural Period

INPUT MOTION		L R B		H D R	
		c=0.7	c=1.0	c=0.7	c=1.0
KAIHOKU RECORD	A	1.04	1.11	0.84	0.88
	B	1.13	1.18	0.90	0.93
HACHIRO-GATA RECORD	A	1.08	1.14	0.80	0.85
	B	1.15	1.20	0.89	0.92

(b) Viscous Damping Ratio

BEARING	INPUT MOTION		c=0.7	c=1.0
L R B	KAIHOKU	A	0.149	0.150
		RECORD	B	0.151
	HACHIRO-GATA	A	0.150	0.151
		RECORD	B	0.152
H D R	KAIHOKU	A	0.111	0.112
		RECORD	B	0.113
	HACHIRO-GATA	A	0.109	0.111
		RECORD	B	0.113

Fig. 16 compares the predicted and measured deck response acceleration for the Kaihoku record. The predicted response assuming $c = 0.7$ and $c = 1.0$ sufficiently assesses the experimental response, and these two values of c do not give meaningful difference on the response. Table 3 compares the peak response between the predicted and the measured. Although the analysis assuming $c = 1.0$ gives a little better outcome compared with the analysis assuming $c = 0.7$, it may be said that the accuracy of both cases are satisfactory enough in practical sense.

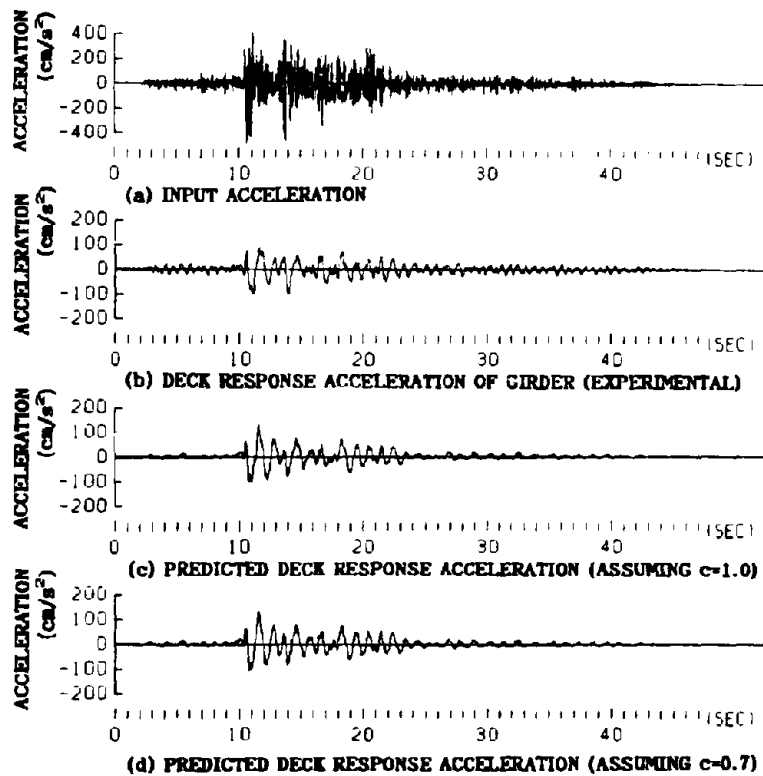


Fig.16 Deck Response Acceleration for Kaihoku Record B

Table 3 Comparison between Experimental and Analytical by Equivalent Linear Analysis

MENSHEIN BEARING	INPUT MOTION		PEAK INPUT ACCELERATION (cm/s ²)	EXPERIMENT		SIMULATION			
				PEAK DECK RESPONSE ACCELERATION (cm/s ²)	PEAK DECK RESPONSE DISPLACEMENT (mm)	c = 0.7		c = 1.0	
						PEAK DECK RESPONSE ACCELERATION (cm/s ²)	PEAK DECK RESPONSE DISPLACEMENT (mm)	PEAK DECK RESPONSE ACCELERATION (cm/s ²)	PEAK DECK RESPONSE DISPLACEMENT (mm)
L R B	KAIHOKU	A	273.2	72.5	21.0	80.2 (1.11)	18.2 (0.87)	80.2 (1.11)	20.8 (0.98)
		RECORD	481.3	101.0	35.8	134.6 (1.33)	36.6 (1.02)	130.4 (1.29)	39.1 (1.09)
	HACHIRO-GATA	A	85.1	81.7	26.1	120.0 (1.47)	30.4 (1.16)	111.5 (1.36)	31.5 (1.21)
		RECORD	115.6	110.2	41.2	163.7 (1.49)	47.5 (1.15)	151.3 (1.37)	47.9 (1.16)
H D R	KAIHOKU	A	276.4	124.6	18.6	125.6 (1.01)	17.9 (0.96)	118.6 (0.95)	18.9 (1.02)
		RECORD	484.7	181.9	33.1	190.9 (1.05)	32.2 (0.97)	182.2 (1.00)	33.1 (1.00)
	HACHIRO-GATA	A	83.1	102.7	14.0	112.5 (1.10)	14.8 (1.06)	113.8 (1.11)	17.0 (1.21)
		RECORD	111.5	170.4	30.4	186.2 (1.09)	31.5 (1.04)	197.3 (1.16)	36.2 (1.19)
AVERAGE OF RATIO						(1.21)	(1.15)	(1.17)	(1.11)

() Represents Ratio of Experimental to Analytical

ANALYTICAL SIMULATION BY BILINEAR ANALYTICAL MODEL

An analysis was also made for the model 1 by idealizing the nonlinear hysteretic behavior of the Menshin bearings by a bilinear analytical model. The initial stiffness k_1 , post-yield stiffness k_2 and the characteristic load Q are the basic parameters for defining the bilinear model. As shown in Figs. 17 - 19, they were estimated from the sinusoidal excitation test results presented in Fig. 4. Empirical equations were derived for k_1 , k_2 and Q

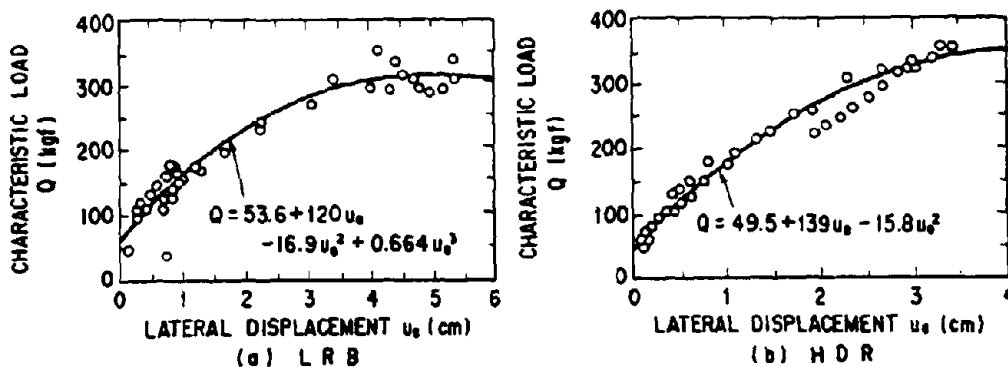


Fig.17 Characteristic Load

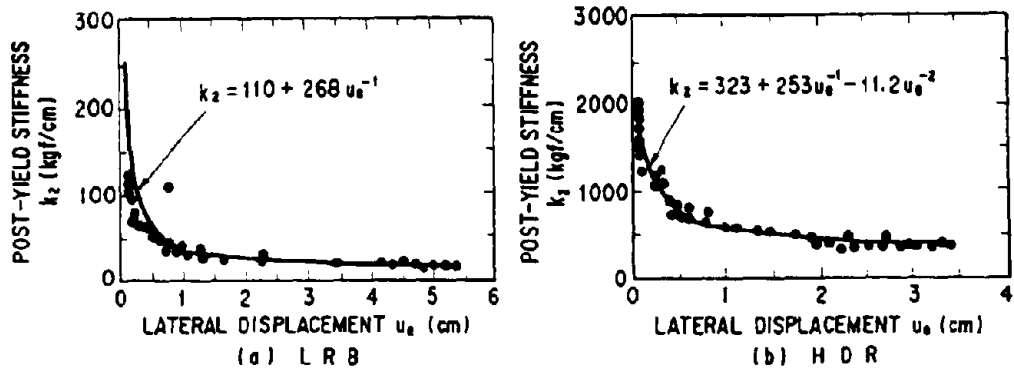


Fig. 18 Post-yield Stiffness

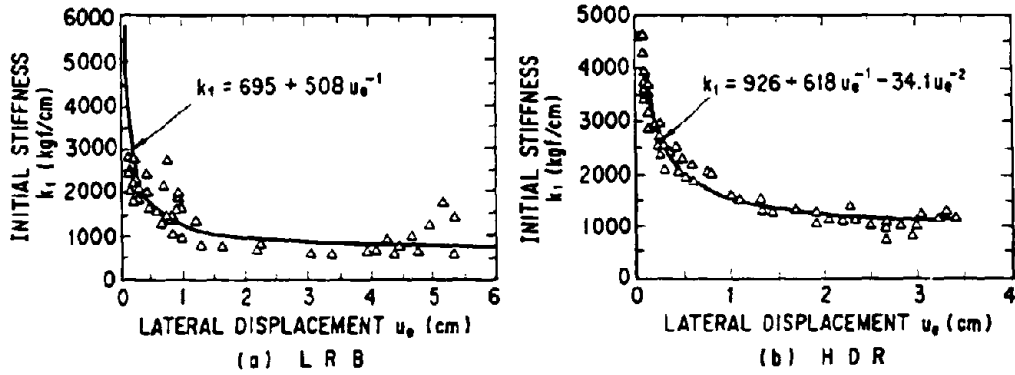


Fig. 19 Initial Stiffness

Fig. 20 compares the hysteresis loop thus idealized with the bilinear model and the experimental result. The model remarkably agrees with the experimental loop.

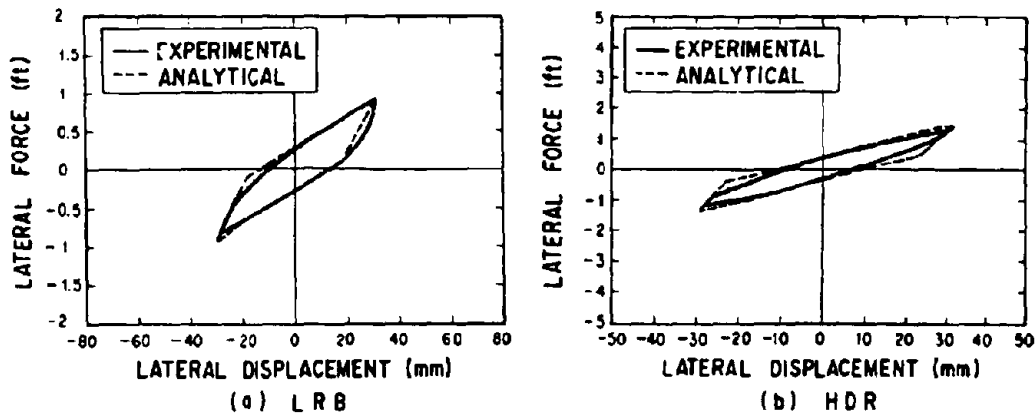


Fig. 20 Analytical Idealization by Bilinear Spring Model

It should be however noted here that because the parameters k_1 , k_2 and Q depend on the shear deformation of the Menshin bearings, the idealization with the bilinear model has to be made depending on the shear deformation developed in the Menshin bearings. Because a computer program in which the displacement-independent bilinear model is assumed was used, iteration similar with the equivalent linear analysis was required to determine the most appropriate shear deformation of the Menshin bearings. Therefore, the response displacement of the Menshin bearings u_e was assumed as

$$u_e = c_{NL} \cdot u_{max} \quad (3)$$

where c_{NL} is a coefficient ($0 \leq c_{NL} \leq 1.0$) and u_{max} is the peak displacement of a Menshin bearing developed during excitation. Although it was anticipated from the preceding analysis by the equivalent linear analysis that the coefficient c_{NL} of 0.7 and 1.0 gives practically small difference, analytical simulation was made assuming these two values for the coefficient c_{NL} . Similar with the equivalent linear analysis, the peak response displacement actually developed in the Menshin bearings during the excitation tests was assigned for u_{max} in Eq. (3), and the iteration was avoided in the analytical simulation.

The same cases studied as in the equivalent linear method were analyzed. To represent energy dissipation at the columns, Rayleigh damping was included. Coefficients of Rayleigh damping were determined so that it gives the mode damping ratio computed by the proportional-to-strain-energy damping computing method for the first and second vibration modes, i.e., $h_1 = 0.0$ and $h_2 = 0.02$.

Fig. 21 compares the deck response between the analysis and the experiment. The analysis gives good agreement with the experiment, and no significant difference can be observed between $c_{NL} = 0.7$ and $c_{NL} = 1.0$. Only slight discrepancy is the decay of the deck response after the main vibration. The tests show faster attenuation than the analysis. This is because the bilinear hysteresis loop of the Menshin bearing was so adjusted to be applicable for the larger shear deformation during the main vibration, and is not fitting for the smaller deformation after that.

Table 4 compares the peak deck response. Defining a ratio of the predicted and experimental peak deck response, the ratio ranges from 0.9 to 1.1 for $c_{NL} = 1.0$, while it scatters widely for $c_{NL} = 0.7$. Based on such evaluation, c_{NL} is proposed to be assigned 1.0.

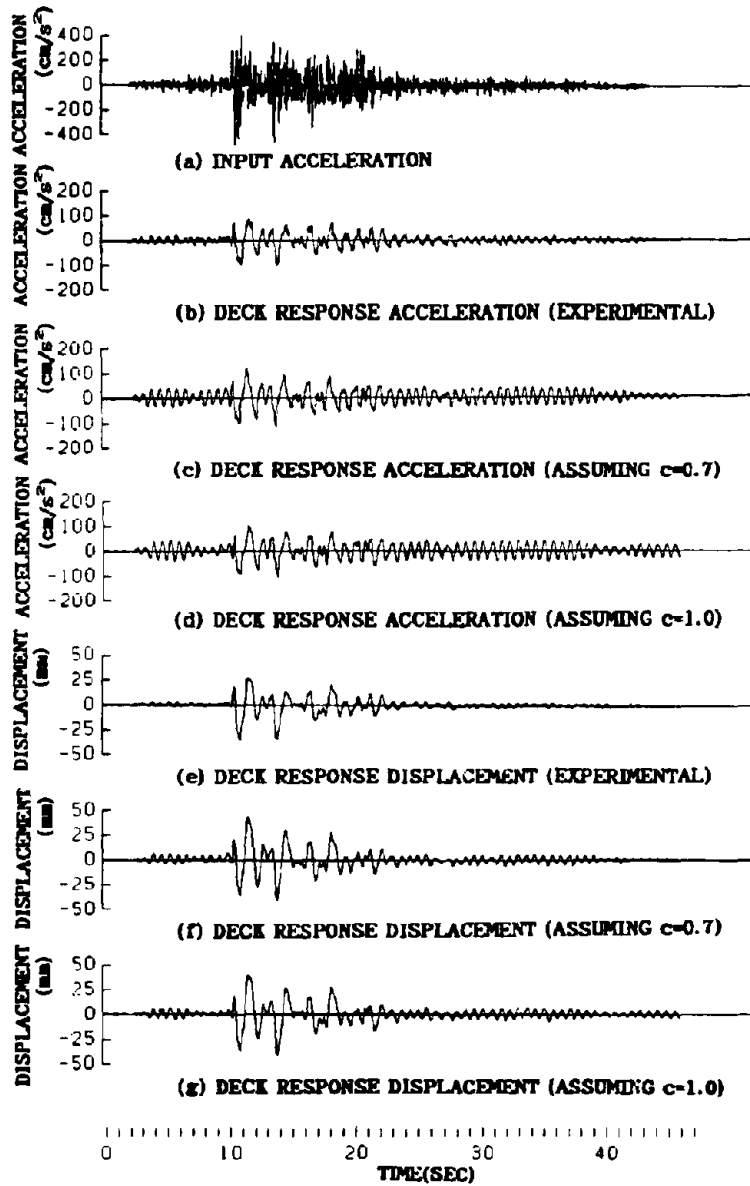


Fig.21 Deck Response for Kauhoku Record B

Table 4 Comparison between Experimental and Analytical by Nonlinear Analysis

MENSJIN BEARING	INPUT MOTION	PEAK INPUT ACCELERATION (cm/s ²)	EXPERIMENT		SIMULATION				
			PEAK DECK RESPONSE ACCELERATION (cm/s ²)	PEAK DECK RESPONSE DISPLACEMENT (mm)	c = 0.7		c = 1.0		
					PEAK DECK RESPONSE ACCELERATION (cm/s ²)	PEAK DECK RESPONSE DISPLACEMENT (mm)	PEAK DECK RESPONSE ACCELERATION (cm/s ²)	PEAK DECK RESPONSE DISPLACEMENT (mm)	
L R B	KAIHOKU	A	273.2	72.5	21.0	92.2 (1.27)	25.3 (1.20)	83.6 (1.15)	25.7 (1.22)
	RECORD	B	481.3	101.0	35.8	118.3 (1.17)	43.4 (1.21)	102.7 (1.02)	40.4 (1.13)
	HACHIRO-GATA	A	85.1	81.7	26.1	123.7 (1.51)	40.3 (1.54)	97.3 (1.19)	34.1 (1.31)
	RECORD	B	115.5	110.2	41.6	148.4 (1.35)	60.7 (1.46)	123.0 (1.12)	53.8 (1.29)
H D R	KAIHOKU	A	276.4	124.6	13.6	128.6 (1.03)	22.1 (1.19)	116.5 (0.93)	20.7 (1.11)
	RECORD	B	484.7	181.9	33.1	172.3 (0.95)	34.4 (1.04)	156.9 (0.86)	31.7 (0.96)
	HACHIRO-GATA	A	83.1	102.7	14.0	95.0 (0.93)	15.6 (1.11)	93.6 (0.91)	15.4 (1.10)
	RECORD	B	111.5	170.4	30.4	189.9 (1.11)	39.3 (1.29)	185.3 (1.09)	39.8 (1.31)
AVERAGE OF RATIO						(1.17)	(1.26)	(1.03)	(1.16)

() Represents Ratio of Experimental to Analytical

ANALYTICAL SIMULATION FOR COLLISION

The stopper of Menshin bridges has to be properly modeled in Menshin design since it would cause great impact force to the columns due to collision. As shown in Fig. 22, the stopper was idealized as a linear spring functioning only when collision takes place. In the range over the gap space Δ_g of the stopper, a spring with the compression stiffness of the rubber installed on the stopper resists for further compression. Energy dissipation due to collision was disregarded in this idealization (Ref. 10).

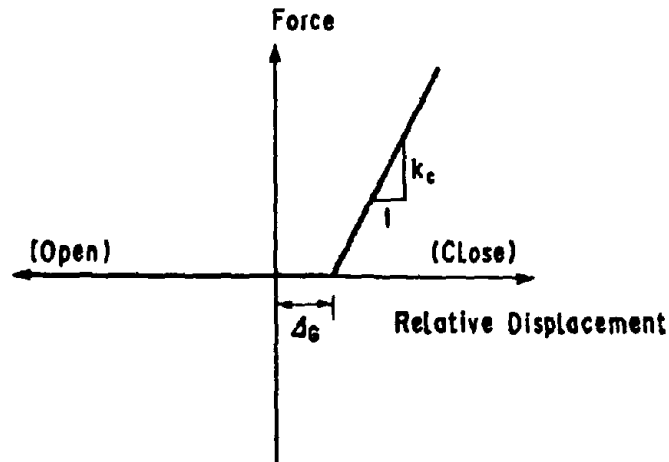


Fig.22 Idealization of Stopper

The width w , height h , thickness t , and young modulus E of the rubber are 40 cm, 20 cm, 7.1 cm and 40.0 kgf/cm², respectively, so that the compression stiffness k_c is obtained as

$$\begin{aligned} k_c &= E \times w \times h / t \\ &= 40.0 \times 40 \times 20 / 7.1 \\ &= 4,507 \text{ kgf/cm} \end{aligned} \quad (4)$$

The deck response of the model 2 supported by the LRB was simulated with nonlinear dynamic analysis. The Menshin bearing was modeled as a bilinear model. The initial stiffness, post-yield stiffness and characteristic load of the Menshin bearing were determined by the method proposed in the preceding chapter. The damping of other structural elements than the Menshin bearings is taken into account by Rayleigh damping with the same method as described also in the preceding chapter.

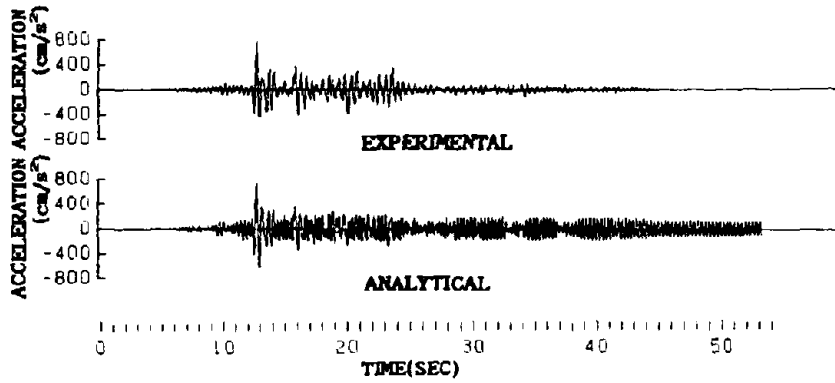
Figs. 23 and 24 compare the deck response acceleration and the response displacement of the bearing between the analysis and the experiments. The analysis can successfully simulate the effect of collision. Figs. 25, 26 and 27 show the hysteresis loops between the force transmitted to the columns and the relative displacement of the bearing. Sudden increase of the force when collision occurred can be realistically predicted by the analysis, although the effect of strain hardening of rubber can not be simulated in the analysis.

Table 5 compares the peak response of the analysis and the experiment. The accuracy of the analytical prediction expressed in terms of a ratio of the peak predicted response to the peak measured response ranges from 0.92 to 0.95 for the acceleration and from 1.03 to 1.16 for the displacement. They are quite sufficient.

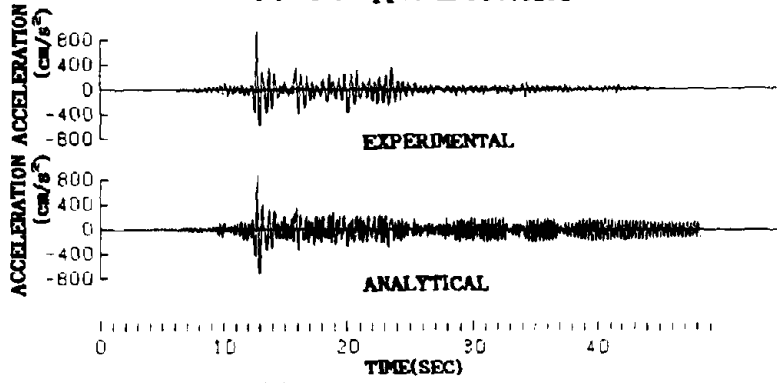
Table 5 Comparison between Experimental Analytical Deck Response

GAP SPACE	PEAK INPUT ACCELERATION (cm/s ²)	EXPERIMENT		SIMULATION	
		PEAK DECK RESPONSE ACCELERATION (cm/s ²)	PEAK DECK RESPONSE DISPLACEMENT (mm)	PEAK DECK RESPONSE ACCELERATION (cm/s ²)	PEAK DECK RESPONSE DISPLACEMENT (mm)
No Stopper	751.6	785.8	43.1	744.7 (0.95)	44.5 (1.03)
3 cm	768.6	937.4	39.1	891.9 (0.95)	44.0 (1.13)
2 cm	787.2	1023.1	35.7	936.8 (0.92)	41.4 (1.16)

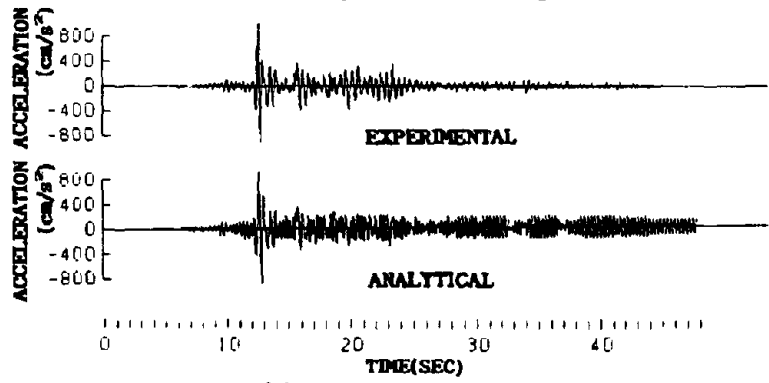
() Represents Ratio of Experimental to Analytical



(a) No Stopper Is Provided

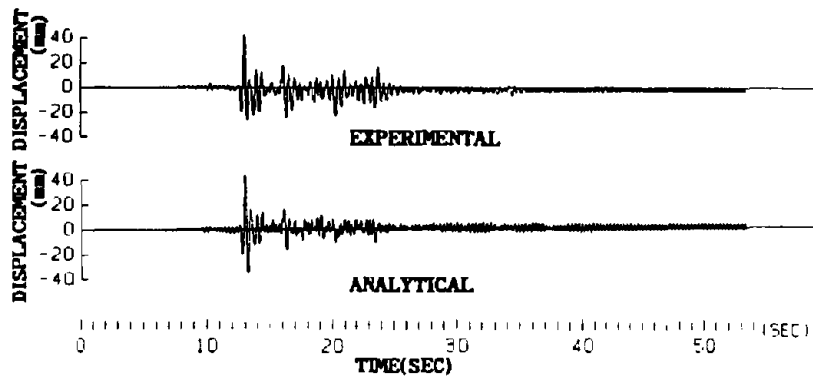


(b) Stopper with 3cm Gap is Provided

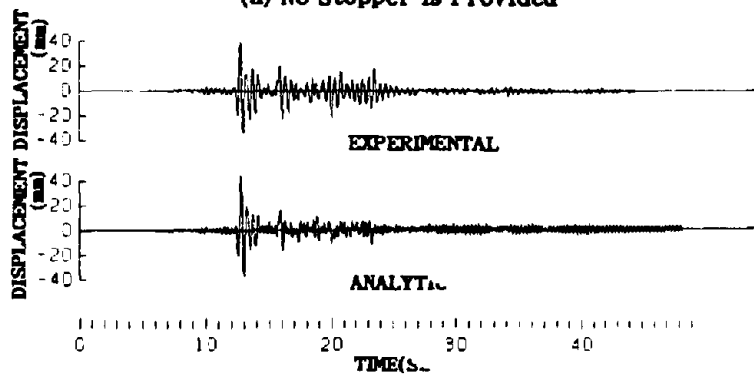


(c) Stopper with 2cm Gap is Provided

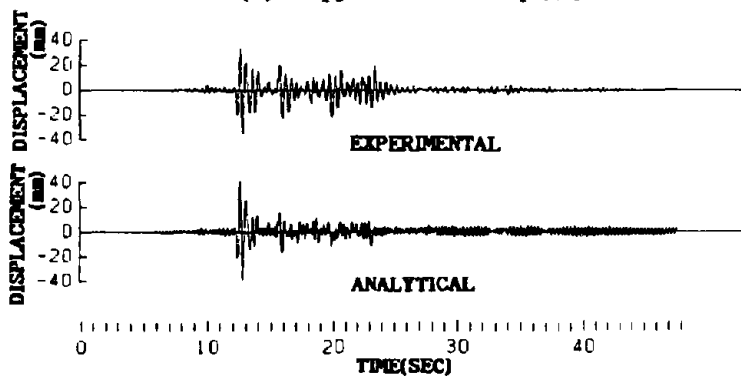
Fig.23 Comparison between Experimental and Analytical Deck Response Acceleration



(a) No Stopper is Provided



(b) Stopper with 3cm Gap is Provided



(c) Stopper with 2cm Gap is Provided

Fig.24 Comparison between Experimental and Analytical Deck Response Displacement

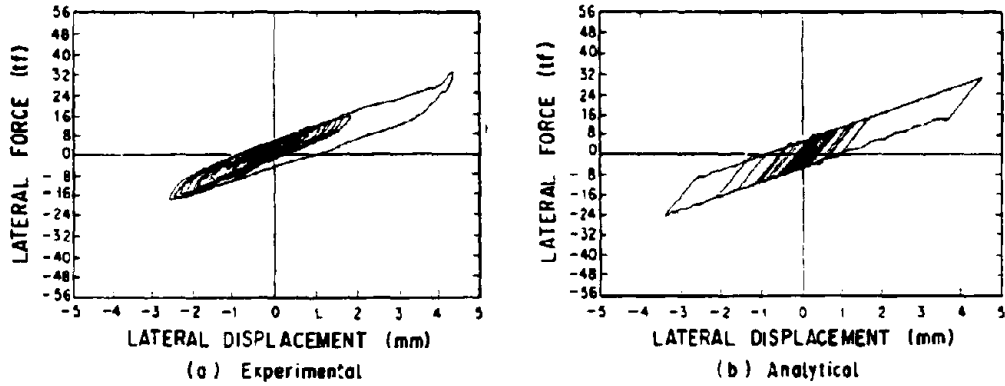


Fig.25 Hysteresis When No Stopper is Provided

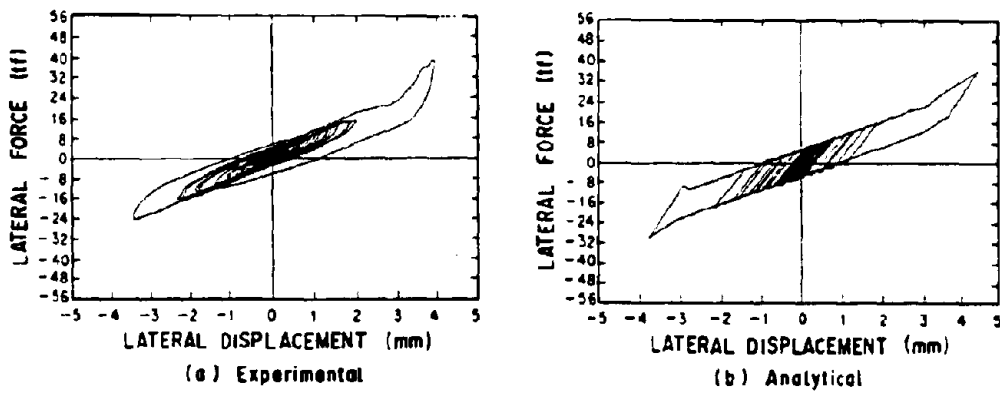


Fig.26 Hysteresis When Stopper with 3cm Gap is Provided

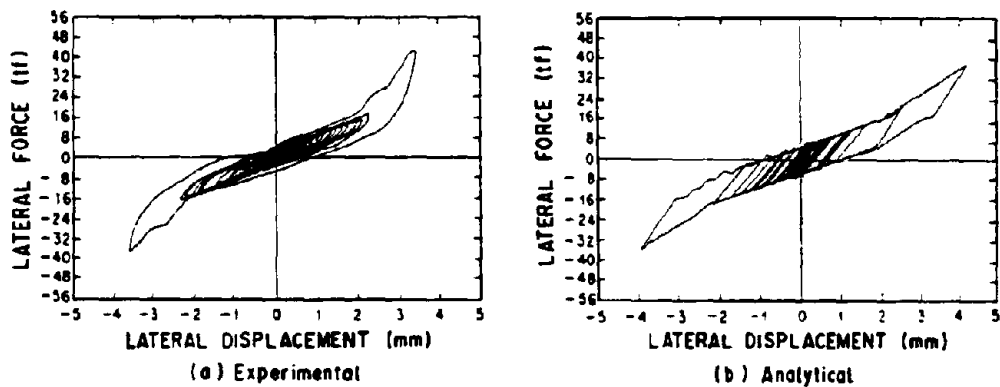


Fig.27 Hysteresis When Stopper with 2cm Gap is Provided

CONCLUSIONS

Response characteristics of two Menshin bridges were investigated through a series of shaking table tests. The response data of the model bridges were analyzed by the equivalent linear and bilinear analysis. The following conclusions may be deduced from the result presented herein.

- 1) The stoppers, which can effectively control the excessive relative displacement between the deck and the column, could develop great impact forces at the columns. Effect of such impact force needs to be considered in the Menshin design. The force and the displacement can be assessed by nonlinear dynamic analysis with the model of stoppers functioning as a linear spring only when the collision occurs.
- 2) Effect of vertical excitation is less significant to lateral response of the deck.
- 3) The response of the Menshin bridge can be successfully simulated by the equivalent linear analysis if the equivalent stiffness and the equivalent damping ratio are appropriately assumed in the analysis. The coefficient c in Eq. (1) is proposed to be assigned as 1.0 although the difference of the response by assuming $c = 0.7$ is small.
- 4) The response of the Menshin bridge can be successfully assessed by idealizing the nonlinear hysteretic behavior of the Menshin bearings with the bilinear model. The coefficient c_{NL} of 1.0 gives better result than c_{NL} of 0.7 to determine the initial stiffness, the post-yield stiffness and the characteristic load of the Menshin bearing.

ACKNOWLEDGEMENT

This study was achieved as a part of joint research program entitled "Development of Menshin System for Highway Bridges" between the Public Works Research Institute and 28 private firms. The shaking table tests shown in this paper were performed under the joint research program between the Public Works Research Institute and the Metropolitan Expressway Public Corporation. The authors express their sincere appreciation for their cooperation to proceed the research.

REFERENCES

- 1)Public Works Research Institute : Report of Joint Research between PWRI and 28 Private Firms on Development of Menshin Systems for Highway Bridges, Technical Report of Cooperative Research, No. 44 and No. 60, Public Works Research Institute, March 1990 and March 1991 (in Japanese)
- 2)Kawashima, K., Hasegawa, K., Yoshida, T., Yamauchi, H. and Kosaka, H. : Shaking Table Test on Dynamic Response of Base-Isolated Bridges, Civil Engineering Journal, Vol. 30-10, pp. 521 - 526, October 1988 (in Japanese)
- 3)Kawashima, K., Hasegawa K. and Nagashima, H. : Seismic Response Analysis of a Base-Isolated Bridge with an Equivalent Linear Analysis, Civil Engineering Journal, to be presented (in Japanese)

- 4) Buckle, I. G. and Mayes, R. L. : Seismic Isolation : History, Application, and Performance - A World View, Earthquake Spectra, Vol. 6, No. 2, pp. 161 - 202, May 1990
- 5) McKay, G. R., Chapman, H. E. and Kirkcaldie, D. K. : Seismic Isolation : New Zealand Applications, Earthquake Spectra, Vol. 6, No. 2, pp. 203 - 222, May 1990
- 6) Robinson, W. H. : Lead-rubber Hysteretic Bearings Suitable for Protecting Structures during Earthquakes, Earthquake Engineering and Structural Dynamics, Vol. 10, pp. 593 - 604, 1982
- 7) Tyler, R. G. and Robinson, W. H. : High-strain Test on Lead Rubber Bearings for Earthquake Loadings, Bull. New Zealand National Society for Earthquake Engineering, Vol. 17, No. 2, pp. 90 - 105, June 1984
- 8) Kojima, H. and Fukahori, Y., : Performance, Durability of High Damping Rubber Bearings for Earthquake Protection, Rubber World, Vol. 202, No. 1, April 1990
- 9) Japan Road Association : Design Specifications for Highway Bridges - Part V Seismic Design -, February 1990 (in Japanese)
- 10) Kawashima, K. : An Analytical Model of Contact and Impact in Dynamic Response Analysis, Proc. Japan Society of Civil Engineers, Vol. 308, pp. 123 - 126, April 1981

ON-LINE EARTHQUAKE RESPONSE TESTS OF HIGH-DAMPING RUBBER BEARINGS FOR SEISMIC ISOLATION

Hirokazu IEMURA¹ Yoshikazu YAMADA² William TANZO³
Yoshifumi UNO⁴ Shizuo NAKAMURA⁵

- ¹ Assoc. Prof., Earthquake Engg. Lab., Dept. of Civil Engg., Kyoto Univ., Kyoto, Japan
² Professor, Earthquake Engg. Lab., Dept. of Civil Engg., Kyoto Univ., Kyoto, Japan
³ Grad. Student, Earthquake Engg. Lab., Dept. of Civil Engg., Kyoto Univ., Kyoto, Japan
⁴ Chief, Bridge Design Section, Kawaguchi Metal Industries Co., Kita-ku, Osaka, Japan
⁵ Chief Engineer, Nitto Engineering Consultants, Nishi-ku, Osaka, Japan

ABSTRACT

On-line hybrid loading tests (pseudo-dynamic tests) have been used to determine earthquake response and resonant response of seismic isolation devices in addition to usual cyclic loading tests. Thus, effectiveness of the seismic isolation system can be evaluated directly in terms of earthquake response characteristics. High-damping rubber (HDR) bearings were tested and have been verified to have energy-absorbing capacity equivalent to about 11–15% damping ratio of the linear elastic models. Response for shear strain level under 100% can be modeled with bilinear hysteretic model. Isolation effectiveness in terms of lower earthquake energy input and high energy-absorbing capacity is evaluated with calculation of energy partitioning in structural systems. In addition, the response of the HDR isolators for extreme load conditions has been experimentally verified in which strain hardening is tapped as an inherent safety measure against excessive deformation.

INTRODUCTION

In recent years, there has been a tremendous amount of interests in using seismic isolation as an effective and practical approach to earthquake-resistant design. New isolator techniques and configurations continue to be developed. For these to be widely accepted for use by the structural engineering profession, their fundamental engineering properties and their expected behavior during earthquakes should be well established. Extensive experimental tests are very much needed to study their behavior and provide data for analytical modeling and design.

Extensive experimental tests on high-damping rubber (HDR) seismic isolators were conducted using an on-line hybrid computer-actuator experimental system for earthquake response analysis developed at the Earthquake Engineering Laboratory, Department of Civil Engineering, Kyoto University. Seismic performance of HDR-supported systems can be evaluated under different earthquake ground motions. Resonant response under frequency-sweeping sine input excitations can also be determined. In addition, the normal procedure of repeated cyclic loading test can be conducted using the same testing facility. Thus, the integrated testing system can test for: (a) fundamental mechanical properties, (b) resonant response, and (c) earthquake response. Effectiveness of the isolators is discussed in terms of structural acceleration and displacement response which is directly connected to design requirements. Earthquake response of equivalent linear elastic models and that of bilinear hysteretic models are numerically simulated and compared to that of the test results for accurate modeling of the isolators. Earthquake input energy and its partitioning in a seismically isolated structure are calculated to investigate seismic effects of the isolators in terms of energy concepts. With these ranges of obtained results, the developed loading system offers a versatile testing system in the early development stage, as well as for final verification and proof tests.

HIGH-DAMPING RUBBER SEISMIC ISOLATORS

A total of four tested HDR isolator specimens are presented in this report. Two different rubber mixtures

were used: compound A with target equivalent damping $\xi=15\%$ and compound B with $\xi=10\%$. Composition of compound A is shown in Table 1 and physical properties are given in Table 2.

Geometrically, the specimens are of 25-cm \times 25-cm square in plan. A 3-layer configuration, a 4-layer configuration, and a 9-layer configuration (Fig. 1) were fabricated to determine differences in stiffness and damping properties due to geometrical effect. All of the specimens tested have the same thickness ($t=12\text{mm}$) for each single rubber layer. The shape factor is then the same ($S.F.=5.2$) for all specimens. Except for a few cases when axial loads were differed to check for effect of axial load level on damping ratios and stiffnesses, the specimens were loaded vertically with 40 tonf giving an axial bearing pressure of 64 kg/cm^2 .

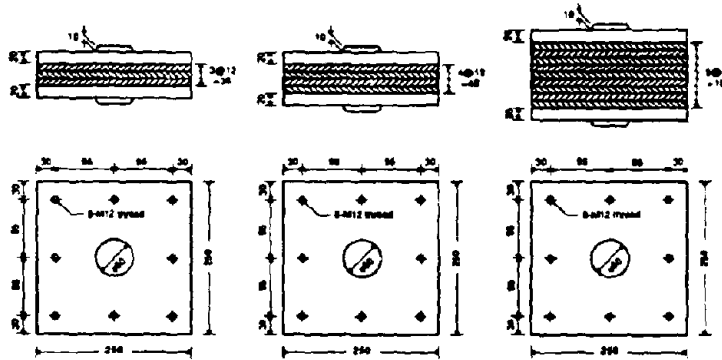


Fig. 1 Plan and Dimensions of HDR Isolator Specimens Tested

TEST SET-UP

The test rig shown in Fig. 2 is used in this experiment. The specimen is bolted to the underside of the load-transfer beam and to a rigid platform that is attached to the rails of the strong reaction floor. Different heights of isolator specimens could be accommodated by inserting spacer plates between the specimen and the test platform. Photo 1 shows a full view of the set-up of loading system.

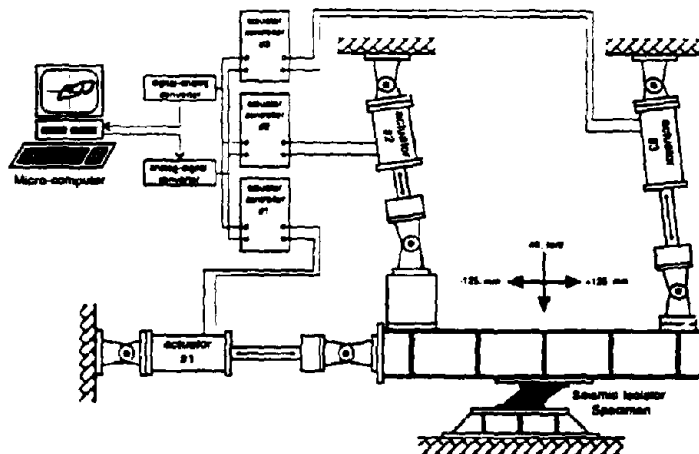


Fig. 2 Specimen is Laterally Displaced, While Sustaining an Axial Load

For general applications to testing of structural components, the load-transfer beam can be commanded to displaced the specimen in three degrees of freedom (lateral δ_x , vertical δ_y , and rotational θ_z). For the present test cases, the load-transfer beam is controlled to impose horizontal displacements while maintaining a

constant axial load on the isolator specimen. The actuator for horizontal motion (labeled no. 1) has a maximum stroke of ± 125 mm and maximum load capacity of 40 tonf. Each of the vertical actuators (no. 2 and no. 3) has load capacity of 40 tonf.

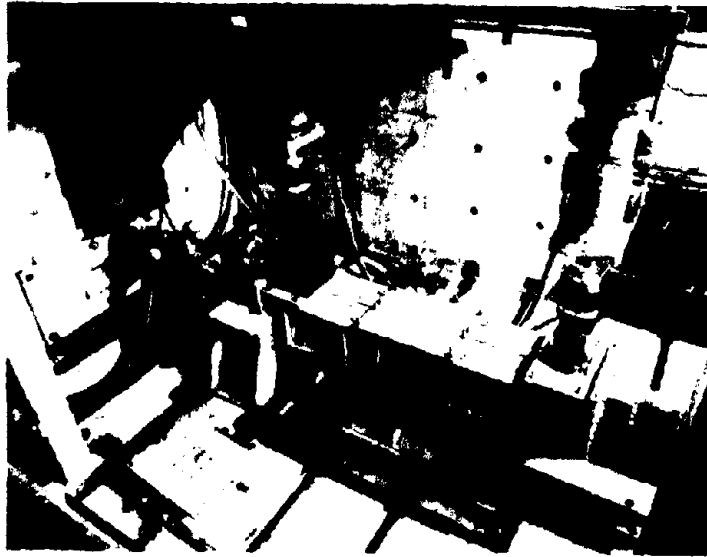


Photo 1 Setup for Testing Seismic Isolators

A computer that can be highly programmed to control instrumentations is used to: (1) control the load actuators; (2) receive feedback forces; (3) do dynamic structural analysis in on-line hybrid tests; and (4) do other data acquisition and recording functions. Digital displacement control values are sent to a digital-to-analog converters (DAC), while analog feedback signals are received through an analog-to-digital converter (ADC). Timing parameters are set within the control program to operate the loading system at the desired loading rate.

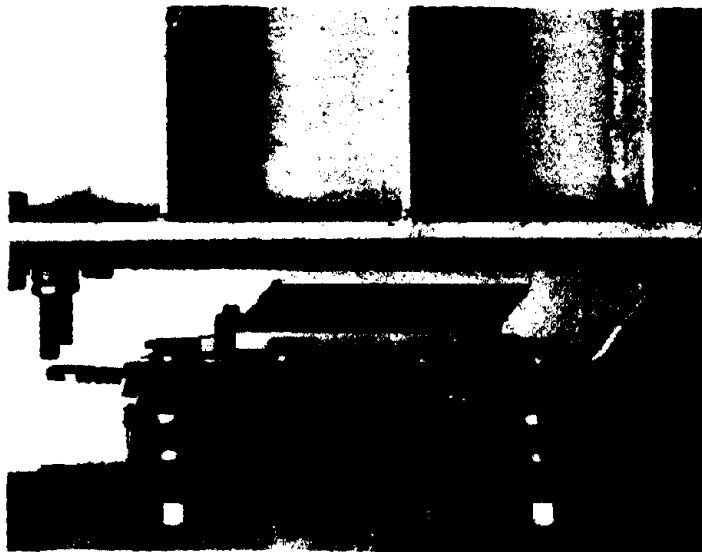


Photo 2 A HDR Seismic Isolators under Test

Table 1 Composition (by Weight) of Rubber Compound A Used

components	A
natural rubber components	58.6%
strengthening agents	29.3%
plasticizers and accelerators	2.0%
age resistors and others	10.0%

Table 2 Physical Properties of Rubber Compound A Used

property	A
hardness (JIS K 6301 Type-A durometer)	64
static elastic shear modulus (kgf/cm ²)	10
tensile strength (kgf/cm ²)	164
elongation at break (%)	510

TEST PROGRAMS

The specimens were tested for: (a) fundamental mechanical properties, (b) resonant response, and (c) earthquake response. The test programs are described in the following.

Cyclic Loading Tests Cyclic loading tests are the most common standard tests for determining mechanical properties of the isolators. These are usually done to evaluate lateral stiffness and equivalent damping ratios of the isolators. In this experiment, the main cyclic loading tests were done first up to 150% shear strain and finally up to 200% shear strain (Fig. 4). Besides the two main cyclic loading tests (QS150 and QS200), cyclic loading tests at different levels of axial loads and constant amplitude sinusoidal tests at different loading speeds done on a few specimens to check effects on lateral stiffnesses and hysteretic behavior.

On-line Hybrid Tests for Earthquake Response On-line hybrid test (pseudo-dynamic test) is a computer-controlled experimental technique in which direct numerical time integration is used to solve the equations of motion. The computed displacement at each step is statically imposed on a specimen through a computer-controlled load actuators in order to measure its restoring forces at the current deformation state. The measured restoring forces are then fed into the equations of motion to compute the next set of displacements. The development, current activities and future prospects of on-line hybrid test methods have been reported by Iemura [1985], Takahashi and Nakashima [1987], and Mahin et al [1989].

On-line hybrid tests were conducted on the HDR isolators in order to determine earthquake response of a seismically-isolated structure. It is to be noted that natural rubber component is used in these specimens and in most currently used laminated bearings. For natural rubber, dynamic stiffness does not vary much with temperature and frequency [Derham and Thomas 1980]. Hence, the specimens are suitable for on-line hybrid tests. A few cyclic loadings tests under different loading speeds were done to verify the insignificant effects of loading speed on the mechanical properties of the tested specimens.

It can be assumed in this very preliminary stage that the isolated superstructure would move as a rigid body. More refined analytical modeling of the superstructure can be implemented in a substructured on-line hybrid test. The structure is modeled as a single-degree-of-freedom (SDOF) system with a natural period of 2 seconds. For this relatively flexible SDOF system, numerical stability of explicit form of direct integration schemes poses no special problem. The central difference scheme is found sufficient for this experiment.

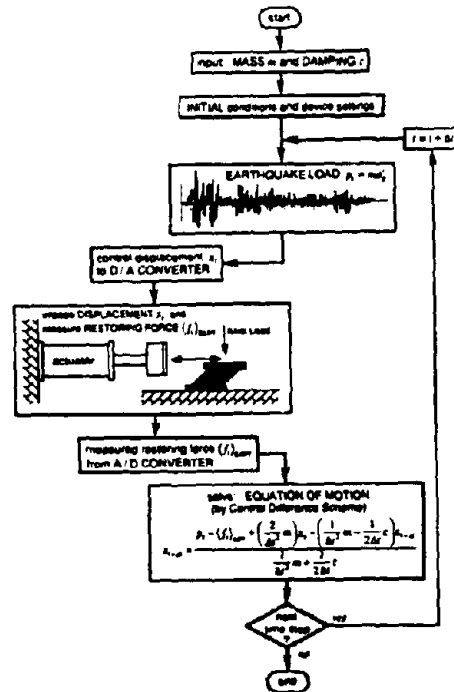


Fig. 3 On-line Hybrid Test Procedure for Earthquake Response

For a nonlinear SDOF system, the equation of motion for on-line hybrid test is expressed as follows:

$$m\ddot{x}_t + c\dot{x}_t + \langle f_t \rangle_{\text{expt}} = p_t \quad (1)$$

where m, c : mass and damping of the SDOF system; $x_t, \dot{x}_t, \ddot{x}_t$: displacement, velocity, and acceleration, respectively, at time t ; p_t : equivalent load due to ground acceleration; and $\langle f_t \rangle_{\text{expt}}$: restoring force of the isolator at time t due to displacement x_t measured directly from a loaded specimen by an on-line computer. Using the velocity and acceleration approximation based on the central difference scheme and substituting these expressions into the equation of motion above and solving for $x_{t+\Delta t}$

$$x_{t+\Delta t} = \frac{p_t - \langle f_t \rangle_{\text{expt}} + \left(\frac{2}{\Delta t^2} m\right) x_t - \left(\frac{1}{\Delta t^2} m - \frac{1}{2\Delta t} c\right) x_{t-\Delta t}}{\frac{1}{\Delta t^2} m + \frac{1}{2\Delta t} c} \quad (2)$$

Effectiveness of seismic isolators are very much dependent on the characteristics of the input earthquake motion and the supported structures. Two representative types of earthquake records are used. These are: (a) the NS-component of the El Centro record during the 1940 Imperial Valley Earthquake (Fig. 6); and (b) the NS-component of the Hachinohe record during the 1968 Tokachi-oki Earthquake (Fig. 7). These records are scaled to evaluate isolator performance at different range; i.e., 100% strain for ideal bilinear behavior and 150% strain for assumed overload range.

On-line Hybrid Sweep Test In order to check for resonance, a model is usually subjected to sweeping-frequency sine input in a shaking-table test. This can also be implemented in an on-line hybrid test. A typical sweeping-frequency sine input is shown in Fig. 5. The first sine wave has a frequency of 0.2 cps or period of $T = 5$ s. The period is then reduced by an decrement of 0.2s until $T = 3$ s. Between $T = 3$ s and $T = 1$ s, the period of the sine wave is decrement by a smaller interval of 0.1s to give better detail to the resonant range. Finally, period is decremented again by 0.2s after $T = 1$ s. In this experiment, the final period used was 0.6s. The input sine waves are discretized at 0.02s, the same integration time step used in the tests. The constant amplitude level is scaled to give response within some desired ranges, e.g., at 100% strain and 150% strain.

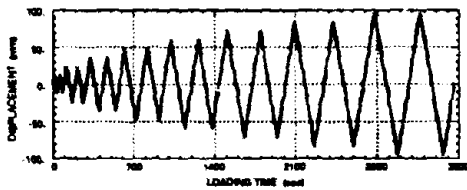


Fig. 4 Displacement History for Repeated Cyclic Loading Test (QS200) of HDR-A(4)



Fig. 5 Input Frequency-Sweeping Sine Ground Excitation for HS100 of HDR-A(4)

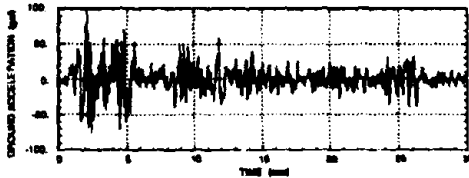


Fig. 6 Input El Centro Earthquake Record ($A_{max} = 0.10g$) for HE100 of HDR-A(4)

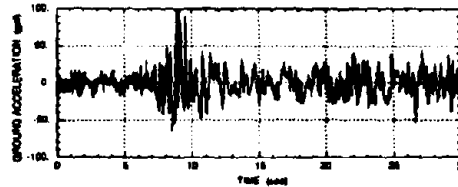


Fig. 7 Input Hachinohe Earthquake Record ($A_{max} = 0.10g$) for HH100 of HDR-A(4)

TEST RESULTS AND ANALYSIS

Only the results of one specimen will be presented in detail to illustrate the features of the loading system developed. Specimen HDR-A(4) is a four-layer steel-reinforced high-damping ($\xi = 15\%$ nominal) rubber seismic isolator (Photo 2). The specimen was subjected to the following sequence of loading programs:

- Cyclic loading up to 150% shear strain QS150
- El Centro record for 100% shear strain HE100
- Hachinohe record for 100% shear strain HH100
- sweeping-sine excitation for 50% shear strain HS050
- sweeping-sine excitation for 100% shear strain HS100
- sweeping-sine excitation for 120% shear strain HS120
- sweeping-sine excitation for 150% shear strain HS150
- and finally, to cyclic loading up to 200% shear strain QS200.

Static Cyclic Loading Tests In this experiment, the main cyclic loading tests were done first up to 150% shear strain and finally up to 200% shear strain (Fig. 4) in the last sequence of the testing program. The specimen was first subjected to the cyclic loading program QS150 to evaluate static cyclic behavior. The displacement loading history consists of cyclic displacements of $\pm 25\%$, $\pm 50\%$, ..., $\pm 150\%$ shear strain (i.e., proportional to specimen height) at two repetitions of each cycle. Fig. 8 shows the hysteretic cyclic behavior. Comparing the curves traced by the two repetitions at each cycle shows stable hysteretic behavior for the specimen. Material hardening can be observed to have been starting to commence at about 125% for this specimen.

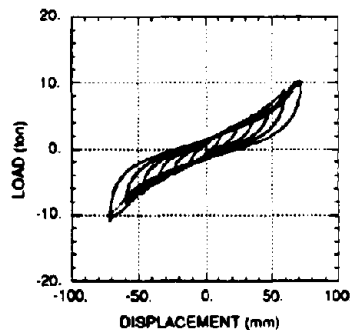


Fig. 8 Hysteretic Behavior of HDR-A(4) under Repeated Cyclic Loading Tests (QS150)

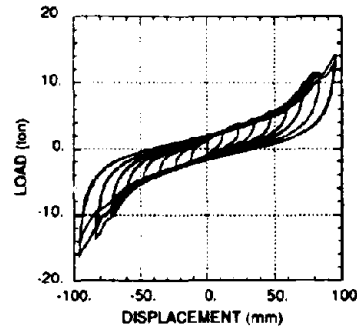


Fig. 9 Hysteretic Behavior of HDR-A(4) under Repeated Cyclic Loading Tests (QS150)

After being subjected to different earthquake and sweep excitations, the specimen HDR-A(4) was finally subjected to cyclic loading up to 200% shear strain (± 96 mm). Fig. 9 shows the hysteretic cyclic behavior. Comparing the two hysteresis curves in Figs. 8 and 9, there is not much degradation in the mechanical properties of the specimen even after the previous tests.

Fig. 10(a) shows the lateral stiffnesses against shear strain for three-, four-, and nine-layer HDR-A isolators. Fig. 10(b) shows the equivalent viscous damping ratio against shear strain for the same set of three-, four-, and nine-layer HDR15-A isolators. Equivalent damping ratios are not much affected by the number of layers for three specimens tested. However, differences in lateral stiffnesses are very much significant between the three specimens of different heights. A more extensive coverage of this plot through testing of more sets of specimens will constitute an important data base for structural design, i.e., specifying a set of isolators giving appropriate flexibility to the total structural system. It can also be observed from Fig. 10(a) that strain-hardening effects are initiated earlier (at about 75% for HDR-A(3) and at about 125% for HDR-A(4)) and stiffer in the shorter specimens.

Effects of axial bearing pressure on lateral stiffnesses and damping ratios were also tested and confirmed using the loading system. For shear strain of 100%, Fig. 11(a) shows the effect of axial bearing pressure on lateral stiffnesses, while Fig. 11(b) shows the effect on damping ratios. The level of axial load (or the axial bearing pressure) is an important factor in both the stiffness and damping properties of an isolator.

In Fig. 11(a), it can be observed that lateral stiffnesses are reduced with higher axial bearing pressure. The reductions in lateral stiffnesses for the same percentage of shear strain are also higher in the more compressed cases. On the other hand, equivalent damping capacities as shown in Fig. 11(b) are higher in specimens subjected to higher axial bearing pressure. However, the reductions in damping capacities for the same percentage of shear strain are not significantly higher for the higher levels of axial bearing pressures.

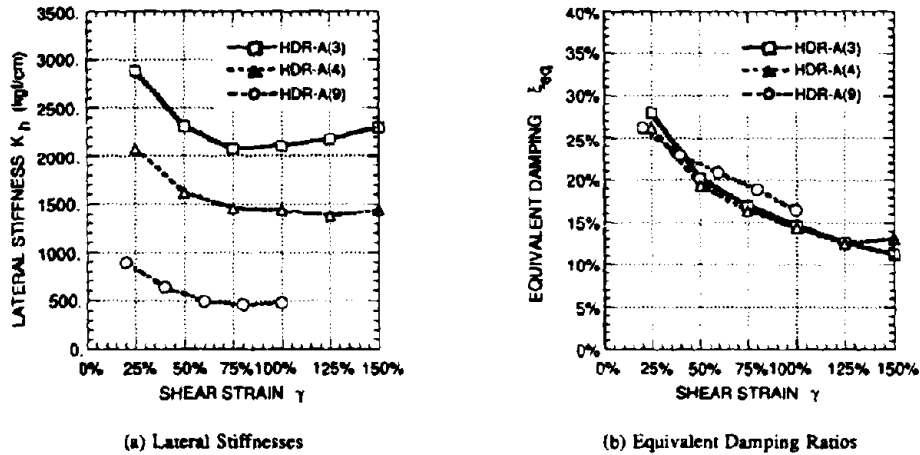


Fig. 10 Effect of number of layers on HDR-A isolators

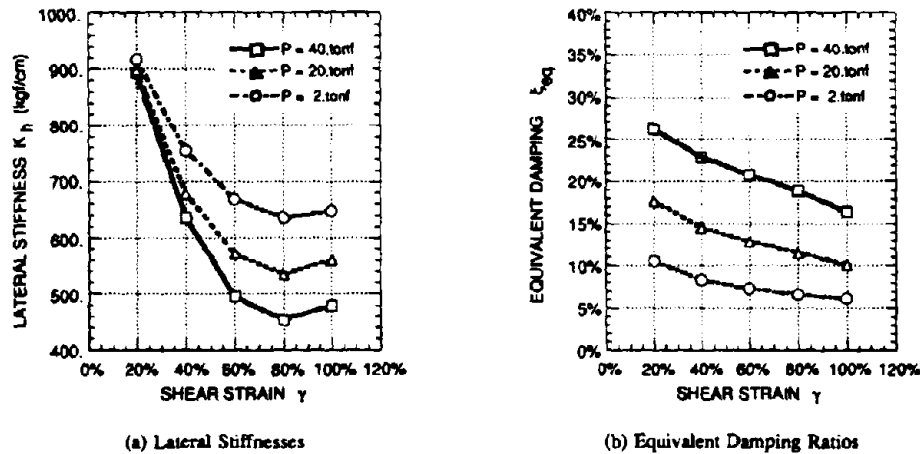


Fig. 11 Effect of Axial Load Level on HDR-A(9)

From the plot of Fig. 11(a), it can be observed that strain hardening effects are initiated at $\gamma=80\%$ and stiffer for the specimen subjected to higher axial bearing pressure. Going back to the plot of Fig. 10(a), it has been mentioned earlier that strain-hardening effects are initiated earlier and stiffer in the shorter specimens than the taller specimens. These are important considerations if strain-hardening property is to be tapped as an extra measure against excessive displacements upon reaching the assumed overload range (say, more than 150% shear strain).

On-line Hybrid Tests for Earthquake Response Performance of the HDR isolator under the two earthquake ground motion input is checked for maximum displacement corresponding to 100% shear strain. For the El Centro earthquake, the earthquake record was scaled to have maximum acceleration of 0.1g (Fig. 6). Displacement and acceleration time histories are shown in Fig. 12. Hysteretic load-deformation behavior of the isolator is shown in Fig. 12(a). Also shown in the same set of plots are the response of an equivalent viscously-damped linear elastic model giving the same level of maximum displacement. It can be said that the

HDR-isolator system has an equivalent viscous damping ratio of 15%. Response of an approximate bilinear model is given in Fig. 13. Overall, good correlations are obtained within 100% shear strain for response under El Centro excitation.

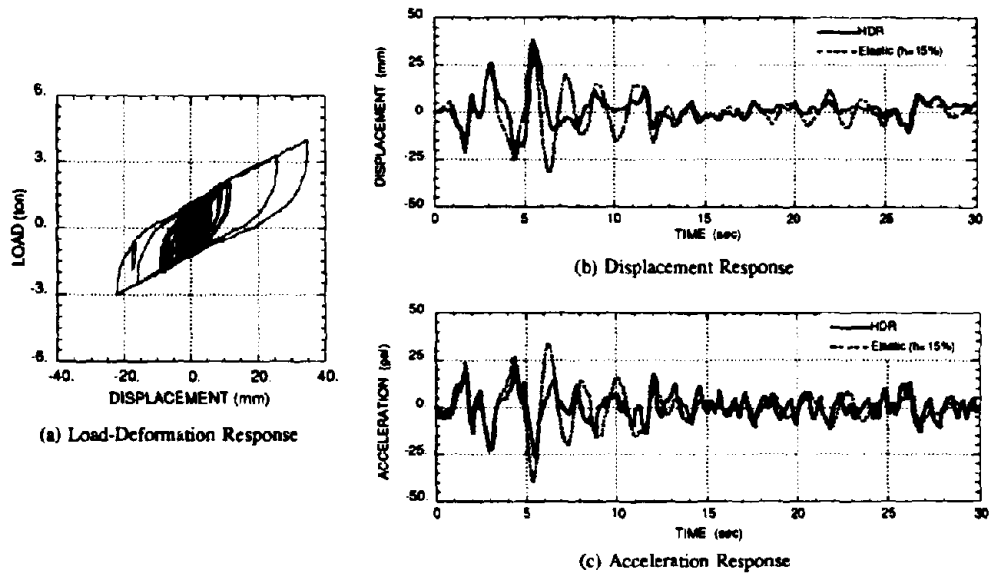


Fig. 12 Earthquake Response of HDR-A(4) under El Centro Excitation

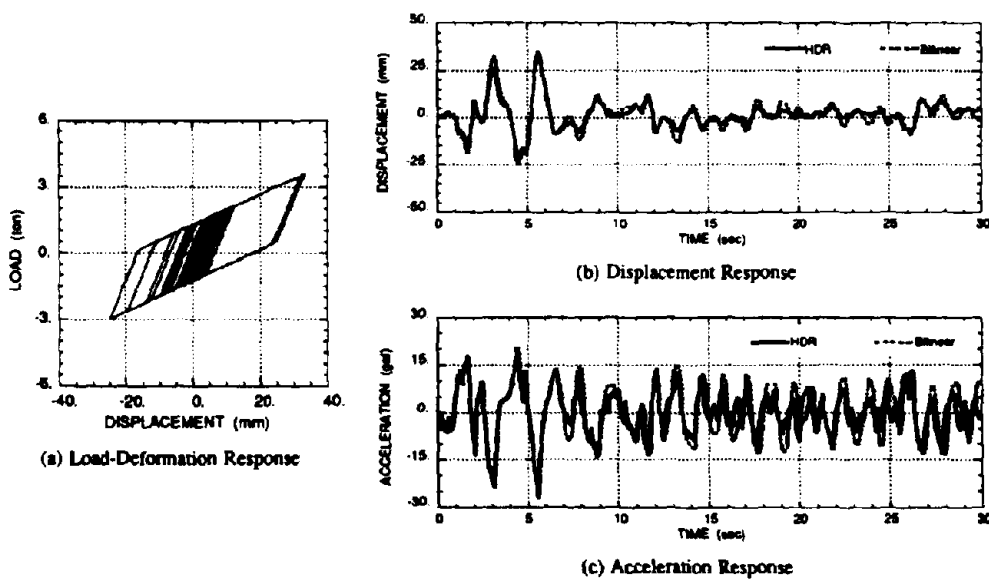


Fig. 13 Bilinear Response of HDR-A(4) under El Centro Excitation

For the Hachinohe earthquake, the earthquake record was scaled to have maximum acceleration of 0.06g (Fig. 7). Hysteretic load-deformation behavior of the isolator is shown in Fig. 14(a). Displacement and acceleration time histories are shown in Fig. 14(b) and (c).

Also shown in the same set of plots are the response of an equivalent viscously-damped linear elastic model giving the same level of maximum displacement. It can be said that the HDR-isolator system has an equivalent viscous damping ratio of 11%. Response of an approximate bilinear model is given in Figs. 15(b) and (c). Overall, good correlations are also obtained within 100% shear strain under the Hachinohe earthquake input.

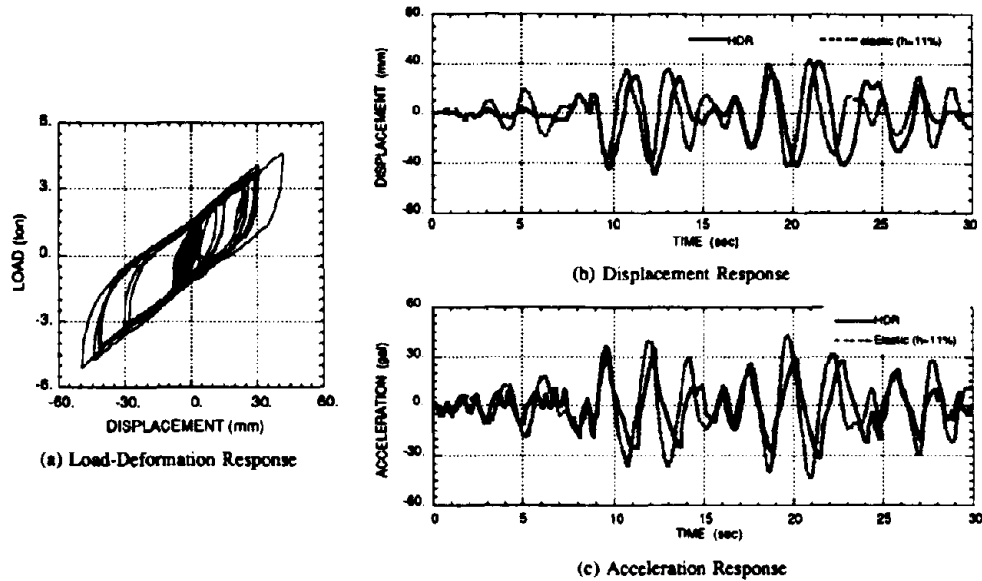


Fig. 14 Earthquake Response of HDR-A(4) under Hachinohe Excitation

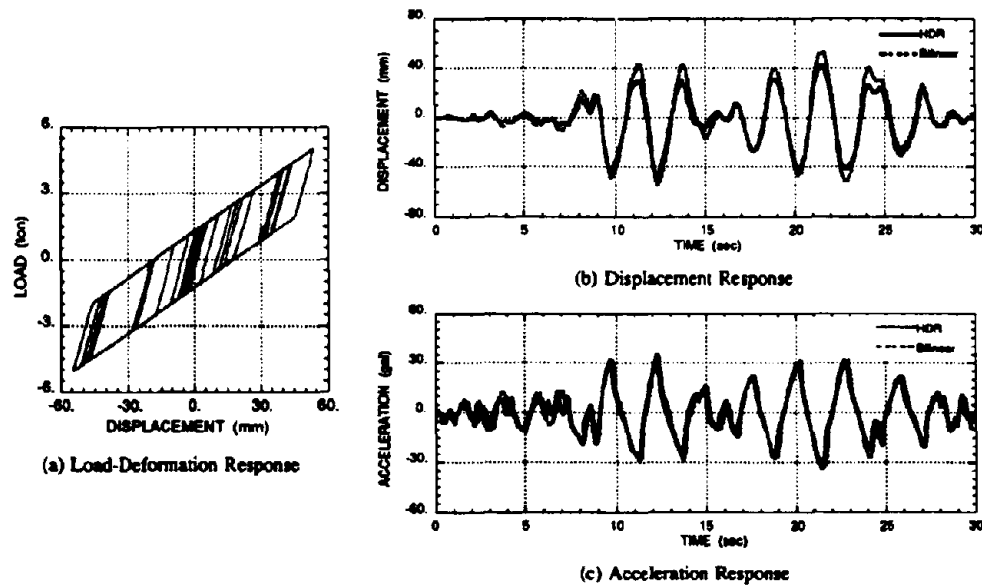


Fig. 15 Bilinear Response of HDR-A(4) under Hachinohe Excitation

On-line Hybrid Sweep Tests For this particular specimen, four resonant-response tests using frequency-swept sine input ground excitation were conducted. Taking the case of HS100, hysteresis is given by Fig. 16(a)

The displacement response is compared to the response of an equivalent viscously-damped linear elastic model giving the same level of maximum displacement as shown in Fig. 16(b). It can be said that the HDR-isolator system has an equivalent viscous damping ratio of 11%. Response of an approximate bilinear model is given in Fig. 17. Overall, good correlations are also obtained.

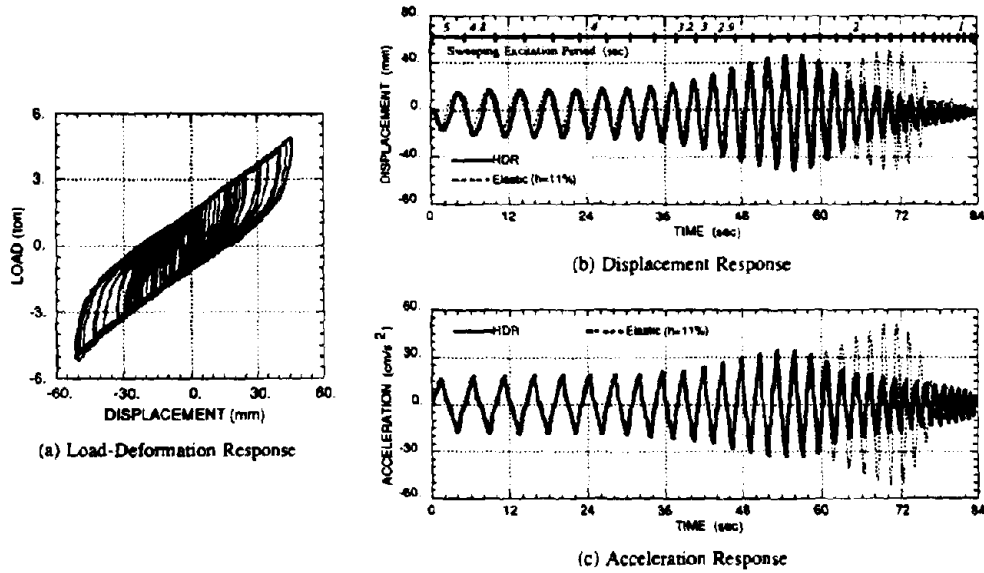


Fig. 16 Resonant Response of HDR-A(4) due to Sweeping-Sine Excitation for Shear Deformation under 100%

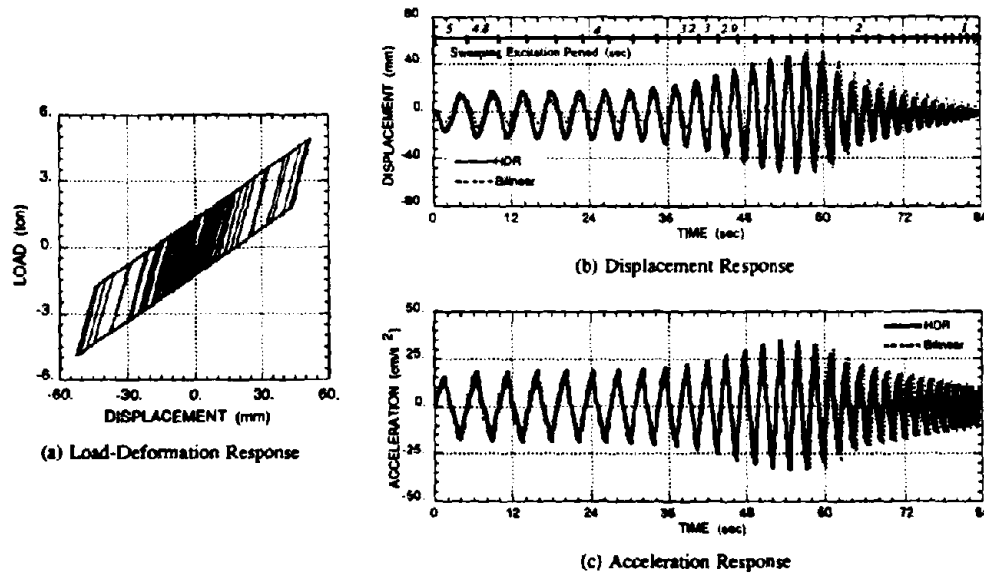


Fig. 17 Bilinear Response of HDR-A(4) due to Sweeping-Sine Excitation for Shear Deformation Under 100%

In the previous response tests, the input earthquakes were scaled such that the isolator would behave within the $\pm 100\%$ shear displacement range. Based on the comparisons of on-line hybrid response with the bilinear response, it can be stated with confidence that the isolator behavior shows ideal bilinear approximation

within the $\pm 100\%$ shear displacement range. Due to its simplicity, structural designers would prefer to have the isolators behave within this displacement range during moderate earthquakes. However, due to the possibility of the occurrence of strong earthquakes, the behavior of the isolators into the overload range (taken as $\pm 150\%$ in this case) should be properly tested and taken into consideration in the design of fail-safe devices such as stoppers or restraints.

For the purpose of establishing the response behavior of the isolator into the overload range, the maximum acceleration amplitude of the input sweeping excitation is taken at 15. gal giving maximum displacement response of about $\pm 150\%$ range. Hysteresis for the case HS150 is given by Fig. 18(a). It can be observed in the hysteresis that strain hardening is induced at about ± 60 . mm. The displacement response is compared to the response of an equivalent viscously-damped linear elastic model giving the same level of maximum displacement as shown in Fig. 18(b). It can be said that the HDR-isolator system has an equivalent viscous damping ratio of 9%.

In order to study the effect of the strain hardening on the response of an isolated system, the on-line hybrid response is compared with the bilinear response analysis. Response of an approximate bilinear model is given in Fig. 19. From the comparison, it can be observed in Fig. 19(a) that strain hardening has the effect of limiting excessive displacements during the overload range of the isolator. In addition, no significant increase in acceleration response is induced by the strain hardening effect comparing the on-line hybrid response with the bilinear response, as can be observed in Fig. 19(c).

It is important to conduct extensive testing on the isolator behavior during the overload range for the purpose of modeling if the advantage of strain hardening effect is to be tapped as a fail-safe system. Using the developed loading system under which cyclic loading tests and on-line hybrid tests for earthquake response can be conducted, mechanical properties and response behavior of isolators under large loads and displacements can be tested and observed.

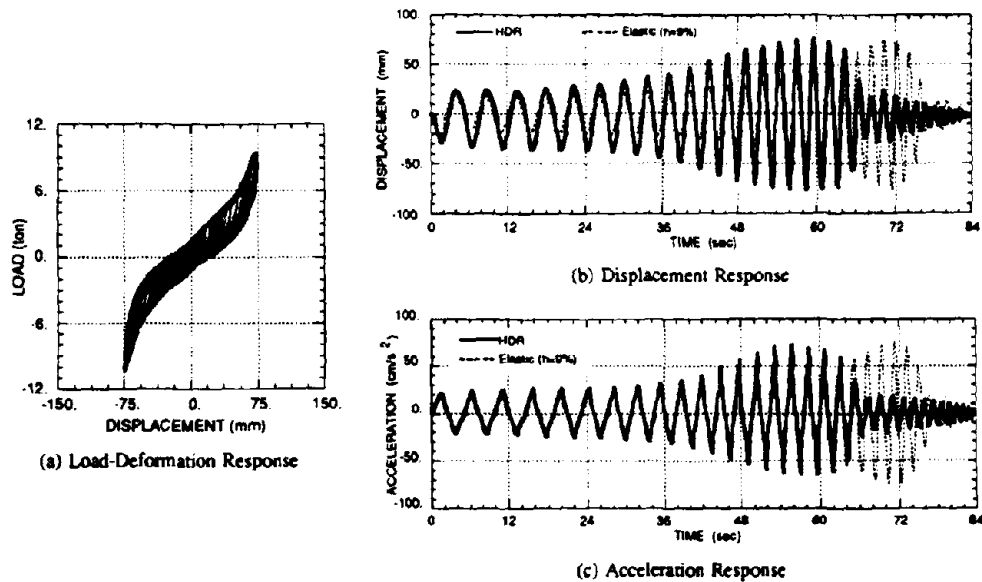


Fig. 18 Resonant Response of HDR-A(4) due to Sweeping-Sine Excitation for Shear Deformation under 150%

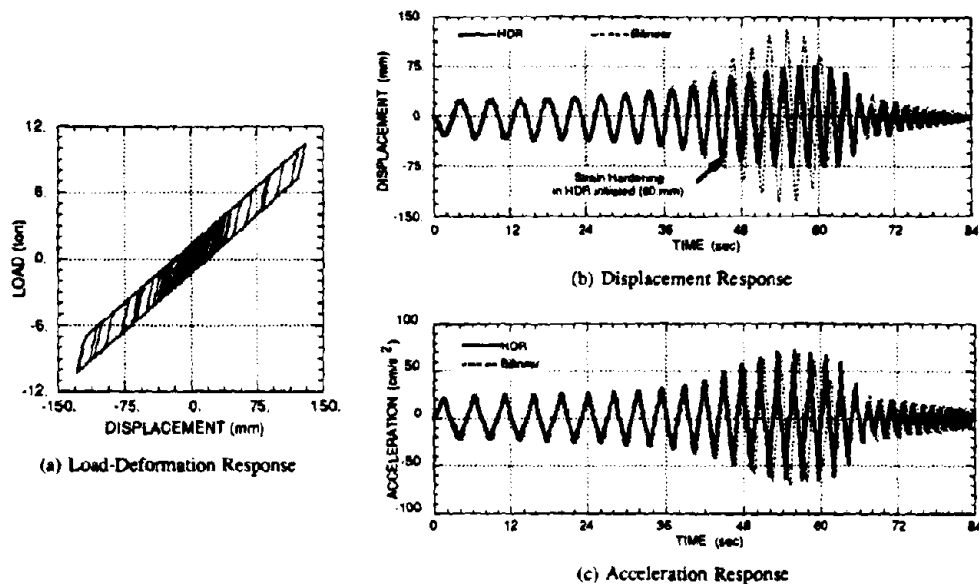


Fig. 19 Bilinear Response of HDR-A(4) due to Sweeping-Sine Excitation for Shear Deformation Under 150%

Earthquake Energy Partitioning in Seismic-Isolated System Two most essential requirements of a seismic isolator are: (1) horizontal flexibility to decouple or detune the structure from the destructive horizontal ground motions, which in effect reduces the seismic loads transferred to the superstructures; and (2) adequate energy-absorbing or damping capacity to limit excessive translational displacements due to the flexibility.

To investigate the functions of seismic isolators from the energy point of view, earthquake input energy and its partitioning in seismic-isolated structures are calculated and compared with linear elastic structures with flexibility and/or damping characteristics. Integrating the equation of motion of a simple structure from time 0 to t_0 , the following energy equation is obtained.

$$\frac{1}{2}m\dot{x}^2(t_0) + \int_0^{t_0} c\dot{x}^2(t) dt + \int_0^{t_0} f(x, t)\dot{x} dt = - \int_0^{t_0} m\ddot{z}(t)\dot{x}(t) dt \quad (3)$$

The above energy equation can be simply rewritten as

$$W_K + W_C + W_E + W_H = -E_T \quad (4)$$

where W_K : kinetic energy at $t = t_0$; W_C : viscous damping energy from $t = 0$ to t_0 ; W_E : strain energy at $t = t_0$; W_H : hysteretic absorbed energy from $t = 0$ to t ; E_T : total input earthquake energy to a structure from $t = 0$ to t_0 .

Using the above energy expressions, energy partitioning in the tested structural model with the HDR isolator subjected to the El Centro earthquake is plotted in Fig. 20(a). It is clearly observed that most of the earthquake input energy is absorbed by hysteretic behavior of the isolator. Consequently, the kinetic energy and viscous damping energy are suppressed to small values.

Similar computation of earthquake energy partitioning is done for the following three linear elastic structures: (1) a stiff lightly-damped structure ($T=0.5s$, $\xi=3\%$); (2) a flexible lightly-damped structure ($T=2.0s$, $\xi=3\%$); (3) a stiff highly-damped structure ($T=0.5s$, $\xi=15\%$). Results are given in Figs. 20(b), (c), and (d). Comparing the results, the following can be observed:

- For the flexible lightly-damped structure in Fig. 20(c), the kinetic and strain energy shows very high values resulting from high dynamic oscillation. However, the total input energy is a little lower than those of stiff systems.

- In stiff structures, the earthquake input energy is found similar for both the light damping system and the high damping system, except that large fluctuation of the kinetic energy in the former case.

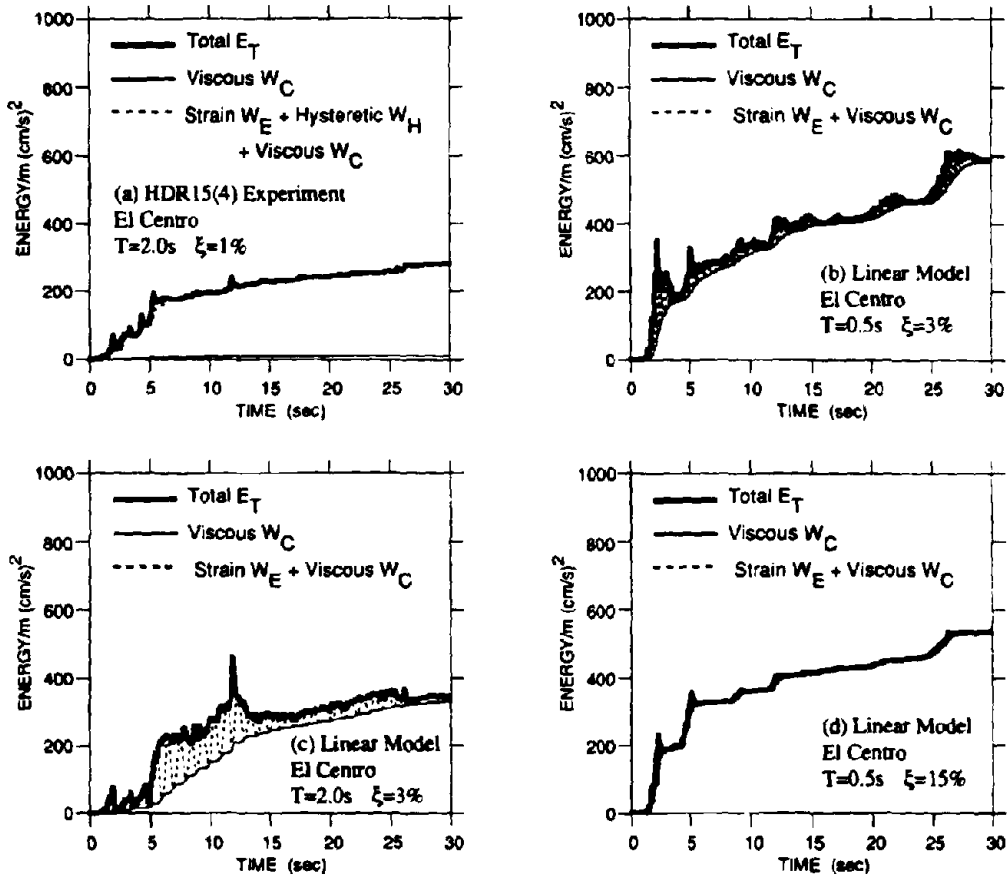


Fig. 20 Energy Partitioning in Seismic-Isolated Structure and Linear Elastic Structures Subjected to El Centro NS (1940) Earthquake

Similar computation of energy partitioning for the seismic-isolated structure and the linear elastic structures subjected to the Hachinohe NS (1968) Earthquake. Results are plotted in Fig. 21. Because of the large amount of inherent damping possessed by the HDR isolator, most of the earthquake input energy is absorbed by hysteretic damping. However, it should be well noted that the earthquake input energy is significantly increased compared to those of stiff structures. This is due to the amplification effects due to resonance of the assumed flexible structures ($T=2.0s$) with the predominant period of around 2.0s of the Hachinohe Earthquake.

Further Considerations In the tests conducted so far, the load-transfer beam of the set-up was controlled to impose lateral displacements on the installed isolator specimen without rotation. This constitute the usual boundary condition for desirable isolator performance. However, in actual situations, rotational strains might be induced due to possibility of bearing uplift. Not much studies have been done on this, although it has been noted that rotational strains have very significant influences on bearing behavior. Tests are important in order to understand this behavior and in order to devise means to prevent them. The set-up developed is capable of testing for bearing uplifts since it has been designed to impose axial, lateral, and rotational deformations on a specimen.

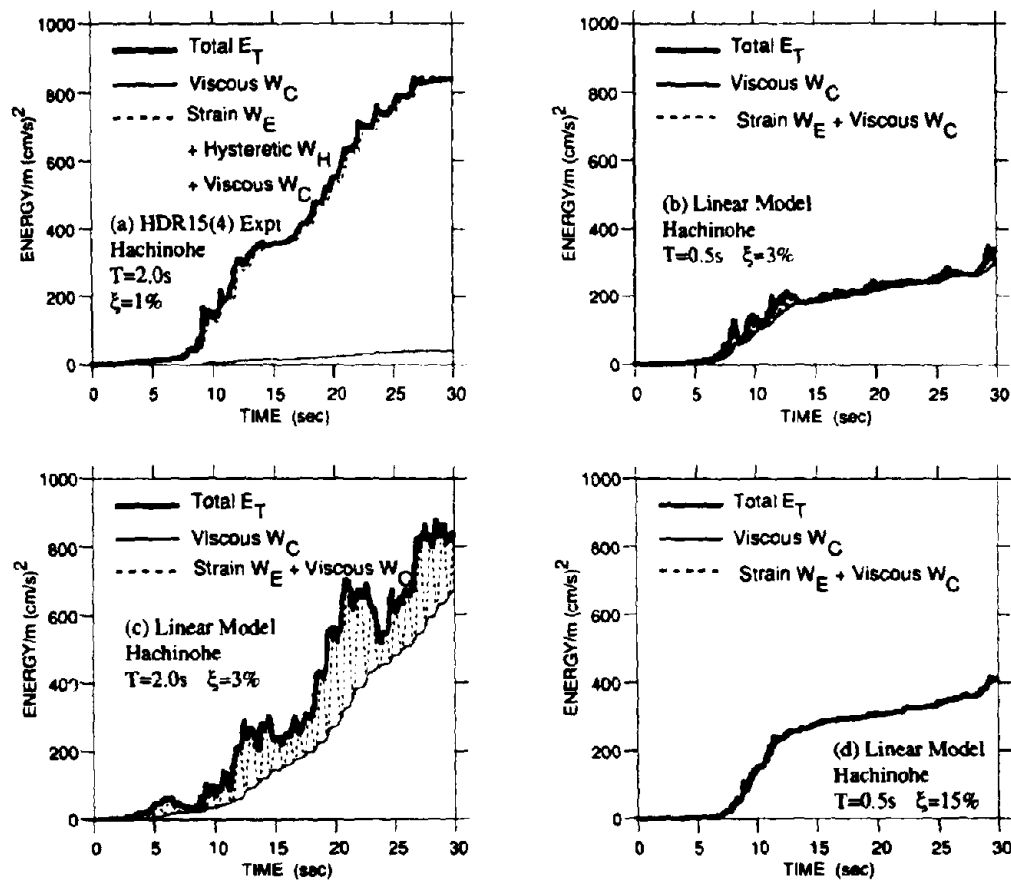


Fig. 21 Energy Partitioning in Seismic-Isolated Structure and Linear Elastic Structures Subjected to Hachinohe NS (1968) Earthquake

It has been shown that axial loads have very significant effects on lateral stiffness and damping properties. Axial loads on isolators may vary during a strong earthquake due to tendency of uplifts especially in exterior columns of frame structures and also due to pounding from vertical accelerations. Testing for this behavior would involve modeling the whole structure. A substructured on-line hybrid procedure has been developed into which the bridge superstructure and substructure are modeled analytically while the restoring force of the isolation system is directly measured from a tested specimen.

Most recently, a substructured hybrid loading system for MDOF structures with seismic isolators has been developed. In the substructured loading test, the isolator elements are taken as experimental substructures and are tested. This test provides a proof test of the effectiveness of the isolator for a specific application. After the verification tests of the HDR isolators presented above, the second phase of the test program on the HDR isolators includes substructured hybrid loading test of the isolator for inelastic earthquake response of a MDOF bridge structural model.

CONCLUSIONS

Extensive tests have been conducted on the developed high-damping rubber seismic isolator bearings to establish the mechanical properties, as well as on response characteristics during earthquakes and resonant conditions. The following conclusions can be stated:

- The new on-line hybrid loading system for earthquake response using three actuators is developed. The system is an ideal and versatile experimental system to verify earthquake behavior of seismic isolators. Most recently, the performance of a MDOF structure with seismic isolation devices can be determined and verified by the newly developed substructured hybrid loading system.
- The HDR seismic isolators were first tested with the usual cyclic loading test. It has been confirmed that the HDR isolators behave as bilinear elements without strain hardening when shear strain is below 100%. Equivalent stiffness and damping decreases with increasing strain. Also, lateral stiffness decreases but damping increases with increasing axial bearing pressure.
- HDR bearings subjected to sweeping sine input acceleration with constant amplitude were tested by the on-line hybrid system. From these tests, resonant response of a 2-sec SDOF HDR system was obtained and has been found to possess sufficient damping to suppress excessive amplification. The beneficial effect of strain hardening at the overload range of 150% shear strain is verified to have controlled excessive displacement.
- The HDR bearings were tested for earthquake response under both the El Centro Earthquake and the Hachinohe Earthquake. Under El Centro earthquake, equivalent damping of about 15% has been observed for strain below 100%, the same level obtained from static tests. However, equivalent damping of only 11% was observed when subjected to the Hachinohe earthquake which contains long-period waves. The simple procedure of using equivalent viscous damping ratio in linear elastic analysis should be used cautiously since the effectiveness of seismic isolation is very much dependent on the input earthquake ground motion.
- In addition to the displacement and acceleration response time histories, seismic effectiveness is evaluated for the tested HDR bearings in terms of energy input earthquake energy and hysteretic damping energy.

ACKNOWLEDGEMENTS

The authors would like to acknowledge the support and cooperation of the following persons and organization: Mr. Kazuyuki Izuno (research associate), Mr. Shinji Nakanishi (laboratory engineer), Mr. Nomura (graduate student) of Kyoto University, Katayama Ironworks Co., and Toyo Tire & Rubber Co.

REFERENCES

- C.J. Derham, A.G. Thomas [1980]: "The Design and Use of Rubber Bearings for Vibration Isolation and Seismic Protection of Structures," *Engineering Structures*, Vol. 2, July, 171-175.
- H. Iemura [1985]: "Development and Future Prospects of Hybrid Experiments," *Trans. Japan Society of Civil Engineers*, No. 356/1-3, 1-10, April. (in Japanese)
- M. Izumi [1988]: "State-of-the-Art Report: Base Isolation and Passive Seismic Response Control," *Proc., 9th World Conference on Earthquake Engineering*, VIII, 385-396, Tokyo-Kyoto.
- P.C. Jennings [1968]: "Equivalent Viscous Damping for Yielding Structures," *Engineering Mechanics Division, ASCE*, Vol. 94, No. EM1.
- J.M. Kelly [1986]: "Aseismic Base Isolation: Review and Bibliography," *Soil Dynamics and Earthquake Engineering*, Vol. 5, No. 3, 202-216.
- S.A. Mahin, P.B. Shing, C.R. Thewalt, R.D. Hanson [1989]: "Pseudodynamic Test Method—Current Status and Future Directions," *Journal of Structural Engineering, ASCE*, Vol. 115, No. 8, August.
- K. Takahashi, M. Nakashima [1987]: "Japanese Activities in On-line Testing," *Journal of Engineering Mechanics, ASCE*, Vol. 113, No. 7, July, 1014-1032.
- Technology Research Center for National Land Development [1989]: "Guidelines for Seismic Isolation Design of Highway Bridges," March. (in Japanese)
- Y. Yamada, H. Iemura, W. Tanzo, K. Endo [1990]: "Substructured Hybrid Loading of Structural Members Under Combined Axial, Shear, and Bending Loads," *8th Japan Earthquake Engineering Symposium*, December 12-14, Tokyo.

4. Active Control and Hybrid Systems for Bridges

Active Control for Bridge Applications: Case Studies
T.T. Soong

A Hybrid Sliding Isolation System for Bridges
Q. Feng, M. Shinozuka, S. Fujii and T. Fujita

Some Thoughts on Hybrid Control of Bridge Structures
J.N. Yang

ACTIVE CONTROL FOR BRIDGE APPLICATIONS

- CASE STUDIES -

T.T. Soong

Department of Civil Engineering
State University of New York at Buffalo
Buffalo, New York 14260

ABSTRACT

Active control research for structures against large environmental loads has received considerable attention in recent years. Large-scale laboratory experimentation and the development of full-scale active protective systems have taken place in the area of building structures. For bridge applications, however, the feasibility of using active control has been limited to studies of analytical and simulation nature. In this paper, three case studies of active bridge control are summarized in order to provide added impetus to conducting more in-depth studies of active control as a possible protective systems principle for bridges against earthquakes and other environmental loads.

INTRODUCTION AND BASIC PRINCIPLES

The possible use of active control systems as a means of structural protection against seismic loads has received considerable attention in recent years. It has now reached the stage where active systems have been installed in full-scale structures [1]. While the applications of active protective systems have so far been directed to building structures, the principle of active control is equally applicable to other types of structures. For bridge applications, several studies have been performed and it is the purpose of this paper to summarize the results of three case studies in order to stimulate further studies of active systems as possible seismic protective systems for bridges.

In terms of basic principles, an active structural control system has the basic configuration as shown schematically in Fig. 1. It consists of (a) sensors located about the structure to measure either external excitations, or structural response variables, or both; (b) devices to process the measured information and to compute necessary control forces needed based on a given control algorithm; and (c) actuators, usually powered by external energy sources, to produce the required forces. When only the structural response variables are measured, the control configuration is referred to as *closed-loop control* since the structural response is continually monitored and this information is used to make continual corrections to the applied control forces. An *open-loop control* results when the control forces are regulated only by the measured excitations. In the case where the information on both the response quantities and excitation are utilized for control design, the term *open-closed loop control* is used.

To see the effect of applying such control forces to a structure under ideal conditions, consider a structure modeled by an n -degree-of-freedom lumped mass-spring-dashpot system. The matrix equation of motion of the structural system can be written as

$$M\ddot{\mathbf{x}}(t) + C\dot{\mathbf{x}}(t) + K\mathbf{x}(t) = D\mathbf{u}(t) + E\mathbf{f}(t) \quad (1)$$

where, M , C and K are the $n \times n$ mass, damping and stiffness matrices, respectively, $\mathbf{x}(t)$ is the n -dimensional displacement vector, the r -vector $\mathbf{f}(t)$ represents the applied load or external excitation, and the m -vector \mathbf{u} is the applied control force vector. The $n \times m$ matrix D and the $n \times r$ matrix E define the locations of the control force vector and the excitation, respectively.

Suppose that the open-closed loop configuration is used in which the control force $\mathbf{u}(t)$ is designed to be a linear function of the measured displacement vector $\mathbf{x}(t)$, the velocity vector $\dot{\mathbf{x}}(t)$ and the excitation $\mathbf{f}(t)$. The control force vector takes the form

$$\mathbf{u}(t) = K_1 \mathbf{x}(t) + C_1 \dot{\mathbf{x}}(t) + E_1 \mathbf{f}(t) \quad (2)$$

where K_1 , C_1 , and E_1 are respective control gains which can be time-dependent.

The substitution of equation (2) into equation (1) yields

$$M \ddot{\mathbf{x}}(t) + (C - DC_1) \dot{\mathbf{x}}(t) + (K - DK_1) \mathbf{x}(t) = (E + DE_1) \mathbf{f}(t) \quad (3)$$

Comparing equation (3) with equation (1) in the absence of control, it is seen that the effect of open-closed loop control is to modify the structural parameters (stiffness and damping) so that it can respond more favorably to the external excitation. The effect of the open-loop component is a modification (reduction or total elimination) of the excitation.

It is seen that the concept of active control is immediately appealing and exciting. On the one hand, it is capable of modifying properties of a structure in such a way as to react to external excitations in the most favorable manner. On the other hand, direct reduction of the level of excitation transmitted to the structure is also possible through active control.

The choice of the control gain matrices K_1 , C_1 , and E_1 in equation (2) depends on the control algorithm selected. A number of control strategies for structural applications have been developed, some of which are based on the classical optimal control theory and some are proposed for meeting specific structural performance requirements. The reader is referred to [1] for discussions of some commonly used structural control algorithms.

CASE STUDIES

A number of feasibility studies using active control principles in strengthening existing bridges or in leading to more efficient designs have been carried out. In what follows, three such studies are summarized which may stimulate more in-depth studies of using active protective systems for bridges against large environmental loads.

A Cable-stayed Bridge [2,3] A cable-stayed bridge is considered in this case study where active control is used to increase its critical speed, thus enhancing its aerodynamic stability. As shown in Fig. 2, cable-stayed bridges are ideal for active control implementation since their existing suspension cables can be used as active tendons to which active feedback control systems are attached.

For the purpose of this feasibility study, the structural model is the Sitka Harbor bridge at Sitka, Alaska. Design information on this cable-stayed bridge provided in [2,3] gives the fundamental natural frequency in flexure $\omega_g = 5.083$ rad/sec, the fundamental natural frequency in rotation $\omega_f = 8.589$ rad/sec, and the critical wind speed $\bar{u}_f = 155.5$ mph (69.52 m/s). For simplicity, the critical wind speed is considered here as the performance criterion. Wind speeds higher than the critical will cause aerodynamic instability in the bridge.

It is of interest to ask whether the critical speed can be significantly increased when the existing suspension cables operate in an active mode. As a possible configuration for active tendons, the bridge cables can be connected to electrohydraulic servomechanisms located at the points of anchorage. One transducer is installed at each anchorage point to sense the motion at that point. The sensed motion, in the form of electric voltage, is used to regulate the motion of a hydraulic ram, thus generating the required control force in each cable. For this configuration, the ram displacement $s(t)$ is related to the feedback voltage $\nu(t)$ by

$$\dot{s}(t) + R_1 s(t) = \frac{R_1 \nu(t)}{R} \quad (4)$$

where R_1 = the loop gain; and R = the feedback gain of the servomechanisms. The feedback voltage $\nu(t)$ is in turn proportional to the sensed motion. Suppose that the sensed motion is the flexure velocity $\dot{w}(t)$ at the anchorage. We then have

$$\nu(t) = p\dot{w}(t) \quad (5)$$

Let the two nondimensional control parameters be defined by

$$\epsilon = \frac{R_1}{\omega_f} \quad \text{and} \quad \tau = \frac{p\omega_f^2}{R} \quad (6)$$

The critical speed \bar{u}_f for the actively controlled structure thus becomes a function of ϵ and τ ; the results are shown in Fig. 3. The case of $\epsilon = 0$ corresponds to the passive structure. It is observed that the value of \bar{u}_f increases as ϵ and τ increase, and this increase can be rather dramatic when certain values of ϵ and τ are chosen. Indeed, the critical wind speed for the actively controlled structure can be raised to any desirable level provided that the required control forces are realizable.

It is also shown that the power required for the active control system in order to increase the critical speed is quite modest [3]. Thus, the required capacity of the servomechanism is small and feasible for practical application.

A Pipeline Suspension Bridge [4] The purpose of this case study is to provide necessary flexural and torsional stiffness to the girder of a large pipeline suspension bridge, as shown in Fig. 4, by the addition of an active stay system. Structures designed to carry low working loads such as a pipeline suspension bridge must be adequately weighed or stiffened in order to withstand large dynamic loads. An active control system for the oscillations of this type of structure, and in general for very slender and light bridge structures may have the following advantages:

- eliminating, or at least reducing, the projected limitations imposed by dynamic effects,
- providing a general control system for oscillations induced by various causes: vortex shedding, buffeting, flutter, crowd action on pedestrian bridges, etc.,
- providing a control system applicable to existing structures with a minimum of intervention.

For practical application of the active control to bridge structures, it is necessary to resolve first the problem of ensuring the functioning of the control devices (if possible independently from an energy network) and of minimizing the size of the force applied. A number of control strategies were considered in this feasibility study. The system depicted in Fig. 5 was chosen as the most efficient which, however, requires the pre-stressing of the control tendons with the aim of providing the structure with both positive and negative control forces.

Figures 6(a) and 6(b) show the control results with respect to the first bending mode and the first torsional mode, respectively, together with required control forces. Two conclusions can be drawn from this study. Firstly, the peak control forces are again shown to be within practical limits. They largely depend on the strategy adopted and become most economical for early control intervention. Secondly, the energy required also depends on the time interval programmed to reduce oscillations to the prescribed values.

A Simple-span Utility Bridge [5,6] This feasibility study addresses a broader issue of optimization of an actively controlled structure. The basic question to be answered here is whether substantial changes in structural configuration can be realized by allowing some members of a structure to become active. The formulation of this problem is more complex than that outlined in Section I since the structural parameters together with control parameters must be simultaneously optimized. As shown in [5,6], a system of nonlinear equations must be solved in this case.

The utility bridge in this case study is modeled as a king-post beam as shown in Fig. 7. The two king-posts, serving as active members, are located along the beam and are capable of applying point forces directly to the beam. Sufficient pre-tensioning of the cables is assumed to allow both upward and downward control forces. A moving load of constant magnitude $P(x)$ and velocity $V(t)$ is applied to the beam.

This feasibility study is investigated through a number of different cases. Specifically, the following four cases are identified.

Case 1. Passive Structure. The only design parameter considered is the beam width b , subjected to the simple bounds: $0.10 \text{ in. (2.254 cm)} \leq b \leq 10.0 \text{ in. (25.4 cm)}$.

Case 2. Two active members (i.e., king-posts) located at $x/L = 0.30$ and 0.70 , as well as the beam width, are the design variables. The two active members are capable of generating both up and down control forces. No bounds are imposed on the magnitude of the control forces. The bounds on b are the same as in Case 1.

Case 3. Identical to Case 2 except that, along with the two active members and the width, the locations of the two active members are also considered as design variables. Hence five design variables are considered with the bounds on the active member locations of: $x/L = 0.0 \leq XL \leq 1.00$; $x/L = 0.0 \leq XR \leq 1.00$, which force the two locations, XL for the left member and XR for the right, to be along the beam.

Case 4. In this variation, the effect of allowing the two active members to change position *with time* is considered. The simple bounds are identical to those of Case 3. Note that while this is a logical extension of the active structure concept, the realization of such a "fully" active structure may be difficult.

The solution to these four cases is obtained using a simultaneous search procedure. The results for each are summarized in Table 1. The quantities listed in Table 1 are the performance index (PI), the beam width (b), the maximum centerline deflection of the beam (y_{max}), the maximum control force (u_{max}), and the active member location (XL and XR). Comparison of the centerline displacement response and required control force in the left king-post is shown in Figs. 8 and 9, respectively. Also, the moving locations of the two king-posts for Case 4 are illustrated in Figs. 10 and 11.

It is seen from Table 1 and Figs. 8 and 9 that Case 4, with a PI of 93.96, represents the optimum configuration of the king-post beam. This is expected since this case has the highest capacity to act as an active structure.

CONCLUDING REMARKS

The case studies presented above are intended to demonstrate the possible use of active systems for bridge protection against large environmental loads or for more efficient structural design. Certain types of bridges, particularly suspension bridges, are shown to be good candidates for active control implementation since existing structural members can be augmented to provide active control capabilities.

As mentioned in Section I, considerable progress in terms of full-scale active control system development has been made in the area of building structures. It is hoped that these successes together with encouraging results obtained in these case studies will provide added impetus to conducting more indepth studies of active control for bridge applications.

REFERENCES

1. Soong, T.T., *Active Structural Control, Theory and Practice*, Logman, London, and Wiley, New York, 1990.
2. Yang, J.N. and Giannopoulos, F., "Active Control and Stability of Cable-stayed Bridge," *ASCE J. Eng. Mech. Div.*, 105, 677-694, 1979.
3. Yang, J.N. and Giannopoulos, F., "Active Control of Two-stayed-cable Bridge," *ASCE J. Eng. Mech. Div.*, 105, 795-810, 1979.
4. Carotti, A., DeMiranda, M. and Turci, E., "An Active Protective System for Wind Induced Vibrations of Pipeline Suspension Bridges," in *Structural Control*, H.H.E. Leipholz (ed.), Martinus Nijhoff, Amsterdam, 76-104, 1987.
5. Soong, T.T. and Manolis, G.D., "Active Structures," *ASCE J. Struct. Eng.*, 113, 2290-2301, 1987.
6. Cha, J.Z., Pitarresi, J.M. and Soong, T.T., "Optimal Design Procedures for Active Structures," *ASCE J. Struct. Eng.*, 114, 2710-2723, 1988.

A HYBRID SLIDING ISOLATION SYSTEM FOR BRIDGES

Qing Feng

Department of Civil Engineering and Operations Research
Princeton University
Princeton, NJ 08544, USA

Masanobu Shinozuka *

National Center for Earthquake Engineering Research
State University of New York at Buffalo
Buffalo, NY 14260, USA

Shunji Fujii

Technology Development Department
Taisei Corporation
1-25-1 Nishi-Shinjuku, Shinjuku-ku, Tokyo, Japan

Takafumi Fujita

Institute of Industrial Science
University of Tokyo
7-22-1 Roppongi, Minato-ku, Tokyo, Japan

Abstract

This study deals with a hybrid isolation system using friction controllable sliding bearings [1]. During earthquakes, this isolation system controls the friction force on the sliding interface between the structure and the ground to confine the sliding displacement within an acceptable range, while keeping the transfer of seismic force to a minimum. This is the advantage of the hybrid sliding isolation system that can not be duplicated by the passive sliding system. Instantaneous optimal control and bang-bang control algorithms are developed for controlling the friction force. Shaking table tests are performed using a bridge model equipped with such a hybrid isolation system. Computer simulations show good agreement with the experimental results, demonstrating the effectiveness of the hybrid sliding control system and the feasibility of its applications for bridges.

*On leave from Princeton University

1 Introduction

The sliding isolation system is beginning to find its applications in civil engineering structures having the advantage that its isolation performance is not influenced by the frequency content of ground excitation. The sliding isolation system, however, has some limitations in its capability; It is not necessarily efficient for small to medium earthquakes, and tends to suffer from a large sliding displacement during large earthquakes.

The objective of this research then is (1) to physically develop a hybrid isolation system using friction controllable sliding bearings, and (2) to experimentally demonstrate that such a hybrid isolation system can indeed control the friction force on the interface between the structure and the ground to confine the sliding displacement in an acceptable range, and at the same time, to minimize the transfer of seismic force to the structure.

Instantaneous optimal control and bang-bang control algorithms are developed for controlling such an isolation system. These algorithms are relatively simple and yet robust for on-line control operations, and they effectively achieve the objective mentioned above.

A model bridge structure equipped with the sliding isolation system is constructed, and shaking table tests are conducted under earthquakes of various intensities. Both experimental and analytical studies demonstrate the advantage of the proposed hybrid isolation system.

2 Hybrid Isolation System

The hybrid isolation system using friction controllable bearings is conceptually depicted in Fig. 1, where a bridge structure is shown to be resting on the bearings. Each bearing has a fluid chamber which is connected to a pressure control system composed of a computer, a servo amplifier, a servo valve and a pump. The friction on the interface between the bearing and the ground is controlled by adjusting the fluid pressure in the chamber. The control of the fluid pressure is based on the observed structural response such as acceleration and sliding displacement. As shown in the section view in Fig. 2, the bearing is of disk shape with the fluid chamber inside which is sealed by an O-ring around the circular perimeter just inside the sliding interface.

3 Control Algorithms

3.1 Analytical Model

The motion of a girder bridge in its axial direction is considered for analysis and experiment. The friction controllable bearings are installed between the girder and piers. Considering the piers to be rigid, the bridge can be modeled as a rigid mass with a single degree of freedom as shown in Fig. 3. The equations of motion of the bridge in the longitudinal direction under earthquake excitation can then be written as follows.

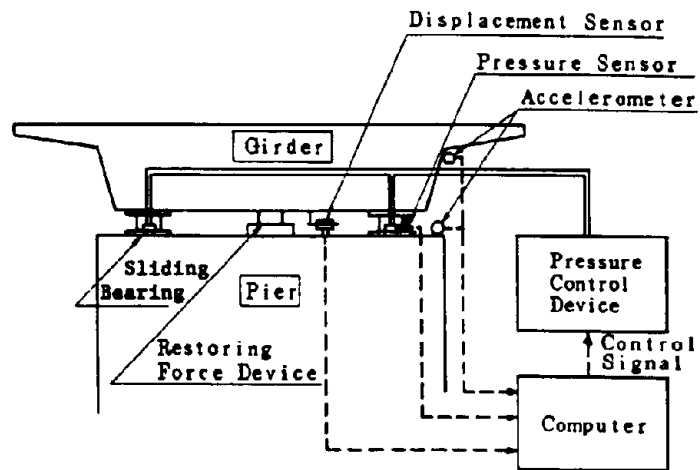


Figure 1: System Concept

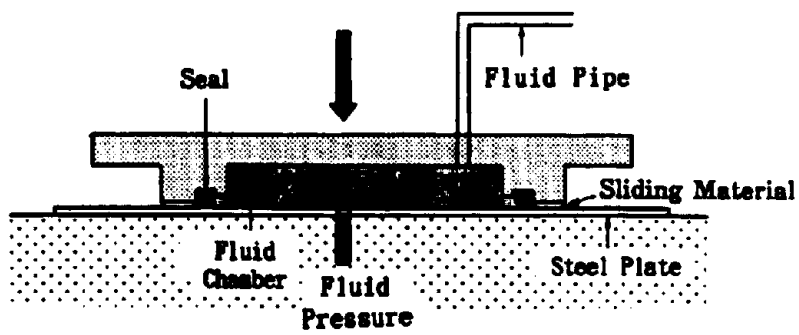


Figure 2: Friction Controllable Sliding Bearing

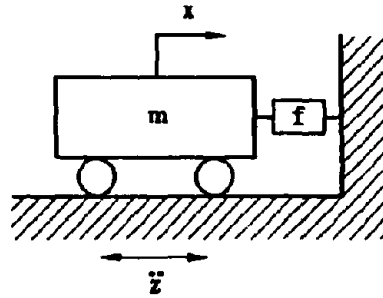


Figure 3: Analytical Model

1. Sticking — Phase I

$$\dot{x} = 0, \quad x = \text{const.} \quad (1)$$

2. Sliding — Phase II

$$\ddot{x} = -\ddot{z} - f \operatorname{sgn}(\dot{x}), \quad f = \mu_k g \quad (2)$$

3. Changing Condition (Phase I → Phase II)

$$|\ddot{z}| > \mu_s g \quad (3)$$

4. Changing Condition (Phase II → Phase I)

$$\dot{x} = 0, \quad |\dot{x} + \ddot{z}| \leq \mu_s g \quad (4)$$

where

- x : sliding displacement of mass relative to ground
- \ddot{z} : input earthquake acceleration
- μ_s : static coefficient of friction
- μ_k : kinetic coefficient of friction

The dynamic characteristics of the pressure control system is assumed to follow the first order time delay model:

$$T\dot{p} + p = u \quad (5)$$

where

- p : pressure in bearing chamber
- u : pressure control signal
- T : time constant

The relationship between the pressure p in the fluid chamber and the friction force f on the sliding interface is idealized by a linear equation:

$$f = -c_1 p + c_2 \quad (6)$$

where c_1 and c_2 are constants.

3.2 Bang-Bang Control

Bang-bang control approach provides a simple and yet often effective algorithm. The particular algorithm used in this study facilitates the following control: When the sliding displacement and velocity of the mass are in the same direction, the pressure control signal $u(t)$ will be decreased to a minimum value u_{min} to increase the friction force. On the other hand, when the sliding displacement and velocity are in the opposite direction, the pressure control signal will be increased to a maximum value u_{max} to decrease the friction force.

$$u(t) = \begin{cases} u_{min}, & \text{if } \text{sgn}(x) = \text{sgn}(\dot{x}) \\ u_{max}, & \text{if } \text{sgn}(x) = -\text{sgn}(\dot{x}) \end{cases}$$

in which u_{min} is set at a level of maximum response acceleration that can be tolerated by the bridge girder and u_{max} is limited by the maximum chamber pressure corresponding to the lifting force equal to the girder weight.

3.3 Instantaneous Optimal Control

The optimal pressure control signal $u(t)$ is determined by minimizing the following time dependent objective function $J(t)$ at every time instant t for the entire duration of an earthquake [2].

$$J(t) = \alpha x^2(t) + \beta f^2(t) + \gamma u^2(t) \quad (7)$$

in which, the friction force f also represents the response acceleration, and α , β and γ indicate the relative importance, in the control objective, of the sliding displacement, response acceleration and pressure control signal, respectively. Assuming that the system motion is always in Phase II (Eq. 2), numerical solutions for Eqs. 2, 5 and 6 are obtained on the basis of the linear acceleration method, and are used as constraints when minimizing the objective function $J(t)$;

$$x(t) = a f(t) \text{sgn}(\dot{x}(t)) + b \ddot{z}(t) + d_1 (t - \Delta t) \quad (8)$$

$$f(t) = -c u(t) + d_2(t - \Delta t) \quad (9)$$

where

$$a = b = -\frac{\Delta t^2}{6}, \quad c = \frac{c_1 \Delta t}{2T + \Delta t} \quad (10)$$

$$d_1(t - \Delta t) = x(t - \Delta t) + \dot{x}(t - \Delta t)\Delta t + \frac{1}{3} \ddot{x}(t - \Delta t) \Delta t^2 \quad (11)$$

$$d_2(t - \Delta t) = \frac{2T}{2T + \Delta t} \left(\frac{c_2 \Delta t}{2T} + f(t - \Delta t) + \frac{1}{2} \dot{f}(t - \Delta t)\Delta t \right) \quad (12)$$

Thus, the generalized objective function is established by introducing Lagrangian multipliers λ_1 and λ_2 :

$$\begin{aligned} H(t) = & \alpha x^2(t) + \beta f^2(t) + \gamma u^2(t) \\ & + \lambda_1 [x(t) - a f(t) \text{sgn}(\dot{x}(t)) - b \ddot{z}(t) - d_1 (t - \Delta t)] \\ & + \lambda_2 [f(t) + c u(t) - d_2 (t - \Delta t)] \end{aligned} \quad (13)$$

The necessary conditions for minimizing the objective function $J(t)$ are:

$$\frac{\partial H}{\partial x} = 0, \quad \frac{\partial H}{\partial f} = 0, \quad \frac{\partial H}{\partial u} = 0, \quad \frac{\partial H}{\partial \lambda_1} = 0, \quad \frac{\partial H}{\partial \lambda_2} = 0, \quad (14)$$

Substituting Eq. 13 into Eq. 14 yields the optimal pressure control signal:

$$u(t) = A_1 f(t) + B_1 x \operatorname{sgn}(\dot{x}(t)) \quad (15)$$

where

$$A_1 = \frac{c \beta}{\gamma}, \quad B_1 = \frac{c a \alpha}{\gamma} \quad (16)$$

In the development of the optimal control algorithm shown above, the time delay of control device shown in Eq. 5 is incorporated. In this case, the control is referred to as "instantaneous optimal control with time delay".

If the response of the control device is so fast that the time delay can be ignored, the relationship between the pressure and the control signal is given by:

$$p(t) = u(t) \quad (17)$$

The control algorithm is also developed for this case, in which, the objective function and Hamiltonian become respectively:

$$J(t) = \alpha x^2(t) + \beta f^2(t) + \gamma u^2(t) \quad (18)$$

and

$$\begin{aligned} H(t) = & \alpha x^2(t) + \beta f^2(t) + \gamma u^2(t) \\ & + \lambda_1 [x(t) - a f(t) \operatorname{sgn}(\dot{x}(t)) - b \bar{z}(t) - d_1 (t - \Delta t)] \\ & + \lambda_2 [f(t) + c_1 u(t) - c_2] \end{aligned} \quad (19)$$

The control based on Eq. 19 is referred to as "instantaneous optimal control without time delay". By letting the following partial derivatives equal to zero,

$$\frac{\partial H}{\partial x} = 0, \quad \frac{\partial H}{\partial f} = 0, \quad \frac{\partial H}{\partial u} = 0, \quad \frac{\partial H}{\partial \lambda_1} = 0, \quad \frac{\partial H}{\partial \lambda_2} = 0, \quad (20)$$

the optimal control signal is obtained as:

$$u(t) = A_2 + B_2 x \operatorname{sgn}(\dot{x}(t)) \quad (21)$$

where

$$A_2 = \frac{c_1 c_2 \beta}{\gamma + \beta c_1^2}, \quad B_2 = \frac{c_1 a \alpha}{\gamma + \beta c_1^2} \quad (22)$$



Figure 4: Structure Model with Isolation Devices

4 Experimental and Analytical Studies

In order to examine the performance of the proposed hybrid isolation system and the feasibility of its applications to the bridges, computer simulations and experiments are performed. For this purpose, a pilot hybrid isolation system with friction controllable bearings has been developed. Installing the system to a bridge model, shaking table tests are carried out at Taisei Technology Research Center in Yokohama, Japan.

4.1 Experimental Devices

Figs. 4 and 5 show the experimental devices. The model representing a rigid bridge girder consists of a steel frame and a number of steel weights. The total weight of the model is 12 tonf. The model is supported equally by four friction controllable bearings. The sliding surface of the bearing is a brass sheet of 1 mm thick, and a rubber O-ring of 5.7 mm in diameter is used as a seal. The sliding plate fixed on the shaking table is made of stainless steel and has a sliding area of 50 cm \times 50 cm. A servo valve is connected to the fluid chamber of each bearing to adjust the fluid flow to and from the chamber.

Sensors are placed to measure (1) accelerations on the shaking table and on the structural model, (2) relative displacement between the table and the model, and (3) fluid pressure at each bearing chamber.

A schematic of the control system is shown in Fig. 6. The controller is a 16 bit microcomputer (80286) with a numerical co-processor (80287) to facilitate faster computation. The response signals measured by the sensors are sent to the microcomputer through 12 bit A/D converters. Then the control signal is calculated according to one of the feedback control algorithms mentioned earlier, and sent to the servo valve through a 12 bit D/A converter and servo amplifier. The sampling

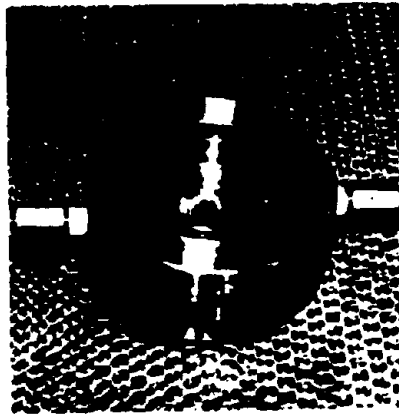


Figure 5: Friction Controllable Bearing

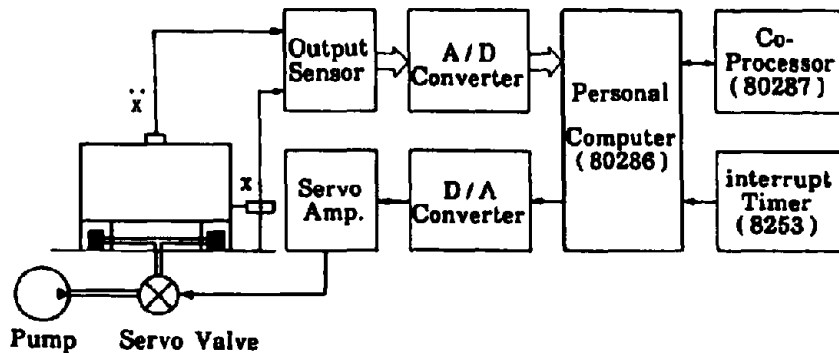


Figure 6: Control System

interval of measurement is 0.002 sec and that of control is 0.004 sec. The control program is written with C language.

4.2 Identification Experiments

The dynamic characteristics of the pressure control system is identified by using (i) step signals and (ii) sinusoidal signals of various frequencies as inputs to the servo valve and then measuring the response pressure in the bearing. It is found that the first order time delay model (Eq. 5) fits the experimental results reasonable well. The value of the time constant T is given in Table 1, in which T_i is the time constant to be used when the pressure is increasing, and T_d is the time constant when the pressure is decreasing.

The relationship between pressure and friction is identified by passive isolation experiments. For this purpose, the El Centro (NS, 1940) record is used as ground motion, and the pressure is

Table 1: Identified Parameters

T_i	20 ms	c_1	$2.5 \text{ cm}^3/(\text{s}^2\text{kgf})$
T_d	40 ms	c_2	135.1 cm/s^2
k	0.3 cm/s	δ	400.0 s/m

kept at a certain value. It is observed that the assumed model shown in Eq. 6 is not really good enough to describe the experimental results. Indeed, the friction force depends not only on the pressure in the bearings but also on the sliding velocity of the mass. Based on the experimental result, the analytical model for the friction is modified as follows:

$$f = (-c_1 p + c_2) \frac{k^2}{\dot{x}^2 + k^2} \quad (24)$$

Where the values of the parameters involved are given in Table 1.

4.3 Computer Simulation

The analytical model shown in Eqs. 1-5 and 24 is used to simulate the response of the physical bridge model isolated passively and with the hybrid device. However, the discontinuous function $\text{sgn}(\dot{x})$ in Eq. 2 is replaced by

$$\text{sgn}(\dot{x}) \doteq \frac{1 - e^{-\delta \dot{x}}}{1 + e^{-\delta \dot{x}}}, \quad \delta \gg 1, \quad (25)$$

which is found to be a reasonable approximation of the actual behavior. The parameter value of δ used in the simulation is shown in Table 1. Also, in the simulation, the kinetic coefficient of friction μ_k is assumed to be equal to the dynamic coefficient of friction μ_d , and the time interval used for numerical intergration is 0.002 sec. The computer simulation demonstrates the effectiveness of the hybrid isolation system, and will be elaborated later.

4.4 Isolation Experiments

The following experiments are performed on the shaking table. The El Centro (NS, 1940) record is used as input earthquake. Its peak acceleration, however, is linearly adjusted to 100, 200, 300 and 400 gal, respectively.

1. Passive isolation

The pressure control signal is kept to a certain value for each shaking table test (at 10, 20, 30, 40 and 45 kgf/cm^2).

2. Hybrid isolation using bang-bang control

The pressure control signal is switched between the following two values: $u_{max} = 45 \text{ kgf/cm}^2$, $u_{min} = 10 \text{ kgf/cm}^2$.

3. Hybrid isolation using instantaneous optimal control

3a. algorithm with time delay

3b. algorithm without time delay

In case 3a, both response acceleration and sliding displacement are used for the feedbacked purpose, while in case 3b only sliding displacement is used for the same purpose. The pressure control signal is bounded by $u_{max} = 45 \text{ kgf/cm}^2$, and $u_{min} = 10 \text{ kgf/cm}^2$ for both cases.

Other earthquakes such as Hachinohe, Akita and Taft are also used for shaking table tests although the results are not shown here.

4.5 Experimental and Analytical Results

Fig. 7 shows the maximum response acceleration, maximum sliding displacement and the residual displacement of the model with passive or hybrid isolation system under different intensities of input seismic motion. Hybrid isolation results shown in this figure used instantaneous optimal control algorithm without time delay. It is evident that the hybrid isolation system performs better than the passive system in the sense that a reduction of response acceleration has been achieved for small to medium seismic inputs, and at the same time, the maximum values of sliding displacement and residual displacement have been reduced considerably.

Some examples of time histories from experiments and computer simulations are shown in Figs. 8, 9 10 and 11. These example time histories show remarkably high degrees of agreement between experiments and simulation results. Fig. 8 is the passive isolation result, in which the pressure in the bearing is kept at 30 kgf/cm^2 with the corresponding values of friction force, $f = \mu_d g = 60.1 \text{ cm/s}^2$. Fig. 9 illustrates the response under bang-bang control. Figures. 10 and 11 respectively depict the responses under instantaneous optimal control with and without time delay. The feedback gains in the former case are $A_1 = 1.0 \text{ kgf s}^2/\text{cm}^3$ and $B_1 = -45.0 \text{ kgf/cm}^3$, and in the later case, $B_2 = -16.4 \text{ kgf/cm}^3$.

The response is numerically simulated always taking into consideration the following factors that involve some modelling and parameter uncertainties: (i) time delay, (ii) influence of sliding velocity on the friction force and (iii) continuous and hence more realistic approximation (Eq. 25) for $\text{sgn}(\dot{x})$. In this respect, it is important to observe that (i) the optimal control algorithms with and without time delay taken into account show little difference in the isolation performance, (ii) the optimal control algorithms are developed under the assumption that the friction force is a linear function of the chamber pressure only, again without adversely affecting the isolation performance and (iii) the continuous approximation used for $\text{sgn}(\dot{x})$ has made it easier to carry out the numerical simulation, and, in spite of its rather arbitrary nature, has resulted in the simulated response in good agreement with the experimental result. These observations clearly indicate that the system is robust particularly with respect to the three critical factors which could otherwise become problematic.

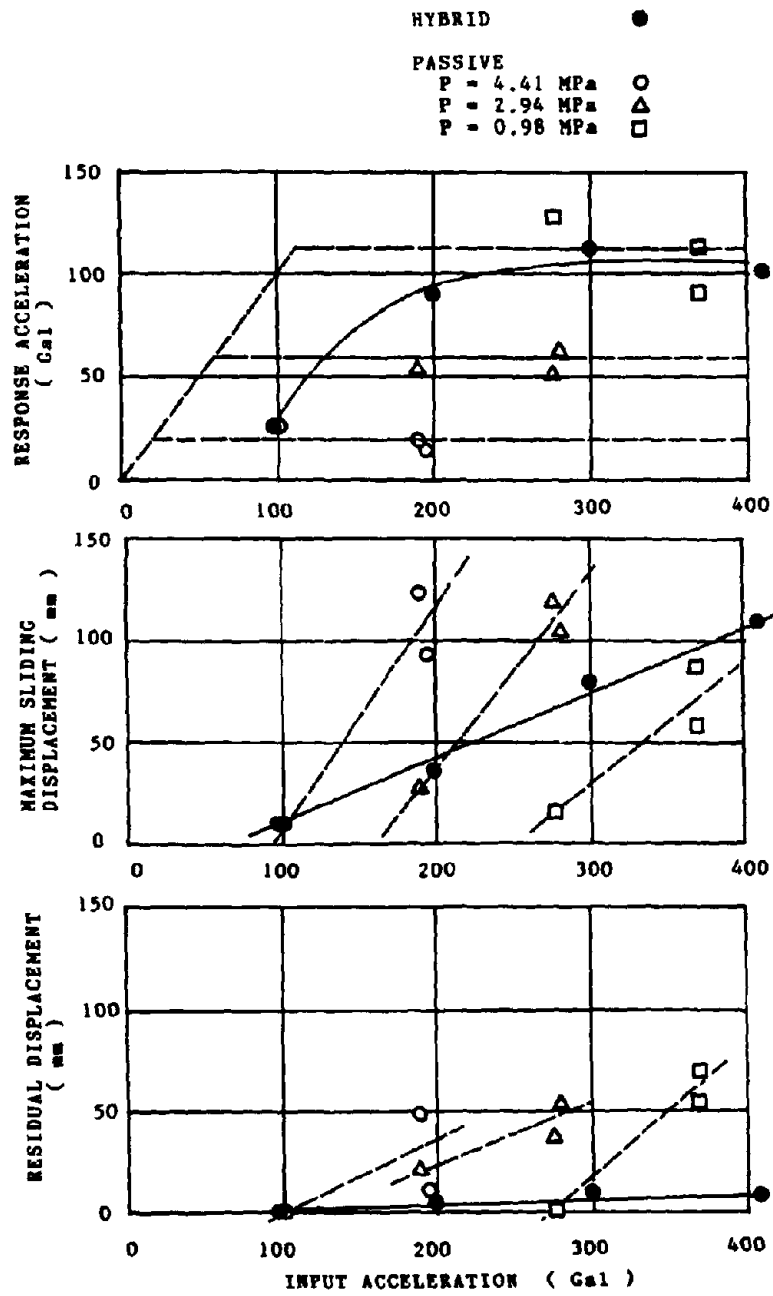


Figure 7: Comparison of Passive and Hybrid Isolation

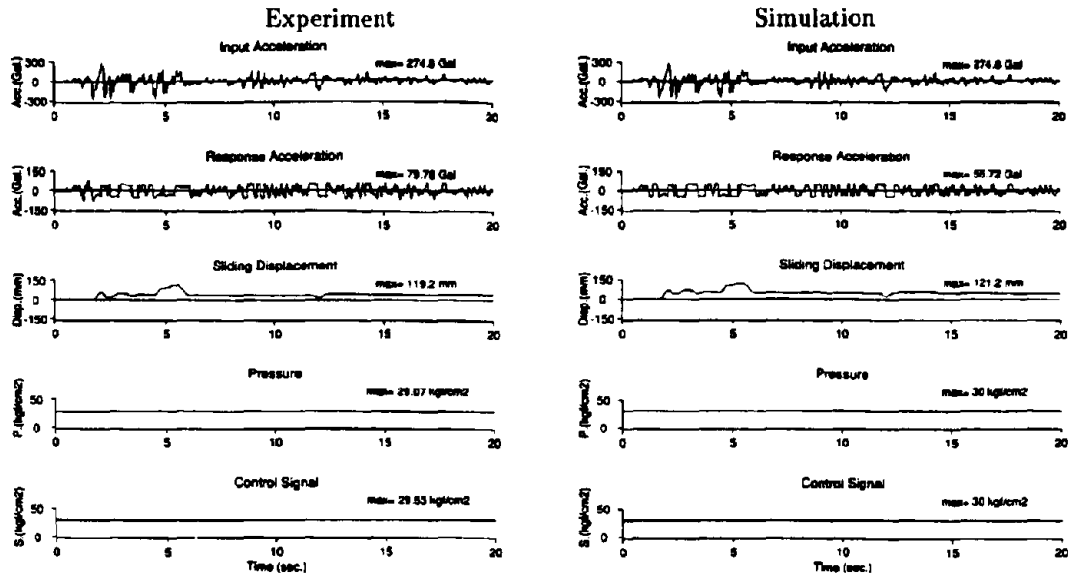


Figure 8: Passive Isolation

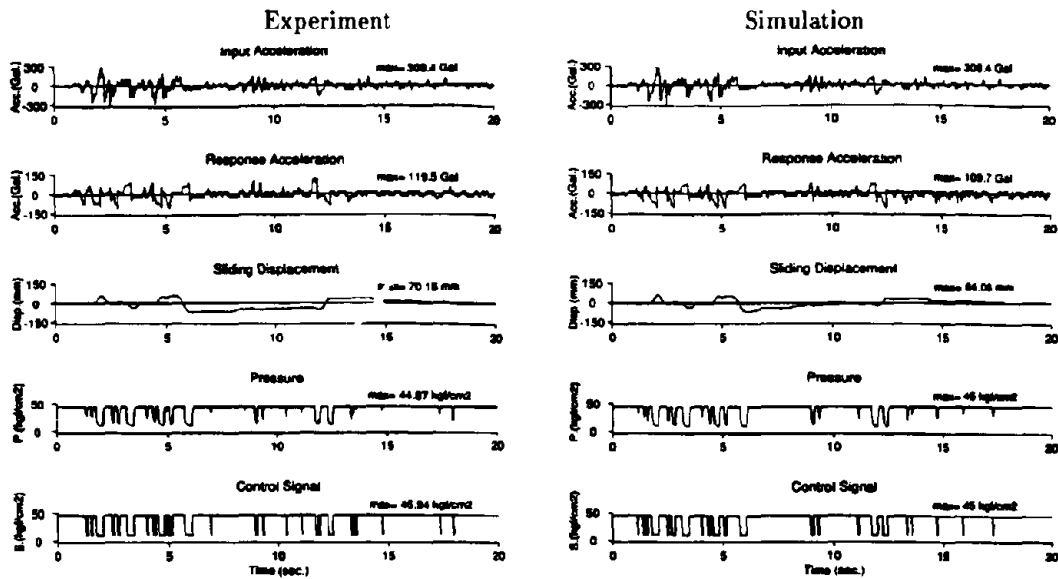


Figure 9: Hybrid Isolation under Bang-Bang Control

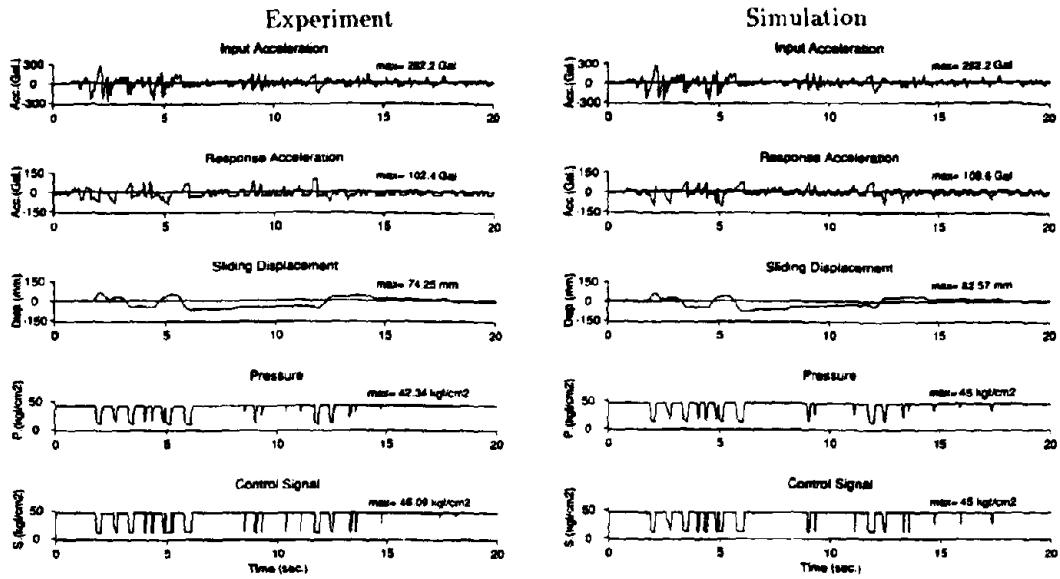


Figure 10: Hybrid Isolation under Optimal Control without Time Delay

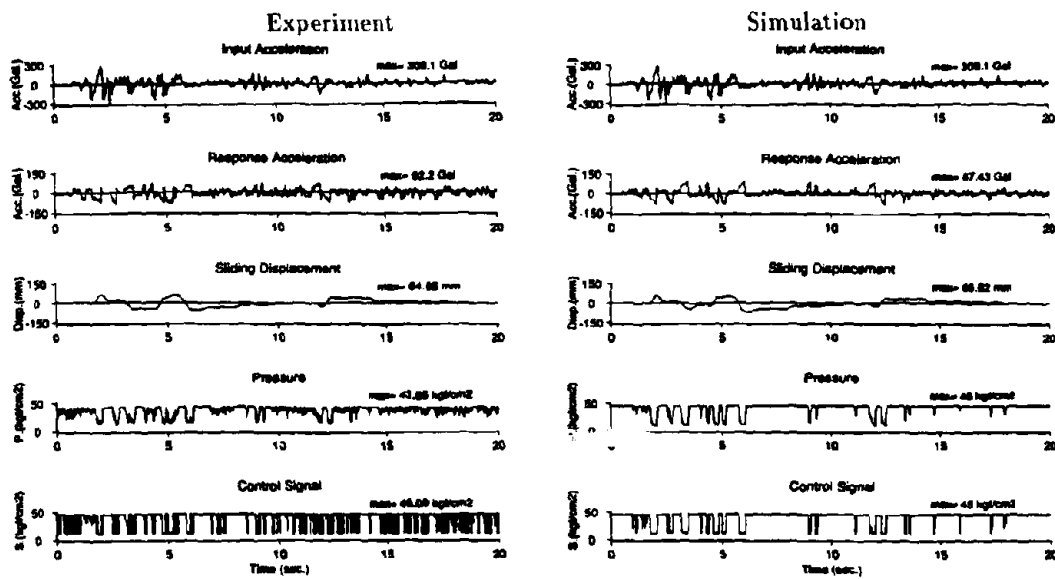


Figure 11: Hybrid Isolation under Optimal Control with Time delay

5 Concluding Remarks

The following conclusions are obtained from the experimental and analytical studies.

1. Significantly beneficial effects of the hybrid control on the reduction of the sliding displacement, residual displacement as well as of the transfer of seismic force, have been verified.
2. The hybrid isolation system using the friction controllable bearings appears to be quite robust in the face of uncertainty involved in various aspects of the control model.
3. Experimental results have good agreement with computer simulations, implying that the analytical model used represents the actual system very well.

In the immediate future, possible implementation of the hybrid sliding isolation system to existing full-size structures such as simple span girder bridges will be explored.

6 ACKNOWLEDGEMENT

This work was supported partially by Taisei Corporation, Tokyo, Japan and partially by the National Center for Earthquake Engineering Research under Grant Number NCEER 90-2204.

References

- [1] Feng, Q., Fujii, S., Shinozuka, M., and Fujita, T., "Hybrid isolation system using friction-controllable sliding bearings," *Eighth VPI&SU Symposium on Dynamics and Large Structures*, Blacksburg, VA, May 6-8, 1991.
- [2] Yang, J.N., et al., "Optimal control of nonlinear flexible structure," *Technical Report NCEER-88-0002*, 1988.

SOME THOUGHTS ON HYBRID CONTROL OF BRIDGE STRUCTURES

Jann N. YANG¹

¹ Department of Civil Engineering, University of California, Irvine, CA 92717, USA

SUMMARY

Investigations on the application of active control systems to long-span bridges subjected to strong earthquakes have been made recently. The results indicate that the application of an active control system alone may not be practical, because the requirements for the stroke of the actuator and for the external energy supply may be excessive. This paper presents some results of the preliminary study for the applications of two types of aseismic hybrid control systems to bridge structures. These include a combined use of rubber bearings and either actuators or active mass dampers. Hybrid control usually involves active control of nonlinear or hysteretic systems. The instantaneous optimal algorithm recently developed for applications to control of nonlinear and hysteretic systems is used in this study. Numerical simulation results demonstrate that performance of the hybrid control systems investigated is quite satisfactory and that the hybrid control systems may be practical for applications to long-span bridges.

INTRODUCTION

Active control of civil engineering structures has progressed to the stage where full-scale implementations are currently underway, in particular for building structures subjected to seismic loads. State-of-the-art reviews in this field have been available [e.g., 1-6]. Early investigations for possible applications of active control systems to long-span bridges subjected to strong wind turbulences can be found, for instance, in Refs. 7-10. Studies for the possible applications of active control to long-span bridges under strong earthquakes were conducted recently by Kawashima et al [e.g., 11-13]. It was found in Refs. 11-12 that the applications of an active control system alone to long-span bridges subjected to strong earthquake ground motions may not be practical, because of excessive external energy requirements and the excessive displacement (stroke) for the actuator.

The passive base isolation systems, such as rubber bearings, are capable of reducing the horizontal seismic force transmitted to the superstructure by lowering the fundamental natural frequency of the bridge [e.g., 14-20]. However, there are limitations for the passive isolation systems for bridge applications: (i) the fundamental natural frequency of the base isolated bridge cannot vary to respond favorably to different types of earthquakes with different intensities and frequency contents, (ii) the fundamental natural frequency cannot be too low, otherwise the relative displacement of the rubber bearings may be too large to satisfy the design requirements, and (iii) when bridges are on a relatively soft ground, the effectiveness of the rubber bearings is limited.

On the other hand, the active control systems are capable of varying both the fundamental natural frequency and the damping coefficient of the structure at every time instant in order to respond favorably to different types of earthquakes, such as strong or weak earthquakes with different frequency contents. The active control systems are independent of the ground (or foundation) condition and are adaptive to external ground excitations. However, when the active control system is used alone as a primary aseismic protective system, the required active control power (or energy) provided by external sources or the required actuator stroke may be excessive as demonstrated by Kawashima et al [11,13]. Likewise, unlike the building structures, there are serious physical limitations for the installation and maintenance of a large active control system on bridges.

Since passive base isolation systems have been used for bridge structures [e.g., 14-20], it is suggested and demonstrated by Kawashima et al [11, 13] that a combined use of active and passive control systems, referred to as the hybrid control system, is beneficial and practical for control of bridge structures under seismic loads. A combination of variable viscous dampers and rubber-bearing isolators was demonstrated to be quite effective [13].

Another type of hybrid control systems for bridge structures was investigated in Refs. 21-25 in which a variable frictional-type sliding isolation system was developed. In this system, the weight of the superstructure can be regulated (or lifted) actively by the oil pressure. This is equivalent to an actively controlled frictional-type sliding system in which the frictional force or the coefficient of friction can be controlled actively. Preliminary experimental and simulation results indicate that such a hybrid control system is effective for seismic-excited bridge structures [21-25].

Various types of hybrid control systems have also been shown, theoretically, to be effective for seismic-excited building structures [e.g., 26-33]. These include the combinations of passive base isolation systems, such as lead-core rubber bearings and frictional-type sliding bearings, and active control devices, such as actuators, active mass dampers and active tendons. The idea of hybrid control systems is to utilize the advantages of both the passive and active control systems to extend the range of applicability of both control systems to protect the integrity of the structure, whereas the required capacity of the active control system is not too large. In particular, under extreme environments, such as strong earthquakes, hybrid control systems are superior. With aseismic hybrid control systems, the advantage of the base isolation system, which is the ability to drastically reduce the horizontal motion transmitted to the superstructure, is preserved, whereas the active devices can be adaptive to different types of earthquake ground motions.

It is well known that most passive control systems behave either nonlinearly, such as sliding isolation systems, or inelastically (hysteretically), such as lead-core rubber-bearing isolation systems. As a result, hybrid control involves active control of nonlinear or inelastic (hysteretic) structural systems. Unfortunately, control theories for nonlinear or hysteretic systems are very limited [e.g., 27, 34, 35, 36]. Recently, instantaneous optimal control algorithms have been proposed and developed for applications to active control of linear, nonlinear and hysteretic structural systems [e.g., 37, 29-33]. These control algorithms have been demonstrated to be suitable to some types of aseismic hybrid control systems [e.g., 29-33] and they have been used in Refs. 21-24.

The purpose of this paper is to explore the feasibility of applying different types of aseismic hybrid control systems to bridge structures. These include the installation of either actuators or active mass dampers at the locations of rubber bearings. The hysteretic behavior of rubber bearings is taken into account and the instantaneous optimal control algorithm recently developed [29-33] for control of nonlinear and hysteretic structural systems is used. Numerical examples are worked out to demonstrate the feasibility and performance of these hybrid control systems for bridge structures subjected to strong earthquakes.

FORMULATION FOR HYBRID CONTROL

Consider a lumped-mass bridge structure equipped with rubber-bearings and active control devices, such as actuators or active mass dampers, as shown in Fig. 1 [13]. The rubber bearings are inelastic and their hysteretic behavior will be described later. The structure is idealized by an n -degree-of-freedom system and subjected to a one-dimensional earthquake ground acceleration $\ddot{X}_0(t)$ in the longitudinal direction. The matrix equation of motion of the entire structural system can be expressed as

$$\mathbf{M}\ddot{\mathbf{X}}(t) + \mathbf{C}\dot{\mathbf{X}}(t) + \mathbf{F}_j[\mathbf{X}(t)] = \mathbf{E}\ddot{X}_0(t) + \mathbf{H}\mathbf{U}(t) \quad (1)$$

in which $\mathbf{X}(t) = [x_1, x_2, \dots, x_n]'$ = an n vector denoting the deformation between adjacent masses, \mathbf{M} = an

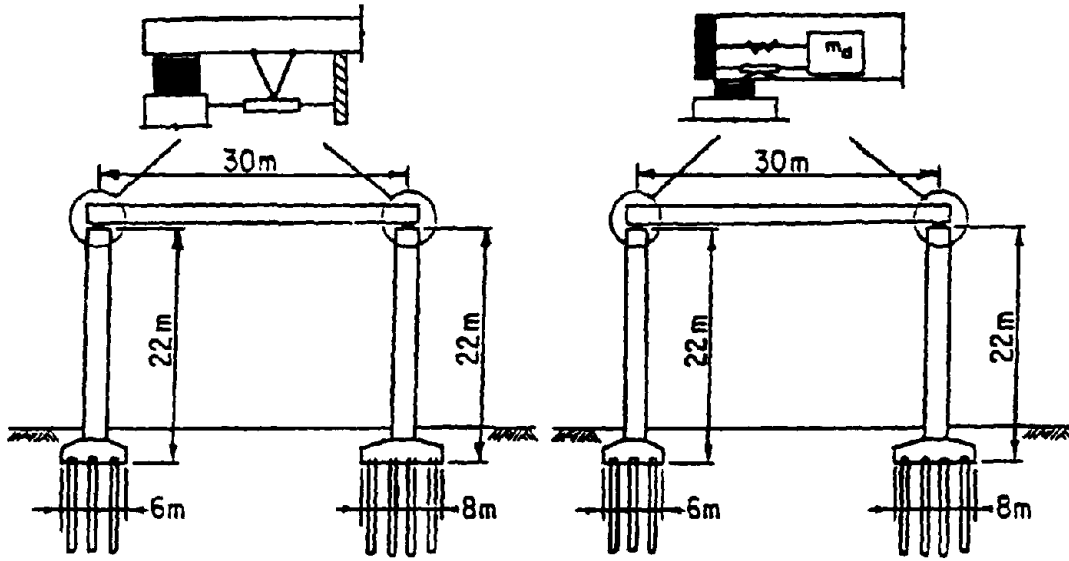


Fig. 1: Highway Bridge With Hybrid Control System; (a) Rubber Bearing and Actuator, (b) Rubber Bearing and Active Mass Damper

($n \times n$) mass matrix, \mathbf{C} = an ($n \times n$) damping matrix, $\mathbf{U}(t)$ = a r -dimensional control vector, \mathbf{H} = an ($n \times r$) location matrix denoting the location of r controllers and \mathbf{E} is an n vector denoting the influence of the earthquake ground acceleration $\ddot{\mathbf{X}}_0(t)$ on each degree of freedom. For the notations above, an under bar denotes a vector or matrix and a prime indicates the transpose of a vector or matrix. In Eq. (1), $\mathbf{E}_s[\mathbf{X}(t)]$ is an n vector denoting the nonlinear (or hysteretic) stiffness restoring force that is assumed to be a function of $\mathbf{X}(t)$.

Introducing a $2n$ state vector $\mathbf{Z}(t)$,

$$\mathbf{Z}(t) = \begin{bmatrix} \mathbf{X}(t) \\ \dot{\mathbf{X}}(t) \end{bmatrix} \quad (2)$$

one can convert the second-order nonlinear matrix equation, Eq. (1), into a first order nonlinear matrix equation as follows:

$$\dot{\mathbf{Z}}(t) = \mathbf{g}[\mathbf{Z}(t)] + \mathbf{B}\mathbf{U}(t) + \mathbf{W}_1 \ddot{\mathbf{X}}_0(t) \quad (3)$$

where $\mathbf{g}[\mathbf{Z}(t)]$ is a $2n$ vector which is a nonlinear function of the state vector $\mathbf{Z}(t)$,

$$\mathbf{g}[\mathbf{Z}(t)] = \begin{bmatrix} \dot{\mathbf{X}}(t) \\ -\mathbf{M}^{-1}[\mathbf{C}\dot{\mathbf{X}}(t) + \mathbf{E}_s[\mathbf{X}(t)]] \end{bmatrix} \quad (4)$$

\mathbf{B} is a ($2n \times r$) matrix and \mathbf{W}_1 is a $2n$ vector

$$E = \begin{bmatrix} Q \\ - \\ - \\ M^{-1}H \end{bmatrix} ; \quad W_1 = \begin{bmatrix} Q \\ - \\ - \\ M^{-1}F \end{bmatrix} \quad (5)$$

Based on instantaneous optimal control, the time dependent objective function is given by [29,32]

$$J(t) = Z'(t) Q Z(t) + U'(t) R U(t) \quad (6)$$

in which Q is a $(2n \times 2n)$ positive semidefinite weighting matrix and R is a $(r \times r)$ positive definite weighting matrix.

The optimal control vector can be obtained as [29, 32]

$$U(t) = -\phi R^{-1} E' Q Z \quad (7)$$

in which $\phi = \Delta t/3$ is a small positive constant. In addition to being a positive semidefinite matrix, Q should also guarantee the stability of the controlled structure [33]. One possible way of choosing the Q matrix using the Lyapunov direct method is presented in Ref. 33.

Substituting Eq. (7) into Eq. (3), one obtains the matrix equation of motion for the controlled structure

$$\dot{Z}(t) = g[Z(t)] - \phi E R^{-1} E' Q Z(t) + W_1 \dot{X}_0(t) \quad (8)$$

To guarantee the stability of the controlled structure, the weighting matrix Q can be determined using the Lyapunov direct method as follows [33]. Let

$$Q = \phi_2 Q_1 \quad (9)$$

in which $\phi_2 > 0$ and consider the Lyapunov function, $V(Z) = \dot{Z}'(t) Q_1 \dot{Z}(t)$, so that its derivative is $\dot{V} = \dot{Z}'(t) Q_1 \dot{Z}(t) + \dot{Z}'(t) Q_1 \dot{Z}(t)$. Taking the derivative of Eq. (8) and neglecting the term $\dot{X}_0(t)$, one obtains $\dot{Z}(t) = [\Delta(Z) - \phi \phi_2 B R^{-1} E' Q_1] \dot{Z}(t)$ where

$$\Delta(Z) = \partial g(Z) / \partial Z \quad (10)$$

is a $(2n \times 2n)$ matrix. Substitution of the expression for $\dot{Z}(t)$ obtained above into the equation for \dot{V} leads to the following results [33]; $\dot{V} = \dot{Z}'(t) [\Delta'(Z) Q_1 + Q_1 \Delta(Z) - 2\phi \phi_2 Q_1 B R^{-1} E' Q_1] \dot{Z}(t)$. For $\dot{V} \leq 0$, one obtains

$$\Delta'(Z) Q_1 + Q_1 \Delta(Z) - 2\phi \phi_2 Q_1 B R^{-1} E' Q_1 = -I_0 \quad (11)$$

in which I_0 is a $(2n \times 2n)$ positive semidefinite matrix. Eq. (11) is a Riccati-type matrix equation from which the Q_1 matrix can be determined. Since the system without control is stable, $\Delta(Z)$ is negative definite and Q_1 is positive definite. Furthermore, since $Q_1 B R^{-1} E' Q_1$ is positive semidefinite, Q_1 can also be obtained from the following linear algebraic equation

$$\Delta'(Z) Q_1 + Q_1 \Delta(Z) = -I_0 \quad (12)$$

In deriving Eqs. (11) and (12), the term $\dot{X}_0(t)$ has been neglected, since it does not affect the stability of the structure.

Simulation of Bridge Response The inelastic stiffness restoring force, $F_m(x_i)$, of the i th element, i.e., between $i-1$ and i nodal points, can be expressed as [29-32]

$$F_m(x_i) = \alpha_i k_i x_i + (1 - \alpha_i) k_i D_{y_i} v_i \quad (13)$$

in which k_i = elastic stiffness, α_i = ratio of the post-yielding to pre-yielding stiffness, D_{y_i} = yield deformation = constant, and v_i is a nondimensional variable introduced to describe the hysteretic component of the deformation, with $|v_i| \leq 1$, where

$$\dot{v}_i = D_m^{-1} [A_i \dot{x}_i - \beta_i |\dot{x}_i| |v_i|^{n_i-1} v_i - \gamma_i \dot{x}_i |v_i|^{n_i}] = f_i(x_i, v_i) \quad (14)$$

In Eq. (14), parameters A_i , β_i and γ_i govern the scale and general shape of the hysteresis loop, whereas the smoothness of the force-deformation curve is determined by the parameter n_i .

The stiffness model given by Eqs. (13) and (14) is capable of describing different types of hysteresis loops, such as those of lead-core rubber bearings. If the i th element is elastic, then α_i in Eq. (13) is set to be 1.0, i.e., $\alpha_i = 1.0$, and the elastic restoring force becomes $F_{ni}(x_i) = k_i x_i$ [29, 32].

With the introduction of the hysteretic model, Eq. (13), the stiffness vector $E_n[\underline{X}(t)]$ in Eq. (1) can be expressed as

$$E_n[\underline{X}(t)] = K_e \underline{X}(t) + K_h \underline{Y}(t) \quad (15)$$

in which $\underline{Y}(t) = [v_1(t), v_2(t), \dots, v_n(t)]'$ is an n vector denoting the hysteretic variables, $v_i(t)$, of each element, and K_e and K_h are $(n \times n)$ elastic stiffness matrix and hysteretic stiffness matrix, respectively. All elements of K_e and K_h are zero except $K_e(i, i) = \alpha_i k_i$, $K_h(i, i) = (1 - \alpha_i) k_i D_{y_i}$ for $i = 1, 2, \dots, n$ and $K_e(i, i+1) = -\alpha_{i+1} k_{i+1}$, $K_h(i, i+1) = -(1 - \alpha_{i+1}) k_{i+1} D_{y_{i+1}}$ for $i = 1, 2, \dots, n-1$.

To simulate the response of the bridge structure equipped with hybrid control systems, the optimal control vector $\underline{U}(t)$ given by Eq. (7) is expressed as

$$\underline{U}(t) = -\phi B^{-1} B' Q Z = \underline{G}_2 \underline{X}(t) + \underline{G}_1 \dot{\underline{X}}(t) \quad (16)$$

in which Eq. (2) has been used, and \underline{G}_1 and \underline{G}_2 are $(r \times n)$ matrices which are functions of the weighting matrix Q . Furthermore, a $3n$ state vector, $\underline{Z}(t)$, a $(3n \times r)$ matrix, \underline{B} , and a $3n$ vector, \underline{W}_1 , are introduced

$$\underline{Z}(t) = \begin{bmatrix} \underline{X}(t) \\ \underline{Y}(t) \\ \dot{\underline{X}}(t) \end{bmatrix}, \quad \underline{B} = \begin{bmatrix} \underline{0} \\ \underline{0} \\ M^{-1} H \end{bmatrix}; \quad \underline{W}_1 = \begin{bmatrix} \underline{0} \\ \underline{0} \\ M^{-1} E \end{bmatrix} \quad (17)$$

Then, the second order matrix equations of motion, Eqs. (1) and (15), can be converted into a first order matrix equation as follows

$$\dot{\underline{Z}}(t) = D[\underline{Z}(t)] + \underline{G} \underline{Z}(t) + \underline{W}_1 \dot{\underline{X}}_0(t) \quad (18)$$

in which $D[\underline{Z}(t)]$ is a $3n$ vector consisting of nonlinear functions of components of the vector $\underline{Z}(t)$, and \underline{G} is a $(3n \times 3n)$ matrix

$$D[\underline{Z}(t)] = \begin{bmatrix} \dot{\underline{X}} \\ \text{-----} \\ f(\underline{X}, \underline{Y}) \\ \text{-----} \\ -M^{-1} (C \dot{\underline{X}} + K_e \underline{X} + K_h \underline{Y}) \end{bmatrix}; \quad \underline{G} = \begin{bmatrix} \underline{0} & \underline{0} & \underline{0} \\ \underline{0} & \underline{0} & \underline{0} \\ M^{-1} H G_2 & \underline{0} & M^{-1} H G_1 \end{bmatrix} \quad (19)$$

where $f(\underline{X}, \underline{Y}) = [f_1(x_1, v_1), f_2(x_2, v_2), \dots, f_n(x_n, v_n)]'$ is an n vector with the i th element, $f_i(x_i, v_i) = \dot{v}_i$ given by Eq. (14).

The response $\underline{Z}(t)$ of the controlled bridge can be simulated by solving Eq. (18) numerically using the Fourth-Order Runge-Kutta method [29-32].

Approximation for $\Lambda(Z)$ By Equivalent Linearization The weighting matrix Q are determined from Eqs. (9) and (11) or (12). In Eqs. (11) and (12), however, the nonlinear matrix $\Lambda(Z) = \partial g(Z) / \partial Z$, Eq. (10), is a function of the response state vector $Z(t)$. Hence, the Q matrix should be computed on-line at every time

instant t when the state vector $\mathbf{Z}(t)$ is measured. To simplify the problem for practical implementations, two equivalent linearization techniques have been proposed in Ref. 33, so that $\Delta(\mathbf{Z})$ can be approximated by a constant matrix Δ . Then, the constant \mathbf{Q} matrix can be determined off-line. For the rubber-bearing isolation system, a linearization of the $\Delta(\mathbf{Z})$ matrix at the equilibrium point, $\mathbf{Z}=\mathbf{Q}$ and $\dot{\mathbf{Y}}=\mathbf{Q}$, is shown to be quite reasonable [33], i.e.,

$$\Delta = \Delta(\mathbf{Z}) \Big|_{\mathbf{Z}=\mathbf{Q}, \dot{\mathbf{Y}}=\mathbf{Q}} = \partial \mathbf{g}(\mathbf{Z}) / \partial \mathbf{Z} \Big|_{\mathbf{Z}=\mathbf{Q}, \dot{\mathbf{Y}}=\mathbf{Q}} \quad (20)$$

Substituting Eq. (15) into Eq. (4), taking the derivative with respect to \mathbf{Z} , and evaluating the resulting $\Delta(\mathbf{Z})$ matrix at $\mathbf{Z}=\mathbf{Q}$ and $\dot{\mathbf{Y}}=\mathbf{Q}$, Eq. (20), one obtains

$$\Delta = \begin{bmatrix} \mathbf{Q} & \mathbf{I} \\ -\mathbf{M}^{-1}\mathbf{K} & -\mathbf{M}^{-1}\mathbf{C} \end{bmatrix} \quad (21)$$

in which \mathbf{C} and \mathbf{K} are $(n \times n)$ band-limited damping and elastic stiffness matrices, respectively, with all elements equal to zero except $C(i,i)=c_i$, $K(i,i)=k_i$ for $i=1,2,\dots,n$ and $C(i,i+1)=-c_{i+1}$, $K(i,i+1)=-k_{i+1}$ for $i=1,2,\dots,n-1$, where c_i and k_i are the damping coefficient and the elastic stiffness, respectively, of the i th element. In Eq. (21), \mathbf{I} is a $(n \times n)$ identity matrix.

Thus, the \mathbf{Q}_1 matrix can either be obtained from Eq. (11)

$$\Delta' \mathbf{Q}_1 + \mathbf{Q}_1 \Delta - 2\phi \phi_2 \mathbf{Q}_1 \mathbf{B} \mathbf{R}^{-1} \mathbf{B}' \mathbf{Q}_1 = -\mathbf{I}_0 \quad (22)$$

or from Eq. (12)

$$\Delta' \mathbf{Q}_1 + \mathbf{Q}_1 \Delta = -\mathbf{I}_0 \quad (23)$$

DEMONSTRATIVE EXAMPLES

The same single-span girder bridge analyzed in Ref. 13, as shown in Fig. 1, is considered, where the strong earthquake is applied in the longitudinal direction. The differences between the bridge system analyzed in Ref. 13 and in this paper are as follows: (i) The rubber bearing considered in Ref. 13 is elastic, while it is considered as inelastic in this paper, and (ii) instead of using variable viscous dampers, actuators and active mass dampers are used, see Fig. 1. As in other feasibility studies, such as Refs. 11 and 21-24, the bridge structure is modeled by a single-degree-of-freedom system, as shown in Fig. 2, for simplicity. The weight of the bridge deck is 241.5 tf. The hysteretic behavior of the rubber bearing is defined by Eqs. (13) and (14), in which $D_{y1}=16\text{cm}$, $k_1=9542\text{ kN/m}$, $\alpha_1=0.8$, $A_1=1.0$, $\beta_1=\gamma_1=0.5$ and $n_1=3.0$. The hysteresis loop

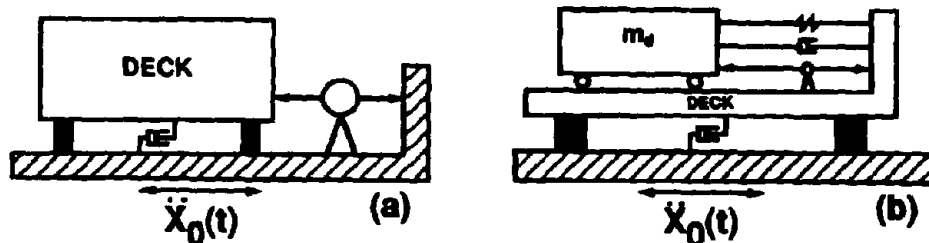


Fig. 2: Idealized Bridge Model; (a) Rubber Bearing and Actuator, (b) Rubber Bearing and Active Mass Damper

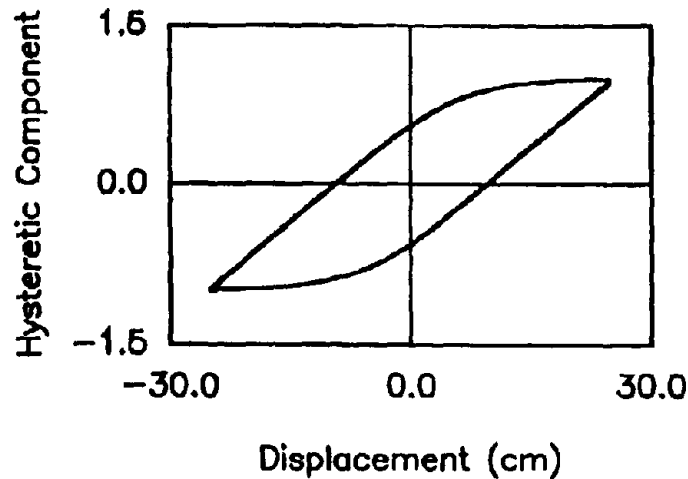


Fig. 3: Hysteresis Loop of Rubber Bearing

of such a rubber bearing, i.e., v_1 versus x_1 , is shown in Fig. 3. For such a bridge structure, the fundamental natural period at small oscillation is 1 second. The damping ratio is assumed to be 2%. A simulated strong earthquake with a maximum ground acceleration of 0.5g shown in Fig. 4 is used for the excitation.

Without active control devices, time histories of the relative displacement and absolute acceleration of the bridge deck have been computed. The time history of the relative displacement of the bridge deck is presented in Fig. 5(a). Within 45 seconds of the earthquake episode, the maximum response quantities are

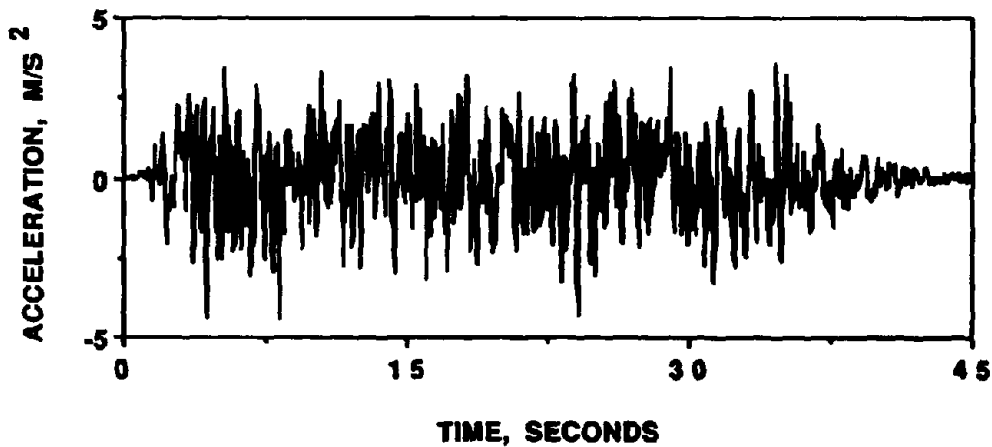


Fig. 4: A Simulated Earthquake Ground Acceleration

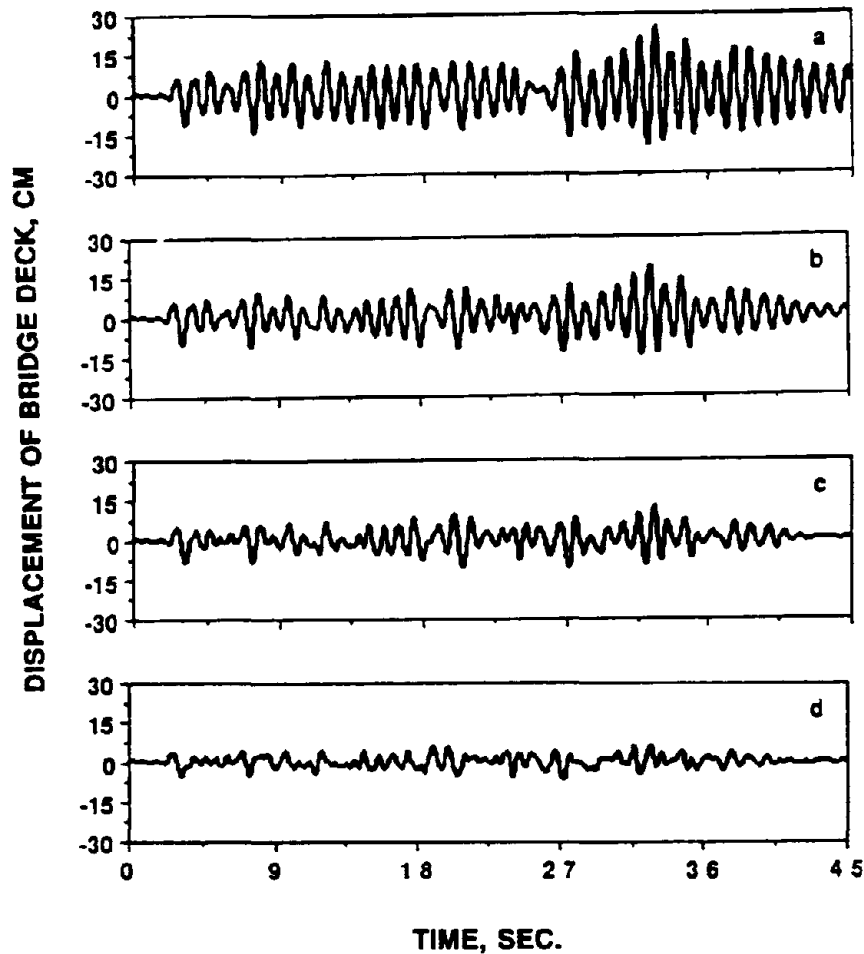


Fig. 5: Time Histories of Relative Displacement of Bridge Deck;
 (a) Inelastic Rubber Bearing, (b) Hybrid Control System (I),
 (c) Hybrid Control System (II), and (d) Hybrid Control System (III)

presented in Table 1, designated as "Inelastic Bearing." When the rubber bearing is considered elastic, the maximum response quantities are shown in Table 1, designated as "Elastic Bearing", for comparison. As expected, the inelastic bearing results in smaller response quantities due to the energy dissipation by the hysteresis loop.

With the application of an actuator, i.e., the hybrid control system shown in Fig. 2(a), the response of the bridge deck depends on the weighting matrices \mathbf{Q} and \mathbf{R} . For the present example with only one controller, the \mathbf{R} matrix consists of only one element, denoted by R_0 , and the dimension of the \mathbf{Q} , \mathbf{Q}_1 and \mathbf{I}_0 matrices, Eq. (23), is (2x2). For illustrative purpose, $R_0=0.005$ and $\phi=\Delta t/3=0.005$ are used. The \mathbf{Q} matrix is obtained from Eq. (9) and (23) in which $\phi_2=1$, $I_0(1,1)=I_0(1,2)=I_0(2,1)=0$ and $I_0(2,2)=50 \times 10^6$.

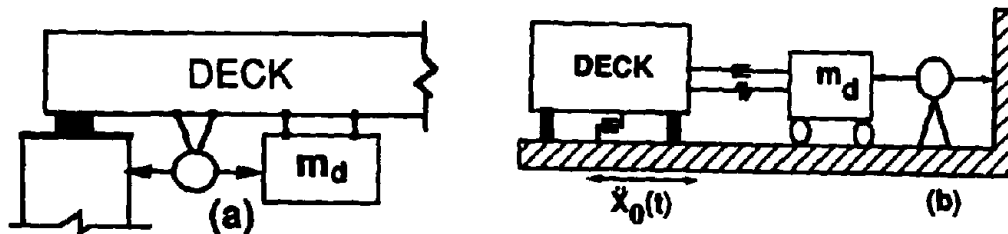


Fig. 6: A Hybrid Control System; (a) Rubber Bearing and Active Mass Damper, and (b) Idealized Structural Model

Although the Q matrix is a full matrix, only elements in the second row are relevant to the control force $\underline{U}(t)$, Eq. (7). These elements are $Q(2,1)=0$ and $Q(2,2)=198.94$, indicating that only the relative velocity of the bridge deck should be measured. The time history of the relative displacement of the bridge deck is simulated using Eq. (18) and the results are presented in Fig. 5(b). The maximum response quantities in 45 seconds of the earthquake episode are shown in Table 1, designated as Case "I", under the hybrid control system (actuator). The maximum active control force of 10.1 tf is also presented in Table 1.

With the increase of $I_0(2,2)$ to 150×10^8 , i.e., $I_0(2,2) = 150 \times 10^8$, we obtain $Q(2,1) = 0$ and $Q(2,2) = 296.83$. The time history of the relative displacement of the bridge deck is shown in Fig. 5(c), whereas the maximum response quantities are shown in Table 1, designated as Case "II", under the hybrid control system (actuator). Finally, for Case III in which $I_0(2,2) = 500 \times 10^8$, we obtain $Q(2,1) = 0$ and $Q(2,2) = 1989$. The resulting time history of the relative displacement of the bridge deck is displayed in Fig. 5(d), whereas the corresponding maximum response quantities are shown in Table 1, designated as Case "III", under the hybrid control system (actuator).

TABLE 1: Maximum Response of Bridge Deck

	Passive System		Hybrid Control System				
	Elastic Bearing	Inelastic Bearing	Actuator			Active Mass Damper	
			I	II	III	I	II
Displacement (cm)	34.5	24.9	18.8	12.2	6.7	11.5	11.4
Acceleration (cm/s ²)	1241.9	912.3	711.1	481.2	313.7	420.6	418.3
Active Control Force(tf)	0	0	10.1	20.2	38.1	13.0	12.2

It is observed from Table 1 that the maximum response quantities of the bridge deck reduce as the control force increases. For Case II, the maximum response quantities are reduced by 50% and the maximum control force is 20.2 tf that is less than 10% of the weight of the bridge deck. For Case III, the maximum displacement is reduced by 73% and the maximum acceleration is reduced by 66%, whereas the maximum control force is 38.1 tf that is about 16% of the weight of the bridge deck. Such a performance of the control system is consistent with that observed in building applications [29-32].

Instead of using an actuator, an active mass damper is used as shown in Figs. 1(b), whereas the idealized structural model is shown in Fig. 2(b). The weight of the mass damper is 5% of that of the bridge deck. The natural period of the mass damper is 1 second and the damping ratio is 10%. Since this is a two-degree-of-freedom system, the dimension of the \mathbf{Q} , \mathbf{Q}_1 and \mathbf{I}_0 matrices is (4x4). For illustrative purpose, $R_0=0.005$, $\phi=\Delta t/3=0.005$ and $\phi_2=100$ are used. The \mathbf{Q} matrix is computed from Eq. (9), in which \mathbf{Q}_1 is computed from the Riccati-type equation given by Eq. (22). In Eq. (22), elements of the \mathbf{I}_0 matrix are zero except $I_0(4,4)=150 \times 10^9$. In this particular case, only the elements in the third and fourth rows of the \mathbf{Q} (or \mathbf{Q}_1) matrix are relevant to the active control force $\mathbf{U}(t)$. These elements are $Q_1(3,i)=[-6736.5, 2336.2, 6061.9, 258.5]$ and $Q_1(4,i)=[-2439.8, 111.2, 258.5, 51.8]$. The maximum response quantities and the maximum active control force within 45 seconds of the earthquake episode are simulated using Eq. (18) and the results are presented in Table 1, designated as Case "II", under the active mass damper.

When the same active mass damper is arranged in a different form as shown in Fig. 6(a), the idealized structural model is given by Fig. 6(b). With such an active mass damper, the active control force $\mathbf{U}(t)$ depends only on the third row of the \mathbf{Q} (or \mathbf{Q}_1) matrix. In this case, $R_0=0.005$, $\phi=\Delta t/3=0.005$ and $\phi_2=100$ are used. Elements of the (4x4) \mathbf{I}_0 matrix are zero except $I_0(4,4)=150 \times 10^9$. The (4x4) \mathbf{Q}_1 matrix is computed from Eq. (22) and the third row of the \mathbf{Q}_1 matrix is as follows: $Q_1(3,i)=[104.9, -2099.4, 41.7, 157.0]$. Within 45 seconds of the earthquake episode, the maximum response quantities and the maximum active control force are simulated using Eq. (18). The results are presented in Table 1, designated as Case "I", under the active mass damper.

It is observed from Table 1 that the performances of the hybrid control systems using an active mass damper for two different configurations are almost the same, and that their performances are quite satisfactory. Because the mass damper is capable of drawing the energy from the bridge system through its own motion, the performance of the active mass damper is better than that of the actuator as indicated in Table 1. However, the hybrid control system using the actuator is easier for practical implementations. Extensive simulation results indicate that, unlike the case for the actuator, the performance of the active mass damper is not satisfactory when the bridge response should be reduced by more than 75%, such as the Case III in Table 1.

CONCLUSION

A preliminary study has been conducted to explore the feasibility of applying two aseismic hybrid control systems to bridge structures. These include a combination of rubber-bearing isolators and actuators or active mass dampers. The inelastic behavior of rubber-bearing isolators is taken into account. Numerical simulation results indicate that these two types of aseismic hybrid control systems are promising for applications to long-span bridges.

One important advantage of hybrid control systems is that the active control devices are capable of responding favorably to different earthquakes that have different magnitudes and frequency contents. For bridge applications, several types of active control devices in combinations with passive isolation systems have been investigated to-date. These include variable viscous dampers [11-13, 21], frictional-controllable sliding bearings [22-25], and actuators and active mass dampers investigated herein. From the standpoint of external energy supplies, the use of either variable viscous dampers or frictional-controllable sliding bearings is very

favorable. For these two systems, the external energy is required to regulate either the oil flow rate or the magnitude of the oil pressure and hence the energy demand may be small. The applications of actuators or active mass dampers, however, require a larger energy supply to produce large control forces in order to counter the motion of the base-isolated bridges. Aseismic hybrid control systems are very promising for applications to bridge structures; however, further research is needed.

ACKNOWLEDGMENT

This research is partially supported by the National Science Foundation Grant No. NSF-BCS-91-96089 and NCEER-90-2202. The author is grateful to Dr. K. Kawashima of PWRJ, Japan, for valuable discussions. The author would like to thank Dr. Z. Li and Mr. S. Vongchavalitkul for their assistance in numerical computations.

REFERENCES

1. Reinhorn, A.M. and Manolis, G.D., "Recent Advances in Structural Control", Shock and Vibration Digest, Vol. 21, 1989, pp. 3-8.
2. Yang, J.N., and Soong, T.T., "Recent Advancement in Active Control of Civil Engineering Structures", J. of Probabilistic Eng. Mech., Vol. 3, No. 4, December 1988, pp. 179-188.
3. Soong, T.T., "State-of-the-Art Review: Active Structural Control in Civil Engineering", Engineering Structures, Vol. 10, 1988, pp. 74-84.
4. Soong, T.T., Active Structural Control: Theory and Practice, New York, Longman, London and Wiley, 1990.
5. Proc. U.S. National Workshop on Structural Control Research, edited by S.F. Masri and G. Housner, Dept. of Civil Eng., USC, October, 1990.
6. Kobori, T., "State-of-the-Art Report: Active Seismic Response Control", Proc. 9th World Conf. on Earthquake Eng., Tokyo/Kyoto, Japan, 1988, pp. 453-446.
7. Yang, J.N. and Giannopoulos, F., "Active Control and Stability of Two Cable-Stayed Bridge", J. of Eng. Mech., ASCE, Vol. 105, No. EM4, August 1979, pp. 677-694.
8. Yang, J.N. and Giannopoulos, F., "Active Control of Two Cable-Stayed Bridge", J. of Eng. Mech., ASCE, Vol. 105, No. EM5, October 1979, pp. 795-810.
9. Ghaemmaghami, P. and Yang, J.N., "Stochastic Dynamic Analysis of Long-Span Bridge With Active Control", Stochastic Structural Dynamics, edited by J.K. Lin and G.I. Schueller, Springer-Verlag, 1987, pp. 136-164.
10. Soong, T.T., "Active Control for Bridge Applications -- Case Studies", paper presented at the First US-Japan Workshop on Earthquake Protective Systems for Bridges, September 4-5, 1991, SUNY, Buffalo, NY; to appear in the Workshop Proceedings.
11. Taguchi, J., Iwasaki, T., Adachi, Y., Sasaki, Y., and Kawashima, K., "U.S.-Japan Cooperative Research Program on Hybrid Control of Seismic Response of Bridge Structures", Proc. 22nd Joint Meeting of U.S.-Japan Panel on Wind and Seismic Effects, UJNR, paper no. 3-4, pp. 1-8, May 15-18, 1990, NTIS, Gaithersburg, MD.
12. Kawashima, K., Hasegawa, K. and Yoshida, T., "Active Control of Seismic Response of Structure by Means of Mass Damper", Japanese Civil Engineering Journal, Vol. 31, No. 5, May, 1989.
13. Kawashima, K., Hasegawa, K., Unjoh, S., Nagashima, H. and Shimizu, H., "Current Research Efforts in Japan for Passive and Active Control of Highway Bridges Against Earthquakes", Proc. 23rd Joint Meeting of U.S.-Japan Panel on Wind and Seismic Effects, UJNR, Tsabuka, Japan, May, 1991.
14. Katayama, T., Kawashima, K. and Murakami, Y., "Current Design Considerations for Reducing Seismic Lateral Force of Highway Bridges in Japan", paper presented at the New Zealand-Japan Workshop on Base Isolation of Highway Bridges, November 1987, Wellington, New Zealand.

15. Guidelines for Design of Base-Isolated Highway Bridges, Final Report of A Committee for Study of Application of Base Isolation to Seismic Design of Highway Bridges (Chairman: Professor T. Katayama), Technology Research for National Land Development, Japan, March, 1989.
16. Kawashima, K., "Development and Future Scope of Seismic Isolation of Structures - A Review", Proc. Japan Society of Civil Engineers, Structural Eng./Earthquake Eng., Vol.398/I-10, 1988.
17. Buckle, I., "Development and Application of Base Isolation and Passive Energy Dissipation - A World Review", Proc. Seminar and Workshop on Base Isolation and Passive Energy Dissipation, San Francisco, March, 1986, pp. 153-174.
18. Buckle, I. and Kelly, J.M., "Shake Table Studies of Base Isolated Bridge Superstructures with Energy Dissipators", Proc. 8th European Conf. on Earthquake Eng., pp. 845-861, 1986.
19. Kelly, J.M., Buckle, I. and Koh, C.G., "Mechanical Characteristics of Base Isolation Bearings for a Bridge Deck Model Test", Report No. UCB/EERC-86/11, Earthquake Engineering Research Center, University of California, Berkeley, November, 1987.
20. Kelly, J.M., "Aseismic Base Isolation: Review and Biography", J. of Soil Dynamics and Earthquake Engineering, Vol. 5, No. 3, 1986, pp. 202-216.
21. Feng, Q., and Shinozuka, M., "Use of a Variable Damper for Hybrid Control of Bridge Response Under Earthquake", Proc. U.S. National Workshop on Structural Control Research, October, 1990, pp. 107-112.
22. Feng, Q., Fujii, S., and Shinozuka, M., "Hybrid Isolation System Using Friction-Controllable Sliding Bearings", Proc. 8th VPI and SU Symposium on Dynamics and Large Structures, May, 1991.
23. Feng, Q., Shinozuka, M., Fujii, S. and Fujita, "A Hybrid Sliding Isolation System for Bridges", paper presented at the First US-Japan Workshop on Earthquake Protective Systems for Bridges, September 4-5, 1991, SUNY, Buffalo, NY; to appear in Workshop Proceedings.
24. Kawamura, S., Shinozuka, M., Fujii, S. and Feng, Q., "Hybrid Isolation Systems Using Friction-Controllable Sliding Bearings", paper presented at the US-Japan-Italy Workshop/Seminar on Intelligent Systems, June 27-29, 1991, Perugia, Italy; to appear in Workshop Proceedings.
25. Kitamura, H., Kawamura, S., Yamada, M. and Fujii, S., "Structural Response Technologies of Taisei Corporation", Proc. U.S. National Workshop on Struct. Control Res., Oct. 1990, pp. 141-150.
26. Kelly, J.M., Leitmann, G., and Soldatos, A.G., "Robust Control of Base-Isolated Structures Under Earthquake Excitation", J. Optimization Theory and Appl., Vol. 53, No. 2, 1987, pp. 159-180.
27. Reinhorn, A.M., Soong, T.T., and Yen, C.Y., "Base Isolated Structures with Active Control", Seismic Engineering, Recent Advances in Design, Analysis, Testing and Qualification Methods, ASME, PVP-Vol. 127, 1987, pp. 413-419.
28. Yang, J.N., Danielians, A., and Liu, S.C., "Aseismic Hybrid Control Systems for Building Structures", Journal of Engineering Mechanics, ASCE, Vol. 117, No. 4, April, 1991, pp. 836-853.
29. Yang, J.N., Li, Z., Danielians, A. and Liu, S.C., "Instantaneous Optimal Control of Nonlinear Hybrid Structural Systems", Proc. 8th VPI&SU Symp. on Dynamics and Control of Large Systems, Blacksburg, Virginia; to appear in conference proceedings, May 6-8, 1991.
30. Yang, J.N., Li, Z., Danielians, A., and Liu, S.C. "Optimal Hybrid Control of Seismic-Excited Nonlinear and Inelastic Structures", Proc. US-Japan-Italy Workshop/Seminar on Intelligent Systems, Perugia, Italy, June 27-29, 1991.
31. Yang, J.N., Li, Z., and Liu, S.C., "Aseismic Hybrid Control of Nonlinear and Inelastic Structures Using Velocity and Acceleration Feedbacks", Proc. IUTAM Symposium on Nonlinear Stochastic Mechanics, July 1-5, 1991, Torino, Italy.
32. Yang, J.N., Li, Z., and Danielians, A., "Hybrid Control of Seismic-Excited Nonlinear and Inelastic Structural Systems", National Center for Earthquake Engineering Research, Technical Report NCEER-TR-91-0020, 1991.
33. Yang, J.N. and Li, Z., "Active and Hybrid Control of Civil Engineering Structures", paper presented at the US-Korea-Japan Trilateral Workshop on Frontier R&D for Constructed Facilities, October 21-24, 1991, Honolulu, Hawaii; to appear in the Workshop Proceedings.

34. Reinhorn, A.M., Manolis, G.D. and Wen, C.Y., "Active Control of Inelastic Structures", Journal of Engineering Mechanics, ASCE, Vol. 113, No. 3, 1987, pp. 315-332.
35. Masri, S.F., Bekey, G.A. and Caughey, T.K., "On-Line Control of Nonlinear Flexible Structures", Journal of Applied Mechanics, ASME, Vol. 49, No. 4, 1981, pp. 871-884.
36. Yang, J.N., Long, F.X., and Wong, D., "Optimal Control of Nonlinear Structures", Journal of Applied Mechanics, ASME, Vol. 55, December, 1988, pp. 931-938.
37. Yang, J.N., Akbarpour, A., and Ghaemmaghami, P., "New Optimal Control Algorithms for Structural Control", Journal of Engineering Mechanics, ASCE, Vol. 113, Vol. 9, June, 1987, pp. 1369-1386.

5. Design Issues and Applications

Selecting Bedrock Motions for the Seismic Design of Bridges

A.W. Taylor and W.C. Stone

AASHTO Seismic Isolation Design Requirements for Highway Bridges

R.L. Mayes, I.G. Buckle, T.E. Kelly and L.R. Jones

Bridge Modeling Method in Menshin Design

M. Shimada, K. Dewa and T. Tamura

Design and Construction of Miyagawa Bridge (First Menshin Bridge in Japan)

M. Yoshiro and H. Koji

Equivalent Linearizing Method of Menshin Devices

K. Takahashi, D. Ozaki, K. Matsubara, K. Takagi, Y. Makiguchi and Y. Suizu

Simplified Determination Method of Substructure Dimensions of Menshin Bridges

Y. Sawauchi, Y. Hishiki and K. Utsugi

Seismic Response Analysis Method of Menshin Bridges

Y. Hamazaki, O. Ohtani and H. Zui

Effect of Nonlinearity of Bridge Columns on Seismic Response of Menshin Bridges

T. Hirai and M. Sugimoto

Seismic Response of Curved Continuous Menshin Bridge

N. Hosoda, I. Kaneko and K. Kuroda

Comparative Design of a Steel Girder Bridge Using Three Different Bearing Systems

M. Okado, M. Komuro, M. Horikawa and F. Kawahara

Selecting Bedrock Motions for the Seismic Design of Bridges

by
Andrew W. Taylor* and William C. Stone*

Introduction

A recent advance in the seismic design of reinforced concrete bridges has been the development of a number of time-step hysteretic failure models [Park et al. (1987), Powell (1990), Rodriguez-Gomez et al. (1990)]. These models have made it possible to track the inelastic behavior, and damage state, of a bridge through the course of an earthquake. While most time-step hysteretic failure models are still in the development stage at this time, and all are computationally intensive by today's standards, these models may soon become the primary method for designing reinforced concrete bridges in seismic regions.

A comprehensive rational seismic design procedure for reinforced concrete bridge piers is currently under development at the National Institute of Standards and Technology (NIST). The procedure is outlined in detail elsewhere [Stone and Taylor (1991)], but can briefly be described as incorporating a time-step hysteretic failure model [Park et al. (1987)] to evaluate the seismic performance of the pier; a shear wave model [SHAKE (1990)] to propagate earthquake bedrock motions upward through the overlying soil layers; and a cost optimization algorithm to determine the most economical design for a given site, earthquake magnitude, and specified acceptable level of damage.

A critical step in the implementation of any time-step analysis is the selection of appropriate earthquake motions to drive the analysis. In order to design a new bridge, evaluate the potential for seismic damage to an existing bridge, or evaluate the effectiveness of earthquake protection systems, it is first necessary to obtain an estimate of the seismic forcing function. In the case of the NIST design procedure, the desired earthquake motions are bedrock acceleration-time records: the motions at the ground surface are obtained by employing the shear wave model [SHAKE (1990)] to propagate the bedrock motions upward through the overlying soil layers. This paper describes a method for selecting site-specific bedrock motions for the seismic design or evaluation of bridges.

Earthquake Record Selection and Scaling Method

There are two common approaches to the selection of site-dependent earthquake bedrock motions. Both methods require that a "design" or "target" acceleration response spectrum first be established. This spectrum serves as the model against which other spectra are compared. The target spectrum is derived from statistical studies of response

*Research Structural Engineer, Building and Fire Research Laboratory, National Institute of Standards and Technology, Gaithersburg, Maryland, 20899.

spectra, calculated from all historically-recorded ground motions in the region of interest. (Development of the target response spectrum used in this study is described in the next section).

In the first approach to record selection, synthetic ground motions are generated which have response spectra similar to the target response spectrum. In many cases an historically-recorded ground motion is selected to serve as a basis for the synthetic motion. This record is then altered (sometimes radically) in frequency content, duration and intensity to arrive at a synthetic motion which has a response spectrum close to the target spectrum. This method is often employed in regions where little or no historic earthquake data are available.

In the second approach, "natural" response spectra, from historically-recorded ground motions, are compared to the target spectrum. The natural response spectrum, or spectra, which best match the target spectrum are chosen for design purposes. If no natural spectra match the target spectrum closely, the natural spectra can be altered to some degree. Amplitude scaling of the natural spectra is accomplished by multiplying the ordinates of each spectrum by a constant scale factor. Once appropriate scale factors have been determined, the acceleration record corresponding to each natural spectrum is multiplied by its scale factor. This approach is best suited for areas where there is a catalogue of historically-recorded ground motions: the more extensive the catalogue, the greater the likelihood of finding natural response spectra which, after minimal scaling, match the target response spectrum.

The second approach has been chosen for use in the NIST seismic design procedure for several reasons. First, the NIST study has focused initially on the San Francisco Bay region. Since there is a relative abundance of historic earthquake data from the West Coast of the United States it is possible to derive relationships for the target response spectrum and attenuation equations in the region of interest. Second, the method relies mainly on natural earthquake records which are minimally altered to match the target response spectrum. It is preferable to make use of natural earthquake records whenever possible, rather than synthetic records, as the natural records may reflect aspects of the ground motions which are not accounted for in the synthetic record generation procedures. Finally, the use of a suite of three to five natural earthquake records, which together span the target spectrum, provides a more realistic loading history than a single synthetic record, which is forced to match the entire target spectrum. In reality, a structure is subjected to a series of earthquakes over its lifetime. Taken together, these earthquakes tend to cover the entire range of the target response spectrum. A single synthetic earthquake record which covers the entire target response spectrum represents an unrealistic agglomeration of earthquake effects.

Target Response Spectrum and Attenuation Relationships

A number of methods for computing site-dependent target response spectra have been proposed [Campbell (1981), Idriss (1985), Joyner and Boore (1988), Youngs et al. (1988)]. The development of the spectral equations of Idriss (1985) was based exclusively on seismic data from California. As part of the present study, these

equations were revised to reflect the seismic data collected from the 1989 Loma Prieta earthquake. Thus the equations represent up-to-date target spectra for the region of interest in this study. Figure 1 illustrates schematically how the target response spectrum is computed, as a function of magnitude and distance. The method of computing the target response spectrum is summarized briefly below. (While the target spectrum equations are presented here in their present complete form, it is anticipated that further research may result in a more compact version of the equations).

The method begins with a basic normalized spectral shape for a magnitude 6.75 earthquake. The ordinates of this curve, shown in Table 1, were determined from a statistical study of historically-recorded earthquake bedrock motions in California.

Period, seconds	Normalized Spectral Ordinates (S_e/a)	Period, seconds	Normalized Spectral Ordinates (S_e/a)
0.03	1.000	0.50	2.170
0.05	1.275	0.55	2.020
0.075	1.635	0.60	1.875
0.10	1.920	0.65	1.724
0.11	2.022	0.70	1.600
0.13	2.210	0.75	1.481
0.15	2.375	0.80	1.375
0.18	2.525	0.85	1.280
0.20	2.610	0.90	1.200
0.22	2.666	1.00	1.065
0.25	2.720	1.50	0.648
0.27	2.769	2.00	0.452
0.30	2.755	3.00	0.266
0.32	2.751	4.00	0.180
0.35	2.690	5.00	0.130
0.37	2.630	6.00	0.100
0.40	2.530	8.00	0.065
0.45	2.340		

Table 1. Bedrock motion, normalized spectral ordinates for magnitude 6.75

The next step is to alter this basic normalized spectrum to account for a magnitude other than 6.75. This is accomplished using Equation 1 below, which was derived from a statistical study of earthquakes in California, and accounts for the variation of spectral amplitude as a function of magnitude, M , and period, T , in seconds.

$$\left(\frac{S_e}{a}\right)_M = \exp[a(M) + b(M) \cdot \ln(T)] \left(\frac{S_e}{a}\right)_{M=6.75} \quad (\text{Eqn. 1})$$

$$\text{where } a(M) = -7.427 + 1.654(M) - 0.082(M^2)$$

$$\text{and } b(M) = -3.224 + 0.718(M) - 0.036(M^2)$$

The peak acceleration, "a" (in g's), is computed using Equation 2, which is a function of magnitude, M, and the surface distance from the earthquake source, D, in kilometers.

$$a = \exp[\alpha(M) - \beta(M) \cdot \ln(D + 20)] \quad (\text{Eqn. 2})$$

$$\text{where } \alpha(M) = \exp[2.261 - 0.083 \cdot M] \text{ for } M \leq 6.0$$

$$\alpha(M) = \exp[3.477 - 0.284 \cdot M] \text{ for } M > 6.0$$

$$\beta(M) = \exp[1.602 - 0.142 \cdot M] \text{ for } M \leq 6.0$$

$$\beta(M) = \exp[2.475 - 0.286 \cdot M] \text{ for } M > 6.0$$

Finally, the normalized spectral ordinates are multiplied by the peak acceleration to obtain the absolute spectral ordinates.

$$S_a = \left(\frac{S_e}{a}\right)_M \cdot (a) \quad (\text{Eqn. 3})$$

Demonstration Computer Program

The method of selecting and scaling bedrock motions outlined above is well suited for implementation in a computer program on a work station with interactive graphics capabilities. Such a program called EARTHGEN was written at NIST for Silicon Graphics IRIS 4D/210VGX work station. It is anticipated that EARTHGEN will make up one module of the comprehensive seismic design procedure for bridge piers currently under development at NIST. A block diagram of EARTHGEN is shown in Figure 2, and the operation of EARTHGEN is summarized below.

Initially, EARTHGEN displays a menu and prompts the designer to enter the distance of the bridge site from the fault of interest, and up to five earthquake

**EARTHGEN could have been implemented on any work station with high resolution graphics.

magnitudes. EARTHGEN then displays the target response spectrum for the first magnitude value. The 84th and 16th percentile limits (the target spectrum plus and minus one standard deviation) are also displayed (Fig. 3).

The designer may then select, from a list, the name of an historically-recorded bedrock motion. EARTHGEN retrieves the corresponding acceleration-time record from a data base, computes the response spectrum, and overlays this natural response spectrum on the target response spectrum already displayed (Fig. 4). (As part of this study some 60 recorded bedrock acceleration records for the state of California were compiled and incorporated into the EARTHGEN data base). The designer may then alter the vertical scale of the natural response spectrum by adjusting a scaling dial (Fig. 5). EARTHGEN continuously updates the display to reflect, in real time, this scaling of the natural response spectrum.

The designer may repeat the record selection and scaling procedure for up to five other historically-recorded bedrock motions, all of which are displayed simultaneously on the screen (Fig. 6). When the designer is satisfied that this suite of scaled natural response spectra adequately covers the target spectrum, a new magnitude value is chosen and the record selection and scaling process is repeated. The designer may re-display and adjust the scaling of the spectra for any of the five magnitudes at any time. An automated scaling option is also incorporated in EARTHGEN. When invoked, this routine determines the scale factor for each natural response spectrum which results in the least total difference between the natural spectra and the target spectrum. The designer may use this feature to provide an objective measure of the agreement of the natural and target spectra.

Finally, when records have been selected and scaled for all five magnitude values, the designer terminates the interactive session, and data is written to an output file. This data includes the initial input data (distance and magnitudes), and up to 25 historically-recorded bedrock motions and their scale factors (up to 5 records for each of 5 magnitudes). The scaled bedrock motions may then be used for later non-linear analyses of the bridge structure subjected to five earthquakes of varying magnitude.

Conclusions

A method has been demonstrated for selecting and scaling bedrock earthquake motions for the seismic design and evaluation of bridges. The method lends itself well to implementation on a computer with interactive graphics capabilities. A demonstration program, EARTHGEN, has been described. EARTHGEN allows a designer to rapidly view response spectra from a large number of historically-recorded ground motions, then select and scale the records which are most appropriate for a particular site and structure. EARTHGEN has been initially configured for the San Francisco Bay region, but could be re-configured for other localities. To do so it would be necessary to supply attenuation relationships (such as those developed in the studies of Idriss (1985), Campbell (1981), Joyner and Boore (1988), and Youngs et al. (1988)) and specify a data base of bedrock motion records which are appropriate for the geology of the region of interest.

References

- Campbell, K. W. (1981), "Near Source Attenuation of Peak Horizontal Acceleration," Bulletin of the Seismological Society of America, Vol. 71, No. 6, 1981, pp 2039-2070.
- Idriss, I.M. (1985), "Evaluating Seismic Risk in Engineering Practice," Proceedings, XIth International Conference on Soil Mechanics and Foundation Engineering, San Francisco, August 1985, pp. 255-320.
- Joyner, W.B.; and Boore, D.M. (1988), "Measurement, Characterization, and Prediction of Strong Ground Motion," Earthquake Engineering and Soil Dynamics II - Recent Advances in Ground-Motion Evaluation, Proceedings of the specialty conference sponsored by the Geotechnical Engineering Division of the American Society of Civil Engineers, Park City, Utah, 1988, pp. 43-102.
- Park, Y.J.; Reinhorn, A.M.; and Kunnath, S.K. (1987), "IDARC: Inelastic Damage Analysis of Reinforced Concrete Frame - Shearwall Structures, (1987)," Department of Civil Engineering, State University of New York at Buffalo, Buffalo, NY 14260, Technical Report NCEER-87-0008, July 20, 1987.
- Powell, Graham H. (1990), "DRAIN-2DX Version 0.01 User's Guide," Department of Civil Engineering, University of California, Berkeley, CA 94720, November 1990.
- Rodriguez-Gomez, S.; Chung, Y.S.; and Meyer, C. (1990), "SARCF-II User's Guide: Seismic Analysis of Reinforced Concrete Frames," Technical Report NCEER-90-0027, National Center for Earthquake Engineering Research, State University of New York at Buffalo, Buffalo, NY 14260, September 1990.
- "The SHAKE System: Earthquake Response Analysis of Horizontally Layered Sites," (1990), User's Manual Version 1.0, Geotech International Ltd., Chicago, IL, 1990.
- Stone, W.C.; and Taylor, A.W. (1991), "System Identification of Spirally Reinforced Circular Bridge Columns Subjected to Cyclic Lateral Loading," Proceedings, 23rd Joint Meeting of the U.S.-Japan Panel on Wind and Seismic Effects, UJNR, Takuba, Japan, May 1991.
- Youngs, R.R.; Day, S.M.; and Stevens, J.L. (1988), "Near Field Ground Motions on Rock for Large Subduction Earthquakes," Earthquake Engineering and Soil Dynamics II - Recent Advances in Ground-Motion Evaluation, Proceedings of the specialty conference sponsored by the Geotechnical Engineering Division of the American Society of Civil Engineers, Park City, Utah, 1988, pp. 445-462.

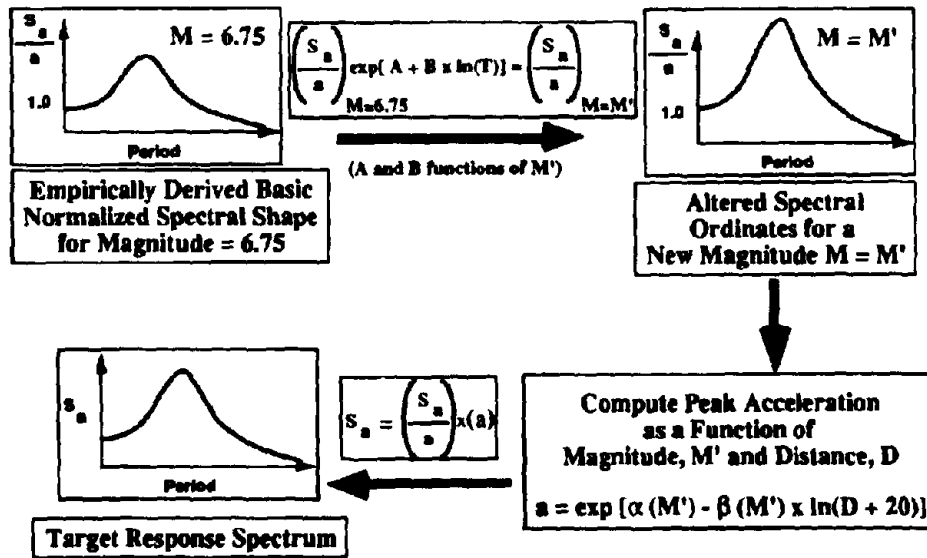


Figure 1. Schematic of the method used for computing the target response spectrum.

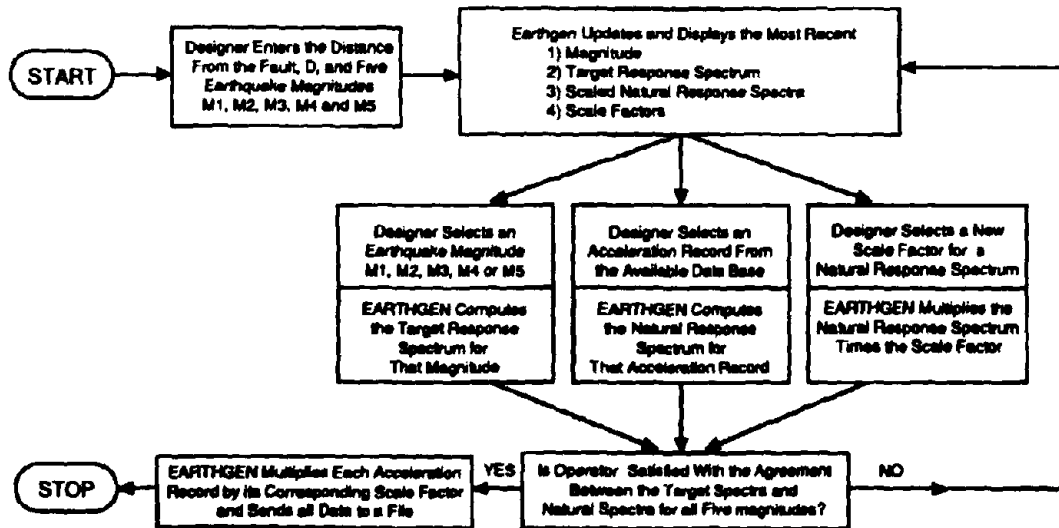


Figure 2. Block diagram of the program EARTHGEN.

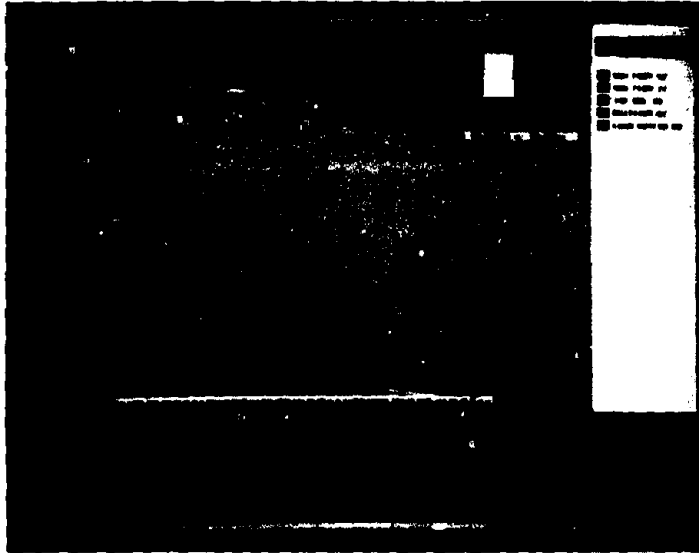


Figure 3. EARTHGEN display of target spectrum and 84th and 16th percentiles.

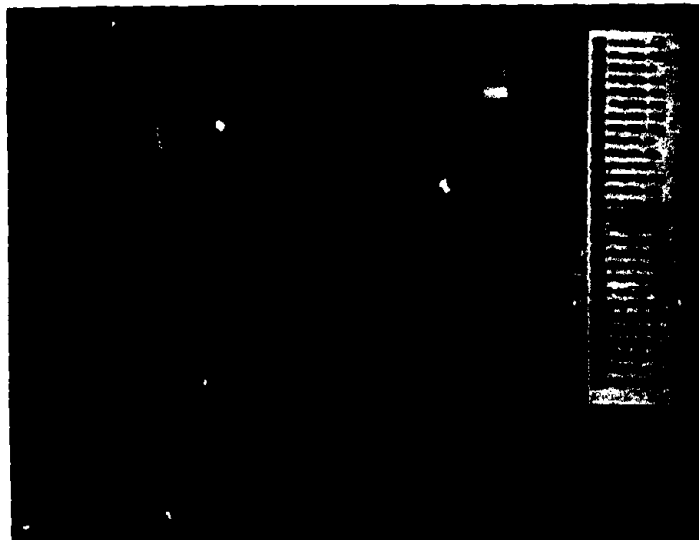


Figure 4. EARTHGEN display of un-scaled natural response spectrum.

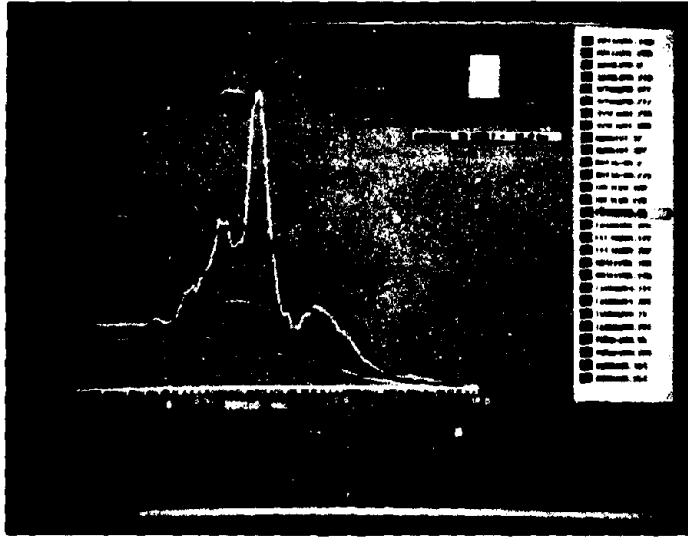


Figure 5. EARTHGEN display of scaled natural response spectrum.

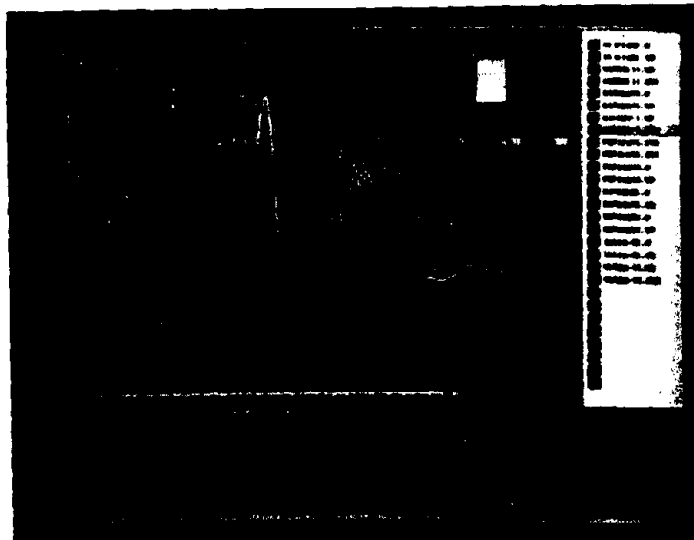


Figure 6. EARTHGEN display of multiple scaled natural response spectra.

AASHTO SEISMIC ISOLATION DESIGN REQUIREMENTS FOR HIGHWAY BRIDGES

Ronald L. Mayes¹, Ian G. Buckle², Trevor E. Kelly¹, Lindsay R. Jones¹
Members, ASCE

Abstract: In October, 1990 the American Association of State Highway Transportation Officials (AASHTO) adopted Guide Specifications for the Seismic Isolation Design of Highway Bridges. This paper overviews the basic concepts and design principles of seismic isolation and discusses the objectives and philosophy of the provisions. A summary of the provisions is presented and the paper concludes with a procedure to compare the performance of isolation systems with different damping values.

Key Words: Base Isolation; Codes; Design Requirements; Highway Bridges; Seismic Isolation

INTRODUCTION

In the past 15 years a relatively new technology called "seismic isolation" has emerged as a practical and economic alternative to conventional design. This concept has received increasing academic and professional attention (ASCE 1989, Applied Technology Council 1986, EERI 1990) and is being applied to a wide range of civil engineering structures. To date there are several hundred bridges in New Zealand, Japan, Italy, Iceland and the United States which use seismic isolation principles and technology for their seismic design. The basic intent of seismic isolation is to increase the fundamental period of vibration such that the structure is subjected to significantly lower earthquake forces.

One of the major impediments to the implementation of seismic isolation has been the lack of code requirements (Mayes 1990). With liability issues being a major concern to design professionals in today's litigious society many firms have been unwilling to use the technology without the protection of professionally

¹ President, Vice President Engineering, Executive Vice President, Respectively, Dynamic Isolation Systems Inc., 2855 Telegraph Ave., Suite 410, Berkeley, CA 94705

² Deputy Director, National Center for Earthquake Engineering Research, State University of New York at Buffalo, Red Jacket Quadrangle, Buffalo, New York 14261

acceptable code provisions. Thus the October, 1990 adoption of Seismic Isolation Design Requirements by AASHTO (AASHTO 1991) is a key step forward in the more widespread use of seismic isolation. This paper summarizes the AASHTO Guide Specifications for Seismic Isolation Bridge Design and provides a comparison of design forces with those obtained with conventional design requirements. A summary of the design issues for isolation systems is also presented.

OBJECTIVES OF THE PROVISIONS

In the development of the seismic isolation design requirements for bridges there were three basic objectives as follows:

- To be as consistent as possible with the recently adopted AASHTO Standard Specifications for conventional seismic design.
- To be as consistent as possible with the recently adopted Uniform Building Code provisions for seismically isolated buildings.
- To be applicable to a wide range of possible seismic isolation systems.

The first objective necessitated that the requirements fit within the Seismic Performance Category (SPC) concept of the new seismic design provisions. This concept provides a gradation of requirements from minimal requirements for the lowest category SPC-A with an acceleration coefficient less than 0.10, to the most stringent requirements for the highest category SPC-D with an acceleration coefficient greater than 0.29. The second objective formed the primary basis for the isolation design requirements. Some modifications were required due to the differences between building and bridge structural form and design loads. Others were required to provide consistency with the first objective.

The third objective necessitated that the requirements remain general and as such rely on mandatory testing of isolation system hardware to confirm the engineering parameters used in the design and to verify the overall adequacy of the isolation system. Some systems may not be capable of demonstrating acceptability by test and, consequently, would not be permitted. In general, acceptable systems will:

- remain stable for required design displacements,
- provide increasing resistance with increasing displacement,
- not degrade under repeated cyclic load, and
- have quantifiable engineering parameters (e.g., force-deflection characteristics and damping).

Both static and dynamic analysis procedures are included (depending on the SPC) and are based on the same level of seismic input and require the same level

of performance from the bridge. The design basis earthquake load corresponds to a level of ground motion that has a 10 percent probability of being exceeded in a 50 year time period, i.e. 475 year return period.

PHILOSOPHY OF THE PROVISIONS

Seismic isolation provides a significant reduction in the elastic seismic forces the bridge must resist when compared to conventional fixed base design (Buckle et al 1986, 1989, 1990). As a consequence there are two possible design philosophies that can be used and both are included in the AASHTO Seismic Isolation Guide Specifications (AASHTO 1991). The first is to take advantage of the reduced forces and provide the most economical bridge design. This option utilizes the same Response Modification Factors (R-Factors) as the recently adopted AASHTO Standard Specifications and thus provides the same level of seismic safety. The advantage of this design option is that if seismic forces are governing the design of the bridge, cost savings up to approximately 10% of the total bridge cost can be realized (Billings 1985).

The second design option is to provide a bridge with much better seismic performance characteristics than that of a conventional design using the AASHTO Standard Specifications. The intent of this design option is to eliminate or significantly reduce damage (inelastic deformation) to the substructure and abutments. In this case an R-Factor of 1 to 1.5 will ensure essentially elastic response by eliminating the ductility demand on the substructure. In bridges this design option can generally be achieved for similar or less cost than a conventional design. Furthermore, it provides protection for earthquakes that may exceed the 475 year design event.

METHODS OF ANALYSIS

The basic premise of the seismic isolation design provisions (consistent with those for buildings and hospitals) is twofold. First, the energy dissipation of the isolation system can be expressed in terms of equivalent viscous damping; and second, the stiffness of the isolation system can be expressed as an effective linear stiffness. These two basic assumptions permit both the single and multimodal methods of analysis to be used for seismic isolation design.

For sliding systems without a self-centering mechanism or for pure elasto-plastic isolation systems the equivalent viscous damping concept is no longer valid. The equivalent viscous damping formula produces a value that is independent of the coefficient of friction for sliding systems or the yield point for elasto-plastic systems. Furthermore, because these systems lack a restoring force, the Total Design

Displacement may be underestimated. Consequently, it is necessary to perform a nonlinear time history analysis for all seismic isolation systems that have no self-centering mechanism.

Statically Equivalent Seismic Force and Coefficient

For the design of conventional bridges the form of the elastic seismic coefficient (C_s) is

$$C_s = \frac{1.2AS}{T^{2/3}} \quad (1)$$

with S (soil type) values that range from 1.0 to 1.2 to 1.5 for different soil types. A is the Acceleration Coefficient and depends on the location of the bridge in the seismic risk map and T is the fundamental period of vibration. Although the ground response spectrum decreases approximately as 1/T for longer periods, the form given above does not decrease as rapidly as 1/T. In fact, at a period of 2.0 seconds, C_s will be approximately 50% greater than the ground acceleration response spectra. The two major reasons for introducing this conservatism in the design of longer period (tall columns, long spans) conventional bridges is stated in the commentary of the AASHTO *Standard Seismic Specifications* as follows:

- a. In longer period conventional bridges, high ductility demands will be concentrated in a few columns.
- b. Instability of a conventional bridge is more of a problem as the period increases.

For seismic isolation design, the elastic seismic coefficient is directly related to the elastic ground response spectra. This is because the intent of seismic isolation design is to introduce flexibility and damping in specifically designed and tested elements with the goal of eliminating or significantly reducing the ductility demand on the substructures. Consequently, the conservatism of the seismic coefficient required for long period (long span, tall column) conventional bridges is not necessary for short span, regular column height isolated bridges. The form of the seismic coefficient is therefore slightly different from that for a conventional design and, for 5% damping, is given by

$$C_s = \frac{AS_i}{T} \quad (2)$$

In this case, A is the acceleration coefficient, S_i is the site coefficient for seismic isolation design and the 1/T factor accounts for the decrease in the ground response spectra ordinates as T increases. The specific S_i values for the isolation requirements reflect the fact that above a period of 1.0 second, there is a 1.0 to 1.5 to 2.0 relationship for the spectral accelerations for Soil Types I, II and III, respectively

(Figure 12 of AASHTO *Standard Seismic Specifications*). Once again, C_s should not exceed a value of 2.5A.

If the effects of damping are included, the elastic seismic coefficient is given by

$$C_s = \frac{AS_i}{TB} \quad (3)$$

where B is the damping term for the isolation system. Note that for 5% damping, B=1.0.

The quantity C_s is a dimensionless design coefficient, which when multiplied by g produces the spectral acceleration. This spectral acceleration (S_A) is related to the spectral displacement (S_D) by the relationship

$$S_A = \omega^2 S_D \quad (4)$$

where ω is the circular natural frequency and is given by $2\pi/T$. Therefore, since $S_A = C_s \cdot g$

$$S_A = \frac{AS_i}{TB} g \quad (5)$$

and

$$\begin{aligned} S_D &= \frac{1}{\omega^2} \frac{AS_i}{TB} g \\ &= \frac{9.79AS_i T}{B} \text{ inches} \end{aligned} \quad (6)$$

Denoting S_D as D, which is the displacement across the elastomeric bearings, equation 6 is approximated by:

$$D = \frac{10AS_i T}{B} \text{ inches} \quad (7)$$

An alternate form for C_s is possible. The quantity C_s is defined by the relationship

$$F = C_s W \quad (8)$$

where F is the earthquake design force and W is the weight of the structure. Therefore,

$$C_s = \frac{F}{W} = \frac{\sum k_{eff} \times D}{W} \quad (9)$$

where Σk_{eff} is the sum of the effective linear springs of all isolation bearings supporting the superstructure segment. The equivalence of this form to the previous form is evident by recalling that $\Sigma k_{\text{eff}} = \omega^2 W/g$, from which

$$C_s = \frac{\omega^2 W}{g} \times \frac{D}{W} = \frac{4\pi^2}{T} \times \frac{1}{386.4} \times \frac{9.79AS_i T}{B} \quad (10)$$

$$C_s = \frac{AS_i}{BT}$$

Thus in summary, equations 7 and 9 are used to determine the statically equivalent seismic force. The isolated period of vibration is given by

$$T = 2\pi \sqrt{\frac{W}{\Sigma K_{\text{eff}} \cdot g}} \quad (11)$$

The base shear (V), (which is equal to the statically equivalent seismic force) is obtained by substituting equations 7 and 11 into equation 8.

$$V = F = \Sigma K_{\text{eff}} \cdot D \quad (9)$$

$$V = \frac{AS}{TB} \cdot W \quad (12)$$

Single Mode Spectral Analysis

The single mode method of analysis given in Section 5.3 of the AASHTO *Standard Seismic Specifications* is also appropriate for seismic isolation design. In fact, use of the method is simplified with seismic isolation. Steps 1, 2 and 3 of the procedure are not necessary since the use of an isolation system will ensure a simple rigid body deformation pattern of the superstructure.

In Step 4 of the procedure the value of $p_e(x)$, the intensity of the equivalent static seismic loading, is determined as

$$p_e(x) = w(x) \cdot C_s \quad (11)$$

where C_s is calculated by Equation 9 and $w(x)$ is the dead load per unit length of the bridge superstructure. In Step 5 of the procedure the loading $p_e(x)$ is applied to the superstructure to determine the resulting member forces and displacements.

Multimode Spectral Analysis

The guidelines given in Section 5.4 of the *AASHTO Standard Seismic Specifications* are also appropriate for the response spectrum analysis of an isolated structure with the following modifications:

- a. The isolation bearings are modelled by use of their effective stiffness properties determined at the design displacement D (Figure 1).
- b. The ground response spectrum is modified to incorporate the damping of the isolation system (Figure 2).

The response spectrum required for the analysis needs to be modified to incorporate the higher damping value of the isolation system. This modified portion of the response spectrum should only be used for the isolated modes of the bridge and will then have the form shown in Figure 2.

Time History Analysis

When a time history analysis is required for systems with a non-centering capability, it is necessary for the time histories to be frequency scaled so they closely match the appropriate ground response spectra for the site. In addition, the analytical model should incorporate the nonlinear deformational characteristics of the isolation system.

DESIGN DISPLACEMENTS FOR SEISMIC AND OTHER LOADS

Adequate clearance shall be provided for the displacements resulting from the seismic isolation analysis in either of the two orthogonal directions. As a design alternate in the longitudinal direction, a knock-off abutment detail may be provided for the seismic displacements between the abutment and deck slab. Adequate clearance for the seismic displacement must be provided between the girders and the abutment. The shear deflections in the isolators resulting from braking loads, wind loads and centrifugal forces will be a function of the nonlinear force-deflection characteristics of the isolators. Adequate clearance at all expansion joints must be provided for these movements.

DESIGN FORCES FOR SEISMIC PERFORMANCE CATEGORY A

The AASHTO Standard Specification (AASHTO 1991) for conventional design has only two requirements for SPC-A. All bearing and column connections are required to be designed for 0.2 times the dead load and the minimum support

length requirements need to be met. In the isolation design requirements the isolation bearing connections are required to be designed for

$$F = K_{\text{eff}}D$$

where

K_{eff} = Effective linear stiffness of the isolation bearing

D = Displacement of the isolated superstructure using a minimum acceleration coefficient, A , of 0.10.

This permits utilization of the real elastic force reduction provided by seismic isolation and will result in a lower connection design force than conventional design.

DESIGN FORCES FOR SPC B, C, AND D

Design forces for a seismically isolated bridge in SPC B, C and D are obtained using the same load combinations as for a conventionally designed bridge. The two design philosophies discussed previously are incorporated in the determination of the design forces. The provisions permit the use of the same R-factors as conventional design with a lower limit on the design forces being the yield level of the isolation system. This option permits a more economic design with the same performance level as conventional design. If a higher level of performance is desired it is recommended that an R-factor of 1.0 to 1.5 is used to ensure essentially elastic response.

A comparison of the design forces for a conventional and an isolated design can be obtained from the lateral force design equations (AASHTO 1991). The lateral force (V) is the uniform load applied in a manner similar to wind loads and calculated as follows:

$$V = C_s W \quad (1)$$

Conventional $C_s = \frac{1.2AS}{T^{2/3}} \quad (2)$

Isolation $C_s = \frac{AS_i}{T_i B} \quad (3)$

where

A = Acceleration coefficient obtained from the seismic risk map. A varies from 0.4 for SPC D to 0.1 for SPC B. A is less than 0.1 for SPC A.

S = Soil Coefficient (1.0, 1.2 and 1.5 for Soil Types I, II and III, respectively).

S_i = Soil Coefficient (1.0, 1.5 and 2.0 for Soil Types I, II and III, respectively).

T = Period, seconds

T_i = Isolated period seconds

B = Damping Coefficient of the isolation system (1.0 for 5%, 1.2 for 10% and 1.7 for 30%).

For most conventional bridges with column heights less than 30 feet the fundamental period calculated for use in the above equation will be less than 0.6 seconds resulting in C_d attaining its maximum value of 2.5A. A comparison of the elastic design forces resulting from Equations 1, 2 and 3 is given in Table 1, together with the ratio of the conventional to isolated (V_c/V_i) base shear value. It will be noted that seismic isolation provides a factor of 3 to 8 reduction in the elastic forces. In order to compare column, foundation and connection design forces, a factor of 5 reduction will be assumed in the value of elastic base shear (V) for the isolation design. The actual reduction in elastic forces will vary between 3 and 8, and depends on several factors including; the isolation period which generally varies between 1.5 and 2.5 seconds; the soil type, with stiffer soils producing higher factors of reduction; and the damping of the isolation system, with higher damping values producing higher factors of reduction.

Table 2 presents a comparison of the design forces for 3 cases. A conventional design where the elastic force $C_d W$ is obtained, assuming the period of the bridge is less than 0.6 seconds resulting in an elastic force of 2.5AW. For SPC B where A may be as low as 0.1, this results in a lateral force of 0.25W. The two isolation design cases are based on the assumption that there is a factor of 5 reduction in the elastic force with $V = 0.5AW$. The two columns of results presented for an isolation design are the two design alternates permitted by the AASHTO Guide Specifications. The first uses the same R-Factors as conventional design, whereas the second uses an R-Factor of 1. The second design alternate will result in an elastic design with no damage, whereas the use of the same R-Factors will produce the same performance as a conventional design.

It will be noted from Table 2 that when the same R-Factors are used for a conventional and isolation design the reduction in design forces for the isolation design are the same as the elastic force reduction, which in this example is a factor of 5. For the no damage isolated design option ($R=1$) a column design force reduction is only obtained for single columns. However, for the foundations, a factor of 2 to 3 reduction is obtained, and the factor of 5 elastic force reduction is also obtained in the connection design forces.

REQUIRED TESTS OF ISOLATION SYSTEM

The code requirements are predicated on the fact that the isolation system design is based on tested properties of prototype isolators. The testing section of the provisions provides a comprehensive set of tests to both establish the design properties of the system and then determine the adequacy of the tested properties. Systems that have been previously tested with this specific set of tests on similar type and size of isolator units do not need to have these tests repeated.

ELASTOMERIC BEARING DESIGN REQUIREMENTS

Elastomeric bearings which are used for seismic isolation will be subjected to earthquake induced displacements and must therefore be designed to safely carry the vertical loads at these displacements. Since earthquakes are infrequently occurring events, the factors of safety required under these circumstances will be different from those required for more frequently occurring loads. Since the primary design parameter for earthquake loading is the displacement of the bearing, the design procedures must be capable of incorporating this displacement in a logical, consistent manner. The requirements of Section 14.2 of the AASHTO *Standard Specifications* limit vertical loads by use of a limiting compressive stress and therefore do not have a mechanism for including the simultaneous effects of seismic displacements. The British Specifications BE 1/76 and BS 5400 recognize that shear strains are induced in reinforced bearings by both compression and shear deformation. In these codes, the sum of these shear strains is limited to a proportion of the elongation-at-break of the rubber. The proportion (1/2 or 1/3 for service load combinations and 3/4 for seismic load combinations) is a function of the loading type.

Since the approach used in BE 1/76 and BS 5400 incorporates shear deformation as part of the criteria, it can be readily modified for seismic isolation bearings. The design requirements given in the seismic isolation code provisions are based on the appropriate modifications to BE 1/76 and BS 5400.

DESIGN ISSUES FOR ISOLATION SYSTEMS

The global design issues for the isolation system involve the desired isolation period, the base shear, the damping of the system and the required margins of safety for the system. There are many interrelated variables involved in an isolation system design and to provide an overview of how these variables impact the structural design process the new AASHTO seismic isolation design requirements are used.

The displacement across the isolators (D), the elastic base shear (V) and the isolation period (T) are given by the following formulas.

$$D = \frac{10AS_i T_i}{B} \quad (4)$$

$$T_i = 2\pi \sqrt{\frac{W}{K \cdot g}} \quad (5)$$

$$V = KD = \frac{AS_i}{T_i B} \cdot W \quad (6)$$

where

- D = Isolator Displacement, Inches
- K = Overall Isolator Stiffness (GA/Tr for plain reinforced elastomeric isolators where Tr is the total elastomer height).
- V = Elastic Base Shear, Kips
- W = Structure Weights, Kips
- G = Shear Modulus of Elastomer, Kips/Inch.
- Tr = Total Elastomer Heights, Inches

The important design variables are impacted by the isolation system properties as follows:

DISPLACEMENT - The isolator displacement is given by equation 4 and the two isolation system properties that impact isolator displacements, D , are the isolated period T and damping coefficient B . D increases as the isolation period T increases and decreases as the damping coefficient B increases.

BASE SHEAR - The base shear, V , is given by Equation 6 and is inversely proportional to the isolation system period T and damping coefficient B . That is V decreases as both the isolation period T and damping coefficient B increase.

PERFORMANCE COMPARISON OF ISOLATION SYSTEMS

In order to compare the relative performance of isolation systems with different damping values a basis for the comparison must be established. There are three possibilities:

- The isolated structure must have the same base shear.
- The isolated structure must have the same displacement.
- The isolated structure must have the same isolated period.

If different isolation systems have different damping values, these three options are mutually exclusive, i.e. only one of these criteria may be satisfied at any one time. From a structural engineering design perspective, the key design parameter is the equal base shear option since the structure will have the same degree of protection and safety margin regardless of the isolation system used.

This option is evaluated and for the purposes of numerical comparison a 10% damped ($B_{10} = 1.2$) and a 30% ($B_{30} = 1.7$) system will be compared since this is the practical range of currently available systems.

If the elastic base shear of two isolated systems are to be equal then the relationship between the isolated periods and resulting displacements of the two

systems, defined by subscripts 1 and 2, can be derived from Equations 4, 5 and 6 as follows:

	Set $V_{e2} = V_{e1}$	<i>Numerical Comparison</i>	if $V_{10} = V_{30}$
then	$T_2 = r \cdot T_1$		then $T_{10} = 1.4T_{30}$
and	$D_2 = r^2 \cdot D_1$		and $D_{10} = 2.0D_{30}$

where $r = \frac{B_1}{B_2}$

and B_1 and B_2 are the damping factors for the two isolation systems.

Thus, for an equal base shear comparison a 10% damped system will require a 40% longer isolated period, and will experience twice the displacement of a 30% damped system. For an equal displacement comparison a 10% damped system will require a 40% lower period and will produce twice the base shear of a 30% damped system. Clearly from a structural design perspective, the damping of the isolation system is an important design variable.

SUMMARY

Seismic isolation offers particular advantages to bridge structures. Reductions in earthquake loads can be significant and savings can be achieved in the foundations of new designs along with improved seismic performance (elastic response). Isolation also offers an elegant solution to many of the common retrofit problems encountered in existing bridges. Limited experience to date has shown that isolation can be adapted and implemented to meet a wide variety of different site and bridge conditions.

The adoption of the seismic isolation code requirements discussed herein is a key step in the implementation of any new technology and these code requirements should significantly increase the implementation phase of the technology. They provide engineers with professionally acceptable procedures without which, liability issues dominate decision making. The lack of code provisions to date has been an impediment to the more widespread use of the technology and thus these new code requirements are a key step forward in the application of this beneficial technology.

REFERENCES

AASHTO (1991), "Standard Specifications for Highway Bridges," American Association for State Highway and Transportation Officials (AASHTO), 15th Edition, 1989 and Interim Specifications 1990, 1991.

ASCE (1989), "Seismic Engineering: Research and Practice," Proceedings ASCE Structures Congress, May 1989.

Applied Technology Council (1986), "Proceedings of a Seminar and Workshop on Base Isolation and Passive Energy Dissipation," ATC Report No. 17, Palo Alto, CA, 1986.

Billings, I.J. and Kirkcaldie, D.K. (1985), "Base Isolation of Bridges in New Zealand," Proceedings US-NZ Workshop on Seismic Resistance of Highway Bridges, Report No. 12-1, Applied Technology Council, May 1985.

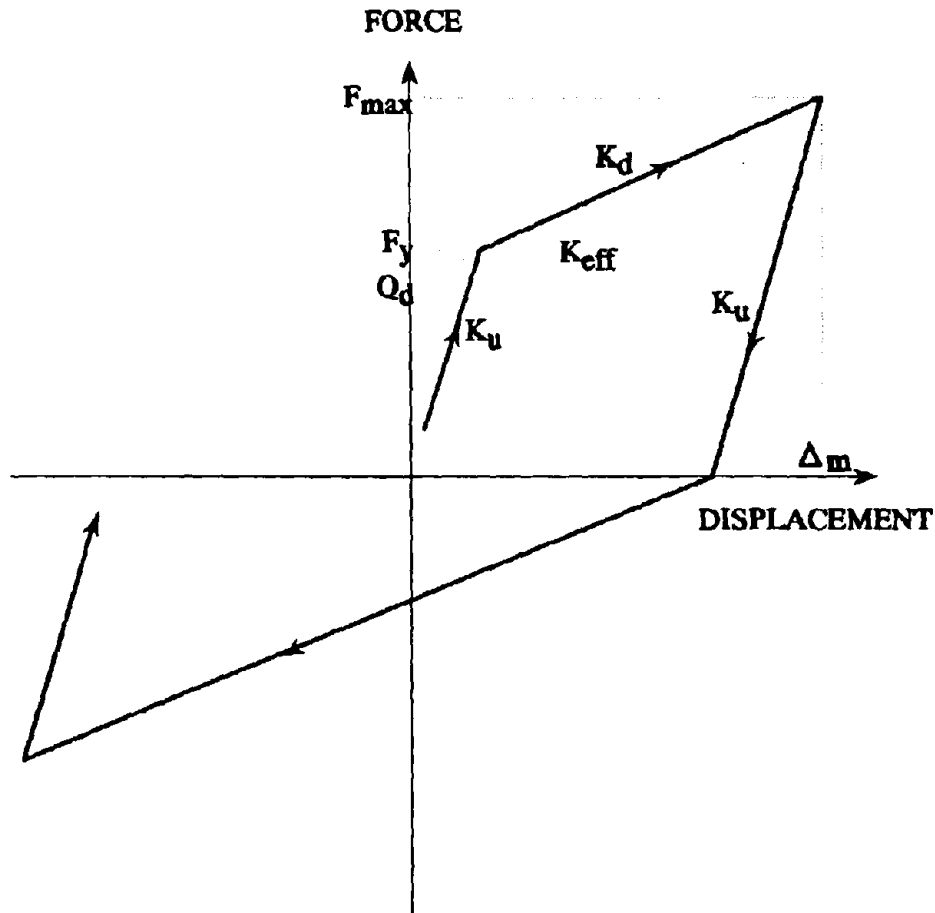
Buckle, I.G., Mayes, R.L. and Button, M.R. (1986), "Seismic Design and Retrofit Manual for Highway Bridges," Computech Engineering Services, Berkeley, CA. Also Published by Federal Highway Administration as Report FHWA/RD-86/006, 1987.

Buckle, I.G. and Mayes, R.L. (1987), "The Application of Seismic Isolation to Bridges," Proceedings ASCE Structures Congress: Seismic Engineering - Research and Practice, pp 633-642, May, 1990.

Buckle, I.G. and Mayes, R.L. (1990), "Seismic Isolation: History, Application and Performance - A World View," Earthquake Spectra, EERI, Vol.6, No.2, May, 1990.

Earthquake Engineering Research Institute (1990), "Seismic Isolation: From Idea to Reality," Earthquake Spectra Journal, Vol. 6, No. 2, May 1990.

Mayes, R.L., Jones, L.R., and Buckle, I.G., (1990), "Impediments to the Implementation of Seismic Isolation," Earthquake Spectra Journal, Theme Issue: Seismic Isolation, EERI, May 1990.



- Q_d = Characteristics strength (kips)
- F_y = Yield force (kips)
- F_{max} = Maximum force (kips)
- K_d = Post-elastic stiffness (kip/inch)
- K_u = Elastic (unloading) stiffness (kip/inch)
- K_{eff} = Effective stiffness
- Δ_m = Maximum bearing displacement

FIG. 1. Characteristics of Elastomeric Bearing with Bilinear Characteristics

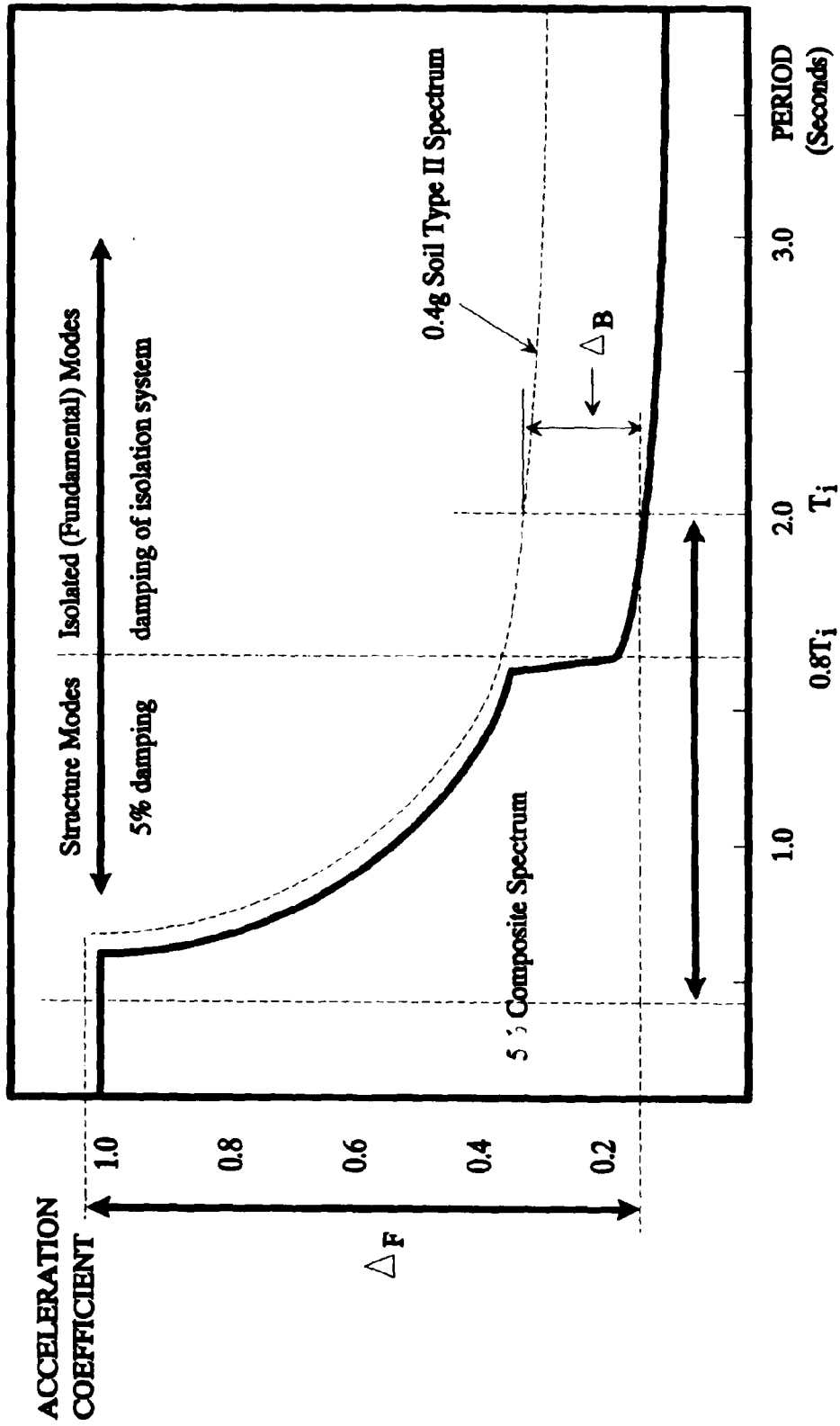


FIG. 2. Development of Composite Response Spectrum

TABLE 1
COMPARISON OF ELASTIC FORCES
($T_{conv} < 0.6$ secs, $B = 1.7$)

Isolation Period T_i	Soil Type I			Soil Type II			Soil Type III		
	V_{conv}	V_{fecl}	$V_c N_i$	V_{conv}	V_{fecl}	$V_c N_i$	V_{conv}	V_{fecl}	$V_c N_i$
1.5 secs.	2.5AW	0.4AW	6.3	2.5AW	0.59AW	4.2	2.5AW	0.78AW	3.2
2.0 secs.	2.5AW	0.3AW	8.3	2.5AW	0.44AW	5.7	2.5AW	0.59AW	4.2

TABLE 2
COMPARISON OF DESIGN FORCES

	Conventional Code R-Factors	Isolation Code R-Factors	Isolation No Damage, $R=1$
Elastic Forces - $C_s W$	2.5A ⁽¹⁾ W	0.5AW	0.5AW
Column Design Forces R = 3 R = 5	$C_s W/R$ ⁽²⁾ 0.8AW 0.5AW	$C_s W/R$ ⁽⁴⁾ 0.2AW 0.1AW	$C_s W$ 0.5AW 0.5AW
Foundation Design Forces ⁽³⁾ R = 3 R = 5	$2C_s W/R$ 1.7AW 1.0AW	$2C_s W/R$ ⁽⁴⁾ 0.3AW 0.2AW	$C_s W$ 0.5AW 0.5AW
Connection Design Forces R = 0.8 R = 1.0	$C_s W/R$ 3.0AW 2.5AW	$C_s W/R$ 0.6AW 0.5AW	$C_s W$ 0.5AW 0.5AW

Notes

1. A = Acceleration coefficient from seismic risk map and varies from 0.1 for SPC B to 0.4 for SPC D.
2. R = Reduction factor. It varies by component and is 3 for a single column, 5 for a multi-column bent, and between 0.8 and 1.0 for all connections.
3. For the purpose of this tabulation, SPC B foundation design forces are used. They are double the column design force. Other values are permitted for SPC C and D.
4. The lower limits on these values are based on the yield level of the isolation system, and these may govern for some Acceleration Coefficients.

BRIDGE MODELING METHOD IN MENSHIN DESIGN

Minoru SHIMADA¹ Katsuyuki DEWA¹ and Tamotsu TANURA²

¹ SHIMIZU CORPORATION, Minato-ku, Tokyo, Japan

² PENTA-OCEAN CONSTRUCTION CO., LTD, Shinagawa-ku, Tokyo, Japan

ABSTRACT

This paper presents the modeling method and the seismic design method of the Menshin bridges. First, comparing the earthquake responses of a Menshin bridge modeled in four simplified frame models, the most appropriate model is proposed. Second, comparing the seismic responses obtained by two types of response spectrum methods, which are "Single-Mode Method" and "Multi-Mode Method", it is observed that there is no remarkable difference between the two methods. The Single-Mode Method is, therefore, recommended to the Menshin design.

INTRODUCTION

Superstructure and substructure are flexibly connected with Menshin bearings. It is, however, expected that the seismic response characteristics of Menshin bridges are more simplified compared with those of non-Menshin bridges.

A frame model is widely used for the seismic design of highway bridges. We have modeled a Menshin bridge in four frame models with different degree of approximation. Through comparing the seismic responses of each model, their differences and characteristics are examined, and the recommended model is proposed accordingly.

The response spectrum method is generally adopted for the seismic design. This method is classified into two methods. One is the Single-Mode Method which considers a fundamental mode of the structure and the other is the Multi-Mode Method which takes into account major modes. Comparing the seismic response accelerations, displacements and response forces obtained by each method, it is observed that there is no remarkable difference between the two methods. As a result the effects of higher vibration modes for Menshin bridges can be definitely negligible.

CHARACTERISTICS OF THE EXAMINED MENSHIN BRIDGE AND STRUCTURE TYPES

Figure 1 shows an examined three-span continuous prestressed concrete bridge. Three types (structure type 1 through 3) of this bridge, with the different pier lengths shown in Table 1, are numerical experimental models. The abutment height is 4.5 m in all models and the cross-section of the abutments and the piers is 2.5 m by 2.5 m. The foundations of abutments and piers are

rigid footings, and they are supposed to be constructed on firm ground. Lead rubber bearings are installed as Menshin devices.

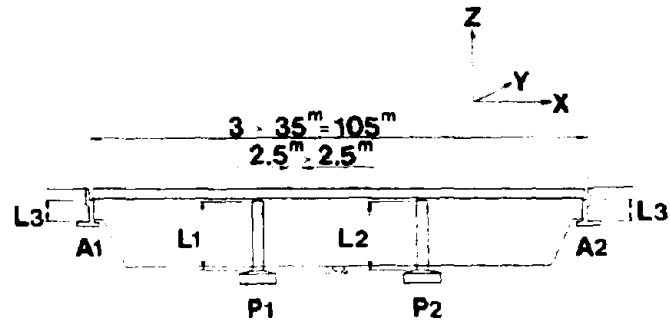


Fig. 1 Dimensions of example bridge

Table 1 Dimensions of structure types

Structure type	Pier P ₁	Pier P ₂	Abutments A ₁ , A ₂
	L ₁ (m)	L ₂ (m)	L ₃ (m)
1	15.0	15.0	4.5
2	7.5	7.5	4.5
3	15.0	7.5	4.5

MODELING OF THE MENSHIN BRIDGE

The Menshin bridge has been modeled by the simplified frame model. Both superstructures and substructures are modeled in beams and lumped masses. The Menshin devices are modeled in equivalent shear springs and substructures are supported by elastic shear and rocking springs of the ground.

To compare the seismic responses and to study the possibility of simplification of the models, four models have been prepared (shown in Figure 2 through 5).

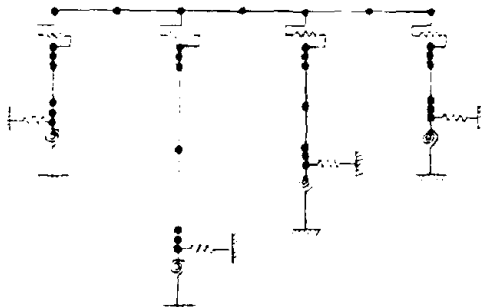


Fig. 2 Bridge design Model 1

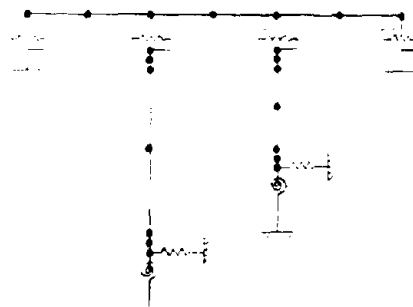


Fig. 3 Bridge design Model 2



Fig.4 Bridge design Model 3

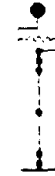


Fig.5 Bridge design Model 4

The characteristics of each model are summarized as follows:
 Model 1 is the strict model of the Menshin bridge.
 Model 2 has neglected the stiffness and mass of abutments, since it is supposed that they have almost no influence on the seismic responses.
 Model 3 has, moreover, neglected the shear and rocking springs of the ground.
 Model 4, the simplest one, is modeled in only one pier of the bridge.

DESIGN ACCELERATION RESPONSE SPECTRUM

Standard acceleration response spectrum ($S_s(T_s)$) is stipulated in Table 2 and Figure 6. Then the design spectrum ($S_A(T_s, h_s)$) is determined by

$$S_A(T_s, h_s) = C_D \cdot S_s(T_s) \quad (1)$$

$$C_D = 1.5 / (40h_s + 1) + 0.5 \quad (2)$$

$$h_s = \frac{\sum (\phi_{s,j}^T \cdot h_j \cdot k_j \cdot \phi_{s,j})}{(\phi_s^T \cdot K \cdot \phi_s)} \quad (3)$$

where

- $S_A(T_s, h_s)$: design acceleration response spectrum corresponds to s-th natural period and s-th damping constant,
- $S_s(T_s)$: standard acceleration response spectrum corresponds to s-th natural period,
- C_D : damping constant factor,
- h_s : s-th modal damping constant,
- $\phi_{s,j}$: s-th modal vector of j-th element,
- h_j : damping constant of j-th element,
- k_j : stiffness matrix of j-th element,
- ϕ_s : s-th total modal vector, and
- K : total stiffness matrix.

The damping constant h_s , which corresponds to each vibration mode, has been calculated to be proportional to strain energy.

Table 2 Standard acceleration response spectrum

Natural Period T (sec)	$T \leq 1.4$	$1.4 < T$
Standard acceleration response spectrum $S_s(T)$ (gal)	700	980/T

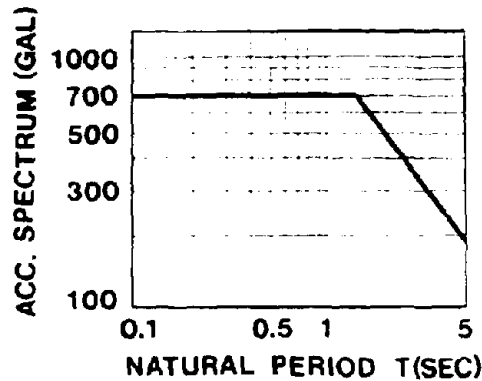


Fig.6 Standard acceleration response spectrum

RESPONSE SPECTRUM METHOD

The Single-Mode Method takes into account a fundamental mode of vibration, while the Multi-Mode Method considers major modes which are considered to be effective to the seismic responses. The Square Root of the Sum of the Squares (SRSS) method is generally applied to this Multi-Mode Method and maximum seismic responses are calculated as follows:

$$\ddot{u}_{max} = (\sum \ddot{u}_s^2)^{1/2} = [\sum (\beta_s \cdot S_a(T_s \cdot h_s) \cdot \phi_s)^2]^{1/2} \quad (4)$$

$$u_{max} = (\sum u_s^2)^{1/2} = [\sum (\beta_s \cdot S_a(T_s \cdot h_s) / \omega_s^2 \cdot \phi_s)^2]^{1/2} \quad (5)$$

$$F_{max} = (\sum F_s^2)^{1/2} = [\sum (K \cdot u_s)^2]^{1/2} \quad (6)$$

where

- $\ddot{u}_s, \ddot{u}_{max}$: response acceleration of s-th mode and maximum response acceleration,
- u_s, u_{max} : response displacement of s-th mode and maximum response displacement,
- F_s, F_{max} : nodal force of s-th mode and maximum nodal force,
- β_s : s-th participation factor, and
- ω_s : s-th natural circular frequency.

RESULTS OF THE BRIDGE MODELING

To study the differences of the bridge modeling, the Multi-Mode Method has been applied to the seismic design. The natural periods, the participation factors and the damping constants of structure type 1 are tabulated in Table 3. From the first to the third natural periods of longitudinal direction (X direction) of the four models are represented. There are slight differences among them, i.e. model 4, the simplest one, indicates the longest first natural period, but, generally, the simpler the model becomes, the shorter the natural periods become (except the case of model 4).

Maximum shear forces, bending moments and relative displacements of the Menshin device are tabulated in Table 4. The percentage of each response value ratio divided by the response of Model 1 is also indicated in the same table.

Figures 7, 8 and 9 show the response accelerations, displacements and relative displacements of the Menshin device, respectively. These results are the responses of structure type 1. Figures 10 and 11 show maximum shear force and bending moment at the bottom of the pier, respectively.

Among the four models, model 4 indicates notable differences. The larger shear forces and bending moments appear particularly in comparison with the other three models. Comparing models 1 and 2, it may be concluded that there is almost no remarkable difference between them. The abutments which are far stiffer than the piers have little influence on the seismic responses and therefore, they can be negligible. On the other hand, when comparing models 1 and 3, there are some differences in both response accelerations and displacements because of the existence of elastic ground springs. However, there is no remarkable difference in the maximum shear forces and the bending moments. Since these differences are less than 9 % compared with those in model 1, both the simpler model 2 and/or 3 can be applicable as a seismic design model.

As for the structure types, though the seismic responses differ, those of all structure types show the same tendency as type 1.

Table 3 Natural periods, participation factors
and damping constants

Model	Mode	Natural period (sec)	Participation factor	Damping constant (%)
1	1st	1.342	1.071	15.32
	2nd	0.290	0.995	18.29
	3rd	0.173	1.436	6.63
2	1st	1.301	1.059	16.53
	2nd	0.290	1.005	17.94
	3rd	0.122	-1.001	5.93
3	1st	1.229	1.043	17.39
	2nd	0.297	0.937	16.60
	3rd	0.072	0.599	5.32
4	1st	1.389	1.062	15.11
	2nd	0.246	0.931	16.85
	3rd	0.072	0.599	5.32
Non- Menshin model	1st	0.720	1.068	5.00
	2nd	0.105	0.782	5.00
	3rd	0.060	-0.261	5.00

Note: Structure type 1

Table 4 Maximum shear forces, bending moments and relative displacements of Menshin device

Model		Maximum shear force (tf)		Maximum bending moment (tfm)	Maximum relative displacement (cm)
		Pier P _i		Pier P _i	P _i Menshin Device
		Top	Bottom	Bottom	
1	Multi Mode	289.9 (100)	351.4 (100)	4931 (100)	9.04 (100)
2	Multi Mode	263.1 (91)	323.8 (92)	4511 (91)	8.21 (91)
3	Multi Mode	287.6 (99)	333.7 (95)	4762 (97)	8.97 (99)
4	Multi Mode	391.2 (135)	437.3 (124)	6333 (128)	12.20 (135)

Note: Structure type 1

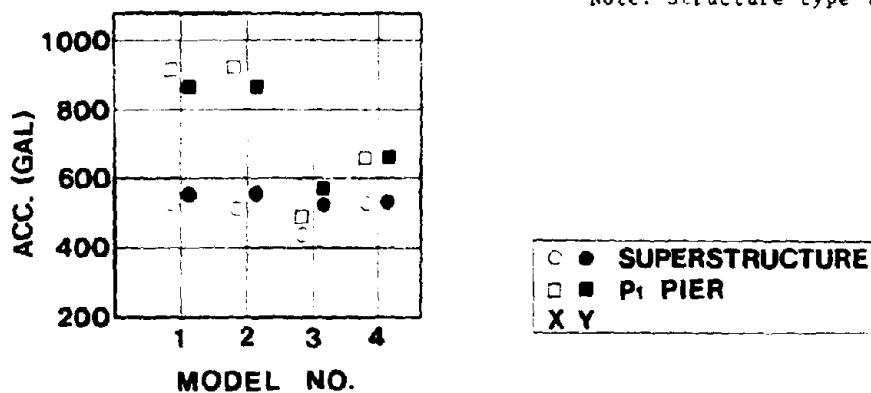


Fig.7 Response accelerations of four models

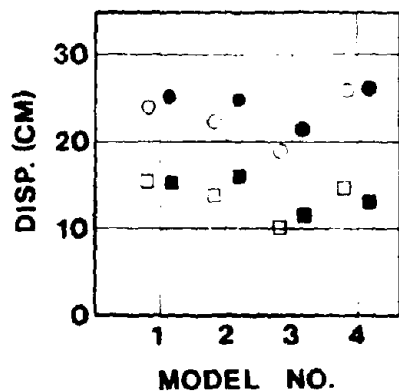


Fig.8 Response displacements of four models

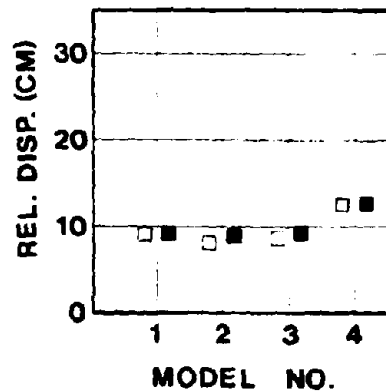


Fig.9 Relative displacements of Menshin device of four models

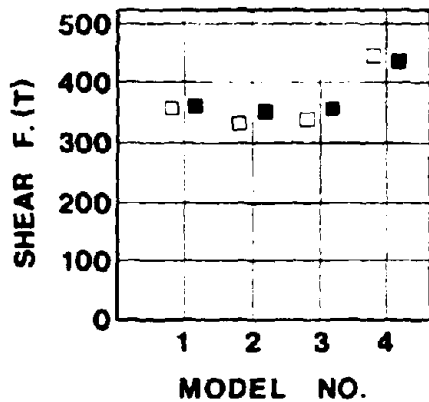


Fig.10 Maximum shear forces of four models

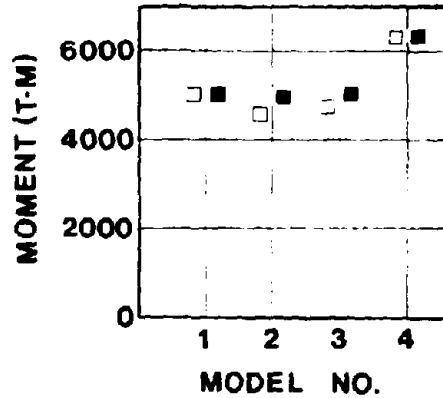


Fig.11 Maximum bending moments of four models

RESULTS OF COMPARING TWO RESPONSE SPECTRUM METHODS

To study the differences of the two response spectrum methods, model 1 has been applied. The maximum shear forces, the maximum bending moments and the maximum relative displacements of the Menshin device for structure type 1 are tabulated in Table 5. The percentage of each Single-Mode response value ratio divided by the Multi-Mode response is also indicated in the same table. A correlation of maximum accelerations obtained by the Single-Mode Method and the Multi-Mode Method is shown in Figure 12. Figures 13 and 14 show correlations of maximum displacements and relative displacements which occur in the Menshin device, and Figures 15 and 16 show correlations of maximum shear forces and maximum bending moments, respectively.

Some of the maximum response accelerations calculated by the Multi-Mode Method are larger than those by the Single-Mode Method, and consequently, it may be considered the response accelerations are influenced by the higher vibration modes. However, there is almost no difference in relative displacements which relate to stiffness and energy dissipation of the Menshin device. While, maximum shear forces and bending moments which decide the cross-section of piers are generally correlative.

The effect of higher vibration modes is less for the Menshin bridge, and hence, the Single-Mode Method is suitable for the seismic design. As for Table 5, there is a high degree of agreement between the responses by the Single-Mode Method and those by the Multi-Mode Method.

Numerical integration time history analysis by the modal method is carried out to compare with the seismic responses by the Single-Mode Method. An artificial earthquake record with the same acceleration spectrum as that of the response spectrum method is applied to this analysis. Figures 17 and 18 show correlations of maximum relative displacements of the Menshin device and the maximum bending moments obtained by these two methods, respectively. There is not significant difference in the seismic responses between the time history analysis and the Single-Mode Method, and hence, this simplified method is recommended to the Menshin design.

Table 5 Maximum shear forces, bending moments and relative displacements of Menshin device

Model		Maximum shear force (tf)		Maximum bending moment (tfm)	Maximum relative displacement (cm)
		Pier P ₁		Pier P ₁	P ₁ Menshin Device
		Top	Bottom	Bottom	
1	Multi Mode	289.9 (100)	351.4 (100)	4931 (100)	9.04 (100)
	Single Mode	288.2 (99)	342.7 (98)	4914 (100)	8.99 (99)
2	Multi Mode	263.1 (100)	323.8 (100)	4511 (100)	8.21 (100)
	Single Mode	261.2 (99)	314.1 (97)	4493 (100)	8.15 (99)
3	Multi Mode	287.6 (100)	333.7 (100)	4762 (100)	8.97 (100)
	Single Mode	286.8 (100)	324.9 (97)	4739 (100)	8.95 (100)
4	Multi Mode	391.2 (100)	437.3 (100)	6333 (100)	12.20 (100)
	Single Mode	390.6 (100)	430.8 (99)	6317 (100)	12.18 (100)

Note: Structure type 1

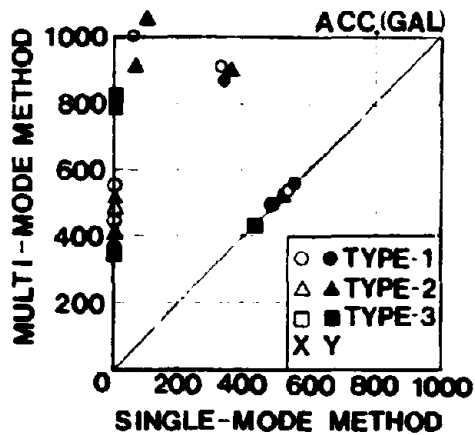


Fig.12 Correlation of maximum accelerations

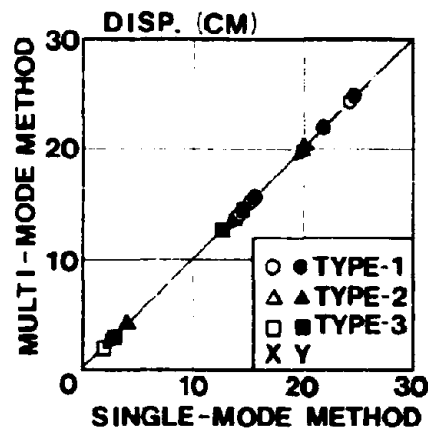


Fig.13 Correlation of maximum displacements

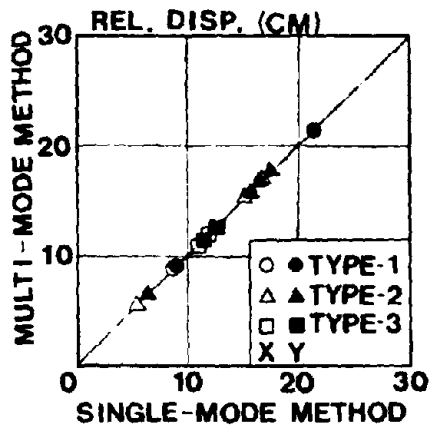


Fig. 14 Correlation of maximum relative displacements of Menshin device

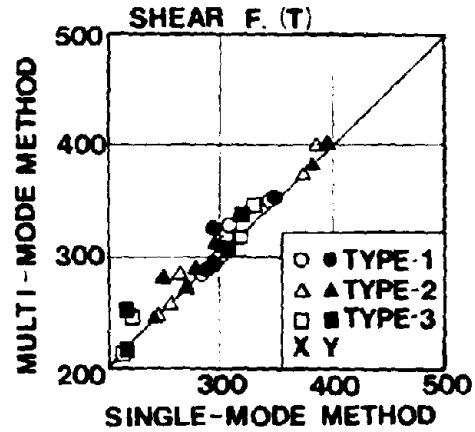


Fig. 15 Correlation of maximum shear forces

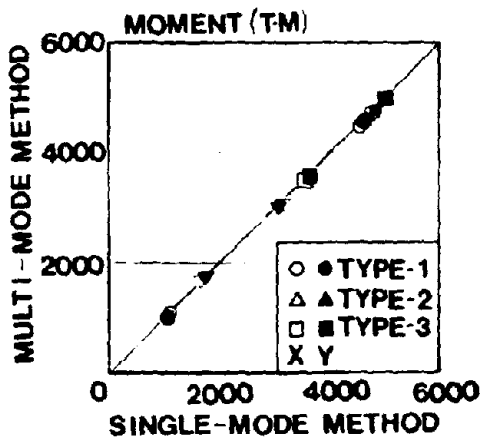


Fig. 16 Correlation of maximum bending moments

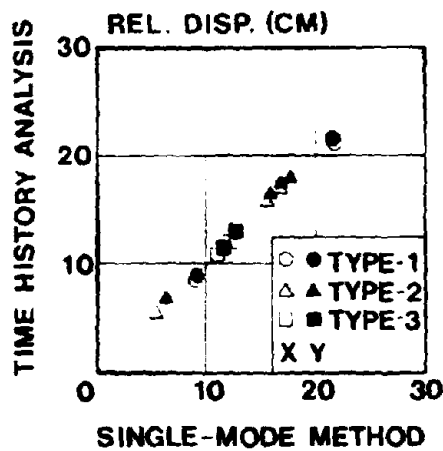


Fig. 17 Correlation of maximum relative displacements of Menshin device

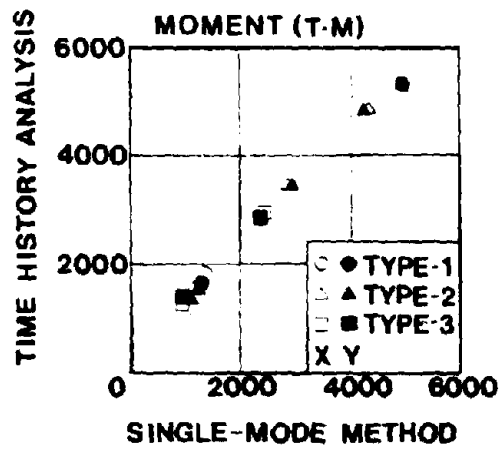


Fig. 18 Correlation of maximum bending moments

CONCLUSIONS

The authors have confirmed that Menshin bridges can be designed using the simplified frame model 2 and/or 3. Because the abutment is far stiffer than the pier and it effects little on the seismic responses of the Menshin bridge. And the shear and rocking springs of the ground can be neglected because seismic displacement of footing on firm ground is negligibly small.

Meanwhile, concerning the design method, it is recommended that the simple Single-Mode Method is an effective design method for the Menshin bridge since there is no remarkable difference in the seismic responses between Single-Mode Method and Multi-Mode Method. That is, the Menshin devices connect the superstructure with the substructure softly, thus the higher vibration modes contribute less to the seismic responses.

ACKNOWLEDGEMENT

This study was made as a part of the joint research program on "Development of Menshin Systems of Highway Bridges" between PWRI and 28 private firms in Japan.

REFERENCES

1. Japan Road Association : "Design Specifications for Highway Bridges, Part V Earthquake Resistant Design, 1990" (in Japanese)
2. Public Works Research Institute (PWRI) and 29 Private Firms : "Development of Menshin Systems of Highway Bridges - Report No.1-", PWRI Joint Research Report No.44, March 1990 (in Japanese)
3. Public Works Research Institute (PWRI) and 28 Private Firms : "Development of Menshin Systems of Highway Bridges - Report No.2-", PWRI Joint Research Report No.60, July 1991 (in Japanese)
4. Tamura,T., Dewa,K., Hosoda,N. and Takahashi,K. : "A Study on Menshin Bridge Design Modeling", Japan Society of Civil Engineers Annual Symposium, 1991 (in Japanese)

DESIGN AND CONSTRUCTION OF MIYAGAWA BRIDGE
(FIRST MENSIN BRIDGE IN JAPAN)

MATSUO Yoshiro¹ and HARA Koji²

1. Director, Road Construction Division, Public Works Department, Shizuoka Prefectural Government,
Shizuoka city, Shizuoka, Japan
2. Technological Staff, Road Construction Division, Public Works Department, Shizuoka Prefectural Government,
Shizuoka city, Shizuoka, Japan

SUMMARY

The Miyagawa bridge in Shizuoka prefecture is the first Menshin bridge constructed in Japan. Although base-isolation bridges have been already constructed in New Zealand and U.S.A., the design method of base-isolation could not be directly applied to the Menshin bridges in Japan because of the different seismic and other conditions such as the higher possibility and larger size of earthquakes, and softer ground. This report introduces the Menshin design method of the Miyagawa bridge to distinguish the difference from the base-isolation design method. Loading tests of the Menshin bearing used in the Miyagawa bridge and field vibration tests of the bridge are also presented briefly, which were carried out prior to the construction and after the completion, respectively, to confirm the dynamic performance of the bearing and the bridge.

INTRODUCTION

All of Shizuoka prefecture where the Miyagawa bridge is located, has been designated as an area under intensified measures against earthquake disasters, since the significant Tokai earthquake is predicted to occur off the coast of Shizuoka in near future. Therefore, the national government and the Shizuoka prefectural government has been already promoting various countermeasures for the prevention of earthquake damages and disasters. As one of the important measures, further improvement of seismic performance of highway bridges is required from the view point of ensuring emergency transportation system during the earthquake.

Under these circumstances, the Miyagawa bridge was selected as one of the pilot Menshin bridges by the "Menshin Highway Bridge Committee", which has been founded in the Road Bureau, Ministry of Construction, in order to discuss the applicability of Menshin design. The bridge was designed and constructed by the Shizuoka prefectural government under supervision of the Ministry of Construction, and opened for public traffic as the first Menshin highway bridge in Japan on March 15, 1991, as shown in Photo 1.



Photo 1 Completed Miyagawa Bridge

DESCRIPTION OF MIYAGAWA BRIDGE

The Miyagawa bridge is a 3-spans continuous bridge with a non-composite steel plate girder, whose total length and width is 108.5m and 10.5m, respectively. The bridge was erected across the Keta river as a renovated bridge of National Highway No.362 in Haruno-cho, Syuchi-gun, Shizuoka prefecture (See Figs.1 to 4). The bridge specifications are shown in the follows.

Horizontal Alignment : $R=\infty$ (Straight Bridge)
Vertical Alignment : $i=0.45\%$
Skew Angle : $\alpha=90^\circ$
Ground Condition : Stiff Ground (Ground Category I in the Specifications (Ref. 1))

Although the Menshin effect could be taken in both longitudinal and transverse direction, the effect only in longitudinal direction was intended in the Miyagawa bridge, and devices for restraining the transverse deformation of Menshin bearings were installed at the bearings. Therefore, the Menshin design was applied in the longitudinal direction while the bridge was designed as an ordinary bridge in the transverse direction.

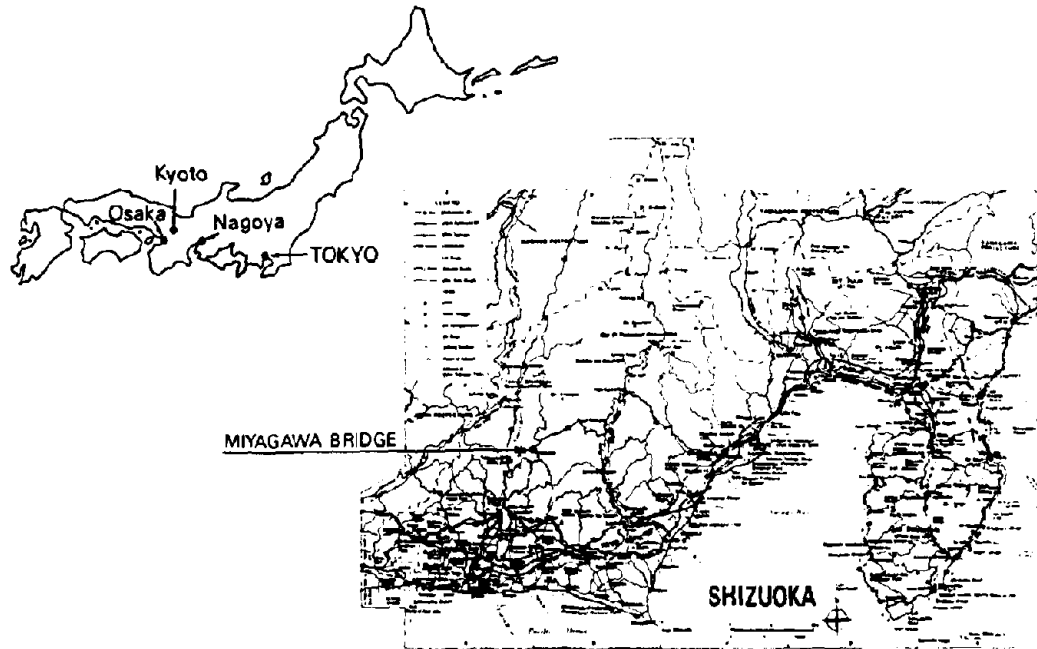


Fig 1 Location of Miyagawa Bridge

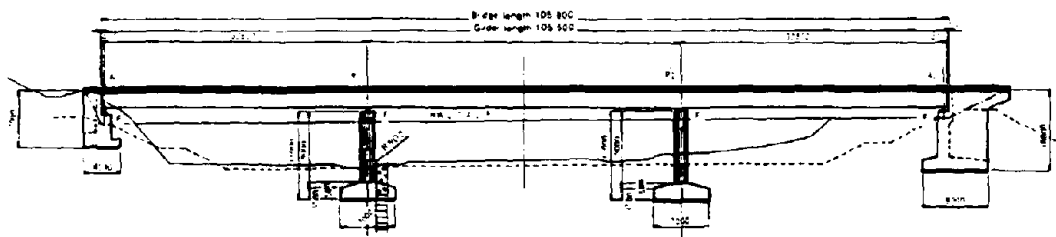


Fig 2 Side View

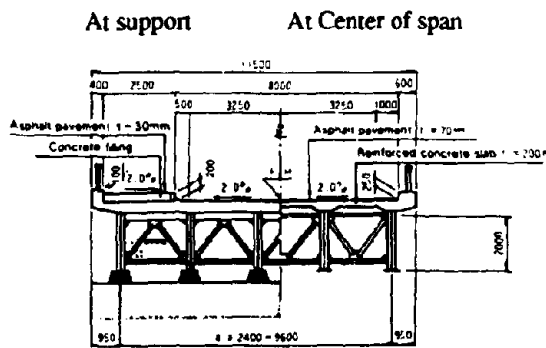


Fig 3 Superstructure

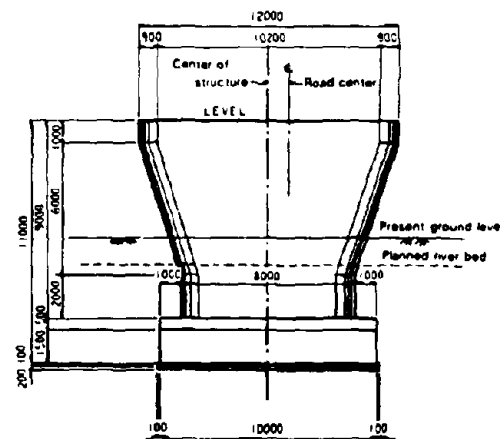


Fig. 4 Bridge Pier

MENSHIN DESIGN OF MIYAGAWA BRIDGE

The Miyagawa bridge was designed in accordance with the regulations of the Design Specifications for Highway Bridges (Ref. 1). We also referred to some items on Menshin design in "Guidelines for Design of Menshin Highway Bridges (Draft)" published by the Technology Research Center for National Land Development in March 1989 (Ref. 2), since there was no previous example of a bridge designed by the Menshin concept in Japan.

Fig. 5 outlines the flow chart of Menshin design used in the Miyagawa bridge. According to the Specifications, two levels of seismic force shall be taken into consideration in the seismic design of highway bridges. The lower level, which is designated hereafter as Level 1, represents the effect of moderate earthquakes which are expected to take place with high possibility. The higher level, which is designated hereafter as Level 2, represents the effect of larger earthquakes with the Richter scale more than 8 which are supposed to take place very rarely, such as the Kanto earthquake ($M=7.9$) of 1923. For the Level 1, allowable stress method is adopted in the Specifications so that the stress developed due to the Level 1 seismic force be less than the seismic allowable stress which is almost equal to the yielding stress. For Level 2, the ductility of reinforced concrete piers shall be checked to avoid brittle failures during significant earthquakes.

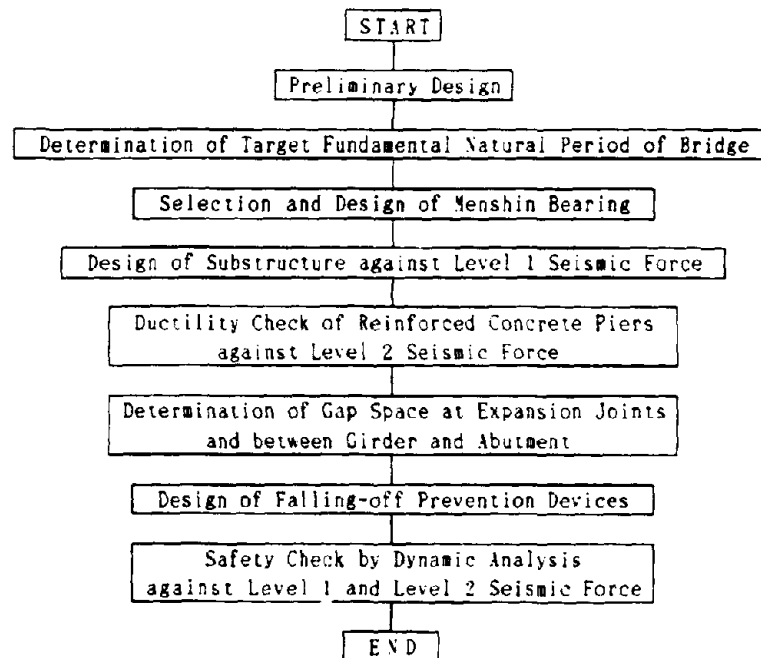


Fig. 5 Flow Chart of Menshin Design

According to the flow chart the preliminary design was done at first to determine the rough configuration, and the Menshin design was performed as follows.

Fundamental Natural Period of Menshin Bridge Since it is significantly required in Menshin bridges to

avoid the resonance vibration between the Menshin deck and the substructure, the fundamental natural period of the Menshin bridge have to be enough longer than that of the non-Menshin bridge where Menshin bearings would be replaced with fixed bearings. The Guidelines recommend that the fundamental natural period of the Menshin bridge should be twice or more longer than that of the non-Menshin bridge to avoid the harmful resonance vibration. As the fundamental natural period of the non-Menshin Miyagawa bridge was computed as 0.30 sec, the target value of the fundamental natural period of the Miyagawa bridge was set at 0.80 sec.

Selection and Design of Menshin Bearing Table 1 shows the Menshin bearings which could be used for highway bridges. After surveying and comparing characteristics of Menshin bearings shown in Table 1, the lead rubber bearing (LRB), which was originally developed in New Zealand and has been often used in many foreign countries, was adopted as Menshin bearings of the Miyagawa bridge. The key point of the comparison was on durability, reliability, compactness, and easiness of being handled during construction and being replaced if damaged.

Table 1 Menshin Devices

No	Description
1	Lead Rubber Bearing (LRB)
2	High Damping Laminated Rubber Bearing (HDR)
3	High Damping Laminated Rubber Bearing with Built-in Plastic Rubber
4	Steel Bar Damper System
5	Laminated Rubber Bearing + Steel Bar Damper + Lead Damper
6	Laminated Rubber + Friction Damper
7	Steel Damper + Laminated Rubber Bearing
8	Slide Bearing + Restoring Spring
9	Laminated Rubber Bearing + Viscous Shear Damper
10	Laminated Rubber Bearing + Steel Bar Damper

Figs. 6 and 7 show the LRB at the abutments and the piers, respectively, which was designed in accordance with the Guidelines. Table 2 gives the specifications of the LRB.

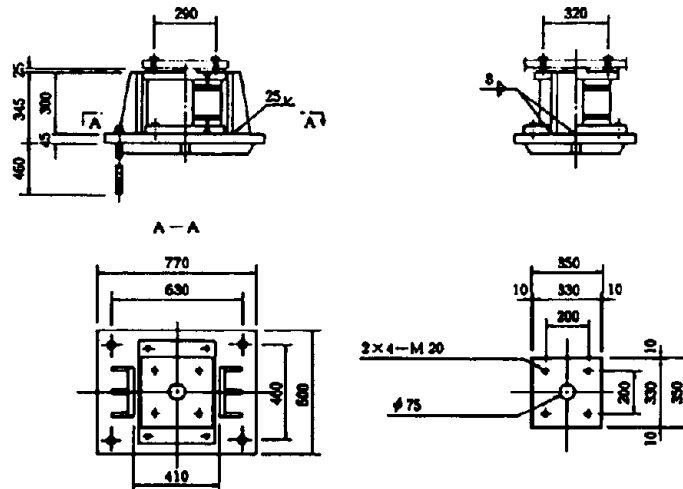


Fig. 6 LRB for Bridge Abutments

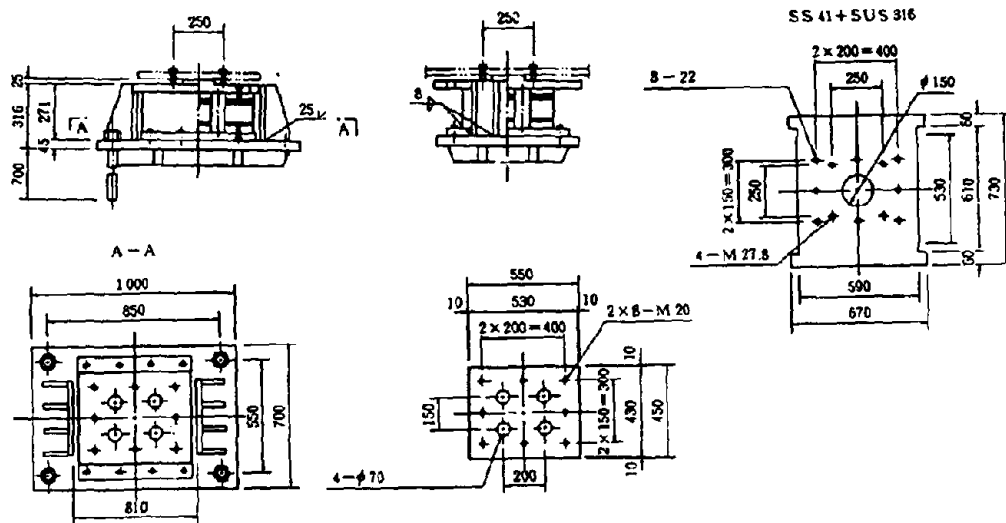


Fig. 7 LRB for Bridge Pier

Table 2 Specifications of LRB

	Notation	Unit	LRB Design Specification	
			Abutment	Pier
Width and Depth of Bearing	$a \times b$	mm	350 × 350	450 × 450
Net Area of Rubber	A_R	cm ²	1,818	2,321
Net Thickness of Rubber	$n \times t_e = \sum t_e$	mm	14 × 9 = 126	10 × 11 = 110
Section of Lead Plug	$N \times \phi$	mm	1 × φ 75	4 × φ 70
Shear Modulus of Rubber	G	kgf/cm ²	8.0	10.0
Shape Factor	S		9.4	10.6
Compressive Stiffness of Bearing	K_V	tf/mm	46.63	156.60
Yield Strength of Lead	Q_d	tf	3.443	12.00
Initial Stiffness	K_u	tf/m	706.3	2463.0
Post-Yield Stiffness	K_d	tf/m	108.7	378.9

Design of Substructures A significant feature of a Menshin bridge is to intentionally distribute the inertia force of a deck to substructures. The distribution ratio of each substructure could be easily adjusted as desired by changing the lateral stiffness of Menshin bearings. Considering the lateral strength of the substructures of the Miyagawa bridge, 38% and 12% of the total inertia force was to be allocated to each pier and each abutment, respectively. The total weight of the deck is 1,320tf and the lateral force coefficient of the Level 1 is 0.2 so that the total inertia force was computed as 264tf by multiplying the weight with the coefficient. The piers and the abutments were designed in allowable stress method against the distributed inertia force of the deck as well as the inertia force of the substructure itself. Figs. 4 and 8 show the configuration and the arrangement of reinforcing bars of the P1 and P2 piers.

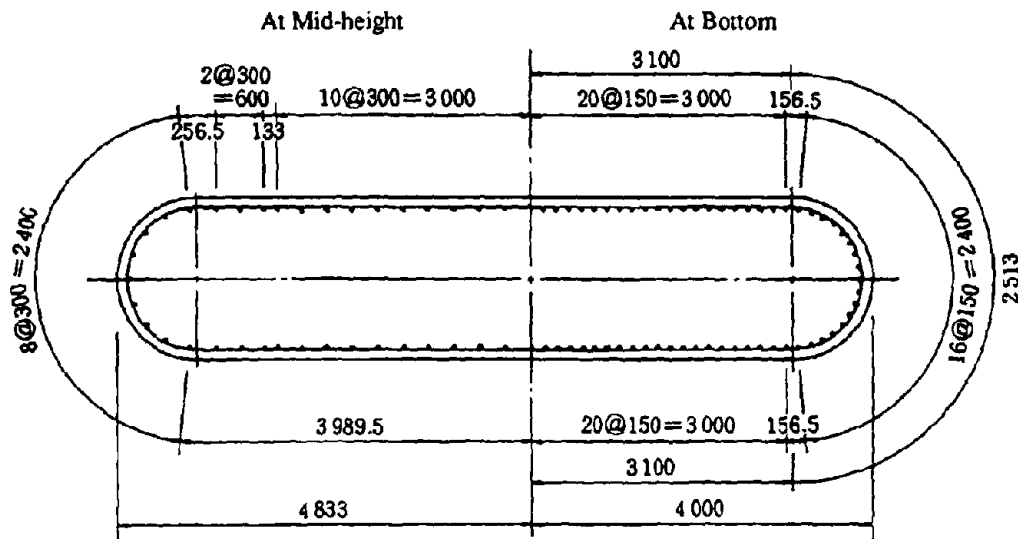


Fig. 8 Cross Section of Piers D 22

Table 3 summarizes the design values of the LRB and the substructures for the Level 1. It should be noted here that the energy dissipation effect of the Menshin bearings was not taken into account when designed against the Level 1 seismic force. The relative displacement in the bearing was about 28mm (22% shear strain in rubber) and 20mm (18% shear strain in rubber) at the abutments and the piers, respectively. The fundamental natural period was computed as 0.76 sec, which is satisfactorily near to the target value of 0.80 sec. The fundamental natural period of 0.76 sec is not so long as that of base-isolation structures. This is because too much elongation would bring problems at the expansion joints discussed later in this paper.

Table 3 Design Values of LRB and Substructures for Level 1

Item	Unit	A 1	P 1	P 2	A 2	
Total of Equivalent Stiffness of Bearing	K_B	tf/m	1,154	4,634	4,685	1,159
Damping Ratio of Bearing	h_B		These are not Considered			
Stiffness of Substructure	K_p	tf/m	40,510	14,090	11,180	31,750
Total Stiffness of Bearing and Substructure	K	tf/m	1,122	3,487	3,718	1,118
Distribution Ratio of Deck Inertia Force	η		0.1231	0.3825	0.3718	0.1226
Fundamental Natural Period of Bridge	T	sec	0.764			
Design Seismic Lateral Force Coefficient	k_n		0.20 (1.0*0.8*1.0*1.25*0.2)			
Design Relative Displacement of Bearing	U_B	mm	28.2	21.8	20.2	28.0
Inertia Force Transmitted to Substructure	F	tf	32.5	101.1	98.2	32.4

Ductility Check of Piers The ductility of the reinforced concrete piers against the Level 2 seismic force was checked to avoid brittle failures during significant earthquakes. Table 4 summarizes the design values of the LRB and the substructures for the Level 2. The relative displacement in the bearing was about 130mm (110% shear strain in rubber) and 110mm (100% shear strain in rubber) at the abutments and the piers, respectively.

Table 4 Design Values of LRB and Substructures for Level 2

Item	Unit	A 1	P 1	P 2	A 2
Total of Equivalent Stiffness of Bearing	K_B tf/m	673	2,450	2,466	676
Damping Ratio of Bearing	h_B	0.117	0.137	0.139	0.119
Stiffness of Substructure	K_p tf/m	40,510	10,300	8,680	17,950
Total Stiffness of Bearing and Substructure	K tf/m	622	1,979	1,920	651.5
Distribution Ratio of Deck Inertia Force	η	0.1270	0.3797	0.3683	0.1250
Fundamental Natural Period of Bridge	T sec	1.010			
Damping Ratio of Entire Bridge	h	0.119 ($C_D=0.760$)			
Design Seismic Lateral Force Coefficient	k_{hc}	0.54 ($1.0 \times 0.7 \times 0.76 \times 1.0$)			
Design Relative Displacement of Bearing	U_B mm	133	109	105	130

The lateral force coefficient for the Level 2 was computed as 0.54 with the fundamental natural period of 1.01 sec, when energy dissipation effect of the LRB was taken into account. However, since the bridge is one of the first Menshin bridges constructed in Japan, the damping effect was disregarded in the ductility check. Therefore, the lateral force coefficient of 0.7 which was obtained by assuming that the energy dissipation of the LRB is zero, was used in the check.

Fig. 9 illustrates the lateral force vs. lateral displacement ($P-\delta$) curve of the piers used for the ductility check. Table 5 shows the result of the check. Since the ultimate flexural strength P_u is lower than the shear strength P_s , the flexural failure is expected to take place. The allowable flexural strength P_a and the allowable ductility ratio μ_a are obtained as :

$$P_a = P_y + (P_u - P_y) / \alpha \quad (1)$$

$$\mu_a = 1 + (\delta_u - \delta_y) / \alpha \delta_y \quad (2)$$

where P_y and δ_y are yielding flexural strength and yielding displacement, P_u and δ_u are ultimate flexural strength and ultimate displacement, and α is a safety factor over yielding to ultimate. Although the safety factor α is usually assumed as 1.5 for an ordinary bridge, α of 3.0 was used for the Miyagawa bridge not to develop progressive plastic hinges at two location, i.e., at the Menshin bearing and at the bottom of the piers, resulting unstable mechanism during significant earthquakes.

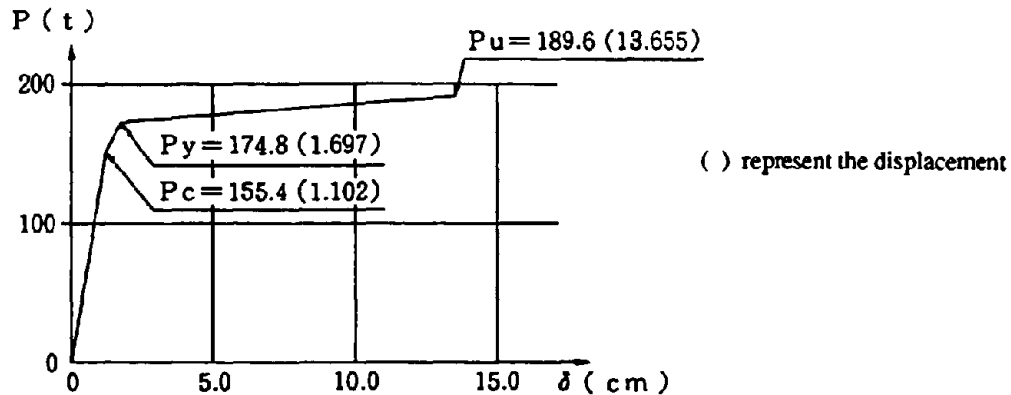


Fig. 9 $P-\delta$ Curve of P1 Pier

Table 5 Result of Ductility Check of Pier

Item	Calculated Value
Ultimate Flexural Strength	$P_U = 189.6 \text{ tf}$
Shear Strength	$P_S = 467.5 \text{ tf}$
Allowable Ductility Ratio	$\mu = 5.672$
Design Seismic Lateral Force Coefficient	$K_{hc} = 1.0 = 1.0 \times 0.7 = 1.0 = 0.7$
Equivalent Seismic Lateral Force Coefficient	$K_{he} = 0.22$
Allowable Flexural Strength	$P_a = 179.7 \text{ tf}$
Lateral Inertia Force	$F = 153.2 \text{ tf} < P_a$

The Level 2 seismic force and the allowable flexural strength was computed as 153.2 tf and 179.7 tf, respectively. By comparing the force and the strength, it was judged that the piers have enough ductility against the Level 2 seismic force.

Determination of Gap Space Since large displacement of a deck relative to a substructure would be developed in Menshin bridges, a sufficient gap should be kept between an abutment and a deck, and at expansion joints. On the other hand, the larger gap at expansion joints would bring vulnerability to the traffic load, especially in Japan due to heavier traffic on highways. Therefore, the following concept on the gap space was adopted in the Miyagawa bridge, that the space between the abutment and the deck should be decided so that the deck would not collide to the abutment when subjected to the Level 2 seismic force, and the space at the expansion joints should be made equivalent to the relative displacement developed there by the Level 1 seismic force. It followed that the space between the abutment and the deck was 150 mm and at the expansion joints was 50 mm. Rubber expansion joints with movable range of ± 115 mm were actually used, considering their installation and size.

Design of Falling-off Prevention Devices Falling-off prevention devices were installed at the deck end and at the bearings on the piers. The device at the deck end consists of two plates fixed to the deck and to the abutment each, and a rod which was inserted into the holes of the two plates to connect them as shown in Fig. 10. When excessive relative displacement between the deck and the abutment is being developed, the collision between the rod and the plates would take place to control the displacement. Since great impact force due to the collision would disturb the Menshin effect, narrower gap space is not appropriate. The gap space of the device installed at the bearing, which is a shear-key restrainer, also should not be too narrow. Therefore, the space of the device at the bearing was set at a value of the relative displacement developed there by the Level 2 seismic force, and the space of the device at the deck end was adjusted at 10mm longer as additional space than the space of expansion joints.

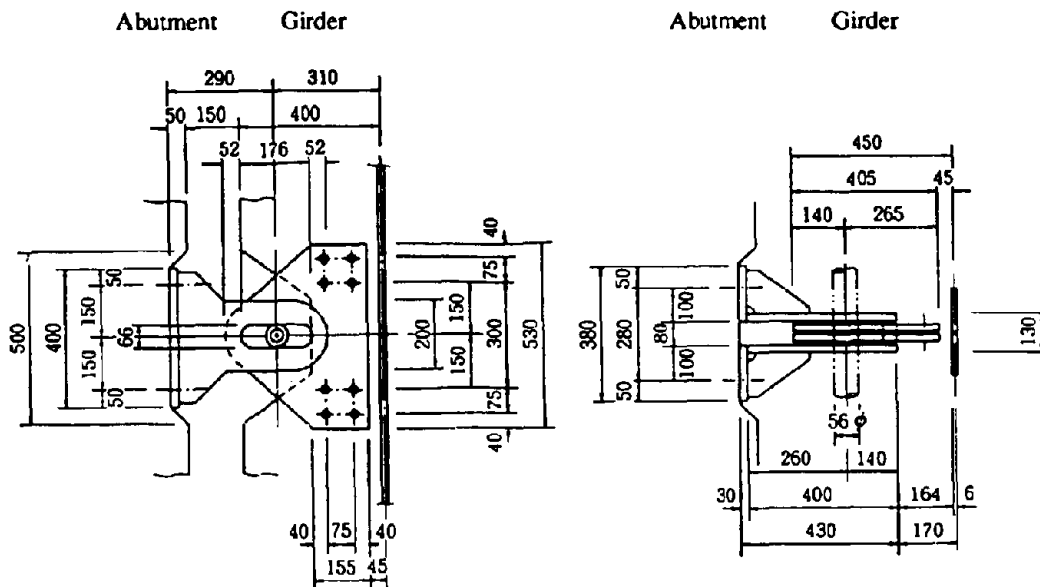


Fig. 10 Falling-off Prevention Devices

Safety Check by Dynamic Analysis The seismic safety as a whole bridge structure was checked by linear dynamic analysis for both the Level 1 and the Level 2, where the LRB was idealized into a linear spring and a linear viscous damper by the equivalent linearizing method. Dynamic analysis was executed by the response spectrum method and the time-history response analysis method which compute the response by the mode-superposition method with eigenvalue analysis. Since the damping effect is of importance in the Menshin design, the damping ratio of each vibration mode have to be properly calculated from the damping ratio of each structural element such as the Menshin bearing and the substructure. The proportional-to-strain-energy damping computing method shown in the Specifications was used, by which the damping ratio of each vibration mode is obtained as a weighted average of damping ratio of each element with proportion to its strain energy.

Table 6 shows the natural period and the damping ratio of each vibration mode. The damping ratio of the LRB, the substructure and the foundation were assumed as 27%, 5% and 10%, respectively, in the Level 1, and 13%, 5% and 10% in the Level 2. The first to fourth vibration modes for the Level 1 are shown in Fig. 11. Since the first is a vibration mode where only the deck is swaying with large shear deformation of the bearing and slight flexural deformation of the substructures, the damping ratio of 24% for the first vibration mode is predominated by the damping ratio of 27% of the bearing.

Table 6 Natural Period and the Damping Ratio

Mode No.	Level 1		Level 2	
	Natural Period (sec)	Damping Ratio	Natural Period (sec)	Damping Ratio
1	0.7724	0.2355	1.0156	0.1216
2	0.2744	0.0324	0.2748	0.0312
3	0.2121	0.1775	1.2419	0.0987
4	0.1941	0.0996	0.2206	0.0938
5	0.1906	0.1080	0.1927	0.0341
6	0.1593	0.0464	0.1594	0.0416
7	0.1425	0.1457	0.1583	0.0848
8	0.1103	0.1523	0.1108	0.1000
9	0.0876	0.1138	0.0885	0.0882
10	0.0812	0.1341	0.0867	0.0790

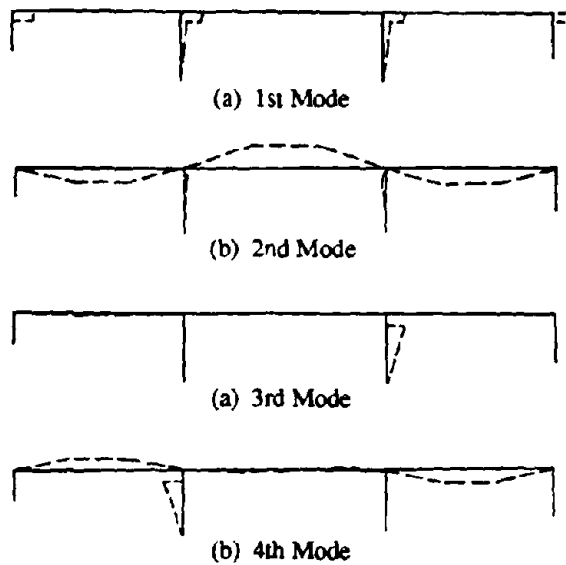


Fig. 11 Vibration Mode

Fig. 12 shows the acceleration response obtained through the time-history response analysis for the Level 1. The wave component with short period is cut in the deck response with reduction of peak response, compared with the pier crest response. Table 7 compares the bending moment and the shear force between the design and the dynamic analysis. The significant difference between the design and the dynamic analysis is the damping effect of the Menshin bearing. While the damping effect was disregarded in the design, it was taken into account in the dynamic response. Therefore, the sectional force developed at the piers, the deck displacement and the relative displacement at the bearing obtained through the dynamic analysis are lower than the design value, and the seismic safety of the Miyagawa bridge as an entire structure was confirmed.

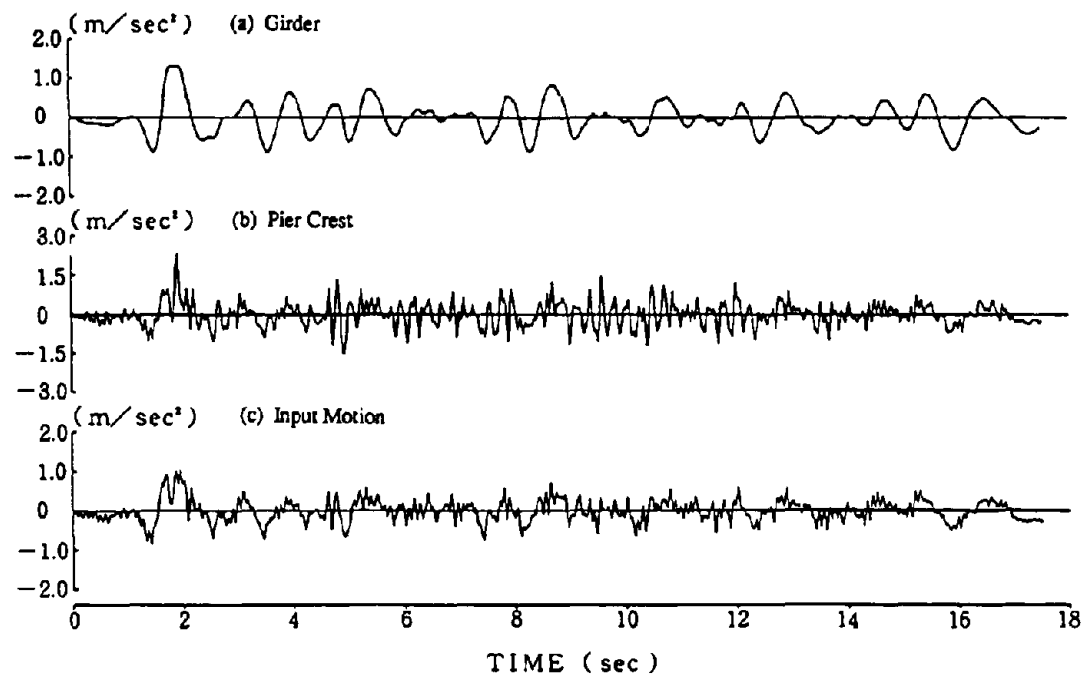


Fig. 12 Acceleration Response

Table 7 Comparison of Sectional Forces of Bridge Piers

Section Number	P 1 Pier				P 2 Pier			
	Shear Force (tf)		Bending Moment(tf·m)		Shear Force (tf)		Bending Moment(tf·m)	
	Design	Dynamic Analysis	Design	Dynamic Analysis	Design	Dynamic Analysis	Design	Dynamic Analysis
1 (Top)	101.0	69.8	0	0	99.0	64.2	0	0
2		72.3	72.2	34.9		68.9	71.3	32.1
3		92.7	288.8	143.3		85.8	285.4	135.3
4		108.8	649.8	367.5		101.2	642.1	342.8
5		123.4	1010.8	642.0		115.1	998.8	595.9
6 (Bottom)	190.0	123.4	1299.6	890.5	189.2	115.1	1284.2	826.0

FIELD TESTS OF MIYAGAWA BRIDGE

Since the Menshin bearing is a key of Menshin design, loading tests of the bearing alone were made prior to the construction and field vibration tests were conducted after the completion to confirm the dynamic performance of the bearing and the bridge.

Loading Tests of Menshin Bearing Prior to the installation of the bearings, the loading tests of the LRB were conducted to confirm the dynamic performance of the bearing alone (See photos 2 and 3). Two kinds of the LRB were manufactured, 11 sets of the LRB were for the abutments and the other 11 sets of the LRB were for the piers. 10 sets of each kind were actually installed in the Miyagawa bridge and each

extra 1 set which was randomly selected among the 11 sets, was used in the loading tests. The tests consists of compression tests, cyclic shear loading tests and shear rupture tests. Table 8 shows the test cases and conditions, and Table 9 summarizes the test results.

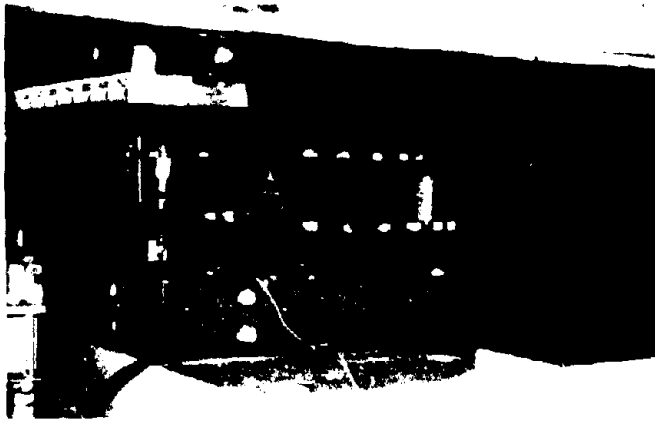


Photo 2 Cyclic Shear Loading Tests

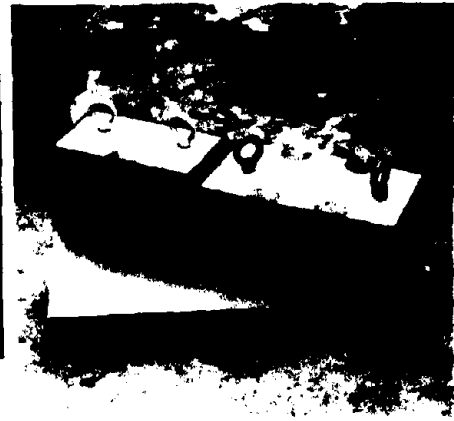


Photo 3 Tested Bearing

Table 8 Test Cases and Condition

(a) Test Cases

Test Item	LRB at Abutment	LRB at Pier
① Compression Test	Done	Done
② Cyclic Shear Loading Test	Done	Done
③ Shear Rupture Test	-	Done

(b) Compression Test

	Units	LRB at Abutment	LRB at Pier
Compressive Load(V)	tf	51.0	161.0
Load Amplitude($R_{max}-R_0$)	tf	± 8.0	± 22.0
Number of Cycles	times	5	5

(c) Cyclic Shear Loading Test

	Units	LRB at Abutment	LRB at Pier	Remarks
Compressive Load	tf	43	139	
Lateral Displacement (Shear Strain)	①	28 (22%)	22 (20%)	Equivalent to Level 1
	②	63 (50%)	55 (50%)	
	③	95 (75%)	83 (75%)	
	④	133 (106%)	108 (98%)	Equivalent to Level 2
	⑤	200 (159%)	162 (147%)	1.5 Times Level 2
Number of Cycles	times	5	5	
Loading Velocity	cm/s	1.5	1.5	
Input Displacement	-	Sinusoidal Wave	Sinusoidal Wave	

Table 9 Test Results

Test Item		Notation	Unit	LRB at Abutment		LRB at Pier	
				Test	Design	Test	Design
Compression Test	Maximum Load	V	tf	58.12	59.00	182.1	183.0
	Compressive Displacement at Maximum Load	δ	mm	1.197	1.270	1.24	1.17
	Static Vertical Stiffness	K_v	tf/mm	48.55	46.63	146.8	156.6
	Dynamic Vertical Stiffness	K_{vd}	tf/mm	100.3	—	312.8	—
Cyclic Shear Loading Test	22% Shear Strain (Corresponding to Level 1)	Q_d	tf	3.80	3.443	11.49	12.00
		K_d	tf/m	103.2	108.7	381.8	378.9
		K_{eq}	tf/m	242.2	231.7	923.0	924.4
		h_{eq}	%	31.7	26.8	30.3	27.7
	50% Shear Strain	Q_d	tf	4.08	3.443	13.98	12.00
		K_d	tf/m	64.8	108.7	233.7	378.9
		K_{eq}	tf/m	130.5	163.4	487.0	597.1
		h_{eq}	%	29.4	19.4	28.8	20.8
	75% Shear Strain	Q_d	tf	4.14	3.443	13.24	12.00
		K_d	tf/m	52.1	108.7	183.0	378.9
		K_{eq}	tf/m	94.6	144.9	342.6	523.5
		h_{eq}	%	27.1	15.0	28.0	16.4
	106% Shear Strain (Corresponding to Level 2)	Q_d	tf	4.06	3.443	12.31	12.00
		K_d	tf/m	48.5	108.7	166.9	378.9
		K_{eq}	tf/m	78.4	134.6	280.3	490.0
		h_{eq}	%	24.0	11.7	26.2	13.7
159% Shear Strain (Corresponding to 1.5 Times Level 2)	Q_d	tf	4.05	—	12.41	—	
	K_d	tf/m	45.7	—	157.3	—	
	K_{eq}	tf/m	65.7	—	235.7	—	
	h_{eq}	%	20.4	—	22.1	—	
Shear Rupture Test	Ultimate Lateral Force at Rupture	F_u	tf	—	—	95.2	—
	Ultimate Lateral Displacement at Rupture	L_u	mm	—	—	307	—
	Ultimate Shear Strain at Rupture	γ_u	%	—	—	278	—

In the cyclic shear loading tests, cyclic lateral force were repeatedly applied to the bearing under a constant compressive load equivalent to the vertical reaction force in the actual bridge in order to examine the stability of the hysteresis loop, the damping ratio, and the dependency of lateral stiffness on lateral displacement. Comparing the test results with the design values shown in Table 9, the damping ratio from the tests drastically exceeds the design value at any lateral displacement. However, the equivalent stiffness gained from the tests was significantly lower than the design value over the shear strain of 75%.

Fig. 13 and Fig. 14 show the hysteresis curves of lateral force and lateral displacement of the LRB. The displacement of the tests shown in Figs. 13 and 14 corresponds to the Level 1 (shear strain of 22%), and the Level 2 (shear strain of 106%), respectively. The hysteresis curve assumed in the design was shown in Figs. 13 and 14 as reference. The above-mentioned difference of the stiffness between the design and the tests in large strain range can be apparently observed in Fig. 14.

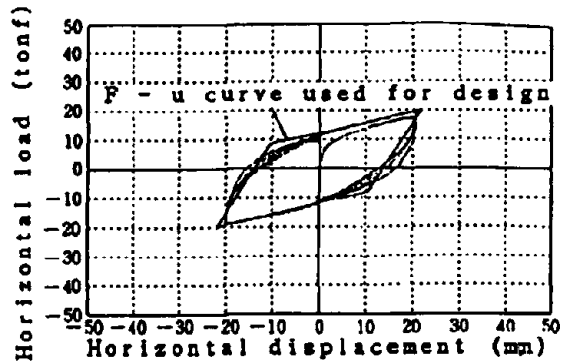


Fig. 13 Load Displacement Curves (Level 1)

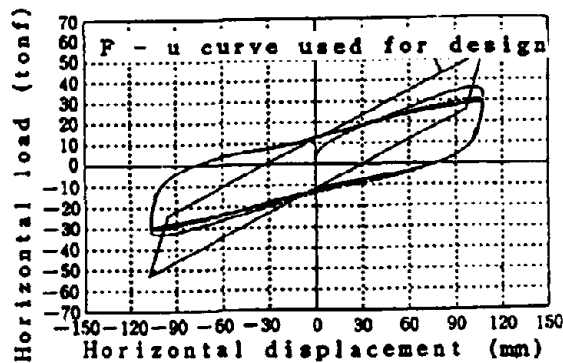


Fig. 14 Load Displacement Curves (Level 2)

The dynamic performance of the whole bridge at the Level 2 was reevaluated with use of the stiffness obtained from the tests, and it was confirmed that the lower stiffness would cause no practical problems on the ductility of the piers and the gap space between the deck and the abutment.

Field Vibration Tests Field vibration tests were conducted under the joint research program with the Public Works Research Institute, Ministry of Construction, in February 1991 prior to the opening in order to verify the Menshin effect. The tests consist of lateral free vibration tests and the traffic vibration tests.

In the lateral free vibration tests, three hydraulic static jacks owned by the Laboratory of Japan Highway Public Corporation were placed between the temporary steel frames assembled under the deck and the A2 abutment as shown in Photo 4. The force capacity of each jack is 180 tf and the maximum stroke is 150mm. The force generated by the jack can be released more rapidly than the regular static jack to develop the free vibration. The deck was forced by the jack to move against the abutment in the longitudinal direction to a certain displacement. The maximum displacement was decided as 8cm so that the total force of the jacks should not exceed the lateral bearing capacity of the abutment. The acceleration on the deck at each substructure (8 points), the acceleration on the crests of the substructures (8 points) and the displacement of the deck relative to each substructure (8 points) were recorded during the free vibration tests.



Photo 4 Hydraulic Static Jack

Fig. 15 shows the relative displacement of the deck at the A2 abutment when the force of the jack was released at 8cm. It is observed in the figure that the free vibration was developed in 0.75 sec after the release, and the deck came nearly to a stop at 4 sec, remaining the residual displacement of 5.4cm by the plastic resistant force of the lead plug. The analysis using single-degree-of-freedom system with a linear spring model and a friction model could successfully assess the field test only in the first 0.75 sec (Ref. 3). The gradual decrease of the relative displacement after 0.75 sec observed in the test, is thought to have to do with the creep of the lead plug. Further analysis is being proceeded to verify the distribution of deck inertia force to the substructures.

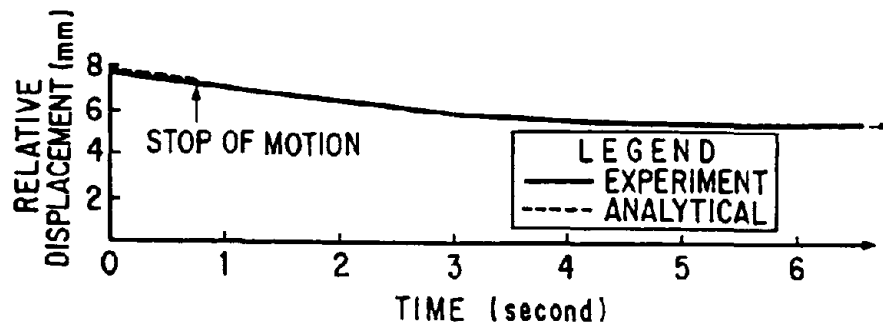


Fig. 15 Relative Displacement of the Deck at A2 Abutment

Traffic vibration tests were carried out by running heavy vehicles with the weight of 20tf. The purpose is to check the harmful vibration of the bridge and surrounding ground. The tests consist of constant speed tests and braking tests. No unusual vibration due to the Menshin bearing was not monitored around the bearing and the surrounding ground.

Strong-earthquake-motion observation is being done to measure the earthquake response and to analyze the dynamic behavior. Accelerometers were installed at three locations, at the deck, at the pier crest and in the bedrock behind the A1 abutment. The analyzed data would be also used to confirm the appropriateness of the Menshin design.

CONCLUDING REMARKES

A short report of the Menshin bridge has been given in this paper, we will be very pleased if this paper becomes a useful reference to assist in the planning for Menshin bridge, which will become more common in future. We hope to report the results of various tests done on the actual bridge, at another time.

ACKNOWLEDGMENT

In conclusion, we'd like to express our sincere gratitude to the many concerned staff members of the Public Works Reserch Institute, and to the Road Bureau in the Ministry of Construction including Dr. Kawashima K and Mr. Hasegawa K of the Public Works Research Institute of the Ministry of Construction, who gave us a kind guidance and encouragement for the various tests, as well as the designing and construction of the Miyagawa bridge, and the Laboratory of Japan Highway Public Corporation. We also hope that they will give us further assistance and guidance. Thank you very much for all your help.

REFERENCES

1. Japan Road Association : "Design Specifications for Highway Bridges, part I~V, 1990" (in Japanese)
2. Technology Research Center for National Land Development : "Guidelines on the Design of Menshin Highway Bridge (Draft) ", A Final Report of A Committee on Menshin Bridge Design Chaired by Pro. Katayama (University of Tokyo), March 1989 (in Japanese)
3. Kawashima K., Hasegawa K., Unjoh S., Nagashima H. and Shimizu H. : Current Research Efforts in Japan for Passive and Active Control of Highway Bridges against Earthquake, 23rd Joint Meeting, U.S.-Japan Panel on Wind and Seismic Effects, U.J.N.R., May 1991
4. Kawashima K., "Present Situation and Future Takes of Menshin Techonology on Highway Bridge", Bridge, Vol. 27, No. 3, March 1991 (in Japanese)
5. Matsuo Y., Oishi A., Hara K. and Yamashita M. : "Design and Construction of Miyagawa Bridge (First Base Isolated Bridge in Japan) ", Bridge and Foundation Engineering, Vol. 25, No. 2, February 1991 (in Japanese)

EQUIVALENT LINEARIZING METHOD OF MENSHTIN DEVICES

Takahashi K.¹, Ozaki D.², Matsubara K.³, Takagi K.⁴,
Makiguchi Y.⁵ and Suizu Y.⁶

- 1 Civil Engineering Division, Okumura Corporation, Minato-ku, Tokyo, Japan
- 3 Civil Engineering Division, Taisei Corporation, Shinjuku-ku, Tokyo, Japan
- 3 Technical Research Center, Hazama-Gumi, Ltd., Yono-shi, Saitama, Japan
- 4 Civil Engineering Division, Nishimatsu Construction Co., Ltd., Minato-ku, Tokyo, Japan
- 5 Technical Dept. 2, Oiles Industry Co., Ltd., Fujisawa-shi, Kanagawa, Japan
- 6 Research and Development Department, Bridgestone Corporation, Kodaira-shi, Tokyo, Japan

SUMMARY

In this paper, the results of seismic response analysis performed on Menshtin devices are presented. This analysis is basically to investigate the validity of the equivalent linearizing method in predicting the seismic response of the Menshtin device. As a result of comparison of equivalent linearizing methods, it was observed that Dynamic Stiffness and Geometrical Stiffness methods are valid for use in equivalent linearization of restoring force characteristics of Menshtin devices.

It was confirmed that the equivalent linear analysis by using these two methods, is a practical analysis for the purposes of design. Reported here are the methods of representing lead-rubber bearing and high-damping rubber bearing in models and also a proposal of a simplified model in determining the properties of Menshtin devices.

INTRODUCTION

In recent years, usage of Menshtin device is expanded by using it in highway bridges, in addition to that in buildings, and successfully applied to practical use¹⁾. While the restoring force characteristics of these Menshtin devices are usually non-linear, the equivalent linearizing method is generally used to facilitate the design of Menshtin bridges.

A fundamental principal of this method is that every hysteresis loop of Menshtin device is first replaced approximately by that of Voigt model with a certain assumed spring constant. Then equivalent damping ratio is defined so as to make the loss of energy per cycle of actual hysteresis loop be equal to that of Voigt body. Jennings²⁾ shows that the equivalent damping ratio defined from a unique hysteresis loop gives different value if the assumed spring constant is different.³⁾

It is the purpose of this paper to examine some of the different equivalent linearizing methods, using six kinds of actual Menshtin devices. And the application of the equivalent linear analysis to seismic response of Menshtin bridge is examined.

DESIGN OF MENSHIN DEVICE

A design was carried out for the Menshin devices for the bridge shown in Fig. 1⁴). The "Guideline on the Design of Menshin Highway Bridge (Draft)"⁵) was referred to in the structural design of the Menshin devices and care was taken to maintain the displacement of the Menshin devices at the seismic force level for ultimate ductility check between 15 and 20cm. The designed Menshin devices and their properties are given in Table 1. They are all hysteresis type Menshin devices and are represented by non-linear models on the basis of the force-displacement curves obtained in tests. Examples of the models for the spiral steel bar damper are given in Fig. 2. The damper can be represented fairly well with a elasto-plastic model, while greater accuracy can be achieved with the Ramberg-Osgood (R-O) model. Test calculations, however, indicate that there is no great difference in the maximum response values, which are of importance in the design, obtained using these two models (Fig. 7). The bi-linear model was selected as a practical non-linear model for use in the design in view of the results Obtained. Similar results were obtained with the other devices listed in Table 1 confirming the decision to use the bi-linear model as the non-linear model.

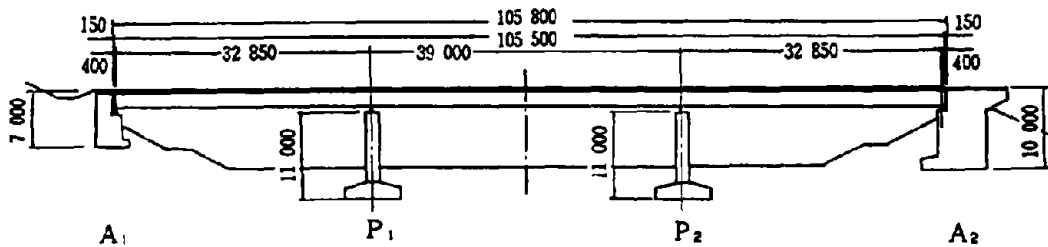


Fig. 1 General View of Three Span Bridge

Table 1 Properties of Menshin Devices

Menshin Devices	Q_v (tf)	K_1 (tf/cm)	K_2 (tf/cm)
Lead Rubber Bearing	60.0	123.2	18.9
High Damping Rubber Bearing	61.1	98.0	19.7
Rubber Bearing + Friction Damper	64.5	46.4	16.9
Elasto Sliding Bearing + Horizontal Spring	49.0	81.7	16.9
Rubber Bearing + Stainless Steel Ring Damper	68.2	32.0	10.8
Rubber Bearing + Spiral Steel Bar Damper	75.9	70.3	15.3

The diagram shows a bilinear hysteresis loop on a Force vs. Displacement graph. The vertical axis is Force (F) and the horizontal axis is Displacement (u). The loop is defined by a yield force Q_v and two stiffnesses: K_1 for the initial elastic portion and K_2 for the post-yield portion.

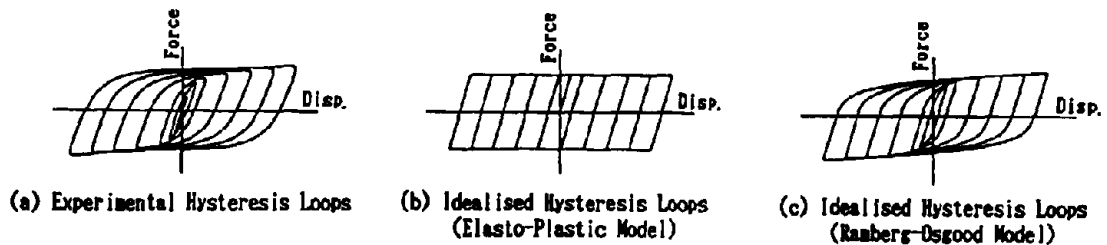


Fig. 2 Hysteresis Loops of Spiral Bar Damper

EQUIVALENT LINEARIZING METHOD FOR MENSHIN DEVICES

There are several methods for equivalent linearizing of the force-displacement curves obtained in tests. Here, the following 3 methods were selected as those appropriate for Menshin devices out of the methods listed by Jennings²⁾. The equations for calculation of the equivalent stiffness and damping ratio when the 3 methods are applied to the bi-linear model are given in Table 2.

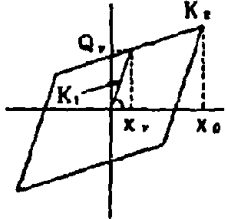
Resonant Amplitude Method (R.A. Method) The initial tangent stiffness is used for the equivalent stiffness. The equivalent stiffness remains constant and the equivalent damping ratio tends to be smaller than in other methods. The calculations involved in this method are the simplest.

Dynamic Stiffness Method (D.S. Method) The equivalent stiffness and damping ratio are determined ensuring an agreement between the stationary resonant frequency and energy absorption. While the non-linearity is evaluated most faithfully, the calculations involved are more complex than in other methods.

Geometrical Stiffness Method (G.S. Method) The gradient of the straight line joining the maximum deformation point on the force-displacement curve and the point of origin is used as the equivalent stiffness. It is the method most widely used.

The equivalent stiffness and damping ratios when the methods are applied to laminated rubber and spiral steel bar dampers are compared in Fig. 3. While there is little difference between the methods in the region with low ductility factors, the differences become greater in the range with ductility factors of 10 to 15 where Menshin devices are used.

Table 2 Equivalent Stiffness and Damping Ratio

1. Resonant Amplitude Method	
$K_{..} = K_1$	$h_{..} = \frac{2}{\pi} \cdot \frac{\mu - 1}{\mu^2} \cdot (1 - \gamma)$
2. Dynamic Stiffness Method	
$K_{..} = K_1 + C_1$	$h_{..} = -\frac{S_1}{2C_1}$
$C_1 = \frac{1}{\pi} \left\{ (1 - \gamma)\theta + \gamma\pi - \frac{1 - \gamma}{2} \sin 2\theta \right\}$	$x_0 > x_v$
$= 1.0$	$x_0 \leq x_v$
$S_1 = -\frac{4(1 - \gamma)}{\pi} \cdot \frac{\mu - 1}{\mu^2}$	$x_0 > x_v$
$= 0.0$	$x_0 \leq x_v$
$\theta = \cos^{-1}(1 - 2/\mu)$	
3. Geometrical Stiffness Method	
$K_{..} = K_1 \cdot \frac{1 + (\gamma - 1)}{\mu}$	$h_{..} = \frac{2}{\pi} \cdot \frac{\mu - 1}{\mu} \cdot \frac{1 - \gamma}{1 + \gamma(\mu - 1)}$
 <div style="display: inline-block; vertical-align: middle; margin-left: 20px;"> $\gamma = K_1 / K_2$ $\mu = x_0 / x_v$ </div>	

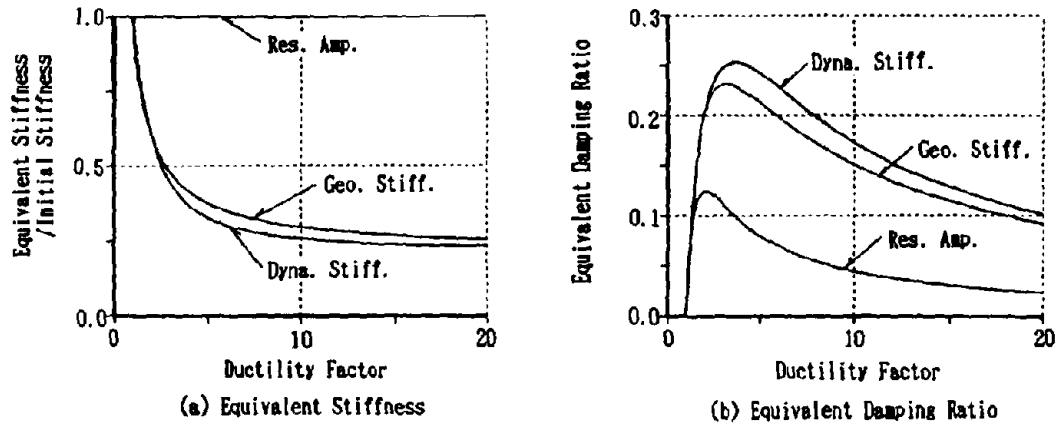


Fig. 3 Ductility Factor vs. Equivalent Stiffness and Damping Ratio

COMPARISON OF RESPONSE RESULTS

Analysis Conditions The pier P_1 in the bridge shown in Fig. 1 was selected for the analytical model and analysis was carried out on the behavior along the bridge axis. The model and its properties are shown in Fig. 4 and Table 3. For the input earthquake motion, the artificial earthquake waves for Group I ground taking into consideration the seismic coefficient method and seismic force level for ultimate ductility check (Levels 1 and 2) in the "Highway Bridge Design Specifications for Highway Bridge - Earthquake Resistant Design" ⁶⁾ were used. The response spectra of the artificial earthquake waves are given in Fig. 5. In the equivalent linear analysis, the maximum response value was used as the effective amplitude and calculations were repeated until the response displacement of the Menshin device agreed with the assumed value.

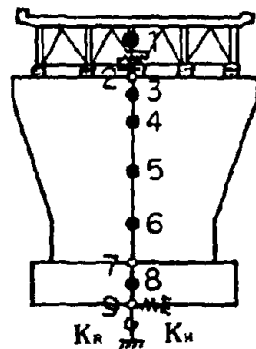


Fig. 4 Analytical Model

Table 3 Properties of Analytical Model

Node No.		E I (t · m ²)	
		Level-1	Level-2
1	2	—	—
2	3	1.423 × 10 ⁷	6.690 × 10 ⁶
3	4	1.381 × 10 ⁷	6.492 × 10 ⁶
4	5	1.233 × 10 ⁷	5.801 × 10 ⁶
5	6	1.023 × 10 ⁷	4.810 × 10 ⁶
6	7	9.173 × 10 ⁶	4.313 × 10 ⁶
7	8	∞	∞
8	9	∞	∞
Spring Const.		K _R = 2.261 × 10 ⁵ (t/m) K _A = 2.770 × 10 ⁶ (t · m/rad)	

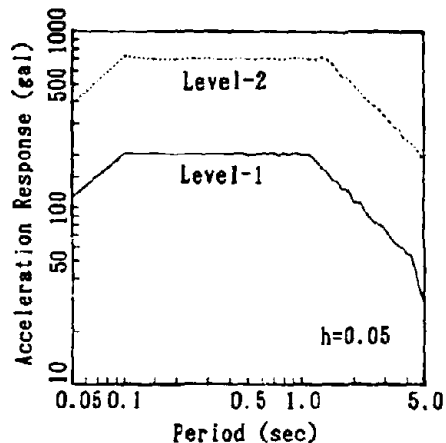


Fig. 5 Acceleration Response Spectra of Input Earthquake Motion

Maximum Response Value The maximum response values obtained through non-linear (bi-linear model) and equivalent linear (R.A, D.S. and G.S. method) analysis are compared in Fig. 6. There was little difference among the equivalent linear analysis values in the response analysis at level 1 and they agree closely with the results of non-linear analysis. It is thought that the small response displacement of the Menshin device (ductility factor: 1 to 5) led to there being no great differences in the external forces accompanying the differences in the frequency characteristics in each method. In the response analysis at level 2, there was little difference in the response values for the D.S. and G.S. methods and both agree closely with the non-linear analysis results. With the R.A. method, however, while there was no great difference in the maximum acceleration, maximum bending moment and shear force, the response displacement was around a half of that obtained in non-linear analysis. This is because the use of the initial stiffness as the equivalent stiffness resulted in a large difference from the non-linear analysis result in the frequency characteristics in regions with large response displacement and indicates that the application range of the R.A. method has been exceeded.

Time History Response Wave The response wave of the superstructure when laminated rubber and spiral steel bar damper are used are shown in Fig. 7 as typical examples. The input earthquake motion was at Level 2. The response waves obtained with the R-O model in Fig. 2 are also shown for reference. The comparison indicates that there is no significant difference between the response waves obtained with the R- and bi-linear models. Although the response waves in the D.S. and G.S. methods agree closely with the non-linear analysis results in the region around the main motion, the long-period components begin to predominate in the small-amplitude region after the main motion, making the results differ from those in the non-linear analysis. This is because the equivalent stiffness and damping ratio are determined using the maximum response value as the effective amplitude. While it is possible to reduce the effective amplitude through use of some reduction coefficient, the methods used here are thought adequate at least for evaluation of the maximum response value.

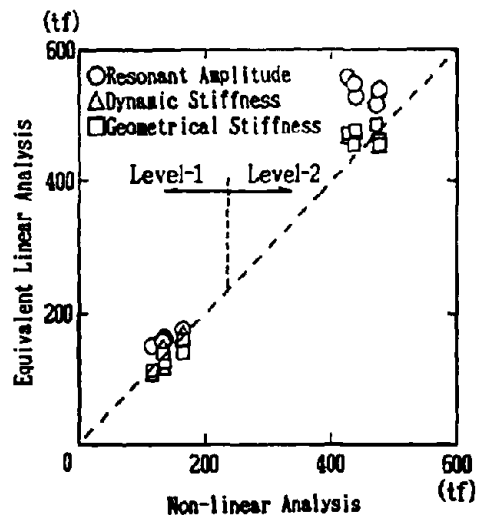
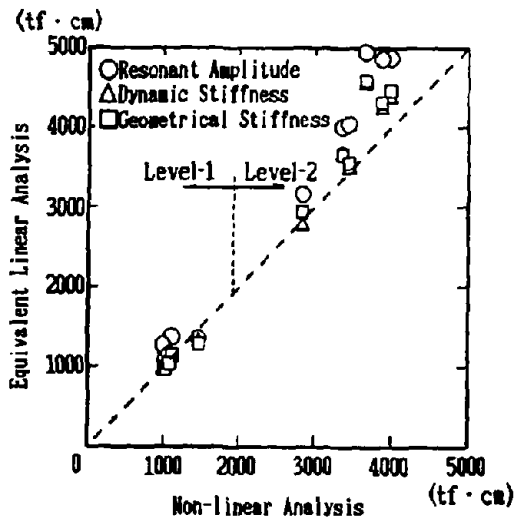
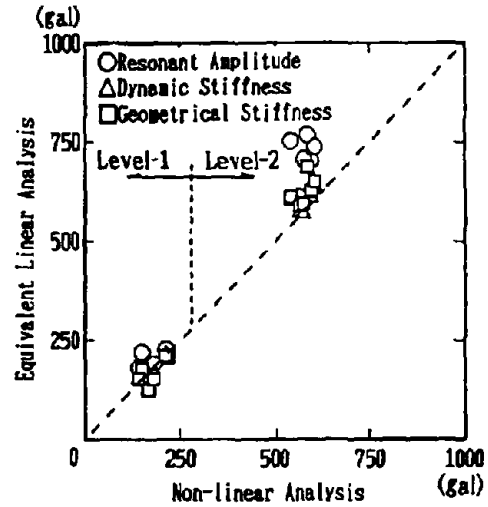
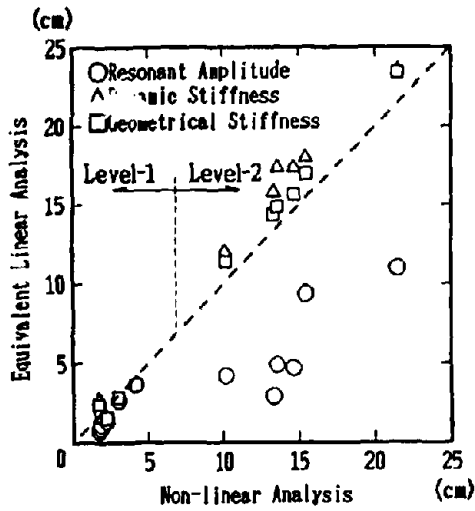


Fig. 8 Comparison between Non-linear Analysis and Equivalent Linear Analysis

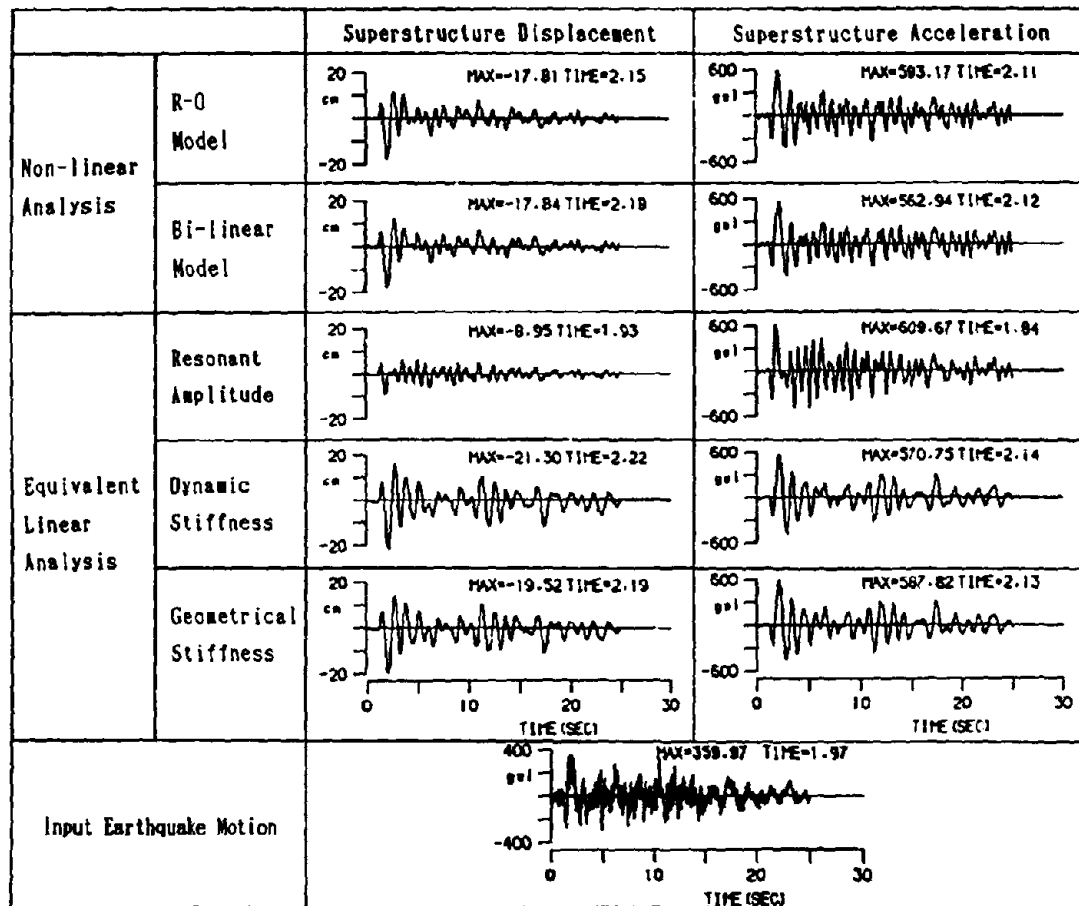


Fig. 7 Response Waves by Non-linear and Equivalent Linear Analysis (Level-2)

MODELING OF FORCE-DISPLACEMENT HYSTERESIS LOOPS FOR LEAD-RUBBER BEARING AND HIGH DAMPING RUBBER BEARING

Lead-rubber bearing (LRB) The modeling of force-displacement hysteresis loop for LRBs adopted in Japan is based on the design guide of the Ministry of Works and Development in New Zealand ⁷⁾. The shape of the idealized hysteresis loop can be defined by three parameters, characteristic dissipator strength: Q_d , post-yield stiffness: K_d and initial stiffness: K_U (see Fig. 8). The methods of estimation for these parameters are shown in the second column of Table 4.

However, the tests carried out recently in Japan to confirm actual dynamic properties of LRBs have made clear that the idealized hysteresis loop disagrees with the actual ones in the following points:

1. Actual characteristic dissipator strength is approximately 10 per cent larger than the idealized one.
2. Actual post-yield stiffness is in good agreement with the idealized one at shearing strain up to 50 per cent. However, it decreases gradually at strain over 50 per cent. In fact, the actual post-yield stiffness at strain of 100 per cent is approximately 50 per cent of that of the idealized one. Accordingly the actual equivalent stiffness is 40 per cent smaller and the equivalent damping ratio is 90 per cent

larger than the idealized ones at the strain of 100 per cent. This means that the post-yield stiffness is not constant but varies depending on the strain.

In Fig. 9, the idealized hysteresis loop is compared with the actual one for the LRB of 450mm*550mm in plain and 110mm in effective thickness of elastomers at 100 per cent strain (110mm displacement). In this paper, a new method is proposed in estimating parameters of the LRB so that the hysteresis loop can be modeled reasonably well.

Based on the test results the characteristic yield stress and shearing stress at the strain γ are taken as Shown in Table 4. These relationships have been substantiated by testings of several LRBs with sizes different to each other at various strain rates. The characteristic dissipator strength, the post-yield stiffness and initial stiffness can be obtained as shown in Table 4.

In Fig. 10, the hysteresis loop estimated by proposed method is shown comparing with the actual one for the LRB of 450mm*550mm in plain and 110mm in effective thickness of elastomers at 100 per cent strain (110mm displacement). The figure shows that they are in good agreement to each other.

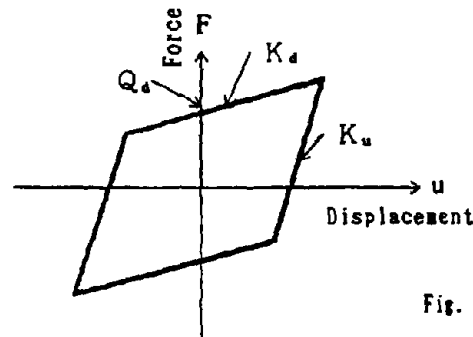


Fig. 8 Idealised Hysteresis Loop

Table 4 Comparison of Method for Estimating LRB Properties

	Present Method	Proposed Method
Characteristic Dissipator Strength Q_d	$Q_d = 78A_p$	$Q_d = 85A_p$
Post-yield Stiffness of Dissipator K_d	$K_d = K_R(1 + 12 \frac{A_p}{A_R})$	$K_d = (F - Q_d) / u$ $F = F_R + F_p$ $F_R = K_R \cdot u$ $F_p = A_p \cdot q(\gamma)$ $q(\gamma) = -283.6\gamma^2 + 183.8\gamma + 85.0$ $(0 \leq \gamma < 0.5)$ $q(\gamma) = 28.3\gamma^2 - 128.1\gamma + 163.0$ $(0.5 \leq \gamma \leq 2.0)$
Initial Stiffness K_u	$K_u = 6.5K_d$	$K_u = 6.5K_d$
where K_R : shear stiffness of without lead (kgf/cm) F : shear force (kgf) A_p : cross-sectional area of lead plug (cm ²) F_R : shear force of rubber without lead (kgf) A_R : area of bearing rubber (cm ²) F_p : shear force of lead (kgf) $q(\gamma)$: shearing stress of lead at strain γ (kgf/cm ²) γ : shearing strain u : displacement (cm)		

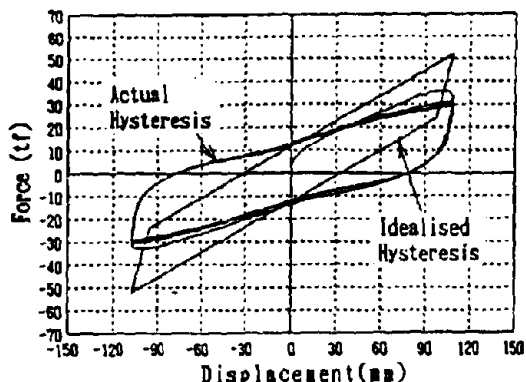


Fig. 9 Comparison of Present Idealised Hysteresis Loop with Actual Hysteresis Loop

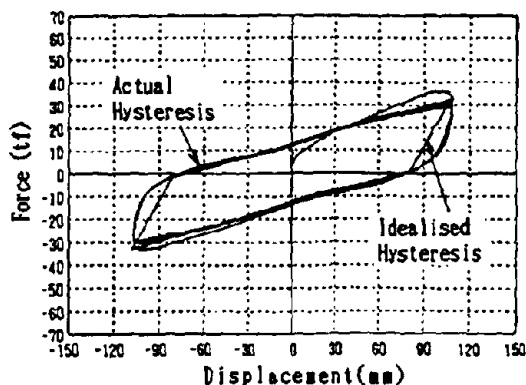


Fig. 10 Comparison of Proposed Hysteresis Loop with Actual Hysteresis Loop

High damping rubber bearing(HDR)

Fig. 11 shows the force-displacement hysteresis curve for HDR, and reveals that restoring force characteristics have a great influence on shearing strains. Fig. 12 shows the test results of the second series carried out subsequent to those of the first series in Fig. 11. Restoring force characteristics vary even in the same strain according to the series: first, second etc., thus indicating its greater dependence on the history of the shearing strain.

Judging from earthquake response analysis, it is quite probable that the maximum acceleration depends on the stiffness of the first series while the maximum displacement, depends on the stiffness of the second series. Consequently, substitution of the equivalent linear model for the hysteresis loop is made in light of shear strains and history of deformation. The formula for calculating the effective stiffness and equivalent damping ratio are as follows: In conformity with the dependence on the history of deformation, the design maximum shear strain is determined beforehand as 200% for high damping rubber to be subjected during earthquakes, and up to 200% as the average of two corresponding values prior to and subsequent to the undergoing of the maximum shear strain. And for the range of over 200% of the strains it is adopted as a given value from the rubber in which no maximum shear strain has over taken place before. (see Fig. 13)

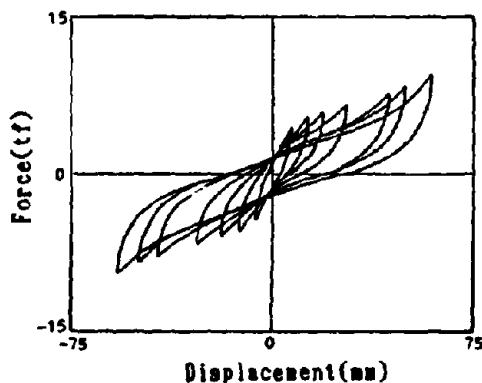


Fig. 11 Hysteresis Loop(1st series)

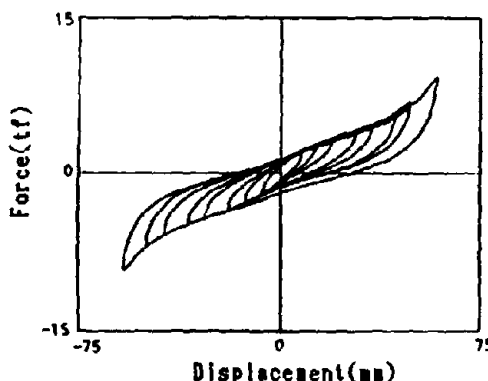


Fig. 12 Hysteresis Loop(2nd series)

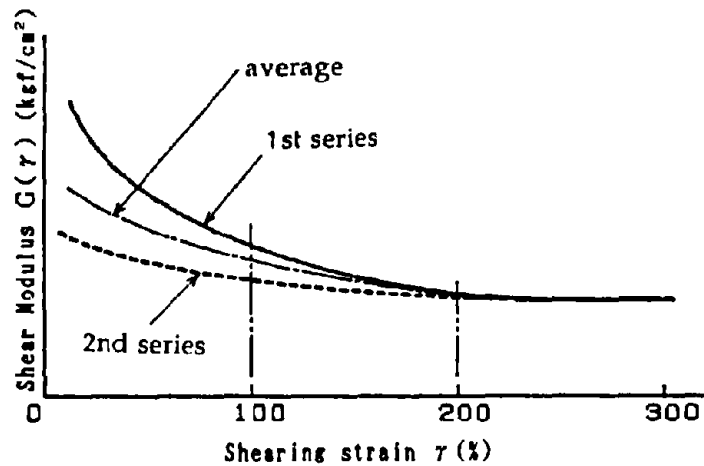


Fig. 13 Influence of Deformation History on Shear Modulus

a. Equivalent stiffness of High damping rubber bearing is estimated from the following Eq. (1).

$$K_B = A \cdot G(\gamma) / t_e \quad (1)$$

where,

K_B : equivalent stiffness of High damping rubber bearing(kgf/cm)

A : area of rubber bearing(cm²)

t_e : total thickness of rubber(cm)

$G(\gamma)$: shear modulus (kgf/cm²)

$$G(\gamma) = a_1 + a_2\gamma + a_3\gamma^2 + a_4\gamma^3 + a_5\gamma^4 \quad (2)$$

a_i : coefficient of influence of strain dimension on shear modulus

γ : shearing strain of rubber

Table 5 Coefficient of Influence of Strain Dimension (case of HDR401 by Bridgestone Corp.)

range of shearing strain	a_1	a_2	a_3	a_4	a_5
$0 \leq \gamma \leq 180\%$	28.3	-48.0	45.7	-21.1	3.88
$180 < \gamma \leq 300\%$	0.31	-6.89	-1.08		
$300 < \gamma$	10.03	0.41			

b. Equivalent damping ratio of High damping rubber bearing is estimated from the following Eq. (3).

$$h_B = b_1 + b_2\gamma + b_3\gamma^2 + b_4\gamma^3 \quad (3)$$

where,

h_B : equivalent damping ratio of High damping rubber bearing(kgf/cm)

γ : shearing strain of rubber

b_i : coefficient of influence of strain dimension on damping ratio

Table 6 Coefficient of Influence of Strain Dimension on Damping Ratio (case of HDR401 by Bridgestone Corp.)

range of shearing strain	b_1	b_2	b_3	b_4
$0 \leq \gamma \leq 200\%$	0.172	-0.00693	0.00276	-0.00694
$200 < \gamma$	0.392	-0.240	0.0618	-0.00561

DETERMINATION OF PROPERTIES OF MENSHIN DEVICE

The equivalent stiffness and damping ratio of the device need to be known for determination of the properties of the Menshin device that would ensure the required Menshin effects. For this, it is vital to evaluate correctly the maximum response generated in the Menshin device during earthquakes. Because of the non-linearity of the restoring force properties of Menshin devices, however, it becomes necessary to repeat the 4 steps of 1. assumption of response in device, 2. determination of equivalent stiffness and damping ratio, 3. response calculations and 4. return to step 1. until the response agrees with the assumed value. It is hardly practical to carry out these complex calculations on the Menshin bridge model (Fig. 14) used for the design of the substructure. Charts have been proposed with calculations already made for various assumed values for factors such as the Menshin device, design input earthquake motion and bridge type but their range of application is extremely limited.

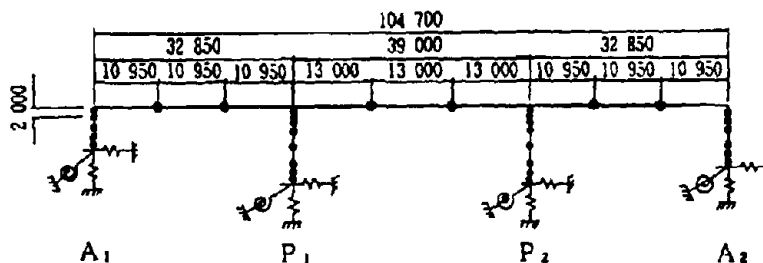


Fig. 14 Multi Degree of Freedom Model

Simplified Model of Menshin Bridge The model shown in Fig. 15 was devised in view of the above with a view to ensuring i) accuracy of the response of the device obtained and ii) simplicity. The primary vibration mode predominates in the response of the device. If the considerations are limited to the primary mode, the superstructure will behave as a rigid body and it was thought possible to represent it with a single degree of freedom model consists of the mass of superstructure and the stiffness calculated from the stiffness of the Menshin device and the substructure. By using such a model, the displacement (u_{Bi}) of the Menshin device can be calculated using the following equation.

$$u_{Bi} = F_i / K_{Bi} \quad (4)$$

where,

F_i : inertia force of each pier ($= K_h \cdot W \cdot K_i / \sum K_i$)

K_h : design lateral seismic force coefficient taking equivalent natural period and damping into account

W : weight of superstructure

$\sum K_i$: equivalent stiffness of Menshin bridge

$$1 / K_i = 1 / K_{Bi} + 1 / K_{Pi} \quad (5)$$

K_{Bi}, K_{Pi} : stiffness of Menshin device and substructure

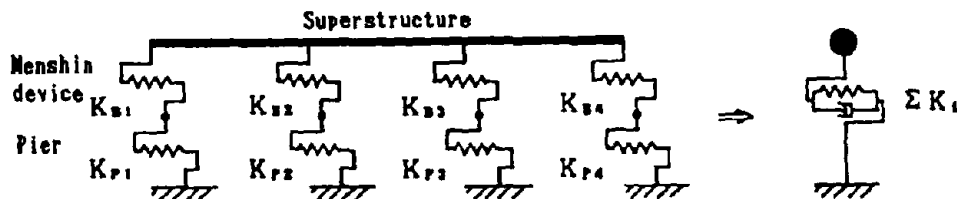


Fig. 15 Single Degree of Freedom Model of Menshin Bridge

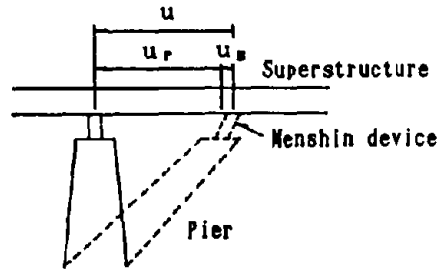


Fig. 16 Displacements of Superstructure and Menshin Device

Investigation of Simplified Model The validity of the proposed simplified model was investigated using the bridge shown in Fig. 1. The spiral steel bar damper in Table 1 was used for the Menshin device and the maximum response value under Level 2 input earthquake motion was sought through repeated calculations. The calculations were made according to 2 methods, one using Eq. (4) for the single degree of freedom model shown in Fig. 15, and the other replacing the bridge as a whole with the frame model shown in Fig. 14 and seeking the response value under statically applied inertia force. The responses obtained with the 2 models are compared in Table 7. The response displacements and equivalent properties agree closely, indicating the validity of the model in Fig. 15. The results indicate that it is possible to determine the properties of the Menshin device and to predict the maximum response through repeated calculations using the single degree of freedom model in Fig. 15. The substructure design can be conducted using the model in Fig. 10 without repeated calculations by using the equivalent stiffness and damping ratio thus obtained.

Table 7 Comparison of Maximum Displacement of Menshin Device

Model	Menshin Device Displacement(cm)				Equivalent Natural Period T_{eq} (sec)	Equivalent Damping Ratio h_{eq} (%)
	A_1	P_1	P_2	A_2		
Static Single Degree of Freedom Model(Fig. 15)	15.6	13.3	12.9	15.3	1.095	11.9
Static Frame Model (Fig. 14)	16.4	13.0	12.3	15.8	1.075	12.0

CONCLUSIONS

1. Comparison was made between the seismic response analysis results when the Menshin device on a single pier multi mass model was represented by a non-linear model and an equivalent linear model. It was discovered that Dynamic Stiffness and Geometrical Stiffness methods are valid methods for use in equivalent linearization of restoring force characteristic of Menshin devices.
2. It was observed that the equivalent linear analysis by using these methods is a practical analysis for the purposes of design.
3. A new method was proposed by which more accurate evaluation than in conventional methods of the properties of lead-rubber bearing and high-damping rubber bearing.

4. The properties of the Menshin device are determined through repeated calculations. A proposal was made for a single degree of freedom model made up of the stiffness calculated from the equivalent stiffness of the substructure and Menshin device and the mass of the superstructure, as a simplified bridge model for accurate prediction of the Menshin device response.

ACKNOWLEDGMENTS

This study was made as a part of the joint research program on " Development of Menshin Systems of Highway Bridges " between PWRI and 28 private firms in Japan.

REFERENCES

- 1) PWRI and 28 Private Firms : " Development of Menshin Systems of Highway Bridges - Report No.2 - ", PWRI Joint Research Report No.60, July 1991 (in Japanese).
- 2) Jennings,P.C." Equivalent Viscous Damping Yielding Structures ", Proc.ASCE,Vol.94,No.EMI,Feb.1968,pp.103-116
- 3) Watanabe,H. et al., " A Consideration on the Equivalent Linearization of Restoring Force Characteristics of Structure ", Proc. of JSCE Vol.2 No.1, April 1985.
- 4) Matsuo,Y. et al., " Design and Construction of Miyagawa Bridge ", Bridge and Foundation Engineering ,Vol.25,No.2,Feb.1991 (in Japanese).
- 5) Technology Research Center for National Land Development : " Guide lines on the Design of Menshin Highway Bridges (Draft) ", March 1989 (in Japanese).
- 6) Japan Road Association : " Design Specification for Highway Bridges, Part V, Earthquake Resistant Design , 1990 " (in Japanese)
- 7) Ministry of Works and Development : Design of Lead-Rubber Bearings, Civil Engineering Division, 818/A, New Zealand , 1983.

SIMPLIFIED DETERMINATION METHOD OF SUBSTRUCTURE DIMENSIONS OF MENSHPIN BRIDGES

Yoshitake SAWAUCHI¹, Yoshihiro HISHIKI² and Kazuhiro UTSUGI³

^{1,2,3} Civil Engineering Design Division, KAJIMA CORPORATION
Minatoku, Tokyo, Japan

SUMMARY

The inertia of the superstructure of a menshin bridge during earthquakes is affected by the characteristics of the substructure and menshin devices of the bridge. It is therefore necessary, in determining the sectional form of the substructure, to perform trial-and-error calculations considering the interaction between the substructure, the menshin devices and the superstructure. This paper proposes a simplified method for determining the initial dimensions of the substructure of a menshin bridge, considering the bridge's dynamic characteristics, describes trial designs based on the proposed method, and discusses the effectiveness of the proposed method.

INTRODUCTION

When an ordinary bridge is designed, spatial, temporal, environmental and other restraints and aesthetic aspects are considered, and the type of structure and details of members which are structurally safe and economical are adopted. In the case of a type of structure which has separate superstructure and substructure, the superstructure is designed first, and based on its reaction and other conditions, the structural type and dimensions of the substructure are determined accordingly. In this case, specifications of the substructure usually do not affect the reaction of the superstructure, and the reaction can be estimated unequivocally. Therefore, the substructure can be designed rather easily.

Also, in the case of a type of structure whose superstructure and substructure are designed as an integral body, structural design can be performed in a similar manner. This comes from the facts that there is a considerable accumulation of design records and data, which the designer can refer to, and those minor design changes of the substructure do not seriously affect sectional forces used for the design of structural members.

However, since a menshin (seismically isolated) bridge is a multiple-point-support continuous bridge which softly supports its superstructure through menshin devices installed on the top faces of the substructure, the dispersibility and the amount of horizontal inertial force of the superstructure during earthquakes are subject to change depending on the characteristics of the substructure and menshin devices. In addition, changes in the stiffness and damping characteristics of the menshin devices are nonlinear. Therefore, even at the stage of preliminary design, the designer is forced to go through a series of trials and errors, which make the design process very time-consuming.

Such a time-consuming trial-and-error approach to the design of menshin bridges could become a serious obstacle to the diffusion and progress of menshin bridges. It is important, therefore, to try to minimize such trials and errors by properly setting the initial dimensions of the substructure at an early stage of menshin (seismic isolation) design. This paper proposes a method for

determination of the initial dimensions of a menshin bridge which can be applied in actual design as easily as in the design of an ordinary bridge.

PROCEDURE

In designing a menshin bridge, the determination of the substructure (cross sections of pier members) and the menshin devices (stiffness of the menshin devices) are of vital importance.

This section describes an efficient design method of a menshin bridge which minimizes trials and errors by simplifying the estimation procedure of the vibration characteristics of the bridge. The proposed method can be applied to designs following the Seismic Coefficient Method of the Japanese Design Specification for Highway Bridges.

According to the Specifications for Highway Bridges, the design lateral force coefficient is calculated as follows:

$$k_h = c_z \cdot c_g \cdot c_i \cdot c_r \cdot k_{h0} \dots \dots \dots (1)$$

where,

- k_h : design lateral force coefficient (to be rounded off to three decimal places)
- k_{h0} : standard design lateral force coefficient (0.2)
- c_z : seismic zone factor
- c_g : ground condition factor
- c_i : importance factor
- c_r : natural period factor

Fig. 1 shows response factors indicated in the Japanese Design Specification for Highway Bridges.

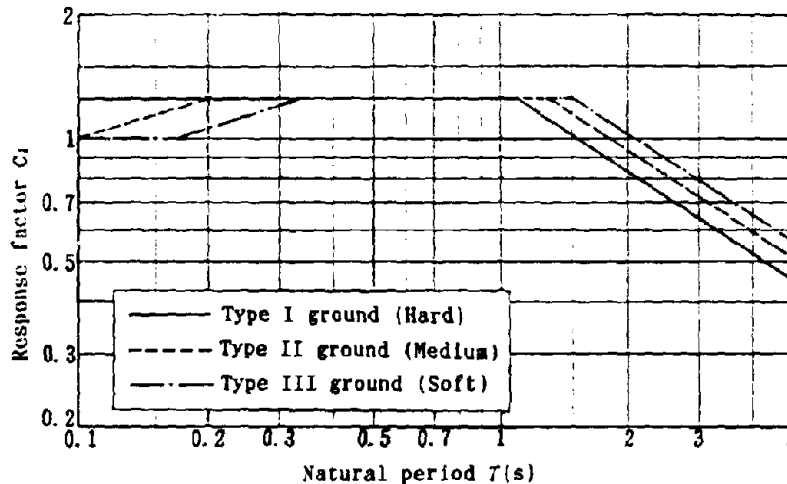


Fig. 1 Response Factor

Assumptions and Basic Understandings The following basic assumptions are made:

- 1) The structural type, structure and spans of the superstructure have already been fixed.
- 2) The cross sections of the substructure are determined by sectional forces

acting on the substructure during earthquakes which are predominant in all loading conditions.

- 3) The predominant vibration mode of the menshin bridge in the bridge axis direction is the primary mode, which dominates the sectional forces of the substructure during earthquakes.
- 4) In the primary mode the girder moves like a swinging log, and relative displacement between the girder and the top face of the pier is absorbed by menshin bearings.

Assumptions 1) and 2) above can be applied to many highway bridges.

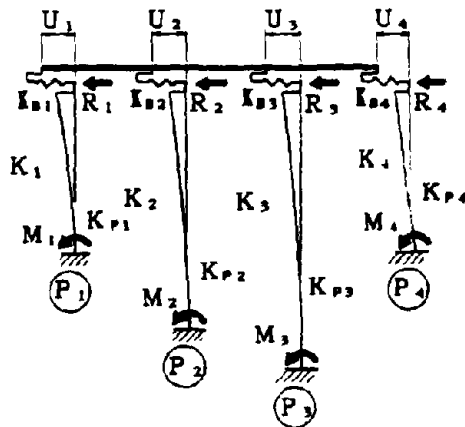
The validity of Assumptions 3) and 4) is indicated in Reference 2.

From Assumptions 3) and 4), the behavior of the menshin bridge during an earthquake can be expressed by an analytical model having one degree of freedom as shown in Fig. 2. As is generally known, in this case natural period T can be expressed as follows:

$$T = 2\pi \sqrt{\frac{W}{G \cdot \Sigma K_i}} \dots \dots \dots (2)$$

where,

- W : total weight of superstructure
- G : gravity acceleration
- K : equivalent stiffness of stiffness K_e of the menshin device at Pier i and stiffness K_p of the pier



- U : design displacement during earthquake
- R : horizontal reaction during earthquake
- K : equivalent stiffness of the menshin device and the pier
- K_e : equivalent stiffness of the menshin device
- K_p : equivalent stiffness of the pier
- M : moment at the bottom of the pier

Fig. 2 Modeling of the Behavior of Menshin Bridge During Earthquake

Using displacement U_i , vertical reaction W_i of the superstructure acting on the piers, and design lateral force coefficient K_h , horizontal reaction R_i of the piers during an earthquake can be expressed by Equations (3) and (4).

$$R_i = U_i \cdot K_h \dots \dots \dots (3)$$

$$W_i = W_i \cdot K_h \dots \dots \dots (4)$$

Therefore, the relationship in Equation (5) can be obtained.

$$W_i = \frac{1}{K_h} U_i \cdot K_h \dots \dots \dots (5)$$

From $W = \sum W_i$ and the fact that U_i becomes constant value U , the relationship in Equation (6) can be obtained.

$$W = \frac{U}{K_h} \sum K_i \dots \dots \dots (6)$$

By substituting Equation (6) in Equation (2), the relationship between natural period T and design displacement U in Equation (7) can be obtained.

$$U = \left(\frac{T}{2\pi} \right)^2 \cdot G \cdot K_h \dots \dots \dots (7)$$

Design Procedure Fig. 3 shows a flowchart for the proposed method. First, natural period T is calculated based on the equations in Section (1), and then sectional force is calculated by assuming design displacement U . After that, the initial dimensions of the substructure are determined, considering the expected stiffness of the menshin devices. Finally, the menshin devices to be used are selected.

The design procedure in the flowchart is described in detail below.

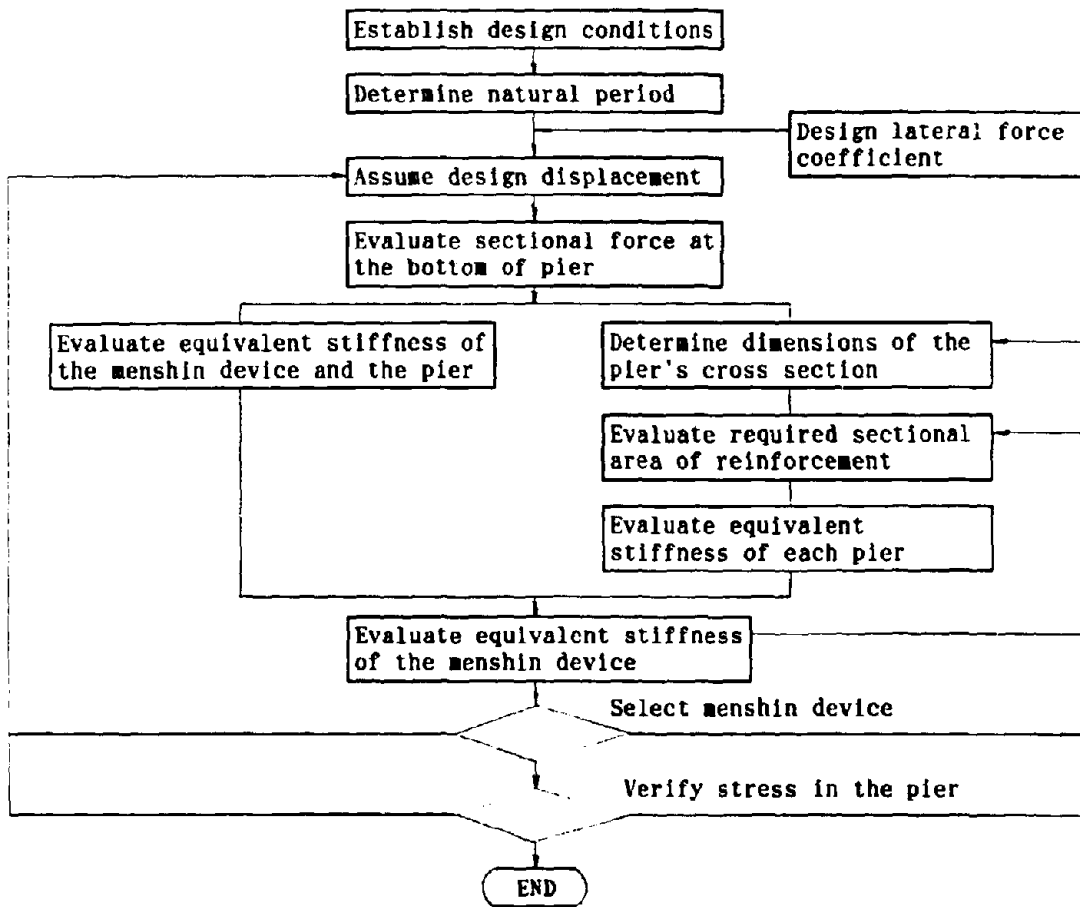
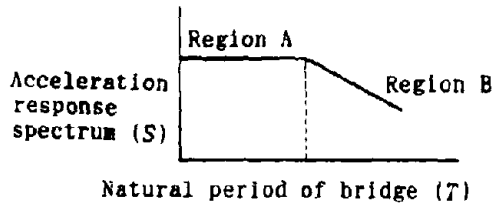


Fig. 3 Flowchart for Determination of the Initial Dimensions of the Pier

(a) Natural Period and Design Displacement

The natural period of the bridge is set so that it falls within either Region A (constant response acceleration spectrum region) or Region B (variable response acceleration spectrum region). In this paper, the proposed method is applied to Region A. Table 1 shows the natural periods of the bridge in Region A for different ground conditions. If the natural period is fixed, design displacement U can be easily estimated using Equation (7).

Table 1 Natural Periods in Region A



Type of Ground	Natural Period
Type I ground	$T < 1.12$ sec
Type II ground	$T < 1.40$ sec
Type III ground	$T < 1.68$ sec

Fig. 4 Acceleration Response Spectrum

(b) Sectional Force at the Bottom of the Pier

Sectional force which is necessary to determine the dimensions of the cross section of the pier and evaluate the equivalent stiffness of the menshin device and the pier is evaluated here.

1) Vertical Reaction of the Superstructure

Assuming that each pier carries the weight of a portion of the superstructure corresponding to a half span on both sides, vertical reaction W_i of the superstructure can be obtained by the following equation:

$$W_i = \frac{(L_i + L_{i+1})}{2} \cdot \frac{W}{L} \dots\dots\dots (8)$$

L_i, L_{i+1} : span lengths on both sides of Pier i
 L : length of the overburden load zone

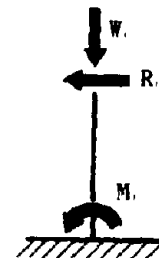


Fig. 5 Forces Acting on Pier

2) Horizontal Reaction During Earthquake

Horizontal reaction R_i acting on pier i during an earthquake can be evaluated, using Equation (4), as the product of vertical reaction W_i of the superstructure and design lateral force coefficient K_h .

3) Bending Moment at the Bottom of Pier

Bending moment M_i acting on the bottom of Pier i can be evaluated by the following equation:

$$M_i = R_i \cdot l_i = W_i \cdot K_N \cdot l_i \dots\dots\dots (9)$$

l_i : height of Pier i

(c) Dimensions of the Pier's Cross Section

By using the sectional force of the bottom of the pier, the dimensions of its cross section were determined and the required reinforcement is calculated. Then, whether the required sectional area of reinforcement satisfies the rules of the maximum and minimum sectional areas of reinforcement is checked. Also, whether the reinforcement can be arranged within the cross section is checked by going over structural details, such as cover and clearance.

(d) Equivalent Stiffness of the Pier

By using the dimensions of the pier's cross section, equivalent stiffness K_{p_i} of Pier i is evaluated by the following equation:

$$K_{p_i} = 3E_i \cdot I_i / l_i^3 \dots\dots\dots (10)$$

- E_i : Young's modulus of Pier i
- I_i : geometrical moment of inertia of Pier i
- l_i : height of Pier i

(e) Equivalent Stiffness of the Menshin Device and the Pier

By using the bending moment at the bottom of Pier i evaluated in (b) above, equivalent stiffness K_i of the menshin device and the pier is evaluated by the following equation:

$$K_i = \frac{M_i}{U_i \cdot l_i} = \frac{R_i}{U_i} \dots\dots\dots (11)$$

For the purpose of verification, the natural period of the bridge is evaluated by Equations (2), using equivalent stiffness K .

(f) Equivalent Stiffness of the Menshin Device

By using the equivalent stiffness K_i of the menshin device and the pier evaluated in (e) above and the equivalent stiffness K_{p_i} of Pier i evaluated in (d) above, required equivalent stiffness K_{S_i} of the menshin device is determined.

Each pier can be modeled as a single-mass, single-degree-of-freedom system with a series spring as shown in Fig. 6. Therefore, the equivalent stiffness of the menshin device can be given by the following equation:

$$K_{S_i} = \frac{K_{p_i} \cdot K_i}{K_{p_i} + K_i} \dots\dots\dots (12)$$

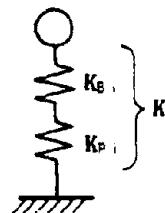


Fig. 6 Modeling of Menshin Device and Pier

(g) Selection of Menshin Device

The relation between yield load Q_1 and secondary stiffness K_2 , which satisfies the required equivalent stiffness K_{eq} of the menshin device is expressed by the following equation:

$$Q_1 = U_1 (K_{eq} - K_2) \dots\dots\dots (13)$$

A combination of the yield load and the secondary stiffness is selected, considering the attainable level of performance and dimensions of the menshin device. When the device that satisfies the required equivalent stiffness is not available, the dimensions of the pier's cross section may be revised. If it is impossible to change the dimensions of the pier's cross section, the assumed design displacement may be revised.

(h) Verification of Stress in the Pier

Stress in the lowest part of the pier is checked using the initial dimensions of the pier determined thus far. Sectional forces acting on the bottom of the pier are axial force, horizontal reaction during earthquake and bending moment at the bottom of the pier.

1) Axial Force

Axial force V_1 is a sum of the vertical reaction W_1 of the superstructure obtained by Equation (8) and the dead loads of the pier.

$$V_1 = W_1 + W_{1,1} + W_{1,2} \dots\dots\dots (14)$$

- $w_{1,1}$: dead load of the projecting portion of the pier
- $w_{1,2}$: dead load of the pier column

2) Horizontal Reaction During Earthquake

Horizontal reaction R_1 during an earthquake is a sum of the horizontal reaction R_1 of the superstructure during an earthquake obtained by Equation (4) and the horizontal reactions of the pier itself during an earthquake.

$$R_1' = R_1 + w_{1,1} \cdot K_h + w_{1,2} \cdot K_h \dots\dots\dots (15)$$

3) Bending Moment at the Bottom of the Pier

Bending moment M_1 at the bottom of the pier is a sum of bending moment M_1 caused by the horizontal reaction of the superstructure during an earthquake which can be obtained by Equation (9), and the bending moments caused by the horizontal reaction of the pier itself during an earthquake.

$$M_1' = M_1 + w_{1,1} \cdot K_h \cdot L_{1,1} + w_{1,2} \cdot K_h \cdot L_{1,2} \dots\dots\dots (16)$$

- $L_{1,1}$: distance from the bottom of the pier to the point of application of the horizontal Reaction of the projecting portion of the pier during earthquake
- $L_{1,2}$: distance from the bottom of the pier to the point of application of the horizontal reaction of the pier column

The step following the stress verification may be one of the following:

- (i) Review of the sectional area of reinforcement
- (ii) Review of the dimensions of the cross section of the pier
- (iii) Review of assumed design displacement U_1 or review of the natural period

If the stresses in concrete or reinforcement do not satisfy their requirements, (i), (ii) and (iii) are considered in this order so that their requirements are satisfied. If the requirements are satisfied, the next step is to move on to (i), (ii) or (iii) to improve economy, performance and workability, or to the design of meshin devices based on the dimensions of the cross section.

EXAMPLE OF APPLICATION

This section exemplifies the determination of the dimensions of the pier's cross section using the proposed method.

Design Conditions A three-span continuous prestressed concrete bridge as shown in Fig. 7 is considered here. Design conditions shown in Fig. 7, and seismic force in the direction of the bridge axis is assumed.

- Type of Bridge:
 - Superstructure
 - Type of structure : 3-span continuous prestressed concrete composite girder bridge (4 piers)
 - Total weight (dead load): 2,884t
 - Substructure
 - Type of structure : Rectangular cantilever-type pier, spread foundation
- Design Seismic Motion: Level 1 seismic motion
- Ground condition : Type I ground
- Direction of seismic motion: Same as the bridge axis

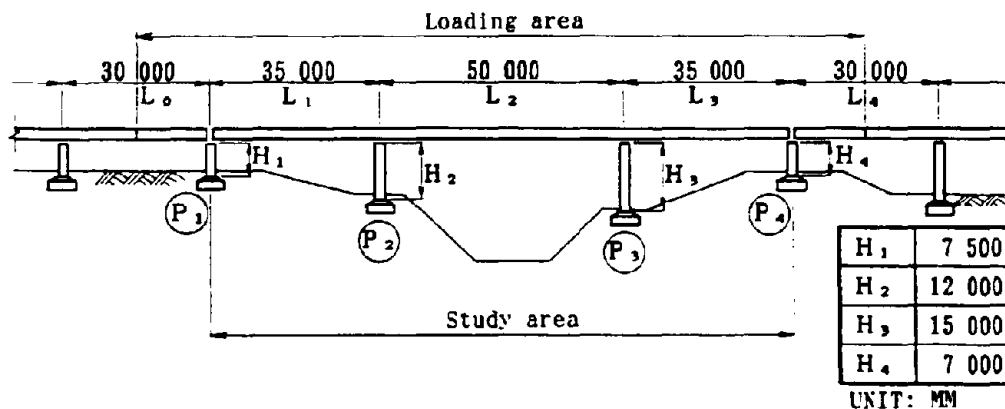


Fig. 7 Meshin Bridge for Analysis

Natural Period and Design Displacement The estimation of the primary natural period of the bridge may be arguable. In this example, following the argument described in Section 2, target natural period T is set as $T=1.12$ seconds.

In this case, according to the Specifications for Highway Bridges, design lateral force coefficient K_h is evaluated as follows:

$$K_h = 1.0 \times 0.8 \times 1.0 \times 1.25 \times 0.2 = 0.2$$

Hence, using Equation (7), displacement is

$$U = 0.062m$$

The subsequent discussion is based on this displacement.

Results Table 2 and Fig. 8 show the results determined by the proposed method. These values can be determined relatively easily.

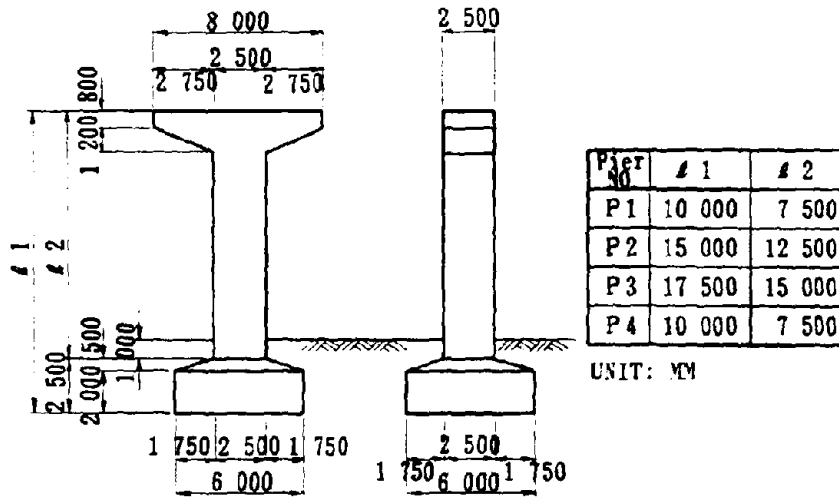


Fig. 8 Configuration of Pier

Table 2 Specifications of Determined Menshin Devices

Pier No.	Characteristic Shear Strength Strength Q(tf)	Post-yield Stiffness K2(tf/m)
P ₁	20.3	200
P ₂	27.2	400
P ₃	32.7	500
P ₄	20.3	200

Comparison of the Simplified Method and the Detailed Method Table 3 compares the displacement of the superstructure and the bending moments at the bottom of the pier determined by the simplified method, with those determined by modeling the menshin bridge as a multiple-mass frame structure and converging the relative displacements of the menshin devices by repeated calculation to reflect the nonlinearity of the stiffness of the menshin devices.

The displacement and bending moments determined by the simplified method falls within a range of ±10% of those obtained by the detailed method. This indicates that the proposed method is an effective method for determining the initial configuration.

Table 3 Comparison of Simplified Method and Detailed Method

Item	Simplified Method	Detailed Method	
Natural Period (sec)	1.10	1.04	
Displacement of Superstructure (cm)	6.00	5.45	
Moment at the Bottom of Pier (tfm)	Pier P ₁	1091	901
	Pier P ₂	2318	2100
	Pier P ₃	2788	3101
	Pier P ₄	1091	901

CONCLUSION

This paper has described a method for easier determination of the configuration of the substructure and menshin devices of a menshin bridge which reduces trials and errors in the design process by simplifying the dynamic characteristics of the bridge, and has indicated the effectiveness of the proposed method.

On the basis of the results of this study, the applicability of the proposed method to other types of bridge and to the synchronous bands of low acceleration spectrum ranges needs to be investigated.

ACKNOWLEDGMENT

This study was made as a part of the joint research program on "Development of Menshin Systems of Highway Bridges" between PWRI and 28 private firms in Japan.

The authors are very grateful to Dr. K. Kawashima, Mr. K. Hasegawa, Mr. S. Unjo and Mr. H. Nagashima of the Earthquake Engineering Division of PWRI for their cooperation.

REFERENCES

1. Japan Road Association, Design Specifications for Highway Bridges, Part V. Earthquake Resistant Design, (1990) (in Japanese)
2. Technology Research Center for National Land Development, Guidelines on the Design of Menshin Highway Bridges (Draft), (1989) (in Japanese)

SEISMIC RESPONSE ANALYSIS METHOD OF MENSHPIN BRIDGES

Yoshihiro HAMAZAKI¹, Osamu OHTANI¹, Hiroshi ZUI²

¹Mechanical Engineering Research Laboratory, Kobe Steel Ltd.
Takatsukadai, Nishi-ku, Kobe, JAPAN

²Department of Civil Engineering, Setsunan University,
Ikedamachi, Neyagawa, Osaka, JAPAN

SUMMARY

The response characteristics of Menshin bridges are examined by several earthquake response analysis such as nonlinear time history response analysis, equivalent linear time history response analysis and response spectrum analysis in which equivalent linear spring constants and damping ratios for Menshin bearings are utilized. Frame models for five span continuous steel girder bridges are utilized. It is confirmed that response spectrum analysis gives appropriate response values.

INTRODUCTION

Response characteristics of Menshin bridges are quite different in comparison with those of ordinary bridges and earthquake response analysis is generally carried out on the seismic design to confirm the response characteristics of such bridges. Response spectrum analysis applicable only for linear structures is usually utilized on seismic design. However, Menshin bearings have nonlinear hysteresis. Therefore, it is necessary to linearize the nonlinear hysteresis in order to utilize response spectrum analysis and to confirm the validity of linearization. Also, it should be confirmed that the equivalent linear response spectrum analysis gives appropriate response values.

In this paper, seismic response analysis are carried out for a multi-span continuous steel girder bridge in order to examine response characteristics of Menshin bridges and appropriateness of the equivalent linear method. Three response analysis methods are utilized. The first one is equivalent linear response spectrum analysis in which equivalent linear spring constants and damping ratios are utilized. The second one is equivalent linear time history response analysis, in which equivalent linear spring constants and damping ratios are also utilized. The last one is nonlinear time history response analysis where nonlinear hysteresis of lead-rubber type Menshin bearings are taken into account accurately by using nonlinear hysteresis elements.

THEORETICAL ANALYSIS

MATHEMATICAL MODEL A five-span continuous steel girder bridge is utilized as an analysis model. Fig.1 shows the general plan of the model bridge. The span is 65m and the total length of bridge is 325m. The classification of ground condition is second class as defined in Design Specifications for Highway Bridges of Japan Road Association¹⁾. Physical properties of superstructure and substructure are shown in Table 1. Lead-rubber type Menshin bearings are installed in the inside supports(P1,P2,P3,P4) and both end supports(A1,A2) are assumed to be movable bearings.

The frame model of this bridge for analysis is shown in Fig.2. Distributed mass beam elements are utilized for steel girders and reinforced concrete piers. Sway-rocking spring constants of the foundation and ground are determined from the stiffness of the foundation piles and soil properties. Damping ratios are assumed to be 2 % for the superstructure, 5 % for the substructure and 20 % for both the sway and rocking ground springs.

The direction of the seismic force is assumed to be along the girder axis. Fig.3 shows the standard acceleration response spectrum utilized, which corresponds to the seismic force level for ultimate ductility check of bridge piers. Modified KAIHOKU bridge record spectrally fitted with the acceleration response spectrum shown in Fig.3 is utilized as the input earthquake motion wave on the time history response analysis.

EQUIVALENT LINEAR RESPONSE SPECTRUM ANALYSIS Fig.4 shows idealized hysteresis characteristics of lead-rubber type Menshin bearing and constants used. The equivalent linear spring constant and the damping ratio of lead-rubber type Menshin bearing are calculated as follows:²⁾

$$\left. \begin{aligned} \mu &= \frac{x}{x_y} , \\ k_{eq} &= \frac{k_1 + k_2(\mu - 1)}{\mu} , \\ h_{eq} &= \frac{2}{\pi} \cdot \frac{1 - k_2/k_1}{1 + k_2/k_1 \cdot (\mu - 1)} \cdot \frac{\mu - 1}{\mu} \end{aligned} \right\} \quad (1)$$

The equivalent linear spring constant k_{eq} is the gradient of the hysteresis loop on maximum displacement and the equivalent damping ratio h_{eq} is equal to energy loss per one cycle.

Modal dampings h_i on the response spectrum analysis are calculated as follows:¹⁾

$$h_i = \frac{\sum_{j=1}^n \phi_{ij}^T \cdot \zeta_j \cdot K_j \cdot \phi_{ij}}{\phi_i^T \cdot K \cdot \phi_i} \quad (2)$$

where

- ϕ_{ij} : modal vector of j element of i-th order vibration mode
- ζ_j : damping ratio of j element
- K_j : stiffness matrix of j element
- ϕ_i : modal vector of total structure of i-th order vibration mode
- K : stiffness matrix of total structure

The damping modification factor c_D in the response spectrum analysis is calculated as follows:¹⁾

$$c_D = \frac{1.5}{40h_i + 1} + 1.5 \quad (3)$$

The acceleration response spectrum is calculated as follows:

$$S = c_D \cdot S_0 \quad (4)$$

where S_0 is the standard acceleration response spectrum given in Fig.3.

Response values on the response spectrum analysis are calculated by taking the root mean square, and 50 modal orders are employed.

EQUIVALENT LINEAR AND NONLINEAR TIME HISTORY RESPONSE ANALYSES

The nonlinear equation of motion can generally be described as following the second order differential equation for a total structure,³⁾

$$[M_L + M_N]\ddot{Z} + [C_L + C_N]\dot{Z} + [K_L + K_N]Z = F + F_N \quad (5)$$

where M_L , C_L and K_L are the linear mass, damping and stiffness matrices respectively, which are constant through each time step. M_N , C_N and K_N are the nonlinear mass, damping and stiffness matrices respectively, which vary at each time step. \ddot{Z} , \dot{Z} and Z are the vectors of response accelerations, velocities and displacements respectively. F is the external force vector and is expressed in this case as $-[M_L + M_N] \cdot [J] \cdot \ddot{u}_g$, where $[J]$ is a matrix which expresses the direction of the seismic force, and \ddot{u}_g is the input earthquake acceleration wave. F_N is the nonlinear force vector which compensates for the structural nonlinearity.

Direct integral method by Newmark β method are utilized for both equivalent linear and nonlinear time history response analyses. In the equivalent linear time history response analysis, same linear spring constants and damping ratios of the Menshin bearing are utilized as those used in the response spectrum analysis. In the nonlinear time history response analysis, nonlinear characteristics of Mensin bearings are taken into account accurately by using bi-linear hysteresis elements.

NUMERICAL ANALYSIS

The maximum response values in each response analysis are shown in Table 2. A1,P1 and P2 show positions of the bridge piers. When relative displacements of the Menshin bearings obtained differ much with assumed relative displacements of the Menshin bearings, equivalent linear spring constants and damping ratios of Menshin bearings should be recalculated. In this case, the difference between assumed and obtained spring constants and damping ratios are not so large that calculations need be repeated.

It can be seen from Table 2 that linear time history response analysis gives smaller response values for both accelerations and displacements by about 30% compared with response spectrum analysis. Bending moments and shear forces at the bottom of the bridge piers calculated by linear time history response analysis are also smaller than those of response

spectrum analysis. Moreover, nonlinear time history response analysis gives smaller response values by about 20 % compared with those given by linear time history response analysis.

Time history response waves of linear and nonlinear time history response analysis are shown in Fig. 5. Nonlinear hysteresis curves of the Menshin bearings obtained by nonlinear time history response analysis are shown in Fig. 6. Menshin bearings are designed to be elastic for small seismic forces which occur often during the life span of a bridge. In Fig.6, however, seismic forces are relatively large corresponding to the seismic force level for ultimate ductility check of bridge piers, and maximum response forces of Menshin bearings exceed by far their yield strength. Therefore, Menshin bearings show much hysteresis behavior.

Maximum lateral acceleration of steel girders by nonlinear time history response analysis is approximately the same as the input maximum acceleration. Therefore, seismic response magnification becomes about 1, and bending moments and shear forces at the bottom of the bridge pier are relatively small compared with those of linear time history response analysis and response spectrum analysis. Maximum acceleration at the top of bridge pier by nonlinear time history response analysis are smaller than those of response spectrum analysis but are larger than those of linear time history response analysis. This means that steel girders and bridge piers move independently after the yielding of the Menshin bearings on the nonlinear time history response analysis. On the other hand, steel girders move integral with bridge piers due to the equivalent linear springs and dampings on the linear time history response analysis.

CONCLUSIONS

It is confirmed that equivalent linear response analysis such as seismic response spectrum analysis which utilize equivalent linear spring constants and damping ratios of the Menshin bearings gives safe side response values.

It is also confirmed that appropriately designed lead-rubber type Menshin bearings have large hysteresis damping effects for large seismic forces and decrease seismic lateral inertia forces.

ACKNOWLEDGEMENTS

This study was made as a part of the joint research program for " Development of Menshin Systems of Highway Bridges " between PWRI and 28 private firms in Japan. The authors appreciate members of the joint research program for their useful advice.

REFERENCES

- (1) Japan Road Association: " Design Specifications for Highway Bridges, Part V, Earthquake Resistant Design, 1990 " (in Japanese)
- (2) PWRI and 28 Private Firms: " Development of Menshin Systems of Highway Bridges-Report No.1 ", PWRI Joint Research Report No.44, March 1990 (in Japanese)
- (3) Zui, H., et al: " A Study of the Simulation of Link Mechanics (1st Report, Analysis on the Dynamic Responses of Large Deformation Elements Including Elastic Vibration) ", Proceedings of the JSME, Vol.52, No.44, November 1986 (in Japanese)

Table 1 Physical Properties of Bridge Members

	Superstructure	Substructure	
		A1,A2	P1~P4
Sectional Area [m ²]	0.729	28.13	15.00
Second Moment of Inertia (Axis) [m ⁴]	0.830	11.87	7.81
Second Moment of Inertia (Right Angle) [m ⁴]	10.840	366.21	45.00
Polar Moment of Inertia of Area [m ⁴]	0.435	42.08	22.97

Table 2 Result of Numerical Calculations

	Response Spectrum Method			Time History Response Analysis (Max. Values)					
				Equivalent Linear			Nonlinear Hysteresis		
	A1	P1	P2	A1	P1	P2	A1	P1	P2
Superstructure Acceleration [gal]	697.8	695.4	694.1	515.8	513.4	512.1	446.5	440.7	439.0
Top of Bridge Pier Acceleration [gal]	677.2	1028.	738.6	230.6	356.0	355.5	217.9	498.9	469.5
Bearing Relative Displacement[mm]	475.9	404.8	405.8	312.1	276.7	274.1	179.7	158.6	155.4
Bottom of Bridge Pier Bending Moment [t·m]	701.6	11760.	11700.	413.1	8175.	8099.	406.8	6071.	5982.
Bottom of Bridge Pier Shear Force [tf]	187.4	999.7	987.1	110.6	698.1	691.9	108.9	530.1	522.7

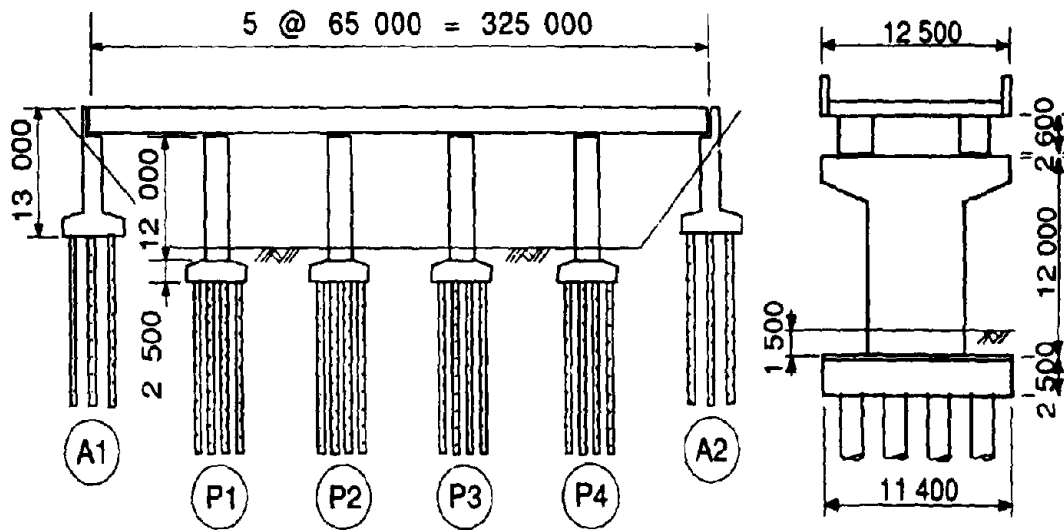


Fig. 1 Configuration of Model Bridge

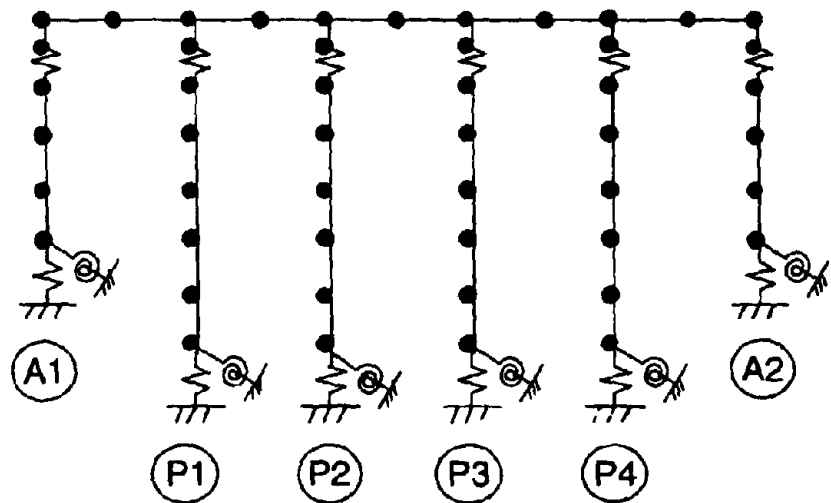


Fig. 2 Frame Model

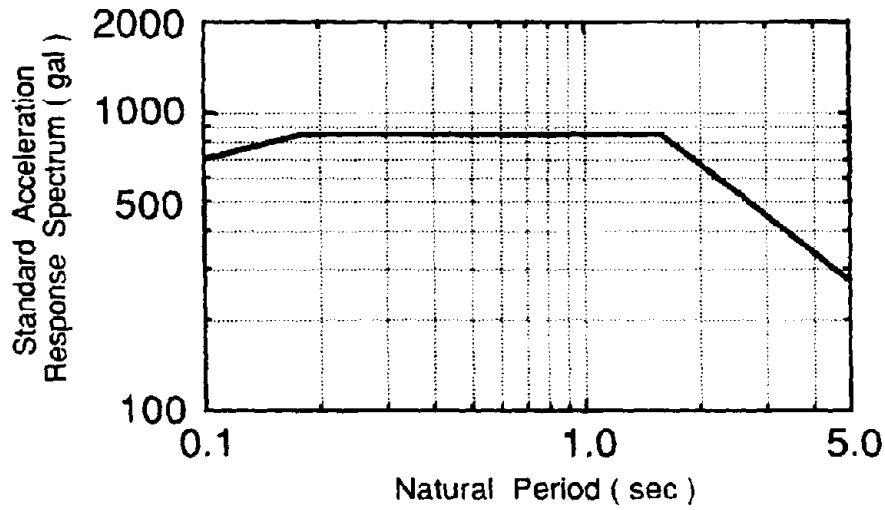


Fig. 3 Standard Acceleration Response Spectrum of The Ground Used for Response Spectrum Analysis

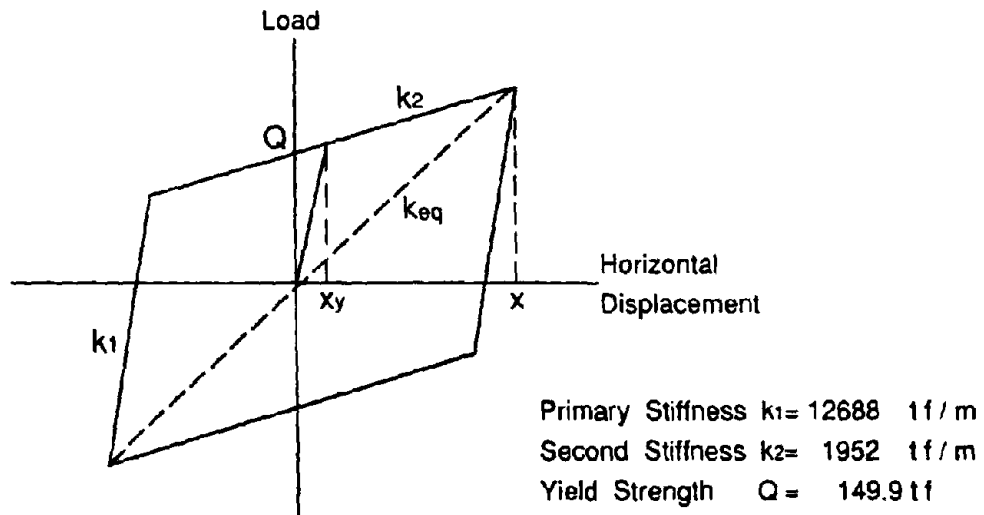


Fig. 4 Idealized Hysteresis Characteristics of Lead-Rubber Type Mensin Bearings

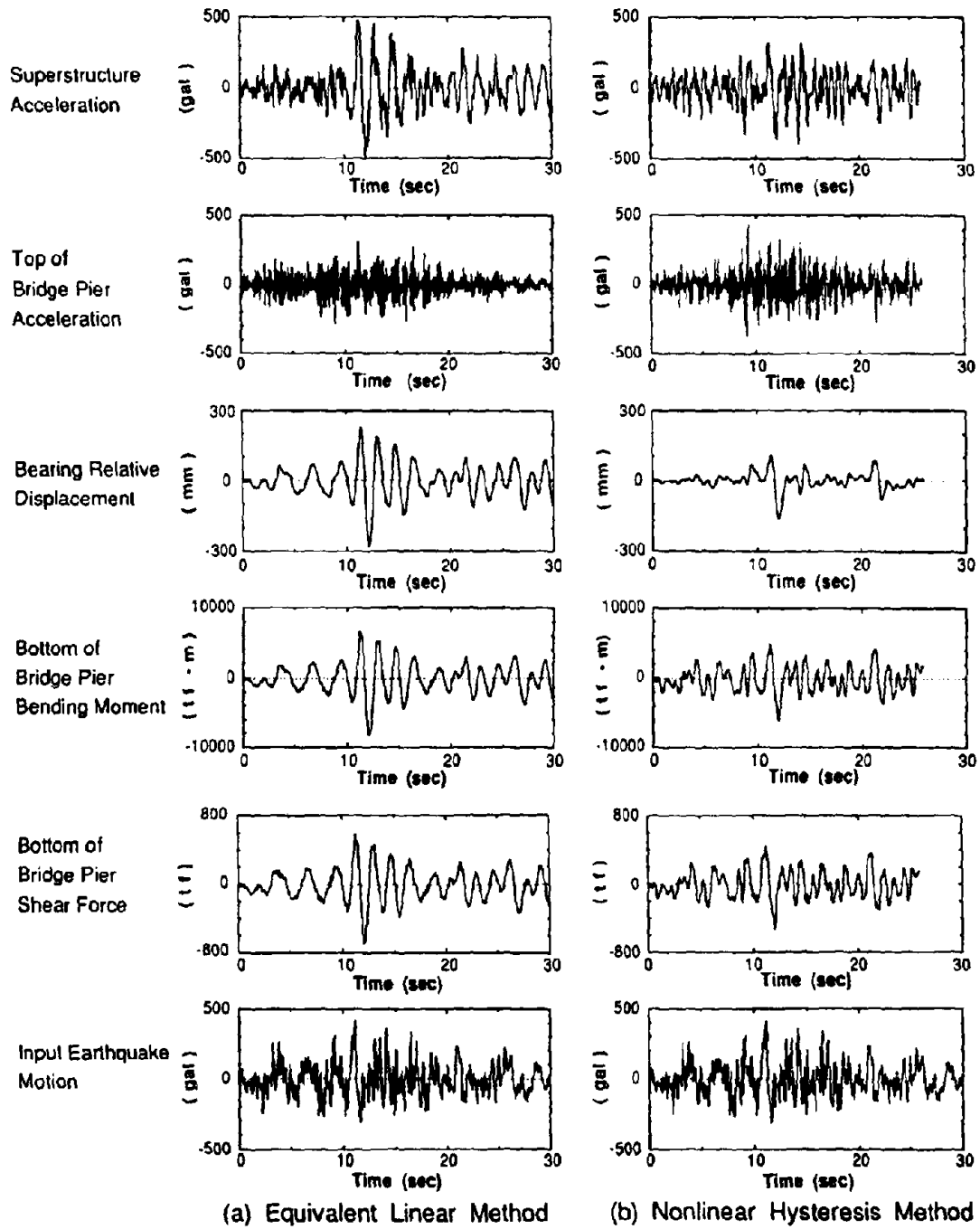
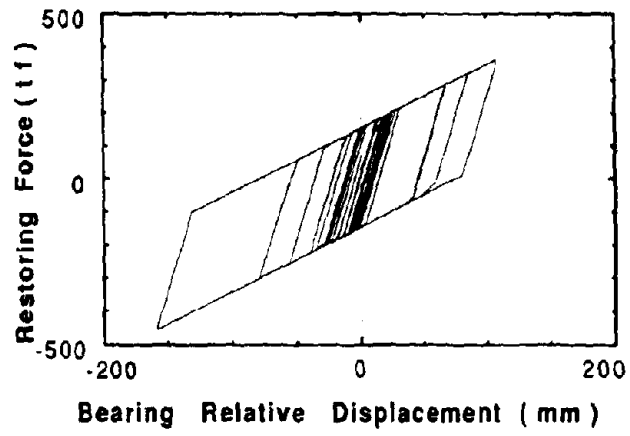
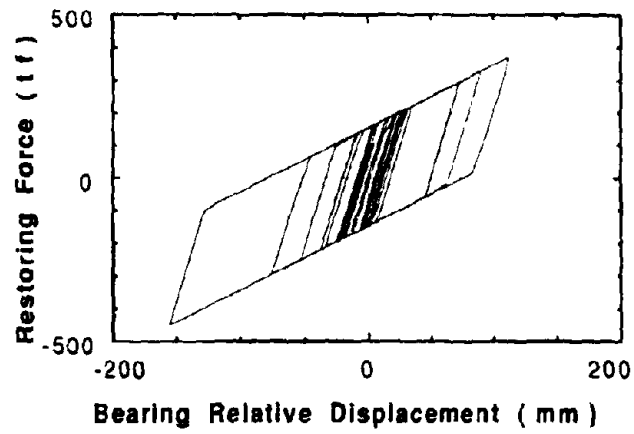


Fig. 5 Time History Response Values (Bridge Pier : P1)



(a) Bridge Pier : P1



(b) Bridge Pier : P2

Fig. 6 Calculated Hysteresis Roops of Lead-Rubber Type Mensin Bearing

EFFECT OF NONLINEARITY OF BRIDGE COLUMNS
ON SEISMIC RESPONSE OF MENSHPIN BRIDGES

Takeshi HIRAI and Michio SUGIMOTO
Takenaka Technical Research Laboratory

SUMMARY

The Menshin bridge which is under consideration in this study has the following two kinds of nonlinear elements in its entire system: the ductile behavior of the Menshin bearings and that of the RC column. The conceptual model used in this study is a one column model, the base of which is fixed. The effect of the nonlinearity of this model is examined. In this paper, the dynamic response of the linear column is compared with that of the nonlinear column in which the plasticity factor is 2.4. From the result, almost no differences are observed in these cases.

INTRODUCTION

Menshin bridges can reduce the lateral load acting on the bearings during earthquakes with a lengthening of the natural period and an increase of the damping characteristics of the bridge structure. When taking the dynamic interaction between the ground and the bridge structure into account, a short column, fixed on hard ground, with a short natural period, is considered to be suitable for the effective functioning of the Menshin bearing. However, during high level seismic motions, there is a possibility of nonlinear characteristics occurring in the columns and on the ground. Due to this, the natural periods of the structures, the columns, and the ground, are lengthened and the functions for the Menshin system may be lowered.

In this paper, the effect of the nonlinear characteristics of the columns is studied through carrying out a dynamic analysis.

NONLINEARITY

The effect of the nonlinear characteristics of the columns on the dynamic behavior of the Menshin bridges is studied through the conduct of a time-history response analysis. The investigation of the nonlinearity of the columns is carried out under consideration of the fact that the stiffness of the columns lowers and the energy absorption increases with the increase of the input seismic motion. As the input seismic motion becomes larger, the Menshin bearings show nonlinearity. Then the reinforced concrete columns begin yielding with the increase of seismic motion. As a result, the nonlinearity of the columns increases. Therefore, it can be predicted that the behavior of the Menshin bridges having two elements with nonlinearity, such as columns and Menshin bearings, becomes complicated during an earthquake. The response characteristics, the maximum response values and the response magnification factors at the top of the columns and the superstructures are closely examined with the aim of clarifying the nonlinear characteristics of the Menshin Bridges.

Then it is discussed just how the aforementioned seismic responses of the Menshin bridges are influenced by the nonlinearity of the entire system.

ANALYTICAL METHOD

Structural Model A spring-mass model used in this analysis is a fixed-base four-mass model corresponding to a Menshin bridge, as illustrated in Table-1.

Model of Hysteretic Elements Menshin bearings and the RC columns which are employed in this study are assumed to have nonlinear characteristics as follows.

Menshin bearings have bi-linear hysteresis characteristics, as shown in Fig.-1. The hysteresis characteristics show linear behavior with relatively large stiffness of K_1 within the area of yields point A. Then the stiffness decreases to K_2 at the place exceeding the yielding displacement (point A). After unloading, the stiffness of K_1 is regained.

The RC columns have the tri-linear characteristics shown in Fig.-2. The characteristics of the columns show linear behavior within the area of the first yield point of A, where concrete breaks due to the tensile stress caused by the bending moment. Only the tension reinforcement resists against the tensile stress in the area between the first yield point and the second yield point of B, where the reinforcement yield and the stiffness becomes smaller.

Input Seismic Motion Fig.-3 shows the time-history characteristics of the input seismic motion. The analysis is made through varying the peak value of the input seismic motion from 10 gal to 360 gal (see Fig.-3) without changing the frequency features shown in Fig.-3.

Models Compared The following two models are compared with each other as shown in Table-2: a linear column model in which the columns of a Menshin bridge are supposed to have linear characteristics, and a nonlinear column model with tri-linear hysteresis characteristics.

RESULTS OF ANALYSIS

In this study, under the assumption that the Menshin bearings have bi-linear type nonlinearity, the response characteristics of the superstructures and the columns for the following two different systems: a system in which the columns have linear characteristics and a system in which the columns have tri-linear type nonlinear characteristics.

Maximum Response of the Superstructure Table-3 shows the maximum displacement of the column-heads and the superstructure respectively, and the maximum acceleration response of the superstructure for the nonlinear and linear column models to the peak acceleration ranging from 10 gal to 360 gal.

From the aforementioned result, it is clarified that the lateral load which acts on the columns during a strong earthquake (peak acceleration = 360 gal) is reduced due to the effect exerted by the nonlinearity of the columns. The degree of the lateral load reduction is approximately 13% of the response value for the linear column model. Fig.-4 shows the relationship between the input seismic acceleration and the maximum acceleration of the superstructure through comparing the two types of models. The values for the maximum response acceleration indicated in Fig.-4 are shown as substituted values based on 100 gal for the input maximum acceleration. This is done in order to examine the degree of the damping and the amplification of the response of the superstructure to each input acceleration. In the area of 50 gal or less for the input maximum acceleration, the maximum acceleration response of the superstructure are approximately 200 gal for both models without regard to the input maximum acceleration. The maximum response acceleration of the superstructure is approximately double the input maximum acceleration. The reason that the values of the maximum acceleration response for both models are equivalent within this area is because the Menshin bearings and the columns have the same linear characteristics in both models.

In the area of 100 gal or more, the corrected response acceleration values of the superstructure for the model in which the column is assumed to have nonlinearity, become smaller than the values for the model in which the column is assumed to have linearity with the increase of the input maximum acceleration. It is considered that this is due to the fact that the nonlinearity of the linear column model becomes different from that of the nonlinear column model in the area of 100 gal or more.

Fig.-5 shows the relationship between the maximum acceleration and the maximum response displacement of the superstructure, which is substituted for the input maximum acceleration of 100 gal. The maximum displacement response shows approximately the same values (40mm) for both models within the area of 50 gal. Beyond 100 gal, the maximum displacement response values for the nonlinear column model become larger than the values for the linear column model as the input maximum acceleration increases. It is considered that the aforementioned tendency for the maximum displacement response is due to the fact that the two models are under the same state as has been described in the explanation of fig.-4.

The maximum displacement response of the Menshin bearing to the input maximum acceleration of 200 gal, 300 gal and 360 gal, shown at points A,B,C, in Fig.-4 and 5, is plotted in Fig.-6 for the linear model and in Fig.-7 for the nonlinear model. As Fig.-6 and 7 show, the relationship between the displacement and the input motion is expressed in a bi-linear skeleton curve for both models. Fig.-8 is obtained by superimposing Fig.-7 onto Fig.-6, showing a comparison between the two models.

Fig.-8 clearly shows that the nonlinear model has a smaller maximum displacement response than the linear model and the difference in the maximum displacement response for both models tends to increase with the increase of the input maximum acceleration. At the input maximum acceleration of 360 gal, point C in Fig.-8, 5.4cm difference in the maximum displacement response is observed between the nonlinear and linear column models. As for the column-head, on the other hand, the maximum displacement response for the nonlinear column model is plotted against the input maximum acceleration in Fig.-9. The relationship between the displacement and the input motion is expressed in a tri-linear skeleton curve. Plasticity factor, μ = maximum response displacement / yielding displacement, increases with the increase of the input maximum acceleration : μ = 0.7 for A, 1.3 for B and 2.4 for C.

As shown in Fig.-4, the maximum acceleration response of the superstructure for the linear column model decreases with the increase of the input maximum acceleration. It is considered that this phenomenon is caused by the fact that the maximum displacement for the Menshin bearing of the model increases, as shown in Fig.-6. From Fig.-8, it can be seen that the maximum relative displacement response of the Menshin bearing for the nonlinear column model is smaller than that for the linear column model at the same value of the input maximum acceleration. From Fig.-4, it is clarified that in the area of 100 gal or more for the input acceleration, despite the fact that the maximum displacement of the Menshin bearing for the linear column model is larger than that for the nonlinear column model, the maximum acceleration response of the superstructure for the nonlinear column model is smaller than that for the linear column model.

It can be considered that this is due to the fact that as for the nonlinear column model, the maximum acceleration of the superstructure is lowered by the nonlinear effects exerted by both the Menshin bearing and the column. For the linear column model, the maximum acceleration decreases due to the nonlinear characteristics of only Menshin bearing.

Time-History Response Characteristics Time history waves of the response displacement of the column-head, the response displacement and the response acceleration of the superstructure are shown in Table-4 for the linear column model and in Table-5 for the nonlinear column model. The input maximum accelerations examined are 200, 300 and 360 gal. The discussions on the time-history response shown in Table-4 and 5 are as follows.

a) The maximum response is observed in the vicinity of 2.0 sec in all cases shown in Table-4 and 5. This is due to the fact that the acceleration wave of the input seismic motion has its maximum value at approximately 2.0 sec.

b) The time-history wave of the displacement response of the column-head for the nonlinear column model is similar in shape to that of the superstructure, since the period of the displacement response wave of the column-head lengthens in the nonlinear column model, unlike in the linear column model, with the increase of the input maximum acceleration.

Therefore, it is supposed that the vibration isolation effect of the Menshin bearing in the nonlinear column model could be smaller than that in the linear column model after the column becomes plastic.

c) In the linear column model, residual displacement is observed in the input maximum acceleration of 360 gal in the column-head and the superstructure. The time-history and the idealized hysteresis loop of the relative displacement of the Menshin bearing are illustrated in Fig.-10 and 11. It is found from these figures that there is no residual displacement in the Menshin bearing. Therefore, it is clarified that the residual displacement observed in the superstructure is caused by the residual displacement in the column-head.

CONCLUSION

a) In the case of 360 gal for the input maximum acceleration, the maximum acceleration response of the nonlinear column model is smaller by 59 gal and the maximum displacement response is larger by 3.9cm, compared with the linear column model. The difference in the maximum acceleration response and the maximum displacement response correspond to 13% of the maximum response of the linear column model. The plasticity factor of the column in the nonlinear column model is 2.4.

b) Considering the differences of the maximum response between each superstructure of the models, these differences tend to increase with the increase of the input peak for the acceleration. The maximum acceleration response becomes smaller in the case of the nonlinear model than in the case of the linear model. On the other hand, the maximum displacement response becomes larger in the case of the nonlinear model.

c) In the area of 100 gal or more, for the input acceleration, the maximum acceleration response of the superstructure for the nonlinear column model is smaller than that for the linear column model. Under this situation, the maximum displacement response value of the Menshin bearing for the linear column model is larger than the value for the nonlinear column model. The larger the displacement for the Menshin bearing, the smaller the maximum acceleration of the superstructure for the linear column model. However, the maximum accelerations of the superstructures for both models can not be compared with each other through the use of each maximum relative displacement of the Menshin bearings. This is due to the fact that in the nonlinear column model the nonlinearity of both the column and the bearing exerts an influence on the maximum acceleration of the superstructure.

d) From the time-history waves of the superstructure and the column-head, it can be recognized that the maximum response is observed at around 2.0 sec in all cases when the input motion is at a high level and the maximum response value of the superstructure is predominant over the other peak values.

e) In the nonlinear column model, the time-history wave of the displacement response of the column-head tends to become similar in shape to that of the superstructure as the input motion increases.

Therefore, it is supposed that the vibration isolation effect of the Menshin bearing and the column of the nonlinear model could be smaller than that of the linear column model when the input motion is in the vicinity of 360 gal.

f) In the nonlinear column model, residual displacement is observed in the superstructure at the input maximum acceleration of 360 gal. This residual displacement observed in the superstructure is caused by the residual displacement in the column-head. Residual displacement can hardly be recognized in the Menshin bearing.

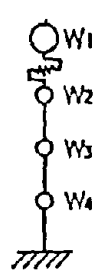
ACKNOWLEDGEMENTS

This study was made as part of the joint research project on the "Development of Menshin System of Highway Bridges" between PWR1 and 28 private firms in Japan.

REFERENCES

1. Japan Road Association: "Design Specifications for Highway Bridges, Part V, Earthquakes Resistant Design, 1990" (in Japanese).
2. PWR1 and 28 Private Firms: "Development of Menshin System of Highway Bridges - Report no. 1 - ", PWR1 Joint Research Report No 44, March 1990 (in Japanese.)

Table-1 Analytical model

Analytical Model	Mass No.	Weight (t)	Mass coordinates
	1	721.4	17.5
	2	113.0	16.67
	3	236.9	9.00
	4	417.1	1.12
	Fixed		0.00

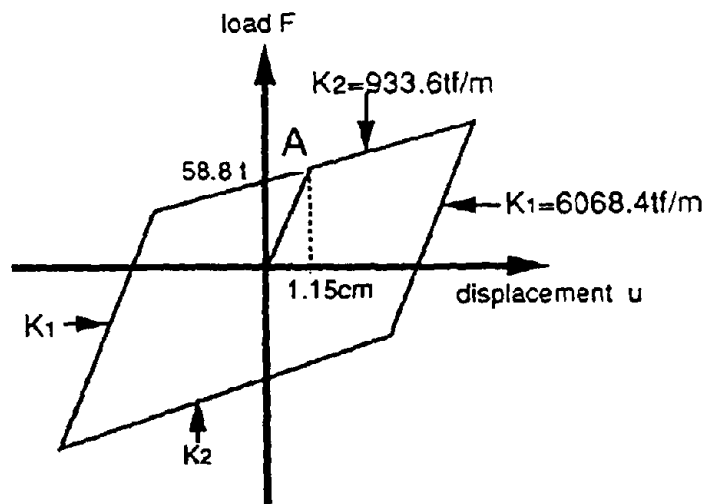


Fig-1 Hysteresis characteristics of a Menshin Bearing

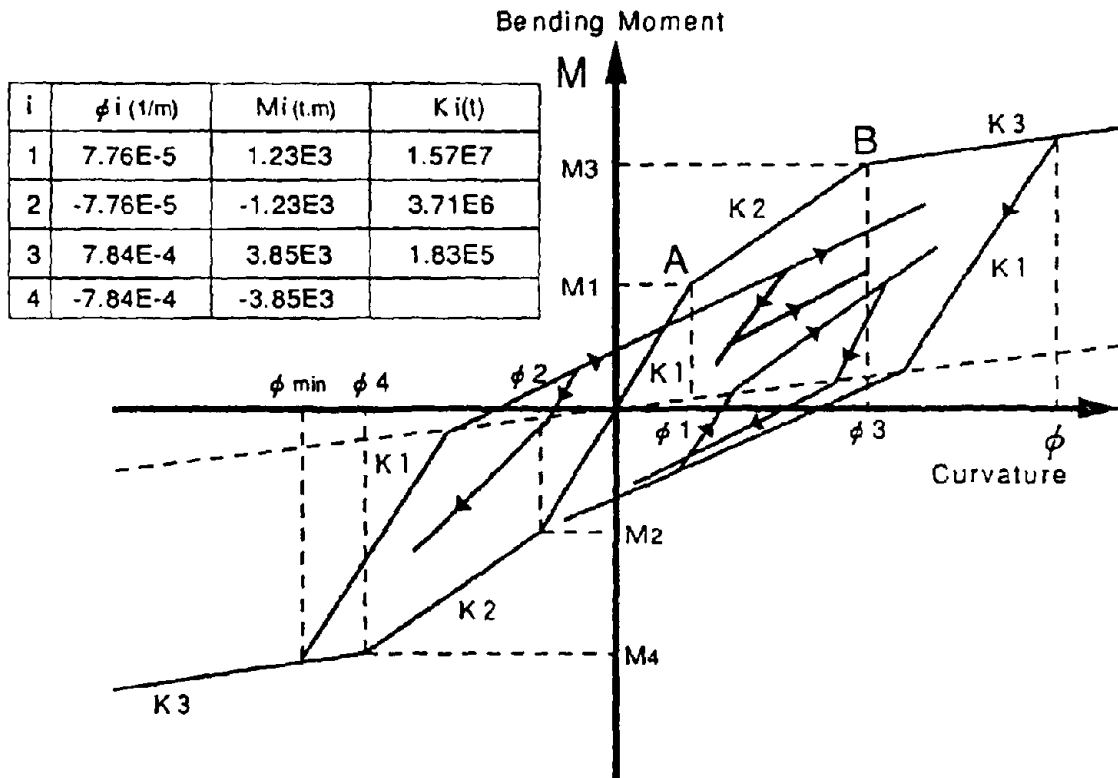


Fig-2 Non-linear characteristics of a RC column

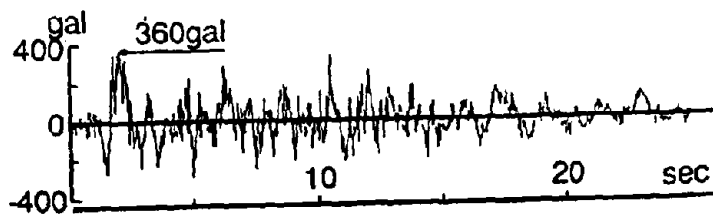


Fig-3 Input seismic motion
(The maximum acceleration is 360gal)

Table-2 Analyzed cases

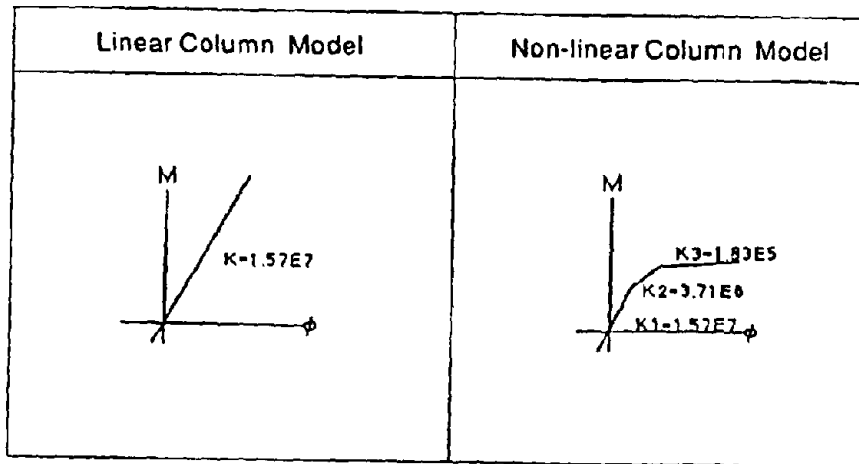


Table-3 The relationship between the maximum acceleration of the input seismic motion and the maximum response

input max. acc. (gal)	max. disp. (column head) (mm)		max. disp. (superstruct.) (mm)		max. acc. (superstructure) (gal)	
	linear column	non-linear	linear column	non-linear	linear column	non-linear
10	1.4	1.4	3.9	3.9	20.8	20.8
20	2.8	2.8	7.8	7.8	41.7	41.7
30	4.2	4.2	11.7	11.7	62.6	62.9
40	5.6	5.6	15.6	15.6	83.5	83.5
50	6.5	7.0	19.6	19.6	97.8	97.7
70	8.2	10.5	30.3	30.9	111.5	108.0
100	10.0	15.2	53.0	55.8	137.9	134.8
200	16.7	35.6	133.5	148.9	236.2	227.5
300	23.8	69.1	231.6	258.3	356.8	327.3
360	27.9	126.9	292.1	331.4	420.7	370.8

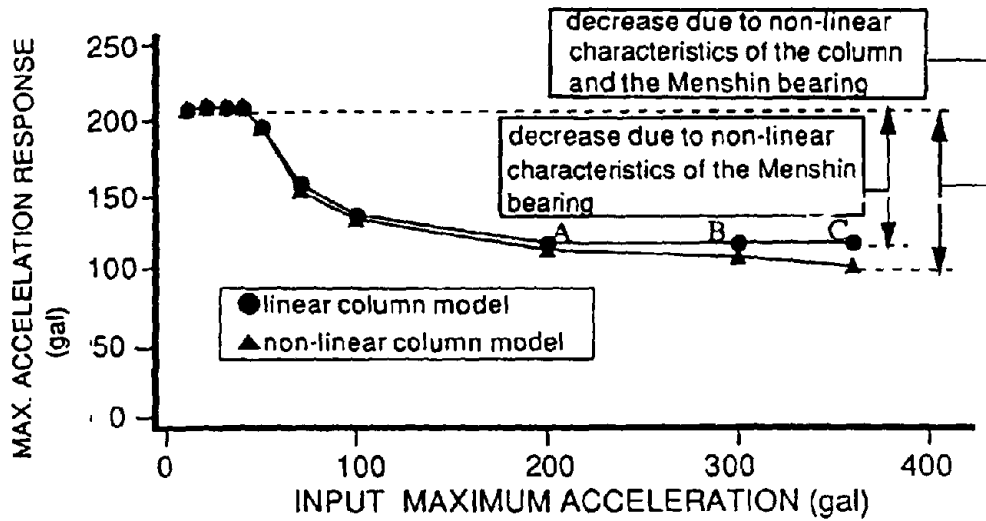


Fig-4 Substituted maximum acceleration response of superstructure as the value based on 100gal for the input maximum acceleration

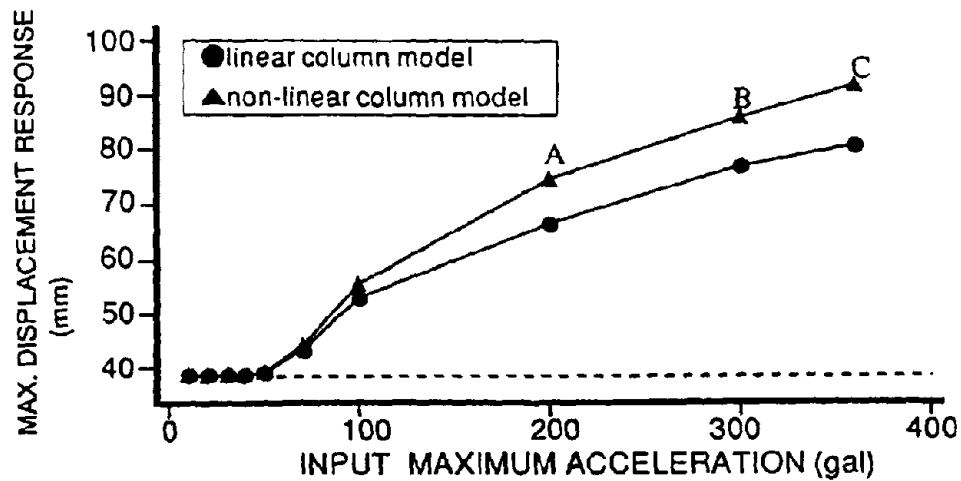


Fig-5 Substituted maximum displacement response of superstructure as the value based on 100gal for the input maximum acceleration

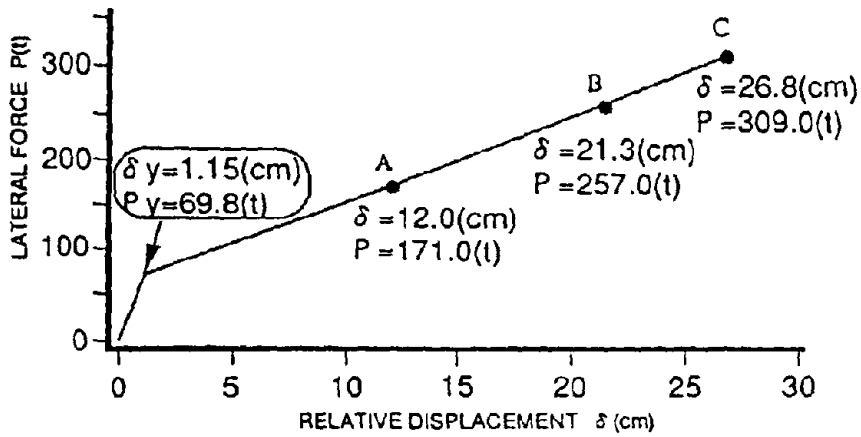


Fig-6 Maximum relative displacement of the Menshin bearing in the linear column model

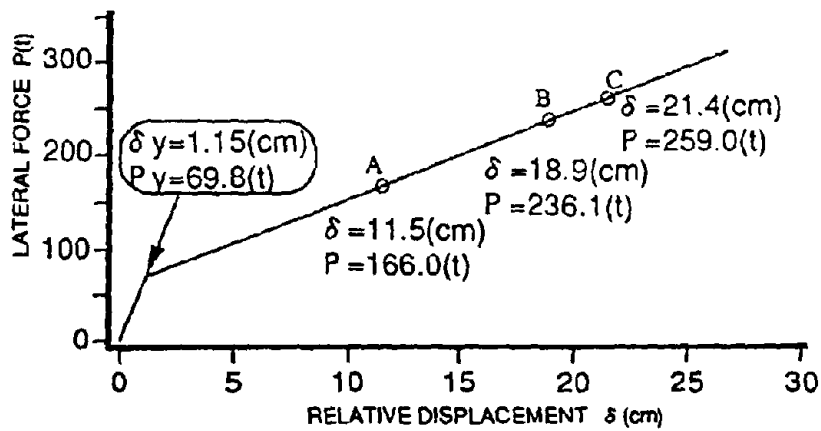


Fig-7 Maximum relative displacement of the Menshin bearing in the non-linear column model

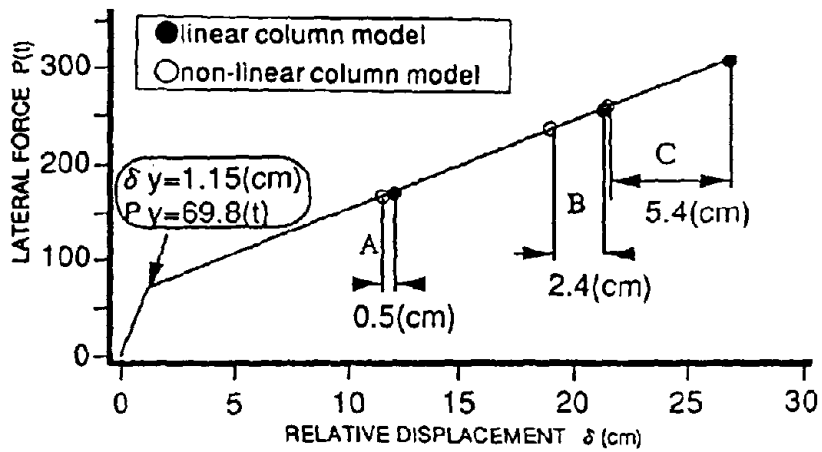


Fig-8 Maximum relative displacement of the Menshin bearing in the linear and non-linear column models

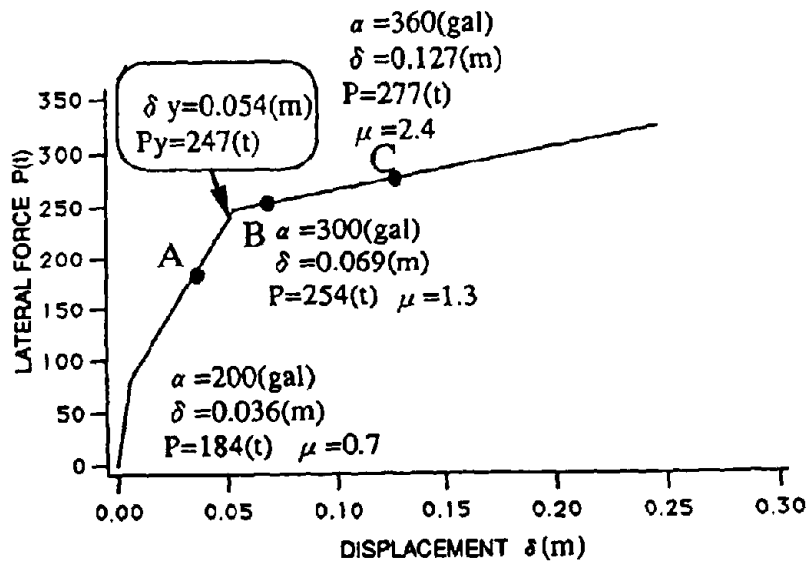


Fig-9 Maximum displacement response of the column-head plotted on the skelton curve

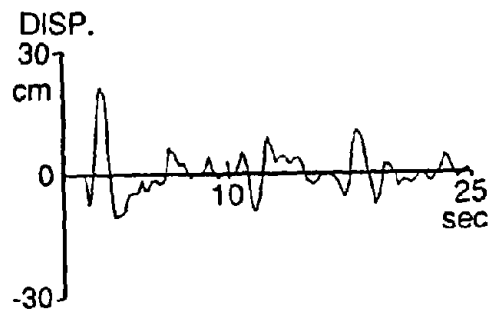


Fig-10 Time-history wave of relative displacement of the Menshin bearing to 360 gal input motion

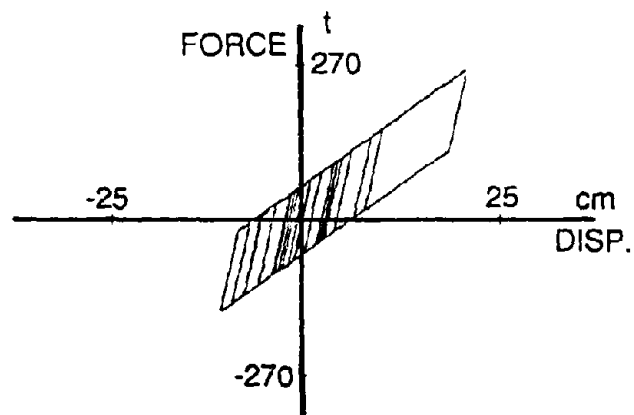
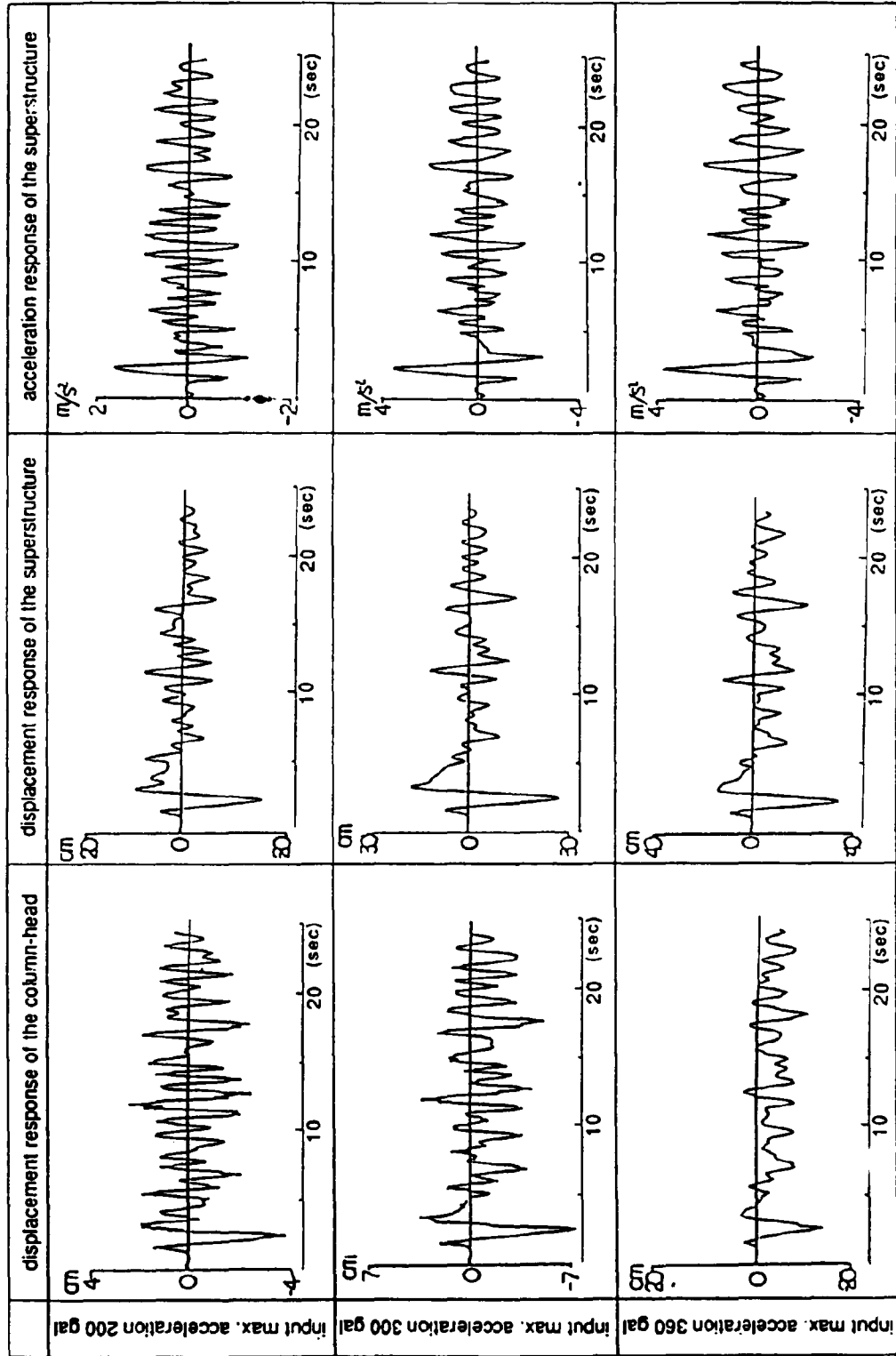


Fig-11 Idealized hysteresis loop of relative displacement of the Menshin bearing nad applied horizontal force for 360 gal input motion

Table-4 Time-history response of the linear column model to various levels of input maximum acceleration

input max. acceleration 200 gal	displacement response of the column-head cm 2 0 -2 10 20 (sec)	displacement response of the superstructure cm 20 0 -20 10 20 (sec)	acceleration response of the superstructure m/s ² 3 0 -3 10 20 (sec)
input max. acceleration 360 gal	cm 3 0 -3 10 20 (sec)	cm 30 0 -30 10 20 (sec)	m/s ² 4 0 -4 10 20 (sec)
input max. acceleration 300 gal	cm 3 0 -3 10 20 (sec)	cm 30 0 -30 10 20 (sec)	m/s ² 5 0 -5 10 20 (sec)

Table-5 Time-history response of the non-linear column model to various levels of input maximum acceleration



SEISMIC RESPONSE OF CURVED CONTINUOUS MENSHIN BRIDGE

Nobumichi HOSODA¹, Isao KANEKO², and Kouki KURODA³

- ^{1,2} Research Department of Civil Structures, Institute of Construction Technology, Kumagai Gumi Co., Ltd., Ibaraki 300-22, Japan
³ Civil Engineering Division, Design and Planning Department, Kumagai Gumi Co., Ltd., Tokyo 162, Japan

SUMMARY

A series of the earthquake response analyses of a curved Menshin bridge were carried out using an analytical approach in which the non-linear behavior in the shear deformation of the Menshin bearing is be able to taken into consideration. It was found that the seismic responses at an individual substructure and Menshin bearing in the tangential direction to the deck axis are larger than the corresponding responses of the straight bridge in the longitudinal direction, while the seismic responses in the normal direction are smaller than the corresponding responses of the straight bridge in the transverse direction.

INTRODUCTION

In conducting a earthquake response analysis, the coupled vibration in plane is a important phenomenon for the curved bridge, and the non-linear behavior in shear deformation of the Menshin bearing is important for the Menshin Bridge. In the case of curved Menshin bridge, it is considered that the non-linear analysis for the simultaneous excitation in orthogonal directions simulates very well the response during a particular earthquake. However, because the direction of principal axes of a substructure is different from the other substructures, it should be necessary to adopt a complex approach in order to estimate the maximum response values of an individual Menshin bearing and substructure. This paper discusses, at first, two analytical approach, which are called as the approach A and B in this paper, for evaluation of the maximum response values of the curved Menshin bridge.

This paper also presents the earthquake responses of a curved Menshin bridge in comparison with those of an idealized continuous bridge where the deck is fixed on all substructures.

ANALYTICAL APPROACHES FOR EVALUATION OF MAXIMUM RESPONSE OF CURVED MENSHIN BRIDGES

Approach A The analytical approach A for evaluation of the maximum response values of the curved Menshin bridge is outlined as follows:

- (a) Idealize the bridge as a three dimensional frame model.
- (b) As illustrated in Fig. 1, conduct a earthquake response analysis due to an excitation in a direction, which has the angle θ in degree from one of the horizontal axis X of the global coordinates. Generally the axis X itself would

be chosen as the direction of excitation. From the outputs of the analysis, pick up the maximum responses on the local coordinates of every Menshin bearing and substructure, for example, as follows;

$\theta F_{i,t}$, $\theta F_{i,n}$: maximum shear forces in the tangential direction and the normal direction, respectively, at an i -th Menshin bearing,

$\theta U_{i,t}$, $\theta U_{i,n}$: maximum relative displacements in the tangential direction and the normal direction, respectively, at an i -th Menshin bearing,

$\theta M_{i,t}$, $\theta M_{i,n}$: maximum bending moments around the tangential direction and the normal direction, respectively, at a bottom of an i -th substructure.

- (c) Conduct the same earthquake response analysis as described in (b) except the direction of the excitation which crosses with that of previous analysis at a right angle. From the analysis due to the excitation of the direction with the angle of $\theta-90$ degrees from the coordinate axis X , the maximum shear forces at the i -th Menshin bearing, $\theta-90 F_{i,t}$ and $\theta-90 F_{i,n}$, the maximum relative displacements at the i -th Menshin bearing, $\theta-90 U_{i,t}$ and $\theta-90 U_{i,n}$, and the maximum bending moment at the bottom of the i -th substructure, $\theta-90 M_{i,t}$ and $\theta-90 M_{i,n}$, would be obtained.
- (d) Evaluate the maximum responses on the local coordinates of every Menshin bearing and substructure by using the square-root-of-sum-of-squares (SRSS) operation to combine the two maximum values which were obtained in (b) and (c) For example, the maximum shear forces and relative displacements at the i -th Menshin bearing and the maximum bending moments at the bottom of the i -th substructure could be evaluated by the Eqs. (1), (2) and (3), respectively:

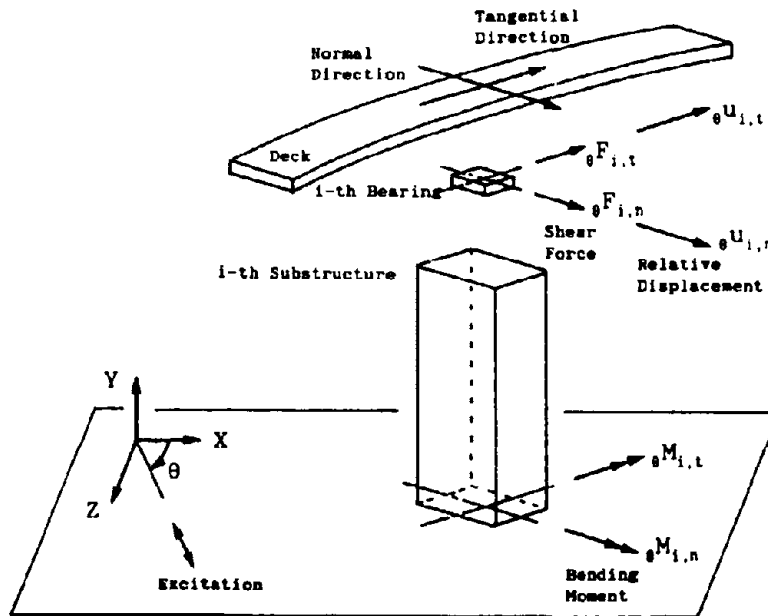


Fig. 1 Definition of the Maximum Responses to be Used in the Approach A

$$F_{i,t} = \sqrt{\left(\theta F_{i,t} \right)^2 + \left(\theta_{.90} F_{i,t} \right)^2} \quad (1-a)$$

$$F_{i,n} = \sqrt{\left(\theta F_{i,n} \right)^2 + \left(\theta_{.90} F_{i,n} \right)^2} \quad (1-b)$$

$$u_{i,t} = \sqrt{\left(\theta u_{i,t} \right)^2 + \left(\theta_{.90} u_{i,t} \right)^2} \quad (2-a)$$

$$u_{i,n} = \sqrt{\left(\theta u_{i,n} \right)^2 + \left(\theta_{.90} u_{i,n} \right)^2} \quad (2-b)$$

$$M_{i,t} = \sqrt{\left(\theta M_{i,t} \right)^2 + \left(\theta_{.90} M_{i,t} \right)^2} \quad (3-a)$$

$$M_{i,n} = \sqrt{\left(\theta M_{i,n} \right)^2 + \left(\theta_{.90} M_{i,n} \right)^2} \quad (3-b)$$

where, $F_{i,t}$ and $F_{i,n}$ are the combined maximum shear forces in the tangential direction and the normal direction, respectively, at the i -th Menshin bearing, $u_{i,t}$ and $u_{i,n}$ are the combined maximum relative displacements in the tangential direction and the normal direction, respectively, at the i -th Menshin bearing, and $M_{i,t}$ and $M_{i,n}$ are the combined maximum bending moments around the tangential direction and the normal direction, respectively, at the bottom of the i -th substructure.

In this approach, the coupled vibration of the curved bridge in plane is able to be taken into consideration. However the non-linear behavior in shear deformation of the Menshin bearing cannot be considered so exactly because the combination as formulated in Eqs. (1), (2) and (3) are not applicable to a non-linear analysis. In order to conduct the linear response analyses in (b) and (c), the Menshin bearing has to be idealized as the combination of the linear spring element with the effective stiffness and the linear viscous damping element with the effective damping ratio. Furthermore the effective stiffness and effective damping ratio have to be given in (a) by assuming a proper relative displacements of the bearing. After the analyses, the assumed relative displacements have to be checked by comparing with those obtained in (d). If the assumed relative displacements are different from the corresponding ones calculated, it is necessary to return to (a) and carry out the procedures once more again.

Approach B The analytical approach B for evaluation of the maximum response values of the curved Menshin bridge is outlined as follows:

- (a) Idealize the bridge as a three dimensional frame model.
- (b) As illustrated in Fig. 2.(a), conduct a earthquake response analysis due to an excitation, the direction of which is tangent to the deck axis at an i -th substructure. From the outputs of the analysis, pick up the maximum responses at the considering Menshin bearing and substructure and regard them as the maximum responses in the tangential direction or around the normal direction,

for example, as follows;

- $F^{i,t}$: regarded maximum shear force at the Menshin bearing in the tangential direction,
- $u^{i,t}$: regarded maximum relative displacement at the Menshin bearing in the tangential direction,
- $M^{i,n}$: regarded maximum bending moment at the bottom of the substructures around the normal direction.

Note: The excitation is considered to exist in the only one direction in the physical sense. But it is dealt with, from the view point of the numerical method, as a simultaneous excitation in orthogonal directions where the input ground motions in two horizontal axes of the global coordinates are in phase with each other.

Note: The directions of these maximum responses, in general, do not correspond to the tangential direction; There may exist some angles $\phi[.]$ as illustrated in Fig. 2. But it seems that the effect of the difference of the directions on the maximum response values should be very little and could be neglected.

- (c) As illustrated in Fig. 2.(b), conduct another earthquake response analysis due to the excitation in the normal direction of the i-th substructure. From the outputs of the analysis, obtain the maximum responses, for example, as follows;

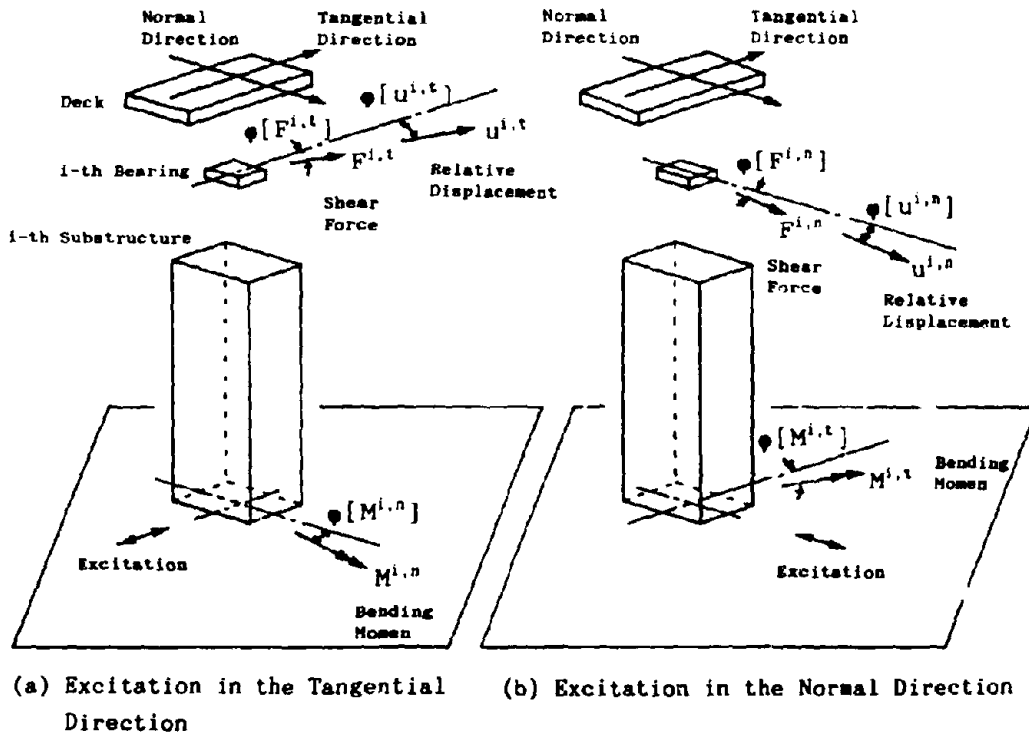


Fig. 2 Definition of the Maximum Responses to be Used in the Approach B

- $F^{i,n}$: regarded maximum shear force at the Menshin bearing in the normal direction,
- $u^{i,n}$: regarded maximum relative displacement at the Menshin bearing in the normal direction,
- $M^{i,t}$: regarded maximum bending moment at the bottom of the substructure around the tangential direction.

(d) Repeat the analyses of (b) and (c) as the same times as the number of the substructures.

In this approach, the non-linear behavior in shear deformation of the Menshin bearing is able to be taken into consideration. However, it cannot but have some errors due to the coupled vibration of the curved bridge, as described in the later note of (b). This approach was applied to a curved Menshin bridge and the result obtained from the analyses is presented below.

OUTLINE OF EARTHQUAKE RESPONSE ANALYSES

Considered Bridge The continuous prestressed concrete girder bridge with four spans was considered in the analyses, as shown in Fig. 3 (Ref.1). It is assumed to be constructed on the site with the stiff ground condition which is classified as the ground condition I in Japan (Ref. 2). Every reinforced concrete column has a square section of 2.5 meters, and the every abutment has a rectangular section of 10.1 by 0.9 meters, and they are settled on the spread foundation. A Menshin bearing used is a lead rubber bearing, and it is installed between the deck and the top of a column or an abutment.

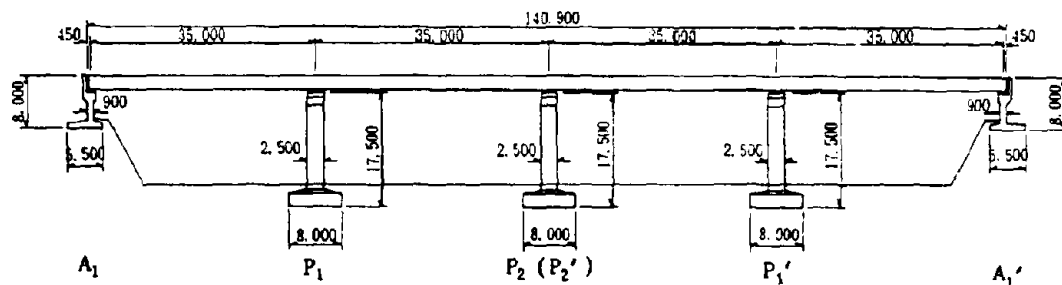


Fig. 3 Schematic Diagram of the Bridge Analyzed

Cases of Analyses Fig. 4 illustrates the schematic diagrams representing the cases of the analyses conducted to evaluate the maximum responses of the curved Menshin bridge. The earthquake response analyses of the curved bridge, two radii of which cross at a right angle, were carried out, changing the direction of excitation in 22.5 degrees interval in plane. In addition, the earthquake response analyses of the straight bridge were also carried out for comparison, due to the excitation in the longitudinal and transverse directions, respectively.

The same cases of the earthquake response analyses of the idealized continuous bridge, where fixed bearings are used in place of Menshin bearings, were carried out, too. This type of bridge is called as the all-point fixed bridge in this paper,

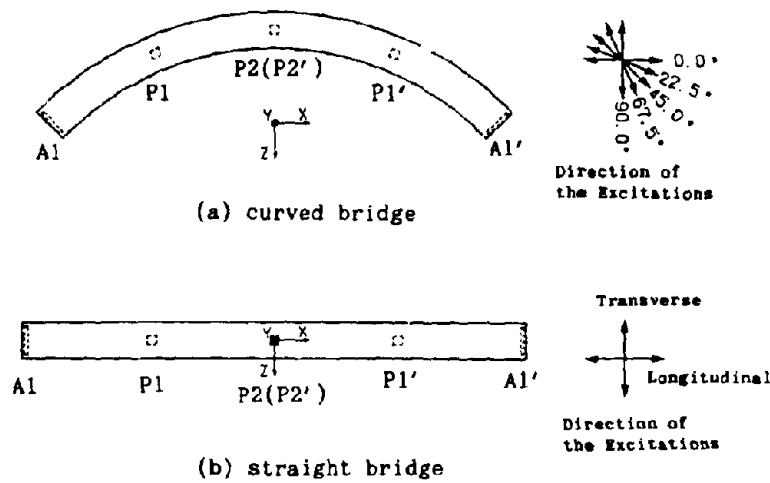


Fig. 4 Schematic Diagrams to Represent the Series of Analyses

and it is considered to be adequate to demonstrate the effect of the Menshin bridge, by comparing the results of response analyses on both type of bridge. Moreover, the maximum response values of the curved all-point fixed bridge are evaluated by the both approaches A and B, and they are compared with each other in order to confirm the applicability of the approach B.

Method of Analyses The bridges are idealized as three dimensional frame models as shown in Fig. 5. A Menshin bearing is assumed to have the force-displacement

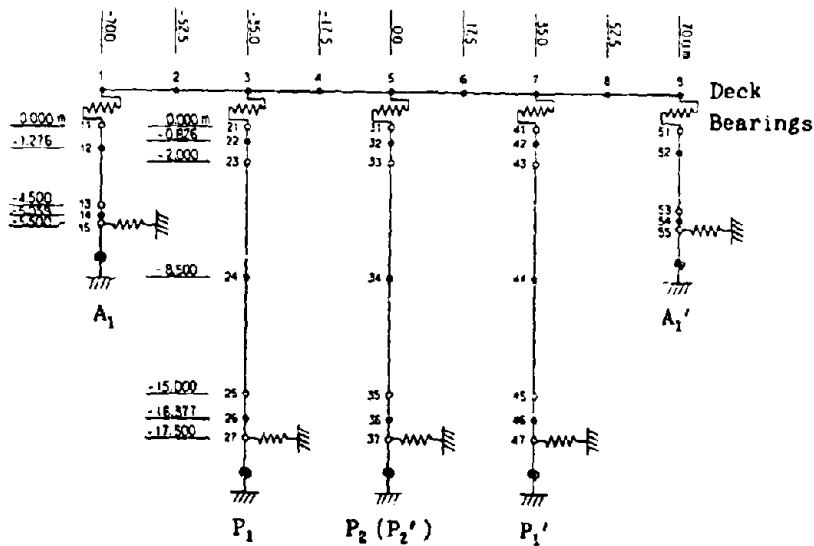


Fig. 5 A Description for the Numerical Method used in the Analyses

relationship of bi-linear type in shear deformation, and it is constituted of eight bi-linear springs in different directions of 22.5 degrees interval in plane so as to have the same deformation characteristics to every directional deformation. A fixed bearing is modeled as two sufficiently stiff springs.

The earthquake response analyses are performed using the numerical integration of Newmark's β method with $\beta=1/4$. The input motion used is modified acceleration record which was recorded on the ground near the Kaihoku bridge during the Miyagi-ken-oki Earthquake of 1978, with the maximum acceleration of 360 cm/sec².

RESULTS OF ANALYSES

Applicability of Approach B Table 1 shows the maximum shear forces at the fixed bearings of the all-point fixed bridge evaluated by Eq.(1) of the Approach A, changing the direction of the couple of excitations. As shown in the table, some maximum shear force is evaluated differently, at most 5 percents, according to the direction of the couple of excitations.

Table 1 Effect of the Direction of the Couple of Excitations on the Maximum Shear Force at the Fixed Bearing Evaluated by the Approach A

(a) Tangential Direction

Angles of the Direction of Excitations (Degree)	$F_{A1,t}$	$F_{P1,t}$	$F_{P2,t}$
I. 0.0 and -90.0	626.8 tf	68.1 tf	65.3 tf
II. 22.5 and -67.5	626.7 tf (1.000)	68.1 tf (1.000)	65.4 tf (1.001)
III. 45.0 and -45.0	626.9 tf (1.000)	68.1 tf (1.001)	65.4 tf (1.001)
IV. 67.5 and -22.5	627.0 tf (1.000)	68.4 tf (1.005)	65.4 tf (1.001)

The value in the parentheses is the ratio of the maximum response to that listed in the row I.

(b) Normal Direction

Angles of the Direction of Excitations (Degree)	$F_{A1,n}$	$F_{P1,n}$	$F_{P2,n}$
I. 0.0 and -90.0	1345.6tf	55.8 tf	80.0 tf
II. 22.5 and -67.5	1344.3tf (0.999)	57.9 tf (1.039)	79.9 tf (1.000)
III. 45.0 and -45.0	1344.8tf (0.999)	58.6 tf (1.051)	80.0 tf (1.000)
IV. 67.5 and -22.5	1345.8tf (1.000)	56.9 tf (1.021)	79.9 tf (1.000)

The value in the parentheses is the ratio of the maximum response to that listed in the row I.

Table 2 shows the comparison of the approach A and B for the maximum shear forces at the fixed bearings of the all-point fixed bridge. Some difference between the maximum values evaluated by two approaches, at most 5 percents, are recognized. As for the maximum bending moments at the bottom of the columns and the abutment,

the difference was at most 2 percents between two approach, but the details will not be shown here. Comparing this result with that as shown in Table 1, it could be concluded that the approach B gave the maximum responses of the all-point fixed

Table 2 Comparison of the Approach A and B for the Maximum Shear Forces at the Fixed Bearing

(a) Tangential Direction

Approach	$F_{A1,t}$ or $F^{A1,t}$	$F_{P1,t}$ or $F^{P1,t}$	$F_{P2,t}$ or $F^{P2,t}$
I. Approach A : $F_{1,t}$	626.8 tf	68.1 tf	65.3 tf
II. Approach B : $F^{1,t}$	634.2 tf	68.0 tf	65.4 tf
III. Ratio : $F^{1,t} / F_{1,t}$	1.012	0.999	1.001

The value listed as the approach A was evaluated from the results for the direction of excitations with the angles θ of 0.0 and 90.0 degrees.

(b) Normal Direction

Approach	$F_{A1,n}$ or $F^{A1,n}$	$F_{P1,n}$ or $F^{P1,n}$	$F_{P2,n}$ or $F^{P2,n}$
I. Approach A : $F_{1,n}$	1345.6 tf	55.8 tf	80.0 tf
II. Approach B : $F^{1,n}$	1341.6 tf	52.9 tf	80.0 tf
III. Ratio : $F^{1,n} / F_{1,n}$	0.997	0.949	1.000

The value listed as the approach A was evaluated from the results for the direction of excitations with the angles θ of 0.0 and 90.0 degrees.

Table 3 Angle of the Direction of the Maximum response from the Tangential or Normal Direction of the Individual Member (in degree)

(a) Maximum Shear Force at the Bearing

Type of Bridge	$\theta[F^{A1,t}]$	$\theta[F^{P1,t}]$	$\theta[F^{P2,t}]$	$\theta[F^{A1,n}]$	$\theta[F^{P1,n}]$	$\theta[F^{P2,n}]$
Menshin Bridge	9.7	7.2	0.0	7.9	0.4	0.0
All-point Fixed Bridge	11.8	0.9	0.0	3.8	0.5	0.0

(b) Maximum Relative Displacement at the Bearing

Type of Bridge	$\theta[u^{A1,t}]$	$\theta[u^{P1,t}]$	$\theta[u^{P2,t}]$	$\theta[u^{A1,n}]$	$\theta[u^{P1,n}]$	$\theta[u^{P2,n}]$
Menshin Bridge	8.8	5.8	0.0	6.0	0.3	0.0

(c) Maximum Bending Moment at the Bottom of the Column or Abutment

Type of Bridge	$\theta[M^{A1,t}]$	$\theta[M^{P1,t}]$	$\theta[M^{P2,t}]$	$\theta[M^{A1,n}]$	$\theta[M^{P1,n}]$	$\theta[M^{P2,n}]$
Menshin Bridge	5.8	0.3	0.0	8.0	8.2	0.0
All-point Fixed Bridge	4.0	1.7	0.0	11.6	10.0	0.0

bridge with a sufficient accuracy in comparison with the approach A.

Table 3 shows the angle of the direction of the maximum response from the tangential or normal direction of the individual bearing and substructure, which was neglected in the evaluation of the maximum response value by the approach B. Since the range of the angles of the Menshin bridge is almost the same as that of the all-point fixed bridge, it seems that the approach B is also sufficiently applicable to the Menshin bridge.

It has not yet been done to compare the result between the approach A and B in the case of Menshin bridge in order to investigate the effect of the difference of analytical methods, a linear analysis and a non-linear analysis, on the resulting maximum response values.

Seismic Response of Curved Menshin Bridge Fig. 6 shows the maximum shear forces at the bearings of the curved bridge evaluated by the approach B in comparison with the straight bridge. In the case of the Menshin bridge, the maximum shear force at any bearing of the curved bridge in the tangential direction is larger than that at the corresponding bearing of the straight bridge due to the excitation in the longitudinal direction, while the maximum shear force of the curved bridge in the normal direction is smaller than that of the straight bridge due to the excitation in the transverse direction. In the case of the all-point fixed bridge, on the contrary, the maximum shear force of the curved bridge in the tangential direction is smaller than that of the straight bridge, while the maximum shear force of the curved bridge in the normal direction is larger than that of the straight bridge.

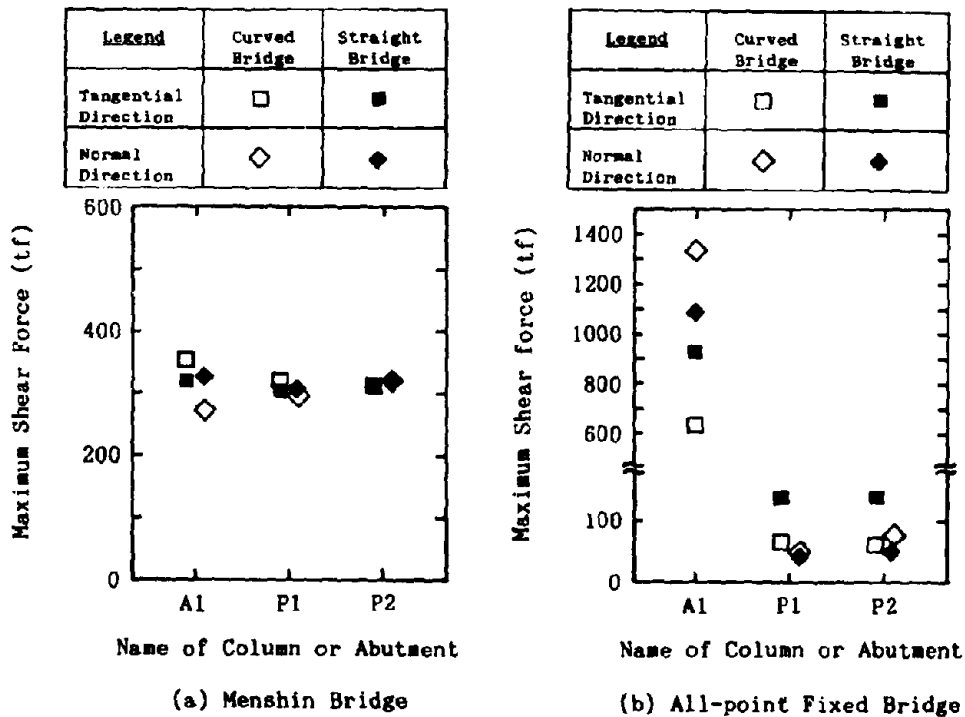


Fig. 6 Maximum Shear Force at the Bearing

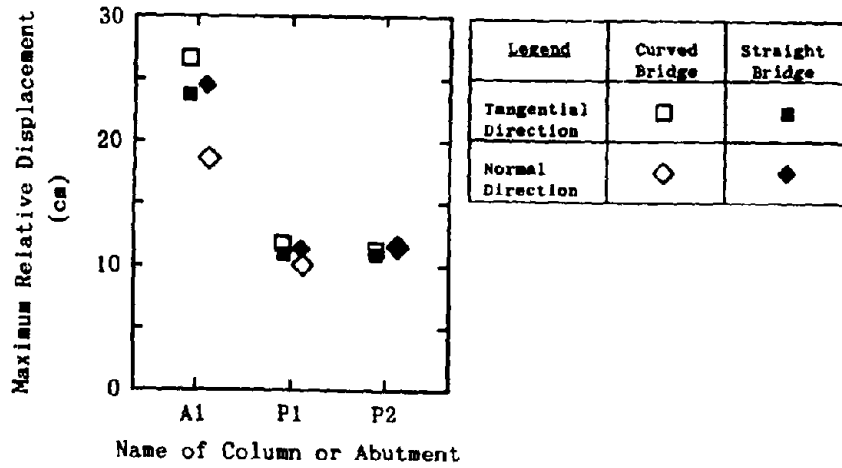


Fig. 7 Maximum Relative Displacement at the Menshin Bearing

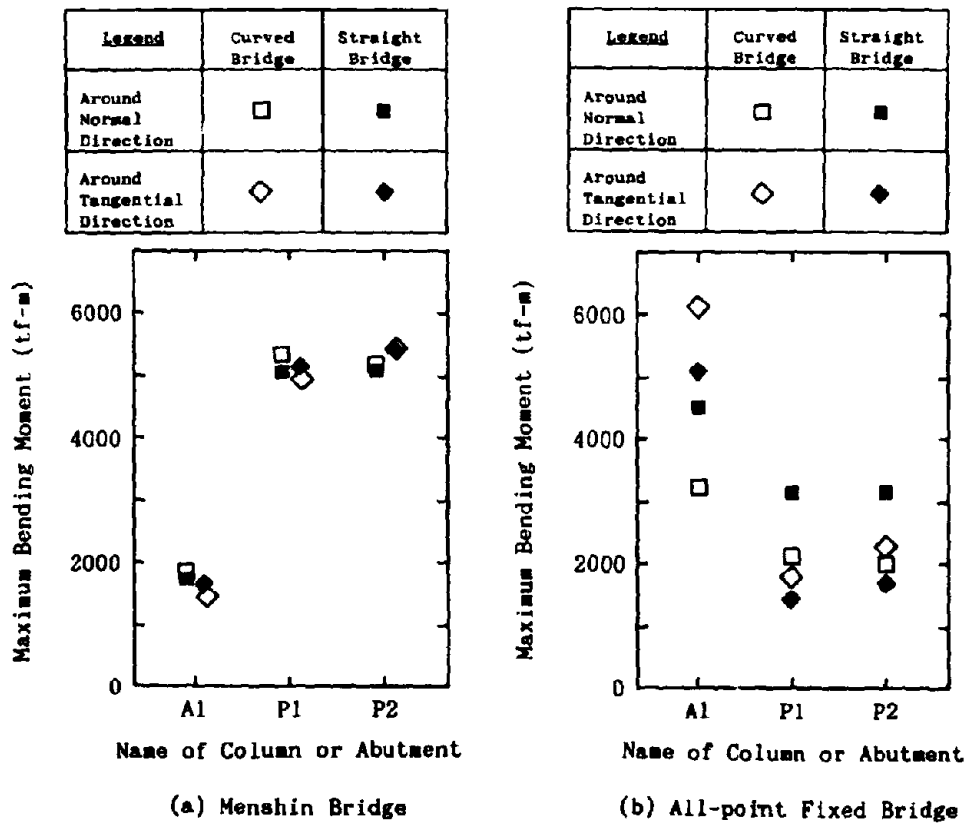


Fig. 8 Maximum Bending Moment at the Bottom of the Substructure

As for the curved bridges considered herein, two radii of which cross at the right angle, the difference in the maximum shear force between the curved bridge and the straight bridge is greatest at the bearing on the abutment A1 in both cases of the Menshin bridge and the all-fixed bridge.

Fig. 7 shows the maximum relative displacements at the bearings of the curved Menshin bridge in comparison with the straight Menshin bridge. Differences in the maximum relative displacements between the curved bridge and straight bridge have the similar tendency with those in the maximum shear forces. The difference is greatest at the bearing on the abutment A1, because the maximum seismic lateral force to be supported by the bearing are larger than the others, as mentioned above, and the bearing was more flexible in the shear deformation than the others.

Fig. 8 shows the maximum bending moments at the bottom of the columns and abutment of the curved bridge in comparison with the straight bridge. The results are analogous to that of the maximum shear force at the bearings.

CONCLUSIONS

1. An analytical approach to evaluate the maximum responses of the curved continuous bridge, in which the non-linear behavior in shear deformation of the Menshin bearing is able to be taken into consideration, was described in detail, and the applicability of the approach was assured.
2. It was found that the seismic responses at an individual Menshin bearing and substructure in the tangential direction to the deck axis are larger than the corresponding responses of the straight bridge in the longitudinal direction, while the seismic responses in the normal direction are smaller than the corresponding responses of the straight bridge in the transverse direction.

ACKNOWLEDGMENTS

This study was made as a part of the joint research program on "Development of Menshin System of Highway Bridges" between the Public Works Research Institute (PWRI) and 28 private firms in Japan. The authors would like to acknowledge the helpful guidance of Dr. K. Kawashima and Mr. K. Hasegawa of the Earthquake Engineering Division of PWRI. Thanks are also due to the members of the joint research program for their fruitful discussion.

REFERENCES

1. PWRI and 28 Private Firms: "Development of Menshin System of Highway Bridges - Report No.2 - ", PWRI Joint Research Report No.60, March 1991. (in Japanese)
2. Japan Road Association: "Design Specifications for Highway Bridges, Part V, Earthquake Resistant Design", 1990. (in Japanese)

COMPARATIVE DESIGN OF A STEEL GIRDER BRIDGE
USING THREE DIFFERENT BEARING SYSTEMS

Mitsuo OKADO¹ Mitsuharu KOMURO² Michihiro HORIKAWA³ Fuminao KAWAHARA⁴

1,2,3,4 New Structural Engineering Ltd. Chiyoda-ku, Tokyo, Japan

SUMMARY

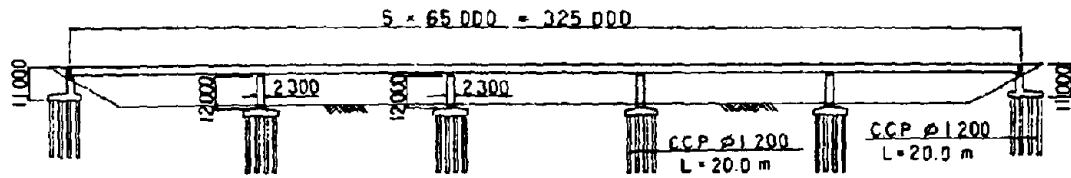
This study investigates the effect of temperature change and the improvement of the seismic response for continuous steel girder Menshin bridge. As the result, it is found that a Menshin bridge can extremely reduce small effect of temperature change, compared with a bridge with multi-point fixed support to the earthquake response, so that multi-span continuous bridge can be designed by using Menshin bearing, and that the seismic response can be improved by Menshin bearing.

INTRODUCTION

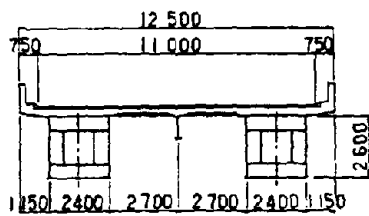
Continuous bridges are often adopted to lessen the number of expansion joints which are vulnerable to traffic load and causing the maintenance problem. However, the inertia force of a girder during an earthquake and the expansion of a girder due to the effect of temperature change increases with increasing the number of the spans. Although the inertia force could be concentrated to one pier with a fixed bearing and the other piers supporting only vertical dead load of a girder with movable bearings, the distribution of the inertia force to some piers with fixed bearings or elastic bearings is usually more reasonable and economical. However, since the effect of temperature change for a steel girder bridge is more larger than that for a concrete girder bridge, the distribution by using fixed bearings is not appropriate to continuous steel girder bridges. This report investigates the applicability of elastic bearings, such as linear rubber bearings and Menshin bearings on continuous steel girders, to reduce the effect of temperature change and improve the seismic response.

ANALYSIS CONDITIONS

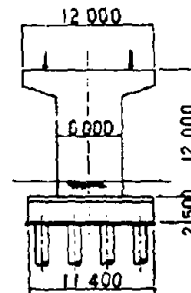
Analysis Model Fig.1 shows the analyzed bridge, whose superstructure is a 5-span continuous steel girder with span length of 65m, and substructure are reinforced concrete piers with pile foundations. The analysis model and the sectional properties of the bridge are shown in Fig.2 and Table 1, respectively.



(a) Side View



(b) Cross Section of Girder



(c) Cross Section of Pier

Fig.1 Dimensions of Analyzed Bridge

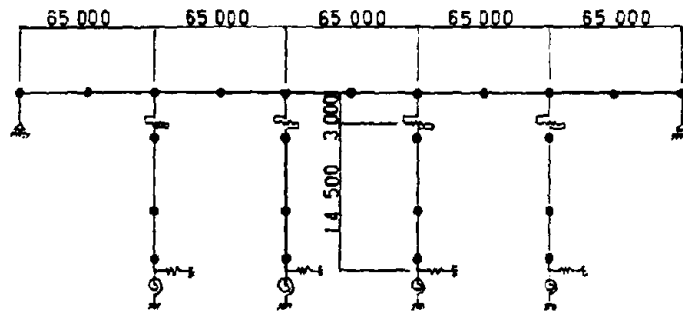


Fig.2 Analysis Model

Table 1 Sectional Properties

(a) Sectional Properties of Bridge Pier

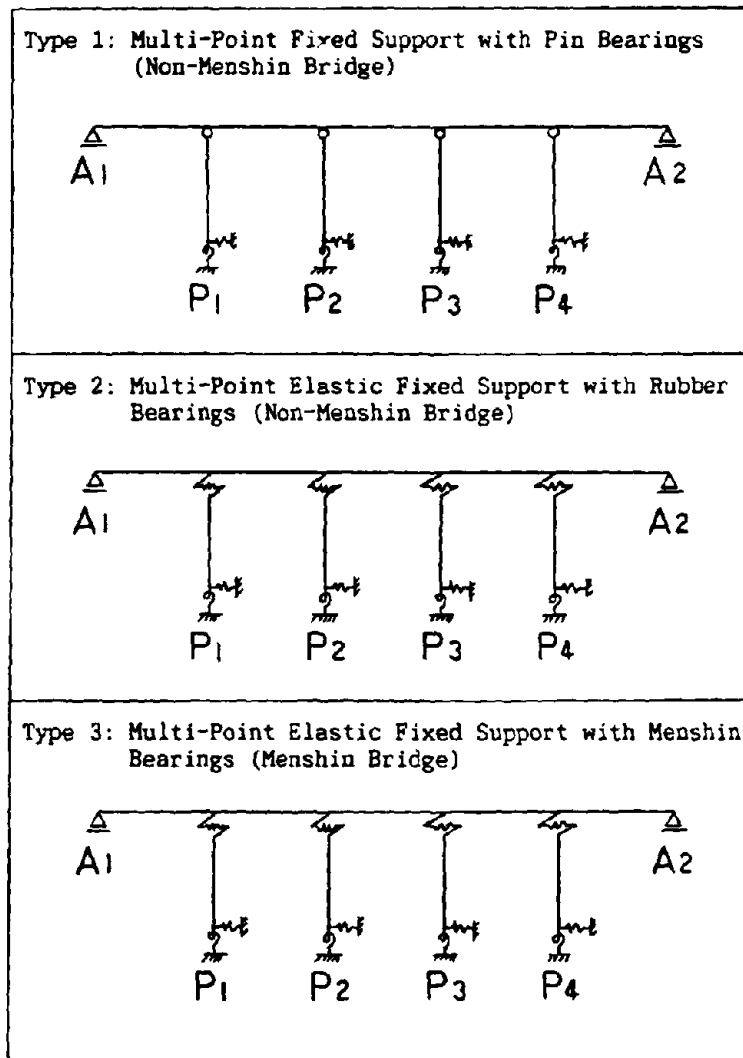
Sectional Area	13.80 m ²
Geometrical Moment of Inertia (longitudinal direction)	6.80 m ⁴
Geometrical Moment of Inertia (transverse direction)	41.40 m ⁴
Torsional Geometrical Moment of Inertia	18.46 m ⁴

(c) Constants for Foundation Spring

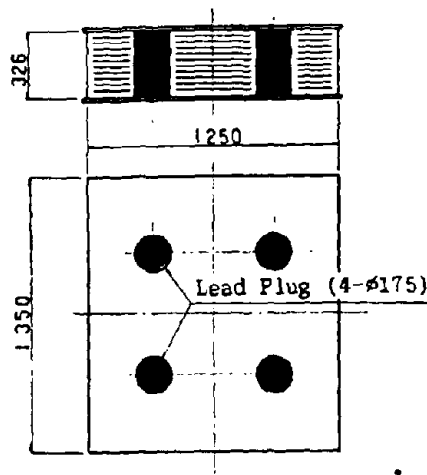
Horizontal Spring Constant	543 900 tf/m
Vertical Spring Constant	829 400 tf/m
Coupled Spring Constant	844 500 tf
Rotational Spring Constant	11 434 800 tf·m

Type of Bearing Support Systems The three types of bearing support systems shown in Table 2 were investigated in order to grasp the effect of temperature changes and earthquake response. The type 1 is a non-Menshin bridge with multi-point fixed support system using pin bearings. The type 2 is non-Menshin bridge with multi-point elastic fixed support system using linear rubber bearings, and the type 3 is a Menshin bridge with multi-point elastic fixed support system using Menshin bearings.

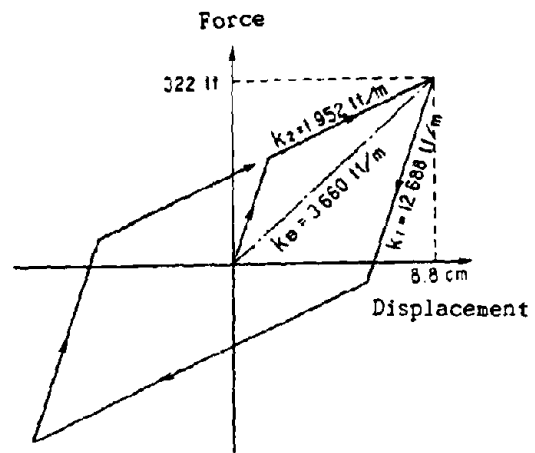
Table 2 Type of Bearing Support Systems



Elastic Bearing Lead rubber bearings (abbreviated as LRB in the following) and used as Menshin devices for the Menshin bridge. The dimensions and the idealized hysteresis loop of the LRB used for the analysis are shown in Fig.3, and the characteristics values of the LRB are shown in Table 3. The stiffness of linear rubber bearing use in the type 2 is equal to the effective stiffness of LRB.



(a) Dimensions of LRB



(b) Idealized Hysteresis Loop

Fig.3 Dimensions of LRB and Idealized Hysteresis Loop

Table 3 Design Values of Menshin Bearing (LRB)

(a) Design Conditions

Design Conditions (per bearing)	Unit	P1,P4	P2,P3
Maximum Vertical Reaction Force	tf	835	737
Dead Load Vertical Reaction Force	tf	608	519
Displacement due to Temperature Change ($\pm 30^{\circ}\text{C}$)	mm	35.1	11.7
Distribution Ratio of Inertia Force of Girder	%	25.0	25.0
Number of Bearings per Bridge Pier	-	2	2
Rubber Shear Modulus	kgf/cm ²	8.0	8.0

(b) Characteristic Values of LRB

Characteristic Values (per bridge pier)	Unit	P1,P2,P3,P4
Effective Stiffness (k_0)	tf/m	3 660
Effective Damping Ratio (H_0)	%	25.0
Initial Stiffness (k_1)	tf/m	12 688
Post-yield Stiffness (k_2)	tf/m	1 952
Characteristic Shear Strength (Q)	tf	150
Design Displacement of Bearing (u_0)	cm	8.8

Analysis Cases Analysis were made in two cases for each of the three types shown in Table 2. One is to investigate the effect of temperature change and other is to study the seismic response by dynamic analysis using the response spectrum method.

The temperature variation from -30°C to $+30^{\circ}\text{C}$ was taken into account and the LRB was idealized by a bi-linear spring model shown in Fig.3 in the analysis for temperature change. The acceleration response spectrum used for the dynamic analysis is shown in Fig.4. The LRB was modeled into a linear spring and a linear viscous damper.

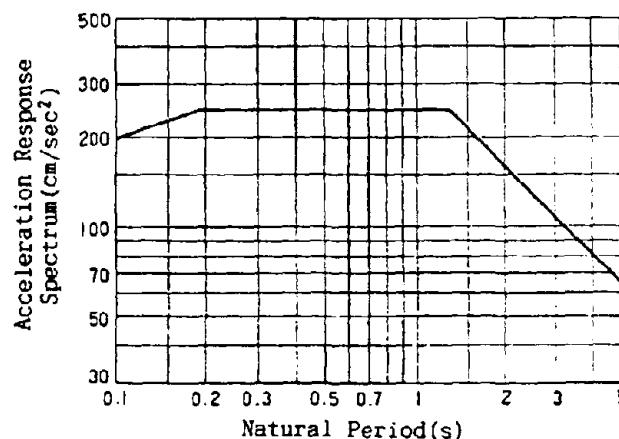


Fig.4 Acceleration Response Spectrum

RESULTS OF ANALYSIS

Effect of Temperature Change Table 4 shows the results of the analysis executed to study for the temperature change effect. The bending moments at bottom of the piers due to temperature change are compared in Fig.5 for each bearing support system. The bending moments of the Type 1 are larger than those of the type 2 and 3. This is because the elastic bearing ca. deform according to the expansion of the girder due to temperature change while the girder is fixed to piers by pin bearing in the Type 1. The effective stiffness of the LRB is inversely proportional to the displacement. An amount of the girder expansion at P1 and P4 piers is larger than that at the P2 and P3 piers. Therefore the bending moment of the type 3 at the P1 and P4 piers is smaller than that of the type 2.

Table 4 Analysis Results of Temperature Change Effect ($\pm 30^{\circ}\text{C}$)

		Type 1	Type 2	Type 3
Displacement at The Girder (mm)		32	34	35
P1	Relative Displacement of The Bearing (mm)	0	28	31
	Displacement at The Top of Pier (mm)	29	6	4
P4	Shear Force at The Top of Pier (tf)	501	102	65
	Bending Moment at The Bottom of Pier (tf.m)	6 018	1 227	775
P2	Relative Displacement of The Bearing (mm)	0	9	9
	Displacement at The Top of Pier (mm)	10	2	2
P3	Shear Force at The Top of Pier (tf)	173	34	40
	Bending Moment at The Bottom of Pier (tf.m)	2 079	412	478

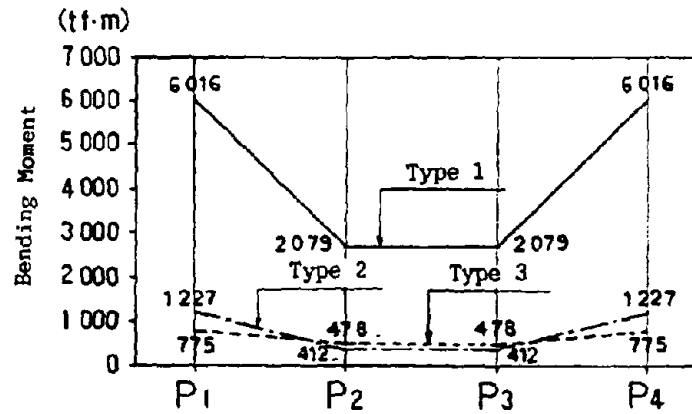


Fig.5 Bending Moment at the Bottom of Pier due to Temperature Change

Seismic Response Table 5 shows the results of the analysis executed to study for seismic response. The vibration modes obtained through the dynamic analysis are shown in Fig.6. An excellent natural period for sway advance mode of the girder is governed by third mode in the type 1 model, and by first mode in type 2 and 3.

Fig.7 shows the bending moments ratio at the pier bottom with 1.0 for the maximum value, according to the response spectrum analysis method for each bearing system. According to this figure, the type 1 and 2 have nearly the same values, while Menshin bridges of the type 3 have value smaller about 30%, which shows the damping effect of Menshin bearing.

The displacement at the girder is compares in Fig.8. According to this figure, the type 1 is smaller values than the type 2 and 3, because only elastic displacement appears at the pier, but no displacement of the bearing. On the other hand, the type 2 and 3 using elastic bearings show large values, but the type 3 using Menshin bearing shows smaller values than the type 2 using linear rubber bearings because of its damping effect. Therefore, it can be understood that Menshin bridges show about 30% smaller values for sectional forces and displacements than non-Menshin bridges. So Menshin bearing is useful for improvement of seismic response and reduction of displacement.

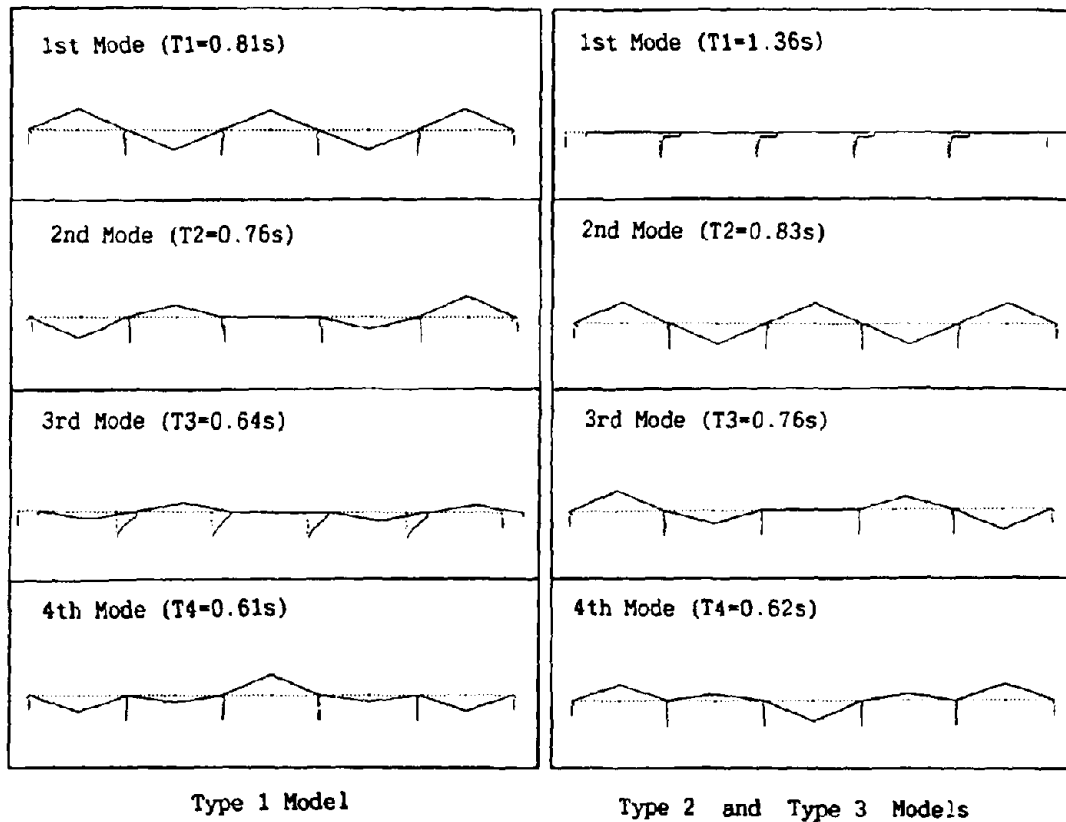


Fig.6 The Vibration Modes

Table 5 Analysis results of Seismic Response

		Type 1	Type 2	Type 3
Natural Period (sec.)		0.64	1.36	1.36
Displacement at the Main Girder (mm)		22	110	79
P1 P4	Relative Bearing Displacement (mm)	0	86	62
	Displacement at Pier Top (mm)	21	21	15
	Shear Force at Pier Top (mm)	295	315	227
	Bending Moment at Pier Bottom (tf·m)	3 961	3 925	2 844
P2 P3	Relative Bearing Displacement (mm)	0	87	62
	Displacement at Pier Top (mm)	20	21	15
	Shear Force at Pier Top (mm)	269	317	228
	Bending moment at Pier Bottom (tf·m)	3 626	3 932	2 845

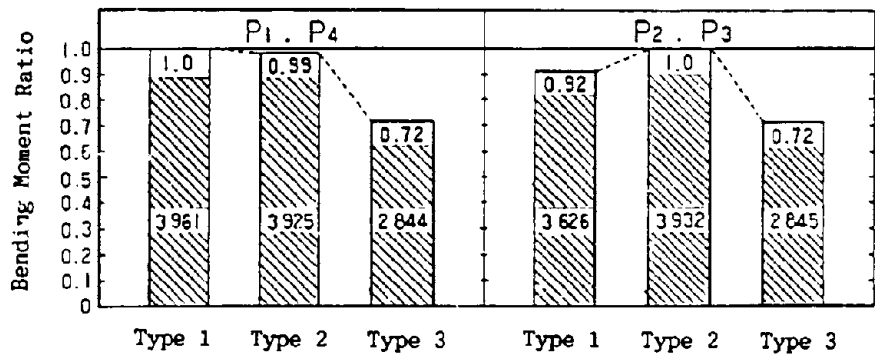


Fig.7 Bending Moment at the Bottom of Pier due to Seismic Response

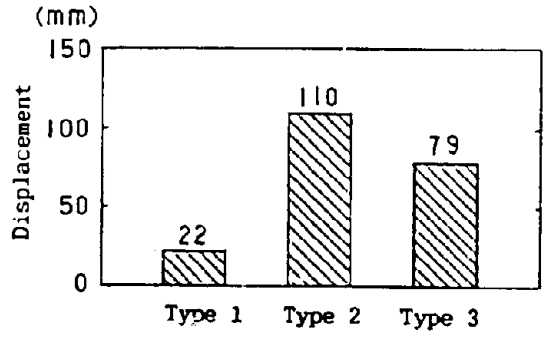


Fig.8 Displacement at the Girder

Relation Between Temperature Change and Seismic Response Fig.9 compare of the bending moments at the pier bottom between the effect of temperature change and seismic response. According to this figure, the bending moment due to temperature change for the type 1 is considerably large in comparison to the type 2 and 3. The bending moments due to the effect of temperature change for the type 2 and 3 is small by about 10% to 30% caused by seismic response, and it can be seen that effect of temperature changes present no problem whatsoever for the design of the substructures for multi-point elastic support.

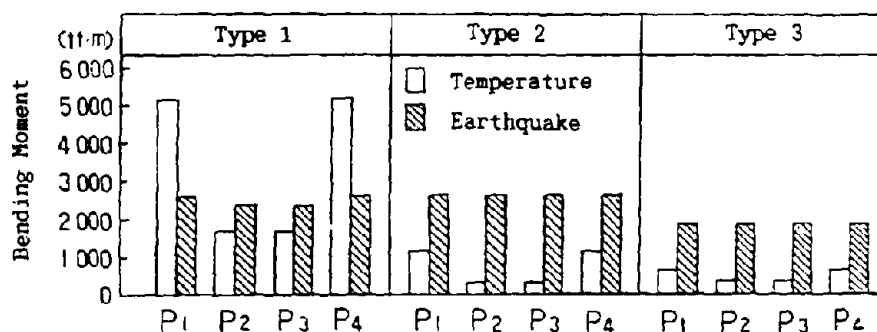


Fig.9 Bending Moment at the Bottom of Pier due to Temperature Change and Seismic Response

CONCLUSION

The effect of temperature change and improvement of the seismic response for steel girder Menshin bridges was investigated, analysing the bridges with the multi-point fixed supports, with elastic fixed support of linear rubber bearing and with elastic fixed support of Menshin bearing. The followings can be derived from the analysis results.

1. In the case of multi-point fixed support, the effect of temperature change is larger than the seismic response, while in the case of elastic fixed support, the effect of temperature change is extremely small in comparison to the seismic response. In particular, for the bridge using Menshin bearing (LRB), the bending moment due to temperature change is even smaller than that of the bridge using rubber bearings by 37% in the analysis models, since the effective stiffness of the bearing is inversely proportional to displacement.
2. The bending moment due to the earthquake response at the pier bottom of a Menshin bridge is about 30% smaller than that of a bridge using rubber bearings because of the damping effect of a Menshin bearing.

ACKNOWLEDGEMENTS

This study was made as a part of the joint research program on "Development of Menshin System of Highway Bridges" between PWPI and 28 private firms in Japan.

REFERENCES

1. Japan Road Association: "Design Specifications for Highway Bridges, Part V, Earthquake Resistant Design, 1990" (in Japanese)
2. Technology Research Center for National Land Development: "Guidelines on the design of Menshin Highway Bridges(Draft)", March 1989(in Japanese)
3. PWPI and 29 Private Firms: "Development of Menshin Systems of Highway Bridges-Report No.1-", PWPI Joint Reserach Report No.44, March 1990 (in Japanese)

6. Applications to Seismic Retrofit

Application of Menshin Design to Seismic Retrofit of Existing Bridges By Concrete Slabs of Adjacent Girders

M. Yanagihara, Y. Makiguchi and I. Kawasaki

Advantages of Isolation Bearings for New Bridges

R. Anderson

Application of Menshin Design to Seismic Retrofitting of Highway Bridge Substructures

T. Tamura, M. Hirai, N. Higuchi and S. Masuda

APPLICATION OF MENSHPIN DESIGN TO SEISMIC RETROFIT OF EXISTING
BRIDGES BY CONCRETE SLABS OF ADJACENT GIRDERS

Mshiro YANAGIHARA¹, Yutaka MAKIGUCHI¹, Iwao KAWASAKI

¹Ishikawajima-Harima Heavy Industries Co.,Ltd

²Oiles Corporation

³Japan Engineering Consultants Co.,LTD

SUMMARY

When the expansion joints of an existing simple girder bridge, which continues over multiple effective spans, are removed, and the concrete slabs of neighboring girders are connected, the flatness of the bridge surface is improved, a drastic reduction of the occurrence of noise and vibration caused by the expansion joints can be achieved, and seismic resistance can be improved. Generally, however, a simple girder bridge is supported by movable bearings and fixed bearings, and therefore, when the method of simply connecting the slabs is used, the bridge will be a multi-bearing fixed structure, and there is therefore a possibility that expansion of girders by temperature change will be obstructed and that excessively great forces will act on the substructure. Therefore, when this method is used, the existing bearings are generally replaced by bearings such as elastomeric bearings, which softly support the superstructure in the horizontal direction. On the other hand, however, the horizontal displacement due to the seismic load will be increased by the soft horizontal spring of the elastomeric bearing, and there is a danger that the horizontal displacement could exceed the floating gap at the girder end section, which is considered to be a maximum of 10cm. Therefore, the application of the menshin bearing, which has higher damping performance than an ordinary elastomeric bearing, can be considered. We have conducted a case study regarding the application of the menshin bearing to construction connecting many effective spans, using an existing elevated bridge in a city as the model case, and we have demonstrated the usefulness of the menshin bearing.

BRIDGE STRUCTURE AND DESIGN CONDITIONS

Structure of bridge Fig.1 shows the entire structure of the existing bridge. The bridge span is 30.0m. This is a composite girder type bridge, constructed of a concrete slab of 22cm thick, and 7 steel plate girders. The maximum reaction force per single supporting point is 80tf. All bearings are made of steel, and the height of each bearing, both movable and fixed, including the height-adjustment mortar, is 180mm.

Design conditions Table 1 shows the design conditions for the bearing sections.

Connection structure and bearing structure Fig.2 shows the slab and girder connection structure, and Fig.3 shows the details of the bearings which are used to replace the existing bearings. Regarding the connection method, there is an example in which the concrete slabs were simply connected, but in this case study, we considered a structure which not only connected the slabs but also connected the girders, with the additional purpose of providing a structure which would prevent the bridge from falling. The connection section is given a rigidity about 1/10 that of the girder. When the rigidity is at this level, it does not generate excessively great tensile stress on the concrete

Table 1 Design Conditions of Bearing

Maximum design vertical force of a bearing	tf	80
Total dead weight of superstructure of one span	tf	606
Temperature change	°C	± 30
Rotation of girder at a bearing	rad	1/450
Allowable bearing stress for maximum design vertical force	kgf/cm ²	80
Allowable shear strain for all design loads except seismic load	%	70
Allowable shear strain for seismic load	%	200

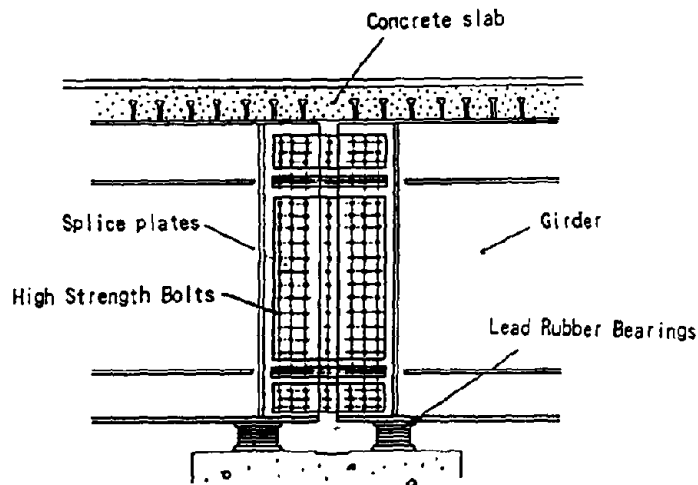


Fig. 2 Details of Connection of Girders

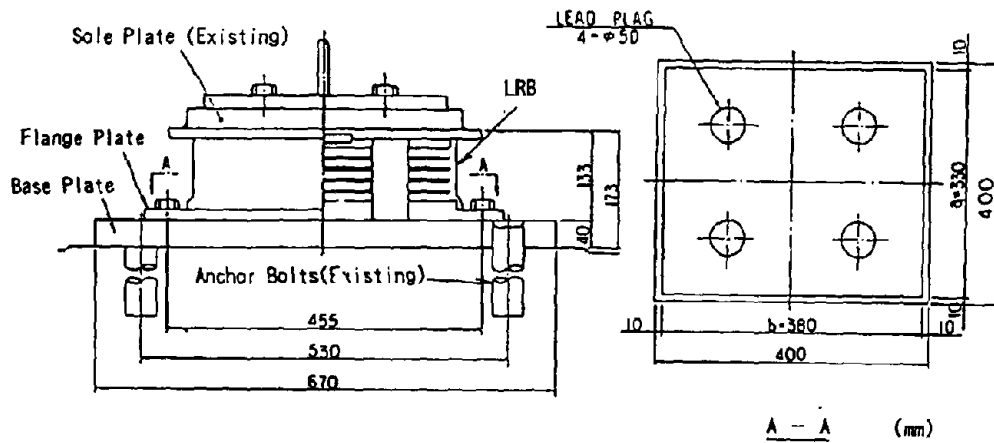


Fig. 3 Lead Rubber Bearing

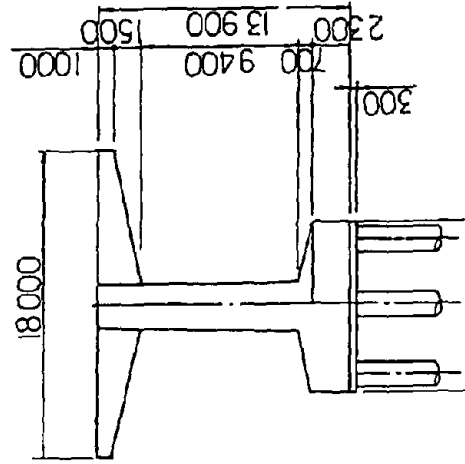
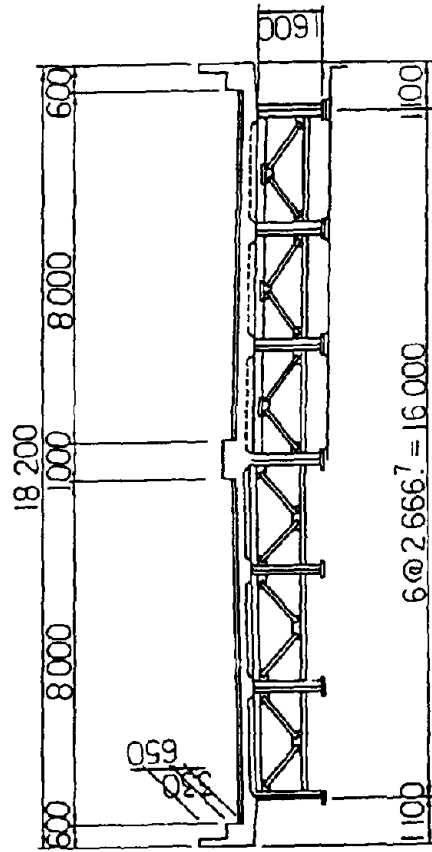
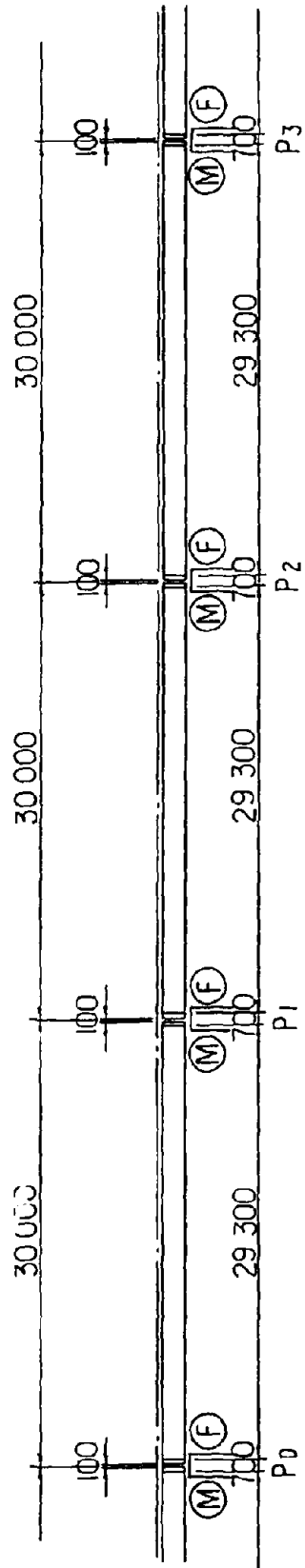


Fig. 1 General View of Existing Bridge

slab even when the girder is connected to the slab. This can also prevent the occurrence of uneven reaction force on the neighboring on the pier. The new bridge used were Lead Rubber Bearing (LRB) which actually have already been used for a menshin bridge in Japan. This new bearing consists of a main unit (height:133mm) and a base plate (thickness: 40mm), which is designed so that it does not exceed the height of existing bearings. The new bearing's main unit is formed from 5 layers of rubber plates (The thickness of each rubber plate is 13mm, and its plane dimensions are 33cm×38cm), 4 reinforcement steel plates each with a thickness of 3mm, top and bottom flange plates with thickness of 28mm each, and 4 lead plugs. (the diameter of each plug is 50mm.) The sides of the bearing are covered by rubber sheet, 10mm thick. The plane shape of the bearing is designed so that the bearing stress against maximum reaction force will be 80kgf/cm² or less. Existing anchor bolts are used as-is, and the base plate of each bearing is fixed in position by welding. The main unit of the bearing is placed on the plate, and fixed there using bolts.

Number of continued effective spans The allowable horizontal displacement by temperature load is 70% of the total thickness of the rubber. The total thickness of rubber is 65mm, and therefor the allowable horizontal displacement is 45.5mm. The horizontal displacement for each 1m of girder length is calculated as 7.0mm. Based on these data, the maximum feasible length l of the girder from the neutral axis, is calculated as shown below.

$$l = \frac{45.5 - 7.0}{0.36} = 106.9 \text{ m} \quad (1)$$

The bridge length can be determined as up to twice the above answer, or $2 \times 106.9\text{m} = 213.8\text{m}$. In other words, up to 7 effective spans can be continued for a 30m span.

$$n = \frac{213.8}{30.0} = 7.1 \quad (2)$$

Where

n : The number of continuous effective spans which can be used.

Earthquake response analysis We carried out a time history response analysis using the analysis model shown in Fig.5. The seismic wave input is the standard wave for the classification of ground condition II, prepared by Public Works Research Institution(PWRI). We also studied the case of a simple laminated rubber bearing after removing the lead plugs from the LRB, for comparison, in addition to the analysis of the LRB itself. The individual constants input for the LRB are the effective stiffness and the effective damping ratio, which can be calculated by equations (3) and (4), using the displacement which was previously estimated.

$$K_{..} = \frac{F}{u} \quad (3)$$

$$h_{..} = \frac{1}{4\pi} \left(\frac{\Delta W}{W} \right) \quad (4)$$

Where,

$K_{..}$: Effective stiffness
 F : Force against estimated displacement, u
 u : Estimated displacement
 $h_{..}$: Effective damping ratio
 $\Delta W, W$: Areas shown in Fig.8

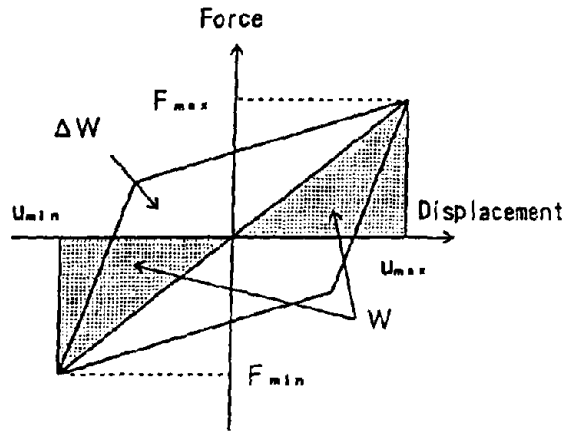


Fig. 4 Force-Displacement Hysteresis Loop

A damping ratio of 5% is also considered, in addition to the spring constant which can be calculated by equation (5), as the constants for the ordinary laminated rubber bearing.

$$K = \frac{A_R \cdot G}{\Sigma t_r} \quad (5)$$

Where,

K :Spring constant of laminated rubber bearing

A_R :Plane area of rubber

Σt_r :Total thickness of rubber

Table 2 shows the input data for earthquake response analysis.

Table 2 Input Data for Earthquake Response Analysis

Item	Unit	Lead Rubber Bearing	Rubber Bearing
Mass of Superstructure : W	tf	606	606
Effective Stiffness of Bearing : K_b	tf/m	3 288	3 037
Effective Damping Ratio of Bearing : h_b	%	14.5	3.0
Mass of Substructure : W_p	tf	180	180
Spring Constant of Substructure : K_p	tf/m	15 000	15 000
Damping Ratio of Substructure : h_p	%	5.0	5.0
Maximum Acceleration of Input Wave at Ground Level	cm/sec ²	413	413

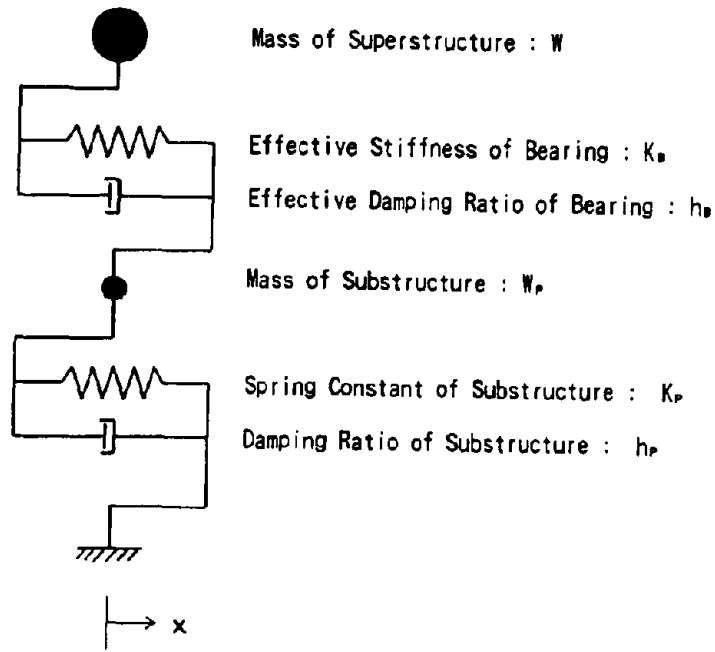


Fig. 5 Model for Earthquake Response Analysis

The results of the analysis are shown in Table 3. As is clearly evident from the table, the maximum response acceleration of the superstructure with the LRBs is 654gal, 70% of the maximum response acceleration with laminated rubber bearing. Also, the maximum response displacement of the superstructure with LRBs is 11.9cm, and the maximum response displacement of the bearing section with LRBs is 9.5cm. these values are 64% of those for laminated rubber bearings. 80% of the displacement is concentrated in the bearing section.

Table 3 Results of Earthquake Response Analysis

	Unit	Lead Rubber Bearing	Rubber Bearing
Natural Period of 1st Mode	sec	1.04	1.04
Maximum Response Acceleration of Superstructure	cm/sec^2	709	1 019
Maximum Response Acceleration of Substructure	cm/sec^2	471	516
Maximum Displacement of Superstructure	mm	119	185
Maximum Relative Displacement between Super- and Substructure	mm	95	152

Bearing replacement method A summary of the procedure for replacing the bearings is given below(See Fig.9).

Stage 1

①Remove the bolts connecting the girder and the existing bearing, and jack up the girder.

②Chip off a layer of concrete (about 10cm thick) from the pier around the bearing, and remove the existing bearing.

Stage 2

③Pre-drill the holes on the base plate for the positions of the anchor bolts, and set the base plate in the designated position. Pre-drill holes and cut screw threads for the bolts which will fix the main body of the bearing to the base plate.

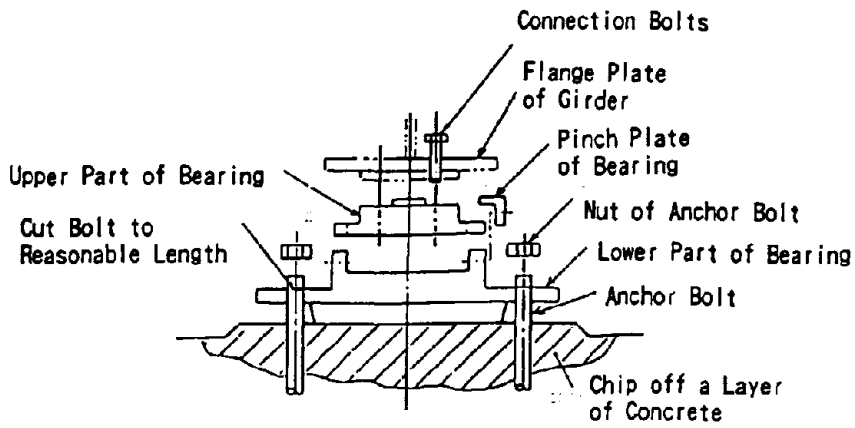
④Weld the base plate and the anchor bolts on-site. After welding has been done, finish the top surface of the base plate so it is smooth.

⑤fill with non-shrinkable mortar, to the bottom of the base plate.

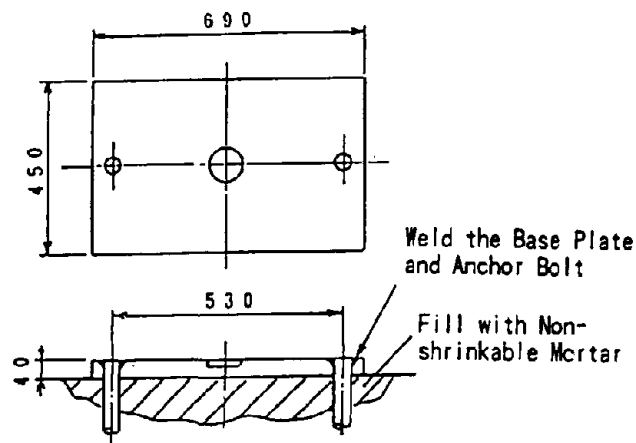
stage 3

⑥Place the main body of the bearing on the base plate, and fix the bearing in place.

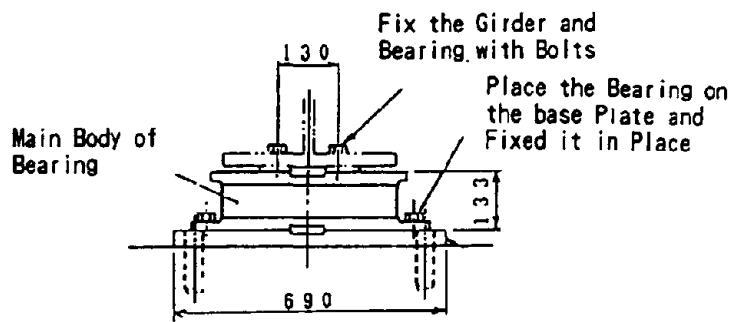
⑦Jack the girder down, and fix the body of the bearing and the girder together, using the bolts.



Stage 1 Removal of the Existing Bearing



Stage 2 Setting of the Base Plate



Stage 3 Setting of the Bearing

Fig. 6 Procedure for Replacing the Bearings

CONCLUSION

The following effects can be expected when menshin bearings are applied in the continuous structure construction method for a simple girder bridge.

①When menshin bearing are used, acceleration response and displacement response can be reduced by 30%~50% from those in cases where ordinary elastomeric bearing have been used. In the case study done at this time, it was possible to minimize the displacement of the girder within the floating gap of the girder end section, by using the menshin bearing.

②When the menshin bearings were used, the microtremors caused by wind load and braking load were very much smaller than in the cases where ordinary elastomeric bearings were used.

③Menshin bearings can disperse the internal force of the superstructure evenly to the piers when an earthquake occurs, just as well as when ordinary elastomeric bearings are used

ACKNOWLEDGEMENT

This study was made as part of a joint research program on the Development of Menshin Systems for Highway Bridges between PWRI and 28 private firms.

REFERENCE

1. PWRI and 28 private firms, "Development of Menshin Systems for Highway Bridges -Report No.1", PWRI Joint Research Report No.44, March 1990 (in Japanese)

ADVANTAGES OF ISOLATION BEARINGS FOR NEW BRIDGES

Ralph E. Anderson¹

¹Engineer of Bridges and Structures, Illinois Department of Transportation,
Springfield, Illinois

SUMMARY

Seismic isolation bearings have been used for the design of two new bridges in the State of Illinois. The bridge over Sexton Creek in Alexander County was designed in-house by the Illinois Department of Transportation. Construction has been completed and the bridge is now open to traffic. There has been insufficient time as of yet, to evaluate bridge performance. The design for the Ramp 1 connector bridge from the M.L. King Bridge in East St. Louis, Illinois is just being completed by Sverdrup Corporation for the Illinois Department of Transportation. Data indicates that the use of isolation bearings is cost effective for both bridges. The magnitude of potential cost savings will vary from bridge to bridge since the extent of savings is affected by many structure and site variables.

INTRODUCTION

A brief description and discussion of the Sexton Creek bridge is first presented. This is followed by a general discussion of the use of isolation bearings for new bridges, using the design of the new Ramp 1 bridge as a case example.

DISCUSSION

The first new bridge in the United States to have seismic isolation bearings was built in Alexander County, Illinois. It is a three span continuous steel plate girder structure with a horizontal curve over Sexton Creek. The spans are approximately 120', 154', and 120' long. The superstructure consists of a 43'-2" wide concrete deck on five, 54" deep plate girders. The substructure members are placed on steel H-piles. The seismic bearing arrangement which was chosen for this bridge consisted of isolation bearings with lead core for the abutments and isolation bearings without lead core at the piers. This resulted in the seismic loads being primarily resisted by the abutments.

One of the reasons this bridge was selected for seismic isolation bearings was its location. It is at the southern tip of Illinois which is closest to the New Madrid Fault and is a Seismic Performance Category C, with an acceleration coefficient of 0.20, soil profile of Type III.

CONCLUSIONS

Our decision to use the Isolation Bearings on a new structure was mainly: (1) To assess the "cost-effectiveness" of these bearings as compared to the conventional design for this seismic zone. (We realized a cost savings of approximately 3%). (2) To evaluate the performance of this type of bearing under normal service conditions.

The bridge at Sexton Creek has been opened to traffic just recently and we have not had the opportunity to evaluate its performance.

Attached is a report by Sverdrup Corporation of St. Louis, Missouri on the use of Isolation Bearings for new bridges. Sverdrup is our consultant performing the rehabilitation study and design of the Poplar Street Complex for Illinois DOT.

USE OF ISOLATION BEARINGS FOR NEW BRIDGES

Stephen S. Steib¹ and Stephen W. Yordy²

¹Structural Engineer, Sverdrup Corporation, St. Louis, MO

²Project Manager and Deputy Bridge Section Manager Sverdrup Corporation, St. Louis, MO

SUMMARY

The scope for the work presented in this report consists of a discussion of reasons why isolation bearings, specifically lead-rubber isolation bearings, should be considered for use when designing new highway bridges that are located in potentially active seismic regions. The discussion presented in the report is specifically applicable when new highway bridges are situated in an area where single or multi-mode dynamic spectral analysis is appropriate in accordance with the AASHTO *Standard Specifications for Seismic Design of Highway Bridges (Ref. 1)*. The report first briefly describes the general advantages and disadvantages of isolation bearings. This is followed by discussion of the use of isolation bearings for new bridges. Economic advantages of isolation bearing use are supported by cost comparisons developed for a specific bridge which Sverdrup Corporation is just completing final design. Estimated costs were computed, tabulated and presented herein for the new Ramp 1 bridge (S.N. 082-0287), which is a new eastbound connector from the M. L. King Bridge to eastbound I-55/70/64 in E. St. Louis, Illinois.

GENERAL ADVANTAGES

The primary advantage of using isolation bearings for bridges designed to resist seismic forces is centered around their ability to significantly reduce the earthquake forces that are transferred to the substructure. This reduction is brought about principally by altering two features of the dynamic response of the bridge to the design seismic event. First, the isolation bearings introduce structural flexibility. Secondly, due to the damping properties of isolation bearings, a modified response spectrum is used for conventional bridges with isolation bearings. Both of these features combine to result in significant reduction in seismic design forces that are transmitted to the substructure.

As the period of a structure increases, the seismic acceleration coefficient and resultant seismic force demand decreases. Additionally, the damping effect of the bearings not only limits horizontal displacements, but also serves to reduce the response spectrum curve. These attributes are shown in Figure 1, which plots the response spectrum curves for a structure on conventional bearings and a structure using isolation bearings.

In Figure 1, the response spectrum for the structure without seismic isolation is taken from Figure 11 in the AASHTO *Standard Specifications for Seismic Design of Highway Bridges (Ref. 1)*. The response spectrum for the structure with seismic isolation is taken from the analysis of new Ramp 1 (Structure No. 082-0287), which Sverdrup is just completing final design for the Illinois Department of Transportation. This particular bridge, which is a new connector from the M. L. King Bridge to eastbound I-55/70/64, is a conventional, continuous, multiple plate girder structure which is partially on a 720-ft radius horizontal curve. Three to five span units are utilized, with a total of 18 spans ranging from 80 feet to 170 feet in span length. Pier heights vary from approximately 20

feet to 55 feet. Bedrock at the site is overlain with approximately 120 feet of Type III soil, which is vulnerable to liquefaction during the design seismic event. The bridge was assigned to Seismic Performance Category B, based upon an assumed Acceleration Coefficient equal to 0.15. When the reference structure just described is seismically isolated, seismic force reductions ranging from 40 percent for the longitudinal component to 60 percent for the transverse component were realized when the resultant increased fundamental period is used in combination with the response spectrum curve for a bridge with seismic isolation.

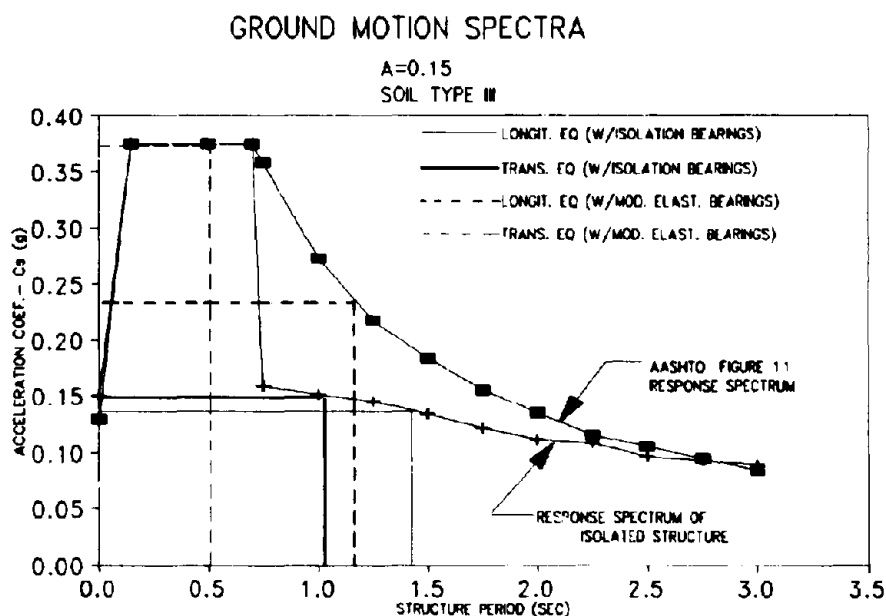


Figure 1

Figure 1 illustrates the relationship between structure period of vibration and the seismic acceleration coefficient. The figure also shows the change in structure period and resultant acceleration coefficient that occurs when changing from the bridge without isolation bearings to the bridge with isolation bearings. The effect of isolation bearing damping is seen when comparing the two response spectra. Note that in the transverse direction, the structure period is doubled when isolation bearings are introduced, significantly reducing the acceleration coefficient. In the longitudinal direction, the structure is relatively flexible even without isolation bearings, and thus the primary benefit of isolation bearings comes from the spectrum shift due to damping.

Advantage can also be realized from the fact that seismic bearings are not specifically "fixed" or "expansion". Since they all act as "fixed" for short-term non-seismic lateral forces, longitudinal forces such as wind or braking are distributed to all of the substructure units, as opposed to only one or two "fixed" piers in a typical structure without seismic isolation. In the case of isolation bearings with lead core that were specifically considered in this report, slowly applied horizontal loads, such

as those due to temperature strains, are reduced by creep of the bearings to approximately 25 percent of the force transmitted from instantaneous loading.

Another potential advantage of seismic isolation bearings is the ability of the designer to "direct" loads to the substructure units most capable of resisting them. By modifying the stiffness properties of the bearings (generally by changing the dimensions of the lead core or elastomer), forces can be directed away from undesirable locations, such as unusually stiff piers or piers founded on "poor" soil.

Lead-rubber isolation bearings have other advantages that can also be credited to various types of conventional elastomeric bearings. These include mechanical reliability, resistance to corrosion, and multi-directional rotation and movement capabilities. The enhanced multi-directional capabilities of isolation bearings is particularly advantageous for horizontally curved bridges, where non-seismic lateral movements are also multi-directional. Thus, careful consideration of bearing orientation is not necessary.

NEW STRUCTURES

The significant reduction in seismic force demand for substructure design that generally results when isolation bearings are used gives the bridge owner and/or designer a potential design philosophy option when considering new bridges. The AASHTO *Standard Specifications for Seismic Design of Highway Bridges* employs a design philosophy where R-factors are used for structure design. These R-factors are used to reduce the theoretical seismic forces to lower design levels that lead to high ductility demand and inelastic structural behavior during the design seismic event. Under such a philosophy, the bridge is designed to avoid collapse, but damage to the substructure may be substantial. Since the use of R-factors significantly reduces the high seismic design forces to which the substructure above the foundation is subjected, it is generally inadvisable (from an economic viewpoint) to design for other than high ductile demand. (Note that the foundation, including footings and piles, is generally designed for an R-factor equal to half of that used for other portions of the substructure, resulting in more elastic behavior and less likelihood of below-ground damage.) When isolation bearings are used, the high theoretical seismic forces are significantly reduced, thus making elastic design of the substructure (minimal expected damage) more economically feasible. In fact, in many instances the substructure of a bridge without isolation bearings and with high ductility demand may be reasonably designed for the same order of magnitude of seismic force demand as a bridge with isolation bearings and low ductility demand. Obviously, in doing so, any higher costs incurred by using isolation bearings to reduce seismic demands for the substructure is traded for investment in a structure that is more damage-resistant. For an essential structure, serious consideration can thus be given to using isolation bearings and at the same time reducing R-factors to as low as 1.0 to 1.5 (as discussed in the Commentary of the AASHTO seismic design specifications), which will result in essentially elastic response, minimizing damage and potentially unacceptable disruption to traffic. The specific bridge used for this report is not considered essential and thus the AASHTO specified R-factors were used, resulting in high ductility demand.

ECONOMIC ADVANTAGES

Overall cost savings experienced when using isolation bearings are often significant, as will be discussed in the following paragraph. However, it must be noted that many items affect the extent of savings. Substructure type and configuration, soil conditions, structure geometry, Acceleration Coefficient (A), and Seismic Performance Category (SPC) are just a few of the variables that can

have an effect on cost savings.

Analysis and design were performed for the previously described proposed new bridge to develop quantity/cost requirements when isolation bearings (lead-rubber type) are used, as compared to quantity/cost requirements when standard Illinois DOT elastomeric bearings, modified (strengthened) to transmit lateral seismic force demands from the superstructure to the substructure, are used. Estimated representative costs for the bridge with and without isolation bearings are presented in Tables 1 and 2, respectively. Overall cost savings of approximately 15% can be achieved for the referenced bridge when using isolation bearings instead of modified elastomeric bearings. The savings is directly a result of the significant reduction in substructure requirements that are a result of the 40% to 60% reduction in seismic force demand transmitted to the substructure. Relatively minor increases in some costs (approximately 2% of overall costs) result when isolation bearings are used, primarily due to the high relative cost of the isolation bearings, but also due to the larger and more costly modular bridge deck expansion devices (approximately 12% increase over standard expansion devices) required for the larger seismic displacement demands that result when isolation bearings are used.

It should be noted that for this particular bridge example a substantial factor in the substructure cost comes from the piling. Since the bridge is located on a site where the top layers of the soil are vulnerable to liquefaction, criteria were established requiring the use of ductile H-piles with tips driven to refusal at, or near, bedrock found approximately 120 feet below ground line. These piles must be designed within their upper portions to support vertical and lateral loads for a significant unsupported length. Thus, pile costs are unusually high even with isolation bearings, and increase quite significantly when the seismic force demand to the substructure is not mitigated by the inclusion of isolation bearings. This will tend to explain why the percentage structure cost savings are estimated to be higher than the 5% to 10% savings typically reported for bridges located in regions of moderate seismic risk, using isolation bearings in place of conventional bearings modified to resist the seismic loads.

CONCLUSIONS

Whether isolation bearings are used for new or retrofit bridges, many advantages can be cited, some of which are common to other types of elastomeric bearings. The high cost of isolation bearings in comparison to modified elastomeric bearings is certainly a disadvantage but this disadvantage is generally overcome by cost savings in the substructure made possible by the significantly reduced seismic force demands that will result. Creep of lead-rubber isolation bearings can also effectively reduce non-seismic, slowly applied horizontal loads, such as those resulting from temperature effects. Additionally, the size and shape of isolation bearings can often be adjusted to economically distribute superstructure lateral loads to the substructure. These reduced force demands are particularly meaningful and cost beneficial for existing structures when such reductions enable existing substructure units to be retrofitted rather than replaced.

Isolation bearings often prove cost-effective for use in new bridges located in moderately to highly active seismic regions. Variable site conditions and structure characteristics can significantly affect the extent of potential savings, as is illustrated by the proposed new structure discussed in this report. Clearly when the right combination of conditions exist, isolation bearings can be shown to be a cost-effective part of new bridges located in seismically active regions. For new bridges, the use of isolation bearings might also be considered so that the seismic force demands are reduced to a level that elastic design of the structure is economically feasible, thus minimizing the potential for significant damage if the design seismic event occurs.

**STRUCTURE COST ESTIMATE
NEW RAMP 1 - STRUCTURE NO. 082-0287
(WITH ISOLATION BEARINGS)**

SUPERSTRUCTURE

STRUCTURE CONCRETE	\$787,000
REINFORCEMENT	\$323,000
STRUCTURAL STEEL	\$1,778,000
MODULAR EXPANSION DEVICES	\$125,000
NEOPRENE EXPANSION DEVICES	<u>\$7,000</u>
TOTAL SUPERSTRUCTURE COST	\$3,020,000

SUBSTRUCTURE

SEISMIC ISOLATION BEARINGS	\$216,000
STRUCTURE CONCRETE	\$543,000
REINFORCEMENT	\$169,000
EXCAVATION	\$27,000
PILES	<u>\$1,382,000</u>
TOTAL SUBSTRUCTURE COST	\$2,337,000

TOTAL COST (SUPERSTR. & SUBSTR.)	\$5,357,000
CONTINGENCY (APPROX. 15%)	\$843,000

TOTAL COST	\$6,200,000
-------------------	--------------------

CONTINGENCY INCLUDES MOBILIZATION AND MISCELLANEOUS BID ITEMS NOT LISTED ABOVE.

Table 1

**STRUCTURE COST ESTIMATE
NEW RAMP 1 - STRUCTURE NO. 082-0287
(WITHOUT ISOLATION BEARINGS)**

SUPERSTRUCTURE

STRUCTURE CONCRETE	\$787,000
REINFORCEMENT	\$323,000
STRUCTURAL STEEL	\$1,778,000
FINGER PLATE EXP. DEVICES	\$112,000
NEOPRENE EXPANSION DEVICES	<u>\$7,000</u>

TOTAL SUPERSTRUCTURE COST	\$3,007,000
----------------------------------	--------------------

SUBSTRUCTURE

MODIFIED ELASTOMERIC BEARINGS	\$54,000
STRUCTURE CONCRETE	\$671,000
REINFORCEMENT	\$204,000
EXCAVATION	\$41,000
PILES	<u>\$2,412,000</u>

TOTAL SUBSTRUCTURE COST	\$3,382,000
--------------------------------	--------------------

TOTAL COST (SUPERSTR. & SUBSTR.)	\$6,389,000
CONTINGENCY (APPROX. 15%)	\$911,000

TOTAL COST	\$7,300,000
-------------------	--------------------

CONTINGENCY INCLUDES MOBILIZATION AND MISCELLANEOUS BID ITEMS NOT LISTED ABOVE.

Table 2

ACKNOWLEDGMENTS

This study and report was prepared for the Illinois Department of Transportation in conjunction with the design of the new Ramp 1 bridge (structure No. 082-0287), which is a new eastbound connector to I-55/70/64 from the M.L. King Bridge in East St. Louis, Illinois.

Sverdrup Corporation is currently under contract with the Illinois Department of Transportation to provide a wide range of engineering services for the rehabilitation and reconstruction of all Illinois approaches to the Poplar Street Bridge over the Mississippi River in East St. Louis, Illinois. The authors would like to express their appreciation to Mr. Ralph E. Anderson of the Illinois Department of Transportation for the opportunity to provide input for the workshop on "Earthquake Protective Systems for Bridges".

REFERENCES

1. American Association of State Highway and Transportation Officials: "Standard Specifications for Highway Bridges" Fourteenth Edition, 1989 and Interim Specifications Through 1991.

APPLICATION OF *MENSHIN* DESIGN TO
SEISMIC RETROFITTING OF HIGHWAY BRIDGE SUBSTRUCTURES

Takashi TAMURA¹ Masao HIRAI² Noboru HIGUCHI¹ Shin'ichi MASUDA³

¹Civil Engineering Design Division, Mitsui Construction Co., Ltd,
Chiyoda-ku, Tokyo, Japan

²Technical Research Institute, Mitsui Construction Co., Ltd, Nagareyama-shi,
Chiba, Japan

³Civil Engineering Department, Japan Engineering Consultant Co., Ltd,
Shinjuku-ku, Tokyo, Japan

SUMMARY

Experimental *Menshin* designs were carried out to determine whether they could be applied to seismic retrofitting of existing highway bridge substructures. Lead rubber bearings (LRB) were used as *Menshin* devices in these experimental designs to reduce the seismic loads acting on the substructures through their high damping rates and through dispersion of the seismic lateral loads by modifying the existing structural system into a multi-point elastic support system. And their effectiveness in seismically retrofitting the substructure was confirmed.

INTRODUCTION

Based on cases of highway bridges sustaining seismic damage, and on the results of seismic inspections in past years, several types of bridges are considered to be seismically deficient. Firstly, bridges whose pier structures require seismic upgrading are:

- Old structures made of unreinforced concrete, piled blocks, and other structural components considered to be seismically vulnerable.
- Bridges whose substructures consist of single line pile bents and the like, and are thus vulnerable to seismic loading.
- Bridges in which the anchorage length of the reinforcing bars in the reinforced concrete (RC) piers are short in the middle sections.
- Bridges whose reinforced concrete piers lack ultimate strength and ductility.

Secondly, bridges whose foundations are considered to be seismically deficient, are:

- Bridges whose foundations are surrounded by soils that may be highly susceptible to liquefaction during an earthquake, or lack bearing strength.
- Bridges whose foundation bearing soils have been scoured and degraded, thus reducing their bearing capacity
- Very old bridges constructed of timber piles and other vulnerable structural components.
- Some bridges whose pile foundations were built before the specifications in 1964, or whose lateral stability had not been confirmed.

To upgrade the seismically deficient bridges described above, conventional measures have been applied to increase the bearing capacity of their substructures and foundation soils. Reinforced concrete linings and steel plates linings, for example, have been widely adopted to strengthen the bearing capacity of the

reinforced concrete piers of highway bridges. Ground improvement by grouting and consolidation of foundations by riprapping with concrete blocks or by coffering with steel sheet piles and steel pipe piles are commonly used to raise the bearing capacity of the foundations themselves. And footing enlargement and extra pile driving are also used to increase the stability of the foundations.

Besides these conventional measures, it is advisable to use *Menshin* devices, which can reduce seismic forces acting to structures. Recently in Japan, several new bridges have been built based on a *Menshin* design in an attempt to improve their seismic resistance. However, no *Menshin* bearing based design has ever been applied to an existing highway bridge to retrofit it. Therefore, we made several experimental *Menshin* designs for upgrading existing seismically deficient bridges, and verified their effectiveness. The following paragraphs first describe the basic concept of *Menshin*-design-based retrofitting of existing bridges, and then, describe how their effectiveness was confirmed.

BASIC CONCEPT OF *MENSHIN*-DESIGN-BASED SEISMIC RETROFITTING

Significance of *Menshin* design *Menshin* devices can directly reduce the seismic inertia forces acting on highway bridge structures to an acceptable level without modifying their piers and foundations, thereby reducing the risk of seismic failure that may be caused by large seismic inertia forces. *Menshin* devices can function in this way because:

- They function as isolators by extending the natural period of bridges, thereby reducing the seismic loads.
- They reduce the seismic forces by functioning as highly efficient dampers.
- They can "change" the entire bridge system from a one-point fixed system to a multi-point elastic support system, thereby dispersing the lateral seismic forces. (see design cases B and C)

However, the natural period of a bridge is extended excessively, the amount by which the superstructures are displaced, will also become excessive. This will require an operation to replace the existing expansion joints and to adjust the expansion spacing. Therefore, it is not practical to depend only on extending the natural period of a bridge. Accordingly, experimental seismic retrofitting designs were executed for case model bridges by utilizing *Menshin* devices with high damping capacity and by dispersing the seismic load.

As a result, the *Menshin* design-based seismic retrofit measures were confirmed to provide the following advantages over conventional measures.

- The seismic loads transferred from the superstructures to the substructures can be reduced, and both the foundations and piers can be retrofitted together.
- The increase in the bridge's weight is negligible.
- Because the main work is to replace the existing bearings with *Menshin* bearings, the scale of work is comparatively small.
- Replacement and maintenance management is easy.
- *Menshin* devices can be installed under much less limiting conditions over a river and in the space under the girders.

Inspecting the Seismic Resistance of Existing Bridges The experimental seismic retrofit designs were executed for case model bridges in accordance with "Design Specifications for Highway Bridges (revised in 1990)" (Ref. 1), and the seismic resistance of their structural components were inspected by giving static seismic loads to the structural components within their elastic response ranges. However, the effective lateral seismic capacity of the reinforced concrete piers only was inspected after taking into account their ultimate strength and ductility during a big earthquake. The specifications do not take into account the effect of the high damping performance of *Menshin* devices on the structural components on the design

seismic intensity. Therefore, this was taken into account by using a modified coefficient of damping (Ref. 2). The *Menshin* devices were checked to ensure that their safety was sufficient to resist large seismic forces equivalent to the effective lateral seismic capacity of reinforced concrete bridge piers.

To determine appropriate seismic retrofitting of existing highway bridges their seismic resistance must first be checked. The structural components requiring seismic retrofitting must then be identified, and the amount by which the identified structural components must be strengthened must be determined (the damping rates required for the *Menshin* devices, for example). The seismic resistance of bridge structures can be assessed from the following safety factor S :

$$S = \frac{\text{Allowable capacity of bridge structures}}{\text{Demand of the external forces on bridge structures}}$$

If the value of S in the above formula is smaller than 1, the structural components of the bridge structures are assessed as seismically deficient, and some seismic retrofitting measures must be considered.

EXAMINING THE APPLICABILITY OF *MENSHIN* DESIGN TO SEISMIC RETROFITTING

First selected as model bridges were following three bridges whose substructures had been to be seismically retrofitted or had already been seismically retrofitted.

- (A) RC columns whose embedded reinforcing bars had insufficient anchorage length at middle sections of the column, and that lacked both bearing capacity and ductility,
- (B) Pile foundations that lacked vertical bearing capacity, and
- (C) Caisson foundations that lacked seismic bearing capacity

The experimental *Menshin* designs were then applied to seismically retrofit these bridges, and the effect on these bridges retrofitted by *Menshin* designs were examined. These examinations were conducted only from a structural and engineering point of view to determine whether make sure if *Menshin* designs can be applied to seismic retrofitting of substructures. The retrofit execution and we selected structural details are briefly described.

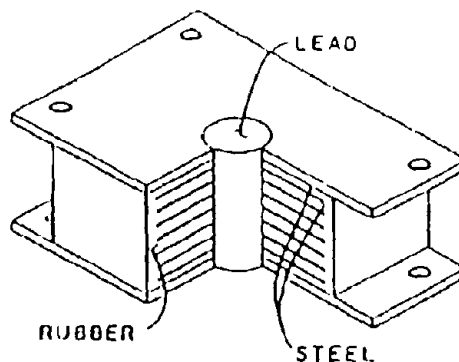


Fig. 1 General View of *MENSHIN* Bearing (LRB)

To the model bridges was applied lead rubber bearings (LRB) as *Menshin* devices, because this type bearing provides excellent performance and the method for designing them has been established. Fig. 1 shows a general view of a LRB. Nevertheless, it is possible that, depending on the type of bridge to be retrofitted and on the type of seismic retrofit measures to be adopted, it may be advisable to use some other type of *Menshin* device.

CASE A - Seismic Retrofitting of RC Columns In both the 1978 Miyagiken-oki Earthquake and the 1982 Uruga-oki Earthquake, the reinforcement concrete columns of some highway bridges sustained a damage at their columns' middle section(s) where the anchorage length of the reinforcing bars was short. According to the results of Seismic Inspections conducted in 1986 for almost all highway bridges in Japan, short anchorage length of reinforcement in some RC columns occurred in the same locations. To strengthen such seismically deficient piers, extra reinforced concrete or steel plate linings have been usually used.

And RC bridge piers and columns are required to provide high ductility, sufficient to retain their bearing capacity even after they have yielded during a large earthquake. The Specifications for Highway Bridges revised in 1990 clearly stipulates that RC piers shall be inspected to ensure that they retain high ductility in their plastic response ranges. Before this requirement was included in these Specifications, in Japan, large-cross-section wall-shaped piers had been adopted to provide potential ductility in the plastic range, but some piers are considered to have been short in their ductility and strength. To seismically retrofit these piers, it is feasible to use RC linings or steel plate linings.

In case A, a seismic inspection revealed that the reinforcing bars of the middle section of the RC columns of an urban expressway viaduct were short in anchorage length. As shown in Fig. 2, the superstructure of this viaduct is a 37-meter-long single steel-concrete composite girder bridge, and its piers are 3-meter-diameter circular RC columns with overhanging beams. As shown in Fig. 3, the main reinforcement of these columns is in four sections where the reinforcing bars end, and are embedded.

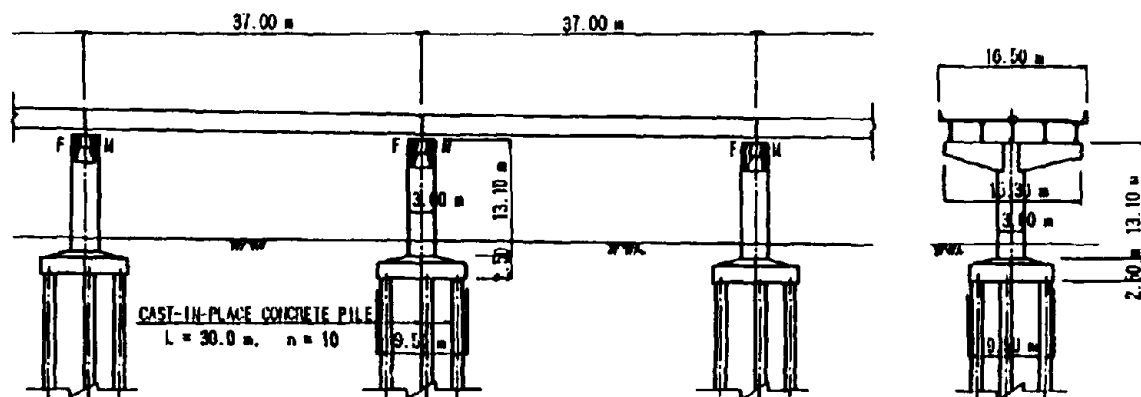


Fig. 2 General View of Case A Model Bridge

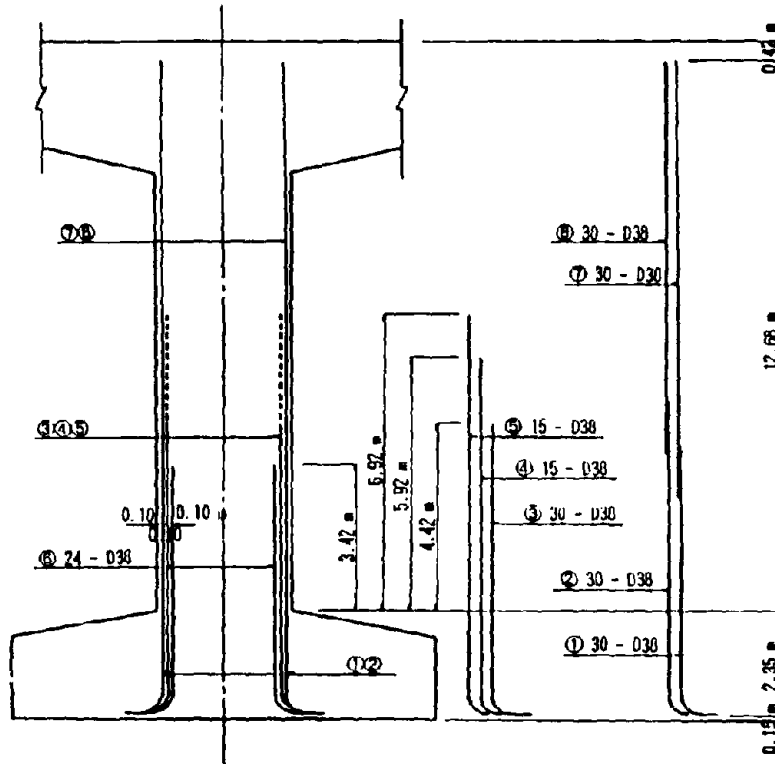


Fig. 3 Arrangement of Main Reinforcement of Case A Model Pier Column

Table 1 The result of the Seismic Inspection (Case A)

	BEFORE RETROFITTING	RETROFITTING WITH WENSHIN DEVICE	RETROFITTING WITH RC LINING
IN TERMS OF MOMENT AT THE SECTION REINFORCEMENT EMBEDDED			
NATURAL PERIOD (sec)	0.75	0.93	0.70
DEMAND (tf·m)	2930	2060	2950
CAPACITY (tf·m)	2330	2330	3050
SAFETY FACTOR	0.80	1.13	1.03
IN TERMS OF EFFECTIVE LATERAL SEISMIC CAPACITY			
NATURAL PERIOD (sec)	0.84	1.39	0.71
DEMAND (tf)	308	248	282
CAPACITY (tf)	251	251	336
SAFETY FACTOR	0.81	1.01	1.19

Table 1 shows the results of the inspection of the seismic resistance of this columns conducted before this viaduct was subject to retrofitting. As shown, the safety factor of the piers in terms of the moment calculated from the stress intensity of reinforcement at the piers's uppermost section, where the reinforcing bars end and are embedded as shown in Fig. 3, is:

$$S = 0.80 < 1.0$$

In addition, the safety factor of the pier in terms of its effective lateral seismic capacity is,

$$S = 0.81 < 1.0$$

Accordingly, this pier does not satisfy the safety requirement either. Since these columns are circular in cross section, they are equally susceptible to seismic forces in all directions.

To ensure the safety of this viaduct, the goals of *Menshin* bearing design were established as follows after taking into consideration the potential decrease in design seismic load due to the damping performance of *Menshin* bearings:

- To give this viaduct a damping ratio of 10 percent, in order to reduce by 20 percent the seismic loads acting on it at the time of inspection of the stress intensity of the reinforcement.
- To give this viaduct a damping ratio of 10 percent, in order to reduce by about 20 percent the seismic forces with respect to the effective lateral capacity of its columns.

In this case, *Menshin* devices were designed to function equally in all directions. Table 2 shows the dimensions of the *Menshin* bearings designed to achieve the above goals.

Table 1 also shows the results of the inspection conducted to examine the seismic resistance of case A model bridge after it was seismically retrofitted using *Menshin* bearings. As shown, the safety factor in terms of the moment in the same section as before is:

$$S = 1.13 > 1.0,$$

The safety factor in terms of the effective lateral seismic capacity is:

$$S = 1.01 > 1.0$$

Accordingly, this viaduct retrofitted with *Menshin* bearings proved to be capable of satisfying the safety requirement.

Whole bridge structural systems are required to allow a design displacement so that *Menshin* devices can function during a design earthquake. In case A, the results of the inspection conducted to determine the effective lateral seismic capacity of the piers of the *Menshin*-device-fitted viaduct showed that the girders had been displaced as much as 261 mm. Furthermore, to allow displacement in the transverse direction, which is usually restrained in existing bridges, the expansion joints and restrainers must be replaced with other suitable devices, and the girder spacing must also be adjusted.

Table 2 Dimension of the *MENSHIN* Bearings (Case A)

NUMBER (PER PIER)	5
PLANE FIGURE	500 mm × 500 mm
LEAD PLUG	5 × φ55 mm
THICKNESS OF RUBBER	16 × 10 mm
WHOLE HEIGHT	265 mm

A retrofitting measure for case A viaduct based on conventional RC lining is designed as an example as shown in Fig. 4. In this case, the safety factor of the columns in terms of the moment at the same section as before is, as shown in table 1:

$$S = 1.03 > 1.0,$$

and in terms of the effective lateral seismic capacity,

$$S = 1.19 > 1.0$$

That is, this bridge satisfies the safety requirement.

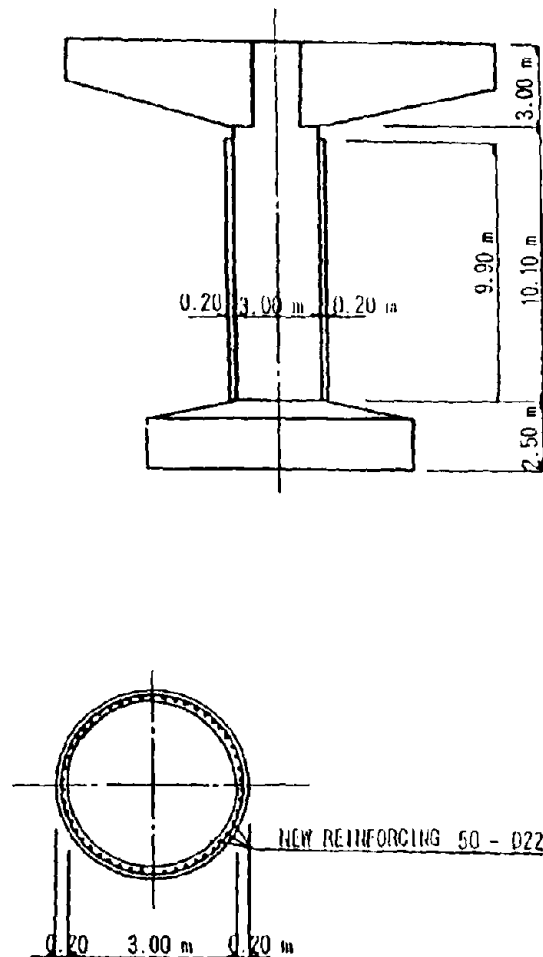


Fig. 4 RC Lining on Case A Model Column

The RC lining operation, which is commonly used, needs rather a small scale of work, and is quite economical, does not cause disruption to bridge traffic. In addition, a weight increase of 12.4 ton-force in the columns lined with the reinforced concrete does not pose any problem in seismic resistance terms, since its foundation has a high degree of redundancy. In case A, the installation of *Menshin* bearings may require replacement of the existing expansion joints and adjustment of the girder spacing. Furthermore, this may involve the disruption to traffic during the replacement operation. Therefore, for case A bridge, the RC lining may be more advantageous than retrofitting with *Menshin* bearings.

However since *Menshin* bearings are comparatively small, and need only small temporary facilities, they may be more advantageous in the following cases:

- Where the cross sections (or weight) of pier foundations can not be increased to seismically strengthen them,
- Where large-scale temporary work is required to erect a temporary cofferdam to retrofit piers in a river.

Moreover, to simplify the maintenance of expansion joints of single girder viaducts, such as the case A bridge, and to improve bridge traffic, a plan is now being pursued to modify the superstructures of such bridges to continuous girders and reduce the number of expansion joints. If this plan is carried out, both bearings and expansion joints must be replaced. At this time, the use of *Menshin* bearings is recommended.

CASE B - Retrofitting of foundation piles The case B model bridge represents a bridge that was seismically retrofitted because its foundation piles has low seismic vertical bearing capacity. As shown in Fig. 5, this bridge is a 43-meter-long, and 3-span cantilever steel plate girder bridge. Each pier is supported on twenty-seven 9-m-long, 30-cm-dia reinforced-concrete piles.

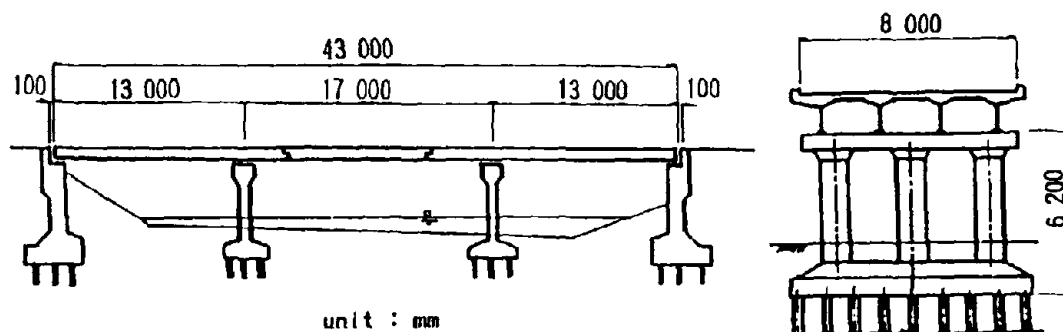


Fig. 5 General View of Case C Model Bridge

Table 3 The Result of the Seismic Inspection (Case B)

	BEFORE RETROFITTING	RETROFITTING WITH MENSIN DEVICE
IN TERMS OF VERTICAL BEARING CAPACITY OF FOUNDATION PILES		
NATURAL PERIOD (sec)	0.37	0.57
DEMAND (tf·m)	23.9	17.6
CAPACITY (tf·m)	17.6	17.6
SAFETY FACTOR	0.74	1.00

The results of the inspection conducted to examine the seismic resistance of the foundations of this bridge before retrofitting, are shown in Table 3. As shown in this table, the safety factor S of these pile foundations in terms of the vertical bearing capacity of the foundation piles with respect to the seismic load in the bridge's longitudinal direction is:

$$S = 0.74 < 1.0$$

That is, the safety factor S of this bridge before retrofitting did not satisfy its safety requirement. In calculating the safety factor of the pier foundation piles it was assumed that the piers themselves were seismically sufficient.

In case B, to ensure the seismic safety of the foundation piles, it was necessary to reduce the seismic lateral load acting on the foundation piles by 33 percent after taking into account the fact that a substantial portion of the reaction force of the piles had been consumed in supporting the weight of the superstructure. Accordingly, the goals of the *Menshin* designs were established as follows, assuming that *Menshin* devices function only in the bridge's longitudinal direction, and that stoppers are installed to prevent them from functioning in the bridge's transverse direction because in that direction, the bearing capacity of the foundations is always working.

- To make this bridge provide a damping ratio for the bridge of about 20 percent.
- To modify the existing structural system of this bridge, or one point fixed system, to a multi-point elastic support system by connecting the existing suspension girders as shown in Fig. 6.

To disperse the lateral seismic loads in the ratio of $A_1 : P_1 : P_2 : A_2 = 1 : 3 : 5 : 1$, approximately in the same ratio as that of the design loads before retrofitting, the lateral stiffnesses of the bearings on each abutment and pier are adjusted. The dispersion of the lateral seismic loads requires that suspension girders be connected to the cantilever girders to transfer the lateral seismic loads. At this time, the suspension girders must be connected so that they do not transmit the moment, for example, using pin-type connectors, in order to prevent the adverse influence of the moments of the adjacent girders.

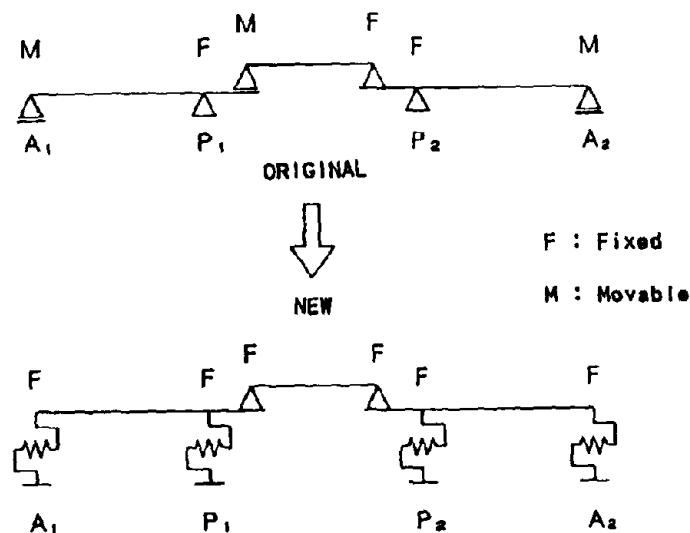


Fig. 6 Modification of Structural System of Case B Model Bridge

Table 4 Dimension of the *MENSHIN* Bearings (Case 5)

	A 1 , A 2	P 1	P 2
NUMBER (PER PIER)	4	4	4
PLANE FIGURE (mm)	250 × 250	250 × 250	250 × 250
LEAD PLUG	1 × ϕ 32 mm	4 × ϕ 30 mm	5 × ϕ 32 mm
THICKNESS OF RUBBER	15 × 6 mm	13 × 8 mm	7 × 7 mm
WHOLE HEIGHT	195 mm	203 mm	129 mm

Table 4 shows the dimensions of *Menshin* bearings designed to achieve the above design goals. Table 3 also shows the seismic resistance of the bridge seismically retrofitted with *Menshin* bearings.

As shown in this table, the seismic safety factor *S* of these foundations piles is:

$$S = 1.00 > = 1.00$$

That is, the safety requirement of the pier foundations of this bridge fitted with this *Menshin* devices are satisfied. Furthermore, this bridge is provided with a damping ratio of about 22.2 percent. The dispersing ratios of the lateral seismic loads at abutments and piers A1, P1, P2, and A2 of this bridge are 1.3, 2.7, 4.6, and 1.3. These ratios show, on the whole, a slight increase in the burden of the seismic loads on the abutments. However, this is considered to be no problem, because the abutments are usually designed to resist, all the year around, earth pressure, and because the effect of the seismic loads, as a whole, has already been mitigated considerably by the damping performance of *Menshin* devices.

The piers of this bridge had already been retrofitted by the improvement of the ground surrounding the foundation piles. As shown in Fig. 7, forty-eight 9-meter-long, 150-mm-dia quick-lime piles were installed for each pier to increase the frictional force of the circumferential surfaces of the existing piles. Assuming that the cohesion of the soils surrounding the piles has increased by 40 percent, the seismic safety factor of these foundation piles will be:

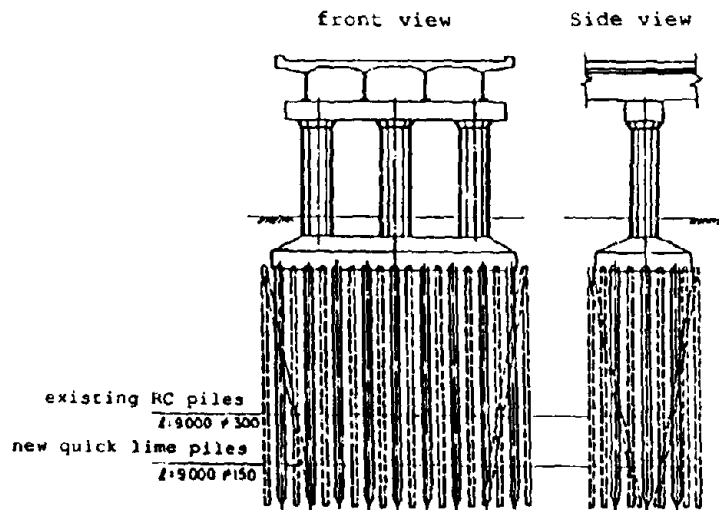


Fig. 7 Ground Improvement for Case B Model Foundation (Ref. 3)

$$S = 1.03 > 1.0$$

Thus, these foundation piles satisfy the safety requirement.

In this case, the economics of *Menshin*-design-based retrofitting does not differ from those of ground-improvement-based retrofitting, because ground improvement by driving of quick lime piles does not require a large-scale operation.

However, where a bridge will be retrofitted by driving extra piles and by installing additional footings (such as the retrofittings of Case-C model bridge as shown in Fig. 9), with operations of a temporary cofferdam in a river, *Menshin* devices will be more advantageous in operation cost terms. Furthermore, this experimental design omits examination of the seismic resistance of the piers. If the piers must also be retrofitted, as for case A, it is advisable to use *Menshin* devices that allow concurrent seismic retrofitting of piers and their foundations.

CASE C - RETROFITTING OF CAISSON FOUNDATIONS As shown in Fig. 8, The case C model bridge is a 385-meter-long 13-span cantilever steel plate girder bridge with oval-shaped caissons. This bridge has already been seismically strengthened by both extra piles and foundation consolidation measures, as shown in Fig. 9. This was necessary because frequent removal of gravel and construction of a weir in the vicinity of this bridge caused its foundations to scour. The river bed surrounding the foundations had degraded by up to 5 meters, reducing the original 11-meter-deep embedment of the pier foundations to as little as 6 meters, and finally to degrade their lateral bearing capacity. The results of the inspection conducted to examine the seismic capacity before retrofitting are shown in Table 5. As shown in this table, the seismic safety factor of the foundations in terms of the vertical bearing capacity of the caisson bottom soils is:

$$S = 0.71 < 1.0$$

and the seismic safety factor of these foundations in terms of the lateral bearing capacity of the caisson front soils is:

$$S = 0.58 < 1.0$$

That is, before retrofitting this bridge did not satisfy these safety requirements.

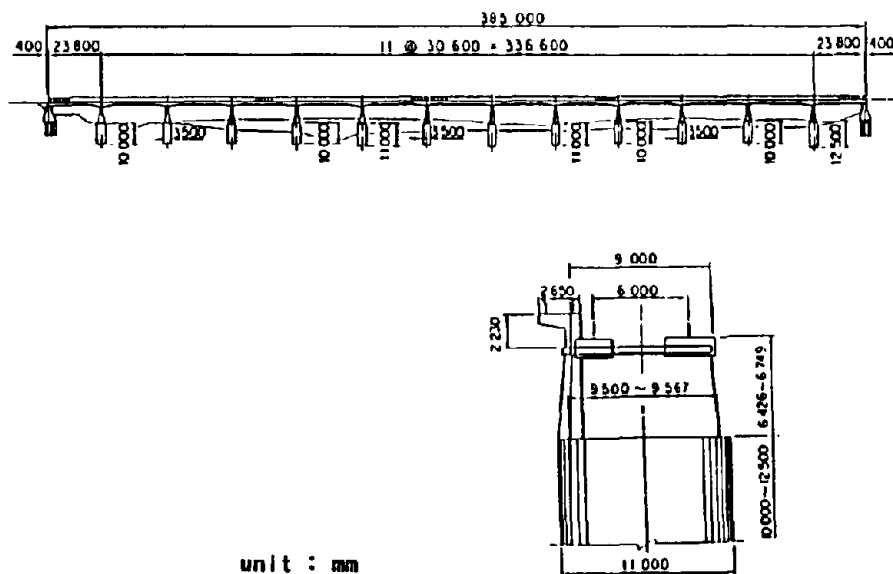


Fig.8 General View of Case C Model Bridge (Ref. 3)

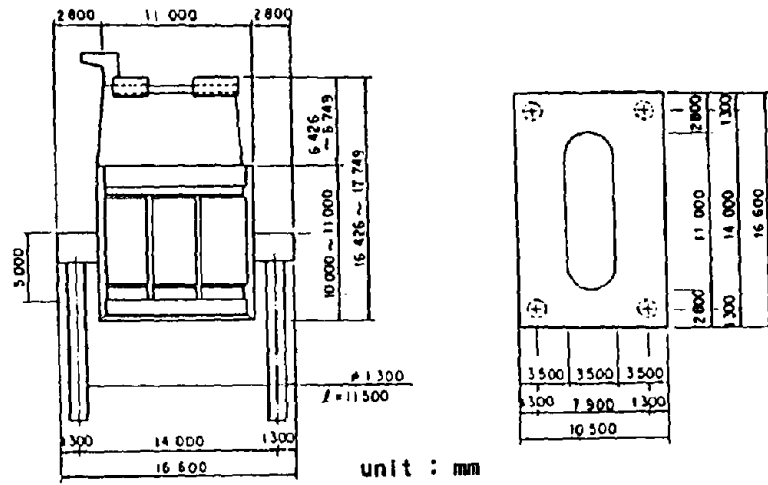


Fig. 9 Extra Pile Driving Practice for Case C Model Foundation (Ref. 3)

Table 5 The Result of the Seismic Inspection (Case C)

	BEFORE RETROFITTING	RETROFITTING WITH MENSIN DEVICE
NATURAL PERIOD (sec)	1.00	0.98
IN TERMS OF VERTICAL BEARING CAPACITY OF CAISSON		
DEMAND (tf)	52.9	33.0
CAPACITY (tf)	43.2	43.2
SAFTY FACTOR	0.82	1.31
IN TERMS OF LATERAL BEARING CAPACITY OF CAISSON		
DEMAND (tf)	17.9	7.4
CAPACITY (tf)	9.4	9.4
SAFTY FACTOR	0.53	1.27

The design goals for retrofitting this bridge were determined using *Menshin* bearings as follows:

- To provide this bridge with a damping ratio of about 16 percent.
- To modify this bridge system to a multi-point elastic support system by connecting the suspension girders as shown in Figure 10, and to replace the existing bearings with *Menshin* bearings equally withstand the lateral seismic loads on each pier.

As in case B, the *Menshin* devices are designed to function only in the bridge's longitudinal direction.

Table 6 shows the dimensions of the *Menshin* bearings designed to achieve the above goals. Table 5 also shows the results of the inspection conducted to examine the seismic resistance of this bridge seismically retrofitted with *Menshin* bearings. As shown in this table, the seismic safety factor of the foundations in terms of the vertical bearing capacity of the caisson bottom soils is:

$$S = 1.3 > 1.0$$

The safety factor of the foundations in terms of the lateral bearing capacity of the caisson front soils is:

$$S = 1.27 > 1.0$$

Thus, the safety requirements of the caisson foundations of this bridge are satisfied.

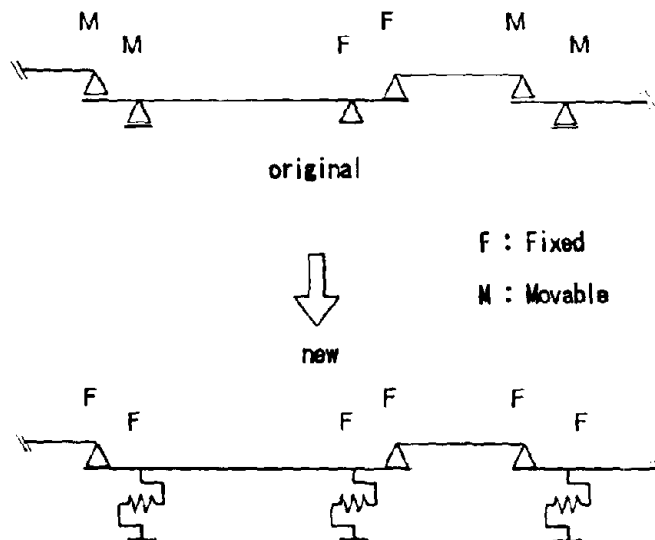


Fig. 10 Modification of Structural System of Case C Model Bridge

Table 6 Dimension of the *MENSHIN* Bearings (Case C)

NUMBER (PER PIER)	2
PLANE FIGURE	500 mm × 500 mm
LEAD PLUG	5 × φ 50 mm
THICKNESS OF RUBBER	4 × 15 mm
WHOLE HEIGHT	129 mm

Since the bearing soils of this model bridge had been degraded to a particularly large extent (as described earlier), and the stiffness of the rotary springs fitted on the foundations had been substantially reduced, the superstructures would have been substantially displaced during an earthquake. If the amount by which the superstructures of this bridge will be displaced is a prime problem, use of *Menshin* devices in this bridge would not be feasible. Even so, *Menshin*-device-based retrofitting measures are economically more advantageous than other conventional seismic retrofitting measures that demand even larger temporary facilities. The seismic retrofitting of this bridge using *Menshin* devices, however, requires foundation consolidation work to prevent further scouring.

CONCLUSION

The following conclusions were led from the experimental *Menshin*-bearing-based retrofitting designs for several model bridges which had to be seismically retrofitted or had already been seismically retrofitted.

(1) It has been verified that *Menshin* design could be applied to seismic retrofitting of the substructures of highway bridges. In the application of *Menshin* design to seismic retrofitting, it is especially effective to disperse the lateral seismic loads by modifying the existing structural system into a multi-point elastic support system with *Menshin* bearings.

(2) In some cases where *Menshin*-bearing-based designs are adopted in seismic retrofitting, such as experimental design case A, existing expansion joints, expansion spaces and restrainers would prevent *Menshin* bearings from acting during an earthquake. Therefore, it would be important to adjust them not to prevent *Menshin* bearings from acting.

(3) In seismic retrofitting of reinforced concrete columns, retrofitting measures with *Menshin* bearings are feasible, but are economically less advantageous than RC lining in most cases. On the other hand, in seismic retrofitting of foundations, retrofitting measures with *Menshin* bearings are more advantageous in cost and ease of execution than conventional seismic strengthening measures that usually demands large-scale works.

(4) It is also effective to use *Menshin* bearings in conjunction with other conventional retrofitting measures to reduce the burden of the structural components in resisting seismic loads. For example, as shown in experimental design case C, *Menshin* bearings cooperated with a foundation consolidation measure to prevent scouring in reducing large-scale extra pile driving.

In the future study, to actualize the seismic retrofitting based on *Menshin* design, it will be necessary to show the design and execution details by using more practical and more detailed cases.

ACKNOLEGEMENT

This *Menshin*-design-based experimental study was made as a part of the joint research program on "Development of *Menshin* Systems of Highway Bridges" between Public Works Research Institute (PWRI) and 28 private firms in Japan. While proceeding with these design experiments, we have been greatly assistend by help and advice from the members of the working group 4.4 in the joint research and Dr. K. Kawashima and his staff of the Earthquake Engineering Division of PWRI, to all of whom, we would like to extend our grateful thanks.

REFERENCES

1. Japan Road Association: "Design Specifications of Highway Bridges, Part V, Earthquake Resistant Design", 1990 (in Japanese)
2. PWRI and 28 Private Firms: "Development of *Menshin* Systems of Highway bridges - Report No.2-", PWRI Joint Research Report No.60, 1991 (in Japanese)
3. Kawashima, K., Unjoh, S. and Azuta, Y.: "Examples of Seismic Retrofittings of Existing Highway Bridges Based on the Result of the Seismic Inspections of 1979", Technical Report, No.2674, PWRI, 1988 (in Japanese)

7. Applications to Medium and Long-Span Bridges

CALTRANS Seismic Isolation Design and Future Concepts
E. Thorkildsen

Earthquake Resistant Design of a Long-Span Cable-Stayed Bridge
Y. Yamada, K. Toki and M. Kitazawa

Passive Seismic Control of Cable-Stayed Bridges
H-E.M. Ali and A.M. Abdel-Ghaffar

Seismic Response of Multi-Span Continuous Bridge with Deck Length of 1 Km
Y. Goto, M. Tokunaga, T. Yosimura and M. Sintaku

Application of Menshin Design to Bridges With Deck Length of 1000 M
H. Mashiko, H. Arai and Y. Fujiwara

CALTRANS SEISMIC ISOLATION DESIGN AND FUTURE CONCEPTS

Eric Thorkildsen

California Department of Transportation, Sacramento, California

INTRODUCTION

The California Department of Transportation (Caltrans) has installed seismic isolation bearings on three bridges since 1985, with plans for another bridge in early 1992. While having no official agenda or policy for future installations, Caltrans is making an effort to keep abreast of the latest seismic isolation technology and opportunities for utilization. Specification development, retrofit applications, and special designs are all progressing. This paper will look at the recent history of Caltrans and seismic isolation, a project ready to be constructed that utilizes these isolation bearings, and a look at future uses of and concerns with the technology.

HISTORY

The first bridge to use seismic isolation bearings was the Sierra Point Overhead in South San Francisco. This overhead structure, initially constructed in 1956, is a 10 span, eight lane welded steel girder bridge with 3' diameter columns. A 0.6 g ground response spectra was applied to the structure computer model revealing severely deficient columns. Thirty six existing steel bearings were replaced with lead filled rubber isolators. The retrofitted bridge was subjected to the 1989 Loma Prieta Earthquake, but the force was not strong enough to activate the isolation system. Sensors installed by the California Strong Motion Instrumentation program measured levels of 0.3g to 0.4g at the column top. No difference in force level was noticed from the sensors above and below the isolation bearing. The abutment backwall haunched top is the fuse that will activate the isolation system, but the force levels were not large enough to sever the backwall haunch allowing displacements to occur.

Another retrofit application of Seismic Isolation was the Eel River bridge in Humboldt County, which is in the northwestern portion of California. This three span steel truss bridge had one of its spans collapse in floods, and the rebuilding effort included earthquake upgrading of the remaining two spans. A 0.5 g response spectra was applied to the structure, and it was decided that lead filled rubber isolators would adequately protect the existing seismic deficient substructure.

The All American Canal bridge in Imperial County was the third California state highway bridge to utilize Seismic Isolation bearings. The original steel truss bridge superstructure was replaced with a wider welded plate girder superstructure. By using lead filled seismic isolation bearings, the existing substructure could be used to support the new superstructure without any modification.

All these three previous applications for Seismic Isolation have been for retrofit purposes. Only recently isolation was considered for new construction. A project that reuses steel girders on a new structure is ready to be constructed. This situation presented an opportune time for the use of seismic isolation bearings on a new bridge.

680/24 OVERVIEW

Interstate 680 intersects State Route 24 in the city of Walnut Creek, California. The 680/24 interchange has an average daily traffic of 280,000 and currently operates at a Level of Service F. Caltrans has undertaken an ambitious seven year \$280 million project to reconstruct the entire interchange and replace every connector with a new structure in order to improve capacity and safety. [1] Due to the high demand to keep traffic moving during construction, a temporary bypass "flyover" structure will be built. It is estimated that the flyover structure will cost \$8 million and will take 15 months to construct.

Since the structure is only temporary, the idea of using salvageable materials for construction was investigated. A planning study was made on the use of welded steel girders. It was found that the expense of using these girders could be justified if the girders could be used again at another location. Fortunately, the first 700 feet of the flyover (about 30% of the total structure length) had a similar profile, superelevation, and roadway curvature of one of the permanent overcrossings to be built in a subsequent construction stage. The remainder of the flyover will be a cast-in-place concrete box girder structure, except at two locations where welded steel "drop-in" girders will span over future connector ramps.

The most common bridge built in California is a cast-in-place concrete box girder. It is a site specific design, very economical, aesthetically pleasing, and has the characteristics desirable in an earthquake resistant structure. However, it is near impossible to dismantle and reuse at another location. The cast-in-place box proposed to be used in the remainder of the structure was estimated as more economical than steel, even with falsework that would exceed 80 feet in height.

A 210' span length is needed for the permanent structure. Since such a long span length was required, welded steel girders was the logical alternative considered. These girders are 84 inches in depth and of composite design. The only girder modifications to be made when they are re-erected at the permanent overcrossing will be the welding of new shear connectors to the girder flange, and new splice plates which will adhere at a slightly different vertical profile.

Walnut Creek's proximity to two separate fault lines led to a seismic design loading corresponding to a peak rock acceleration coefficient of 0.6 g. A seismic design of this magnitude on a structure 2200' long required the columns to act collectively along with other substructure components, to provide an evenly distributed stiffness response. A cast-in-place concrete box girder provides this naturally with its monolithic connection between the column and the superstructure. The connection between a welded steel girder superstructure and its supporting bent is more difficult. Bolted connections work for short spans, but longer steel spans require many bolts to adequately transfer the seismic shear force from the superstructure to the support bent. One method that is commonly used in Seismic retrofit is to tie the girders to the support bent by means of restrainer devices, such as cables, bars, or shear blocks. We found this method to be aesthetically displeasing and difficult to dismantle and reuse. After studying the problem and reviewing possible solutions more closely, it was decided the Seismic Isolation bearings would be used for this situation. What was needed was a product that could adequately soften the force of the anticipated seismic event as well as being simple enough to remove and reuse in the permanent structure.

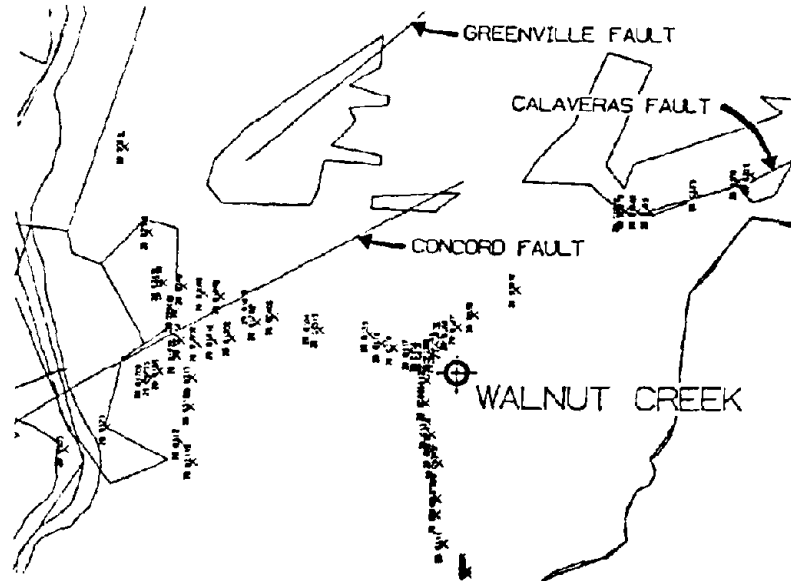


FIGURE 1

STRUCTURE MODELING

The Olympic Boulevard Off Ramp Separation is the permanent structure for which the welded steel girders and the isolation bearings will be reused. It is 700 feet long, has four spans with the maximum being 210 feet crossing the eastbound Route 24 to southbound Interstate 680 connector at a 70 degree skew. The substructure consists of single column bents on pile footings. The abutments are seat type with expansion joints that allow movements up to four inches. The girders are built up on 84" deep web plates with 24" maximum width top and bottom flanges. Two computer models of this structure were developed to illustrate the non-isolated and isolated responses to a seismic event.

The earthquake model was analyzed by the "Strudl" computer program using a response spectrum type analysis. The peak dynamic response of all modes having significant contributions are statistically combined to obtain the total structural response. Computer modeling currently used by Caltrans is an elastic response, with the nonlinear behavior of the structural members controlled by the use of a ductility force reduction factor

The non-isolated model considered elastic restraints at the top of the bents and at the abutments in both the transverse and longitudinal directions. The Caltrans 5% damped elastic acceleration response spectrum (ARS) with depth of alluvium between 10 feet to 80 feet below the ground line was used. Soil response at the abutments was modeled with linear springs. The computer model produced a structure period of 0.8 seconds, which places the ARS gravity force near the peak of the response curve for the 0.6 g acceleration coefficient. Seismic Isolation is a good consideration when the non-isolated structure period is near the peak of the ARS curve. Superstructure displacements were about six inches for the non-isolated model.

The parameters for the isolated model included the effective stiffness of the isolators, K_{eff} , the axial stiffness of the bearings, K_a , and the hysteretic damped response spectrum. Usually damping in elastic structural materials is assumed to be viscous in nature and is expressed as a percentage of critical. Critical damping is the minimum damping for which a vibrating system has no oscillatory motion. When structural materials begin to behave plastically such as Seismic Isolation bearings with damping capabilities, a force-deflection curve will show as hysteretic. The energy dissipation or damping of the device is equal in magnitude to the area of the hysteresis loop. [2]

Non-isolated modes use the Caltrans ARS spectrum for 5% damping. A non-isolated modal response is one in which the displacement is not large enough to activate the non-linear behavior characteristics of the bearing. Isolated modes use a spectrum that reflects the 20-30% hysteretic damping of the seismic isolation bearing. The combination of both of these curves form the Composite Response Spectrum, with the shift from one curve to another arbitrarily chosen at 80% of the isolated structures period. [2] The composite response spectrum assumes that the seismic isolation bearing will supply the higher damping, which must be verified with a rigorous testing procedure that is incorporated into the bearing construction specifications.

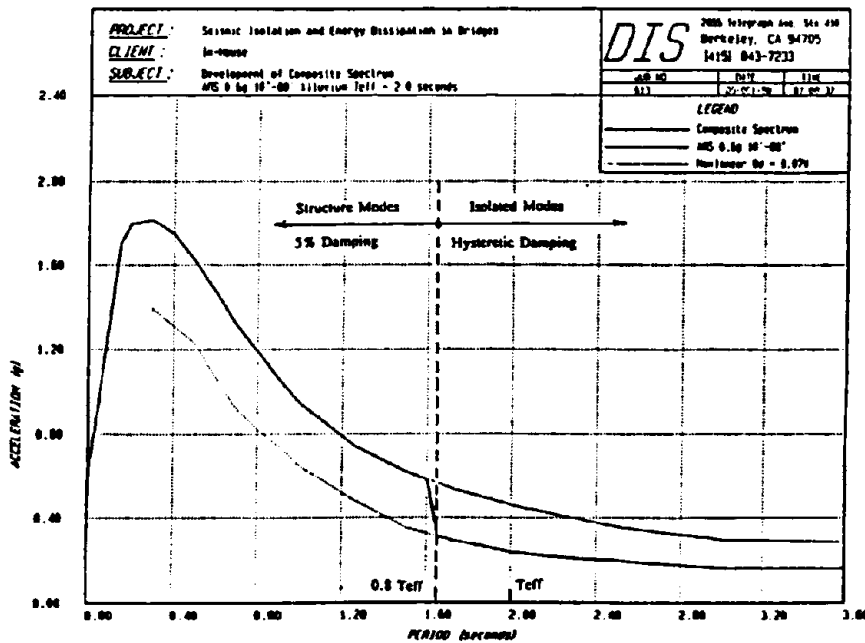


FIGURE 2

The computer model of the isolated structure produced the anticipated results of greater flexibility, with maximum superstructure movements increasing from six inches to nine inches, and a longer structure period that increased to 1.8 seconds. Maximum shear resulting at the top of the pier reduced from 1500 kips to 400 kips. Bottom of column moments were greatly

reduced. Design of the columns and footings could proceed using the elastic forces from this analysis, rather than the higher plastic values caused by yielding columns.

A displacement of this magnitude was not considered a problem except at the abutments. A seat type abutment with a backwall that would break off and displace when impacted by a seismic force was designed. This would limit any further damage to the lower portion of the abutment, where repair would be difficult. The bridge approaches were connected to the backwall in case severe settlement behind the abutment might occur.

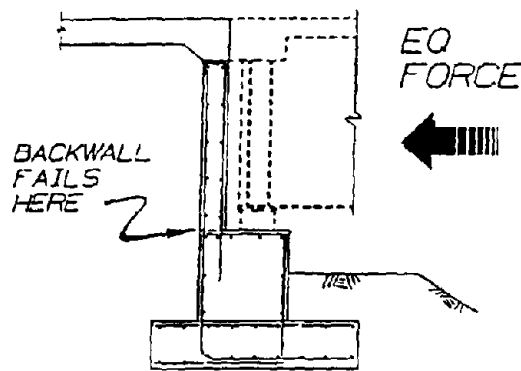


FIGURE 3

The results of the computer model for the isolated structure were arranged in tabular form and placed on the structure plans as Seismic Isolation Design Parameters (see FIGURE 5). These seismic design forces are what the bearing transfers from the superstructure to the substructure. A maximum seismic displacement of nine inches was given along with a corresponding lateral force. The lateral non-seismic forces shown are the approximate maximum loads which would be applied from braking or wind loads. The 1/2 inch displacement cannot be exceeded as the 28 kips is applied laterally. This satisfies the requirement that the bearing have a high elastic stiffness for service loads. If we assume that the isolator will act elastic, by prorating out the non-seismic force deflection to a nine inch displacement, a force of 500 kips will be applied to the substructure. The 135 kips allowable lateral seismic force indicates that some kind of plastic behavior must occur. The maximum allowable rotation of the bearing is also given, to assure that it meets various stability requirements.

SUBSTRUCTURE DESIGN

The primary benefits of Seismic Isolation are received in the design of the substructure. The column-footing connection is fixed to aid stability under seismic conditions. Earthquake moments derived from the computer model at the column-footing connection are compared to the overstrength moment that the column can generate, called the probable plastic moment. For well confined sections, the probable plastic moment is usually assumed to be 1.3 times the nominal moment strength of the column. The footing is designed to resist the smaller of the two

moments, the probable plastic or the elastic earthquake. The isolated structure's column earthquake moments was significantly less than the probable plastic moment from the non-isolated structure's column. The reduction in the size of the footing for the isolated structure resulted in a 38% cost savings. This savings pays for the increased cost of the Seismic Isolation bearings which are generally more expensive than standard bridge bearings. The secondary benefit of isolation are the serviceability and minimal repair costs following a major earthquake because serious damage is prevented.

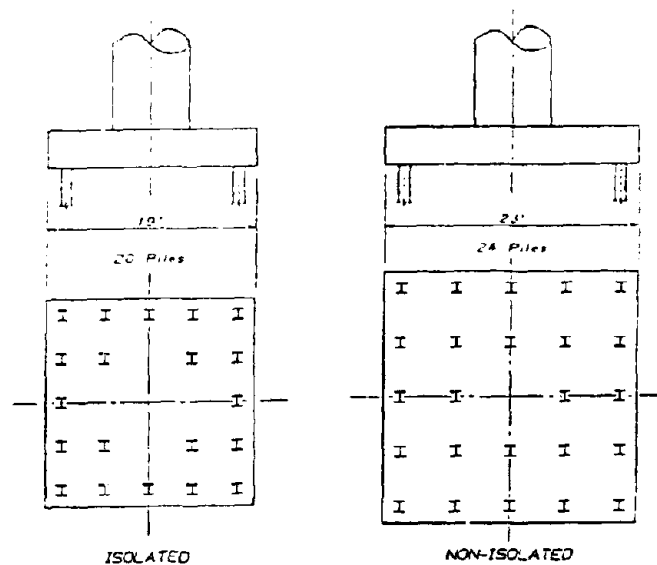


FIGURE 4

SPECIFICATION DEVELOPMENT

Seismic Isolation bearings have been used on three California state bridges. All three contracts listed the bearings as a sole source proprietary item, using the Dynamic Isolation Systems lead core elastomeric bearing. This is referred to as the "directed purchase" method, whereby an agreed price is published in the special provisions of the final bid documents. The Federal Highway Administration's rules governing the use of proprietary products allows this occurrence up to three times as a test installation, with subsequent contracts to include provisions for competitive bidding with equally suitable unpatented items. Caltrans decided to develop a generic specification which would apply to both proprietary and non-proprietary Seismic Isolation bearings.

The specifications were modeled after the proposed provisions for Seismic Isolation Design in the Guide Specifications for Seismic Design of Highway Bridges. Performance and material oriented, these specifications frequently refer to requirements listed on the structural plan. Items that are unique to each structure are listed in tabular form, such as dead and live loads, allowable lateral seismic and non-seismic displacements and their corresponding maximum force levels.

The specifications direct the contractor to supply two full-size specimens of each type of isolator to be subjected to four performance tests.

- (1) Twenty full reversed cycles of loads at the lateral non-seismic force shown on the plans.
- (2) Three full reversed cycles of loading at each of the following increments of the seismic displacement shown on the plans: 0.25, 0.50, 0.75, 1.0, and 1.1.
- (3) Ten full reversed cycles of loading at the seismic displacement shown on the plans.
- (4) Three full reversed cycles of loading at each of the following increments of the seismic displacement shown on the plans: 1.25 and 1.5.

The first prototype test determines if the displacements caused by the lateral non-seismic forces meet acceptable limits. The bridge cannot be too flexible under service loads, especially if it may be perceived as a structural problem. If any elastic restraint is to be applied to the seismic isolator, this test will check the durability of this restraint.

Prototype Test (2) checks the incremental stiffness of the bearing during each cycle, evaluating the consistency of the stiffness with each subsequent cycle as displacements increase.

Prototype Test (3) obtains 10 effective stiffness values at the specified seismic displacement, checking if this cyclic loading effects the stiffness behavior of the bearing.

Prototype Test (4) checks the overall stability of the isolator in a seismic event. Displacements 50% greater than anticipated are used to cover uncertainties in the initial displacement calculation. This is an important check as most seismic isolation bearings have height to width ratios that exceed normal bearing code limitations.

The prototype tests will be performed at the calculated period of the isolated structure. The hysteretic behavior of the bearings will be recorded and compared to the target value that is shown on the structure plans. If the energy dissipated per cycle shown by the hysteresis loop is within tolerance of the specified value, our prior assumption for the composite response spectrum made in computer modeling will be justified. If the prototype tests are not performed at the period of vibration shown on the plans, the contractor will have to perform additional physical tests to demonstrate that the requirements for hysteretic behavior at the specified frequency are satisfied.

The specifications list the available types of Seismic Isolation bearings for a structure by their material composition, such as elastomeric bearing with lead core type or elastomeric bearing type with non-linear hysteresis. Relevant material property requirements are given along with test procedures. The bearings will be measured and paid for by the unit, which will include full compensation for furnishing all labor, materials (including the sample bearing used for testing), tools, equipment, and incidentals.

FUTURE CONCEPTS

A. Opportunities for use of isolation

The use of Seismic Isolators for the Olympic Boulevard structure comes at an opportune time as design is about to start on the third phase of the Caltrans Earthquake Retrofit program. The first phase, which lasted from 1971 to 1987, tied superstructure segments together with restrainer cables to prevent excessive relative movement. Phase two currently in progress strengthens the columns of single column monolithic concrete bridge structures. Phase three currently involves 700 bridges with multiple column bents in definite need of retrofit, many of which are candidates for isolation. Bridges where the superstructure is supported by rocker type bearings is one example. By replacing the existing bearings with Seismic Isolation bearings, the risk of bearing failure is eliminated, the problem of inadequate girder support length is solved, and the need to strengthen columns and footings as in Phase two is mitigated. In some circumstances where bearing replacement is not feasible, or where the structure is monolithic with no bearings, the installation of Seismic Isolation bearings in a gap cut in the columns can be the economical alternative to strengthening the columns and footings. Elimination of substructure retrofits by isolation is especially attractive because many times there is just no room to retrofit existing columns. Existing traffic lanes, utilities, lack of right of way, or other existing facilities such as retaining walls and buildings prevent use of standard retrofit details. The potential for more frequent use of seismic isolation bearings in California bridges goes beyond the 700 bridges mentioned earlier. A risk analysis and prioritization completed in September 1990, identified some 7,500 state and 5,000 local bridges that potentially are seismically deficient, but need further evaluation. The list of 700 will likely grow significantly.

B. Future design policies

Since the Loma Prieta Earthquake, Caltrans has been urged to implement state-of-the-art analysis procedures and emerging technologies such as seismic isolation. [6] Serviceability of bridges after earthquakes has become a major issue, conflicting with Caltrans' basic philosophy of ductility design and acceptance of repairable damage. Caltrans will address these issues in the near future. In establishing seismic design guidelines, the Applied Technology Council has contracted to review all of Caltrans' current seismic design criteria and make recommendations for improvements. The use of seismic isolation will certainly be an item of scrutiny. A seismic advisory board of outside professionals has been formed to approve all proposed changes and additions.

C. Design Manuals and Bearing Selection

The future of seismic isolation design at a production oriented organization like Caltrans depends on clearly established guidelines and procedures which currently do not exist. Design manuals establishing a hand procedure along with examples showing bearing selection would be helpful. The designer could choose a bearing size that would be verified by the supplier at time of successful bid award. The various types and components of isolation bearings currently available to the designer is very confusing, with all suppliers in heavy competition and claiming product supremacy. A single entity representing the interests of all seismic isolation suppliers is one possible solution.

D. Construction Specification and Bid Procedures

The future of Caltrans's generic specifications will include further refinement and development. As more products enter the market, the specifications will have to be broadened, which will be a difficult task considering all the different component materials that make up an isolation bearing. Presently, the only elastomer material included in the specifications is natural rubber, although there have been proposals to include neoprene and polyurethane. Materials used in the manufacture of the bearings must be scrutinized for sensitivity to dust, dirt, temperature change, oxidation, or other forms of contamination. Establishing test procedures to check the long term durability of the bearings will be needed. Performance testing of these large bearings is a problem that must be addressed. The lack of acceptable facilities could cause serious construction delays as the bearings wait their turn to be tested. Caltrans could establish working agreements with a nationwide network of testing laboratories reserving allotted times to ensure performance testing without delay to the project critical path. The specimens could be shipped at Caltrans costs to the various sites. Presently the specifications allow the contractor to choose the isolation bearing supplier. This can be changed so Caltrans can directly select the product based on the overall performance/cost evaluation. The advertised contract would establish a contingency fund for purchasing bearings based on cost proposals submitted by the prospective suppliers.

E. Summary

Caltrans will continue to look for opportunities to use isolation where taxpayer interests appear best served. With each use, the design and selection process by competitive bidding will be evaluated. Feedback from rejected suppliers will be reviewed to determine that viable and effective products have not been eliminated by an arbitrary restrictive specification clause.

REFERENCES

1. 680/24 Project Public Information Office, "Project Handout", 1990.
2. Dynamic Isolation Systems, Inc., "Seismic Isolation and Energy Dissipation Implementation in Bridge Analysis and Design", December 1990.
3. Computech Engineering Services, "Seismic Design and Retrofit Manual for Highway Bridges." Also published by FHWA Report FHWA-IP-86-6, July 1986.
4. "California Department of Transportation Bridge Design Specifications", 1990.
5. Figures (2) and (3) Dynamic Isolation Systems, Inc., "Seismic Isolation and Energy Dissipation Implementation in Bridge Analysis and Design", December 1990.
6. "California Governor's Board of Inquiry on the 1989 Loma Prieta Earthquake", 1990.

EARTHQUAKE RESISTANT DESIGN OF A LONG-SPAN CABLE-STAYED BRIDGE

Yoshikazu Yamada^a, Kenzo Toki^b, and Masahiko Kitazawa^c

^aEarthquake Engineering Laboratory, Department of Civil Engineering, Kyoto University, Yoshida Honmachi, Sakyo-ku, Kyoto 606, Japan

^bDynamics of Foundation Structures Research Section, Disaster Prevention Research Institute, Kyoto University, Gokasho, Uji, Kyoto 611, Japan

^cHigashi-Kobe Construction Office, Kobe Construction Division, Hanshin Expressway Public Corporation, 5 Chome, Uozakiminami-machi, Higashinada-ku, Kobe 658, Japan

Abstract

The Higashi-Kobe Bridge is a long-span cable-stayed bridge in which the unique feature is that the main girder is supported by towers and piers in such a way that the girder is movable in the longitudinal direction. This supporting method was adopted with the aim of lengthening the fundamental period of the bridge to a relatively longer period. By using this supporting method, the effects of the inertial forces due to the superstructure on the bridge towers and the caisson foundations will be greatly reduced, thereby resulting in a more rational and economical bridge design.

1. OUTLINE OF THE HIGASHI-KOBE BRIDGE

The Higashi-Kobe bridge, a steel cable-stayed bridge presently under construction, is one of the several large-scale bridges that will form the Osaka Bay Route of the Hanshin Expressway Public Corporation. The features of this bridge (Figure 1) can be summarized as follows:

- Center span length: 485m
- Width of bridge: 13.5m (3 lanes each for upper and lower decks)
- Main girder: 9m high Warren truss with no vertical chords
- Tower: H-shaped tower with 146.5m high columns and curved cross beams tied at relatively low positions
- Cable: Double-plane multiple cable system with harp pattern arrangement
- Floor system: Steel deck composite with the main girder truss
- Foundations: Pneumatic caissons for the towers ($L \times B \times H = 32 \times 35 \times 25$ m); Cast-in-place piles for the end piers and the pendulum piers.

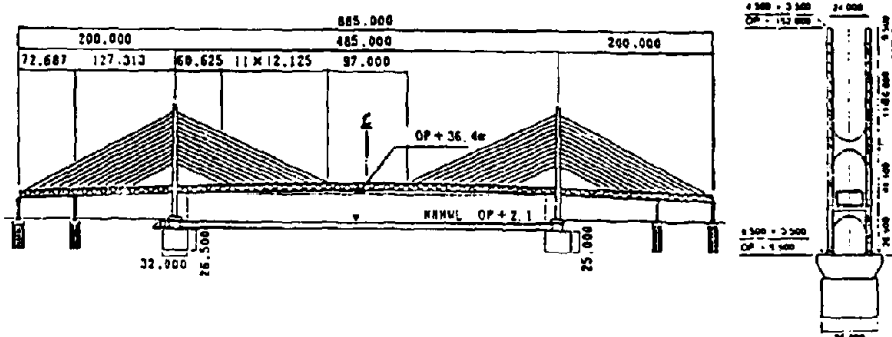


Figure 1. General View of the Higashi-Kobe Bridge

2. EARTHQUAKE RESISTANT DESIGN OF A LONG-SPAN CABLE-STAYED BRIDGE

2.1 General Concepts of Aseismic Design of Higashi-Kobe Bridge

Upon completion, the Higashi-Kobe Bridge will be one of the longest cable-stayed bridges in Japan. Because of high seismicity in Japan, earthquake-resistant design of the bridge is a critical issue in the general design process of the bridge. Cable-stayed bridges are so highly redundant (statically indeterminate) that sophisticated computer analysis is needed. General concepts of the aseismic design are given as follows:

- Keep the bridge structure flexible to a reasonable level in order to reduce seismic inertia, but provide safety devices to suppress excessive deformation.
- Adopt multi-mode response analysis to determine sectional forces due to the design earthquake loads in order to properly model the bridge behavior.

2.2 Selection of the Basic Structural Configuration

In order to determine the ideal support system for the Higashi-Kobe Bridge, the earthquake response of several configurations of structural system were considered and the comparison is shown in Table 1.

The advantages and disadvantages of these supporting systems can be summarized as follows:

- The use of one fixing support or two fixing supports, case 1 and case 5 in Table 1, causes large forces in the fixed piers. And, even multiple fixing support system (case 2), cannot disperse earthquake forces.
- The use of elastic supports (case 3) makes it possible to adjust natural period of the bridge adequately enough to reduce earthquake forces in the towers. However, using such system will require careful maintenance.
- The use of all movable supports (case 4) where the main girder is supported by towers via cables (herein referred to as "all free") gives the bridge a rather longer natural period, and therefore reduces earthquake forces of the tower considerably. However, the displacement of the main girder can be quite large.

Acceleration response spectrum for the superstructure design was determined against the most unfavorable case at the construction site especially in the longer period range. Table 2 shows forces and displacements categorized according to design loads. Adopting the all-free support system, wind loads (rather than earthquake loads) governs in the design of the towers.

As a result, the size of the caisson for the all-free system can be made about 10m smaller than that designed for a two-fixed support system.

Table 1 Comparison of different supporting systems

Support Configuration	Natural Period sec.	Section Forces (tower base) kN, kN-m	Displacement (girder) cm
(1). Two Supports Fixed <i>M+F+F+M</i>	1.42	M=608000 N=90000 S=24000	20
(2). All Supports Fixed <i>F+F+F+F</i>	1.26	M=609000 N=85000 S=24000	18
(3). Spring Supports <i>M+S+S+M</i>	3.01	M=308000 N=88000 S=10000	37
(4). Supports All Free <i>M+M+M+M</i>	8.69	M=155000 N=90000 S= 2000	56
(5). One Support Fixed <i>M+F+M+M</i>	2.21	M=602000 N=97000 S=23000	22

- N.B. - Load combination: $D + L_{EQ} + EQ_L + T_{15}$
 - Fan pattern cable arrangement is assumed
 - Design Spectrum for Ajigawa Bridge is used
 - Forces are given per column
 - 'M' movable; 'F' fixed; 'S' elastic

Table 2. Forces and Displacements by design Loads

	Tower base force and girder displacement			
	All Free		Two Fixing System	
	S (kN)	M (kN*m)	S (kN)	M (kN*m)
W	9200	440000	9300	219000
EQ	7600	406000	25000	600000
Critical Design load	7200	348000	22900	400000
	$(D + W + T)/1.35$		$(D + L + EQ + T)/1.50$	
Plate Thickness at Tower Base	36mm		45mm	
Caisson Size (L×B)	32m × 35m		40m × 35m	

- N.B. - Harp pattern cable arrangement is assumed
 - Forces are given per column

2.3 Countermeasures for Large Displacements

Having selected the all-free configuration, the following problems should be properly addressed:

1. accurate and reliable evaluation of the earthquake response of long-period structure;
2. disadvantage due to out-of-plane buckling of the tower column not fixed to the main girder;
3. large longitudinal displacement of the main girder due to earthquake and wind.

The latter two problems can be solved by arranging the cables in a harp pattern. Arranging cables in harp pattern has the effect of constraining rotational movement of the towers and also of constraining longitudinal movement of the girder. The remaining part of this paper addresses the first stated problem.

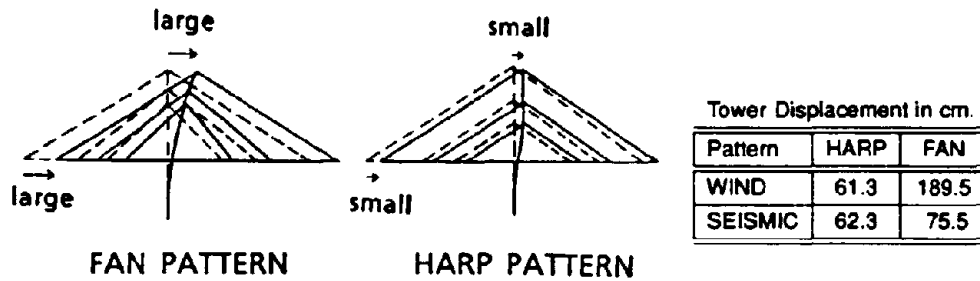


Figure 2. Displacements of Fan and Harp Cable Pattern

2.4 Design Acceleration Response Spectra

The design spectrum was provided with a relatively large safety margin in the long period range. This is because the Higashi-Kobe bridge has an unprecedented long natural period of longitudinal sway mode oscillation. The design spectrum range around the natural period plays a critical role in determining the structure response to earthquakes. The design spectrum was determined by the following procedure:

1. In formulating the design acceleration response spectrum, a 1000 meter deep bedrock at the construction site was assumed from the fact that a granite layer lies at that depth. By taking the deep bedrock, there occurs a possibility of the seismic wave and bridge oscillation frequencies coinciding and causing amplification in the long period range. The bedrock was assumed to be somewhat deeper than usual to increase the safety margin.
2. The maximum acceleration of seismic waves at the bedrock was assumed to be 160 gal as an expected value during a 100-year return period. For the input waves W1 at the bedrock, three earthquake records including Taft were used as data which were reliable up to the range of 0.07 Hz. These are then converted to their equivalent bedrock motion (Figure 3).
3. Waves W2 at the 80m deep design ground base, which will be used for the earthquake response analysis using finite element method, were obtained by multiple wave reflection analysis in which strain dependency of soil properties was considered (Figure 4).
4. The acceleration response spectra for the superstructure were obtained from the tower base waves W3 in the above analysis in which the superstructure, substructure and the surrounding ground are modeled. These spectra have peaks at natural periods of the ground coinciding with that of the bridge.
5. The design spectrum was determined by taking an envelope curve of mean spectrum of these three in longer period range. The shorter and intermediate part of the spectrum was determined by referring to the specifications for highway bridges in Japan and other standards for bridges (Figure 5).

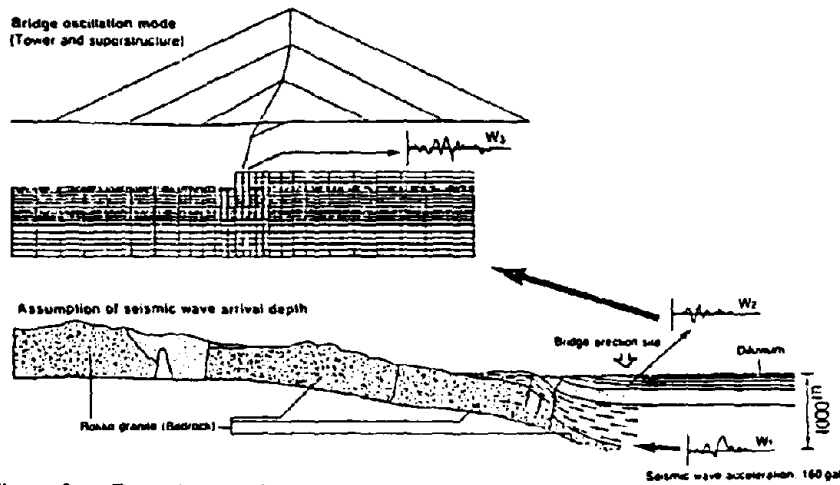


Figure 3. Procedure for Determining Design Spectrum

Depth (m)	Layer	Thickness (m)	Soil description		Average corrected shear modulus (dynes/cm ²)		
			Symbol	Unit weight (kN/m ³)	1000 Hz	10 Hz	1 Hz
0	air	1.00	0.125	1.2	1.2	1.2	1.2
10	all	1.175	1.000	1.2	1.2	1.2	1.2
20	slmp	1.00	15,100	1.5	1.5	1.5	1.5
30	slmp	1.00	15,100	1.5	1.5	1.5	1.5
40	slmp	1.00	15,100	1.5	1.5	1.5	1.5
50	slmp	1.00	15,100	1.5	1.5	1.5	1.5
60	slmp	1.00	15,100	1.5	1.5	1.5	1.5
70	slmp	1.00	15,100	1.5	1.5	1.5	1.5
80	slmp	1.00	15,100	1.5	1.5	1.5	1.5
90	slmp	1.00	15,100	1.5	1.5	1.5	1.5
100	slmp	1.00	15,100	1.5	1.5	1.5	1.5
110	slmp	1.00	15,100	1.5	1.5	1.5	1.5
120	slmp	1.00	15,100	1.5	1.5	1.5	1.5
130	slmp	1.00	15,100	1.5	1.5	1.5	1.5
140	slmp	1.00	15,100	1.5	1.5	1.5	1.5
150	slmp	1.00	15,100	1.5	1.5	1.5	1.5
160	slmp	1.00	15,100	1.5	1.5	1.5	1.5
170	slmp	1.00	15,100	1.5	1.5	1.5	1.5
180	slmp	1.00	15,100	1.5	1.5	1.5	1.5
190	slmp	1.00	15,100	1.5	1.5	1.5	1.5
200	slmp	1.00	15,100	1.5	1.5	1.5	1.5
210	slmp	1.00	15,100	1.5	1.5	1.5	1.5
220	slmp	1.00	15,100	1.5	1.5	1.5	1.5
230	slmp	1.00	15,100	1.5	1.5	1.5	1.5
240	slmp	1.00	15,100	1.5	1.5	1.5	1.5
250	slmp	1.00	15,100	1.5	1.5	1.5	1.5
260	slmp	1.00	15,100	1.5	1.5	1.5	1.5
270	slmp	1.00	15,100	1.5	1.5	1.5	1.5
280	slmp	1.00	15,100	1.5	1.5	1.5	1.5
290	slmp	1.00	15,100	1.5	1.5	1.5	1.5
300	slmp	1.00	15,100	1.5	1.5	1.5	1.5

Figure 4. Multiple Wave Reflection Analysis of Deep Ground

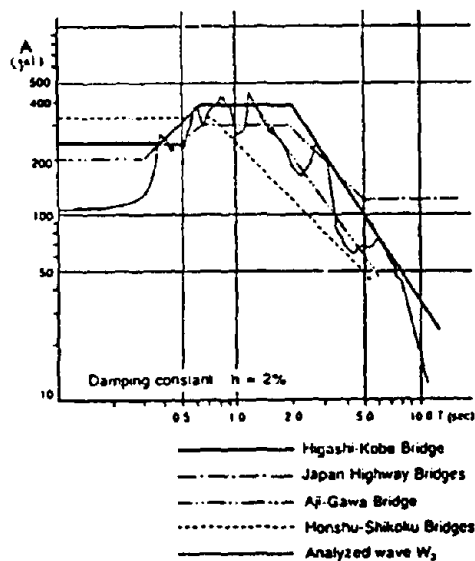


Figure 5. Design Acceleration Response Spectrum

As a result, the design acceleration at 4.4 seconds which corresponds to the natural period of the sway mode oscillation of the structure becomes 120 gal., which is nearly 1/3 of that used in standard bridges in Japan. The sectional forces and displacements using this design criterion have already been shown in Table 2.

Seismic forces taken into consideration were those from any direction that would trigger maximum stress on tower members, in addition to those applied longitudinally and transversely to the bridge. It was confirmed from a 1/100-scale full model vibration test that such stress

is the resultant of those caused by longitudinal and transverse seismic forces.

The design spectrum was confirmed by another study in which records by Japan Meteorological Agency Seismometer and the same records by SMAC were first compared to find differences in both waves and to find recording error of the SMAC. It was found that the error was caused by the spring which controls the SMAC pen movement. Since the ground moves slowly during a long period earthquake, the spring cannot have the power to pull the pen. The error which should be removed turned out to be the minimum value of the smoothed Fourier Spectrum. An attenuation equation was obtained from the relation between magnitude, epicentral distance and SMAC acceleration data modified by the above method. By supposing the Nankaido Earthquake that will cause the worst possible effect for the bridge site, the expected spectrum on the ground was obtained. As a result, it was found that the design spectrum already determined corresponds to the expected value of the mean plus 1σ (standard deviation) and was judged suitable for design use (Figure 6).

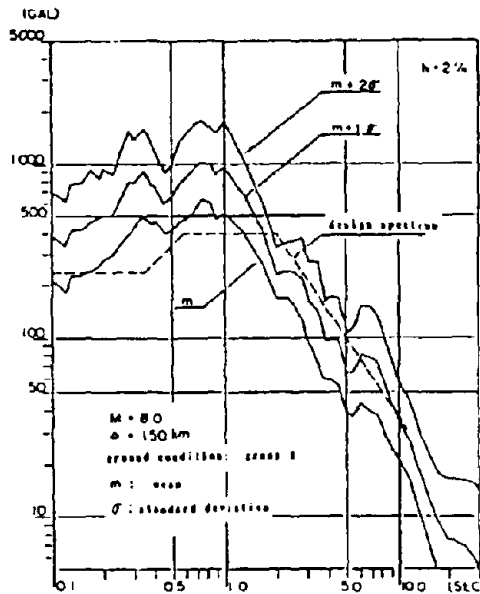


Figure 6. Confirmation of Design Spectrum

2.5 Earthquake Safety Devices — Development and Design

As there is not much data on earthquake resistant design for a cable-stayed bridge with a long natural period, it was decided to install a vibration-resisting device to prevent excessive girder movement which might result in tower collapse. A case in which a simple stopper is installed on each end pier was analyzed. The result indicated that because of the low rigidity of the piers, the movement of the heavy girders cannot be controlled.

After considering several devices, the vane-type oil damper was selected. The damper contains oil in its drum which is divided into two compartments. When the girder moves, the oil moves from one compartment to the next through an orifice in the partition. The turbulent flow generated when the oil passes through the orifice produces the power that moderates the girder movement (Figure 7). The characteristics of the vane-type oil damper are as follows:

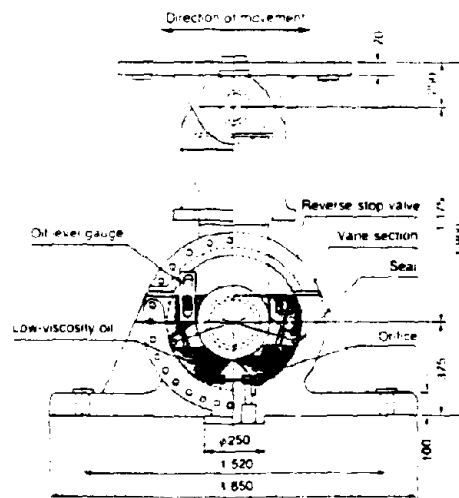


Figure 7. Vane-type Oil Damper

- The damper does not have the problem found in the case of simple stoppers in which small difference in clearance setting often results in big difference in reaction force.
- The effect of the damper increases as girder movement becomes larger and faster. This indicates that the damper is very effective in preventing excessive amplitude.
- The damper increases the safety margin without changing the characteristics of the natural period of the bridge.
- A well-designed damper reduces the girder movement and controls the reaction forces on the end piers.

Considerations for damper design and maintenance should include the following:

- There must not be a gap between the vane and the cylinder to prevent oil leakage.
- A dust cover is required to prevent oil contamination.
- The volume of the oil must be checked periodically.
- The effect of oil temperature on the damper performance is negligible.

To examine the characteristics and applicability of the damper, a 1/2-scale model was fabricated for performance testing. The test was conducted with different movement velocities and orifice sizes. The test results reveals that the turbulent flow resistance characteristic is given by the following expression:

$$F = 1840V^2 \times 2 \quad (\text{in case the orifice angle is } 15^\circ) \quad (1)$$

where V : girder movement velocity

F : resistance which is equivalent to the reaction on the pier.

In designing the damper, an earthquake that is 1.4 times stronger than that considered in the bridge design is assumed. Since the design spectrum corresponds to the expected value of the mean plus 1σ , the value of mean plus 2σ was considered to be suitable for design due to an unexpectedly strong earthquake. Using the characteristics of the vane-type oil damper and this earthquake input, nonlinear time history earthquake response analysis was conducted. The input earthquake used was that of the Izu Peninsula Earthquake.

Table 3. Effect of Vane-type Damper on Girder Displacement

Earthquake Level	Damping Constant (%)	Relative Girder Displacement (cm)	Maximum Response Velocity (cm/sec)	Damper Reaction (kN)
whole structure design level (1.0EQ)	2*	61*	—	—
	1	72	—	—
	2	61	98	—
	1+4.8**	48	75	1480
girder stopping device design level (1.4EQ)	1	102	231	—
	1+6.2**	64	99	3620

N.B. - Values marked with * were obtained using the design spectrum

- Damping constant marked with ** indicates damping of the whole structure plus damping due to the damper

The results are given in Table 3 and can be summarized as follows:

- If an earthquake 1.4 stronger than the design spectrum occurs on the bridge without the dampers (structural damping ratio of 1% is assumed), the displacement of the girder will be $72 \times 1.4 = 102$ cm. This will be over the critical displacement of 74 cm at which the tower buckles.
- If the dampers are installed, the girder displacement will be reduced to 64 cm, which is in the range of the design displacement of 61 cm. This is below the critical displacement for the tower to buckle. In this case, the equivalent damping constant due to the damper is calculated to be approximately 6% based on the displacement response.

2.6 Verification of Dynamic Behavior of the Bridge by Shaking Table Tests

The appropriateness of the method adopted to evaluate the bridge response to the earthquake and the effectiveness of the damper were confirmed by vibration tests using a three-dimensional 1/100-scale elastic model. The model was made of steel satisfying the similarity of stiffness and weight. The natural frequency and mode shapes of the model in several low modes agreed well with the analytically predicted ones. The structural damping of the model without the damper is adjusted to 1~2%, reflecting fairly light damping of a large flexible structure. An electro-magnetic damper is attached to the girder of the model to substitute the vane-type oil damper.

Modified long-period predominant and short-period predominant earthquake records were used for input earthquake ground motion. Results are shown in Table 4. All values are converted to the prototype for comparison. Displacement response due to the short period predominant earthquake (El Centro NS, 1940) record is found to be much less than the design values.

Table 4. Maximum Displacement Response (given in cm.) for Cases with and without Damper

Input Earthquake		Input Along Long'l Axis		Input Along Transverse Axis	
		Top of Tower		Girder Center	Top of Tower
		No Damper	W/ Damper	No Damper	W/ Damper
Long Period	Izu-oki Earthquake	64.0	50.0	65.0	56.0
	Synthesized Wave		(53.9)		
	Chiba-oki Earthquake Corrected Wave	63.0	52.0 (51.6)	44.0	60.0
Short Period	El Centro Earthquake	18.5	17.0	35.0	30.0
Design Value by Response Spectra		60.4	—	79.4	82.0

N.B. - Tabulated values are corresponding to real bridge

- Viscous damping coefficient of 2% is assumed for cases without damper

- Values () are those calculated from time history response analysis

Displacement response at the top of the tower due to the long period predominant earthquake motion without the damper is observed to be nearly equal to the design values. Moreover, energy dissipation of the damper suppressed the response fairly well to the design values. Close agreement of the experimental and numerically calculated results verifies both methods.

In addition to the above vibration tests, following two tests were conducted. Recent earthquake observation in soft ground suggests long duration sinusoidal-type ground motion with relatively small amplitude. Hence, the frequency matched sinusoidal input motion with 10 gal (cm/sec^2) amplitude and 10 cycles are used for the resonance test of the model. The results shown in Figure 8 verifies that the damper is very effective in suppressing resonant-type response to one-third level.

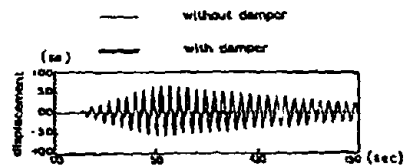


Figure 8. Effectiveness of Damper in Suppressing Resonant-Type Response

To investigate complex 3-D dynamic behavior of the bridge, single component vibration tests in three orthogonal directions and simultaneous three-component vibration tests were conducted and compared. Figure 9 shows the dynamic response of the bridge subjected to the motion in the EW (transverse) direction. From the results, it was confirmed that no interaction between the three directions exists. Comparing with the single component tests, it was found that 3-D results can be predicted from the linear superposition of the single component tests.

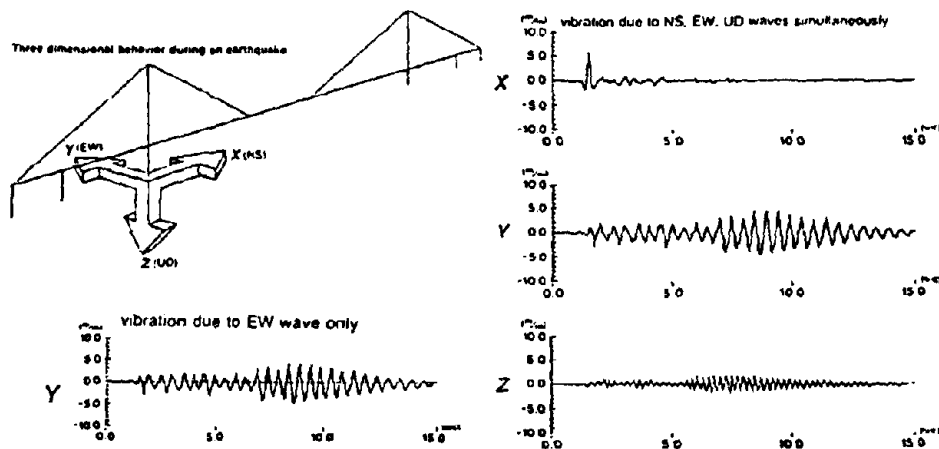


Figure 9. Three-Dimensional Behavior During Earthquake

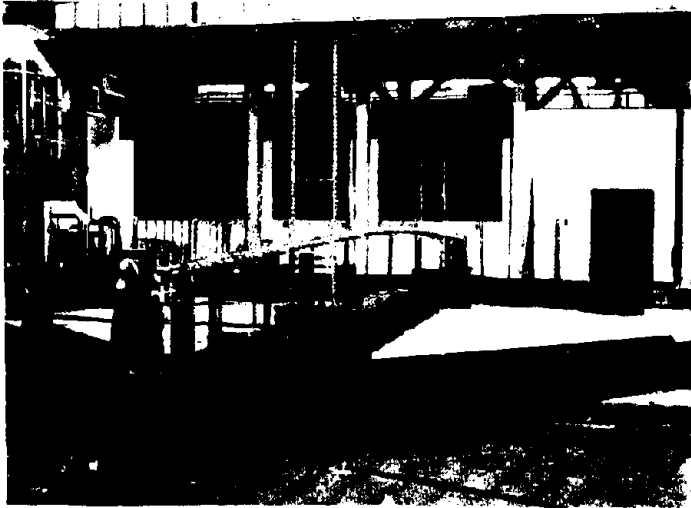


Figure 10. Full Model Vibration Test

3. VIBRATION TEST OF THE ACTUAL TOWERS

In earthquake resistant design process of the Higashi-Kobe Bridge, damping characteristics of the tower itself is assumed as $h = 0.01 \sim 0.02$ (damping ratio). This value is adopted based on previous design practices when relatively large damping capacity is expected due to large amplitude of vibration when subjected to severe earthquake excitation.

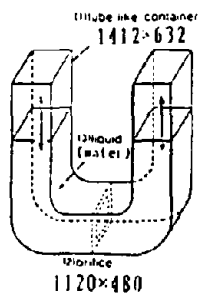


Figure 11. Tuned Liquid Column Damper

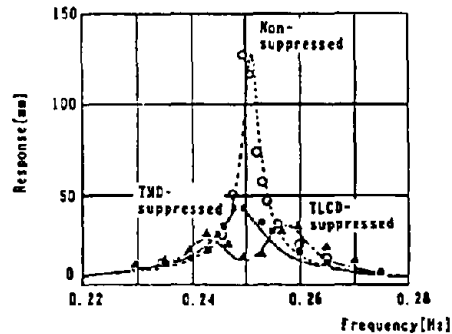


Figure 12. Resonance Tests

Table 5. Natural frequencies and Damping Capacity of the Towers

Mode	Frequency (cps)	Logarithmic Decrement		
		Tower only	with TMD	with TLCD
1st	0.256 (0.249)	0.028 ~ 0.040	0.098	0.110
2nd	1.107 (1.050)	0.094 ~ 0.099	—	—

* Values in () obtained by analysis

Vibration experiments of the actual tower of the Higashi-Kobe Bridge using a pair of exciters were employed to verify the dynamic property assumed in the design and the efficiency of the vibration suppressing devices used only during construction, namely TMD (Tuned Mass damper) and TLCD (Tuned Liquid Column Damper) as shown in Figure 11. The exciters and the dampers were attached to the top of the tower.

The natural frequency and damping of the tower are shown in Table 5. Calculated and measured natural frequency agrees fairly well in 1st and 2nd modes. The logarithmic decrement was found to be about 0.03 for the first mode without dampers.

The frequency response curves of the tower with and without dynamic dampers are shown in Figure 12. The maximum response of the TMD- and TLCD-suppressed cases are reduced to almost 1/3 of that of non-suppressed case. It is verified that logarithmic decrements of those devices are more than 0.1 and effective to control wind-induced excitation.

4. CONCLUSIONS

Main conclusions obtained in this study on aseismic design of a long-span cable-stayed bridge are as follows:

- The main girder is supported by the towers through cables in such a way that the girder is movable in the longitudinal direction. By this supporting method, the fundamental period of the bridge is lengthened to reduce seismic design forces. Consequently, the size of the foundations of the tower was significantly reduced.
- To avoid large displacement due to the all-free girder supports, harp pattern arrangement of the cable was adopted. In addition, harp pattern is considered to be aesthetically favorable due to no visual criss-crossing of the cables when viewed from the sides.
- To prevent failure of the towers due to excessive displacement by exceptionally large earthquake ground motion, vane-type oil damper has been developed and installed between the main girder and the end piers.
- The logarithmic decrement of the tower was determined to be 0.03 and that for the tower with TMD or TLCD was found to be more than 0.10.

5. REFERENCES

1. Toki and Nakase [1986]: "Reliability of Long Period Component of SMAC Accelerograms," *Proc., 7th Japan Earthquake Engineering Symposium*.
2. Kitazawa, Ishizaki, Emi, and Nishimori [1990]: "Characteristics of Earthquake Responses and Aseismic Design on the Long-Period Cable-Stayed Bridge (Higashi-Kobe Bridge) with All Movable Shoes in Longitudinal Direction," *Proc., Japan Society of Civil Engineers*, 422(10).
3. Kitazawa, Noguchi, Nishimori, Izeki [1991]: "Earthquake Resistant Design of a Long Period Structure and Development of Girder Displacement Stopper (Higashi-Kobe Bridge)," *Innovations in Cable-Stayed Bridges*.

PASSIVE SEISMIC CONTROL OF CABLE-STAYED BRIDGES

Hosam-Eddin M. Ali¹ and Ahmed M. Abdel-Ghaffar²

¹ Civil Engineering Department, University of Southern California, Los Angeles, CA 90089-2531, U.S.A.

² Civil Engineering Department, University of Southern California, Los Angeles, CA 90089-2531, U.S.A.

ABSTRACT

Elastomeric and lead-rubber bearings are proposed as a passive control system for cable-stayed bridges. A developed analytical model is used to investigate the effect of the devices on the seismic behavior of such long span bridges. Appropriate locations and properties of the hysteretic-type bearings can achieve significant reduction in seismic forces and relatively better control of displacements.

INTRODUCTION

The increasing popularity and the future trend in constructing cable-stayed bridges with longer center spans make the need for advanced methods of analysis and techniques to suppress vibrations induced by service and environmental loads inevitable. Moreover, the fact that very few bridges have been subjected to strong earthquake shaking makes such need even urgent. Most of the applications in the energy dissipation field are oriented toward buildings with relatively fewer proposals for short and medium span highway bridges. On the other hand, only very few studies [1] have been presented for long span cable-supported bridges in the United States.

The main approach that can be used to reduce the seismic inertial forces of cable-stayed bridges is to isolate the superstructure as much as possible from the ground motion by supporting the bridge deck only by the cables. However, this kind of isolation produces large vibrations in the bridge deck during day-to-day performance. Accordingly special consideration has to be given to the deck connections at abutments and towers.

The objective of this study is to improve the seismic performance of new and existing cable-stayed bridges by using elastomeric and lead-rubber bearings which have not been considered for cable-supported bridges applications. An efficient analytical model is developed for structural components of the bridge and the hysteretic-type energy dissipation devices. The developed model is used to investigate the important parameters that affect the efficiency of lead-rubber bearings as a passive control system.

MODELING OF CABLE-STAYED BRIDGES

The behavior of cable-stayed bridges can be placed in the context of large displacements but small strains. Geometrical nonlinearity originates from: (1) the cables sag which governs the elongation of cables and the corresponding axial tension, (2) the action of compressive loads, due to the inclination of cables, on the bridge deck and towers in terms of their interaction with bending moments, and (3) the effect of the relatively large deflection of the structure on stresses and forces. The material nonlinearity depends on the type of materials (steel or concrete) used in construction. However, it is usually attempted not to allow plastic deformations for such structures for economical and structural stability reasons.

In this study, the geometrical nonlinear behavior is considered using the Total Lagrangian approach of three-dimensional beam elements for deck and tower modeling and a truss element for cables idealization. By adopting a continuum approach and employing four-node isoparametric elements, the formulation is applicable to structures consisting of straight or curved members.

In order to accurately model the deck, the main girders and the towers of the bridge to obtain the response of each part and section of the structure, very large number of finite elements are required including plate and beam elements. The problem becomes unsolvable within the today-computer capabilities. Instead, the global behavior of different sections along the structure will be dealt with. The details of the local parts of the bridge can then be estimated out of the global behavior. The approach is practically adequate and can provide a reasonable alternative to predict the dynamic properties of cable-supported bridges. Beam elements can therefore be used to idealize the deck and towers without great loss of accuracy.

The formulation of a typical beam element stiffness matrix and load vectors is general and includes the possibility of modeling sections with different cross section shapes as shown in Fig. 1-c. Among the cross sections that can be dealt with are the box sections with multiple vents and cut-off corner sections as well as different combinations of rectangular shape parts such as I-beams and plate sections. It should be mentioned that the cut-off corner sections can be used for towers for wind resistance reasons while the box sections may be used for main girders and towers as well.

The analysis of cables under different configurations and loading conditions is extremely complex. These structures are generally elastic in nature but are highly nonlinear in the geometric sense. Fortunately, in cable-stayed bridges, vibrations of cables are not very large (compared to the size of the structure) and the geometry of the cables is somewhat well defined before the analysis. The use of the general and complicated algorithms will always be correct; however, the use of a more restrictive formulation can be more effective and may also provide more insight into the response prediction. A four-node isoparametric cable element, as shown in Fig. 1-b, is proposed for cables idealization. The element can predict both in plane and out of plane responses. In addition, the cable element takes into consideration the effect of pretension which is one of the features of cable-stayed bridges.

In modeling cable-stayed bridges, cables are connected to the tower beam elements and deck beam elements at an eccentricity from the middle plane of the beam as schematically

shown in Fig. 1-a. Accordingly, end nodes of the cable don't coincide with nodes of beam. The problem becomes more pronounced if one beam is used to model the whole deck where consideration of offset becomes inevitable. In this analysis, the cable nodes are treated as slave nodes where degrees of freedom can be expressed in terms of those at the corresponding master nodes of the beam elements by means of transformation.

During the solution process of equilibrium equations, the internal nodes of both beam and cable elements can be eliminated using a condensation technique. However, the responses can be retrieved at their locations without approximations or loss of accuracy [2].

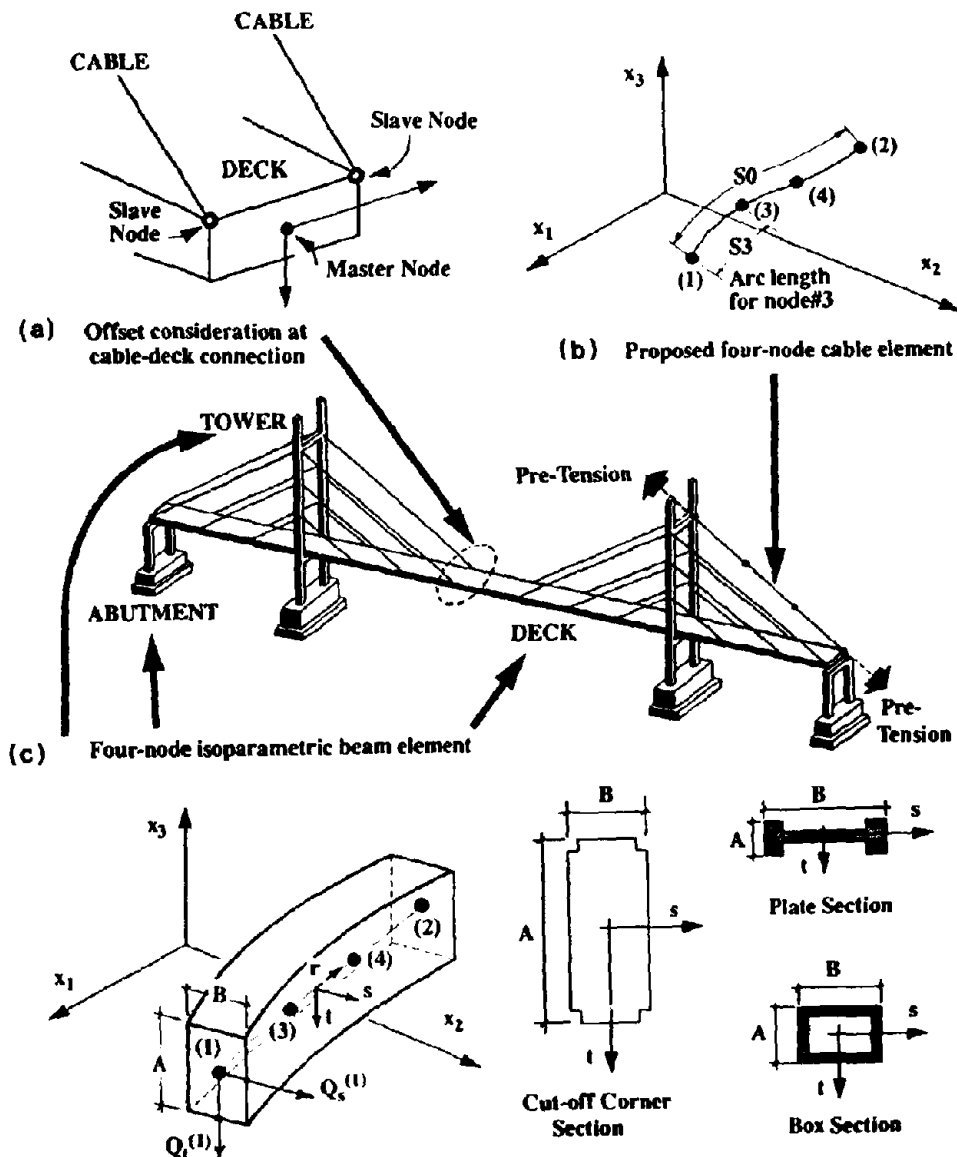


Figure 1: Modeling of cable-stayed bridges

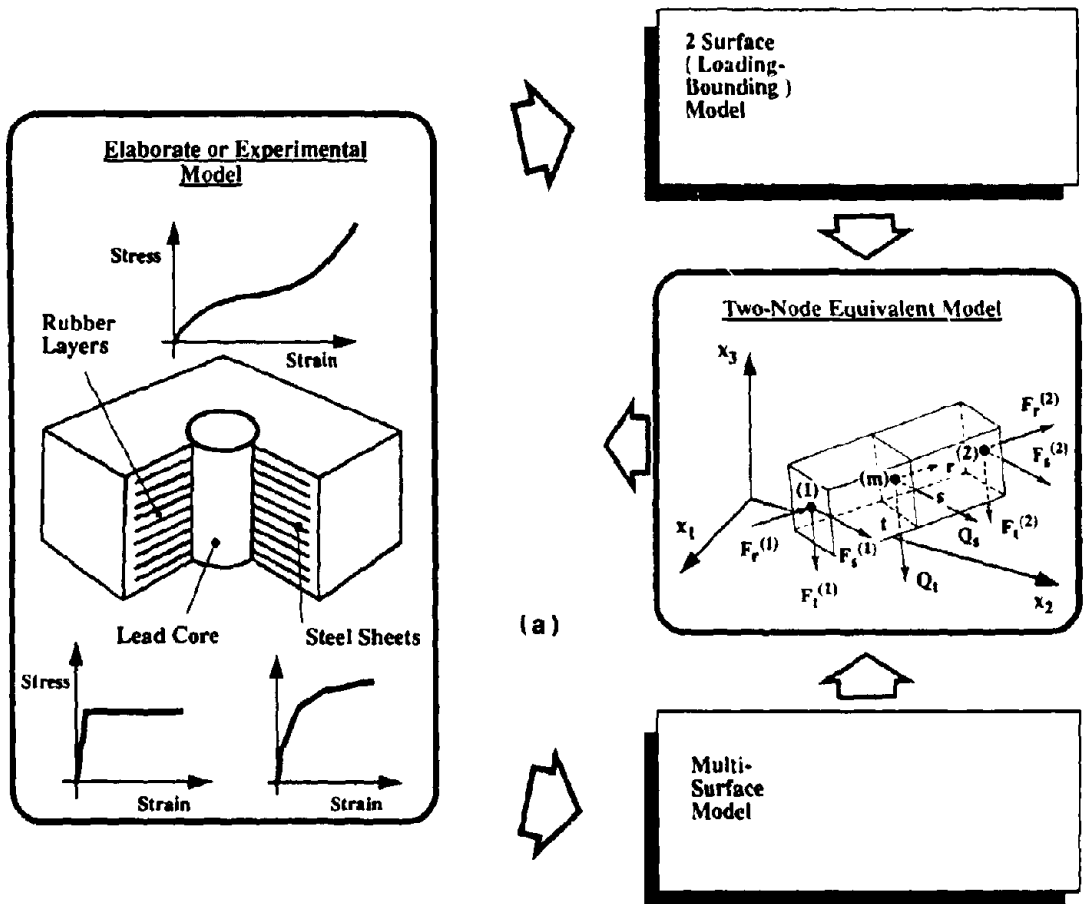
MODELING OF ELASTOMERIC AND LEAD-RUBBER BEARINGS

Elastomeric bearings are widely used as supports for bridge girders of many types. They are also increasingly used as seismic isolation devices. There are quite a few techniques that are used for base-isolation. However, the case of lead-rubber bearings, in which a laminated elastomeric bearing is modified by placing a lead plug down its center, provides a relatively inexpensive and reasonable solution. The bearing carries, in part, the weight of the structure and supplies a horizontal restoring force. The plastic deformation of the lead produces hysteretic damping. Thus, one component provides the stiffness under day-to-day loadings, flexibility under severe earthquake excitations, and damping which are the basic elements required in most base-isolation systems.

Analytical modeling and formulation of the bearing behavior is not an easy task. The device is composed of steel sheets, rubber layers, and the lead plug. Most of the difficulties encountered in modeling the behavior, result from the material nonlinearity of lead and the material, geometric and boundary nonlinearities associated with the rubber parts. In addition, rubber is virtually incompressible during the deformation process which leads to numerical instability in standard linear elastic analysis [3]. Practically, the force-displacement hysteresis loop of elastomeric bearings without a lead plug was broadly assumed elastic with a constant shear stiffness and a small amount of hysteresis. These hysteretic properties provide useful damping for seismic applications, but they are not so well defined as to justify their inclusion in the analysis. Thus, linear elastic analysis is widely acceptable for most bridge elastomeric bearing applications.

In this study, both geometrical and material nonlinearities are considered to model rubber, steel and lead which are the three basic materials in passive devices. For rubber materials, large displacement/large strain finite element model is proposed based on the Total Lagrangian formulation and different strain energy functions that cover wide spectrum of assumptions from restrictive to complicated representation of stress-strain relationship. The incompressibility is handled by using a consistent penalty method in which a solution is efficiently reached by approaching the equilibrium state through a series of decreased compressibility. For steel and lead materials, a loading-bounding stress point plasticity model is developed. Moreover, a multi-yield surface model can be optionally used dependent upon the experimental results of stress-strain relationship. The analytical model is checked against experimental results for lead-rubber bearings where satisfactory agreement is generally obtained [2].

The control and improvement of the vibrations of cable-stayed bridges necessitates the inclusion of energy dissipation devices at certain locations as shown in Fig. 2-b. The problem becomes difficult to solve with the very large number of degrees of freedom associated with accurate modeling for both bearings and bridge components. A simplified model is accordingly proposed for the dissipation devices in which a two-node element is introduced for a stiffness-type approach, as shown in Fig. 2-a. The element is capable of withstanding axial and shear forces. The parameters that control the hysteretic behavior of the element can be estimated out of analytical and/or experimental results. The model has the capability of considering an eccentric installation with regard to the bearing nodes. In order to check the analytical model, the responses of different bearings are compared to experimental results. One of these results is shown in Fig. 3-b.



(b) Tower-deck connection with lead-rubber bearings

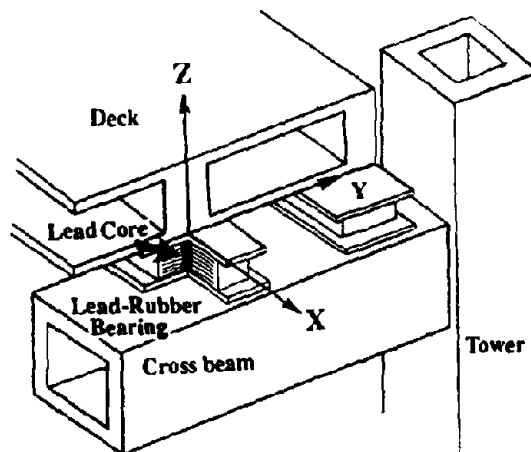
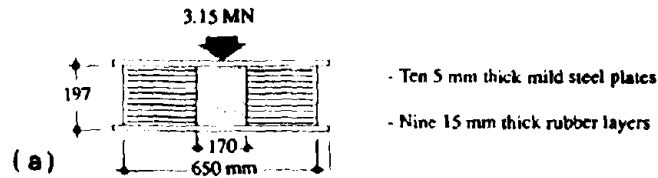
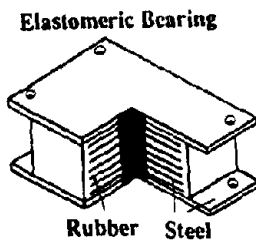


Figure 2: Location and practical model for bearings



(b)

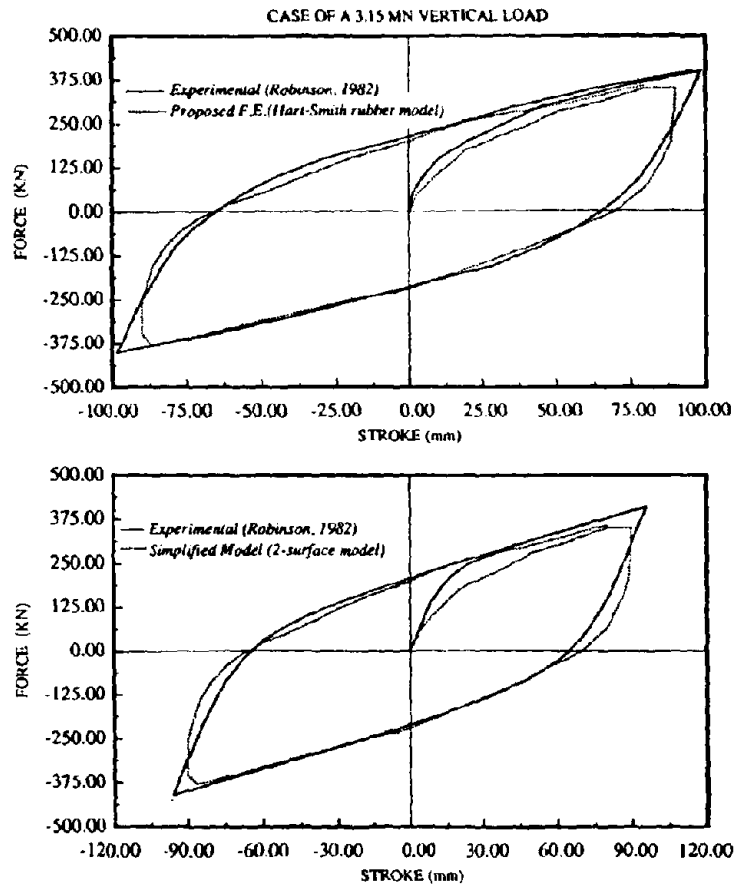


Figure 3: Hysteretic behavior of a lead-rubber bearing

BRIDGE MODEL AND ANALYTICAL PROCEDURE

In order to investigate the sensitivity of cable-stayed bridges response to different parameters of passive control systems, a bridge model is proposed to represent most of the bridge systems and the effective spans. The three-dimensional view of the model is shown in Fig. 4-a. The bridge has a center span length of 1100 ft (330 m), and two side spans of 450 ft (135 m) each. A double plane multi-cable harp system is chosen for the bridge. The finite element nodes and different elements along with the cross sections are shown in the same figure. In the models, cables are anchored to concrete pylons and steel box section-type deck. It can be

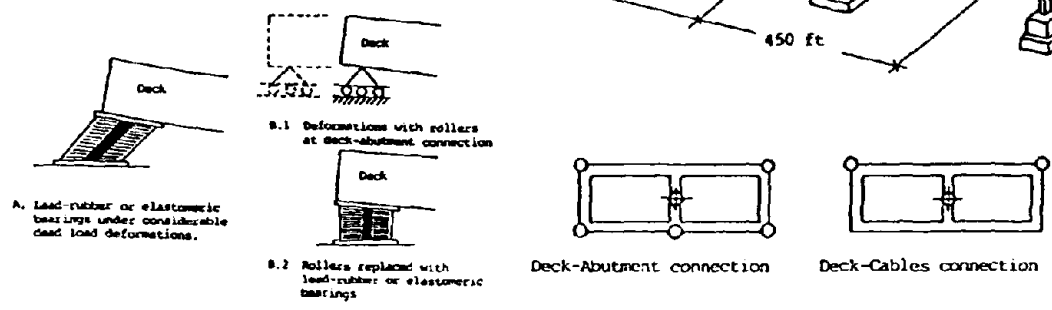
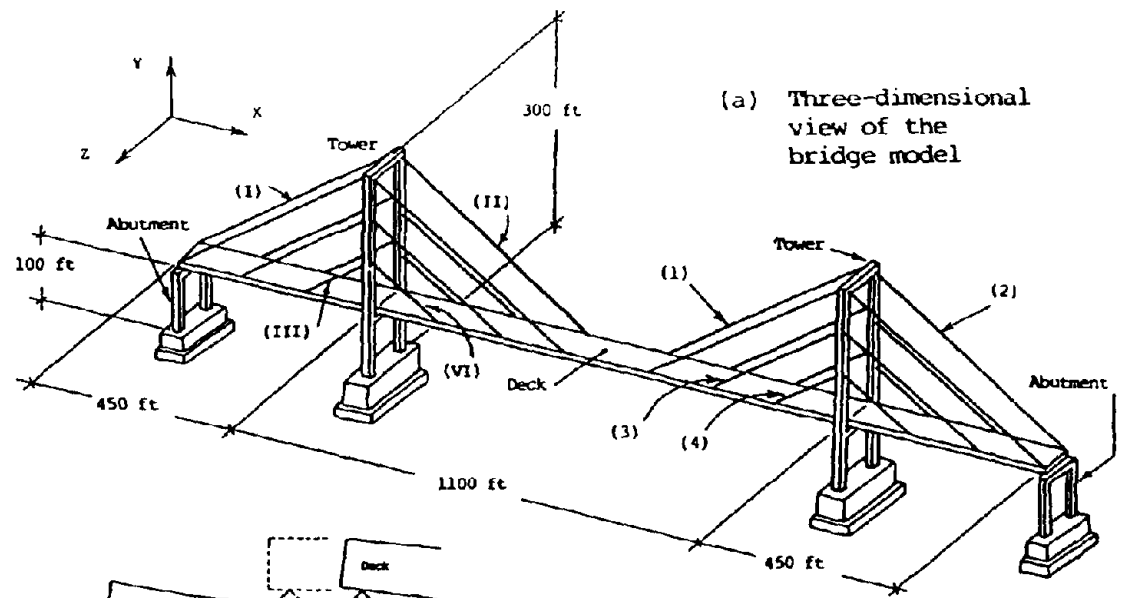
noticed that one beam element is used to idealize the deck accompanied with different slave nodes at various locations along the bridge to take care of the offset associated with cable-deck connections and the eccentric installation of devices with respect to nodes of beams as shown in Fig. 4-b.

In the seismic analyses presented in this study, it is assumed that the bridge starts motion at rest in the dead load deformation position. It is therefore necessary to perform a nonlinear static analysis to compute the tangent stiffness matrix, mass matrix, internal forces, displacements and rotations, and the stress distribution of the bridge structural components. The rationale for the nonlinear static analysis is the fact that cables are pre-taut which significantly affect deflections of the structure and accordingly its dynamic characteristics. In case of lead-rubber bearings, the bearings may undergo considerable shear and compression deformations under the bridge own weight as shown in Fig. 4-c. Excessive deformations of the bearings due to creep, specially in shear, can jeopardize their performance. It is proposed that the bridge be constructed and consequently analyzed with rollers provided at the deck-abutment connections. Once the bridge settles in its dead load deformed shape, bearings can be installed and rollers may then be removed. Some simple construction details have to be provided in order to achieve this task. It may be argued that the structure may suffer more deformations, with the rollers, than elastomeric bearings had they been mounted from the beginning. However, the magnitude and distribution of deformations can be controlled by changing magnitude and distribution of initial tensions in cables.

In the dynamic analysis, the Newmark's constant average acceleration method is used for a 0.01 sec time step. Damping matrix is evaluated considering the Rayleigh approach utilizing the first two eigenvalues with 2% damping ratio. Array no. 6 of Imperial Valley earthquake is used for the ground motion input [2]. Components *S40°E*, *S50°W* and *DOWN* are used for longitudinal, lateral and vertical directions respectively. This array is the strongest among the other recorded arrays. Ideally, a number of earthquake records, which cover the range of frequencies and peak values of interest, should be chosen as input. The choice of these records must be based on geological and local soil conditions of different seismic zones and the expected ground motion characteristics. Based on only one earthquake, the results can nevertheless explain the physics of the problem and evaluate the different parameters that are still applicable to different excitations as well.

LOCATION OF LEAD-RUBBER BEARINGS

The structural synthesis of cable-supported bridges provides few options for mounting the passive control devices. The deck-abutment and deck-tower connections are among the few practical locations for such installation. The option becomes however whether to have all the devices at one connection-type location or to rather distribute them. One more possibility of installing the devices would be at tower-pier connection. However, the construction pattern, stability behavior and bearings performance at this location are practically questionable. This case is therefore not considered in this study.



(c) Precautions during construction

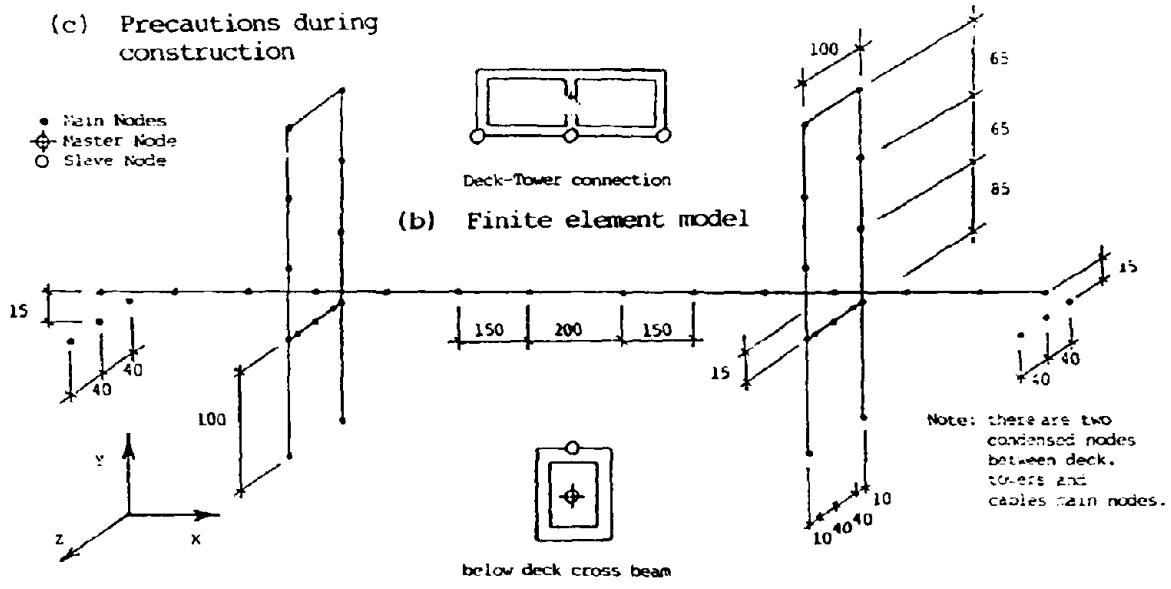


Figure 4: Bridge model and suggested construction procedure for bearings

The seismic energy dissipation capability of an isolation unit depends on the force required to have the device behave in the plastic range. In case of lead-rubber bearings, the process becomes related to the yielding of the lead plugs. Accordingly and in a very simplified way, given the total shear force required to yield all lead plugs at the abutment and the tower combined, V_{all} , and the lead yield stress ($10 - 10.5 \text{ MPa}$), the total area of the lead plugs can be obtained. The shear force required to yield the lead plugs located in bearings at the deck-tower is termed V_{dt} . The ratio of the area of the lead plugs located at the deck-tower connection to the total lead area, (V_{dt}/V_{all}) may vary between zero and one. A ratio of zero represents the case when all the lead plugs are located at the deck-abutment connection only, while a ratio of one represents the case when all the lead plugs are located at the tower-deck connection only. By varying the ratio (V_{dt}/V_{all}) between zero and one, the effect of the location of the lead-rubber bearings on the response of cable-stayed bridges can be investigated in order to identify the most suitable location of the hysteretic-type units.

In order to have a clear picture of the location parameter, different structural properties and non-related parameters of bearings should be kept unchanged. In the analysis, the yield strength of all isolation units is taken equal to 5% of the deck weight, W . For each lead-rubber bearing, the ratio of the initial stiffness to the plastic stiffness is taken equal to ten. For each case of the location parameter, the response of different quantities is normalized to the corresponding response for the non-isolated bridge as shown in Fig. 5. Another parameter of interest is the idealization of the hysteretic loop. Shown in the same figures are the results for two different idealization cases. In the first case, the force-displacement curve for each device element is represented by a two surface (loading-bounding) model. For the second idealization, a bi-linear force-displacement curve is adopted.

The introduction of energy dissipators significantly reduces the earthquake induced forces as compared to the non-isolated bridge case. However, displacements generally increase but with slower rates. Installing lead-rubber bearings only at the abutments reduces dramatically the forces in towers compared with the case of introducing all lead plugs at the towers only associated with relatively slight increase in the displacements of the towers. The deck displacements are least if all hysteretic-type devices are not concentrated at the towers only. More forces are noticed at the abutment side of the deck as well when all lead plugs are placed at the abutments while forces in sections of the deck near the mid-span decrease.

The difference in the bridge performance for different idealizations of the bearing hysteretic response, as shown in Fig. 5, illustrates the importance of the careful and accurate prediction and representation of the bearings behavior. The results obtained in this section can provide a solution for existing towers, piers and abutments with inadequate strength. Installing energy dissipators at the abutment, for instance, attracts more forces to the abutment rather than to the towers and piers which provides an alternative way to strengthening towers and their foundation. The supporting structures along with the approach spans (which is referred to as abutment side) may be, for some existing bridges, among areas most vulnerable to earthquake induced damage. Appropriate choice of location of hysteretic-type devices can create new avenues for seismic response control of these parts.

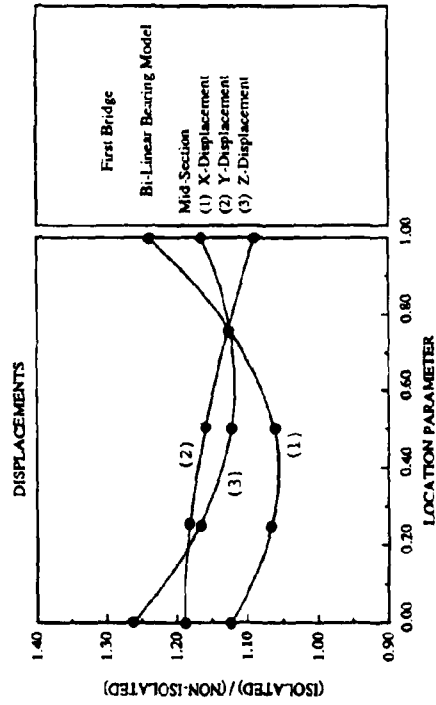
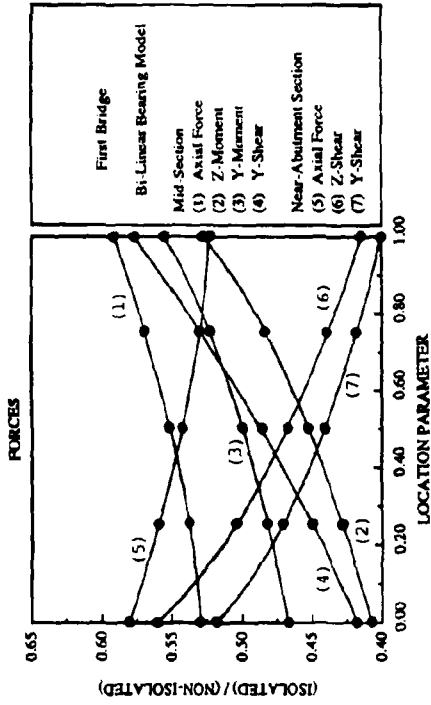
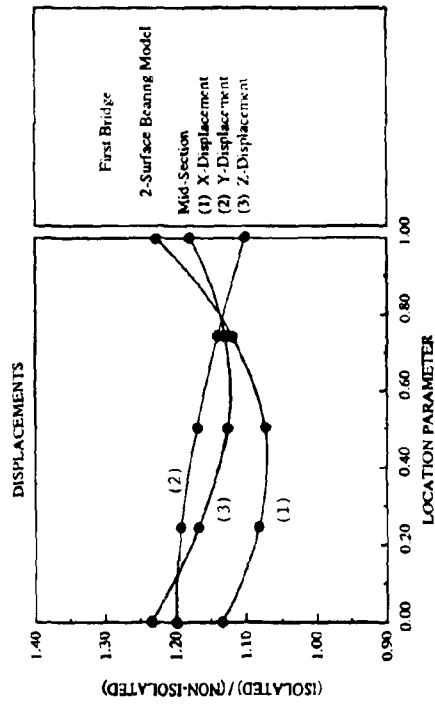
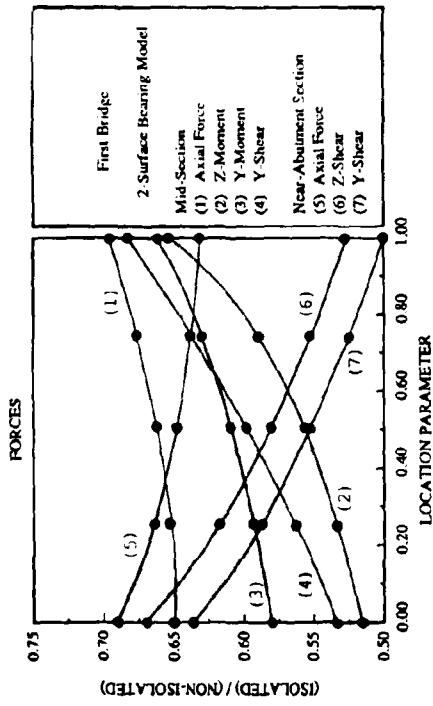


Figure 5: Effect of location of lead-rubber bearings on deck and towers

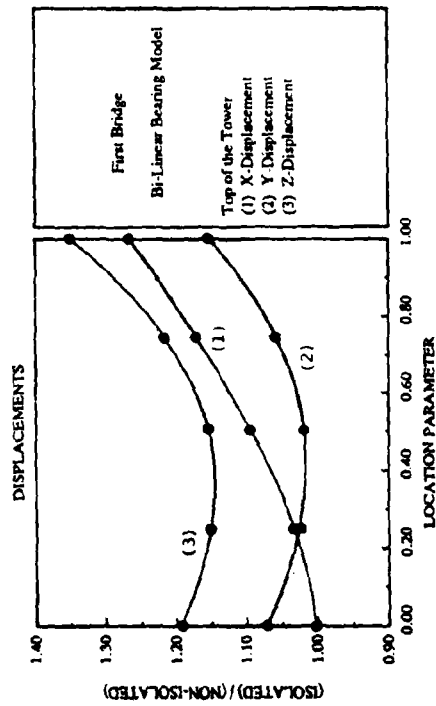
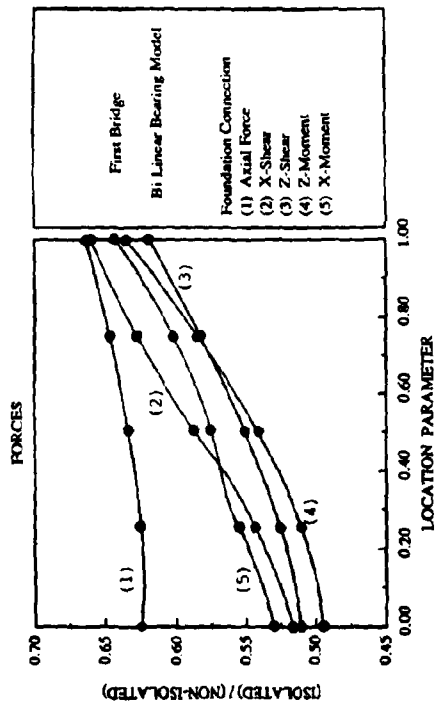
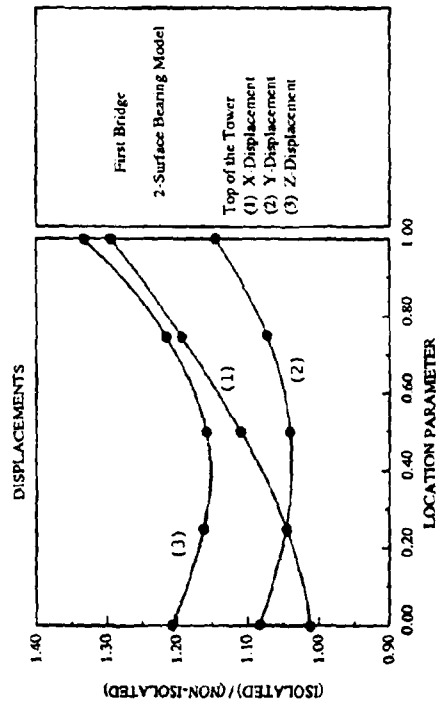
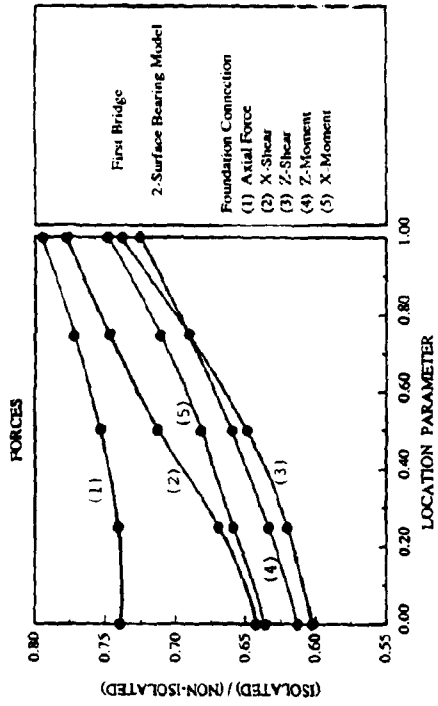


Fig. 5 continued

SHEAR STRENGTH OF LEAD PLUGS

The shear force at which plastic behavior of hysteretic-type units becomes predominant is an important parameter in the design philosophy of energy dissipators. In the case of lead-rubber bearings, given the shear force level and the lead yielding strength, the number and cross sectional area of the lead plugs can be approximately designed. The level of the devices shear strength depends on the mechanism by which all lateral loads, including those arising from sources other than earthquakes, are resisted [5]. Such shear force level should be selected to achieve two objectives. First, the device is required to be stiff under the action of wind, traffic forces, and small earthquakes. Second, during severe seismic events where forces exceed the design shear strength, the level of forces and displacements of the structure are required to remain within acceptable limits to ensure that the bridge continues to function satisfactorily.

The response for different cases with varying yield shear force of lead dissipators are investigated. Various ratios of shear strength of combined devices at the abutment and the tower, V_{all} , to the weight of deck, W , up to 15% were considered in the numerical analysis. The results are normalized to those of the non-isolated bridge. One case of the energy dissipation devices locations are attempted where all lead plugs are inserted in the bearings located at the abutment. The different bridge response quantities are shown in Fig. 6.

The main advantage of lead plugs, as devices that provide a force limiting mechanism for the supporting structure, is quite clear in Fig. 6. The effect of dissipators may be regarded as similar to that of extra equivalent viscous damping. It can be seen that incorporating higher ratios of yield strength at the abutments reduces significantly the forces in the tower and the displacements of the deck and towers but increase the forces on the abutment (for the considered location parameter).

The choice of the shear strength of the isolation system should achieve relatively a good balance between magnitude of forces along the bridge and control of deck and tower vibrations. In small to medium span highway bridges, a lead yield force of about 5% of the superstructure weight, seems to be an optimum value for bridge design applications [4]. In long-span cable-stayed bridges, a comprehensive statistical study is needed for analytical and experimental results using different ground motion time histories. The analysis presented herein suggests a ratio of 8 – 9%. Insignificant change in response quantities can be noticed for higher ratios. Moreover, higher ratios may create problems for the required sizes of lead plugs that can be accommodated in elastomeric bearings.

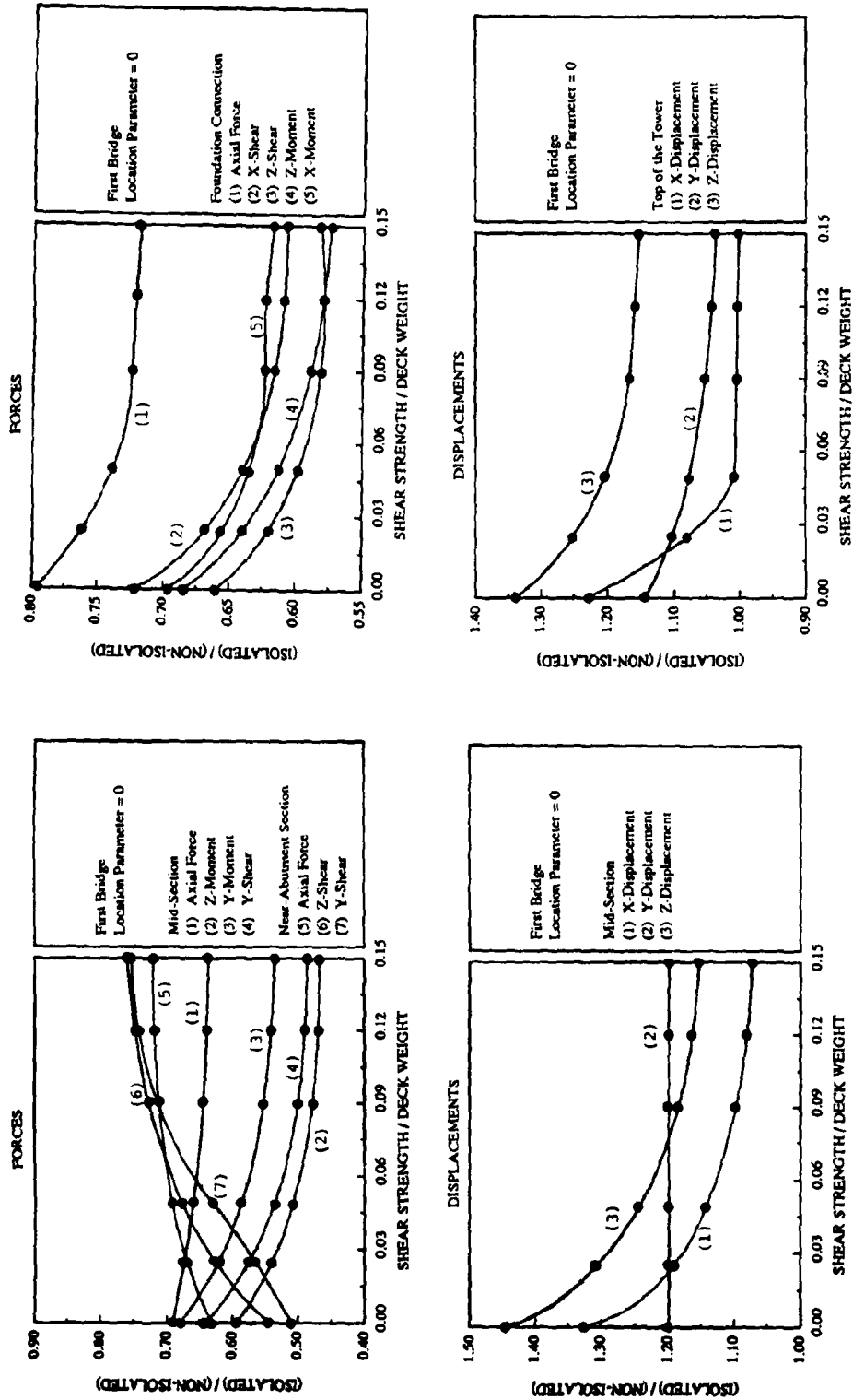


Figure 6: Effect of shear strength of lead plugs on deck and towers

CONCLUSIONS

The use of passive energy dissipation devices offers a potential advantage for the design of earthquake resistant bridges. Generally, the magnitude and distribution of forces for the bridge structural components can be controlled by proper choice of properties and locations of the devices. However, an increase in displacements is to be expected.

The effect of lead inserts in lead-rubber bearings can be regarded as similar to providing extra equivalent viscous damping. A bi-linear representation of the lead-rubber hysteretic loop may overestimate the effectiveness of the bearing. An accurate modeling of the force-displacement relationship based on either experimental or analytical procedure is therefore essential for reliable prediction of the structural performance.

The yield strength of the hysteretic-type devices can be conveniently expressed as a ratio of the superstructure's weight. A ratio of 8 – 9% can be recommended as a practical value. Higher percentages don't help improve the performance significantly.

The distribution of forces transmitted to the towers, deck girders and cables depends on the location of hysteretic-type devices. Incorporation of lead plugs, as energy dissipating devices in the lead-rubber bearings, at the abutments rather than at the towers, for instance, reduces the seismic forces generated in the towers and consequently on the foundations. Displacements can be controlled if hysteretic-type devices are not fully concentrated at the deck-tower connections. The appropriate choice of the location of energy dissipation devices can create new avenues for retrofitting inadequate supporting parts of the bridge.

REFERENCES

1. Abdel-Ghaffar, A.M. and Ali, H.M. (1991), Energy Dissipation Devices for Cable-Stayed Bridges, Proceedings of the second Workshop on Bridge Engineering Research in Progress, pp. 221-224, Reno, Nevada.
2. Ali, H.M. (1991), Nonlinear Seismic Analysis of Cable-Stayed Bridges with Passive Energy Dissipation Devices, Ph.D. Dissertation, Department of Civil Engineering, University of Southern California, Los Angeles.
3. Chang, H. (1988), Nonlinear Elastomer Analysis - Survey of Computer Codes and Case Study for Caliper Seal, Computers and Structures, Vol. 30, No. 5, pp. 1165-1173.
4. Ghobarah, A., and Ali, H.M. (1990), Seismic Design of Base-Isolated Bridges Utilizing Lead-Rubber Bearings, Canadian Journal of Civil Engineering, Vol. 17, No. 3, pp. 413-422.
5. Mayes, R.L., Jones, L.R., Kelly, T.E., and Button, M.R. (1984), Base Isolation Concepts for Seismic Bridge Retrofit, Proceeding of a symposium sponsored by the Technical Council of Lifeline Earthquake Engineering of the ASCE, San Francisco, California.
6. Robinson, W.H. and Tucker, A.G. (1981), The Results of Lead-Rubber Bearings for W.M. Clayton Building, Toe Toe Bridge and Waiotukupuna Bridge, Bulletin of the New Zealand National Society for Earthquake Engineering, Vol. 14, No. 1, pp. 21-33.

SEISMIC RESPONSE OF MULTI-SPAN CONTINUOUS BRIDGE WITH DECK LENGTH OF 1 KM

Yozo GOTO¹, Masahiro TOKUNAGA², Takashi YOSIMURA³
and Masamichi SINTAKU³

¹Technical Research Institute, Obayashi Corporation, Kiyose-shi, Tokyo, Japan
²Information System Center, Obayashi Corporation, Chiyoda-ku, Tokyo, Japan
³Osaka Research Institute, Shimizu Corporation, Minato-ku, Tokyo, Japan

SUMMARY

Earthquake response characteristics of a Menshin designed 1 kilometer multi-span continuous bridge were analyzed by time history response calculations. An analysis was performed of the response under the input of a seismic wave occurring with a phase delay from one end of a 1 kilometer continuous bridge to the other, as well as occurring without a phase delay. As a result, only the girder response section force and the girder end component response acceleration and displacement in the lateral direction to the bridge axis were found to increase from the phase delay effect. Conversely, the girder response acceleration and displacement in the direction of the bridge axis were found to decrease substantially. As the increases mentioned above are not important in engineering point of view, it became evident that the application of the Menshin design in multi-span continuous bridges is advantageous.

INTRODUCTION

The expansion joints built into highway bridges not only adversely affect the stability of running automobiles, but also harm the surrounding environment by causing noise and vibration. Moreover, frequent breakage requires constant repair work, and this repair work causes traffic jams from stopped traffic, leading to a desire in highway technology that reduces the number of expansion joints from bridges in Japanese cities. In order to make girders without expansion joints in multi-span continuous bridges, a structure is necessary that supports the girder while it expands or shrinks in the direction of the girder axis caused by temperature changes as well as concrete shrinkage and creep. Previously, multi-span continuous bridges with support structures such as slip bearings, roller bearings with damper stopper and elastomeric bearings as well as flexible columns have been constructed in Japan, and the longest continuous girder length attained was an extension of 600 meters.

On the other hand, supporting the girder with a Menshin bearing with small stiffness in a lateral direction to realize the Menshin design also enables the passing on of the expansion of the girder from temperature changes and other factors. So the adoption of the Menshin design enables multi-span continuation at the same time. This is a clear example of the proverb "killing two birds with one stone."

Based on this concept, a research has been conducted to investigate the increase in earthquake safety from the adoption of the Menshin design together with the possibility of actually developing a multi-span continuous bridge with a continuous girder length in excess of 1 kilometer. As little previous research has been conducted in Japan, one objective of the research is to clarify what kind of response characteristics the extremely long continuous girder supported by the Menshin bearing has and how it will respond during an earthquake. This report presents the results of an analysis of the seismic response of the multi-span Menshin bridge with continuous girders of 1 kilometer in length by time history response calculations of multi-point inputs taking into account the phase delay of the input seismic waves.

BRIDGE CONFIGURATION

Analyses were performed concerning a steel girder bridge and a prestressed concrete girder bridge. The rough drawings of the bridges are presented in Figures 1 and 2, respectively. Using existing bridges as prototypes, the continuous span number has increased. The steel girder bridge has 16 spans and the prestressed concrete girder bridge possess 26 spans, both of which have an extension of 1 kilometer. The foundation, consisting of substructures which are all made of reinforced concrete bridge piers, is supported by cast in place concrete piles. The surface subsoil layer with a shear wave velocity of 172m/sec has a thickness of 22m and is on the bed rock. This type of ground condition is classified as Group 2, i.e. stiff ground, by the Japanese "Design Specifications for Highway Bridges (Ref. 1)."

Table 1 shows the specifications of the Menshin bearing as determined by the Menshin design. In order to reduce the stress arising from girder expansion due to temperature changes and concrete shrinkage, a lead laminated rubber bearing is used considering its small stiffness under low-velocity load.

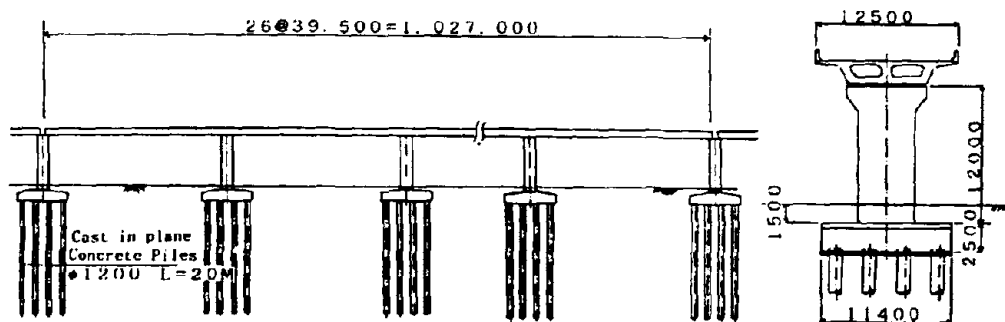


Fig. 1 Multi-Span Bridge with 1 kilometer
Continuous Prestressed Concrete Girder

METHOD OF ANALYSIS

Input Earthquake Motion Seismic calculations for common buildings and bridges have generally been performed assuming that unified seismic waves are input simultaneously to their substructures. Up until now, this assumption has been accepted in light of observed phenomena and to simplify analyses, but this assumption cannot be applied to our research in which structures with an extension in excess of 1 kilometer are studied. As is well known, there is seismic wave scattering from soil irregular lineament and local nonhomogeneity, differences in propagation routes, and surface wave propagations. For these reasons, it is thought that it is sufficient to input different seismic waves to each bridge pier.

On the other hand, the correlation and disparity of point-to-point earthquake motion is still a topic of research, and both a theoretical expression method and a design evaluation method have yet to be established. In particular, there are an infinite number of reasons for making the time history wave form different at each bridge pier. Therefore, in this analysis, the point-to-point difference among seismic waves is assumed to come from only the idealized occurrence of wave propagation and it is thought that the unified seismic wave having a phase delay from the idealized wave propagation in the direction of the bridge axis input to each bridge pier.

There are three kinds of phase delay in the seismic wave considered at the time of the analysis : 0.002sec/m, 0.001sec/m and without phase delay. As the phase delay increases, in other words, the propagation velocity slows down, the strain occurring in the horizontal direction of ground becomes large and the time delay of earthquake motion input to adjoining bridge piers increases. A ground strain in the horizontal direction calculated from observed earthquake waves of around 2×10^{-4} has been reported at a point with an observed acceleration of approximately 120 gal. Even during a strong earthquake, as long as the ground is not very soft and is not destroyed, it is thought that the horizontal strain on the inner surface of the ground will be limited to the order of 10^{-4} . The maximum horizontal strain values in the hypothesized ground conditions of this analysis at phase delays of 0.002sec/m and 0.001sec/m are 3.6×10^{-4} and 1.8×10^{-4} , respectively.

The wave form and power spectrum of the input seismic wave are shown in Figure 3. The response spectrum of the wave at 5% damping is regulated to fit the standard response spectrum for dynamic analysis for Group 2 on Ground Condition as outlined in the "Design Specifications for Highway Bridges (Ref. 1)." Furthermore, in order to perform an analysis according to phase delay input, response calculations based on the absolute coordinate system, not the relative coordinate system, are necessary requiring an input wave expressed at displacement. Since the drift of the obtained displacement wave form from the integration of the input acceleration wave becomes a problem, a careful zero line modification of the previous acceleration wave was carried out.

Modeling for Response Analysis As Figure 4 shows their concept, all bridge spans are modeled into the continuous spring-mass system establishing two kinds of two-dimensional models consisting of an in plane response model and an out of plane response model. When the seismic force action is in the direction of the bridge axis, the in plane response model is used, and when it is in a direction lateral to the bridge axis, then the out of plane model is used. Total degrees of freedom of the analysis models are

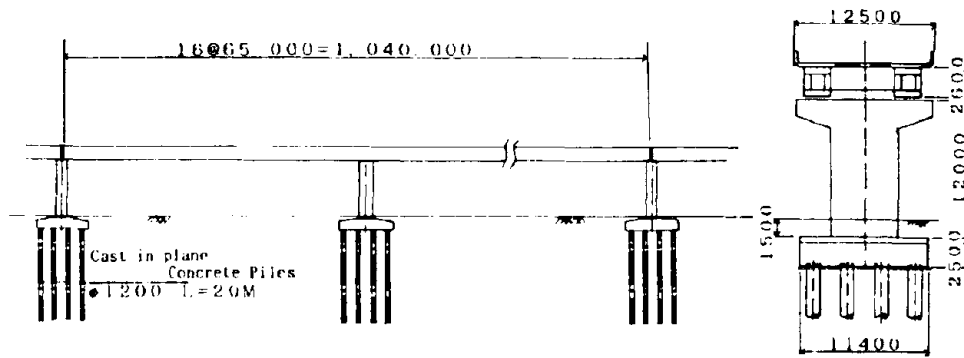


Fig. 2 Multi-Span Bridge with 1 kilometer Continuous Steel Girder

Table 1 Dimension of Menshin Bearing (LRB)

Pier No.	P.C.Girder Bridge		Steel Girder Bridge		
	P1, P27	P2~P26	P1, P17	P2~P5 P13~P16	P6~P12
Dead Load (tf/Bearing)	220.	525.	212.	519.	519.
Plane Dimension (cm)	90×90	100×100	85×85	110×110	105×105
Total Thickness of Rubber (cm)	24.	42.	22.	49.	46.
Dimension of Load (cm)	φ20×1	φ19×4	φ20×1	φ19×4	φ19×4
Yield Strength (tf)	23.5	84.	24.5	88.5	88.5
Stiffness for Low Velocity Loading (tf/m)	294.	286.	280.	300.	300.
Initial Stiffness (tf/m)	2630.	2770.	2500.	2600.	2630.
* Effective Stiffness (tf/m)	650.	1300.	617.	1230.	1230.
* Effective Damping Ratio	0.21	0.27	0.21	0.27	0.27

*Effective for Level-1 Input Earthquake (Standard design level)

shown in Table 2. In addition, the details of modeling the bridge pier components are shown in Figure 5.

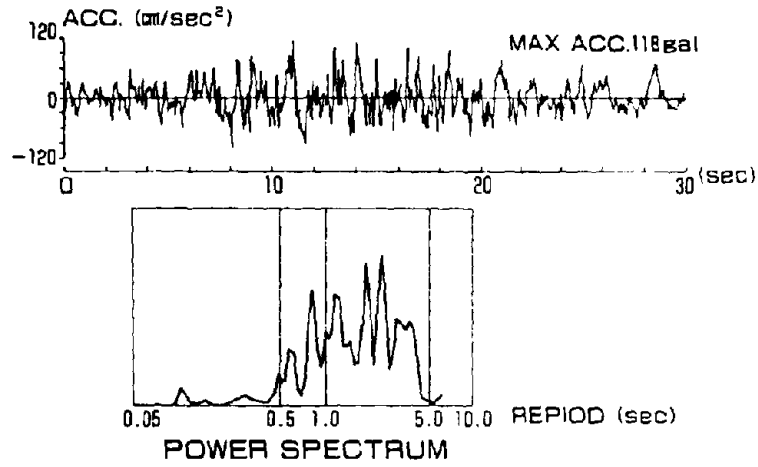


Fig. 3 Input Seismic Wave

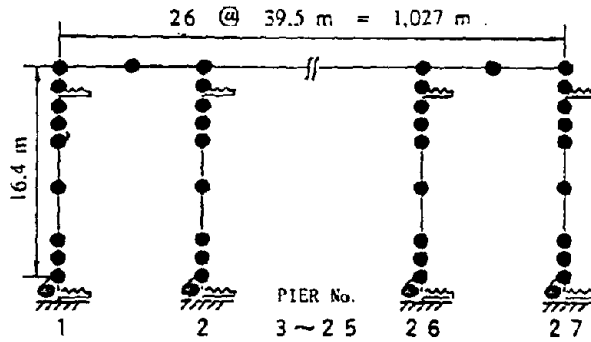


Fig. 4 Concept of Total Spring-Mass System

Table-2 Numbers of Degrees of Freedom

	In Plane Model	Out of Plane Model
P.C. Girder Bridge	484	304
Steel Girder Bridge	779	489

The Menshin device was converted into a model using a visco-elastic spring equivalent to the hysteresis characteristic. The effect of interaction between ground and bridge pier foundation was taken into a model by attaching an equivalent visco-elastic spring to the footing. Since damping is different in each structural component, it is expressed as viscous damping proportional to the stiffness of each component. Table 3 and Table 4 show the main property of material values used in the models.

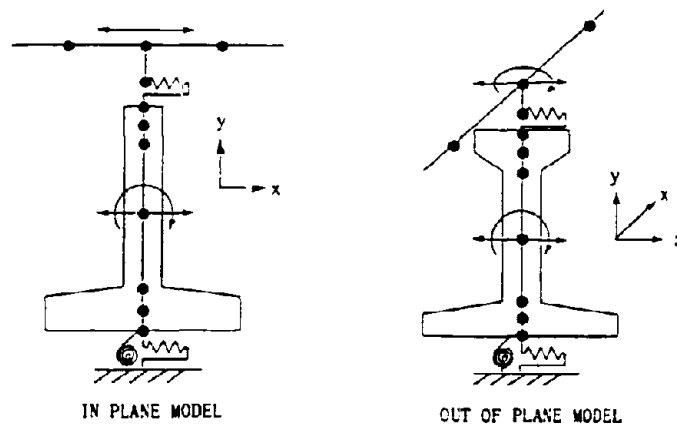


Fig. 5 Concept of Modeling the Pier Components

Table 3 Constants for Girder and Pier

		P. C. Girder Bridge		Steel Girder Bridge		
		Girder	Pier	Girder	Pier	
					P1, P17	P2~P16
Young's modulus (tf/m ²)		3.1×10 ⁶	2.5×10 ⁶	2.1×10 ⁷	2.5×10 ⁶	
Moment of inertia of section (m ⁴)	In plane	3.69	6.51	0.830	13.50	7.80
	Out of plane	71.99	26.04	10.840	54.00	45.00
Polar moment of inertia (m ⁴)		9.61	17.89	0.435	37.08	22.97
Sectional area (m ²)		7.01	12.50	0.729	18.00	15.00
Damping ratio (m ⁴)		3.	5.	2.	5.	

Table-4 Constants for Foundations





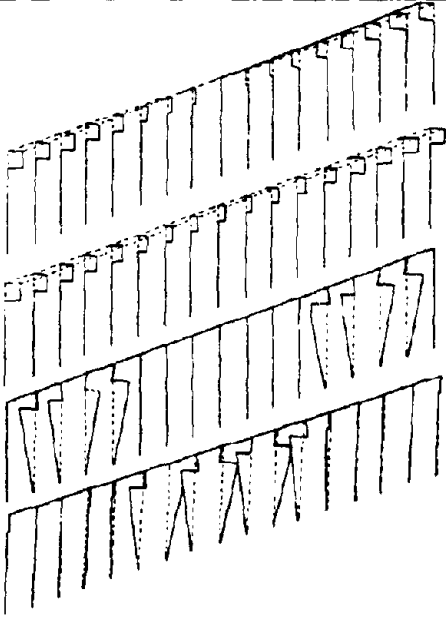
		P. C. Girder Bridge	Steel Girder Bridge	
		P1~P27	P1, P17 P6~P27	P2~P5 P13~P16
Coefficient of subgrade reaction	Sway (t/m)	5.43×10^6	4.67×10^6	5.34×10^6
	Rotation (t·m/rad)	1.15×10^7	1.14×10^7	1.19×10^7
Damping (%)	Sway (t/m)	30.	30.	
	Rotation (t·m/rad)	10.	10.	

RESULTS OF ANALYSES

Natural Periods and Vibration Modes An eigen value analysis was performed in order to grasp the vibration characteristics of the analysis models. From the vibration isolating effect of the Menshin device, a clear division appears between the mode in which the girder components shake greatly and the mode in which the bridge pier components shake greatly. Table 5 shows those results, and in each case there are a primary mode with a natural period of approximately 1.4 seconds to the sway advance mode of the girder and post-secondary several modes in which girder expansion or bending predominantly occur. On the other hand, modes in which bridge piers shake violently comes out as short period, high-degree modes with natural periods of approximately 0.2 seconds.

According to the power spectrum of the input seismic wave shown in Figure 3, the seismic wave possesses a predominant component in the period from 0.8 to 2.5 seconds with a small component in the period less than 0.8 seconds. Therefore, when considered together with the eigen value analysis results, it is supposed that the vibration mode in which the bridge piers shake violently will be virtually absent from earthquake response.

Table-5 Results of the eigen value analysis (Steel girder bridge)

	Mode No.	Period (sec)	Mode shape	Comment
In plane analysis	1	1.377		Sway of girder
	2	0.617		Tension & Compression of girder
	12	0.217		Bending of pier
	15	0.213		Bending of pier
Out of plane analysis	1	1.372		Yawing of girder
	2	1.316		Sway & Bending of girder
	28	0.186		Bending of pier
	33	0.181		Bending of pier

Earthquake Response The following is a report of steel girder bridge response calculation results :

Figures 6 and 7 depict time histories of response acceleration of pier top and girder at representative bridge piers. In addition, Figure 8 shows the distribution of maximum response acceleration. The wave form for the pier top is only slightly amplified, which is almost the same as the input seismic wave form. Owing to the action of Menshin device, the short period component is eliminated from the girder response. When there is no phase delay in the input seismic wave, the response wave forms in directions both along and lateral to the bridge axis are almost the same, but when the phase delay is present, different response tendencies appear depending on the direction.

When there is a phase delay, the response acceleration in the direction of the bridge axis decreases both uniformly and abruptly. This is because the girder responds like a stiff body with a single degree of freedom even when the bridge girder is 1 kilometer long, since the stiffness in this direction is great and it is supported at the Menshin device, so the input seismic forces from each bridge pier cancel each other out due to the phase delay and there is a decrease in the so-called "effective input."

On the other hand, in a direction lateral to the bridge axis, there is little stiffness since the girder is deformed by bending and the girder response on each bridge pier is almost independent. For that reason, even if there is a phase delay in the input seismic wave, a decrease in the response acceleration does not occur. Conversely, when the phase delay is large, the large amplitude of response of a bridge pier (No. 17) at one end attracts attention. This is due to the occurrence of so-called "whipping vibration" in which bending mode wave motion occurs in girder due to seismic wave action with a phase delay along the bridge axis and the wave energy propagated to far end of the girder becomes concentrated, causing a large response.

Figure 9 shows the relative displacement that occurs in the Menshin bearings, and the section force that occurs in the girders and the moment of the pier bases taken from bridge pier numbers on the horizontal axis. The relative displacement that arises in the Menshin device at both ends of the 1 kilometer girder when there is a phase delay in the input seismic wave increases 20% of those when the phase is the same, but is small overall in the intermediate of the 1 kilometer expansion. Girder section force exhibits a greater response when there is a phase delay than when there is not. However, stress arising from axial force and bending moment from the effect of phase delay input is limited to 10% of the allowable stress for girder materials.

Figure 10 shows the analysis results concerning prestressed concrete girder bridges. These results are almost the same both qualitatively as well as quantitatively. The reason is that the weight of prestressed concrete girders is greater than that of steel girder, but its span is shorter and the number of bridge piers is greater, so the superstructure dead load corresponding to one Menshin bearing and one bridge pier becomes almost the same and the bridge vibration characteristics also become the same as a result.

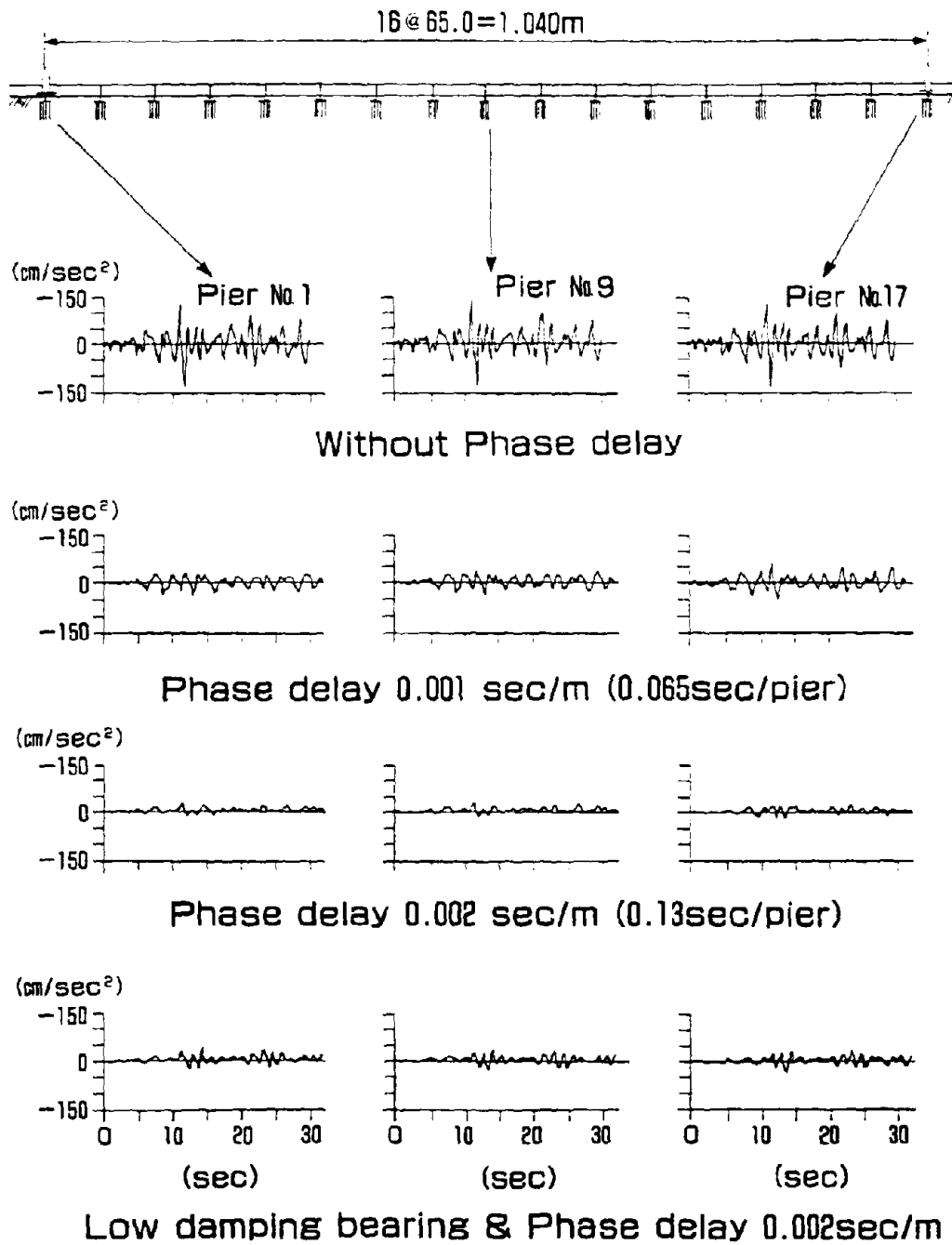


Fig. 6 Response Acceleration Wave Forms (In Plane Response)

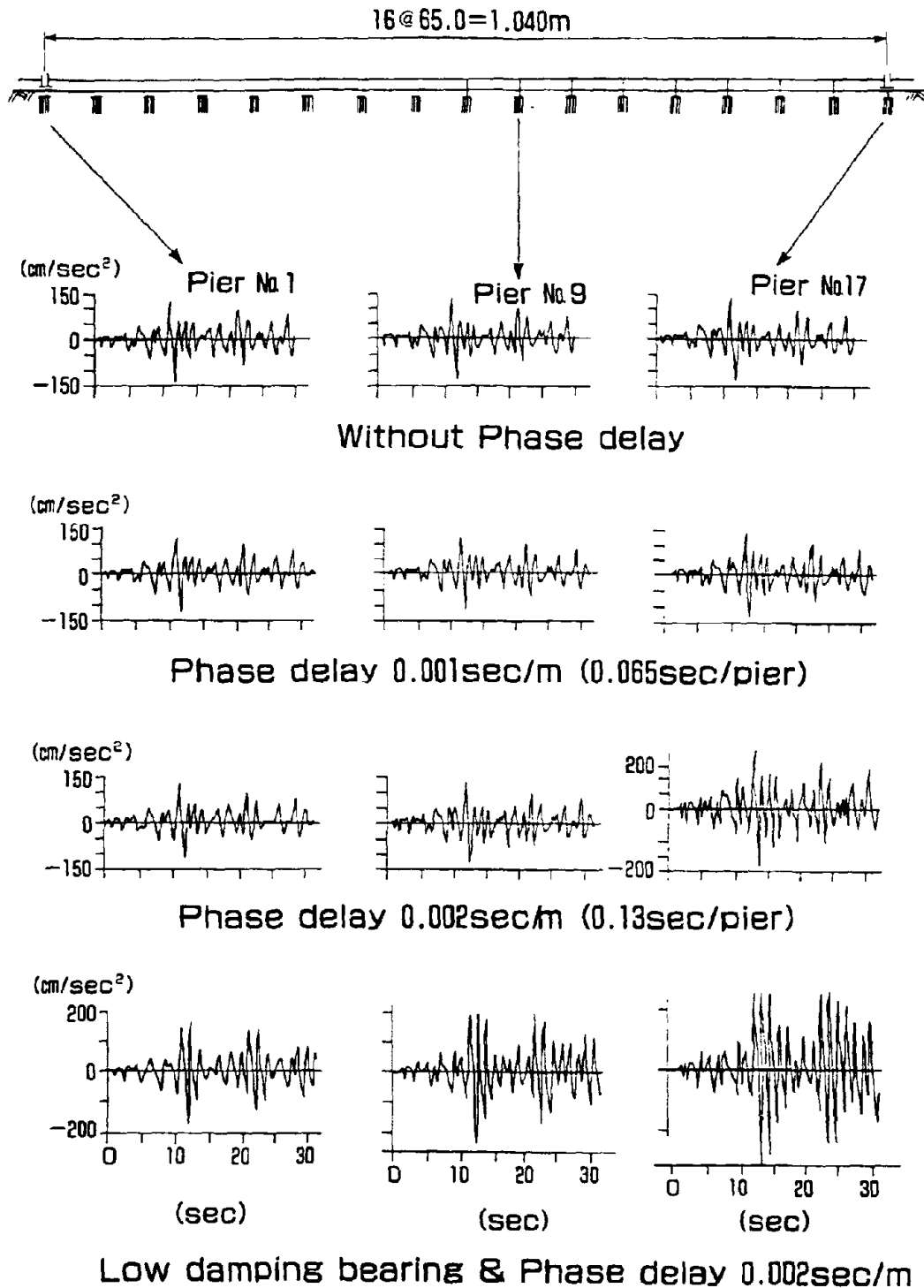


Fig. 7 Response Acceleration Wave Forms (Out of Plane Response)

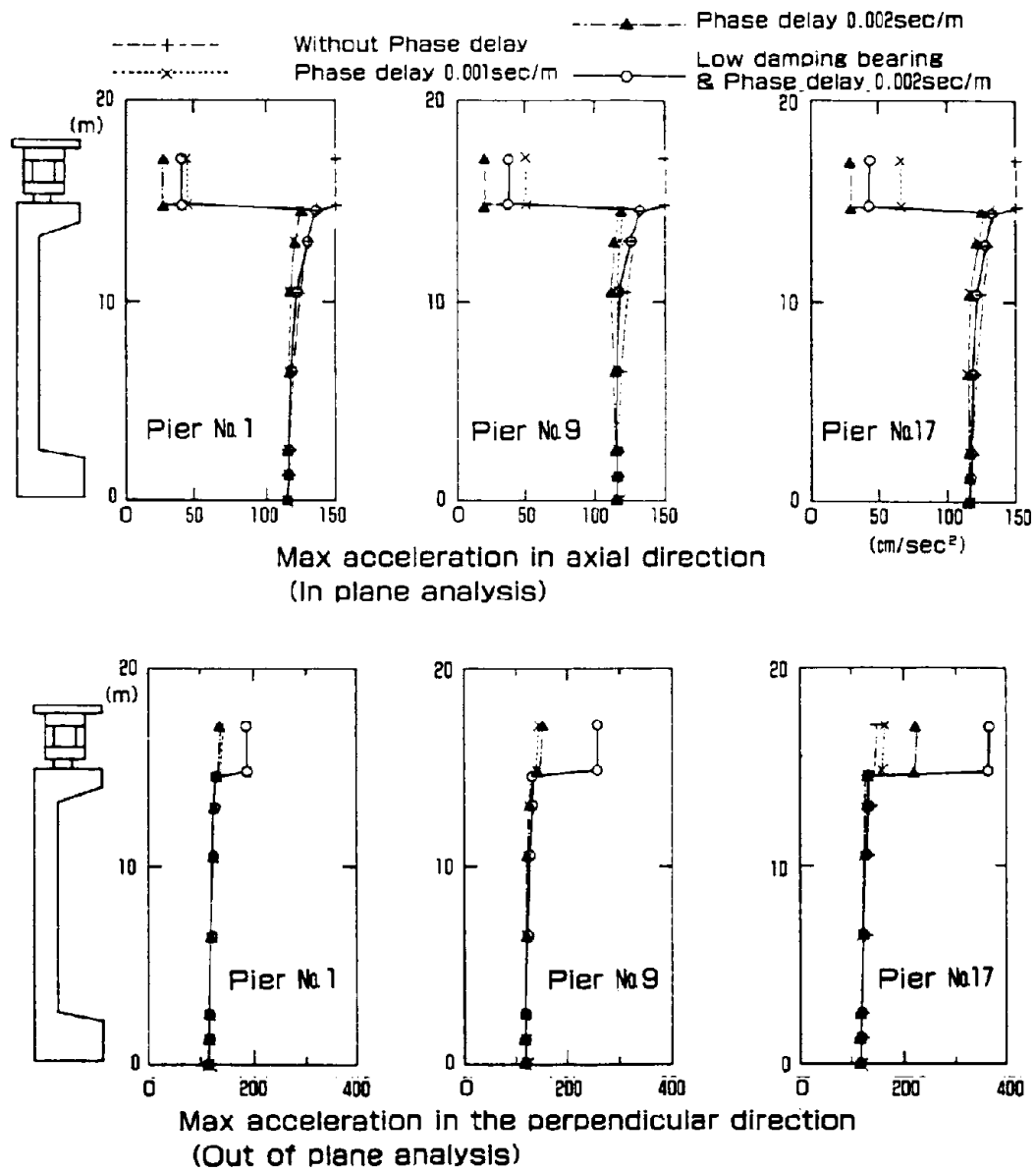


Fig. 8 Distributions of Max. Response Acceleration

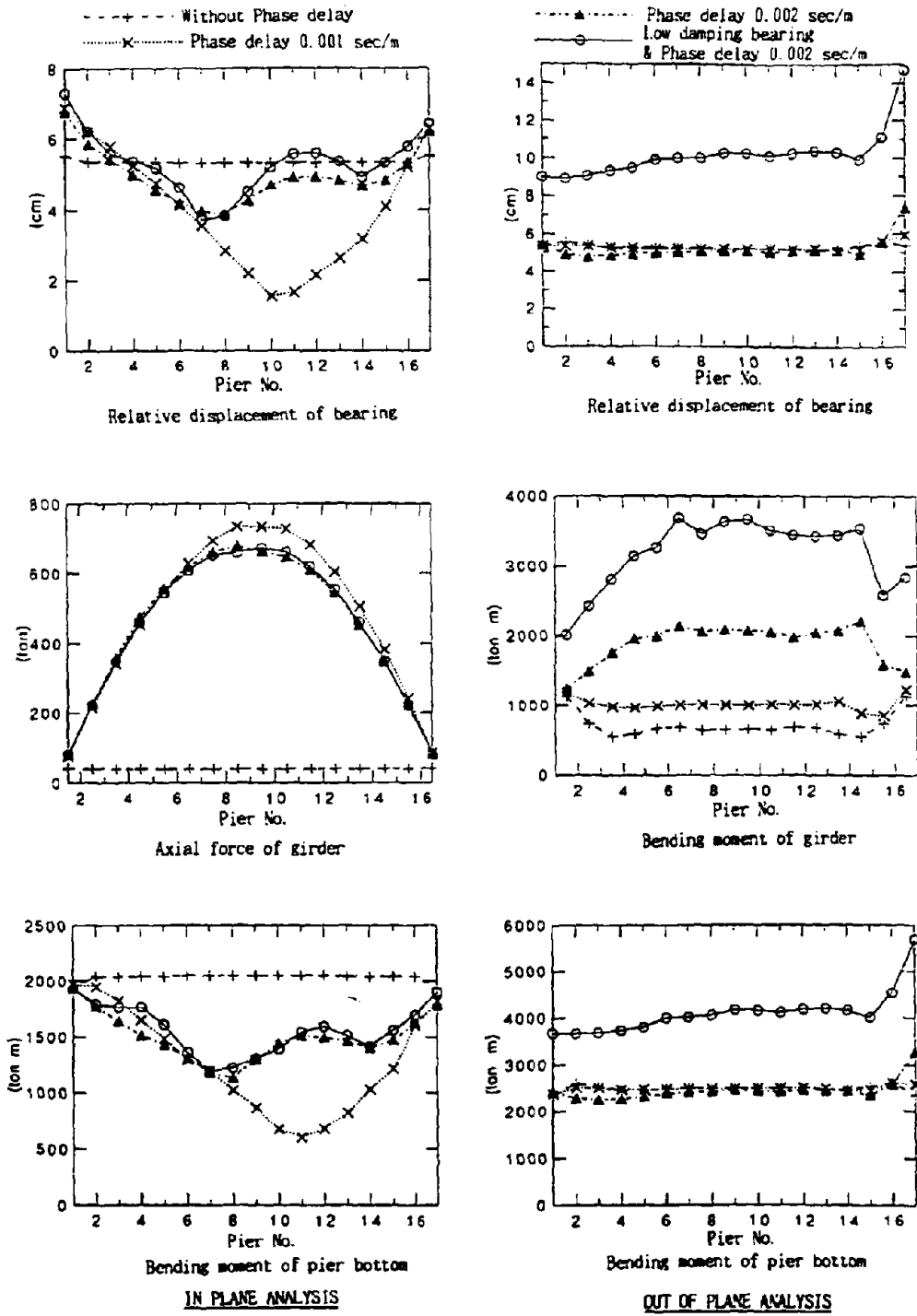


Fig. 9 Max. Response Value Distributions along Bridge Axis (Steel Girder)

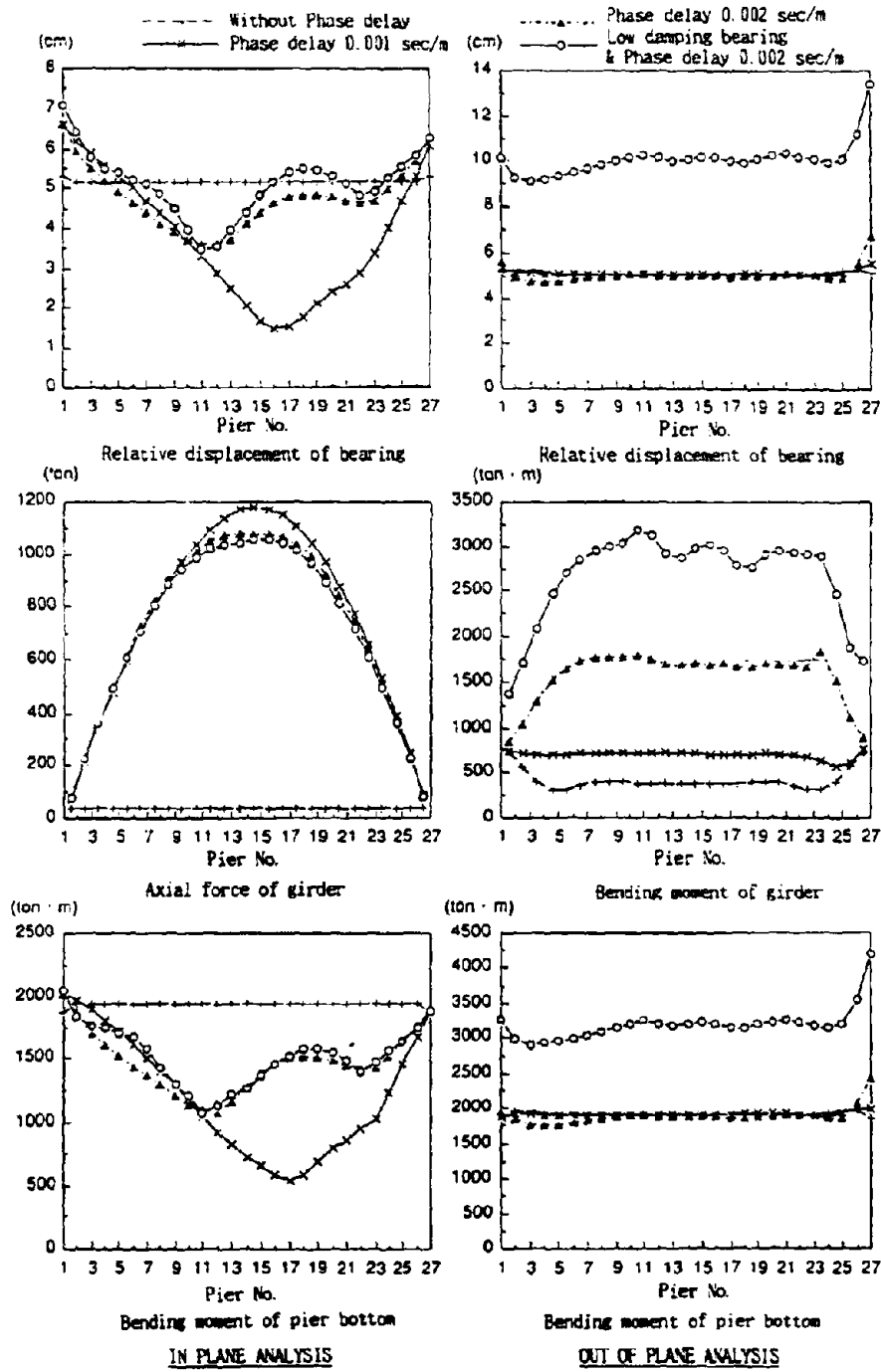


Fig. 10 Max. Response Value Distributions along Bridge Axis (P. C. Girder)

CONCLUSIONS

1. A comparison of prestressed concrete girder bridge with steel girder bridge reveals that the response characteristics of Menshin designed multi-span continuous bridges with 1 kilometer long continuous girders are almost the same for both girder types.
2. A comparison of response in the direction of the bridge axis with those in a direction lateral to it reveals that the effect of the phase delay input appears noticeably in response acceleration and displacement in the axial direction and that these values decrease substantially. This means that the Menshin design can be effectively applied in this direction in multi-span continuous bridges with long girder lengths since the effective input of the earthquake motion on the girders decreases from the phase delay effect.
3. On the other hand, the section force arising in the girders increase from this phase delay input. However, this increase is only 10% of allowable stress.
4. There is a tendency for the response of girders in the direction lateral to the bridge axis to increase at the end section of the 1 kilometer continuous girders. This is thought to arise from the response amplification due to the bending mode wave motion arising in the girder that is propagated in the direction of the girder axis and is reflected at the girder end. This response increase represents an increase of about 30% on most components, but since the improvement of earthquake resistance of bridge piers in the direction lateral to the bridge axis is relatively easy, the problem is solved by slightly strengthening the end bridge piers at the girder ends and bearings on them.
5. Topics for further research concerning multi-span continuous bridges include the response of the bridge having curvilinear axis and the response when the ground conditions change greatly in the direction of the bridge axis. More research of this type is planned for the future.

ACKNOWLEDGEMENT

This study was made as a part of the joint research program on "Development of Menshin Systems of Highway Bridges" between PWRI and 28 private firms in Japan. Grateful acknowledgement is made to Dr. K. Kawashima, Mr. K. Hasegawa, Mr. K. Unjou and Mr. H. Nagashima of PWRI and members from 28 private firms for their valuable discussions on this research.

REFERENCE

1. Japan Road Association : "Design Specifications for Highway Bridges, Part V, Earthquake Resistant Design, 1990" (in Japanese)

APPLICATION OF MENSHPIN DESIGN TO BRIDGES WITH DECK LENGTH OF 1000M

Hiroshi Mashiko¹, Hideo Arai² and Yasuhisa Fujiwara³

^{1, 2, 3}Bridge Design Section, Civil Engineering Department,
SUMITOMO CONSTRUCTION CO., LTD, Shinjuku-ku, Tokyo, Japan

SUMMARY

In recent years, Menshin have been adopted for highway bridges and some of them are already completed in Japan. In this paper, we study application of Menshin design for a multi-span continuous bridge with deck length of 1000 m. As the result of this study, it might be feasible for bridges longer than 1000m to adopte Menshin design.

INTRODUCTION

In Japan, multi-span continuous bridges have been adopted in many cases as viaducts in cities and as highway bridges to reduce unpleasant shocks to drivers and to prevent noise by reducing the number of expansion joints. A multi-point fixing method and a method to distribute the seismic lateral forces in longitudinal direction to each pier by using rubber bearings (hereafter called lateral force distribution method), are increasingly adopted in recent years. Highway bridges with continuous rigid frame are also being employed in mountainous areas. Continuous rigid frame bridges are superior from the point of construction cost and for reducing unpleasant shocks to drivers. As shown in Table 1, there are several bridges of this type with total deck length over 500m in Japan, and construction of this type of bridge is considered to be progressively made.

Based on these facts, applicability of Menshin bearings to approximately 1000m-long multi-span continuous bridges are discussed in this paper. Prestressed concrete bridge is considered for the analysis.

DESIGN REQUIREMENT ON CREEP AND DRYING SHRINKAGE

Although the lateral force distribution method has been adopted, it would have several problems for applying to a highway bridge with total length over 1000m. It is necessary to consider longitudinal elongation of deck due to creep and drying shrinkage for prestressed concrete bridges. The amount of elongation for 1000m bridges is about 300mm for prestressed concrete bridges. Although deck deformation of about $\pm 200\text{mm}$ is developed due to temperature change (design temperature change is $\pm 20^\circ\text{C}$ for prestressed concrete bridge), it is not critical.

Table 1. Multi-Span Continuous Bridges with total length over 500m-long constructed in Japan

Bridge name	Bridge length (m)	Numbers of span	Maximum span length(m)	Bridge type	Super-structure type	Pier type	Average height of piers (m)
Metropolitan Expressway KS-44 Section Bridge	500.0	10	50.0	Continuous girder bridge	Steel box girder	Steel	12.6
Metropolitan Expressway KT-38 Section Bridge	507.5	12	44.0	Continuous girder bridge	Steel box girder	reinforced concrete	11.5
Douou Expressway Ishikarigawa Bridge	543.8	8	74.6	Continuous girder bridge	Prestressed concrete box girder	reinforced concrete	19.3
Tyuou Expressway Okaya-Kouka Bridge	593.0	5	148.0	Continuous rigid frame bridge	Prestressed concrete box girder	reinforced concrete	50.0
Tomei Expressway Shin-Kawato Bridge	605.0	7	95.0	Continuous rigid frame bridge	Prestressed concrete box girder	reinforced concrete	33.3

Lateral force developed due to creep and drying shrinkage depends on lateral stiffness of bearing. For the 1000m multi-span continuous bridge, a large lateral force would be developed at the end piers, and it would develop large bending moment at the bottom of the piers. The situation is the same even in the Menshin design, and the consideration for large elongation of the deck becomes the key issue for applying the Menshin design to the 1000m multi-span continuous bridge.

APPLICATION OF MENSCHIN DESIGN FOR A 1000M MULTI-SPAN CONTINUOUS BRIDGE

For showing the application of Menshin design to a 1000m multi-span continuous bridge, a prestressed concrete continuous box girder with a span of about 40m was considered. This type of structure is often employed in viaducts in cities. The superstructure has a same section with reinforced concrete piers and cast-in-place concrete piles. The site condition is the II class (moderate soil) based on the " Design Specifications for Highway Bridges, Part V, Earthquake Resistant Design, 1990 " .

Fig.1 shows the bridge analyzed. The original dimensions of the model bridge were determined according to the seismic coefficient method assuming the lateral force coefficient of 0.25. This bridge was originally designed so that the seismic lateral force be distributed to each pier using rubber bearings.

In the Menshin design, lead rubber bearings (LRB) are used. Half of the elongation due to creep and drying shrinkage is given to LRB as pre-shear deformation, so that the effects of creep and drying shrinkage would not cause lateral internal force in the substructure. Fig. 2 shows the effect of pre-shear deformation. The LRB assumed are provided in Table 2. The pile was idealized by a set of linear springs with vertical, horizontal and rotating springs.

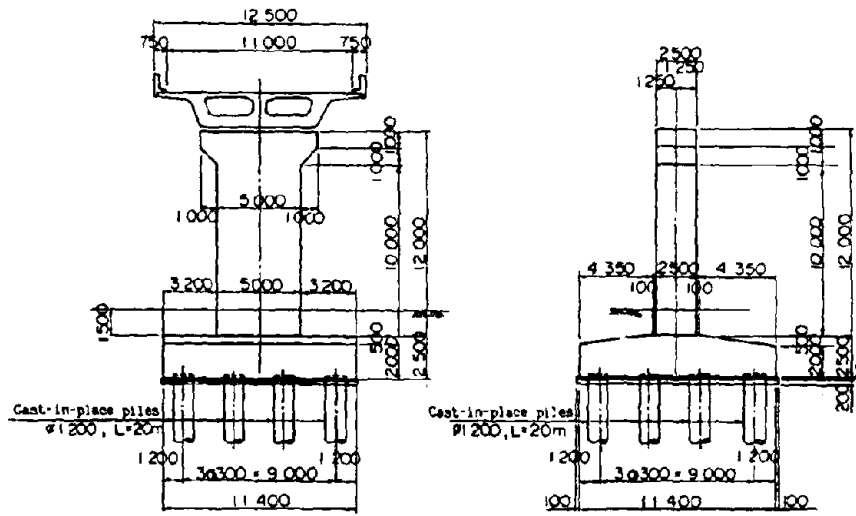
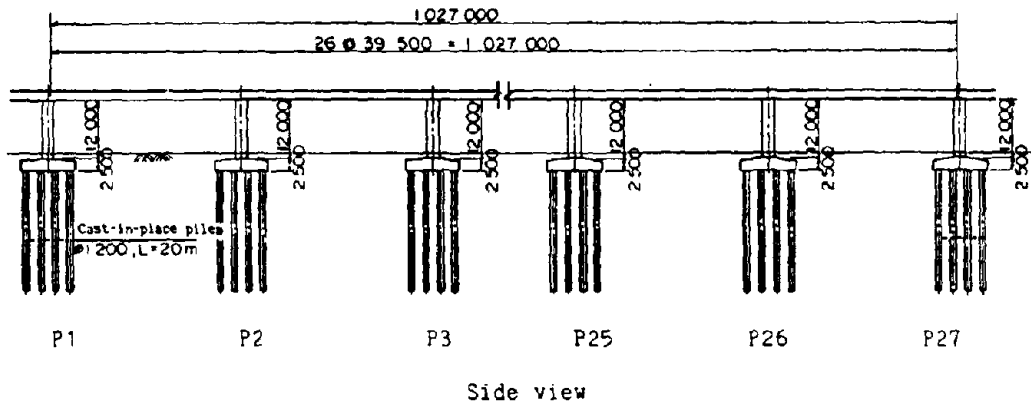
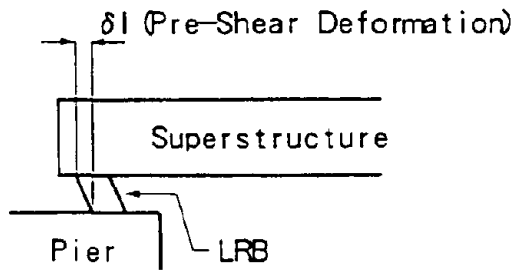


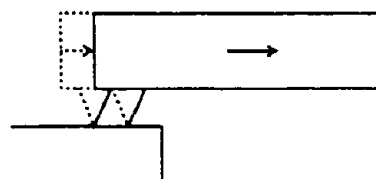
Fig. 1 Prestressed Concrete Bridge with Total Length of 1027m

Table 2. LRB assumed in design

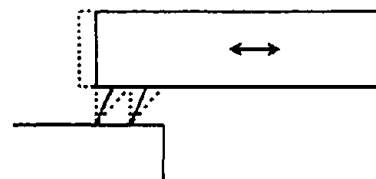
	P1(P27)	P2~P26
Shear modulus of rubber (kgf/cm ²)	8.0	8.0
Plane shape (cm)	90×90	100×100
thickness of rubber (cm)	24.0	42.0
diameter of lead (cm)	20.0×1	19.0×4



(1) At the Time for Setting LRB



(2) Rest Point when Creep and Drying Shrinkage Completed



(3) Excitation during an Earthquake

Fig. 2 Effect of pre-shear deformation

Table 3. Properties of LRB

		P1 (P27)	P2~P26
Effective stiffness	K_B (kgf/cm)	6,503	13,005
Initial stiffness	K_1 (kgf/cm ²)	26,240	77,730
Characteristic shear strength	Q (tf)	23.49	83.95
Design displacement	U_B (cm)	9.55	9.55
Effective damping ratio	h_D (%)	21.4	26.8

The LRB was idealized by the equivalent linear method as shown in Fig. 3. The equivalent spring stiffness of the LRB was evaluated as

$$K_b = Q / U_b + K_2 \quad (1)$$

Where

- K_b : Equivalent stiffness during an earthquake
- Q : Characteristic shear strength
- K_2 : Post-yield stiffness
- U_b : Relative displacement during an earthquakes

The equivalent stiffnesses K_b as well as other parameters is shown in Table 3. Lateral force of LRB associated with deck movement caused by creep and drying shrinkage was evaluated as

$$F_s = 0.2 Q + K_r \cdot u_s \quad (2)$$

Where

- F_s : Lateral force of LRB for low velocity shear deformation
- K_r : Stiffness of rubber
- u_s : Lateral displacement caused by creep and drying shrinkage

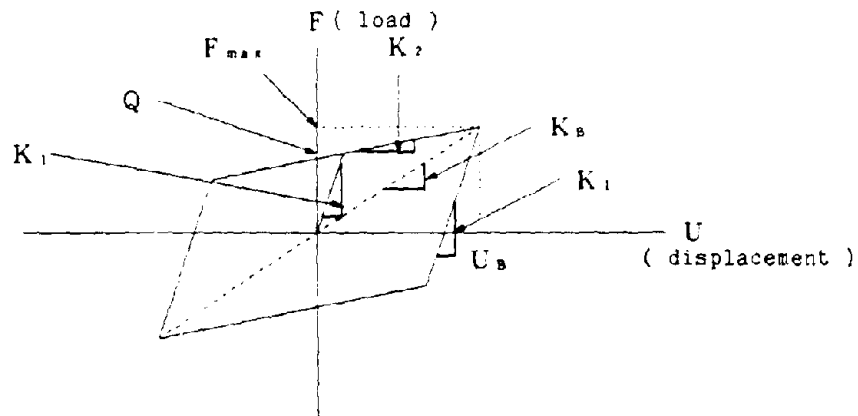


Fig. 3 Idealization of LRB by Equivalent Linear Method

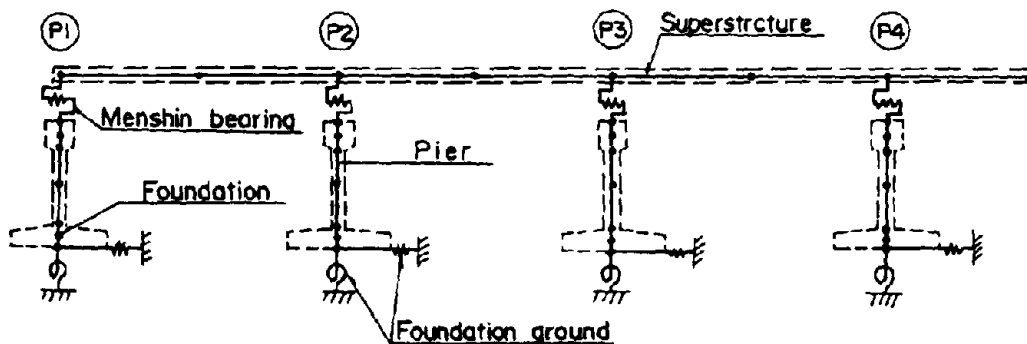


Fig. 4 Analytical computed model

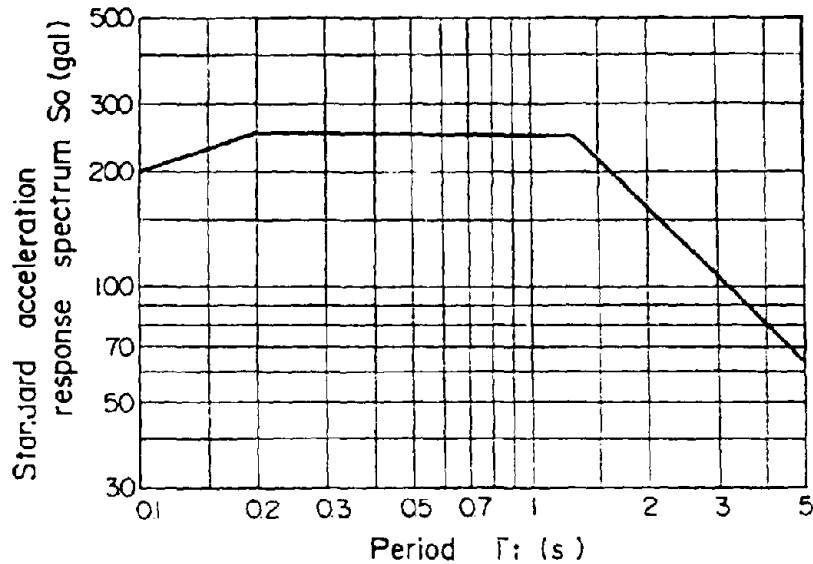


Fig. 5 Standard acceleration response spectrum

Analytical model used for static and dynamic analyses is shown in Fig. 4. Force and displacement developed due to creep and drying shrinkage were computed by static analysis, and the seismic response against as response spectrum as shown in Fig. 5 was by the response spectrum method. The fundamental natural period of the bridge is 1.35 second in longitudinal direction and 1.31 second in transverse direction.

The modal damping ratio was evaluated based on the proportional-to-strain-energy damping method as

$$h_i = \frac{\sum_{j=1}^n \phi_{ij}^T h_j K_j \phi_{ij}}{\phi_i^T K \phi_i} \quad (3)$$

where h_i is the damping ratio of i -th mode, ϕ_{ij} is an i -th mode vector for j -th structural element, h_j is damping ratio of j -th element, K_j is the stiffness matrix of j -th element, ϕ_i is i -th mode vector, K is stiffness matrix of the entire structure and n is the number of elements. The damping ratio of each structural element was assumed as 3% for the superstructure, 5% for the piers and 10% for the foundations.

For examining the effect of energy dissipation, one more bridge was designed for comparison. This bridge has the same characteristics with the bridge described above with only the LRBs being replaced with rubber bearings. The rubber bearings have the same lateral stiffness with LRB as shown in Table 4. Because there is small energy dissipation, the damping ratio of the rubber bearing was assumed as 5%.

Table 4. Properties of rubber bearings

	P1 (P27)	P2~P26
Shear modulus of rubber (kgf/cm ²)	8.0	8.0
Elastic stiffness of rubber K (kgf/cm ²)	6,503	13,005
Damping ratio h (%)	5.0	5.0

APPLICABILITY OF MENSJIN DESIGN

Bending moment developed at bottom of the pier is shown in Figs 6 and 7. Lateral force associated with creep and drying shrinkage was evaluated by Eq.(2). From Fig. 6, it is seen that the bending moment due to creep and drying shrinkage increase as piers get closer to the end, while the bending moment caused by seismic effect is approximately the same for all piers. It is important to note here that the bending moment due to seismic effect is three times as large as that due to creep and drying shrinkage. It should be noted here that the seismic effect is still critical for design of multi-span continuous bridge with the total deck length over 1000m. The bending moment in the transverse direction is almost the same for all piers but the end piers.

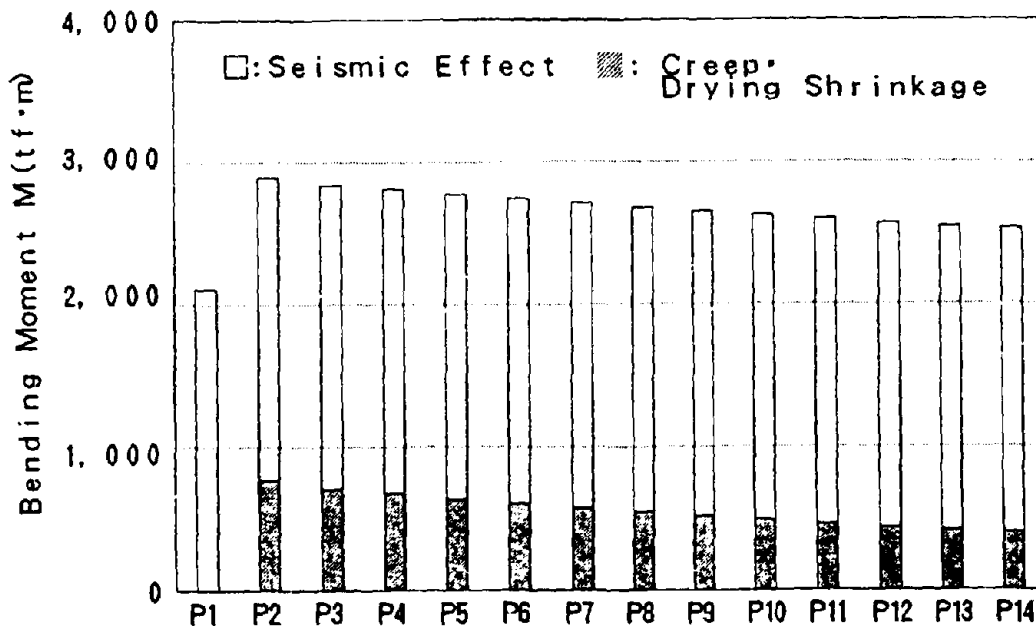


Fig. 6 Bending moment developed at bottom of pier (longitudinal excitation)

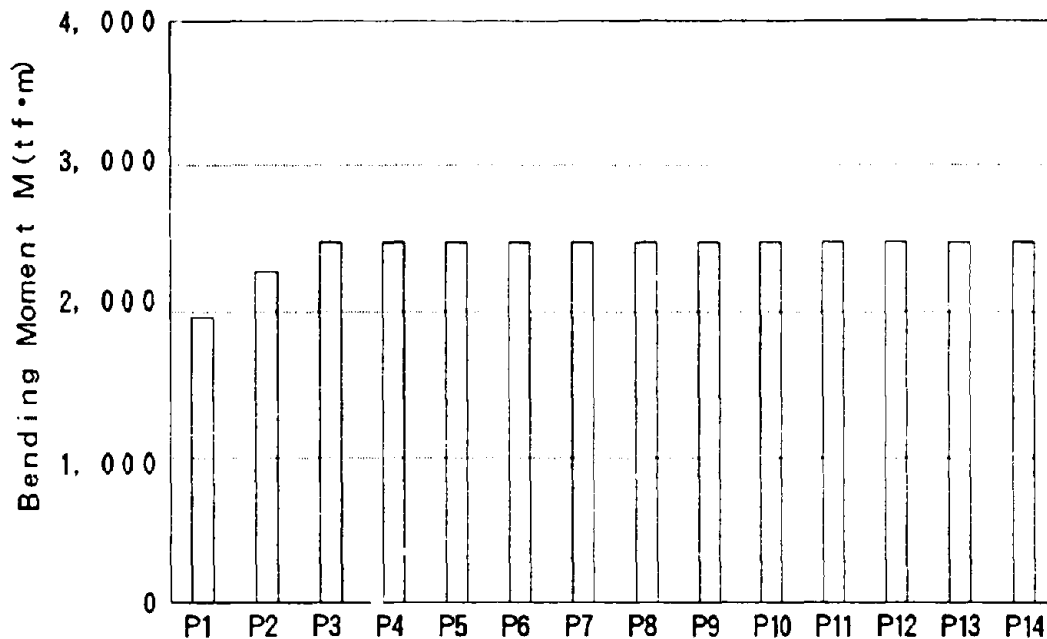


Fig. 7 Bending moment developed at bottom of pier (transverse excitation)

The peak response displacement of the superstructure is about the same for all piers at around 75mm in longitudinal direction. Because deck movement due to creep and drying shrinkage is about 150mm at both end, the pre-shear deformation with amount of 75mm seems effective. In transverse direction, the peak displacement is about 76mm at the middle piers and about 58mm at the end piers.

Based on the design presented here, it may be said that no difficulty would be encountered for construction highway bridge with deck length of 1000m. Highway bridge with more longer deck length would be feasible.

EFFECT OF ENERGY DISSIPATION OF LRB

Effect of energy dissipation of bearing is shown in Fig. 8 in terms of the maximum bending moment developed at the bottom of pier. It is clear from the figure that the bending moment is reduced about 30% due to energy dissipation effect at lead plug. Because Fig. 8 shows the bending moment developed only by seismic effect, the total bending moment caused by seismic effect, creep and drying shrinkage was evaluated as shown in Fig. 9. Lateral force developed by creep and drying shrinkage effect was evaluated by Eq.(2) for LRB. It was evaluated based on stiffness of rubber for bridge supported by the rubber bearings. The reducing rate of the bending moment depends on the piers, and it is from 17% to 20%.

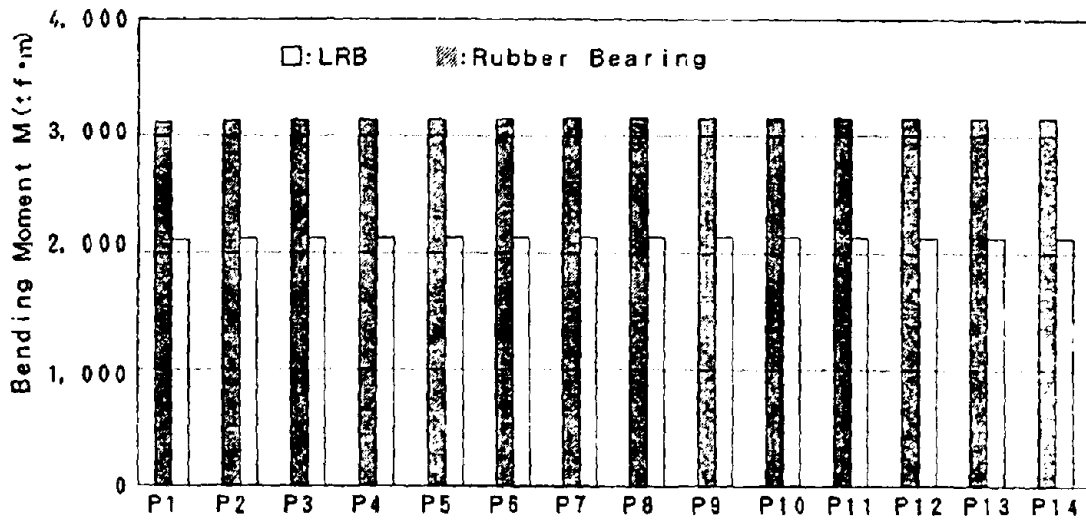


Fig. 8 Comparison of bending moments developed at bottom of pier due to seismic effect

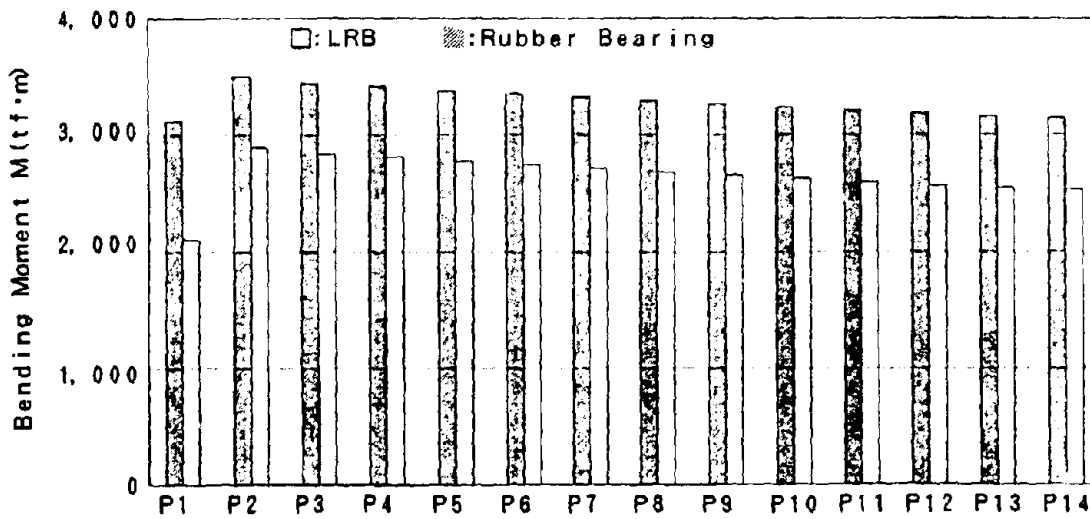


Fig. 9 Comparison of total bending moments developed at bottom of pier (seismic effect + creep + drying shrinkage)

CONCLUSION

From the results presented herein, the following conclusions were obtained.

- 1) For designing a multi-span prestressed concrete continuous bridge with deck length of 1000m, the primarily important point is how to reduce the member forces due to creep and drying shrinkage. It is effective to adopt LRB which has less restoring force for low velocity movement and to set-up the bearings with pre-shear deformation. As a result, the maximum member forces due to creep and drying shrinkage is about 35%, compared with that due to seismic effect.
- 2) Effect of energy dissipation at the bearing in terms of bending moment developed at bottom of pier is about 30% for seismic effect, and about 20% for seismic effect, creep and drying shrinkage.

To realize a multi-span continuous Menshin bridge with deck length of 1000m, there are other problems to be solved, such as expansion devices, restrainers, effect of different pier height, effect of curvature, response against differential ground motion, etc. However, it was found from this study that Menshin design can be applied to highway bridges with deck length about 1000m. It is also anticipated that further elongation of deck length could be made.

ACKNOWLEDGMENTS.

This study was made as a part of the joint research program on "Development of Menshin Systems of Highway Bridges" between PWRI and 28 private firms in Japan.

REFERENCES

1. Japan Road Association : "Design specifications for Highway Bridges, Part V. Earthquake Resistant Design, 1990" (in Japanese)
2. Technology Research Center for National Land Development, "Guidelines on the Design of Menshin Highway Bridges (Draft)", March 1989 (in Japanese)
3. PWRI and 29 Private Firms : "Development of Menshin System of Highway Bridges - Report No.1 -", PWRI Joint Research Report No.44, March 1990 (in Japanese)

Appendix A

Workshop Program

Workshop Participants

First US-Japan Workshop on Earthquake Protective Systems for Bridges

September 4-5, 1991

US Participants

Ahmed Abdel-Ghaffar
University of Southern California
School of Engineering
Los Angeles, CA 90089-0242
Phone: 213-743-6915
FAX: 213-744-1426

Ralph E. Anderson
Engineer of Bridges and Structures
Illinois Department of Transportation
2300 South Dirksen Parkway
Springfield, IL 62764
Phone: 217-782-2124
FAX: 217-782-7960

L.J. Billings
Room 245 Engineering Laboratory
University of California-Irvine
Irvine, CA 92717
Phone: 714-856-7393
FAX: 714-856-5051

Ian G. Buckle
Deputy Director
National Center for Earthquake
Engineering Research
State University of New York at Buffalo
105 Red Jacket Quadrangle
Buffalo, NY 14261
Phone: 716-645-3391
FAX: 716-645-3399

George Christian
New York State Department of Transportation
State Office Campus, Bldg. 5, 6th Floor
1220 Washington Avenue
Albany, NY 12232
Phone: 518-457-6825
FAX: 518-485-7826

M.C. Constantinou
Associate Professor
Civil Engineering
243 Ketter Hall
State University of New York at Buffalo
Buffalo, NY 14260
Phone: 716-645-2480
FAX: 716-645-3733

R.J. Fecarotta
Room 245 Engineering Laboratory
University of California-Irvine
Irvine, CA 92717
Phone: 714-856-7393
FAX: 714-856-5051

Shunji Fuji
Research Associate
136 Ketter Hall
State University of New York at Buffalo
Buffalo, NY 14260
Phone: 716-645-3001
FAX: 716-645-3733

Qing Feng
Department of Civil Engineering
and Operations Research
Engineering Quadrangle
Princeton University
Princeton, NJ 08544
Phone: 609-258-4600
FAX: 609-258-1270

He-Liu
Research Associate
144 Ketter Hall
State University of New York at Buffalo
Buffalo, NY 14260
Phone: 716-645-3964
FAX: 716-645-3733

Ms. M.A. Jacak
Dynamic Isolation Systems
Field Engineer
2855 Telegraph Ave., #410
Berkeley, CA 94705
Phone: 415-843-7233
FAX: 415-843-0366

John Kowalski
New York State Department
of Transportation
125 Main Street
Donovan Office Building
Buffalo, NY 14203
Phone: 716-847-3204
FAX: 716-847-5014

George C. Lee
School of Engineering and
Applied Sciences
412 Bonner Hall
State University of New York at Buffalo
Buffalo, NY 14260
Phone: 716-645-2771
FAX: 716-645-2495

H.S. Lew
National Institute of Standards and Technology
Center for Building Technology
Building 226
Gaithersburg, MD 20899
Phone: 301-975-6060
FAX: 301-975-4032

Albert Lin
National Institute of Standards and Technology
Center for Building Technology
Building 226, Room 158
Gaithersburg, MD 20899
Phone: 301-975-6060
FAX: 301-975-4032

S.C. Liu
Earthquake Hazard Mitigation
Biological and Critical Systems
National Science Foundation
1800 G Street, NW
Washington, DC 20550
Phone: 202-357-9500
FAX: 202-357-9803

Dr. Stephen Mahin
Professor
Civil Engineering
721A Davis Hall
University of California, Berkeley
Berkeley, CA 94720
Phone: 415-642-4021
FAX: 415-643-5264

Ayaz Malik
New York State Department of Transportation
State Office Campus, Bldg. 5, 6th Floor
1220 Washington Avenue
Albany, NY 12232
Phone: 518-457-6825
FAX: 518-485-7826

Ronald L. Mayes
President
Dynamic Isolation Systems, Inc.
2855 Telegraph Ave., #410
Berkeley, CA 94705
Phone: 415-843-7233
FAX: 415-843-0366

Satish Nagarajaiah
Research Associate
132 Ketter Hall
State University of New York at Buffalo
Buffalo, NY 14260
Phone: 716-645-2186
FAX: 716-645-3733

Andrei M. Reinhorn
Professor
Civil Engineering
231 Ketter Hall
State University of New York at Buffalo
Buffalo, NY 14260
Phone: 716-645-3491
FAX: 716-645-3733

Tim Roach
New York State Department
of Transportation
125 Main Street
Donovan Office Building
Buffalo, NY 14203
Phone: 716-847-3204
FAX: 716-847-5014

Robin Shepherd
Professor
Room 245 Engineering Laboratory
University of California-Irvine
Irvine, CA 92717
Phone: 714-856-7393
FAX: 714-856-5051

Masanobu Shinozuka
Director
National Center for Earthquake
Engineering Research
State University of New York at Buffalo
109 Red Jacket Quadrangle
Buffalo, NY 14261
Phone: 716-645-3391
FAX: 716-645-3399

Arun Shirole
Deputy Chief Engineer, Structures
New York State Department
of Transportation
State Office Campus, Bldg. 5, 6th Floor
1220 Washington Avenue
Albany, NY 12232
Phone: 518-457-6825
FAX: 518-485-7826

T.T. Soong
Professor
Civil Engineering
238 Ketter Hall
State University of New York at Buffalo
Buffalo, NY 14260
Phone: 716-645-2469
FAX: 716-645-3733

Eric Thorkildsen
Division of Structures
California Department of Transportation
Sacramento, CA 95814
Phone: 916-322-6395
FAX: 916-445-0574

Jann N. Yang
Department of Civil Engineering
University of California-Irvine
Irvine, CA 92717
Phone: 714-856-4246
FAX: 714-725-2117

I-Chou Tsai
Professor
National Center for Earthquake
Engineering Research
National Taiwan University
Taipei, Taiwan
Republic of China
Phone: (02)3633554
FAX: (02)3633520

Huei-Tsyr Chen
Professor
National Center for Earthquake
Engineering Research
National Taiwan University
Taipei, Taiwan
Republic of China
Phone: (02)3633554
FAX: (02)3633520

First US-Japan Workshop on Earthquake Protective Systems for Bridges

September 4-5, 1991

Japanese Participants

Nobuyuki Doro
Assistant Manager
Technical Department
Chemical/Industrial Products Division
Toyo Tire & Rubber Co., Ltd.
Saitama Plant: 302 Sayamagahara, Iruma-shi
Saitama-ken 358, Japan

Yozo Goto
General Manager
Civil Engineering Department No. 5
Technical Research Institute
Obayashi Corporation
4-640, Shimokiyoto, Kiyose-shi
Tokyo 204, Japan

Yoshihiro Hamazaki
Researcher
Dynamic & Acoustics Research Station
Mechanical Engineering Research Laboratory
Kobe Steel, Ltd.
1-5-5 Takatsukadai, Nishi-ku
Kobe 651-22, Japan

Koji Hara
Technological Staff
Road Construction Division
Public Works Department
Shizuoka Prefectural Government
9-6, Ohtemachi, Shizuoka-shi
Shizuoka-ken 420, Japan

Kinji Hasegawa
Senior Research Engineer
Earthquake Engineering Division
Earthquake Disaster Prevention Department
Public Works Research Institute
Ministry of Construction
1 Asahi, Tsukuba-shi
Ibaraki-ken 305, Japan

Akio Hayashi
Senior Engineer
Construction Department
Pacific Consultants Co., Ltd.
2-40-1 Kameido, Koutou-ku
Tokyo 136, Japan

Takashi Hirai
Research Engineer
Technology Development Department
Office of Technology Development
Takenaka Civil Engineering and
Construction Co., Ltd.
5-14 Minamisuna 2-chome, Koto-ku
Tokyo 136, Japan

Hirokazu Iemura
Department of Civil Engineering
Kyoto University
Kyoto 606, Japan

Takamura Iguchi
Manager
Engineering Department
BBM Co., Ltd.
Tokyo Tatemono Building
1-9-9 Yaesu, Chuo-ku
Tokyo 101, Japan

Tomoyuki Inukai
Research Engineer
Structural - Dynamics Unit
Technical Research Laboratory
Takenaka Corporation
5-14, 2 chome, Minamisuna, Koto-ku
Tokyo 136, Japan

Hiroshi Kamiya
Chief Engineer
Environmental Research Section
Research Department
Technical Research and Development Institute
Nishimatsu Construction Co., Ltd.
2570-4, Shimotsuruma, Yamato-shi
Kanagawa-ken 242, Japan

Isao Kaneko
Institute of Construction Technology
Kumagai Gumi, Ltd.
1043 Shimoyama, Onigakubo, Tsukuba-shi
Ibaraki-ken 300-22, Japan

Iwao Kawasaki
Structural Engineer
Civil Engineering Department
Japan Engineering Consultants Co., Ltd.
(Nihon Gijutsu Kaihatsu K.K.)
2-6 Okubo 2-chome, Shinjuku-ku
Tokyo 160, Japan

Kazuhiko Kawashima
Head
Earthquake Engineering Division
Earthquake Disaster Prevention Department
Public Works Research Institute
Ministry of Construction
1 Asahi Tsukuba-shi
Ibaraki-ken 305, Japan

Teruo Kimishima
Vice Manager
Engineering Design Department
Engineering Division
Nippon Chuzo K.K.
2-1 Shiraishi-cho
Kawasaki-ku, Kawasaki-shi
Kanagawa-ken 210, Japan

Tetsuhisa Kobayashi
Sectional Chief
Engineering Department 2
Kansai International Airport Company, Ltd.
3-11-10 Minami-senba, Chuo-ku
Osaka 542, Japan

Masahiro Koshitohge
Engineer
MB Material Development Department
The Yokohama Rubber Co., Ltd.
Hiratsuka Plant, 2-1 Oiwake, Hiratsuka-shi
Kanagawa-ken 254, Japan

Eiichi Kuribayashi
Department of Construction
Toyohashi University of Technology
Toyohashi-shi
Aichi-ken 440, Japan

Yutaka Makiguchi
Staff Manager
Technical Development Department 2
Oiles Corporation
8 Kiri-hara-cho, Fujisawa-shi
Kanagawa-ken 252, Japan

Hiroshi Mashiko
Deputy Head
Bridge Design Section
Civil Engineering Department
Sumitomo Construction Co., Ltd.
13-4 Araki-cho, Shinjuku-ku
Tokyo 160, Japan

Masaaki Nakanishi
Assistant Manager
Bridge Department
Public Works Bureau
Osaka City Government
1-2-2-500 Umeda, Kita-ku
Osaka 530, Japan

Ichiro Nishikawa
Manager
Information Machines & Equipment
Department
Showa Electric Wire & Cable Co., Ltd.
4-1-1 Minamihashimoto, Sagami-hara-shi
Kanagawa-ken 229, Japan

Mituso Okado
Assistant Manager
Structural Design Department
New Structural Engineering, Ltd.
12 Nibancho, Chiyoda-ku
Tokyo 102, Japan

Daisuke Ozaki
Assistant Manager
Design Department
Civil Engineering Division
Taisei Corporation
Shinjuku Center Building
25-1 Nishi-shinjuku 1-chome, Shinjuku-ku
Tokyo 163, Japan

Yoshitake Sawachi
Assistant Manager
Engineering Development Department
Civil Engineering Design Division
Kajima Corporation
5-30 Akasaka 6-chome, Minato-ku
Tokyo 107, Japan

Minoru Shimada
Assistant Manager
Design Department of Civil
Engineering Division
Shimizu Corporation
Seavens South, 2-3 Shibaura 1-chome,
Minato-ku,
Tokyo 105-07, Japan

Chiaki Sudo
Engineer
Civil Engineering
Marine Products Development Department
Bridgestone Corporation
1 Kashio-cho, Totsuka-ku
Yokohama 244, Japan

Yoji Suizu
Senior Research Engineer
Research and Development Department
Bridgestone Corporation
3-1-1 Ogawahigashi-cho, Kodaira-shi
Tokyo 187, Japan

Tatsumasa Takaku
Head
Design Engineering Section
Steel Construction & Engineering Department
NKK Corporation
2-1 Suehiro-cho, Tsurumi-ku
Yokohama 230, Japan

Isao Takaturi
Earthquake Engineering Division
Earthquake Disaster Prevention Department
Public Works Research Institute
Ministry of Construction
1 Asahi, Tsukuba-shi
Ibaraki-ken 305, Japan

Takashi Tamura
Civil Engineering
Design Section 2
Civil Engineering Division
Mitsui Construction Co., Ltd.
3-10-1 Iwamoto-cho, Chiyoda-ku
Tokyo 101, Japan

Tetsuo Takeda
Senior Research Engineer
Civil Engineering Department
Kajima Institute of Construction Technology
Kajima Corporation
19-1 Tobitakyu 2-chome, Chofu-shi
Tokyo 182, Japan

Tamotsu Tamura
Civil Engineering Development Division
Engineering Research Institute
Penta-Ocean Construction Co., Ltd.
1-11-25 Higashi-ohi, Shinagawa-ku
Tokyo 140, Japan

Kenzo Toki
Disaster Prevention Research Institute
Kyoto University
Uji-shi
Kyoto 611, Japan

Yohifumi Uno
Manager
2nd Designing Section
Design & Engineering Department
Kawaguchi Metal Industries Co., Ltd.
2-7-18 Shibata, Kita-ku
Osaka 530, Japan

Kazushige Yoshikawa
Structure Engineer
Bridge Design Section
Structure Department
Pacific Consultants Co., Ltd.
2-40-1 Kameido, Koutou-ku
Tokyo 136, Japan

**NATIONAL CENTER FOR EARTHQUAKE ENGINEERING RESEARCH
LIST OF TECHNICAL REPORTS**

The National Center for Earthquake Engineering Research (NCEER) publishes technical reports on a variety of subjects related to earthquake engineering written by authors funded through NCEER. These reports are available from both NCEER's Publications Department and the National Technical Information Service (NTIS). Requests for reports should be directed to the Publications Department, National Center for Earthquake Engineering Research, State University of New York at Buffalo, Red Jacket Quadrangle, Buffalo, New York 14261. Reports can also be requested through NTIS, 5285 Port Royal Road, Springfield, Virginia 22161. NTIS accession numbers are shown in parenthesis, if available.

- NCEER-87-0001 "First-Year Program in Research, Education and Technology Transfer," 3/5/87, (PB88-134275/AS).
- NCEER-87-0002 "Experimental Evaluation of Instantaneous Optimal Algorithms for Structural Control," by R.C. Lin, T.T. Soong and A.M. Reinhorn, 4/20/87, (PB88-134341/AS).
- NCEER-87-0003 "Experimentation Using the Earthquake Simulation Facilities at University at Buffalo," by A.M. Reinhorn and R.L. Ketter, to be published.
- NCEER-87-0004 "The System Characteristics and Performance of a Shaking Table," by J.S. Hwang, K.C. Chang and G.C. Lee, 6/1/87, (PB88-134259/AS). This report is available only through NTIS (see address given above).
- NCEER-87-0005 "A Finite Element Formulation for Nonlinear Viscoplastic Material Using a Q Model," by O. Gyebi and G. Dasgupta, 11/2/87, (PB88-213764/AS).
- NCEER-87-0006 "Symbolic Manipulation Program (SMP) - Algebraic Codes for Two and Three Dimensional Finite Element Formulations," by X. Lee and G. Dasgupta, 11/9/87, (PB88-218522/AS).
- NCEER-87-0007 "Instantaneous Optimal Control Laws for Tall Buildings Under Seismic Excitations," by J.N. Yang, A. Akbarpour and P. Ghosemaghami, 6/10/87, (PB88-134333/AS).
- NCEER-87-0008 "IDARC: Inelastic Damage Analysis of Reinforced Concrete Frame - Shear-Wall Structures," by Y.J. Park, A.M. Reinhorn and S.K. Kunnath, 7/20/87, (PB88-134325/AS).
- NCEER-87-0009 "Liquefaction Potential for New York State: A Preliminary Report on Sites in Manhattan and Buffalo," by M. Budhu, V. Vijayakumar, R.F. Giese and L. Baumgras, 8/31/87, (PB88-163704/AS). This report is available only through NTIS (see address given above).
- NCEER-87-0010 "Vertical and Torsional Vibration of Foundations in Inhomogeneous Media," by A.S. Veletsos and K.W. Dotson, 6/1/87, (PB88-134291/AS).
- NCEER-87-0011 "Seismic Probabilistic Risk Assessment and Seismic Margins Studies for Nuclear Power Plants," by Howard H.M. Hwang, 6/15/87, (PB88-134267/AS).
- NCEER-87-0012 "Parametric Studies of Frequency Response of Secondary Systems Under Ground-Acceleration Excitations," by Y. Yong and Y.K. Lin, 6/10/87, (PB88-134309/AS).
- NCEER-87-0013 "Frequency Response of Secondary Systems Under Seismic Excitation," by J.A. HoLung, J. Cai and Y.K. Lin, 7/31/87, (PB88-134317/AS).
- NCEER-87-0014 "Modelling Earthquake Ground Motions in Seismically Active Regions Using Parametric Time Series Methods," by G.W. Ellis and A.S. Cakmak, 8/25/87, (PB88-134283/AS).
- NCEER-87-0015 "Detection and Assessment of Seismic Structural Damage," by E. DiPasquale and A.S. Cakmak, 8/25/87, (PB88-163712/AS).

- NCEER-87-0016 "Pipeline Experiment at Parkfield, California," by J. Isenberg and E. Richardson, 9/15/87, (PB88-163720/AS). This report is available only through NTIS (see address given above).
- NCEER-87-0017 "Digital Simulation of Seismic Ground Motion," by M. Shinozuka, G. Deodatis and T. Harada, 8/31/87, (PB88-155197/AS). This report is available only through NTIS (see address given above).
- NCEER-87-0018 "Practical Considerations for Structural Control: System Uncertainty, System Time Delay and Truncation of Small Control Forces," J.N. Yang and A. Akbarpour, 8/10/87, (PB88-163738/AS).
- NCEER-87-0019 "Modal Analysis of Nonclassically Damped Structural Systems Using Canonical Transformation," by J.N. Yang, S. Sarkani and F.X. Long, 9/27/87, (PB88-187851/AS).
- NCEER-87-0020 "A Nonstationary Solution in Random Vibration Theory," by J.R. Red-Horse and P.D. Spanos, 11/3/87, (PB88-163746/AS).
- NCEER-87-0021 "Horizontal Impedances for Radially Inhomogeneous Viscoelastic Soil Layers," by A.S. Veletsos and K.W. Dotson, 10/15/87, (PB88-150859/AS).
- NCEER-87-0022 "Seismic Damage Assessment of Reinforced Concrete Members," by Y.S. Chung, C. Meyer and M. Shinozuka, 10/9/87, (PB88-150867/AS). This report is available only through NTIS (see address given above).
- NCEER-87-0023 "Active Structural Control in Civil Engineering," by T.T. Soong, 11/11/87, (PB88-187778/AS).
- NCEER-87-0024 "Vertical and Torsional Impedances for Radially Inhomogeneous Viscoelastic Soil Layers," by K.W. Dotson and A.S. Veletsos, 12/87, (PB88-187786/AS).
- NCEER-87-0025 "Proceedings from the Symposium on Seismic Hazards, Ground Motions, Soil-Liquefaction and Engineering Practice in Eastern North America," October 20-22, 1987, edited by K.H. Jacob, 12/87, (PB88-188115/AS).
- NCEER-87-0026 "Report on the Whittier-Narrows, California, Earthquake of October 1, 1987," by J. Pantelic and A. Reinhorn, 11/87, (PB88-187752/AS). This report is available only through NTIS (see address given above).
- NCEER-87-0027 "Design of a Modular Program for Transient Nonlinear Analysis of Large 3-D Building Structures," by S. Srivastav and J.F. Abel, 12/30/87, (PB88-187950/AS).
- NCEER-87-0028 "Second-Year Program in Research, Education and Technology Transfer," 3/8/88, (PB88-219480/AS).
- NCEER-88-0001 "Workshop on Seismic Computer Analysis and Design of Buildings With Interactive Graphics," by W. McGuire, J.F. Abel and C.H. Conley, 1/18/88, (PB88-187760/AS).
- NCEER-88-0002 "Optimal Control of Nonlinear Flexible Structures," by J.N. Yang, F.X. Long and D. Wong, 1/22/88, (PB88-213772/AS).
- NCEER-88-0003 "Substructuring Techniques in the Time Domain for Primary-Secondary Structural Systems," by G.D. Manolis and G. Juhn, 2/10/88, (PB88-213780/AS).
- NCEER-88-0004 "Iterative Seismic Analysis of Primary-Secondary Systems," by A. Singhal, L.D. Lutes and P.D. Spanos, 2/23/88, (PB88-213798/AS).
- NCEER-88-0005 "Stochastic Finite Element Expansion for Random Media," by P.D. Spanos and R. Ghanem, 3/14/88, (PB88-213806/AS).

- NCEER-88-0006 "Combining Structural Optimization and Structural Control," by F.Y. Cheng and C.P. Pantelides, 1/10/88, (PB88-213814/AS).
- NCEER-88-0007 "Seismic Performance Assessment of Code-Designed Structures," by H.H-M. Hwang, J-W. Jaw and H-J. Shau, 3/20/88, (PB88-219423/AS).
- NCEER-88-0008 "Reliability Analysis of Code-Designed Structures Under Natural Hazards," by H.H-M. Hwang, H. Ushiba and M. Shinozuka, 2/29/88, (PB88-229471/AS).
- NCEER-88-0009 "Seismic Fragility Analysis of Shear Wall Structures," by J-W Jaw and H.H-M. Hwang, 4/30/88, (PB89-102867/AS).
- NCEER-88-0010 "Base Isolation of a Multi-Story Building Under a Harmonic Ground Motion - A Comparison of Performances of Various Systems," by F-G Fan, G. Ahmadi and I.G. Tadjbakhsh, 5/18/88, (PB89-122238/AS).
- NCEER-88-0011 "Seismic Floor Response Spectra for a Combined System by Green's Functions," by F.M. Lavelle, L.A. Bergman and P.D. Spanos, 5/1/88, (PB89-102875/AS).
- NCEER-88-0012 "A New Solution Technique for Randomly Excited Hysteretic Structures," by G.Q. Cai and Y.K. Lin, 5/16/88, (PB89-102883/AS).
- NCEER-88-0013 "A Study of Radiation Damping and Soil-Structure Interaction Effects in the Centrifuge," by K. Weissman, supervised by J.H. Prevost, 5/24/88, (PB89-144703/AS).
- NCEER-88-0014 "Parameter Identification and Implementation of a Kinematic Plasticity Model for Frictional Soils," by J.H. Prevost and D.V. Griffiths, to be published.
- NCEER-88-0015 "Two- and Three- Dimensional Dynamic Finite Element Analyses of the Long Valley Dam," by D.V. Griffiths and J.H. Prevost, 6/17/88, (PB89-144711/AS).
- NCEER-88-0016 "Damage Assessment of Reinforced Concrete Structures in Eastern United States," by A.M. Reinhorn, M.J. Seidel, S.K. Kunnath and Y.J. Park, 6/15/88, (PB89-122220/AS).
- NCEER-88-0017 "Dynamic Compliance of Vertically Loaded Strip Foundations in Multilayered Viscoelastic Soils," by S. Ahmad and A.S.M. Israil, 6/17/88, (PB89-102891/AS).
- NCEER-88-0018 "An Experimental Study of Seismic Structural Response With Added Viscoelastic Dampers," by R.C. Lin, Z. Liang, T.T. Soong and R.H. Zhang, 6/30/88, (PB89-122212/AS). This report is available only through NTIS (see address given above).
- NCEER-88-0019 "Experimental Investigation of Primary - Secondary System Interaction," by G.D. Manolis, G. Juhn and A.M. Reinhorn, 5/27/88, (PB89-122204/AS).
- NCEER-88-0020 "A Response Spectrum Approach For Analysis of Nonclassically Damped Structures," by J.N. Yang, S. Sarkani and F.X. Long, 4/22/88, (PB89-102909/AS).
- NCEER-88-0021 "Seismic Interaction of Structures and Soils: Stochastic Approach," by A.S. Veletsos and A.M. Prasad, 7/21/88, (PB89-122196/AS).
- NCEER-88-0022 "Identification of the Serviceability Limit State and Detection of Seismic Structural Damage," by E. DiPasquale and A.S. Cakmak, 6/15/88, (PB89-122188/AS). This report is available only through NTIS (see address given above).
- NCEER-88-0023 "Multi-Hazard Risk Analysis: Case of a Simple Offshore Structure," by B.K. Bhartia and E.H. Vanmarcke, 7/21/88, (PB89-145213/AS).

- NCEER-88-0024 "Automated Seismic Design of Reinforced Concrete Buildings," by Y.S. Chung, C. Meyer and M. Shinozuka, 7/5/88, (PB89-122170/AS). This report is available only through NTIS (see address given above).
- NCEER-88-0025 "Experimental Study of Active Control of MDOF Structures Under Seismic Excitations," by L.L. Chung, R.C. Lin, T.T. Soong and A.M. Reinhorn, 7/10/88, (PB89-122600/AS).
- NCEER-88-0026 "Earthquake Simulation Tests of a Low-Rise Metal Structure," by J.S. Hwang, K.C. Chang, G.C. Lee and R.L. Ketter, 8/1/88, (PB89-102917/AS).
- NCEER-88-0027 "Systems Study of Urban Response and Reconstruction Due to Catastrophic Earthquakes," by F. Kozin and H.K. Zhou, 9/22/88, (PB90-162348/AS).
- NCEER-88-0028 "Seismic Fragility Analysis of Plane Frame Structures," by H.H.-M. Hwang and Y.K. Low, 7/31/88, (PB89-131445/AS).
- NCEER-88-0029 "Response Analysis of Stochastic Structures," by A. Kardara, C. Bucher and M. Shinozuka, 9/22/88, (PB89-174429/AS).
- NCEER-88-0030 "Nonnormal Accelerations Due to Yielding in a Primary Structure," by D.C.K. Chen and L.D. Lutes, 9/19/88, (PB89-131437/AS).
- NCEER-88-0031 "Design Approaches for Soil-Structure Interaction," by A.S. Veletsos, A.M. Prasad and Y. Tang, 12/30/88, (PB89-174437/AS). This report is available only through NTIS (see address given above).
- NCEER-88-0032 "A Re-evaluation of Design Spectra for Seismic Damage Control," by C.J. Turkstra and A.G. Tallin, 11/7/88, (PB89-145221/AS).
- NCEER-88-0033 "The Behavior and Design of Noncontact Lap Splices Subjected to Repeated Inelastic Tensile Loading," by V.E. Sagan, P. Gergely and R.N. White, 12/8/88, (PB89-163737/AS).
- NCEER-88-0034 "Seismic Response of Pile Foundations," by S.M. Mamoon, P.K. Banerjee and S. Ahmad, 11/1/88, (PB89-145239/AS).
- NCEER-88-0035 "Modeling of R/C Building Structures With Flexible Floor Diaphragms (IDARC2)," by A.M. Reinhorn, S.K. Kunnath and N. Panahshahi, 9/7/88, (PB89-207153/AS).
- NCEER-88-0036 "Solution of the Dam-Reservoir Interaction Problem Using a Combination of FEM, BEM with Particular Integrals, Modal Analysis, and Substructuring," by C-S. Tsai, G.C. Lee and R.L. Ketter, 12/31/88, (PB89-207146/AS).
- NCEER-88-0037 "Optimal Placement of Actuators for Structural Control," by F.Y. Cheng and C.P. Pantelides, 8/15/88, (PB89-162846/AS).
- NCEER-88-0038 "Teflon Bearings in Seismic Base Isolation: Experimental Studies and Mathematical Modeling," by A. Mokha, M.C. Constantinou and A.M. Reinhorn, 12/5/88, (PB89-218457/AS). This report is available only through NTIS (see address given above).
- NCEER-88-0039 "Seismic Behavior of Flat Slab High-Rise Buildings in the New York City Area," by P. Weidlinger and M. Ettouney, 10/15/88, (PB90-145681/AS).
- NCEER-88-0040 "Evaluation of the Earthquake Resistance of Existing Buildings in New York City," by P. Weidlinger and M. Ettouney, 10/15/88, to be published.
- NCEER-88-0041 "Small-Scale Modeling Techniques for Reinforced Concrete Structures Subjected to Seismic Loads," by W. Kim, A. El-Attar and R.N. White, 11/22/88, (PB89-189625/AS).

- NCEER-88-0042 "Modeling Strong Ground Motion from Multiple Event Earthquakes," by G.W. Ellis and A.S. Cakmak, 10/15/88, (PB89-174445/AS).
- NCEER-88-0043 "Nonstationary Models of Seismic Ground Acceleration," by M. Grigoriu, S.E. Ruiz and E. Rosenblueth, 7/15/88, (PB89-189617/AS).
- NCEER-88-0044 "SARCF User's Guide: Seismic Analysis of Reinforced Concrete Frames," by Y.S. Chun, C. Meyer and M. Shinozuka, 11/9/88, (PB89-174452/AS).
- NCEER-88-0045 "First Expert Panel Meeting on Disaster Research and Planning," edited by J. Pantelic and J. Stoye, 9/15/88, (PB89-174460/AS).
- NCEER-88-0046 "Preliminary Studies of the Effect of Degrading Infill Walls on the Nonlinear Seismic Response of Steel Frames," by C.Z. Chrysostomou, P. Gergely and J.F. Abel, 12/19/88, (PB89-208383/AS).
- NCEER-88-0047 "Reinforced Concrete Frame Component Testing Facility - Design, Construction, Instrumentation and Operation," by S.P. Pestiki, C. Conley, T. Bond, P. Gergely and R.N. White, 12/16/88, (PB89-174478/AS).
- NCEER-89-0001 "Effects of Protective Cushion and Soil Compliancy on the Response of Equipment Within a Seismically Excited Building," by J.A. HoLung, 2/16/89, (PB89-207179/AS).
- NCEER-89-0002 "Statistical Evaluation of Response Modification Factors for Reinforced Concrete Structures," by H.H-M. Hwang and J.W. Jaw, 2/17/89, (PB89-207187/AS).
- NCEER-89-0003 "Hysteretic Columns Under Random Excitation," by G-Q. Cai and Y.K. Lin, 1/9/89, (PB89-196513/AS).
- NCEER-89-0004 "Experimental Study of 'Elephant Foot Bulge' Instability of Thin-Walled Metal Tanks," by Z-H. Jia and R.L. Ketter, 2/22/89, (PB89-207195/AS).
- NCEER-89-0005 "Experiment on Performance of Buried Pipelines Across San Andreas Fault," by J. Isenberg, E. Richardson and T.D. O'Rourke, 3/10/89, (PB89-218440/AS).
- NCEER-89-0006 "A Knowledge-Based Approach to Structural Design of Earthquake-Resistant Buildings," by M. Subramani, P. Gergely, C.H. Conley, J.F. Abel and A.H. Zaghaw, 1/15/89, (PB89-218465/AS).
- NCEER-89-0007 "Liquefaction Hazards and Their Effects on Buried Pipelines," by T.D. O'Rourke and P.A. Lane, 2/1/89, (PB89-218481).
- NCEER-89-0008 "Fundamentals of System Identification in Structural Dynamics," by H. Imai, C-B. Yun, O. Maruyama and M. Shinozuka, 1/26/89, (PB89-207211/AS).
- NCEER-89-0009 "Effects of the 1985 Michoacan Earthquake on Water Systems and Other Buried Lifelines in Mexico," by A.G. Ayala and M.J. O'Rourke, 3/8/89, (PB89-207229/AS).
- NCEER-89-R010 "NCEER Bibliography of Earthquake Education Materials," by K.E.K. Ross, Second Revision, 9/1/89, (PB90-125352/AS).
- NCEER-89-0011 "Inelastic Three-Dimensional Response Analysis of Reinforced Concrete Building Structures (IDARC-3D), Part I - Modeling," by S.K. Kunnath and A.M. Reinhorn, 4/17/89, (PB90-114612/AS).
- NCEER-89-0012 "Recommended Modifications to ATC-14," by C.D. Poland and J.O. Malley, 4/12/89, (PB90-108648/AS).
- NCEER-89-0013 "Repair and Strengthening of Beam-to-Column Connections Subjected to Earthquake Loading," by M. Corazao and A.J. Durrani, 2/28/89, (PB90-109885/AS).

- NCEER-89-0014 "Program EXKAL2 for Identification of Structural Dynamic Systems," by O. Maruyama, C-B. Yun, M. Hoshiya and M. Shinozuka, 5/19/89, (PB90-109877/AS).
- NCEER-89-0015 "Response of Frames With Bolted Semi-Rigid Connections, Part I - Experimental Study and Analytical Predictions," by P.J. DiCorso, A.M. Reinhorn, J.R. Dickerson, J.B. Radziminaki and W.L. Harper, 6/1/89, to be published.
- NCEER-89-0016 "ARMA Monte Carlo Simulation in Probabilistic Structural Analysis," by P.D. Spanos and M.P. Mignolet, 7/10/89, (PB90-109893/AS).
- NCEER-89-P017 "Preliminary Proceedings from the Conference on Disaster Preparedness - The Place of Earthquake Education in Our Schools," Edited by K.E.K. Ross, 6/23/89, (PB90-207895/AS).
- NCEER-89-0017 "Proceedings from the Conference on Disaster Preparedness - The Place of Earthquake Education in Our Schools," Edited by K.E.K. Ross, 12/31/89, (PB90-108606). This report is available only through NTIS (see address given above).
- NCEER-89-0018 "Multidimensional Models of Hysteretic Material Behavior for Vibration Analysis of Shape Memory Energy Absorbing Devices, by E.J. Graesser and F.A. Cozzarelli, 6/7/89, (PB90-164146/AS).
- NCEER-89-0019 "Nonlinear Dynamic Analysis of Three-Dimensional Base Isolated Structures (3D-BASIS)," by S. Nagarajah, A.M. Reinhorn and M.C. Constantinou, 8/3/89, (PB90-161936/AS). This report is available only through NTIS (see address given above).
- NCEER-89-0020 "Structural Control Considering Time-Rate of Control Forces and Control Rate Constraints," by F.Y. Cheng and C.P. Pantelides, 8/3/89, (PB90-120445/AS).
- NCEER-89-0021 "Subsurface Conditions of Memphis and Shelby County," by K.W. Ng, T-S. Chang and H-H.M. Hwang, 7/26/89, (PB90-120437/AS).
- NCEER-89-0022 "Seismic Wave Propagation Effects on Straight Jointed Buried Pipelines," by K. Elhadi and M.J. O'Rourke, 8/24/89, (PB90-162322/AS).
- NCEER-89-0023 "Workshop on Serviceability Analysis of Water Delivery Systems," edited by M. Grigoriu, 3/6/89, (PB90-127424/AS).
- NCEER-89-0024 "Shaking Table Study of a 1/5 Scale Steel Frame Composed of Tapered Members," by K.C. Chang, J.S. Hwang and G.C. Lee, 9/18/89, (PB90-160169/AS).
- NCEER-89-0025 "DYNA1D: A Computer Program for Nonlinear Seismic Site Response Analysis - Technical Documentation," by Jean H. Prevost, 9/14/89, (PB90-161944/AS). This report is available only through NTIS (see address given above).
- NCEER-89-0026 "1:4 Scale Model Studies of Active Tendon Systems and Active Mass Dampers for Aseismic Protection," by A.M. Reinhorn, T.T. Soong, R.C. Lin, Y.P. Yang, Y. Fukao, H. Abe and M. Nakai, 9/15/89, (PB90-173246/AS).
- NCEER-89-0027 "Scattering of Waves by Inclusions in a Nonhomogeneous Elastic Half Space Solved by Boundary Element Methods," by P.K. Hadley, A. Askar and A.S. Cakmak, 6/15/89, (PB90-145699/AS).
- NCEER-89-0028 "Statistical Evaluation of Deflection Amplification Factors for Reinforced Concrete Structures," by H.H.M. Hwang, J-W. Jaw and A.L. Ch'ng, 8/31/89, (PB90-164633/AS).
- NCEER-89-0029 "Bedrock Accelerations in Memphis Area Due to Large New Madrid Earthquakes," by H.H.M. Hwang, C.H.S. Chen and G. Yu, 11/7/89, (PB90-162330/AS).

- NCEER-89-0030 "Seismic Behavior and Response Sensitivity of Secondary Structural Systems," by Y.Q. Chen and T.T. Soong, 10/23/89, (PB90-164658/AS).
- NCEER-89-0031 "Random Vibration and Reliability Analysis of Primary-Secondary Structural Systems," by Y. Ibrahim, M. Grigoriu and T.T. Soong, 11/10/89, (PB90-161951/AS).
- NCEER-89-0032 "Proceedings from the Second U.S. - Japan Workshop on Liquefaction, Large Ground Deformation and Their Effects on Lifelines, September 26-29, 1989," Edited by T.D. O'Rourke and M. Hamada, 12/1/89, (PB90-209388/AS).
- NCEER-89-0033 "Deterministic Model for Seismic Damage Evaluation of Reinforced Concrete Structures," by J.M. Bracci, A.M. Reinhorn, J.B. Mander and S.K. Kunath, 9/27/89.
- NCEER-89-0034 "On the Relation Between Local and Global Damage Indices," by E. DiPasquale and A.S. Cakmak, 8/15/89, (PB90-173865).
- NCEER-89-0035 "Cyclic Undrained Behavior of Nonplastic and Low Plasticity Silts," by A.J. Walker and H.E. Stewart, 7/26/89, (PB90-183518/AS).
- NCEER-89-0036 "Liquefaction Potential of Surficial Deposits in the City of Buffalo, New York," by M. Budhu, R. Giese and L. Baumgrass, 1/17/89, (PB90-208455/AS).
- NCEER-89-0037 "A Deterministic Assessment of Effects of Ground Motion Incoherence," by A.S. Veletsos and Y. Tang, 7/15/89, (PB90-164294/AS).
- NCEER-89-0038 "Workshop on Ground Motion Parameters for Seismic Hazard Mapping," July 17-18, 1989, edited by R.V. Whitman, 12/1/89, (PB90-173923/AS).
- NCEER-89-0039 "Seismic Effects on Elevated Transit Lines of the New York City Transit Authority," by C.J. Costantino, C.A. Miller and E. Heymsfield, 12/26/89, (PB90-207887/AS).
- NCEER-89-0040 "Centrifugal Modeling of Dynamic Soil-Structure Interaction," by K. Weissman, Supervised by J.H. Prevost, 5/10/89, (PB90-207879/AS).
- NCEER-89-0041 "Linearized Identification of Buildings With Cores for Seismic Vulnerability Assessment," by I-K. Ho and A.E. Aktan, 11/1/89, (PB90-251943/AS).
- NCEER-90-0001 "Geotechnical and Lifeline Aspects of the October 17, 1989 Loma Prieta Earthquake in San Francisco," by T.D. O'Rourke, H.E. Stewart, F.T. Blackburn and T.S. Dickerman, 1/90, (PB90-208596/AS).
- NCEER-90-0002 "Nonnormal Secondary Response Due to Yielding in a Primary Structure," by D.C.K. Chen and L.D. Lutes, 2/28/90, (PB90-251976/AS).
- NCEER-90-0003 "Earthquake Education Materials for Grades K-12," by K.E.K. Ross, 4/16/90, (PB91-251984/AS).
- NCEER-90-0004 "Catalog of Strong Motion Stations in Eastern North America," by R.W. Busby, 4/3/90, (PB90-258062/AS).
- NCEER-90-0005 "NCEER Strong-Motion Data Base: A User Manual for the GeoBase Release (Version 1.0 for the Sun3)," by P. Friberg and K. Jacob, 3/31/90 (PB90-258062/AS).
- NCEER-90-0006 "Seismic Hazard Along a Crude Oil Pipeline in the Event of an 1811-1812 Type New Madrid Earthquake," by H.H.M. Hwang and C-H.S. Chen, 4/16/90(PB90-258054).
- NCEER-90-0007 "Site-Specific Response Spectra for Memphis Sheahan Pumping Station," by H.H.M. Hwang and C.S. Lee, 5/15/90, (PB91-108811/AS).

- NCEER-90-0008 "Pilot Study on Seismic Vulnerability of Crude Oil Transmission Systems," by T. Ariman, R. Dobry, M. Grigoriu, F. Kozin, M. O'Rourke, T. O'Rourke and M. Shinozuka, 5/25/90, (PB91-108837/AS).
- NCEER-90-0009 "A Program to Generate Site Dependent Time Histories: EQGEN," by G.W. Ellis, M. Srinivasan and A.S. Cakmak, 1/30/90, (PB91-108829/AS).
- NCEER-90-0010 "Active Isolation for Seismic Protection of Operating Rooms," by M.E. Talbott, Supervised by M. Shinozuka, 6/8/9, (PB91-110205/AS).
- NCEER-90-0011 "Program LINEARID for Identification of Linear Structural Dynamic Systems," by C-B. Yun and M. Shinozuka, 6/25/90, (PB91-110312/AS).
- NCEER-90-0012 "Two-Dimensional Two-Phase Elasto-Plastic Seismic Response of Earth Dams," by A.N. Yiagos, Supervised by J.H. Prevost, 6/20/90, (PB91-110197/AS).
- NCEER-90-0013 "Secondary Systems in Base-Isolated Structures: Experimental Investigation, Stochastic Response and Stochastic Sensitivity," by G.D. Manolis, G. Juhn, M.C. Constantinou and A.M. Reinhorn, 7/1/90, (PB91-110320/AS).
- NCEER-90-0014 "Seismic Behavior of Lightly-Reinforced Concrete Column and Beam-Column Joint Details," by S.P. Peasiki, C.H. Conley, P. Gergely and R.N. White, 8/22/90, (PB91-108795/AS).
- NCEER-90-0015 "Two Hybrid Control Systems for Building Structures Under Strong Earthquakes," by J.N. Yang and A. Danielians, 6/29/90, (PB91-125393/AS).
- NCEER-90-0016 "Instantaneous Optimal Control with Acceleration and Velocity Feedback," by J.N. Yang and Z. Li, 6/29/90, (PB91-125401/AS).
- NCEER-90-0017 "Reconnaissance Report on the Northern Iran Earthquake of June 21, 1990," by M. Mehrain, 10/4/90, (PB91-125377/AS).
- NCEER-90-0018 "Evaluation of Liquefaction Potential in Memphis and Shelby County," by T.S. Chang, P.S. Tang, C.S. Lee and H. Hwang, 8/10/90, (PB91-125427/AS).
- NCEER-90-0019 "Experimental and Analytical Study of a Combined Sliding Disc Bearing and Helical Steel Spring Isolation System," by M.C. Constantinou, A.S. Mokha and A.M. Reinhorn, 10/4/90, (PB91-125385/AS).
- NCEER-90-0020 "Experimental Study and Analytical Prediction of Earthquake Response of a Sliding Isolation System with a Spherical Surface," by A.S. Mokha, M.C. Constantinou and A.M. Reinhorn, 10/11/90, (PB91-125419/AS).
- NCEER-90-0021 "Dynamic Interaction Factors for Floating Pile Groups," by G. Gazetas, K. Fan, A. Kaynia and E. Kausel, 9/10/90, (PB91-170381/AS).
- NCEER-90-0022 "Evaluation of Seismic Damage Indices for Reinforced Concrete Structures," by S. Rodriguez-Gomez and A.S. Cakmak, 9/30/90, PB91-171322/AS).
- NCEER-90-0023 "Study of Site Response at a Selected Memphis Site," by H. Desai, S. Ahmad, E.S. Gazetas and M.R. Ot, 10/11/90, (PB91-196857/AS).
- NCEER-90-0024 "A User's Guide to Strongmo: Version 1.0 of NCEER's Strong-Motion Data Access Tool for PCs and Terminals," by P.A. Friberg and C.A.T. Susch, 11/15/90, (PB91-171272/AS).
- NCEER-90-0025 "A Three-Dimensional Analytical Study of Spatial Variability of Seismic Ground Motions," by L-L. Hong and A.H.-S. Ang, 10/30/90, (PB91-170399/AS).

- NCEER-90-0026 "MUMOID User's Guide - A Program for the Identification of Modal Parameters," by S. Rodriguez-Gomez and E. DiPasquale, 9/30/90, (PB91-171298/AS).
- NCEER-90-0027 "SARCF-II User's Guide - Seismic Analysis of Reinforced Concrete Frames," by S. Rodriguez-Gomez, Y.S. Chung and C. Meyer, 9/30/90, (PB91-171280/AS).
- NCEER-90-0028 "Viscous Dampers: Testing, Modeling and Application in Vibration and Seismic Isolation," by N. Makris and M.C. Constantinou, 12/20/90 (PB91-190561/AS).
- NCEER-90-0029 "Soil Effects on Earthquake Ground Motions in the Memphis Area," by H. Hwang, C.S. Lee, K.W. Ng and T.S. Chang, 8/2/90, (PB91-190751/AS).
- NCEER-91-0001 "Proceedings from the Third Japan-U.S. Workshop on Earthquake Resistant Design of Lifeline Facilities and Countermeasures for Soil Liquefaction, December 17-19, 1990," edited by T.D. O'Rourke and M. Hamada, 2/1/91, (PB91-179259/AS).
- NCEER-91-0002 "Physical Space Solutions of Non-Proportionally Damped Systems," by M. Tong, Z. Liang and G.C. Lee, 1/15/91, (PB91-179242/AS).
- NCEER-91-0003 "Seismic Response of Single Piles and Pile Groups," by K. Fan and G. Gazetas, 1/10/91, (PB92-174994/AS).
- NCEER-91-0004 "Damping of Structures: Part 1 - Theory of Complex Damping," by Z. Liang and G. Lee, 10/10/91, (PB92-197235/AS).
- NCEER-91-0005 "3D-BASIS - Nonlinear Dynamic Analysis of Three Dimensional Base Isolated Structures: Part II," by S. Nagarajah, A.M. Reinhorn and M.C. Constantinou, 2/28/91, (PB91-190553/AS).
- NCEER-91-0006 "A Multidimensional Hysteretic Model for Plasticity Deforming Metals in Energy Absorbing Devices," by E.J. Graesser and F.A. Cozzarelli, 4/9/91, (PB92-108364/AS).
- NCEER-91-0007 "A Framework for Customizable Knowledge-Based Expert Systems with an Application to a KBES for Evaluating the Seismic Resistance of Existing Buildings," by E.G. Ibarra-Anaya and S.J. Fennes, 4/9/91, (PB91-210930/AS).
- NCEER-91-0008 "Nonlinear Analysis of Steel Frames with Semi-Rigid Connections Using the Capacity Spectrum Method," by G.G. Deierlein, S-H. Haeh, Y-J. Shen and J.F. Abel, 7/2/91, (PB92-113828/AS).
- NCEER-91-0009 "Earthquake Education Materials for Grades K-12," by K.E.K. Ross, 4/30/91, (PB91-212142/AS).
- NCEER-91-0010 "Phase Wave Velocities and Displacement Phase Differences in a Harmonically Oscillating Pile," by N. Makris and G. Gazetas, 7/8/91, (PB92-108356/AS).
- NCEER-91-0011 "Dynamic Characteristics of a Full-Size Five-Story Steel Structure and a 2/5 Scale Model," by K.C. Chang, G.C. Yao, G.C. Lee, D.S. Hao and Y.C. Yeh," 7/2/91.
- NCEER-91-0012 "Seismic Response of a 2/5 Scale Steel Structure with Added Viscoelastic Dampers," by K.C. Chang, T.T. Soong, S-T. Oh and M.L. Lai, 5/17/91 (PB92-110816/AS).
- NCEER-91-0013 "Earthquake Response of Retaining Walls; Full-Scale Testing and Computational Modeling," by S. Alampalli and A.W.M. Elgarnal, 6/20/91, to be published.
- NCEER-91-0014 "3D-BASIS-M: Nonlinear Dynamic Analysis of Multiple Building Base Isolated Structures," by P.C. Tsopelas, S. Nagarajah, M.C. Constantinou and A.M. Reinhorn, 5/28/91, (PB92-113885/AS).

- NCEER-91-0015 "Evaluation of SEAOC Design Requirements for Sliding Isolated Structures," by D. Theodossiou and M.C. Constantinou, 6/10/91, (PB92-114602/AS).
- NCEER-91-0016 "Closed-Loop Modal Testing of a 27-Story Reinforced Concrete Flat Plate-Core Building," by H.R. Somaprasad, T. Toksoy, H. Yoshiyuki and A.E. Aktan, 7/15/91, (PB92-129980/AS).
- NCEER-91-0017 "Shake Table Test of a 1/6 Scale Two-Story Lightly Reinforced Concrete Building," by A.G. El-Attar, R.N. White and P. Gergely, 2/28/91, (PB92-222447/AS).
- NCEER-91-0018 "Shake Table Test of a 1/8 Scale Three-Story Lightly Reinforced Concrete Building," by A.G. El-Attar, R.N. White and P. Gergely, 2/28/91, (PB93-116630/AS).
- NCEER-91-0019 "Transfer Functions for Rigid Rectangular Foundations," by A.S. Veletsos, A.M. Prasad and W.H. Wu, 7/31/91.
- NCEER-91-0020 "Hybrid Control of Seismic-Excited Nonlinear and Inelastic Structural Systems," by J.N. Yang, Z. Li and A. Daniellians, 8/1/91, (PB92-143171/AS).
- NCEER-91-0021 "The NCEER-91 Earthquake Catalog: Improved Intensity-Based Magnitudes and Recurrence Relations for U.S. Earthquakes East of New Madrid," by L. Seeber and J.G. Armbruster, 8/28/91, (PB92-176742/AS).
- NCEER-91-0022 "Proceedings from the Implementation of Earthquake Planning and Education in Schools: The Need for Change - The Roles of the Changemakers," by K.E.K. Ross and F. Winslow, 7/23/91, (PB92-129998/AS).
- NCEER-91-0023 "A Study of Reliability-Based Criteria for Seismic Design of Reinforced Concrete Frame Buildings," by H.H.M. Hwang and H-M. Hsu, 8/10/91, (PB92-140235/AS).
- NCEER-91-0024 "Experimental Verification of a Number of Structural System Identification Algorithms," by R.G. Ghanem, H. Gavin and M. Shinozuka, 9/18/91, (PB92-176577/AS).
- NCEER-91-0025 "Probabilistic Evaluation of Liquefaction Potential," by H.H.M. Hwang and C.S. Lee, 11/25/91, (PB92-143429/AS).
- NCEER-91-0026 "Instantaneous Optimal Control for Linear, Nonlinear and Hysteretic Structures - Stable Controllers," by J.N. Yang and Z. Li, 11/15/91, (PB92-163807/AS).
- NCEER-91-0027 "Experimental and Theoretical Study of a Sliding Isolation System for Bridges," by M.C. Constantinou, A. Kartoum, A.M. Reinhorn and P. Bradford, 11/15/91, (PB92-176973/AS).
- NCEER-92-0001 "Case Studies of Liquefaction and Lifeline Performance During Past Earthquakes, Volume 1: Japanese Case Studies," Edited by M. Hamada and T. O'Rourke, 2/17/92, (PB92-197243/AS).
- NCEER-92-0002 "Case Studies of Liquefaction and Lifeline Performance During Past Earthquakes, Volume 2: United States Case Studies," Edited by T. O'Rourke and M. Hamada, 2/17/92, (PB92-197250/AS).
- NCEER-92-0003 "Issues in Earthquake Education," Edited by K. Ross, 2/3/92, (PB92-222389/AS).
- NCEER-92-0004 "Proceedings from the First U.S. - Japan Workshop on Earthquake Protective Systems for Bridges," Edited by Ian Buckle, 2/4/92.